Petroleum Derived Carbons

Marvin L. Deviney, EDITOR
Ashland Chemical Co.

Thomas M. O'Grady, EDITOR
Standard Oil Co. (Indiana)

A symposium co-sponsored by

the Division of Petroleum

Chemistry, Inc. and the

Division of Industrial and

Engineering Chemistry at

the 169th Meeting of the

American Chemical Society,

Philadelphia, Penn.,

April 9–11, 1975

ACS SYMPOSIUM SERIES 21

ACS Symposium Series

Robert F. Gould, *Series Editor*

FOREWORD

The ACS SYMPOSIUM SERIES was founded in 1974 to provide a medium for publishing symposia quickly in book form. The format of the SERIES parallels that of the continuing ADVANCES IN CHEMISTRY SERIES except that in order to save time the papers are not typeset but are reproduced as they are submitted by the authors in camera-ready form. As a further means of saving time, the papers are not edited or reviewed except by the symposium chairman, who becomes editor of the book. Papers published in the ACS SYMPOSIUM SERIES are original contributions not published elsewhere in whole or major part and include reports of research as well as reviews since symposia may embrace both types of presentation.

PREFACE

Over the past 35 years the industrial carbon and graphite fields have expanded greatly both in the technology available and in the volume of production. Not only has modern technology demanded major improvements in the properties of older, more conventional manufactured-carbon products, but the great advances in nuclear, aerospace, and medical sciences have required the development and continued improvement of new carbon and graphite materials. Over the past decade or so, the use of precursors from petroleum in industrial carbon and graphite manufacturing has grown rapidly. Two reasons for this growth are

1. the plentiful (until very recently) supplies of heavy ends or residua from refineries geared to a gasoline-type economy and operating with emphasis on catalytic cracking

2. the recent development and commercial availability from refineries of selectively manufactured carbon precursors, particularly petroleum pitches, of well defined, reproducible qualities.

The manufacture of carbon and graphite is not only scientifically interdisciplinary but can be improved only through close cooperation and understanding between raw material suppliers, industrial fabricators, and end-product users. The latter two groups have worked closely together for many years. However, the very important role of the raw material producer perhaps has been less fully appreciated, especially by the producer himself. In the past, almost all carbon precursor suppliers —whether from the coal, petroleum, wood, or paper areas (and the expected-to-emerge synthetic crude area should be included here, also) —have considered these raw materials to be mainly by-products to be processed at as low a cost as possible, subjected to a minimum of quality control, and sold as inexpensive commodity materials.

In the past decade, however, new factors have required a reevaluation of these previous concepts. One reason for this reassessment has been, of course, the stringent quality and end-use performance demands associated with recent developments in the general nuclear and aerospace areas and in certain specialty areas (e.g., electronics, biomedical, and electrical discharge machining). A second reason, rapidly becoming more important, is the changing situation regarding raw material availability. Both the increased demands for higher quality carbon and graphite precursors and the petroleum shortage (especially in the United States)

vii

directly affect the refiner. Thus, it was very appropriate that the Division of Petroleum Chemistry of the American Chemical Society decided to sponsor this state-of-the-art symposium.

The 31 papers in this volume deal predominantly with carbon and graphite derived from petroleum, but some overlap with carbons derived from coal is not only inevitable but desirable for comparing the properties of intermediate and final products (e.g., the several papers dealing with mesophase and coke formation, electrode performance, fabrication of carbon–carbon composite materials, machined fabricated products, and high pressure impregnation technology).

The main objective of this symposium was to obtain papers which would cover the full scope of the current field of petroleum-derived carbons. The papers roughly fall into eight groupings as summarized below.

1. Introductory chapters on the business outlook, both projected costs and the anticipated supply and demand situation (Stokes) and an overview of the entire field by a well known senior scientist, engineer, and author with many years of experience in the carbon and graphite field (Mantell).

2. Refinery processes, particularly coke manufacturing (Metrailer, Gotshall), production of a new type of high quality petroleum pitch carbon precursor (Newman) and its analytical characterization (Smith), preparation of activated carbon from acid sludge (Messman), and the mechanisms of adsorption with activated and impregnated charcoal (Magee).

3. Fabrication and manufacturing techniques: large volume products, e.g., electrodes and refractories, and specialty products, such as brushes, nozzles, vanes, dies, seals, bearings, and brakes (Shobert); aluminum production anodes prepared from petroleum pitch (Pendley); machine fabrication of carbon and graphite (Corah); specialty (particularly nuclear grade) graphites from special green cokes (Horne) and by high pressure impregnation and carbonization techniques (Burns, Chard); characterization of the structure of graphites prepared for extreme thermal shock (Bradshaw); experimental design techniques used for preparing graphites for thermostructural (ballistic reentry) applications (Pratt); pyrolytic infiltration techniques in the preparation of carbon–carbon composite materials (Gebhardt); factors affecting the mechanisms of formation of pyrolytic carbons (Cullis); and pyrolytic carbon coatings in medical and bioengineering applications (Bokros).

4. Mesophase transformations and properties and their industrial relevance (Marsh, White). Although the sequence leading to graphitization covers a wide temperature range, ultimately reaching nearly 3000°C, the plastic mesophase region (comprising only a few percent of the total temperature span) is the critical region in which the molecular processes take place which govern the morphology and microstructure of the final graphite product.

5. Methods of fabricating carbon fibers (Diefendorf) and techniques for modifying their surface chemistry to improve adhesion in plastic composite applications (Ehrburger).

6. Carbon black formation mechanisms (Lahaye, Cullis), microstructure and morphology (Ban), and applications of a special type prepared from petroleum coke (Gotshall). In terms of both volume produced and total sales revenue, carbon black is one of the most important chemical products manufactured in the United States. Ninety-four percent of carbon black production is consumed by the rubber industry. Most of this is used in tires where carbon black enhances a number of rubber physical properties (great improvement in tread abrasion resistance being the most important).

7. Electrical and thermal properties of carbon and graphite, with a comprehensive review (Woollam) and a discussion of the use of intercalation techniques to increase greatly the electrical conductivity of graphites, particularly fibers (Vogel, Fischer).

8. Recent developments in the coal derivatives field (Joseph, Kimber), to provide recognition that active research is progressing in this area as well as in the field of the upgrading and finding new uses for petroleum derived carbons.

Finally, many acknowledgments should be extended to several scientists and organizations without whose assistance the symposium and this book would not have been possible. An expression of appreciation is due to Ashland Chemical Co. and Ashland Oil, Inc., particularly to James E. Lewis, for encouragement and permission to undertake the duties of symposium co-chairman and principal editor. The advice and counsel of Joe W. Hightower, John S. Ball, and Robbin C. Anderson are also acknowledged. Likewise, appreciation is also extended for the important contributions of the symposium co-chairman, Thomas M. O'Grady. Finally, special gratitude is expressed to the following industrial organizations for providing support which made it possible for three overseas scientists to make presentations at the Philadelphia symposium. These sponsoring corporations include: Airco Speer, AMOCO, ARCO, Ashland Chemical, Cabot, Cities Service, Continental Carbon, FMC, J. M. Huber, Mobil, Pfizer, SOHIO, Stackpole Carbon, Sun Oil, and Union Carbide.

Ashland Chemical Co.
Columbus, Ohio
October 6, 1975   MARVIN L. DEVINEY

Manufacture of Industrial Carbons from Petroleum Raw Materials

CHARLES A. STOKES

Charles A. Stokes Consulting Group, Princeton, N. J. 08540

This paper is concerned with an important but little known group of highly useful materials which can be described as *high purity industrial carbons* and which will be spoken of simply as *industrial carbons* for convenience. We are not dealing with the final end use products that are made from highly pure carbons. Rather, we are dealing with the forms of carbon that serve as key components in the manufacture of such end use items as tires, plastic building materials, amorphous and graphitized electrodes, and the literally hundreds of very essential small volume items made from carbon. It is the purpose of this paper to place in perspective for you these various forms of industrial carbons indicating not only the opportunities for their growth but the problems that will be encountered in maintaining adequate supplies of proper quality source materials for their manufacture. The problems that are now surfacing present both a continuing technical challenge and a continuing opportunity to enterprising companies who may want to maintain or improve their competitive position in the making of such carbons or their raw materials.

It is appropriate to examine the several industrial carbons as a group because they not only come largely from petroleum sources but also, to a very considerable extent, they stem from the same limited part of the barrel of refined oil. If this part of the barrel finds other uses or becomes too small to take care of demand, problems could arise quickly that would be felt throughout a large segment of industry.

We are not concerned with the technical details of processes to manufacture carbons nor with the small nuances in product quality resulting from raw material changes. Instead, we are concerned with the broad raw material supply/demand picture and the economic effects of a raw material shortage should one occur in the near future.

Definitions

While we have to be to some degree arbitrary in defining an

1

industrial carbon, the definition is nonetheless necessary and
useful in setting apart a certain distinct class of materials
from what will be merely solid carbon or a highly carbonaceous
material of little if any value other than for fuel. The mate-
rials under consideration here are often difficult to make and
require careful control for a useful level of properties. This
paper is mainly concerned with industrial carbons made from petro-
leum source materials, but it is recognized that similar materials
can be and are made from coal tars or various kinds of "syn
crudes" that may be made in the future from coal, tar sands, and
the like. With these limitations in mind, we can define an indus-
trial carbon as:

    (1)   Essentially pure carbon, i.e. approximately
           95% or more carbon content on an ash, sulfur,
           nitrogen, oxygen, and moisture-free basis.

    (2)   Normally a solid at room temperature but, in
           some cases, containing enough hydrogen to be
           liquefiable at elevated temperatures.

    (3)   In the case of liquefiable materials, the end
           use is normally to make solid carbon by elim-
           ination of practically all volatiles at the
           first stage of chemical conversion or altera-
           tion in the end use process. That is, the
           liquefiable carbon is tailored so that it
           will convert easily to solid carbon as nearly
           quantitatively as possible on heating, usually
           to the extent of at least 50% and often up to
           60 to 70%.

    (4)   Sulfur content usually under 2% and desirably
           much lower down to a few tenths of one percent.
           Occasionally, materials of 3 - 5% sulfur are
           included because of shortages of lower sulfur
           carbons.

    (5)   Non-combustible residue below 0.1%, but in some
           cases a few tenths can be tolerated.

    (6)   Metallic contaminants usually less than 0.01%
           for each separate constituent.

This definition excludes carbonaceous materials in which the
carbon can be used chemically without regard to a reasonable
amount of contaminants that do not interfere with the chemical
function of the carbon or the chemical composition of the end
product. Thus, we exclude, for examples, coke designed for blast
furnace use (which isn't made from petroleum anyway), and the
petroleum coke used to make calcium carbide. Included in our def-
inition are such important materials as:

    (1)   Carbon black.
    (2)   Selected petroleum coke, green or calcined.
    (3)   Needle coke, green or calcined.
    (4)   Electrode pitch.

(5) Pitch for structural carbon manufacture
     including graphite shapes for atomic
     reactors.
(6) Carbonaceous reducing agent for the new
     Alcoa primary aluminum process.
(7) Activated carbon.
This list is not necessarily an all inclusive one.

As pointed out earlier, industrial carbons are, in general,
raw materials for further conversion rather than the manufactured
or fabricated article itself.

Some of the carbon materials listed above are by-products,
and some are products made deliberately and to carefully con-
trolled specifications. However, all of them are either petro-
leum refinery by-products or they are made from petroleum
refining by-products. This is a very important point as will be
brought out in the discussion to follow.

We will not dwell on activated carbon from petroleum raw
materials as the volume of raw materials required is so small.
Further, activated carbon is made from many other raw materials
which dominate the field relegating petroleum to a relatively un-
important position as yet. Activated carbon is an important
material and will become more so. However, raw material supply
poses no critical problems for this field. The subject of
activated carbon is well covered in other papers by specialists
in this field.

Carbon Black

In total value, probably our most important industrial
carbon is carbon black. We have to say "probably" because it is
so difficult to get accurate figures on the physical volumes and
dollar values of some of the industrial carbons. World output
value of carbon black will cross the $1 billion mark well before
1980. Carbon black is better than 99% carbon. It is an ex-
tremely finely divided material with the unique property of dis-
persing readily in elastomers to produce a highly strengthened or
"reinforced" end product. About 95% of its use is in rubber. The
largest single rubber use is tires; the use in replacement tires
is about 80% or more of the total consumption for tires, a factor
lending stability to the market.

The carbon black process is essentially a carefully con-
trolled partial combustion of heavy aromatic oils in a refractory
lined and insulated furnace. All processes in use are highly
proprietary and therefore cannot be discussed here. For esti-
mating raw material requirements, it is satisfactory to multiply
the weight of the carbon black by two. In Figure 1, we show the
raw material requirement for carbon black arrived at by doubling
the expected consumption of carbon black. The needs of the Com-
munist countries are almost surely understated as reliable infor-
mation is not available.

To achieve practical yields and plant outputs, as well as for product quality considerations, it is necessary to use as raw material pure, heavy petroleum aromatics containing a preponderance of fused aromatic ring compounds composed mainly of 3 or more rings. The atomic hydrogen to carbon ratio usually falls in the range of 0.9 to 1.1 and very seldom goes above 1.2. Alkali and alkaline earth metals must be in the low ppm range. High molecular weight resins, commonly called asphaltenes in the industry because the standard test method was adapted from the measurement method used on other materials, must be limited, but no definite number can be given. Sulfur is a problem because of loss of yield, plant maintenance, and potential stack discharge considerations. Most raw materials now used fall in the 1 to 3% range. The exact specifications of these materials are considered to be proprietary by most producers.

A better insight into carbon black raw material is gained by recognizing that these materials are synthetic. They are not naturally present in petroleum but are synthesized in the processing of petroleum to gasolene or olefins. Thus, the great bulk of such raw materials come from catalytic cracking to make gasolene and from thermal cracking to make olefins. This means that the carbon black producer must accept what comes out of the cracking processes with only slight alterations being possible at the source. For example, the materials are referred to as fuel oil or tars by the producer which indicates the degree of importance he attaches to their properties. These tars can be altered at the source by better stripping to remove light ends and better settling to remove catalyst fines. Beyond this, about all that the user can demand is the avoidance of contaminants and a reasonable amount of blending to smooth out fluctuations in quality. Nevertheless, the suppliers and users have worked out their mutual problems so that the carbon black industry has been able to function smoothly and grow.

Carbon black today is made largely from a catalytic cracking by-product -- decant oil also called fractionator bottoms. As long ago as the early 1950's, some carbon black was made from ethylene tars. Recently, increasing amounts of ethylene tars have been used, particularly in Europe. In the past, extracts of decant oils and lighter catalytic recycle oils were used, but these products are made only in a few plants scattered throughout the world. Tars from thermal cracking of gas oils to make gasoline are still used in one or two cases, but there is no increase in sight from this source.

Finally, heavy creosotes and anthracene oils produced by coal tar distillation are used especially in Europe, Japan, and in some Eastern Bloc countries.

However, the real work horse raw material for carbon black is decant oil from catalytic cracking of petroleum gas oils. Typical properties of a suitable carbon black raw material based on decant oil are:

API	-2 to +2
Asphaltenes	2 to 6%
Sulfur	2.5% maximum
Benzene Insolubles	0.05% maximum
Sodium	10 ppm maximum
Potassium	1 ppm maximum
Bureau of Mines Correlation Index	125 ± 5
Pounds of carbon per gallon	Not less than 8.0

In the case of ethylene tars, the sulfur tends to be lower and the asphaltenes considerably higher, this latter property becoming the limiting factor in allowing the use of such tars. Also, the carbon content per gallon may drop below the desired level which penalizes the yield somewhat.

While natural, refinery and coke oven gases are widely used as auxiliary heat sources, these materials are not essential. All major producers have processes that use part of the liquid feed as the auxiliary fuel. Plant residue gas is used as a fuel for steam generation and drying the carbon beads produced by wet beading processes.

More will be said about the supply/demand relationships of the feedstocks in a following section.

Electrode Pitch

This product is a highly polymerized hydrocarbon that is processed to the stage of incipient coking. At the next stage of use as a binder for solid carbon, coking is made to occur. At room temperature, these electrode pitches are normally solids, and hence we can justify the terminology as solid carbons. Carbon content is 95% or greater on an inert free basis. In making binder pitch of this kind, one is literally trying to get as nearly to pure carbon as possible while still retaining a material that can be melted and mixed with solid carbon aggregate to form an extrudable or moldable mass. As will be brought out in other papers, the final product must wet the carbon aggregate, give good green strength to the electrode, and, on coking, give a strong, dense electrode or carbon shape that will resist spalling in high temperature service.(1)

Such pitches come from three sources: from specially processed coal tar pitch from high temperature coal tars, from the processing of cat cracked decant oils and from processing ethylene tars. The first two sources are the most important. The coal tar source originally accounted for all electrode pitch. Now the supply of high temperature coal tar is no longer adequate to meet world demand. Consequently, the chemists have turned to polymerizable oils from petroleum cracking, i.e. to our old friends, decant oil from catalytic cracking and ethylene tars from naphtha and gas oil cracking. These materials may be processed by a combination of heat soaking and air blowing to give the kind of highly condensed polymers needed for electrode

binder pitch. (2), (3), (4), and (5) For example, Witco Chemi-
cal and Ashland Oil have built such plants and Koppers, a long
time producer of pitch from coal tars, has modified its Houston
plant to take petroleum feedstocks. Ashland is building a
second plant adjacent to its carbon black plant near Franklin, La.
The yield of pitch is 50 - 60% of the decant oil fed. Most of
the other 40 - 50% is recovered as a heavy aromatic distillate
usable as carbon black feedstock. The latest Ashland petroleum
pitch plant will use the off gas from the adjacent carbon black
plant as fuel for the pitch process. It is quite interesting to
see this close integration finally achieved between two indus-
trial carbons of such importance. Each uses the same starting
material, and the by-products of each are exchanged in the re-
spective conversion processes.

For the new Alcoa aluminum process, a type of pitch is re-
quired, and it replaces both the pitch and coke of the older Hall
electrolytic process. The hydrocarbon is sprayed into a fluid
bed of alumina particles forming a coke layer around the alumina.
The carbon coated alumina is then reacted with chlorine to form
aluminum chloride by the reactions used for many years to produce
this chemical. The aluminum chloride is then put through a cell
in which aluminum is recovered from the chloride by electrolysis
using graphitized electrodes. Chlorine is recycled. Since the
basic reaction still involves transferring oxygen to carbon from
alumina:

$$3Cl_2 + Al_2O_3 + 3C = 2AlCl_3 + 3CO$$
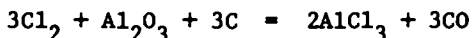
the overall carbon requirement is similar to the presently used
Hall process. Then, of course, carbon is used in the graphite
electrodes.

Supply/demand factors and forward estimates are given in the
Section "Petroleum Feedstock Supplies Related to Demands For
Industrial Carbons" below.

Petroleum Coke

General Considerations. Not all the industrial carbons are
made from synthetic tars. Ordinary or amorphous petroleum coke
is made from the direct residues of crude oil distillation. The
principal process is the well known delayed coking. In recent
years, fluid coking has come in on appreciable scale. Delayed
coke is strongly preferred for industrial carbon uses, but some
fluid coke is gradually finding its way into industrial carbon
uses.

The total amount of delayed and fluid coke made in the world
is on the order of 2 to 3 fold the industrial carbon use if coke
quality is ignored. However when quality is considered, the
picture changes rapidly. Much of the coke is high in sulfur and
metals and is totally unsuited for industrial carbon uses.

Most of the coke is calcined before industrial carbon use.

In this step, 25 - 30% loss occurs further concentrating inorganic impurities although sulfur may be marginally lowered.

In the U.S., coke laid down on cat cracking catalyst is reported in the Government statistics, but this coke never sees the light of day as it is burned to CO and CO_2 in the regeneration step. It is important not to confuse this coke with that actually produced as such and, in fact, the coke burned off catalyst is comparable in quantity to that actually recovered as salable coke.

Most of the world petroleum coke production occurs in the U.S. because we have a gasolene dominated refining output and, until lately, a plentiful supply of natural gas and cheap coal to replace heavy fuel oil. Coking fitted this pattern as nowhere else in the world. Until really successful lower cost processes are found to desulfurize the bottom of the barrel and until gasolene becomes less important in respect to other refinery products, this trend to coking will not be completely reversed in the U.S. In other regions of the world, there is no particular trend toward coking although a few cokers have been installed here and there, and in time there will be a few more. However, these cokers will generally be on Middle East crudes producing cokes not suited for industrial uses. Because of the U.S. domination of coke production, exports have risen exponentially since the end of World War II and in 1970-71 accounted for about 45% of U.S. marketable coke output.

Amorphous Coke. When the charge stock to a delayed coker is largely virgin bottoms, the coke produced is the ordinary or amorphous type used for non-graphitized electrodes. The principal use of this type coke is in anodes for the manufacture of primary aluminum, but such coke is also used in graphitized electrodes and in carbon shapes whether merely baked or graphitized as well. There are other uses for amorphous coke in which purity is not crucial, including fuel, but these are not considered as industrial carbon uses, and other materials can be substituted when petroleum coke is too expensive or unavailable.

A delayed coker is merely a short contact time heater coupled to a large drum in which the preheated feed "soaks" on a batch basis and gradually forms coke until the drum is filled. The filled drum is then discharged by hydraulic cutters while a second drum is being filled. The refiner has relatively little control over the properties of the coke; his object is to maximize gasolene and gas oil yield as these are ordinarily the more valuable products. Coking is often justified on zero value for the coke. However as heavy fuel oil value rises, it becomes less attractive to coke unless the fuel oil is too high in sulfur to be salable. In this case, the coke will not be very salable either except for fuel, particularly in export to a country with no sulfur restrictions on stack discharge.

The coke as made is called green coke and contains 20 - 25% volatile matter. Most of it is calcined to 0.5% or less volatile

matter before use as industrial carbon.

In the manufacture of aluminum, there are required 0.67 tons of green coke per ton of aluminum of which 0.4 ton is used as calcined coke. Purity requirements are high as outlined below:

Typical Specifications for Calcined Petroleum Coke For Aluminum Manufacture

Volatile matter	2.5% max.
Ash	0.05% max.
Metals	
Silicon	0.02
Iron	0.02
Vanadium	0.001
Nickel	0.001
Manganese	0.001
Sulfur	1% or less when EPA rulings are enforced

These specifications cannot always be met and still have adequate coke supply. No one knows the exact average degree of deviation, but directionally it will become larger as supplies become scarcer.

For graphitized electrodes as used in electric arc furnaces, purity requirements are generally not as high. For electrolytic cell carbons, purity requirements may be even higher at times than for aluminum depending upon the product being made. In making graphite moderator elements for atomic reactors, carbon specifications are extremely strict.

Needle Coke. For graphitized electrodes, the preferred carbon is a so-called crystalline coke known as needle coke. It is manufactured by a variation of the delayed coking process employing the very pure synthetic petroleum tars as feedstock. The high aromaticity of the feed is the key variable. Until recently, the operating know how was a carefully guarded secret. Apparently, the know how can now be purchased from selected engineering companies. Needle coke is also calcined before use in most cases.

This product sells on a green basis for in excess of $100 per ton whereas amorphous green coke sells for about half as much. These values are in reference to about $9 per bbl. average U.S. crude cost and are subject to change with crude oil and with the ratio of heavy fuel oil price to gasolene and gas oil values.

Petroleum Feedstock Supplies Related to Demands for Industrial Carbons

The Overall Supply Picture. Petroleum tars and distillation residues are the most important single source of feedstock for industrial carbons.

Crude petroleum as fed to a refinery is essentially CH_2; a closer estimate might be $CH_{1.9}$ or 86.2% carbon on an ash and sulfur free basis. If gas oil is fed to a catalytic cracker or an ethylene plant thermal cracking section, there is produced a certain amount of tar with a composition ranging from $CH_{1.05}$ to $CH_{1.15}$ which we will call $CH_{1.1}$, or 91.5% carbon on a sulfur free basis (ash is negligible in such tars). The tar resulting from naphtha cracking is very similar. These tars, which are made entirely from previously distilled feedstocks, are in essence synthetic polymers. In the case of catalytic cracking, the yield of tar, usually termed decant oil or fractionator bottoms in the trade, is typically 2-1/2% of the fresh feed. The fresh feed to cat crackers in the U.S. is about 30% of crude runs giving an overall yield of 0.75% of the crude run. For the free world as a whole, the fraction of crude fed to catalytic cracking is smaller being on the order of 14% which would give only 0.35% of cracked tar on the crude run. If we exclude the Western Hemisphere from the figures, the figures are very much smaller -- about 5% of crude runs fed to cat cracking and 0.13% of cracked tar on crude.

Synthetic tar produced in refineries by severe thermal cracking of gas oils is negligible in comparison to tars from cat cracking.

On the other hand, synthetic tars made in ethylene plants from naphtha and gas oil feeds are not negligible and are growing at a more rapid rate, although from a smaller base than synthetic tars from petroleum. Typical yields are 10 to 20% of ethylene production for naphthas up to 80 to 120% of ethylene production for gas oils. If these yields are put on the basis of feed to the ethylene plant and are corrected for low boiling oils included in the tars (about 15%), they become:

naphtha feed	2 - 4%
gas oil feed	16 - 24%

Translated back to crude oil, the yields are 0.5 to 1.0% and 5 - 7%, respectively, assuming that all of the naphtha and all of the lighter virgin gas oils from a typical barrel of crude are fed to the ethylene plant.

From these rough figures, we can easily conclude that tars from gas oil fed ethylene units could become very much more important as time goes on. Likewise, the naphtha based tars could be relatively more important since the amount on crude is comparable to cat cracking, and the ethylene plant growth rate is almost an order of magnitude greater than cat cracking growth.

On an absolute basis, the figures are quite different. Cat cracked tars, based on 1974 capacities, were about 191,000 bbls./day in the free world, 115,000 bbls./day in the U.S. alone, and 149,000 bbls./day in the Western Hemisphere. The last figure reflects primarily the high gasolene demand as a percentage of crude runs in the U.S., Canada, and Brazil. Ethylene tar

production in the U.S., including Puerto Rico, if ethylene were
produced at capacity in 1974, would have been at the rate of
some 24,000 bbls. per day of which nearly all (19,500 bbls./day)
would have come from gas oil sources. For the rest of the free
world, ethylene tar production at 1974 capacity would have been
about 44,000 bbls./day mostly from naphtha feed.

        These figures are summarized in Table I. Recognition of two
factors is important: (1) these are estimates and are probably
not closer than ± 15 - 20%, there being no way to improve on
these estimates other than a plant-by-plant detailed study, and
(2) not all of the material produced is suitable for carbon black
or for other industrial carbon uses to be discussed later. Never-
theless, the figures are accurate enough to allow meaningful con-
clusions as to the possible future supply/demand pinch.

        Feedstock Requirements for Carbon Black. Bearing in mind
the dangers of forecasting growth rates after a quantum jump in
energy costs, we have put together in Figure 1 a projection of
world carbon black feedstock requirements through 1985. Data
are actual through 1973 except for Eastern Bloc countries for
which the data are educated estimates. Growth rates from 1973 on
have been lowered to allow for the effect of increased energy
costs on world economies. From these data and the data for free
world cat cracking capacity, we can compare supply and demand
factors to see how they match up as in Table II. (The Eastern
Bloc countries are not included in Table II as the cat cracking
capacity data are not available.) The conclusion is clear that
some time in the next few years, carbon black feedstock demand
will outstrip supply from the decant oil source. This is more
particularly true because not all of the decant oil is suitable
for carbon black or available for this use. We know that little
of the European material is suitable and that consequently the
U.S. exports heavily to supply Europe. Exports also go to South
America and other areas. In Europe, ethylene tar is used as well
as coal tar oils which further emphasizes Europe's deficit posi-
tion on good feedstocks. All of this points to a free world
supply/demand deficit soon. The Eastern Bloc countries are more
apt to be in a deficit than in a surplus position in the years
ahead.

        It is also to be noted that decant oil is a growing source
of raw material for electrode pitch and needle coke and that these
uses can apparently buy feedstock away from carbon black under
today's price structures.

        Feedstock Requirements for Electrode Pitch. Up until about
1973, practically all electrode pitch came from coal tar sources
world wide. Starting about 1975, we believe substantially all
the growth will stem from petroleum sources. Consequently, we
estimate 1985 consumption on this basis, assuming a 50% yield of
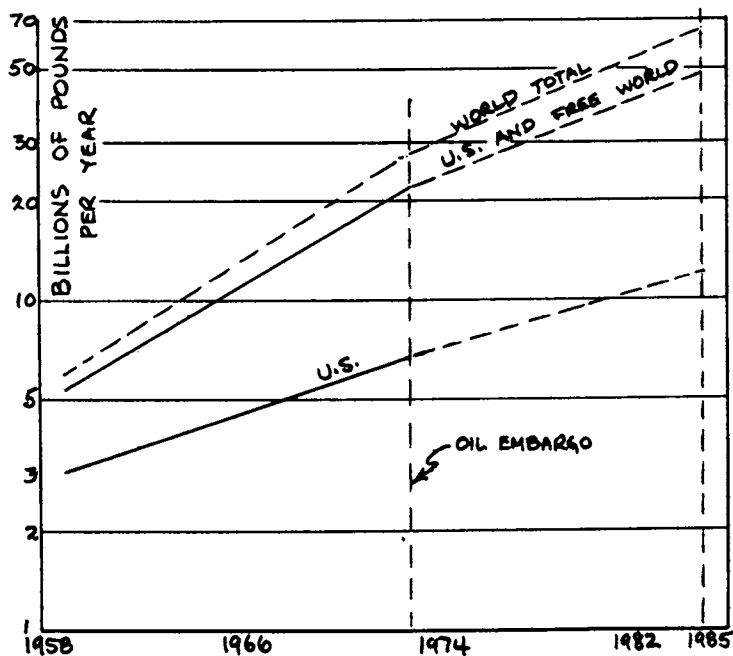pitch on decant oil. Our estimating factors are 0.1 ton of pitch

Figure 1. World feedstock needs for carbon black

TABLE I

ESTIMATED
FREE WORLD PRODUCTION OF PETROLEUM
DERIVED TARS FOR INDUSTRIAL CARBON USES IN 1974

	BARRELS PER CALENDAR DAY			
	U. S.	WESTERN HEMISPHERE	FREE WORLD EX. U. S.	FREE WORLD
CATALYTIC CRACKING	115,000	149,000	76,000	191,000
ETHYLENE TARS	24,000[1]	- - - -	44,000	68,000

ESTIMATED ACCURACY ± 15 - 20%

(1) INCLUDES PUERTO RICO

per ton of aluminum and 0.25 ton of pitch per ton of graphitized
carbons. By 1985, the world petroleum pitch demand will increase
by 1.87 MM tons for aluminum and 650,000 tons for graphitized
electrodes corresponding to 28,000 bbls./da. and 9,700 bbls./da.,
respectively, of decant oil needed or a total of roughly 38,000
bbls./da. This means a cat cracking capacity of 1.5 MM bbls./da.
to supply this amount of decant oil.

In 1975, we estimate that only 200,000 tons of petroleum
pitch will be produced, all in the U.S., requiring 6000 bbls./da.
of decant oil.

As noted below under Petroleum Coke Supply and Demand, there
are certain other possibilities for raw material supply by 1980 –
1985, but these are by no means certain from either an economic
or a technological standpoint.

Petroleum Coke Supply and Demand. It is possible to make a
good estimate of petroleum coke consumption for aluminum, by far
the largest industrial use, in 1985 based on extrapolation of the
historical data up through 1973. Over the period 1963 – 73, world
aluminum production grew at an 8.5% rate, U.S. at 6.3%, and the
world excluding the U.S. at 10.5%. The respective green coke re-
quirements were in short tons per year 8,900,000; 3,040,000; and
5,860,000. We project world consumption of coke for aluminum in
1985 at 17,500,000 tons per year based on an average growth rate
of 7%, down from the past 8.5% rate. Almost all of this must
come from the U.S.

For graphitized electrodes and other baked and structural
carbons, we project a 1985 green coke requirement of 4,400,000
tons, bringing the total industrial carbon uses of green coke to
roughly 22,000,000 tons per year.

The growth rate of marketable coke production in the U.S.
was 8.7% over the period 1954 – 1971. This growth rate is not
likely to be sustained due to the gradual shift in the U.S. back
to fuel oil production in refineries. The coke that will be made
will be increasingly from sour, high metals content crude oils.
Coke exports have been growing faster than coke production and if
both growth rates were sustained, exports would require all U.S.
marketable coke by about 1980 which obviously can't be allowed to
happen. These trends are brought out in Figure 2 which relates
available coke supply after exports to aluminum needs. In ar-
riving at this curve, we assumed that both marketable coke pro-
duction and exports continued to grow along long established
trends. The 1973 and 1974 data on coke production actually show
a pronounced drop in production compared to the trend. We be-
lieve this leveling off will continue. When it is considered
that some 25 – 50% of the coke is unfit for industrial use by
present standards and when all trends are viewed at once, it is
clear that petroleum coke supplies for industrial carbon use will
become a major problem in 5 years or so unless some new coke
sources are found. It is not likely that aluminum growth will be

TABLE II

MILLIONS OF BARRELS PER DAY OF CAT CRACKING CAPACITY
REQUIRED TO PRODUCE CARBON BLACK FEEDSTOCK

	1973 (ACTUAL)	1985 (EST'D)
DEMAND FACTORS		
U. S.	1.7	3.1
FREE WORLD EX U. S.	3.9	9.3
TOTAL	5.6	12.4
SUPPLY FACTORS		
U. S. ACTUAL CAT CRACKING CAPACITY	4.6	5.1
FREE WORLD ACTUAL CAT CRACKING CAPACITY INCLUDING U. S.	7.5	9.0
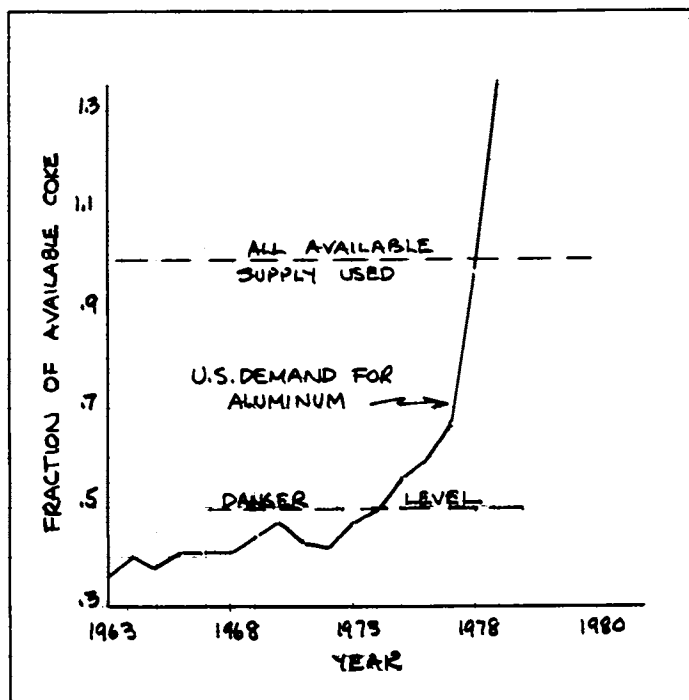
Figure 2. *U.S. supply/demand trends for aluminum coke*

sharply curtailed whether it is energy intensive or not. New
coke sources could come from other countries going to a high gaso-
lene yield on crude via coking relying on coal and nuclear power
for more of their basic energy load. This is not likely within
5 years, but nearly anything can happen in 10. The other possi-
ble source would be the coking of heavy pitches made by coal liq-
uefaction. Here, the removal of inorganics to very low levels
presents a difficult problem for which we have no solutions as
yet. This source could not be important in less than about 10
years as the liquefaction of coal is not even remotely commer-
cially feasible today. The other more likely source of pure car-
bon would be the delayed coking of Lurgi tar from western SNG
plants. This source could become operative in a really important
way over the period 1980 - 1985. All depends upon the regulatory
authorities who hold the whole coal to SNG program in their grasp
now. If they approve, the next hurdle is the capital markets,
not an insignificant hurdle at that.

So far, we have made no distinction between amorphous and
needle coke. The demand for the latter is not very well known.
It is preferred for graphite electrodes, but before being de-
liberately produced, the world got along without it except for
accidental quantities. However, we can guess that a demand of
500,000 tons per year exists now and 1,000,000 by 1985, green
coke basis. Translated back to decant oil at 50% coke yield,
this means 15,000 bbls./day in 1975 and 30,000 bbls./day in 1985.
In terms of cat cracking capacity required, these figures are
0.6 MM bbls./day and 1.2 MM bbls./day, respectively, in 1975 and
1985. While these needs do not overwhelm the potential supply,
they are, nonetheless, quite significant when supplies become a
little thin for other reasons. If half of graphitized carbon
went over to this basis, these figures would slightly more than
double.

Conclusions

As we indicated at the beginning, this paper is not about
technical problems or the latest research findings. It concerns
the problem of whether we have enough of the right raw material
to make what we know well how to make in the way of industrial
carbons of which we want a lot more in the future to keep world
economics going.

The answer is an emphatic "no, we will not have enough in-
dustrial carbon raw materials from petroleum or any other source
without real effort to use all available supplies and to create
new sources." We emphasize these finding by Table III which
presents the overall world picture on petroleum feedstocks for
3 of the 4 important industrial carbons in 1975 and 1985. The
data for 1975, which admittedly are estimates but are based on
near at hand trends and facts, show a close balance between
supply and demand. If one looks at the exports of U.S. carbon

TABLE III

OVERALL WORLD SUPPLY/DEMAND BALANCE
FOR CAT CRACKER DECANT OIL AND ETHYLENE TAR

| | BARRELS PER DAY | |
	1975	1985
DEMAND FACTORS		
CARBON BLACK	238,000	491,000
ELECTRODE PITCH	6,000	38,000
NEEDLE COKE	30,000	120,000
	274,000	649,000
SUPPLY FACTORS		
DECANT OIL	200,000	250,000
ETHYLENE TAR	90,000	690,000
	290,000	940,000

ESTIMATED ACCURACY ± 15 - 20%

black feedstocks and U.S. needle coke, this conclusion is rein-
forced. Likewise, in Europe there is considerable use of coal
tar liquids for carbon black in order to round out supply.

If all trends continue with some allowance for tempering of
growth due to rising crude oil costs, it tells us that ethylene
tars will be the most important feedstock by far in 1985 and that
their importance will grow each year from now on.

Petroleum coke is the other important industrial carbon. It
too will reach a severe shortage position as early as the late
1970's. This will be a major problem for U.S. planners since the
U.S., as in the case of carbon black raw materials, is the major
feedstock supplier to the world. We need the trade, but we also
need the aluminum production at home.

Our common sense tells us that important industries will
somehow be supplied. One answer is to allow ordinary green coke
to become a premium product for the refiner so he will have every
incentive to make it. In the case of carbon black feedstocks, we
can solvent extract heavy catalytic cycle oils which will improve
cat cracker economics but will mean more expensive carbon black
feedstocks. Before this happens, we will upgrade all available
decant oils by proper stripping, adequate catalyst removal, and
perhaps even alteration of cat crackers and their operation con-
ditions to keep conversion at high levels. Likewise, ethylene
tars can be upgraded by removing light and heavy ends.

Finally, we will turn back to coal for heavy aromatics and
begin to look at every process that can produce both a fuel and
an industrial carbon raw material. Conventional coal tar sources
will fade into a minor position just as they have done in regard
to basic chemicals such as BTX. For the next 10 years, however,
we had better pray each day for the discovery and production of
adequate crude oil to keep the industrial machinery going until
coal can again become "the King" if indeed this can ever happen
again.

Addendum

This paper was prepared many months ago when our expectations
of the future growth of the carbon black industry was consider-
ably more optimistic than current opinions will support. Even in
our projections used in this paper, we had diminished the rate of
growth somewhat below historical trends. However, now we would
anticipate that the actual growth of carbon black consumption
over the next 5 years or so would be as much as 20 to 40% below
the trends we have used. This does not mean that there is no
chance that the growth will equal our earlier expectations. It
only means that it is too early to be sure so that we have to in-
troduce this note of caution with respect to the forecast.

In respect to yield of carbon black from carbon black feed-
stock, we have used the factor of 2 times carbon black production
to estimate the carbon black fuel consumption. Government

statistics for the United States carbon black industry do not support a factor of 2 but more nearly a factor of 1.7. We have used the factor of 2 for distinct reasons. First, it is a rounded, conservative figure and therefore avoids disclosing anyone's particular confidential yield data. Second, the use of natural gas to supply a large part of the heat load in a carbon black furnace will diminish over the years ahead in favor of processes based on oil only. In the latter case, part of the carbon black feedstock is burned up to supply heat resulting in a lower yield of carbon based on liquid feedstock.

Literature Cited

(1) Thomas, B. E. A. Gas World (April 2, 1960) "Electrode Pitch"
(2) Kinnaird, Robert N., Jr. U.S. 3,707,388 (December 26, 1972)
(3) Crean, Robert B. U.S. 3,510,328 (May 5, 1970)
(4) Baum, Lester A. H. U.S. 3,725,240 (April 3, 1973)
(5) Alexander, Stephen H.; Butler, Robert C.; and Juhl, William G. U.S. 3,537,976 (November 3, 1970)

2

Petroleum Based Carbon

CHARLES L. MANTELL

447 Ryder Rd., Manhasset, N.Y., 11030

Petroleum-derived carbon is a huge industry, based on the heavy residual oils from vacuum fractionation or solvent extraction. These oils are feed stock for electrode coke or fuel for steam and power generation.

Figure 1 shows the pyrolysis of residual hydrocarbons with severity of cracking. Table I shows transformations during coking. Table II shows commercial coke processes. Figure 2 shows a flowchart for delayed coking operations. Figure 3 shows interrelated petroleum coke quality variables. Table III shows typical analyses of petroleum coke. Figure 4 shows industrial utilization of pet coke. Table IV shows typical properties of calcinated petroleum coke. Figure 5 shows outlets for calcined petroleum coke. Table V gives analyses of calcined petroleum coke.

A generalized flow sheet of electrode manufacture where petroleum coke is the preferred and almost exclusive raw material, is calcined, ground, mixed with binders, shaped, baked into amorphous forms and later graphitized, is shown in Figure 6.

Petroleum coke is the life blood of the electro-process industries. Coking is practiced by the petroleum industry to improve yields. The electro-process industries consume more than a quarter of our annual power production.

Petroleum coke is preferred in its low volatile, low sulfur, low metal content for electrolytic anodes, electrodes for aluminum and magnesium, pastes for linings of fused salt electrolysis cells and self-baking units, electric furnace electrodes for copper, steel, cast iron melting; preparation of ferro alloys of wide variety, manufacture of calcium carbide and synthetic abrasives, refractories for blast furnaces, dies for continuous casting of metals; lumber and vessel linings, chemically resistant equip-

18
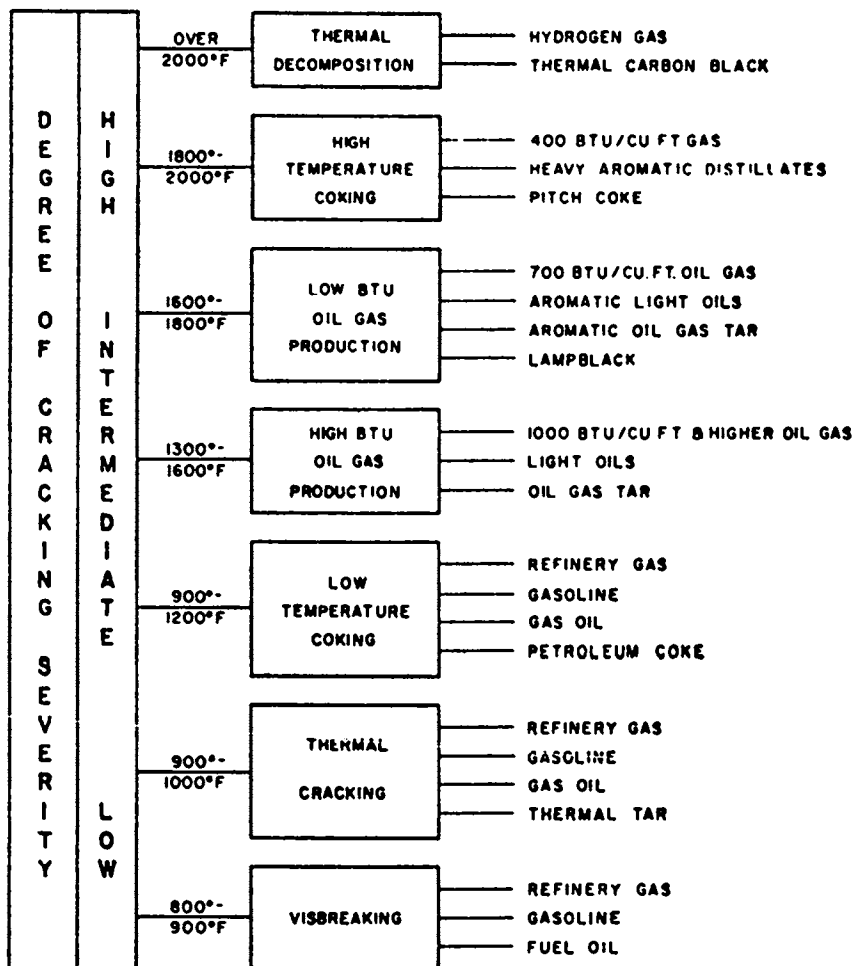
Figure 1. Pyrolysis of residual hydrocarbons with severity of cracking

TABLE I
Transformations During Coking

	Product				
Characteristics	Asphalt →	Pitch →	Semi-→ pitch	Asphaltic→ coke	Carboid coke
Volatile matter, %	45	30-45	20-30	7-20	Less than 7
Solubility in trichlor-ethylene, %	100	60-100	40-60	2-40	Less than 2
Carbon-hydrogen ratio	10-14			18-24	Greater than 24

TABLE II
Commercial Coking Processes

		Coking temperatures	
Method	Type	Type	Range, °F
Atmospheric still coker	Batch	Low	900–1000
Delayed coker	Semicontinuous	Low	900–935
Broad-oven coker	Batch	High	Greater than 1600
Contact coker	Continuous	Low	900–960
Fluid coker	Continuous	Low	900–950
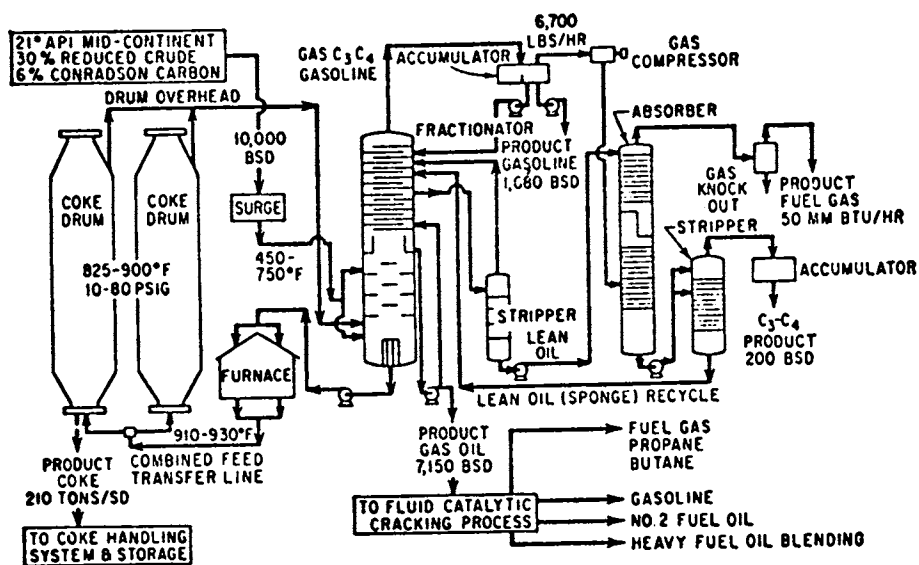
Figure 2.   Delayed coking operations

TABLE III
Typical Analyses of Petroleum Cokes

Source	Type	Moisture, wt %	Volatile matter, wt %[1]	Sulfur, wt %[1]	Ash, wt %[1]	Iron, wt %[1]	Silicon, wt %[1]	Calcium, wt %[1]	Nickel, wt %[1]	Titanium, wt %[1]	Vanadium, wt %[1]	Reference
Middle West[2]	Delayed	0.81	13.5	2.9	0.30	0.043	0.026	0.020	0.0094	0.0003	0.019	(32)
Middle West[2]	Delayed	0.14	11.7	1.3	0.15	0.038	0.013	0.0084	0.0041	0.0003	0.011	(32)
Ohio[2]	Delayed	7.0	11.0	0.77	0.14	0.011	0.0097	0.020	0.0086	0.0003	0.0038	(32)
Mid-Continent[2]	Delayed	3.2	12.3	1.49	0.13	0.008	0.014	0.0088	0.0031	0.0002	0.027	(32)
Mid-Continent[2]	Delayed	6.0	12.8	1.08	0.11	0.012	0.021	0.0060	0.0007	0.0003	0.0019	(32)
Arkansas[2]	Delayed	5.5	12.9	4.51	0.51	0.166	0.053	0.055	0.0042	0.0006	0.0021	(32)
California[2]	Delayed	6.0	10.2	1.15	0.40	0.025	0.054	0.0283	0.0284	0.0010	0.040	(32)
Pennsylvania[2]	Batch	7.8	9.2	0.10	0.14				0.0004	0.0001	0.0006	(32)
American Gilsonite Co.	Delayed	1.8	13–18	0.21	0.37	0.031	0.066		0.071	0.008	0.0009	(32)
South Louisiana	Fluid			1.4	2.8	0.11			0.01		0.01	(34)
Elk Basin	Fluid		5.3	6.4	0.7	0.08			0.06		0.17	(34)
Hawkins	Fluid		5.0	7.0	0.7	0.04			0.01		0.02	(34)
West Coast	Fluid		7.2	1.2	0.3	0.05	0.02	0.014	0.01	0.008	0.021	(35)

[1]Moisture-free basis.
[2]Determinations made in accordance with Great Lakes Carbon Corp. analytical methods.
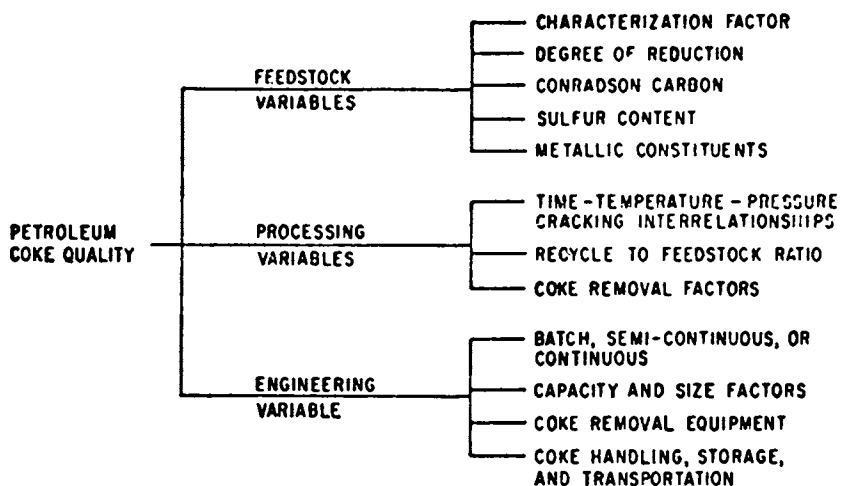
Figure 3.   Interrelated petroleum-coke quality variables
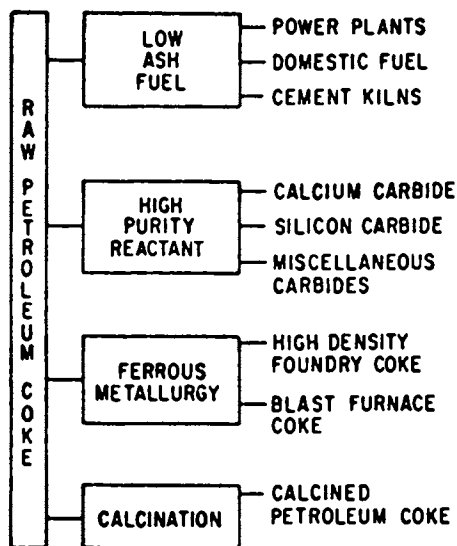
Figure 4.   Utilization of raw petroleum coke

TABLE IV
Typical Properties of Petroleum Coke Used in Carbon and Graphite Manufacture

Property	Raw coke	Coke calcined to 1300°C
Aluminum, ppm[1]	15-100	15-100
Ash, %	0.1-1.0	0.2-1.5
Boron, ppm	0.1-0.5	0.2-0.7
Calcium, ppm	25-500	25-500
Fixed carbon, %	87-97	97-99
Hydrogen, %	3.0-4.5	<0.1
Iron, ppm	50-2,000	50-2,000
Manganese, ppm	2.0-100	2.0-100
Magnesium, ppm	10-250	10-250
Moisture, %	0.5-2.0	Negligible
Nickel, ppm	10-100	10-100
Nitrogen, %	0.1-0.5	<0.1
Real density, g/cc	1.6-1.8	2.08-2.13
Silicon, ppm	50-300	50-300
Sulfur, %	0.2-2.5	0.2-2.5
Titanium, ppm	2.0-60	2.0-60
Vanadium, ppm	5.0-500	5.0-500
Volatile matter, %	5.0-15	<0.2

[1]ppm - parts per million
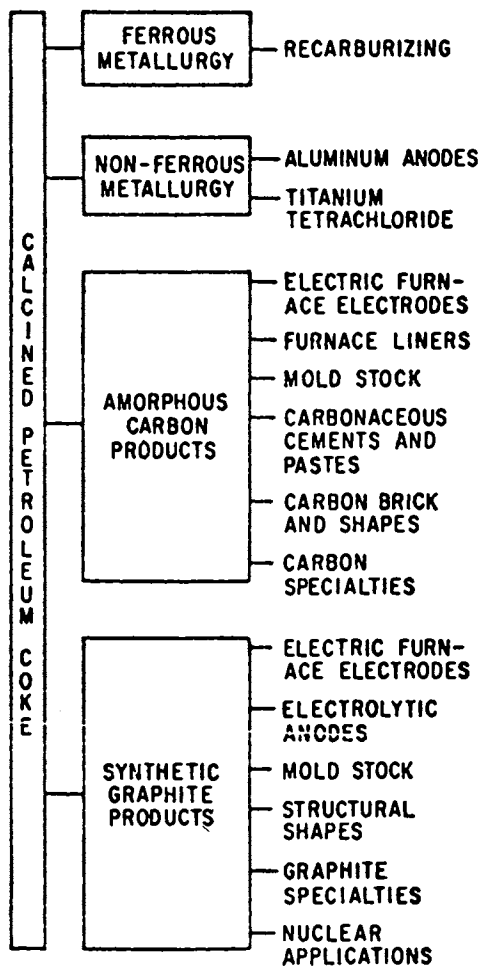
Figure 5. *Outlets for calcined petroleum coke*

TABLE V
Analyses of Calcined Petroleum Cokes

Characteristics						
Moisture, wt%	0.09	1.0 max		0.10	0.10	0.50 max
Volatile matter, wt%	0.75	0.5 max		0.38		0.50 max
Ash, wt%	0.38	0.5 max	0.70	0.33	0.35	0.50 max
Sulfur, wt%	1.06	0.21		1.10	1.5	2.5 max[1]
Real density, g/cc	2.06	2.04		2.07	2.05	2.05 ± 0.03
Electrical resistivity, ohm-in.	0.0019[2]			0.038[3]	0.044[3]	
Bulk density, lb/cu ft				52	52	
Trace elements:						
Iron, wt%	0.03	0.031	0.050	0.048	0.06	0.06 max
Silicon, wt%	0.040	0.066	0.030	0.052	0.02	0.06 max
Calcium, wt%	0.04		0.026	0.0059		
Nickel, wt%	0.05	0.071	0.004	0.034		
Titanium, wt%	0.0004	0.008	0.001	0.0016	0.0014	
Vanadium, wt%	0.040	0.0009	0.007	0.040	0.0003	
Aluminum, wt%	0.012	0.017	0.015			
Manganese, wt%	0.001	0.009	0.002			
Magnesium, wt%	0.006	0.009	0.005			
Boron, wt%		0.0015	0.00004			
Sodium, wt%	0.040	0.006				
Potassium, wt%	0.005	0.002				
Barium, wt%	0.001	0.0009				
Lead, wt%	0.006	0.00004				
Chromium, wt%	0.005	0.0006				
Cobalt, wt%	0.001	0.006				
Molybdenum, wt%	0.001	0.002				
Zinc, wt%		0.0005				

[1]Specifications cited by Klemgard.
[2]Applied pressure 70,000 psi.
[3]GLC C-12A. Applied pressure 150 psi.
[4]Unpublished data, Great Lakes Carbon Corp.

HISTORICAL ASPECTS OF MANUFACTURED CARBON
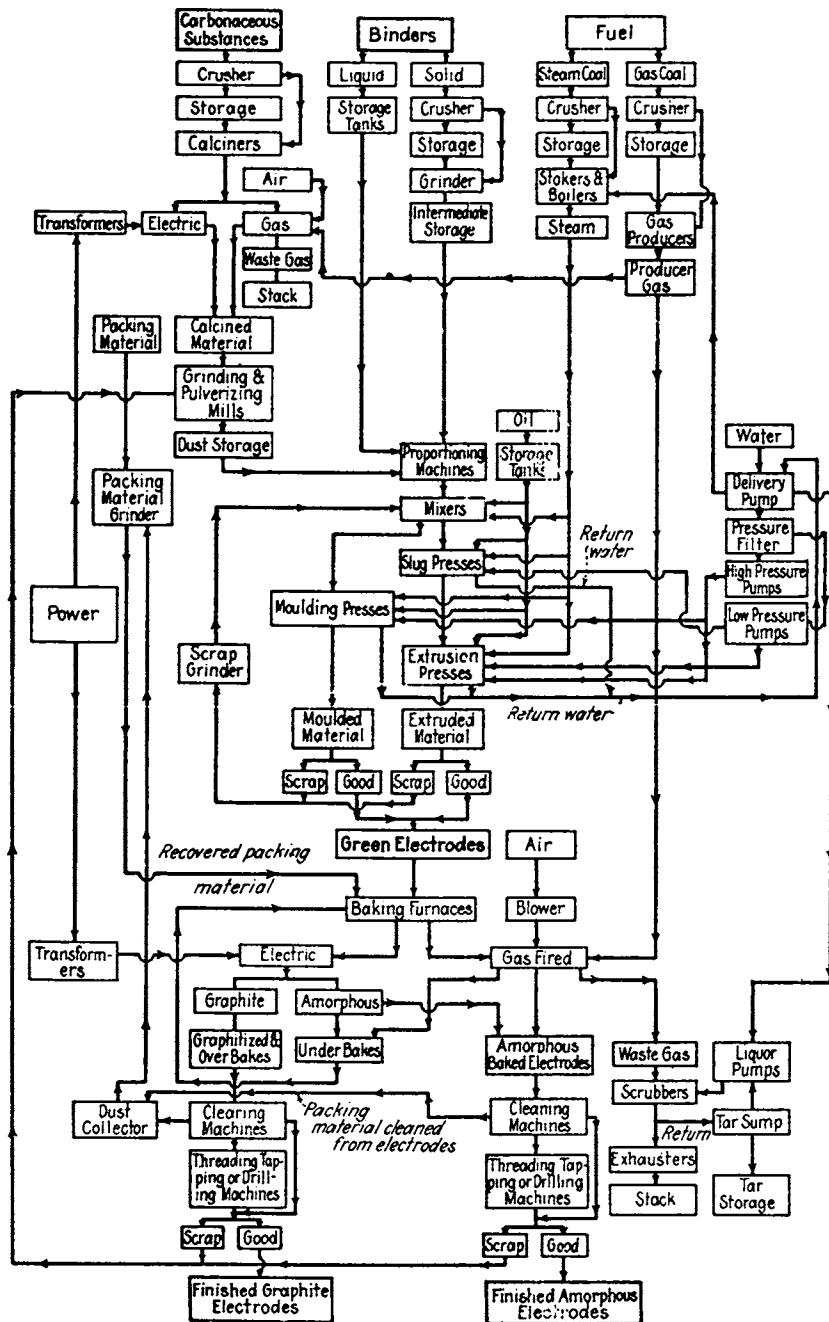
Figure 6.   Flowsheet of electrode manufacture

ment; synthetic and reactor graphite, electrical machinery brushes, contacts and electronic shapes.

High volatile, high sulfur petroleum coke finds use as fuel or fuel additives.

Production of commercial carbides places a premium on high-quality, high-purity carbonaceous raw materials which are involved in the reaction:

$$MeO \text{ (solid} + C \text{ (solid)} \longrightarrow MeC \text{ (solid)} + CO \text{ (gas)}$$

where "Me" represents a metal and "C" represents carbon.

Carbide specifications call for a yield of 4.5 cu ft of acetylene per lb (at 60°F and 20 in. barometric pressure), and the acetylene must contain not more than 0.05 volume percent of phosphine. Since 0.65 - 0.70 lb of coke is required per pound of carbide, carbon quality is a determining factor. Most carbide plants use a mixture of petroleum coke and metallurgical coke breeze.

Percentages up to 40% have been used in some instances. With carbide specifications for sulfur fixed at less than 1%, any high-sulfur petroleum coke is ruled out.

Silicon carbide is prepared by heating a charge of carbon and silica in a resistance furnace. The carbon is a low-sulfur, low-ash anthracite coke or petroleum coke. Sulfur is avoided because SO_2 is produced during the operation of the furnace. The manufacture of 1 ton of silicon carbide requires 1.4 tons of carbon.

Boron carbide is the hardest known synthetic abrasive and is manufactured by heating a mixture of boric acid, petroleum coke, and kerosene in a gastight resistance furnace to about 2500°C.

The reduction of iron ores to molten iron in a blast furnace is, by far, the largest single outlet for metallurgical coke. Petroleum cokes made to a uniform volatile content of 16–20% and agglomerating on heating to 950°C, can be blended to as high as 20% with high-volatile coal to produce blast-furnace coke.

The largest user of petroleum coke is the aluminum industry which makes its own electrodes from calcined petroleum coke. The aluminum industry is the largest calciner. Considering calcining losses, handling and transport losses, losses in baking, preparation and machining, and crediting butt return and pot lining, allowing for somewhat widely varying operating practices, shutdowns and start-ups, power failures, etc., a rough estimate is that 4 million tons a year production of aluminum in the United States require about the same tonnage of petroleum coke. Mag-

nesium is less than 1% of the aluminum production. Figures 7 and 8 show the electrolytic aluminum furnaces. Table VI gives manufacturing data.

TABLE VI
Prebaked and Soderberg Electrodes

	Prebaked	Soderberg
Cell size, amp	90,000	
Current density, busbar	161 asi	
anode, amp/cm^2	0.7	0.7
anode, asi	4.52	4.52
Voltage drop, bus to lower surface of anode, volts	0.25-0.3	0.5-0.6
Bath voltage, volts	3.35	3.15
Over-all cell voltage	4.0 -4.1	4.3-4.4
Current, efficiency, %	90-91	87-88
Power consumption,		
kwhr/kg	14	15
kwhr/lb	6.37	6.8
Anode consumption,		
kg/kg	.45	.52
Baking loss,		
kg/kg	.05	
Total carbon consumption,		
kg/kg	.50	.52

Iron and steel castings, nonferrous metal melting, ferro alloys of wide variety and composition, calcium carbide, phosphorus, scrap and secondary metals consume higher amounts of electrodes per ton than does steel, alloy steels and stainless.

Electric furnace electrodes are made and supplied by the carbon companies.

Electric furnaces and their petroleum coke-based electrodes account for more than 20% of our annual steel production of more than 100 million tons a year, with expected growth to 25% by 1980. Each ton of steel requires from 20 to 30 pounds of electrodes per ton or 20,000,000 x 25, or 5,000,000,000 pounds of electrodes or 250,000 tons. Consumption of carbon and graphite electrodes (per pound of 1,000 pounds of product) is shown in Table VII.
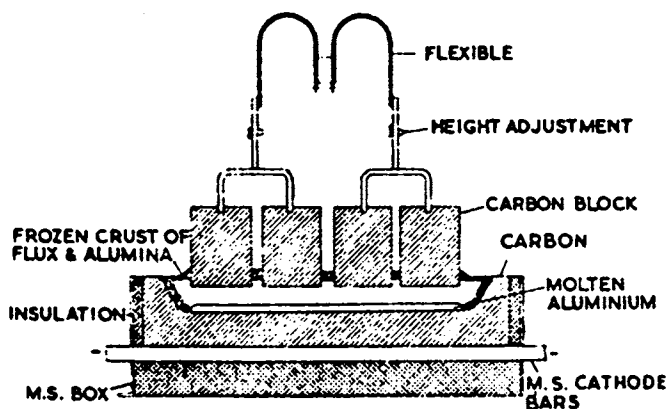
Figure 7. *An electrolytic furnace with baked block electrode*
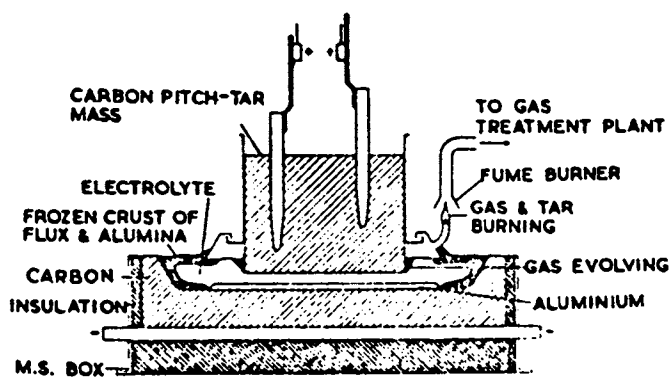
Figure 8. *Electrolytic furnace with vertical stubs*

TABLE VII
Consumption of Carbon and Graphite Electrodes (Expressed in lb/1,000-lb Product)

Application	Carbon	Average	Graphite	Average	Carbon-graphite ratio
Nonferrous metals	-	-	1.25-5	3.12	-
Iron castings, cold scrap	-	-	2.50-5	3.75	-
Same (duplex, hot charge)	-	-	1.50-7	4.25	-
Steel castings	4.5-10	7.25	2.25-5	3.62	2
Steel ingots	8.5-15	11.0	5-10	7.5	1.57
Ferrosilicon, 15%	10-22	16.5	-	-	-
50%	22-33	27.5	-	-	-
80%	35-52	43.5	-	-	-
80% Ferromanganese	-	31.2	-	-	-
High-silicon ferro-silicon	45-145	90	-	-	-
Ferrochromium	-	45	-	-	-
Calcium carbide	15-100	57.5	-	-	-
Phosphorus	-	30	-	-	-
Iron ore (production of pig iron in the electric furnace)	9-13.5	11.25	-	-	-

For those who are statistically minded, an overall figure for coke for the aluminum industry is roughly one ton of raw coke per ton of aluminum. Aluminum production is of the order of copper, zinc and lead combined.

The steel industry is now the major consumer of electrodes.

During the 1960's, the world steelmaking community established the basic oxygen furnace as becoming the dominant production process as shown in Table VIII.

Table VIII
World Steel Production by Process

	1960		1970	
	MM/Tons	%	MM/Tons	%
Open Hearth and All Other	308.3	86.3	268.1	45.1
Basic Oxygen Furnace	13.6	3.8	245.2	41.2
Electric Arc Furnace	34.4	9.7	81.3	13.7
Total	356.3	100.0	594.6	100.0

During that decade, the basic oxygen furnace process grew some 20 fold, and increased its share of total world steel production to 41.2 percent from a level of only 3.8 percent just 10 years earlier.   In the United States, the BOF now accounts for more than 56 percent of steel production, having surpassed open hearth production in the fall of 1969.   In fact, most of the growth of the BOF, at least in the U.S. and Europe, came at the expense of hot metal open hearth capacity in existing integrated steel mills.

The dramatic surge of the BOF process tended to obscure the fact that the electric arc furnace grew some 2.5 times during the 1960's.   Its projected rate of growth shows it accounting for 25 percent of total world steel by 1980 as new technology, new economics, and new thinking pervade the steel industry.

Electric arc furnace steelmaking is increasing throughout the world, and Table IX shows where much of that growth is taking place.

As shown, western Europe is the largest electric arc furnace area, but significant growth has occurred in Japan and the United States.   Also of interest is the fact that the IIAFA countries of Central and South America have the highest percentage of electric arc furnace steel in the world.

Consumption rates multiplied by the electric furnace steel rates, give electrode consumption which, when multiplied by electrode to raw petroleum coke ratio of 1.5, gives a first approximation of petroleum coke, shown in Table VII.

Manufactured carbon for decades was a black and secret art.

Furnace carbon blacks were developed largely by the petroleum distillers and their associates and marketed since World War II to the exclusion of natural gas grades.   Natural gas is too expensive for carbon black; it is a chemical raw material primarily and in the future probably will be too expensive as a fuel.

Carbon black is made in millions of pounds annually for a multiple of uses in inks, rubber and plastics reinforcement, mechanical rubber goods, paints, varnishes, etc.   The inks are for our newspapers, books, magazines, and communications. Plants all over the world have been built from American designs and operation procedures.

Petroleum coke is basic for chlorine and halogen production of about 50,000 tons annually of electrolytic electrodes.   There has been replacement of graphite by dimensionally stable anodes of titanium plated with precious metals and oxides.

Carbon and graphite refractories, electronic materials, nuclear graphite for control rods in nuclear reactors, battery elec-

Table IX
World Electric Arc Furnace Production of Steel and Percentage of Total Steel Produced

| | 1960 | | 1970 | | 1972 | |
	MM/Tons	% Total	MM/Tons	% Total	MM/Tons	% Total
Latin America	1.3	26.2	3.0	23.9	4.5	28.4
Western Europe	12.4	11.4	26.9	16.6	30.9	18.7
Eastern Europe	2.2	10.5	4.0	10.3	6.0	14.0
U.S.S.R.	5.8	8.9	10.6	9.3	12.5	10.0
Japan	4.5	20.2	15.4	16.2	17.2	18.1
United States	7.6	8.4	18.1	15.3	21.2	17.6
Canada	.6	11.4	1.6	14.0	1.8	15.9
All Other	.05	.05	1.6	7.4	6.8	28.4
Total	34.45	9.6	81.2	13.7	100.9	17.5

TABLE X
Processes for Carbon Blacks (9)

Type	Process features	Raw material
Channel	Impingement of unconfined partial combustion of diffusion flames on cool surfaces; black exposed to oxidizing temperature after it is formed	Natural gas Town gas Hydrocarbons
Furnace	Controlled turbulence condition, confined partial combustion in refractory chambers (furnaces)	Natural gas Petroleum distillates and residues Mixed oil + gas
Thermal	Regenerative cracking in a refractory brick checkerwork (cyclic operation, no oxygen present)	Natural gas
Lampblack	Confined partial combustion, low turbulence followed by surface oxidation	Coal tar distillates Petroleum distillates & residues and various carbonaceous materials
Acetylene	Confined exothermic cracking Of C_2H_2 (no oxygen present)	Acetylene

TABLE XI
Commercial Yields of Processes

Process	Raw material	Commercial yields	% Yield carbon of theoretical carbon content
Channel	Natural gas	1.0-2 lb/1000 cu ft gas	3-6[1]
Gas furnace	Natural gas	9.0-12.0 lb/1000 cu ft gas	28-37[1]
Oil furnace	Petroleum fractions	2.5-4.5 lb/gallon oil	35-60[2]
Thermal	Natural gas	10-15 lb/1000 cu ft gas	30-47[1]

[1]Based on feed + fuel
[2]Based on oil feed

trodes, searchlight carbons, brushes and contacts, are estimated to consume 25 to 50,000 tons of petroleum coke annually.

Carbon black has long been the preferred reinforcing agent for rubber in automotive tires and mechanical rubber goods. Originally it was made by restricted combustion of cheap natural gas. Later processes were developed for carbon black from residual petroleum, highly aromatic. These were often not economically processible. Table X gives processes, Table XI the yields, Figure 9 a typical process.

Acid coke is made as a byproduct of sulfuric acid recovery from waste gases resulting from sulfuric acid refining of petroleum products such as lubricants and white oils.

A typical sludge is:

$H_2SO_4\%$	54
$H_2O\%$	8
Hydrocarbons	38
Viscosity (seconds)	
Soybolt Universal at 100°F	6400
Color	black

from which a gas and a coke are produced, as given in Table 12.

This coke may be devolatilized by thermal processing and be activated to filter carbon for cigarettes.

TABLE XII
Analysis of Coke from Prototype Sludge

		%
Fixed Carbon		70
Volatile		29
Acid		1
	Total	100
Screen analysis:		
Retained on No. 5		0.3
10		26.9
20		67.9
30		4.1
40		0.4
60		0.2
80		0.1
Dust		0.1
	Total	100.0
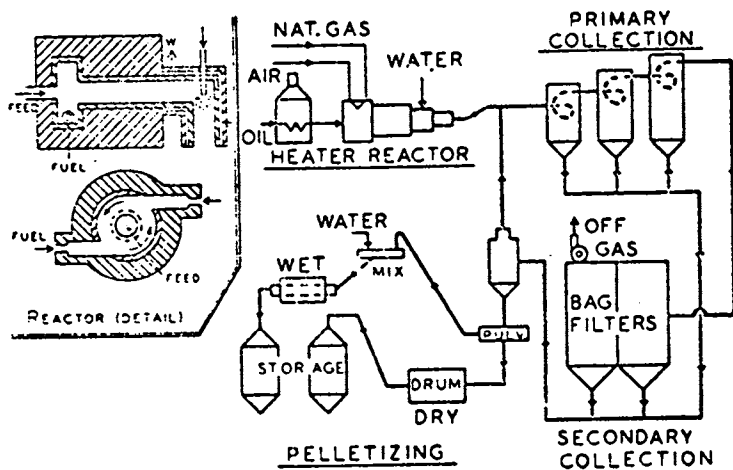
Figure 9.   Phillips oil furnace process

① INSULATION MATERIAL
② PAYLOAD
③ RESISTOR MATERIAL
④ CONCRETE FURNACE STRUCTURE & SUPPORT PIERS
⑤ CONCRETE SIDE BLOCKS
⑥ BUS BARS

PLAN VIEW
SECTION KEY

⑦ GRAPHITE HEAD ELECTRODES   ⑪ FIRE BRICK
⑧ HIGH CONDUCTANCE MATERIAL   ⑫ RAW COKE
⑨ INSULATION BED MATERIAL   ⑬ CONCRETE RUNNING BLOCKS
⑩ COOLING WATER
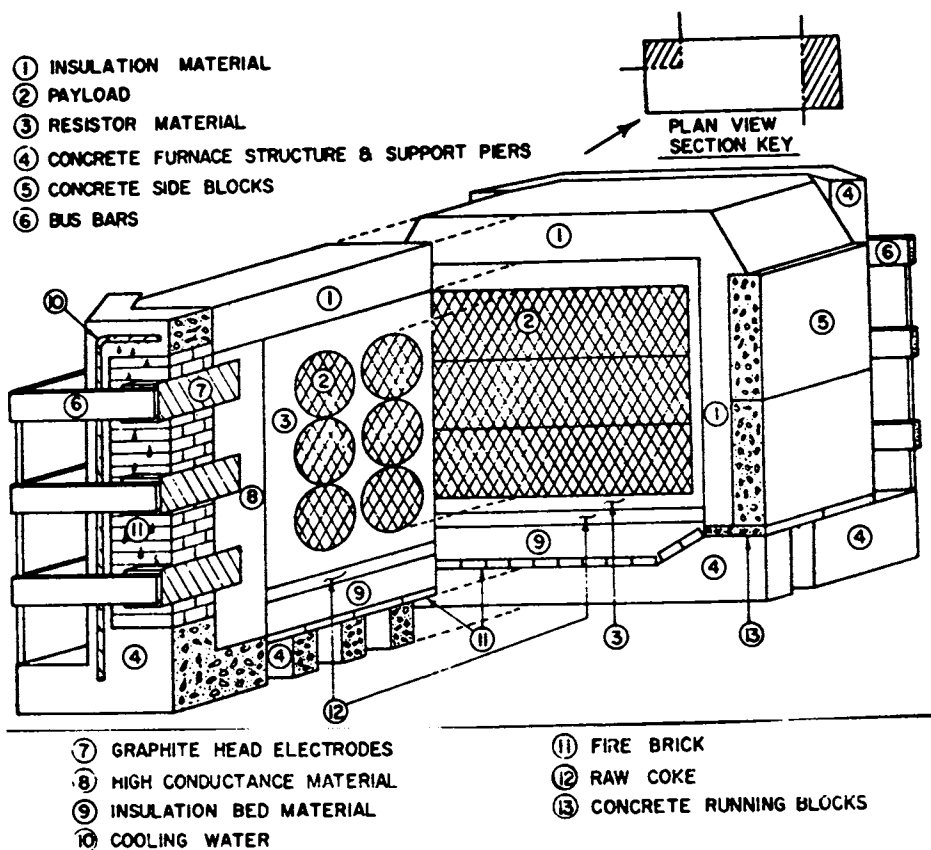
Figure 10.   Schematic plan of graphite furnace

TABLE XIII
Density Change by Graphitization

Amorphous carbons		Graphitized carbons	
Apparent density	Resistivity (ohms per in. cube)	Apparent density	Resistivity (ohms per in. cube)
1.53	.00172	1.58	.00056
1.56	.00158	1.62	.00057
1.56	.00161	1.65	.00051
1.52	.00170	1.64	.00047
1.57	.00162	1.65	.00042
1.54	.00146	1.65	.00046
1.57	.00131	1.64	.00035

TABLE XIV
Changes in Ash Constituents by Baking and Graphitization

	Ash	% of Total ash removed	% Si	% Total Si removed	% Fe	% of Total Fe removed	% Cu	% Cu removed
1. Green electrode	9.89		0.20		0.12		0.38	
1. Amorphous baked carbon	10.72		0.23		0.19		0.33	
1. Graphitized electrode	0.83	92.0	0.03	85.0	0.03	75.0	0.03	92.0
2. Green electrode	7.79		0.06		0.08		0.18	
2. Amorphous baked carbon	7.92		0.20		0.17		0.20	
2. Graphitized electrode	0.89	88.3	0.02	66.4	0.02	75.0	0.04	77.5
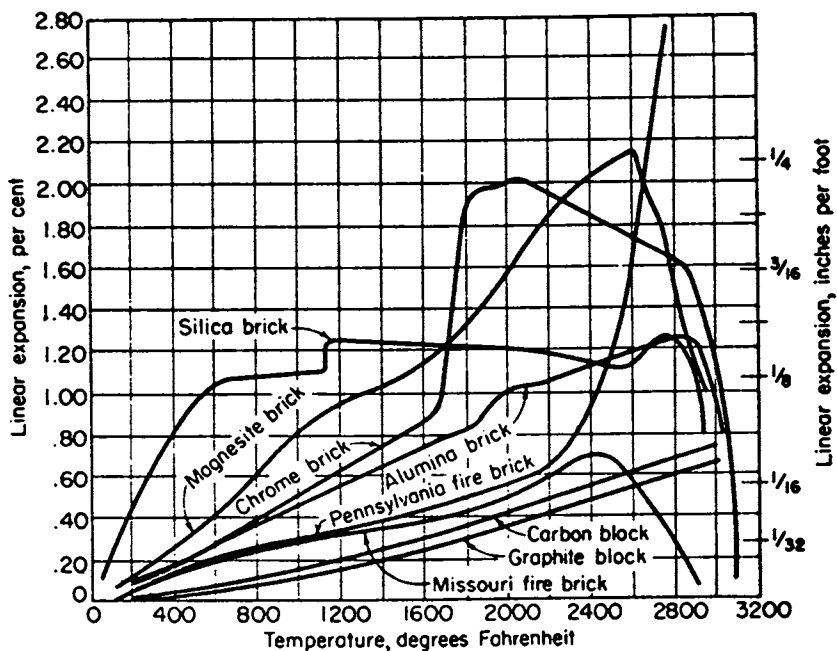
Figure 11. Expansion and stability of refractories

Figure 10 is a schematic plan of a graphite furnace. Tables XIII and XIV show density and ash composition changes during graphitization.

Raw petroleum coke for industrial purposes is calcined. The principal outlets for calcined coke are for the electrolytic industries and for export to foreign manufacturers in the same field. Preparation of carbon and graphite articles is directly by the aluminum and magnesium industry in their own plants, as well as organizations devoted to industrial carbon and graphite articles such as electrodes for others, particularly for electric furnaces.

Figure 11 shows the expansion and stability of refractories which includes carbon pastes, preformed blocks and graphite forms. Almost all blast furnaces are carbon block, lined from the hearth, the tuyere zone and the mantle. Ford Motor Company had a 20-year service life of blast furnace hearths and had 56 inches left of the original 88 inches.

With aluminum at 4 million tons requirement of raw petroleum coke, chlorine and associates at 30,000 tons of product per day, the requirement is 50,000 tons; with electric furnace electrodes at 250,000 tons,and 4 to 5 million tons of calcined coke exported per year, petroleum based carbon is a huge business even if the figures are only $\pm$ 50%.

References:
Mantell, C. L., "Industrial Carbon," D. Van Nostrand Co., New
    York, N. Y. 1928; 2nd Ed. 1946
Mantell, C. L., "Carbon and Graphite Handbook," J. Wiley & Sons,
    New York, N. Y. 1968
Mantell, C. L., "Electrochemical Engineering," 4th Ed., McGraw-
    Hill Co., New York, N. Y. 1960
Mantell, C. L., Engineering Materials Handbook," McGraw-Hill
    Co., New York, N. Y. 1958
Mantell, C. L., "Solid Wastes: Origin, C ollection, Processing
    and Disposal," J. Wiley & Sons, New York, N. Y. 1975

3

Properties of Cokes Produced in the Flexicoking Process

W. J. METRAILER
Exxon Research and Development Laboratories, Exxon Co., U.S.A.,
P.O. Box 2226, Baton Rouge, La. 70821

R. C. ROYLE
Exxon Research and Engineering Co., P.O. Box 51, Linden, N.J. 07036

G. C. LAHN
Exxon Research and Engineering Co., P.O. Box 101, Florham Park, N.J. 07932

FLEXICOKING is a process designed to convert high boiling
petroleum fractions (residua) into more valuable light hydro-
carbons, low sulfur fuel gas and coke. The coke produced in
the FLEXICOKING process is quite different from cokes produced
by conventional Fluid Coking or Delayed Coking. In any petroleum
coking process essentially all of the non-volatiles (metals) and
much of the sulfur in the residuum feed ends up in the coke
product. In Delayed Coking, the coke product is accumulated in
a drum and then mechanically removed. Therefore, the quality of
the coke is primarily related to the quality of the residuum
feed. In Fluid Coking, typically about twenty-five percent of
the coke product is burned to supply process heat. This burning
concentrates the metals somewhat but does not reduce the sulfur
content of the coke product. Gasification of the coke in FLEXI-
COKING produces a substantial concentration of metals in the
coke product with a high coke gasification operation. Gasifica-
tion of the coke also affects significant desulfurization of the
residual coke. The unique system employed in the FLEXICOKING
process permits operation to give substantial coke desulfurization
even at reduced gasification levels. Thus coke gasification
can be minimized when there is an attractive outlet for the low
sulfur petroleum coke. This paper will give a brief description
of the FLEXICOKING process and then discuss 1. the mechanism
of FLEXICOKE formation and desulfurization, 2. the characteristics
of the coke, and 3. potential uses for the coke product.

Process Description

The FLEXICOKING process has been described in detail in
other publications (1, 2). A brief description of the process,
shown in Figure 1, will help to explain the unique mechanism of
coke formation and how the mechanism of the process affects coke
properties. FLEXICOKING is a continuous coking-gasification
process carried out in three vessels containing fluidized solids
(coke) which are interconnected to permit transfer of solids from

38

one vessel to another. In the reactor, steam is injected into
the bottom of the reactor to fluidize the solids and coke is
circulated to and from the heater to maintain the reactor at
925-1000°F. Residuum feed is sprayed into the fluidized bed
where it is cracked to form light hydrocarbons that pass overhead
and are recovered in conventional fractionating equipment. The
coke formed is deposited on the external surface of the "seed"
coke in the fluid bed. The deposited coke causes the particle
size of the seed coke to increase and, as in Fluid Coking (3),
internal attrition is supplied in the system to maintain a
fluidizable particle size range. The coke which is generated in
the reactor passes through the heater where it is partially
devolatilized and then is circulated to the gasifier. Here the
coke is gasified to the extent desired with air and/or oxygen
and steam. In Fluid Coking, only sufficient coke is burned to
provide heat for the process. In FLEXICOKING, additional coke
is burned to provide heat needed for gasification. The amount
of coke gasified can be varied depending on the needs of the
refiner. Hot gases from the gasifier pass overhead and into the
bottom of the heater where they provide fluidization gas for this
vessel. The heater recovers most of the heat from the gases and
provides control of the temperature in the fluid solids system.

Mechanism of Flexicoke Formation and Desulfurization

A fluid coke particle is formed by repeated deposition of
a thin film of fresh coke on "seed" coke particles as they pass
to and from the reactor and gasifier. This is illustrated in
Figure 2. Seed coke is circulated through the reactor/heater
system where made coke C_M is deposited on the seed to build up
a film of new coke. The thickness of this film will vary some-
what with feedstock and operating conditions but typically the
new coke deposit C_M is about 5 microns thick. The reactor/
heater coke represented as R-1 is transferred to the gasifier
where part of the coke is gasified with steam/air mixture. The
amount of coke gasified is designated as C_G. The net product
coke ($C_P = C_M - C_G$) remains on the initial seed as a thin deposit
and this material R-2 is returned to the reactor heater where
additional coke is deposited. Since the "seed" coke particles
are internally generated when the system reaches equilibrium,
the composition of the coke in the system will be that of the net
coke product C_P.

FLEXICOKING operations have been carried out in both a
2 B/D pilot plant and a 750 B/D Prototype unit. Analysis of the
circulating coke from the FLEXICOKER prototype during 60 days of
operation with a residuum containing 28% Conradson carbon and
4.6 wt. % sulfur are shown in Figure 3. The initial "seed" coke
(from a commercial Fluid Coker) contained 4.3 wt. % sulfur. As
the run progressed, the coke in the system is replaced by
FLEXICOKER coke product and the sulfur content of the coke lined
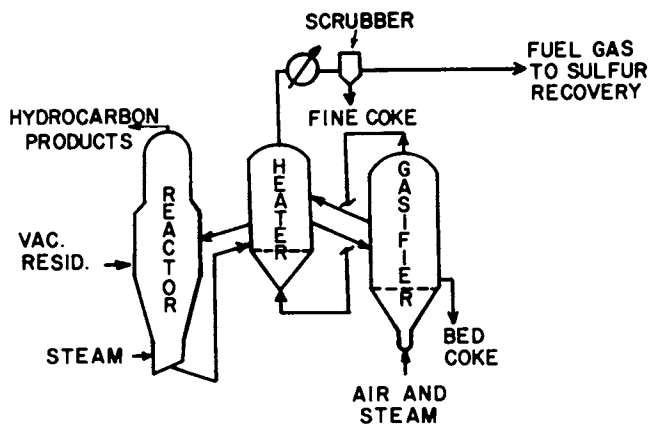
Figure 1.   Flexicoking design flow plan
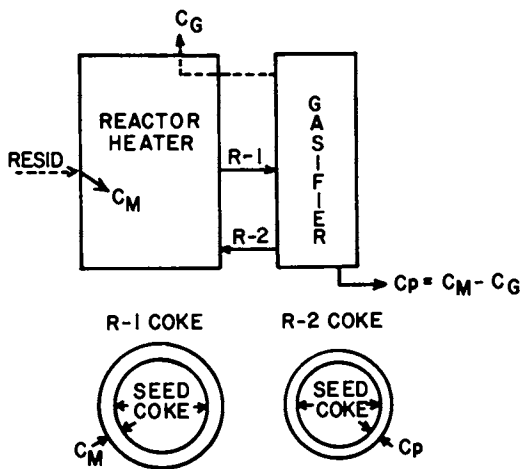
Figure 2.   Flexicoke growth mechanism

out at about 2 wt. %. Normal Fluid Coking of this residuum
would produce a coke containing about 6.0 wt. % sulfur. The 66%
coke desulfurization obtained would not be predicted based on
previous experience in hydrodesulfurization of cokes. It is known
that coke can be hydrodesulfurized (4); however, most of the
studies reported have been carried out at relatively high hydro-
gen partial pressures. The hydrogen partial pressure in the
gasifier-heater system during this FLEXICOKER operation was only
about 5 psia. The fact that coke desulfurization can be affected
at these mild conditions is attributed to the thin film like
nature of the new coke described above.

Electron probe analyses of a cross-section of a coke particle
obtained from operations in the 2 B/D FLEXICOKER pilot plant
(shown in Figure 4) confirm that the desulfurization is occurring
on the layers of the new coke. This operation started with a
"seed" coke containing 5.8 wt. % sulfur. At the time the sample
shown was taken, the unit had not operated long enough to dis-
place all of this "seed" coke from the system. The core of the
coke particle had undergone little or no desulfurization. How-
ever, the new shell of FLEXICOKE had been desulfurized to about
1.2 wt. % sulfur. The residuum feed employed in this operation
contained 4.6 wt. % sulfur and would have produced a coke
containing about 8.0 wt. % sulfur in normal Fluid Coking. Thus,
the equivalent of 85% coke desulfurization was obtained in this
experimental pilot plant FLEXICOKING operation.

Characteristics of Flexicoke

Two types of coke can be obtained from a FLEXICOKER (see
Figure 1). The fine coke carried over from the heater can be
removed with a scrubber and recovered as a product. The metals
in the coke tend to concentrate in this stream. If a larger
quantity of coke is desired, coke product can be withdrawn from
one of the beds. The Prototype FLEXICOKER operation discussed
earlier was carried out at about 95% coke gasification. Here
the fine coke leaving the system with the gas from the heater
made up a major portion of the coke product. The operation in
the 2 B/D pilot plant discussed earlier was carried out at about
60% coke gasification. In this type of operation most of the
coke product would be withdrawn from one of the fluidized coke
beds.

Analyses of the fine coke from two high gasification runs
and bed coke from a low gasification operation are shown in
Table I. The fine coke from high gasification represents about
2 wt. % of the residuum feed, however, this may be 50 to 100 T/D
of useful coke product from a typical size FLEXICOKER. The
metals are concentrated in this product. In the run with West
Texas residuum, the vanadium in the product is 1.17 wt. % which
represents a seventy fold concentration of the vanadium in the
feed. In the other high coke gasification run with Boscan
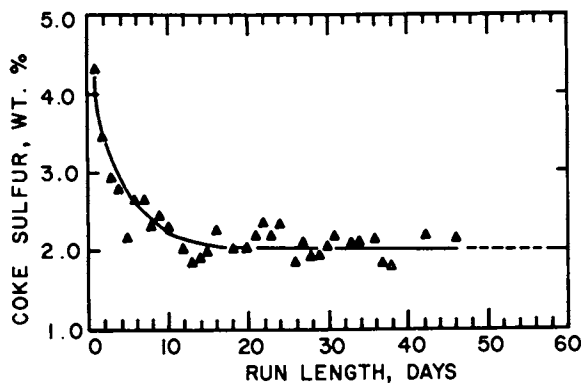
Figure 3.   *Flexicoker prototype circulating coke sulfur level*
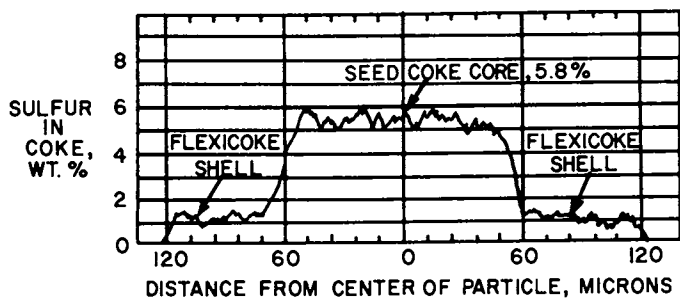
Figure 4.   *Electron probe analyses of coke particle*

(Venezuelan) residuum feed, a fine coke product containing
15 wt. % vanadium was obtained. Metal contents of this level
should be of interest for metals recovery (5). The sulfur content
of the fines stream has been slightly higher than the circulating
coke, however, it still has undergone sufficient desulfurization
to reduce the sulfur level to less than 3 wt. %. The fine
particle size of the coke should permit use without grinding
where fine coke is required.

Coke produced during the pilot plant FLEXICOKING operation
at 60% coke gasification is also compared in Table I to coke
that would be produced by conventional Fluid Coking of the same
material. The density and the particle size of the two cokes
would be about the same. The sulfur content of the coke from
FLEXICOKING is indicated to be less than 2.0 wt. %. As shown
earlier in Figure 4, the coke product from this particular
operation contained only 1.2 wt. % sulfur. In addition to the
lower sulfur content, the coke from FLEXICOKING has a surface
area of 100 m^2/gm compared to less than 10 m^2/gm for Fluid Coke,
and the metals content of FLEXICOKE is higher reflecting the
higher consumption of coke by gasification.

Combustion characteristics are important in many processes
employing coke. Combustion profiles have been obtained on coke
from the low gasification operation. This is a test which has
been proposed by some furnace manufacturers (6). In the test
a sample of coke is placed on a continuous weighing device and
heated at a constant rate while exposed to air. In Figure 5
the results from the FLEXICOKE sample are compared to data on
a low volatile bituminous coal and an anthracite coal. All
tests were on pulverized material. The coke is slightly easier
to burn than anthracite but more difficult than the low volatile
bituminous coal. Thus, FLEXICOKE should perform satisfactorily
in furnaces designed to handle anthracite coal. Other combustion
comparisons show FLEXICOKE to be similar to Fluid Coke which is
currently being used for power generation.

Potential Uses

FLEXICOKING at reduced coke gasification could produce
over a thousand tons per day of coke product in a typical plant.
The operation can be moved in this direction if an attractive
market for the additional coke is available. In addition to
use of this coke as fuel, it could be used in blast furnaces,
foundries, and other ferrous metallurgical processes, in the
manufacture of Portland cement, and to make carbon electrodes
for use in aluminum production.

The fairly low sulfur content of FLEXICOKE could make it a
useful material in ferrous metallurgical processes. Petroleum
coke is reportedly already being used to make metallurgical
grade coke for use in foundries (7). In order to be used as
part of the burden to a blast furnace, coke of a fluidizable

TABLE I

COKE PRODUCT INSPECTIONS

RESIDUUM FEED	WEST TEXAS	BOSCAN	HEAVY ARABIAN	
SULFUR, WT. %	4.6	5.2	4.6	
VANADIUM, PPM	160	1150	104	
TYPE OF OPERATION	------------FLEXICOKING----------		FLUID COKING[1]	
COKE CONSUMED, WT. %	95	95	60	25
COKE PRODUCT STREAM	FINE COKE	FINE COKE	------BED COKE--------	
COKE INSPECTIONS				
DENSITY, L8S/CU. FT.[2]	90	120	98	95
SURFACE AREA, M^2/G	--	--	100	<10
AVERAGE SIZE, MICRONS	<10	<10	--------200-----------	
SULFUR, WT. %	2.8	2.3	<2.0	8.0
VANADIUM, WT. %	1.17	15.0	0.12	0.07
VOLATILES, WT. % @ 950°C	<2	--	<1	~6

(1) PREDICTED
(2) BY DISPLACEMENT IN VARSOL
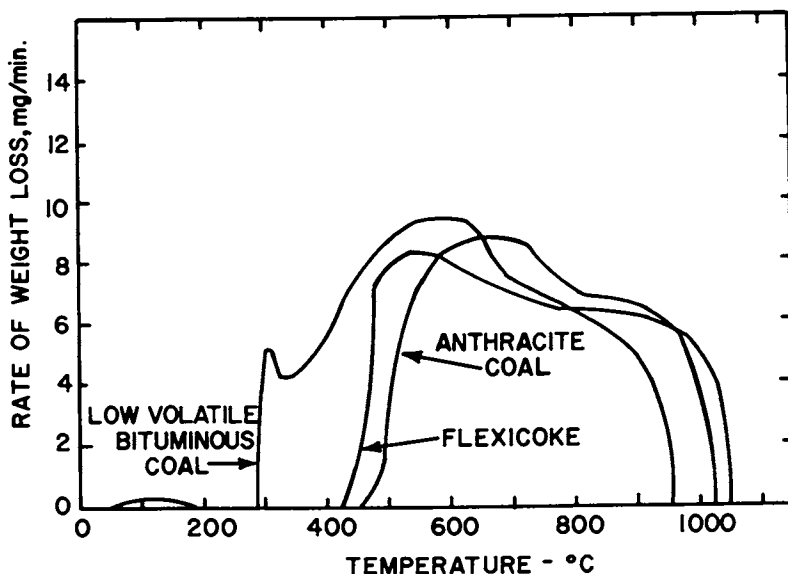
Figure 5.   *Combustion profiles of flexicoke vs. coals (pulverized samples)*

particle size would have to be formed into a sufficiently coarse and strong aggregate to prevent it from being carried out of the burden before reacting. An interesting alternative is to inject the coke into the tuyeres of the blast furnace. The bed coke in a FLEXICOKER has particle size distribution which is fluidizable and is readily transportable in a pneumatic system. Therefore, we believe, it could be handled satisfactorily in a solids injection system without further sizing and grinding. The low volatility of FLEXICOKE should reduce problems associated with solids injection in this very high temperature zone.

Most Portland cement is produced in rotary kilns which may be fired with solid, liquid or gaseous fuel. Most of the sulfur in the fuel usually ends up in the cement product, however, some also leaves as emission sulfur in the kiln stack. The amount of sulfur that leaves with the cement depends on the properties of the stone fed to the process and the type of process used. The sulfur specification on Portland cement may vary from 1.5 to 3.0 wt. % thus the permissible sulfur in the fuel is limited. FLEXICOKE which would be 2 to 3 wt. % sulfur should meet most current producers' requirements. In some cases it may also permit the use of a higher sulfur supplementary fuel which probably will be needed to burn the low volatility FLEXICOKE. The particle size of the fine coke should be suitable for burning without grinding. The bed coke probably will require additional grinding.

Petroleum coke is also used extensively to make carbon electrodes for use in aluminum production. Fluid cokes are being used in electrodes when metals content of the coke is low. Coke from FLEXICOKING at low coke gasification levels where the metals in the residua feed are low may meet the metals specification. It is possible that coke withdrawn from the gasifier may not require additional calcining to give it satisfactory electrical conductivity.

As mentioned earlier, recovery of the vanadium in FLEXICOKE product from high gasification operation may be economically attractive (5). This is especially true when a high metals Venezuelan residuum feed is processed. Laboratory investigations have confirmed that conventional leaching technology can be applied to extract the vanadium from the FLEXICOKER product coke. High vanadium recoveries are possible, resulting in high purity grade vanadium pentoxide. Exploratory studies have also indicated the feasibility of producing other forms of vanadium product, such as ferrovanadium and vanadium oxychloride which are raw materials for other applications in the industry.

Summary

In FLEXICOKING, depending on the needs of the refiner and available markets for the coke, both the quantity and quality of the coke product can be varied independent of residuum

feedstock. A significant amount of coke desulfurization is obtained in the FLEXICOKING process due to the unique method of coke formation. The lower sulfur content of the coke will attract markets that would not be interested in the higher sulfur coke produced by delayed or fluid coking of a high sulfur residua. FLEXICOKING at high coke gasification levels can result in a high concentration of metals in the fine coke product. This high metals content coke is potentially a source of valuable vanadium and nickel when processing certain residua.

Literature Cited

(1) Matula, J. P., Weinberg, H. N. and Weissman, W., Oil and Gas Journal, (1972), 70, (38), 67-71.
(2) Kett, T. K., Lahn, G. C. and Schuette, W. L., FLEXICOKING A Versatile Residuum Conversion Process, Presented 67th Annual AIChE meeting, December 2, 1974, Washington, D. C.
(3) Dunlop, D. D., Griffin, L. I., Jr., and Moser, J. F., Jr., Chem. Eng. Prog., (1958), 54, (8), 39-43.
(4) Mason, R. Burgess. Industrial and Engineering Chemistry, (1959), 51, (9), 1027-30.
(5) Fuentes, F. A., Pagel, J. F., and Rionda, J.A. Presented at International Symposium on Vanadium and Other Metals in Petroleum, University of Zulia, Maraciabo, Venezuela, August 19-22, 1973.
(6) Wagoner, C. L. and Winegartner, E. C. Transactions of ASME Journal of Engineering for Power, (1973), 1, 119-123.
(7) Metallurgical Coke Will Be Made From Granular Petroleum Coke, Chemical Week, p. 35, October 28, 1970.

Characteristics of Petroleum Cokes Suitable for Manufacturing of Carbon Black

WILLIAM W. GOTSHALL

Carbon Development Corp., 2891 Haggerty Rd., Walled Lake, Mich. 48088

In 1964, Marathon Oil Company embarked on a research program to increase the markets for, and value of, petroleum coke.

At that time, Marathon Oil Company had two cokers operating in their domestic refineries. One was a delayed coker operating with a relatively low sulfur feedstock at their Robinson, Illinois refinery, and a fluid coker operating on a high sulfur Wyoming residuum at their Detroit, Michigan refinery. Marketability of the Robinson coke has always been quite strong because of its quality and also its low sulfur content. On the other hand, those from the fluid coker in Detroit suffered because of low prices and limited markets because of its analysis:

Figure I
Typical Analysis - Detroit Fluid Coke

Fixed Carbon	87.30%
Sulfur	5.64
% volatile matter	7.00
Ash	0.06
	100.00%

Analysis of volatiles

Oxygen	4.00%
Hydrogen	1.50%
Methane	1.50%
	7.00%

Fluid coke has several characteristics which make it quite undesirable for most petroleum coke markets. These characteristics are; sulfur content, low volatility, poor crystalline structure, and low grindability index.

The sulfur content of most fluid cokes will vary anywhere from five to eight percent, which obviously makes it rather undesirable for fuel uses and also for metallurgical use. Most fluid cokers were installed in refineries operating on high sulfur feedstocks because of the lower capital investment required for the same throughput with a fluid coker versus delayed coker and the fact that it is a continuous process rather than batch. Because of the savings in capital and lower operating costs, and

also because the cokes would normally be quite undesirable due to
sulfur content, many refiners chose fluid coking.

The volatile content of fluid coke is extremely low because
the material has been partially calcined in the burner portion of
the process where temperatures usually vary between 1125° and
1175° F. Because of this, the volatile combustible matter is only
about 3%. If fluid coke is used as a fuel, a minimum of 10% of
other fuels must be used to sustain combustion since the volatile
content is so low combustion cannot be maintained by burning fluid
coke alone.

The crystalline structure of fluid coke is considerably dif-
ferent than that of delayed coke because of the nature of the coke
formation in the process. Delayed coke formed in the coke drum
has time for the coke crystals to orient themselves upon one
another so that a much more uniform crystallinity can be obtained
which improves its characteristics for most electrode uses. Fluid
coke is formed by spraying residuum on a hot particle of coke. The
residuum is formed almost immediately into coke with complete dis-
orientation with the crystallites in the hot coke particle. Be-
cause of this disorientation of the crystalline structure, grain
density maximums for fluid petroleum coke upon calcining are in
the range of 1.9 to 2.0 grams per cc, whereas delayed cokes can be
calcined to reach grain densities as high as 2.1 grams per cc. Be-
cause of this crystalline disorientation, the electrical conduc-
tivity of fluid coke is considerably less than that of delayed
coke.

Another problem which limits the marketability of fluid coke
is its extreme hardness and low grindability index. A soft, fri-
able bituminous coal has a grindability index of 100 and Pennsyl-
vania anthracites will vary from 30 to 40 on the Hardgrove scale.
Delayed petroleum coke will also have a grindability index approx-
imating 100, whereas fluid petroleum coke normally is in the range
of 20 to 30. Because of this extremely low grindability index, it
cannot be co-ground with most coals because of separation problems
in the pulverizer, and because other fuels are required to sustain
combustion.

One of the areas of research to upgrade fluid petroleum coke
was its use to manufacture a rubber filler. It was felt that it
was desirable for this non-fuel use because of its high fixed car-
bon content, low ash content, and the fact that the sulfur was
tied up in carbon-to-sulfur-to-carbon bonds which would render
the sulfur inactive in rubber compounding. The carbon black mar-
ket was also attractive because of its size. Carbon black is the
seventh largest dollar volume chemical sold in the United States.
The world-wide market approaches 7 billion pounds per year, which
could very easily use the 180 tons per day of fluid coke manufac-
tured in Marathon's Detroit refinery.

It was initially felt that particle size was the principal
criteria. Methods of pulverizing were investigated, resulting in
the selection of a Majac Fluid Energy Mill. Initial samples, how-
ever, showed an anomaly in that the finer particles did not im-

prove the reinforcing qualities of the filler and in some cases
actually decreased it. These samples were produced using air as
the pulverizing fluid. It was suggested that in pulverizing, car-
bon crystals were being broken, exposing free radicals which re-
acted immediately with oxygen in the air, eliminating the surface
activity essential for rubber reinforcement. It was decided to
pulverize the material in steam, [a non-oxidizing fluid at the
temperature used], and subsequently protecting the surfaces ex-
posed until the ground carbon could be compounded into rubber. The
coating which we used was an oil having a high solvency in rubber
so that the active surfaces were exposed after mixing with the
rubber to allow the chemical activity on the surface to perform
similarly to the reinforcing properties of carbon black.

The ground carbons produced exhibited properties which were
not easily catagorized with existing blacks, which is not sur-
prising, being made from an entirely different approach and also
containing a spectrum of particle sizes rather than the narrow
particle size range of most carbon blacks, however, the product
produced from raw fluid coke shows that it is slightly more rein-
forcing than thermal black and less reinforcing than semi-rein-
forcing furnace black as the following test in Styrene-Butadiene
Rubber indicates:

Figure II
Test Formulation

SBR 1502	100.00
Zinc oxide	5.00
Stearic acid	2.00
Sulfur	1.75
Santocure	1.30
Ground carbon @ 65 parts*	
MT @ 75 parts*	

307° F cure

		300% Mod	Tensile	Elong	Set	Hard-creep	Tear
	15'	340	720	650	58	53-42	216
GC	30'	1490	1810	440	9	62-59	150
	50'	1740	1850	330	4	66-63	138
	15'	320	1390	950	42	51-44	288
MT	30'	1000	1490	400	8	61-59	165
	50'	1110	1670	450	10	61-58	124

* Equal volume loading – compounded stock SpGr = 1.150 for
GC vs. 1.230 for MT. Therefore, equivalent volumes equal
152 for GC vs. 148 for MT

Subsequent work covered other sources of carbonaceous mate-
rial such as coal, both anthracite and bituminous, coke made from
coal, coal char, and char from carbonization of rubber products.
Among the technology are several patents covering alteration
of the surface chemistry of the ground particles which allow a
flexibility to manufacture several grades of reinforcing fillers

using the same basic raw materials.

Some of this work will be shown so that this control of the surface chemistry will become apparent.

There are two methods of achieving this control. One is by changing the crystalline structure of the carbon before pulverization, the other is the alteration of the surface after grinding.

Carbon has three basic structures, amorphous, graphite and diamond. The amorphous carbon can be converted to synthetic graphite by a time-temperature relationship. This allows the growth of crystallites on each plane, an ordering of these crystallites, and a reduction of the inter-planar spacing. Raw petroleum coke can have a specific gravity as low as 1.4 and can be calcined to a specific gravity of 2.1. Ground carbons made from primarily amorphous carbons have much lower reinforcing abilities in rubber than the same carbon after calcining.

An example of the differences achieved by this pretreatment of the carbon follows:

Figure III
Test Formula

Natural rubber	100.00
Stearic acid	3.00
Zinc oxide	3.00
Benzothiazyl sulphide	0.60
Sulfur	2.50

Black as noted

	300% Mod	Tensile	Elong	Set	SpGr
Raw fluid coke					
65 phr					
30' cure	1330	1850	390	16	1.116
Calcined fluid coke					
80 phr					
30' cure	1950	2100	330	12	1.216

[It should be noted that the specific gravity of raw fluid coke is 1.5 while calcined is 1.9 which explains the weight difference in loading. The two compounds yield the same volume based upon compounded stock specific gravity.]

These two blacks were made with the same basic raw material, except that the second was calcined at 2300° F for 1/2 hour, while the first had reached a maximum temperature of 1150° F in the coking process.

Alteration of the surfaces of the ground carbons after grinding can be obtained by oxidizing the surfaces of the carbon which reduces reinforcement and lengthens vulcanization time. To reduce and stabilize vulcanization time, the addition of small amounts of methanol to the surface and the subsequent evaporation of the methanol results in constant cure times. Because of the abundance of active sites on the surface of the ground carbons, it is amenable to various other surface treatments.

Marathon Oil Company shut down their fluid coker in 1970, and

felt that this technology was too far afield from their activities to continue their development. Carbon Development Corporation was formed in 1971 and licensed the world-wide rights to this technology.

In summation, the following characteristics of the carbonaceous raw materials required for manufacture of carbon black substitutes from our technology are as follows:

1. <u>Ash content</u> - Obviously the higher the ash content, the lower fixed carbon content which will be available on the surfaces of the finished product, resulting in less reinforcement.

2. <u>Crystallinity</u> - The more crystalline the carbon feedstock, the higher its reinforcing characteristics. This crystallinity can be increased by high temperature treatment such as calcining.

3. <u>Volatile combustible matter</u> - The higher the volatile combustible matter in the raw material the more staining the resultant carbon black is. One of the features of carbon blacks made from fluid petroleum coke, calcined petroleum coke, or metallurgical coke breeze is the extreme non-staining characteristic of the resulting carbon black. This test is made by extracting the oils from the surface of carbon black with either benzene or toluene and measuring the percent of discoloration of the solvent. This is important for uses in tire products, especially white wall tires.

4. <u>Price and availability</u> - Although yields from the raw material used in these processes approximate 100%, price of the raw material is important. Therefore, relatively undesirable materials, such as fluid petroleum coke are particularly advantageous, not because of their characteristics, but strictly because of price and availability.

5

What Is Petroleum Pitch?

JOHN W. NEWMAN

Research and Development Department, Ashland Petroleum Co.,
Ashland, Ky. 41101

The term petroleum pitch can have many definitions, and the
most general is pitch derived from petroleum. What, then, is
pitch? Pitch can be defined as thick, dark colored bituminous
substances obtained as a result of industrial destructive dis-
tillation processes, obtained as deposits on the earth surface,
or, of primary interest here, manufactured from a specially
selected feedstock.

Natural pitch was known to the ancients and Noah probably
used it to calk the ark. Wood tars were widely used to calk the
early sailing vessels. The earliest reference to the possibility
of commercial recovery of tar from coal appeared in British
Patent No. 214 issued in 1681 to Beker and Surley. At this time,
no attempt was made to commercialize the process as ample supplies
of wood tar were available. During the American Revolution, how-
ever, Great Britain could not depend on the American colonies to
supply her wood tar requirements and interest was revived in the
use of coal tar as a wood tar substitute. In 1781, British
Patent No. 1291 was granted to Archibald Cochran on a method of
extracting or making tar pitch, essential oils, volatile alkali,
mineral acids, salts and cinders from pit coal. Since World War
II, many of the same or related coal tar products have become
increasingly available from petroleum and pitch is no exception.

The patent literature (1, 2, 3) contains numerous examples
of petroleum pitch manufacturing processes. Examples of feed-
stocks that could be used to produce a petroleum derived pitch
include decant oil from a fluid catalytic cracking unit, by-
product aromatic extracts from lube oil processes, asphaltic
residues from vacuum stills, hard asphalt from solvent deasphalt-
ing units, and the tar-like bottoms from the pyrolysis of naphtha
and gas oils for the manufacture of ethylene. Obviously, there
can be many petroleum pitches, each quite different from another.
Examples of three different petroleum pitch processes, taken from
the patent literature, and using decant oil as feedstock are sum-
marized in Figures 1 through 8. The differences in physical pro-
perties among two different petroleum pitches and a coal tar pitch

52
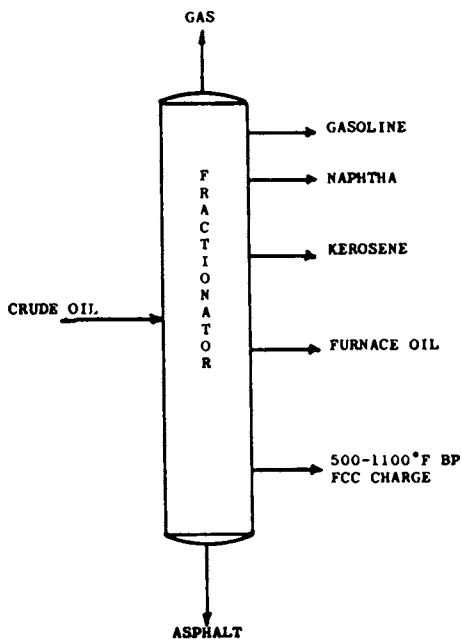
Figure 1. Petroleum pitch manufacture—crude oil fractionation
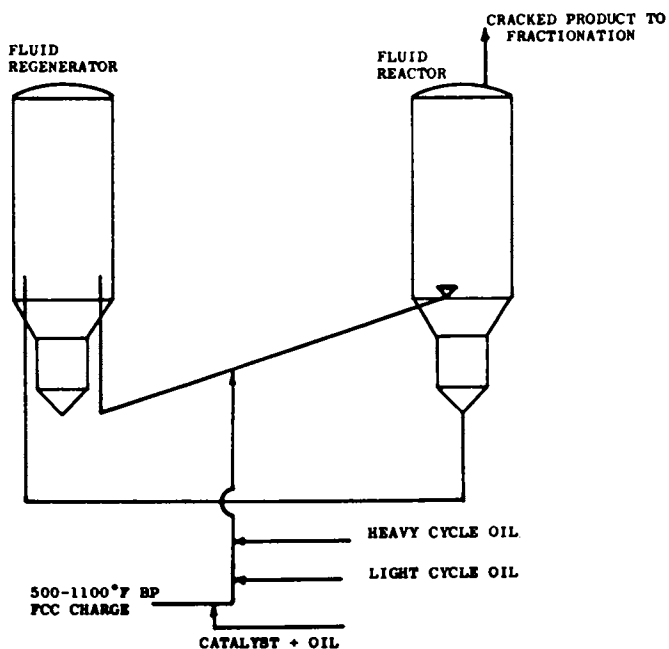
Figure 2. Petroleum pitch manufacture—fluid catalytic cracking
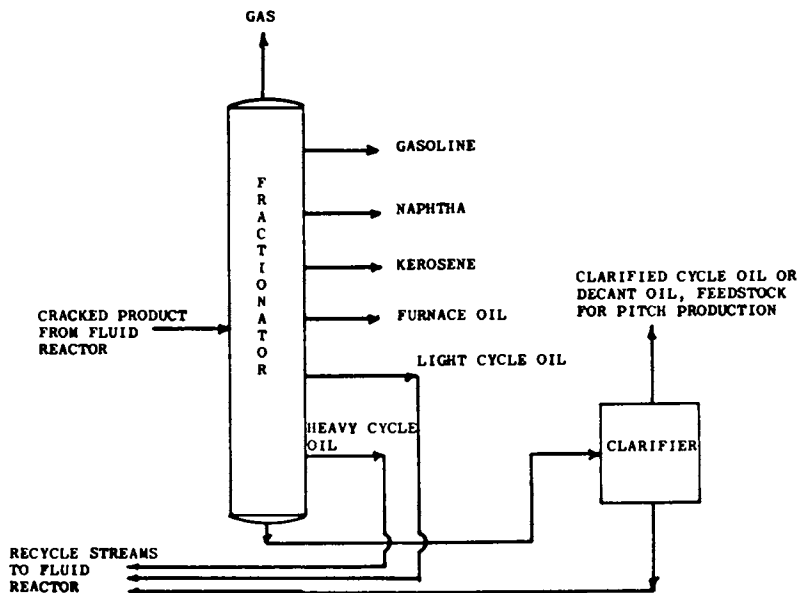
Figure 3.   Petroleum pitch manufacture—production of pitch feedstock
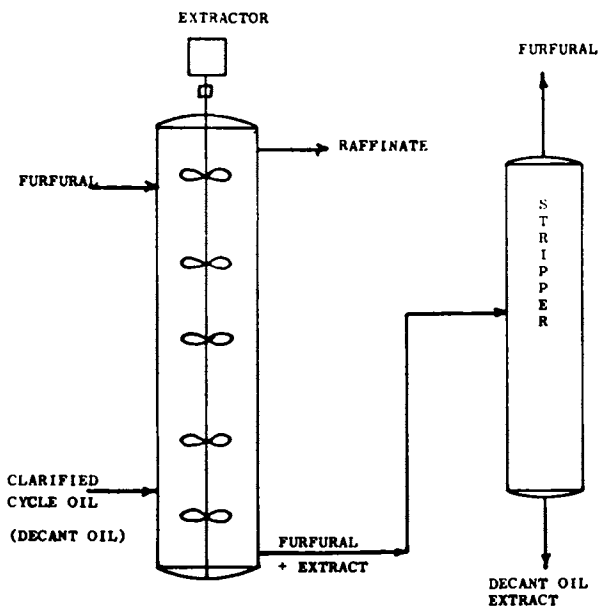
*Figure 4.   Petroleum pitch manufacture—concentration
of aromatics by solvent extraction*
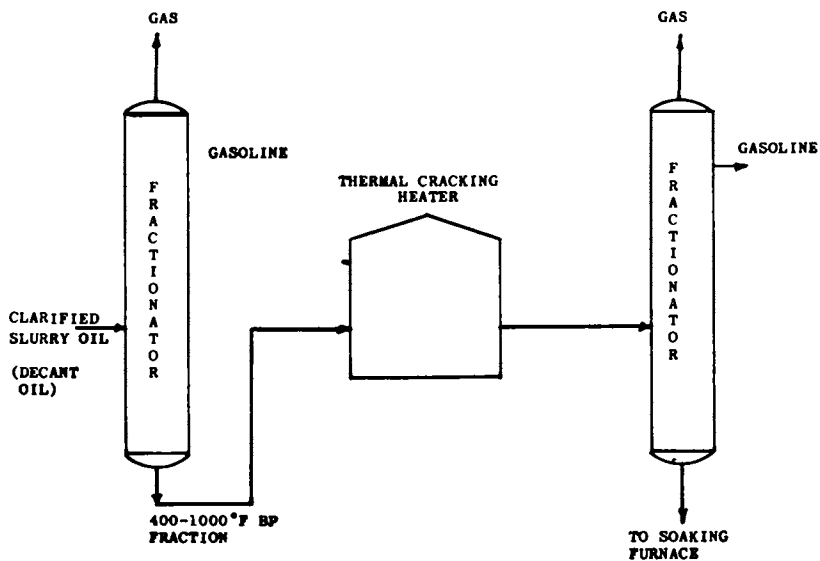
Figure 5.   Petroleum pitch manufacture—thermal process, initial step
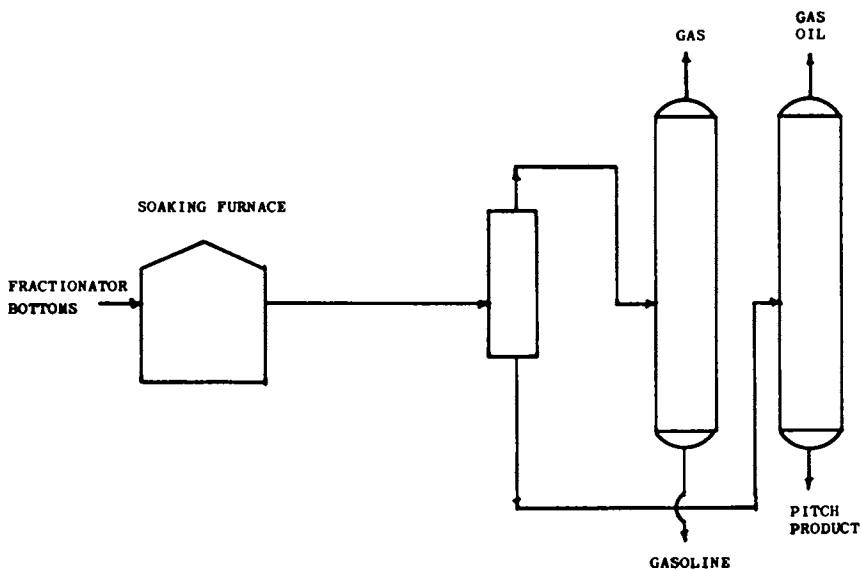
Figure 6.   Petroleum pitch manufacture—thermal process, final step
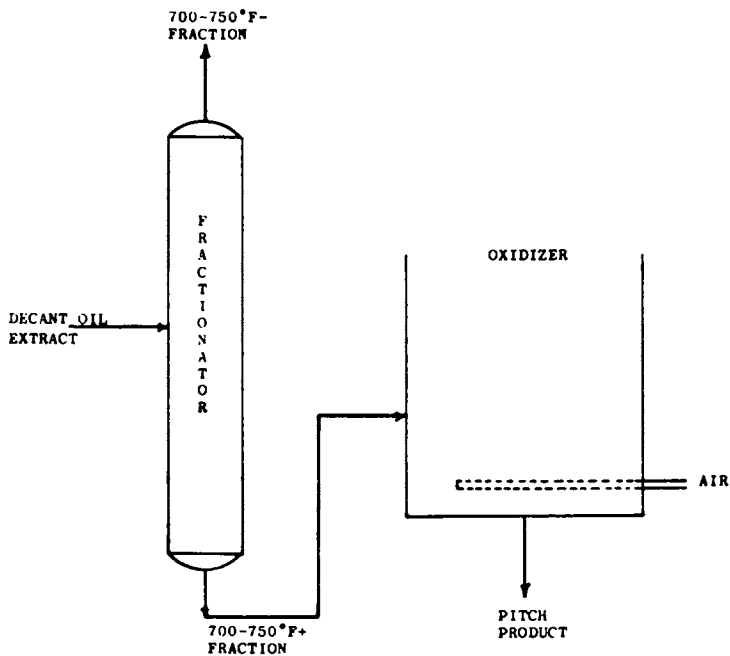
Figure 7.   Petroleum pitch manufacture—oxidation process
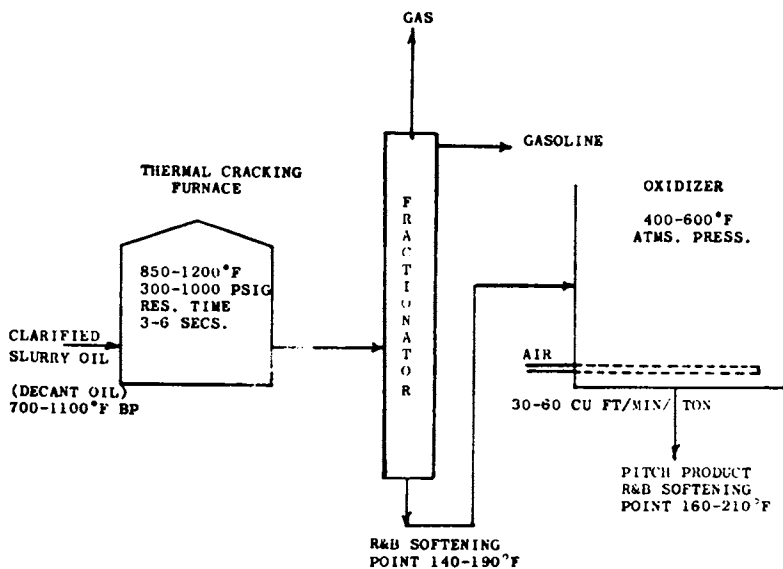
Figure 8.   Petroleum pitch manufacture—combination of thermal and oxidation routes
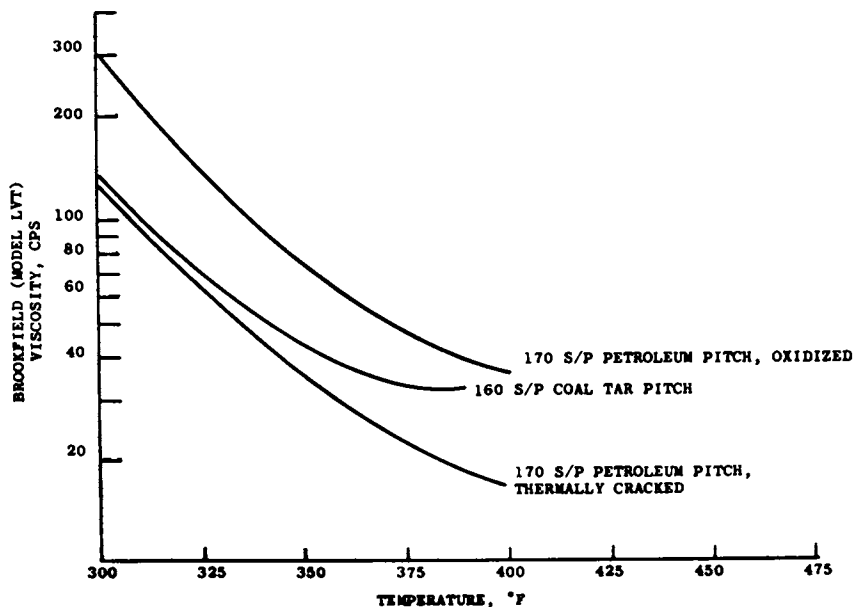
Figure 9. Comparison of Brookfield viscosity—petroleum and coal tar low softening point pitch
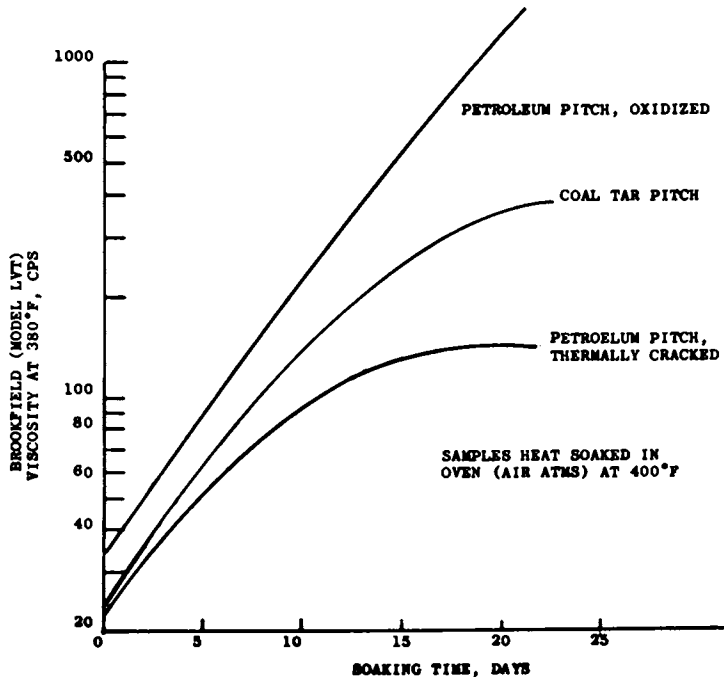
Figure 10. Comparison of thermal stability—fiber pipe impregnant—nominal 170°F S/P (R and B)
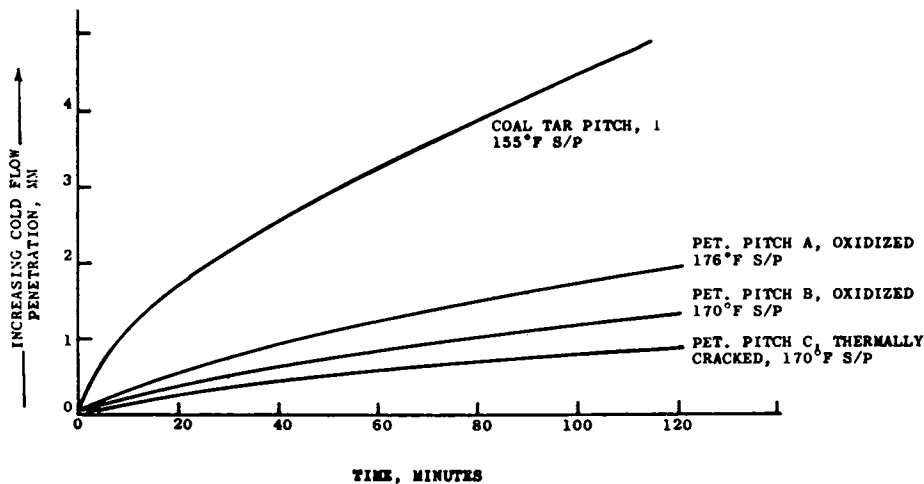
Figure 11. Comparison of cold flow properties commercially available fiber pipe impreg-nants—grease cone penetrometer, 200 g load, 77°F
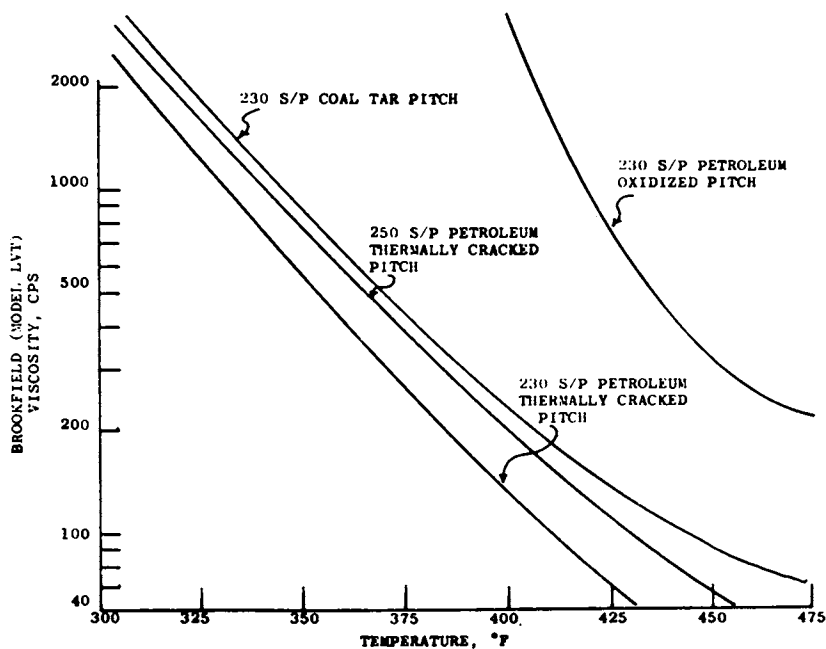
Figure 12. Comparison of Brookfield viscosity—petroleum and coal tar high softening point pitch

TABLE 1

COMPARISON OF TYPICAL PROPERTIES – ASHLAND PETROLEUM PITCHES

Test Method	Ashland 170 Pitch	Ashland 240 Pitch	Ashland Purified Carbon Precursor
Softening Point, °F (ASTM D 2398)	170	240	240
Softening Point, °C (ASTM D 3104)	81	120	120
Coking Value, % (ASTM D 2416)	36.3	50.3	50.4
Quinoline Insolubles, % (ASTM D 2318)	Nil	Nil	Nil
Benzene Insolubles, % (ASTM D 2317)	3.5	5.5	2.5
Specific Gravity (ASTM D 2320)	1.185	1.228	1.210
Ash, % (ASTM D 2415)	0.1	0.1	0.02
Sulfur, % (LECO)	2.8	2.8	0.25
Brookfield Viscosity, cps.			
350°F	35	395	315
375°F	–	180	178
400°F	–	88	88
425°F	–	50	48
450°F	–	31	30

that are commercially available to the fiber pipe industry are
shown graphically in Figures 9 through 11. A graph comparing the
viscosity-temperature relationship of two different types of
petroleum pitch and a coal tar pitch that are typical of electrode
binder pitches is shown in Figure 12.

In the early 1960's, Ashland Petroleum Company began to
experiment with different petroleum pitch manufacturing processes
in their Research & Development laboratory. It soon became evi-
dent that there was a place in the market for a high quality,
consistent, manufactured petroleum pitch as opposed to pitches
which were simply by-products or inconsistently manufactured by
batch processes. By the mid 1960's, Ashland had developed a pro-
prietary commercial, petroleum pitch manufacturing process. The
electrode binder pitch produced by this process became the first
commercial petroleum pitch to be fully approved as an electrode
binder pitch by a major U.S. aluminum company (4, 5). Ashland
petroleum pitch was introduced into the specialty graphite area
through the Nerva Program and is now being used by the country's
leading specialty graphite companies as a high quality carbon pre-
cursor for graphites and graphite and carbon fibers (6,7,8,9,10,
11,12,13,14 15,16,17,18,19,20,21,22,23,24). Typical laboratory
inspections of plant produced A-240 grade electrode binder and
A-170 grade fiber pipe impregnating petroleum pitch (25) and a
new high purity carbon precursor produced from a new pilot unit
are shown in Table 1. The purified carbon precursor now available
in drum quantities from Ashland Petroleum Company was developed
in response to a request from the specialty carbon industry for a
consistent, high purity petroleum pitch.

What is petroleum pitch? Petroleum pitch can be an incon-
sistent, low quality, black carbonaceous mass derived from petro-
leum, or it can be a consistent, high quality carbon precursor
manufactured to specification from selected hydrocarbon feed-
stocks.

Literature Cited

1. Bell, J. F., et al., "Process for Preparing Binder Pitches,"
    U.S. Patent 3,140,248, July 7, 1964.
2. Baum, L. A. H., "Process for Producing Electrode Binder
    Asphalt," U.S. Patent 3,725,240, April 3, 1973.
3. Alexander, S. H., et al., "Production of Petroleum Base Pitch
    and Aromatic Oils," U.S. Patent 3,318,801, May 9, 1967.
4. Alexander, C. D., et al., "Laboratory and Plant Performance
    of Petroleum Pitch," AIME Paper No. A71-29, AIME and WAAIME
    100th Annual Meeting, New York City, February 1971, Published
    by AIME, 345 East 47th Street, New York, New York 10017.
5. Ball, G. L., et al., "Petroleum Pitch - A Major New Carbon
    Source," Proceedings of Sessions-101st AIME Annual
    Meeting, San Francisco, California, February 1972, Published
    by AIME, 345 East 47th Street, New York, New York 10017.

6. Smith, W. E., et al., "Characterization and Reproducibility of Petroleum Pitches," Oak Ridge Y-12 Plant, Published by U.S. Department of Commerce, Report No. Y-1921.
7. Overholser, L. G., "Nerva Fuel Element Development Program Summary Report-July 1966 through June 1972, Oak Ridge Y-12 Plant, Published by U.S. Department of Commerce, Report No. Y-1857.
8. Horne, O. J., et al., "Properties of Carbon Derived from Petroleum Pitches," Oak Ridge Y-12 plant, Published by U.S. Department of Commerce, Report No. Y-1875.
9. Netherlands Patent Application 73-04398, "Process for Preparation of Carbon Fibers from Pitch in the Mesophase State with a High Modulus of Elasticity and a Great Strength," Date open to Inspection October 2, 1973.
10. Newman, J. W., "Petroleum Pitch - A Consistent Carbon Precursor," 11th Biennial Conference on Carbon, Extended Abstracts, 1973, p. 104, Published by NTIS, U.S. Department of Commerce, Springfield, Virginia 22151.
11. Jones, S. S. and Hildebrandt, R. D., "Reactivity of Selected Carbons with Oxygen and Carbon Dioxide," 11th Biennial Conference on Carbon Abstracts, p. 84.
12. Smith, W. E., "Structural Characterization of Petroleum Derived Carbon Precursors," 11th Biennial Conference on Carbon Abstracts, p. 106.
13. Whittaker, M. P., and Miller, F. C., "Unique Binder Systems for the Fabrication of Graphite," 11th Biennial Conference on Carbon Abstracts, p. 110.
14. Kennedy, C. R. and Eatherly, W. P., "The Development of Thermal Shock Resistant Graphite," 11th Biennial Conference on Carbon Abstracts, p. 131.
15. Gilliam, H. G., and Whittaker, M. P., "Mesophase Graphite," 11th Biennial Conference on Carbon Abstracts, p. 211.
16. Bradley, R. A., and Sease, J. D., "The Slug Injection Process for Fabricating HTGR Fuel Rods," 11th Biennial Conference on Carbon Abstracts, p. 239.
17. Hammer, R. L., et al., "Development of Continuous-Matrix Fuel Rods for Advanced HTGR," 11th Biennial Conference on Carbon Abstracts, p. 259.
18. Kennedy, C. R., and Eatherly, W. P., "Development of Graphites for Resistance to Irradiation Damage," 11th Biennial Conference on Carbon Abstracts, p. 304.
19. Kennedy, C. R., "Irradiation of Graphite at 950°C," 11th Biennial Conference on Carbon Abstracts, p. 312.
20. White, J. L., et al., "Mechanisms of Formation of Needle Coke," 12th Biennial Conference on Carbon Extended Abstracts, 1975, p. 221.
21. Rester, D. O., "Factors Controlling the Mesophase Microstructure Produced During Pyrolysis of Aromatic Hydrocarbons," 12th Biennial Conference on Carbon Extended Abstracts, 1975, p.227.

22. Horne, O. J. and Kennedy, C. R., "Graphites Fabricated From Green Petroleum Pitch Cokes," 12th Biennial Conference on Carbon Extended Abstracts, 1975, pp. 255-256.
23. Lewis, I. C. and Jackson, G. W., "Heat of Reaction for Mesophase Formation," 12th Biennial Conference on Carbon Extended Abstracts, 1975, pp. 267-268.
24. Didchenko, R., et al., "High Modulus Carbon Fibers From Mesophase Pitches, Parts One and Two," 12th Biennial Conference on Carbon Extended Abstracts, 1975, pp. 329-332.
25. Gannon, C. R., Australian Patent Number 451,613, Pending in U.S.A., Impregnated Articles, Method for Making Same, and Impregnant Composition.

Characterization of Petroleum Pitches Used for Coke Production

W. E. SMITH, B. NAPIER, and O. J. HORNE

Union Carbide Corp., Nuclear Division, Oak Ridge Y-12 Plant,
Oak Ridge, Tenn. 37830

This report describes the use of nuclear magnetic resonance (NMR) spectrometry as an aid in structural characterization of pitch materials and was part of a larger study on characterization and reproducibility of petroleum-derived products. (1) Discovery and implementation of pitches as bonding agents are recorded in some of the earliest known documents, and their usage in all probability long predates recorded history. Current usage reflects the desirable properties of pitch materials as numerous industries have been built around such applications as road surfacing, roofing materials, various adhesive and sealant formulations, and electrode fabrication.

Though the use of pitch is an ancient art and represents a high-volume market today, characterization and control of pitches have not been emphasized since typical high-volume applications do not warrant such an emphasis. However, pitch from natural sources represents a complex mixture of structures and varies in composition with the location of the source and with the methods used to extract the pitch. The latter can be standardized, but must also compensate for variations in the source if a reproducible pitch is to be made. Currently, some specialty applications require a high degree of characterization and control of starting materials, and it has been these users who continue to support efforts designed for that purpose. Fabricators of specialty items, in general, face less cost restraints and have a higher degree of precision in design and fabrication efforts.

An application in which pitch materials are being widely used is as a binder in the fabrication of specialty composite structures which can subsequently be pyrolyzed to yield carbon. Such fabrication schemes place emphasis on pitch materials that exhibit appropriate properties both as plastics at fabrication temperatures and as ceramic-type materials after carbonization. Since the properties of the latter are quite dependent on the characteristics of the raw material and the chemical and mechanical events that accompany carbonization, the fabrications engineer becomes interested in such subjects as pitch properties,

impurity contents, coke yields, and volume yields as they relate
to the mechanical and electrical properties of the end product.
To optimize and insure reproducibility of such a fabrication
scheme, close control of both materials and processing is re-
quired.

This, in turn, suggests the need for better characterization
of pitch materials which will necessitate the adaptation and
development of more sophisticated analytical techniques than have
traditionally been used for describing these materials. NMR
spectrometry promises to aid in characterization of pitch
materials by providing considerable information about the mole-
cular structure and composition of quite complex mixtures. Using
the method of NMR data analysis developed by Williams (2,3),
information on the aliphatic, alicyclic, and aromatic content
in a sample of petroleum feedstock and a derived pitch was deter-
mined and is presented in the following paragraphs.

Experimental Studies

Materials. Petroleum materials used in this study were
supplied by the Ashland Oil Company, Ashland, Kentucky. The
feedstock sample was fluid and was analyzed as received. Prior
to analysis, the pitch sample was powdered and dried under a
vacuum of < 100 μm for 20 hours at 25° C. Properties of these
materials are compared in Table I.

Analytical Methods. Average molecular weight data were ob-
tained using a Hewlett-Packard Model 302 vapor pressure osmo-
meter. Sucrose octaacetate was used as a standard. Prior to
analysis, chloroform insolubles were removed by a standard pro-
cedure. Samples were analyzed as tetrahydrofuran solutions.

Benzene insolubles were determined as per ASTM D-2317.
Carbon and hydrogen contents were determined by combustion in a
carbon train using quantities of evolved carbon dioxide and water
to calculate the carbon and hydrogen contents, respectively.

Oxygen contents were determined by neutron activation
analysis using a Kaman Model 711 neutron generator and beryllium
as a standard.

Analysis for the sulfur content involved combustion in a
bomb followed by a gravimetric determination of sulfur as barium
sulfate.

Ash contents were determined by firing samples to 900° C in
air and weighing the residuals.

High-resolution spectra were obtained using a Bruker HFX-
15 90-megahertz spectrometer. Other instrument conditions are
listed in Table II.

Method of Data Analysis. This approach follows that de-
scribed by Williams (2,3) and makes use of elemental composition
and molecular-weight data in conjunction with proton distributions

TABLE I

PROPERTIES OF PETROLEUM-DERIVED MATERIALS

	Average Molecular Weight	Benzene Insolubles (%)	Carbon Content (%)	Hydrogen Content (%)	Oxygen Content (%)	Sulfur Content (%)	Ash Content (%)
Feedstock (RD-79 P)	301	---	89.77	8.99	---	0.67	0.08
A-170 Pitch	415	1.8	91.80	5.98	0.70	0.84	0.02

that may be obtained from high-resolution NMR spectra. Since the
input data that were used represent average properties, the re-
sults of the study should be considered as averaged over all
molecular species in the sample.

TABLE II

STANDARDIZED INSTRUMENT CONDITIONS FOR
NUCLEAR MAGNETIC RESONANCE ANALYSIS

Concentration	5% in CCl_4
Standard (internal)	TMS (tetramethylsilane)
Temperature	55°C
Time Constant	0.25 sec.
Sweepwidth (+)	20 Hz/cm
Sweep time	500 sec.
Offset	0
Attenuation f_0	60
f_1	45

Williams ([2,3]) divides the protons into three groups:
aromatic (H_A^*), α-alkyl (H_α^*), and other alkyl ($H_\beta^* + H_\gamma^*$). As noted
in Figure 1, the NMR response of protons associated with aromatic
carbons is easily distinguished from that of the aliphatic pro-
tons. Likewise, the response of α-alkyl protons is readily dis-
tinguished from that of other aliphatic protons. The α-alkyl re-
sponse accounts for protons that are on aliphatic carbon atoms
which are adjacent to aromatic nuclei. Protons on carbons which
are beta or higher to aromatic nuclei yield a variety of NMR
signals due to the complex structures that characterize petroleum
materials.
Calculations associated with this NMR method do not require
the separate classification of H_β^* and H_γ^* protons, but do require
a peak-height ratio of H_γ^* and H_β^*. These data are easily cal-
culated for feedstock materials, but are less accurate for pitch
spectra due to reduced resolution. Equations associated with
this method of data analysis are detailed in Table III. Assump-
tions associated with the method are detailed elsewhere ([1,2]).

Analysis of Petroleum Feedstock. The high degree of spectral
resolution of feedstock samples made these materials amenable to
detailed characterization using NMR techniques. Feedstocks showed
good resolution between the two bands that were collectively
classified as "other alkyl". One proton type (H_β^*) corresponds to
methylene hydrogen while the second (H_γ^*) corresponds to terminal
methyl groups. There would, of course, be some exceptions to such
a simple classification. For example, methyl groups that are
beta-to-aromatic nuclei would probably be measured as H_β^* proton
types.

TABLE III

TERMS AND EQUATIONS FOR EXPRESSING NUCLEAR MAGNETIC RESONANCE DATA

Notation	Description	Equation
$H_A^\bullet$	Normalized integrated intensity of aromatic hydrogen.	
$H_\alpha^\bullet$	Normalized integrated intensity of hydrogen on alkyl carbons, alpha to aromatic nuclei.	α - Alkyl
$H_\beta^\bullet$	Normalized integrated intensity of methylene hydrogen on alkyl carbon beta or higher to aromatic nuclei. Probably includes beta-methyl groups also.	Other Alkyl
$H_\gamma^\bullet$	Normalized integrated intensity of methyl hydrogen on alkyl carbon gamma, or higher, to aromatic nuclei.	Other Alkyl
C	Carbon content . (%)	
H	Hydrogen content . (%)	
MW	Average molecular weight.	
BI	"Branchiness index".	Peak-Height Ratio of Methyl to Methylene Hydrogen
n	Average number of carbon atoms per alkyl substituent.	$\dfrac{H_\alpha^\bullet + H_\beta^\bullet + H_\gamma^\bullet}{H_\alpha^\bullet}$
r	Average number of naphthene rings per substituent.	$\dfrac{[0.250\,(BI + 4.12) - 1]\,(n-1)}{2}$
f	Average carbon-hydrogen weight ratio of alkyl groups.	$\dfrac{12\,n}{2n + 1 - 2r}$
C_s	Fraction saturate carbon. (%)	$f(H_\alpha^\bullet + H_\beta^\bullet + H_\gamma^\bullet)\,H$
C_A	Fraction aromatic carbon. (%)	$C - C_s$
f_a	Aromaticity or ratio of aromatic to total carbon.	$\dfrac{C_A}{C}$
$\#C_A$	Average number of aromatic ring carbon atoms per average molecule.	$\dfrac{C_A \times MW}{1,200}$
C_1	Fraction of nonbridge aromatic ring carbon. (%)	$(12.0\,H_A^\bullet + f\,H_\alpha^\bullet)\,H$
$\#C_1$	Average number of nonbridge aromatic ring carbon atoms per average molecule.	$\dfrac{C_1 \times MW}{1,200}$
AS	Percent substitution of alkyl groups on nonbridge aromatic ring carbons . (%)	$\dfrac{(f\,H_\alpha^\bullet\,H)\,100}{C_1}$
R_s	Average number of alkyl substituents per average molecule.	$\dfrac{(AS)\,(\#C_1)}{100}$
R_A	Average number of aromatic rings per average molecule.	$\dfrac{\#C_A - \#C_1}{2} + 1$
R_N	Average number of naphthenic rings per average molecule.	$\dfrac{(AS)\,(\#C_1)\,r}{100}$

In general, the aliphatic proton distribution shown in Figure 1 suggests: (1) comparatively short aliphatic chains (high values for H_α^* relative to values for $H_\beta + H_\gamma^*$), (2) a low degree of chain branching (relatively small values for H_γ^*), and (3) cyclic structures (high values for H_α^* and H_β relative to H_γ^*).

Information obtained for the feedstock sample will allow construction of a molecular formula and will show correlations between the measured properties and those calculated from NMR data. Data in Table IV indicate an average alkyl group composition of $C_{3.0}H_{6.9}$ with 3.1 of these substituent groups in an average molecule. Other data indicate the presence of 13.3 aromatic ring carbon atoms per average molecule.

Using the generalized molecular formula shown in Table V, the calculated molecular formula is in good agreement with that determined from molecular-weight and elemental-composition data only. The aromatic proton distribution data in Table V were included to demonstrate, in part, the validity of the equations used in the calculations in that the value of H_A^* obtained from the calculated molecular formula was no different than that obtained directly from NMR spectra and used as input in the calculations.

In attempting to visualize the possible aromatic structures of an average molecule of the feedstock sample, models were constructed and were correlated with the observed data. The models, as given in Table IV, represent relatively simple aromatic structures. Thus, the average molecule can be visualized as consisting of three fused aromatic rings with approximately three alkyl substituents, each composed of approximately three carbon atoms.

A-170 Pitch. A sample of A-170 pitch was subjected to NMR analysis similar to that discussed for the feedstock sample (Figure 2).

Significant generalized observations from the aliphatic proton distribution are:

(1) Aliphatic chains are quite short; much shorter than those observed for feedstocks (based on a high value of H_α^*).

(2) Considering H_β^* to represent methylene and beta-methyl protons, there are relatively few alkyl groups containing two carbon atoms.

(3) Considering H_γ^* to represent terminal methyl groups in the gamma (or higher) positions, an even smaller number of the alkyl groups consist of three or more carbon atoms.

Collectively, the data in Table VI allow visualization of a structure representing an average of all molecules in the A-170 pitch sample. The alkyl group composition was $C_{1.4}H_{3.7}$, and 3.3 of these groups are present as substituents in an average molecule. Aromatic moieties average 6.7 aromatic rings per molecule and are composed of 27.3 aromatic carbon atoms. Using the generalized molecular formula shown in Table V, the calculated
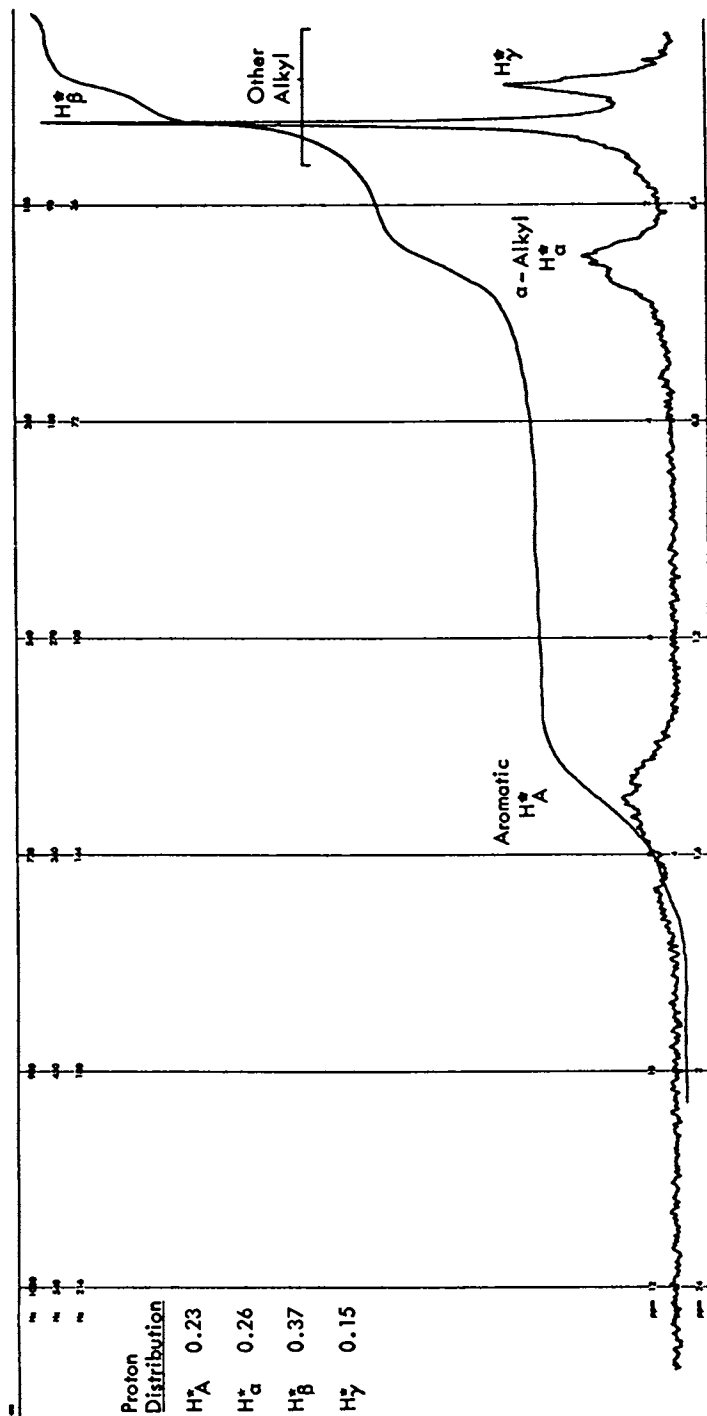
Figure 1. NMR spectrum of petroleum feedstock (RD-79P)

TABLE IV

AVERAGE PROPERTIES CALCULATED FOR FEEDSTOCK RD-79P

	Property	Notation	Value	Models
Aliphatic/Alicyclic	Number of C Atoms per Alkyl Group	n	3.0	$(-C_3H_7)_3$
	Number of H Atoms per Alkyl Group	nx	6.9	
	Number of Alkyl Groups per Molecule	R_S	3.1	
	Naphthenic Rings per Molecule	R_N	0.30	
	Saturated Carbon Content (%)	C_S	37	
Aromatic	Aromatic Carbon Content (%)	C_A	53	
	Aromaticity	f_a	0.59	
	Aromatic Rings per Molecule	R_A	3.0	Anthracene Phenanthrene
	Aromatic Ring Carbon Atoms per Molecule	$^\#C_A$	13.3	
	Non-Bridge Aromatic Carbon Content (%)	C_1	37.2	
	Non-Bridge Aromatic Carbon Atoms per Molecule	$^\#C_1$	9.3	
	Fraction Non-Bridge Aromatic Carbon Atoms with Alkyl Substituents (%)	AS	33.2	

TABLE V

COMPARISON OF MEASURED AND CALCULATED PROPERTIES
FOR FEEDSTOCK RD-79P

Property	Measured	Calculated[1]
Molecular Formula	$C_{22.5}H_{27.1}$ [2]	$C^{\#}_{C_A}H_{(\#_{C_1}-R_s)}(C_nH_{nx})_{R_s}$
		$C_{13.3}H_{6.2}(C_{3.0}H_{6.9})_{3.1}$
		$C_{22.6}H_{27.6}$
Molecular Weight	301	299
Carbon Content (%)	89.8	89.6 [3]
Hydrogen Content (%)	9.0	9.1
Aromatic Proton Content (H_A)	0.23 [4]	0.22

(1) Using the technique of Williams (2).

(2) Obtained by using elemental composition and average-molecular-weight data.

(3) Corrected to account for the constituents other than carbon and hydrogen.

(4) From the NMR Spectrum.

TABLE VI

ANALYSIS OF PETROLEUM PITCH A-170 BY NMR TECHNIQUES

C	Carbon Content (%)	91.80
H	Hydrogen Content (%)	5.98
	Proton Distribution	
H_A^*	Aromatic	0.51
H_α^*	α-Alkyl	0.36
H_β }	Other Alkyl	0.10
H_γ^* }		0.03
C_s	Sat'd Carbon Content (%)	13.0
f	C/H Weight Ratio of Alkyl Groups	4.42
x	H/C Atom Ratio of Alkyl Groups	2.72
n	No. of C Atoms per Alkyl Group	1.35
nx	No. of H Atoms per Alkyl Group	3.68
R_s	No. Alkyl Substituents per Molecule	3.29
C_A	Aromatic C Content (%)	78.82
f_A	Molar Ratio Aromatic to Total C	0.86
R_A	No. Aromatic Rings per Molecule	6.66
$^\#C_A$	No. Aromatic Ring C Atoms per Molecule	27.26
C_1	Non-Bridge Aromatic C Content (%)	46.11
$^\#C_1$	No. Non-Bridge Aromatic Ring C Atoms per Molecule	15.95
AS	Fraction of Non-Bridge Aromatic Ring C Atoms with Alkyl Substituents (%)	20.62
R_N	No. Naphthenic Rings per Molecule	0.06
r	No. Naphthenic Rings per Substituent	0.02
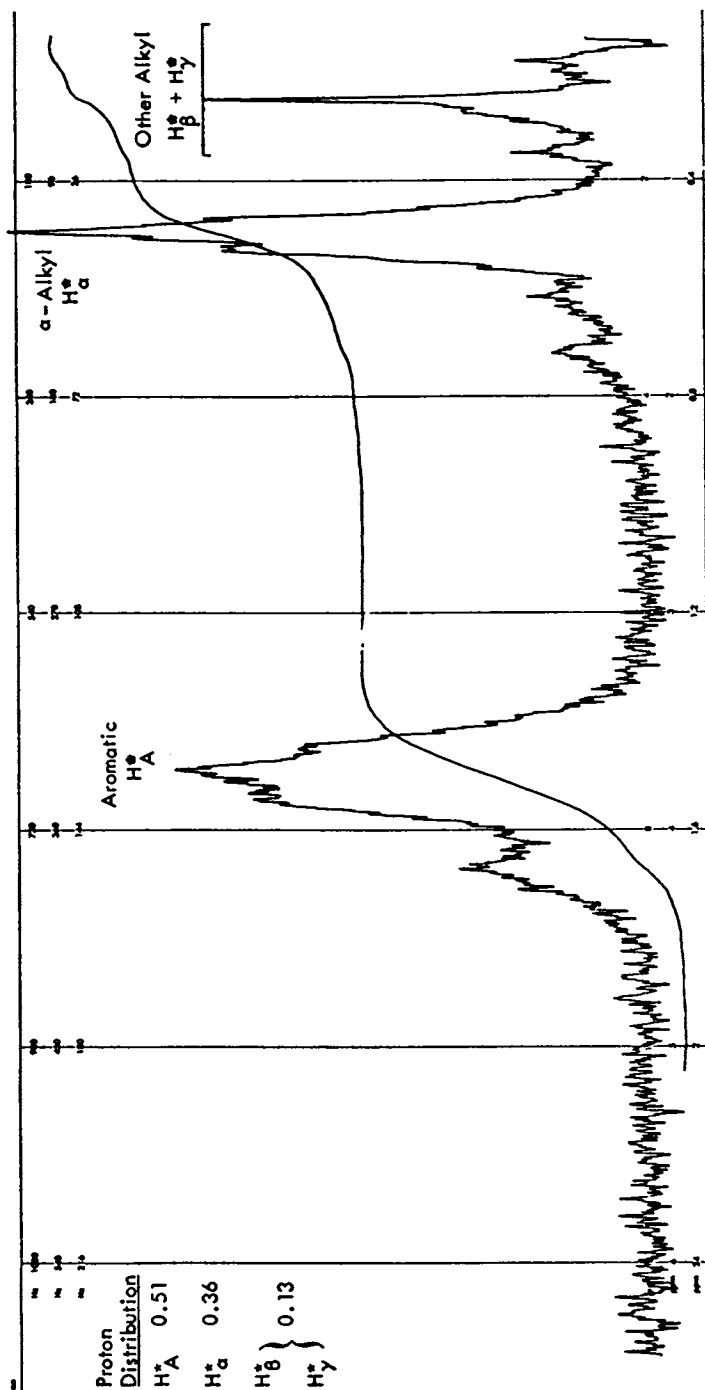
Figure 2. NMR spectrum of petroleum pitch (A-170)

molecular formula from these data is $C_{27.3}H_{12.7}(C_{1.4}H_{3.7})_{3.3}$.
This and other calculated properties may be compared with the
measured properties in Table VII. A comparison of the measured
and calculated proton distribution data show identical values
for H_A^*, and indicate that the equations used in the calculations
did not distort the NMR input data.

TABLE VII

COMPARISON OF MEASURED AND CALCULATED
PROPERTIES FOR PETROLEUM PITCH A-170

Property	Measured	Calculated[2]
Molecular Formula	$C_{32.4}H_{25.4}$ [1]	$C_{31.7}H_{24.7}$
Molecular Weight	415	405
Composition (CH only)		
Carbon (%)	91.80	91.82 [4]
Hydrogen (%)	5.98	5.96 [4]
Aromatic Proton Distribution (H_A^*)	0.51 [3]	0.51

(1) Obtained from elemental composition and average-
     molecular-weight data.
(2) Calculated from NMR data using technique of
     Williams(2).
(3) Measured from NMR spectra.
(4) Corrected to account for constituents other than
     C and H.
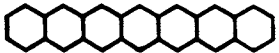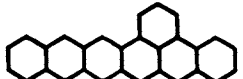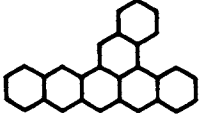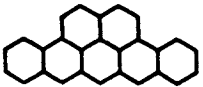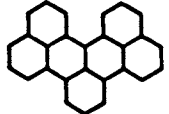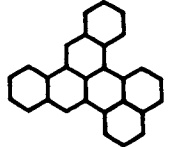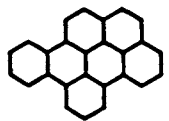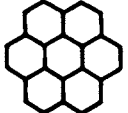
Models of aromatic structures similar to the average stru-
ture determined from NMR data are listed in Table VIII. The
models are all based on seven-ring systems, and progress from a
linear structure (Model 1) with a high content of peripheral or
non-bridge carbon atoms to a symmetrical structure (Model 10)
having a high degree of condensation and a low content of non-
bridge carbon atoms. Table VIII does not include all the
structural isomers for the seven-ring systems, but does represent
the degrees of ring condensation that are possible. Included in
Table VIII are H/C atom ratios for the model structures, allowing
a comparison with the value obtained by NMR calculations. Though
NMR data indicate that 3.34 hydrogen atoms in a seven-ring mole-
cule are substituted by alkyl groups; for the sake of simplicity,
values of H/C atom ratios in Table VIII assume no substitution.
This assumption does not invalidate the comparisons that were
made.

TABLE VIII
SEVEN-RING AROMATIC MODELS CORRESPONDING TO AVERAGE NMR PROPERTIES OF A-170 PETROLEUM PITCH

Model Number	Models	Number of Bridge Carbon Atoms Per Molecule	Number of Nonbridge Carbon Atoms Per Molecule	H/C Atom Ratio[1]
	Required for the Seven-Ring System as Per NMR Data on A-170 Pitch	11.90	16.75	0.585
1		12	18	0.600
2		12	17	0.586
3		12	16	0.571
4		12	16	0.586
5		12	15	0.556
6		12	15	0.556
7		12	16	0.571
8		12	14	0.538
9		12	13	0.520
10		12	12	0.500

Increasing Degree of Condensation

[1] Calculated as ratio: Number of Nonbridge Carbon Atoms/Number of Nonbridge Carbon Atoms + Number of Bridge Carbon Atoms. Values assume no substitution.

Hydrogen-to-carbon atom ratios in aromatic systems containing as many as seven rings are almost independent of the number of aromatic rings per molecule, and the effect decreases with an increasing number of rings. For example, in going from one ring to two rings, the H/C atom ratio changes from 1 to 0.8, or decreases by 20%. In going from a linear arrangement of seven rings to a linear arrangement of eight rings, the H/C atom ratio decreased by only 0.2%. However, as can be seen in Table VIII, the H/C atom ratios of aromatic ring systems can be significantly influenced by the degree of ring condensation; and, for a seven-ring system, can undergo a decrease of 16.7% in changing from linear (Model 1) to its most highly condensed structure (Model 10). Though the molecular distribution in the pitch will include systems containing more and less than seven rings, it seems reasonable to ignore this lesser effect on the H/C atom ratios; and, rather, associate with the atom ratio values the degree of condensation. Of the structures shown in Table VIII, Model 1 would be highly improbable, as would Model 10 and perhaps Model 9. Statistical distributions would not tend to include many molecules with such high degrees of order. Thus, if H/C atom ratios of other models are compared with that calculated from NMR data, two of the isomeric structures (Models 2 and 4) having the next highest H/C atom ratios (0.586) almost exactly duplicate that calculated (0.585), and contributions of other structures having lower H/C atom ratio values would seem to be quite small.

Conclusions

The models suggested in this study are not presented in order to prove specific molecular structures, but rather to demonstrate a technique for characterization and to show average or probable properties. The technique is extended and data are made more specific by fractionation of samples with subsequent analysis of each fraction. Likewise, computer programs to handle the data analysis and molecular modeling further extend the capabilities of this method.

Literature Cited

(1) Smith, W. E., Horne, O. J., Jr., Napier, B., Jr.; "Characterization and Reproducibility of Petroleum Pitches," Y-1921, Union Carbide Corporation, Nuclear Division, Oak Ridge Y-12 Plant, Oak Ridge, TN., June 21, 1973.

(2) Williams, R. B.; "Symposium on Composition of Petroleum Oils, Determination and Evaluation," ASTM Spec Tech Publication, (1958) 224, 168-94.

(3) Clutter, D. R., et al.; Analytical Chemistry (1972) 44, pp. 1395-1405.

Active Carbon Can So Be Made Out of Petroleum

HENRY C. MESSMAN

Box 267, Mamaroneck, N.Y. 10543

In the early pages of the 1951 edition of an authoritative text (1), there appears the clause, "----whereas coke, formed from hydrocarbons, resists most known methods of activation." This is still generally true, although on occasion it has been rather too broadly interpreted as meaning that active carbon can not be derived from petroleum. Pyrolyses of heavy hydrocarbons, that have not first been mixed with or reacted with other materials, do indeed yield coke residues that are quite refractory with respect to the selective oxidation that we call activation. For practical purposes, it is virtually impossible to make usefully active carbon out of delayed coker or fluid coker petroleum coke after it has been calcined to 1000° C. Much the same is true of coal coke, incidentally.

Terminology employed in the activated carbon industry can be confusing and some clarification is in order: 'Active' and 'activated' are commonly used interchangeably to describe usefully adsorptive carbon. The term, 'reactive', however, retains its conventional chemical meaning; so that 'regeneration' is employed to indicate renovation of spent active carbon. 'Char' signifies a carbonaceous residue from pyrolysis of solid organic matter, whereas 'coke' refers to a corresponding residue from pyrolysis of fluid organic matter. Incidentally, 'coke' made from coal is consistent with this usage, because coking coal passes through a plastic (fluid) temperature range before it begins to carbonize. Pyrolysis of non-coking coal yields coal char.

Ordinary wood charcoal exhibits appreciable adsorptive capacity, which was recognized during Biblical times. The first modern active carbon was bone char, developed for sugar processing at Napoleon's behest. It still is employed to some extent by the cane sugar

77

industry, even though it typically assays 10% or less
carbon and has a BET-nitrogen (2) pore surface area of
only about 100 square meters per gram. For compar-
ison, many commercial activated carbons on the market
today have corresponding pore surface areas of 1000 or
more sq. meters/gram.

   The development of active carbon was given great
impetus by the introduction of chemical warfare in
War I. Effective gas masks had to be provided for
troops at the front, and adsorptive carbons had to be
developed for their cannisters.

   With respect to the art of making and using active
carbon, the first rule is that there are nearly always
at least a few exceptions to every pertinent rule.
For this reason, most statements in this paper must be
more or less qualified. One such rule is that chars
are more amenable to activation than cokes. Chars
usually are somewhat porous at the outset, because in
shrunken form they tend to retain the general struc-
ture pattern of their parent raw material, whereas
most cokes exhibit relatively few small pores. And
chars are commonly more reactive than cokes; so that
they may be oxidized more readily.

   In commercial production of active carbon, no two
manufacturers employ the same process or even the same
raw material, with a few exceptions. And all manu-
facturers guard their process details as proprietary
secrets. This accounts for the aura of mystery or
'black magic' that characterizes active carbon pro-
duction technology, as well as for the dearth of
useful process 'know-how' to be found in the
literature.

   If there is such a thing as a conventional
approach to making a new active carbon, perhaps it is
depicted by Don W. Green et al in their work (3) at
the University of Kansas during 1970. These men
experimentally attempted to make granular active
carbon out of green Mid-Continent delayed petroleum
coke with various combinations of chemical treatment
and steam activation at around 1550°F (843°C). At
relatively high burn-off rates they were able to
approach commercial quality. The principal reason
for citing this reference, however, is to illustrate
the difficulty of acquiring background for R. & D. in
the active carbon field. Its authors were doubtless
well-trained and conscientious; so we may assume that
they started with a competent search of conventional
literature. Yet many of their observations would be
judged quite amateurish by technical personnal
experienced in the practical production and utilization

of active carbon. For one example, they state that,
"Materials that contain mineral ingredients (e.g.
bones) are ideal for making decolorizing carbons."
From this, a reader may conclude that bone char is a
popular and efficient decolorizing carbon, which is
not the case. The fact that some bone char continues
to be employed by the cane sugar industry, is not due
to its decolorizing capacity. Another example is the
statement that, "A quality of the micropore structure
(100 angstroms or less) is shown by the iodine test
and the macropore structure of the carbon (100
angstroms or larger) is indicated from the molasses
test." Actually, substantial molasses color can be
adsorbed in micropores between 28 Å and 100 Å. And
with respect to definition, one reputable U.S. manu-
facturer has published: "Micropores may be arbitrarily
defined as pores whose diameters range from 10 to 1000
Å." (4) On the other hand, Dubinin (5) classifies
MICROPORES as those having effective radii less than
18 – 20 Å, TRANSITIONAL pores as larger up to about
500 – 1000 Å and MACROPORES as having effective radii
greater than about 500 – 1000 Å. In support of Don
Green and his associates, however, old references often
suggested 100 Å as the effective radius distinguishing
micro- from macropores. This comment is intended
solely to indicate difficulties inherent in the field
of research on which these authors reported and it is
in no way any reflection on their ability or integrity.

Delayed coker coke is usually less reactive than
most char, while fluid coker coke tends to be even less
reactive than delayed coke. Still, it is possible to
make active carbon out of green fluid coker coke. This
was observed in the course of developing a method for
desulfurizing coke (6) impregnated with an alkali metal
compound, by steam fluidization at around 1400°F
(760°C). The possibility was not pursued because it
appeared at the time that materials of construction
were not available to withstand commercial process
conditions. Cast alumina refractories being offered
today, however, may contain the reaction satisfactor-
ily. Accordingly it would appear that an on-40-mesh
fraction of high sulfur fluid coker coke might warrant
a new look as a possible raw material for spheroidal
'granular' active carbon production. Perhaps this is
not surprising because, grossly in its onion-layered
spheroidal form, fluid coke tends to be more isotropic
than delayed coke. Figures 1, and 2, are electron
microphotographs (replica technique) of fluid coker
coke particles before and after such treatment. If one
assumes that inner layers of the coke in Fig. 2, are
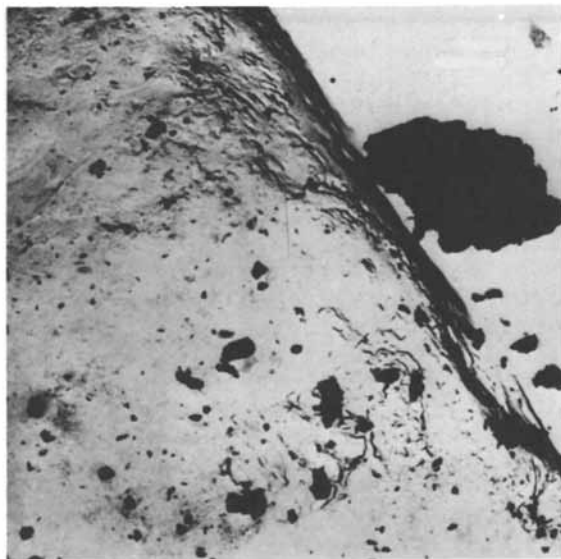
Figure 1.   (3800×)
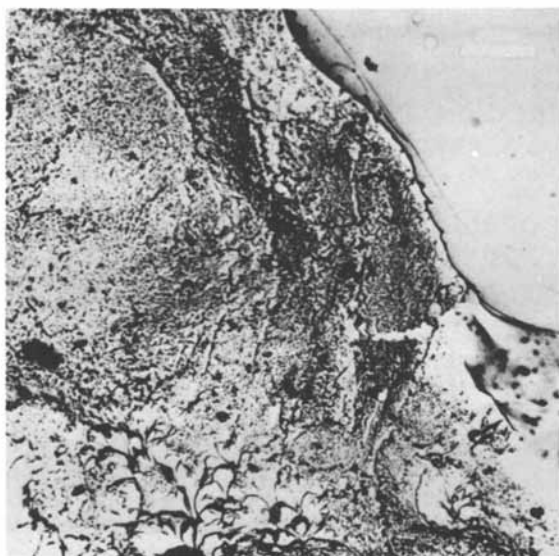
Figure 2.   (3800×)

etched in much the same manner as its exterior surface,
the potential for development of useful pore surface
area is apparent.

It is also noteworthy that a by-product of this
method showed promise as an active carbon in powder
form: Following desulfurization, the alkalized, steam
treated coke was leached with water to remove alkali-
metal compounds. When the (dark green alkali-metal-
organic) washings were evaporated to dryness and the
solid reidue was pyrolized to around 1600°F (871°C),
it could be cooled and washed to yield a remarkably
active carbon powder. Indeed it was found that simple
leaching of raw fluid coke with hot caustic soda (or
potash) resulted in greater yield of a similar residue.

As an example of current commercial production
based on petroleum, one U.S. manufacturer (7) makes
about 5,000,000 annual pounds (8) of durable, regener-
able, spheroidal active carbon out of (sulfuric) acid
sludge resulting from the refining of white mineral
oil. While its process is proprietary, we may specu-
late that it is something about as follows:

Acid sludge preheated to around 500°F (260°C) is
continuously mixed with hot, previously coked parti-
cles. The hot coke particles become coated with
sludge, which is simultaneously desulfurized. The
coated particles recycle to a coking zone operating at
some 1000°F(538°C), from whence the make is continu-
ously elutriated to subsequent conventional gas activ-
ation, which likely employs more or less steam at a
temperature on the order of 1500°F(816°C), depending
on the type of carbon being produced.

Another U.S. manufacturer (9) is known to have
employed acid sludge as one of its raw materials and
probably makes a substantial portion of its gas phase,
granular carbon in a somewhat similar manner. There-
fore, in this country we presently have commercial
production of at least one, and probably of two, active
carbons derived from petroleum. Perhaps it is signif-
icant that both are granular.

As a rule, active carbon powder is easier to make
than granular form. Accordingly, granular material
typically commands two or three times the unit-weight
price of corresponding material in powder form. The
corollary question is, why not mix powder with a car-
bonizable binder, compact the mix and pyrolize the
compacts to make granular active carbon? Hundreds of
attempts to implement this logical approach have been
unsuccessful. The problem appears to be twofold:
Binders tend to block the pores of filler carbons. And
cokes resulting from pyrolysis of binders are usually

less reactive than filler carbons; so that subsequent
activation (selective oxidation) of product granules
tends to burn the filler carbon preferentially. At
least one European manufacturer (10) has an exception
(11). It has developed a process that employs hard-
wood tar for binding particulate hardwood or charcoal
powder to make granular active carbon.

Some of your colleagues in the petroleum industry
appear to have made an important contribution by em-
ploying acid sludge as a binder. In their case, the
sludge is not a by-product. Rather, it is tailored to
its purpose by acid treatment of a selected refinery
stream. Coal char, wood charcoal, acid sludge coke or
some similar material, preferably sized to pass
through 100 mesh or finer, is mixed with the sludge.
Even powdered active carbon may be the filler carbon.
Some uncarbonized bituminous coals are also suitable.
Proper formulation and mixing uniquely permit forma-
tion of rounded granules in the mixer. The resulting
grains are strong enough to withstand screening, hand-
ling and pyrolysis. Bonding of the sludge to the
filler material survives carbonization, which converts
the sludge to a hard, strong, porous carbon matrix
that does not blind pores of the filler carbon to any
serious extent. Finally, the product is gas-activated
by conventional means to develop pore size distribu-
tions suitable for gas phase or for liquid phase
applications, as desired. This process has been
patented, piloted and made available for license (12)
by a leading U.S. oil company (13).

A Japanese process that has been under develop-
ment for several years, is currently emerging (14).
It is reported to make high quality, active, petroleum
pitch carbon in spherical grain form and may be brief-
ly described about as follows:
1. Pitch is melted and mixed with a 'modifier' in a
   heated mixer.
2. The molten mixture is dispersed in hot water, where
   it forms into discrete spherical grains under con-
   trolled temperature and pressure (probably with
   some sort of mechanical agitation).
3. Water is drained off and the grains are dried.
4. The thermoplastic grains are thermoset by oxidative
   heat treatment.
5. The thermoset grains are then carbonized, probably
   to about 900° C.
6. Finally, the carbonized grains are more or less
   conventionally gas-activated to develop required
   pore size distribution. (Steps 5, and 6, probably
   can be combined in one unit, perhaps a multiple

hearth furnace.)

We may speculate that the 'modifier' is a filler, possibly -100 mesh low-rank coal char or wood charcoal in a weight proportion at least equal to the pitch. Or it could be a cheap carbonizable material such as fine sawdust or pulverized coal that co-carbonizes with the pitch. And it is likely that high-sulfur pitch, not suitable for binder pitch or for electrode quality coke production, may be employed because considerable desulfurization doubtless occurs during activation with steam; so that residual sulfur in the active carbon product is tightly bound and tolerable.

Each of the many activated carbons on the market, has properties distinguishing it from others that are made from different raw materials and/or by different process patterns. Most such carbons readily oxidize at moderately elevated temperature, especially in the presence of incidental catalysts, lead compounds for example. One distinguishing feature of active carbons derived from petroleum, is that they generally tend to be somewhat more temperature resistant with respect to oxidation, than corresponding carbons based on other raw materials. This can be an important advantage in some applications.

If active carbon technology is a bit confusing, researching its market is scarcely less so. A horrible example appeared nearly three years ago, when a feature article in a reputable publication (15) quoted a presumably competent authority as stating: "Present consumption for activated carbon made from petroleum coke is approximately 250 tons/day. But there is a great potential for increase in this market by 1975,-----." Considering volatile loss and burn-off, this implied a new and growing market for some 500 tons green coke per day. Worse still, some readers jumped to the conclusion that substantially all of the active carbon produced in the U.S. during 1971, must have been made out of petroleum coke, because 250 tons/day is equivalent to about 180 million lbs./yr. If one assumes the common commercial definition of petroleum coke, which refers only to delayed coker and fluid coker coke, the quoted statement was completely false. More charitably, its estimate was only some 900% high, if acid sludge coke is included.

While not conducive to errors of such magnitude, there is another potential pitfall for those who would estimate actual production from nominal plant capacity. Particularily in the case of manufacturers that have only one production line, there is a relatively wide discrepancy between nameplate capacity and actual pro-

duction, even when business is good. For example, a
fairly recent publication (8) listed one producer's
capacity as 250% of its actual 1974 production and
commented that it was enjoying a good year.

In conclusion, perhaps some (hopefully better)
estimates are in order: Discounting the possibility of
a long business recession, my carbon-filled crystal
ball projects an average annual growth rate of about
11% for all active carbon production in the U.S. over
the coming ten years. This includes a growing propor-
tion of cheap, recycleable, active carbon powder to be
made from waste for waste-water treatment (16).

The same crystal ball shows a figure of 110,000
tons of actual 1974 U.S. production, including powder,
grain and bone char. During 1985, therefore, the
United States may use over a half billion pounds of the
black magic that has enjoyed your kind attention today.

Literature Cited

1) Hassler, John W. "ACTIVE CARBON" 12 Chemical
   Publishing Co., N.Y. 1951
2) Brunauer, Emmett & Teller, J.ACS (1938) 60 309
3) Green, Hardy, Berl & Vickburg "Hydrocarbon
   Processing" (1971) 50 (1) 105-108
4) Pittsburgh Activated Carbon Co., "Basic Concepts
   of Adsorption on Activated Carbon" 3
5) Dubinin, M.M. "Uspekhi Khim" (1955) 24 3
6) Murphy, R.M. et al "Process for Desulfurizing Car-
   bonaceous Materials" U.S.Pat.3,387,941 (6-11-68)
7) Witco Chemical Co.,Inc., N.Y. 10017
8) "Activated Carbon Heads for Sell-Out Year"
   C&EN (1974) 52 (29) 7&8
9) Carbon Prod. Div., Union Carbide Corp., Chicago
10) Degussa, Frankfurt (Main), West Germany
11) Smisek & Cerny "ACTIVE CARBON" Chap.2 American
    Elsevier Publishing Co.,Inc. (1970)
12) Kiikka, Oliver A. "Acid Sludge as Binder for the
    Production of Shaped Carbonaceous Articles and
    Activation Thereof" U.S.Pat.3,592,779 (7-13-71)
13) The Standard Oil Company(Ohio), Cleveland 44115
14) "New Process Uses Thermal Cracking of Residual
    Oils" Oil & Gas Jour. (1975) 73 (21) 96-103
15) "Juggling Crude-Oil Bottoms" Chemical Engineering
    (1972) 79 (9) 29
16) Nickerson, R.D. et al "Making Active Carbon from
    Sewage Sludge" U.S.Pat.3,887,461 (6-3-75)

Analysis of Accelerated and Natural Aging of Impregnated Charcoals

WILLIAM S. MAGEE, JR.

Development and Engineering Directorate, Edgewood Arsenal,
Aberdeen Proving Ground, Md. 21010

Abstract
     This paper presents an analysis of kinetic data for degrada-
tion during accelerated and natural aging of activated charcoals
impregnated with salts of copper, silver and chromium. The
degradation, as measured by decreased ability to remove cyanogen
chloride from humidified air streams, appears to consist of two
simultaneous processes. Although the rate constants for these
processes differ by an order of magnitude, they each have a
second order dependence upon the initial moisture content of the
charcoals and virtually identical simple Arrhenius activation
energies. The analysis suggests an aging mechanism based upon
non-degrading physi-sorptive sites and fast and slow degrading
chemi-sorptive sites. A mathematical model for the mechanism
well approximates both accelerated and natural aging data within
the appropriate temperature and humidity ranges. An extension
to the model for seasonably variable temperatures gives rise to
integrals which can be evaluated only by numerical techniques.

Introduction
     The general adsorbent used in respiratory protective systems
is activated charcoal. For removal of toxic <u>vapors</u> from air,
such systems prove more than adequate as measured by service
times. However, for removal of toxic <u>gases,</u> such systems do not
match the performance with vapors.
     Fortunately, impregnation of activated charcoal with various
substances markedly improves performance with respect to gases.
A typical case, studied[1]extensively during World War II, is the
enhancement of service lives for removal of hydrogen cyanide,
arsine and cyanogen chloride by the impregnation of charcoal with
an ammoniacal solution containing compounds of copper, silver and

chromium. Interest in these materials has again arisen in connec-
tion with several aspects of environmental protection.

Although freshly impregnated charcoal and that from dry
storage exhibit the improved service lives, impregnated sorbent
which contains moisture deteriorates during sealed storage
eventually down to the level of unimpregnated material. The
deterioration is virtually irreversible, only a fraction of the
lost service capability being recoverable.

As a basis for an attempted elimination (or at least allevia-
tion) of the deterioration during storage, this paper presents an
analysis of sealed aging data for both natural storage and
accelerated aging of experimental charcoals. The analysis
suggests a mechanism for deterioration which is used to formulate
a mathematical model. The model yields results which compare
favorably with data within the appropriate ranges of temperature
and virtually all physically realizable moisture contents. An
extension of the model for seasonably variable storage tempera-
tures leads to integrals which can be evaluated only by numerical
techniques. The use of the extension is briefly discussed in
terms of realistic long term storage.

Development of the Model

Jonas and coworkers[2,3,4] modified an equation developed by
Wheeler and Robell[5] and applied the result to studies of service
lives of fixed beds of sorbents exposed to a variety of gases and
vapors. The modified equation based on simple mass balance has
the form

$$t_b = D[(W/C_o Q) - (d/C_o K)\ln(C_o/C)] \tag{1}$$

where t_b is the service life (or breakthrough time) as determined
by a concentration C of the toxic material appearing in the
effluent air stream, C_o is the influent concentration of the toxic,
D is the dynamic saturation capacity of the bed (weight of toxic
picked up per unit weight of charcoal in the bed), Q is the volu-
metric flow rate, d is the bulk density of charcoal as packed in
the bed of weight W and K is a mass transfer coefficient for the
rate of removal of the toxic by the charcoal. Similar
equations[6,7] have appeared in the literature, each being a limit-
ing simplification of more elaborate results[8,9] obtained from
continuity and/or conservation considerations. These equations
differ in their parametric dependencies according to which
elementary process or combination of processes is rate control-
ling. Relations in the form of equation (1) arise for a number
of different rate controlling situations and, therefore, do not
provide unequivocal means for determination of the rate control-
ling processes. In any case, equation (1) does describe the
behavior of the charcoals in the present study.

However, equation (1) is only applicable to systems in which
the instantaneous effluent concentration C can be determined.

Experimentally in our laboratory, cyanogen chloride service lives
are determined by the collection of a specified cumulative amount
passing through the bed into a bubbler. Calling this amount m,
I can write the relation

$$m = \int_o^t CQdt'$$

(2)

where t is the service life defined by the cumulative amount m of
cyanogen chloride passed through the bed and C is the instant-
aneous effluent concentration given by rearranging equation (1).
Performing the integration at constant Q and collecting terms, I
have the relation

$$t = (Dd/C_oK)\ell n[1 + (mK/QDd)\exp(WK/Qd)] \cdot$$

(3)

From the experimental data on both aged and unaged samples, the
various quantities in equation (3) permit the excellent approxi-
mate form

$$t \cong D[(d/C_oK)\ell n(mK/DdQ) + (W/C_oQ)] \cdot$$

(4)

(Details on a derivation of equation (4) from (3) are given in
the Appendix.)
     The quantity D is assumed to be a direct measure of the
number of active sites for removal of cyanogen chloride per unit
weight of charcoal. Unequivocal experimental evidence as to the
precise chemical nature of these sites is difficult to obtain,
so no clear-cut mechanism for their disappearance is available.
Aging data indicate a number of different types of sites. There
are physi-sorptive sites which do not deteriorate with aging
(these are the only sites on unimpregnated charcoal) and a
number of types of chemi-sorptive sites, each type deteriorating
with its own characteristic pseudo-first order rate constant.
Therefore, D can be written in the form

$$D = D_p^o + \sum_{j=1}^N D_j^o \exp(-k_j t_a)$$

(5)

where D_p^o is a measure of the non-deteriorating physi-sorptive
sites, D_j^o is a measure of the $j\underline{th}$ type of chemi-sorptive site
at zero aging time, k_j is the pseudo-first order rate constant
for deterioration, t_a is the time of aging and N is the total
number of types of chemi-sorptive sites.
     Again because of the numerical values of the various quanti-
ties in equation (4) and the fact that the mild logarithmic
functionality of t on D is negligible compared to the strong
linear dependence, I can write equation (4) after insertion of
(5) in the form

$$t = MD_p^o + \sum_{j=1}^N MD_j^o \exp[-k_j t_a]$$

(6)

where $\underline{M}$ is by definition

$$M \equiv (d/C_oK)\ell n(mK/D\rho Q) + (W/C_oQ) \neq f(t_a) \cdot \qquad (7)$$

As mentioned, for all practical purposes $\underline{M}$ is virtually independent of aging time and is treated as a constant of the system in the remainder of this paper.

Analysis of aging data[10] with equation (6) under several conditions of moisture loadings and temperatures yields the following relation for $\underline{k_j}$:

$$k_j = (A/10^{j-1})(H_2O\%)^2 \exp(-E/RT) \qquad (8)$$

where $\underline{A}$ is an apparent Arrhenius pre-exponential factor, $(H_2O\%)$ is the weight percentage of water on the charcoal, $\underline{E}$ is an apparent Arrhenius activation energy for the degradation processes, $\underline{R}$ is the gas constant and $\underline{T}$ is the absolute temperature of storage. The epithet "apparent" is used because $\underline{k_j}$ is most likely the product of an equilibrium and a rate constant.

Combining equations (5), (6) and (8) and rearranging I have the relation

$$r = r_o + \sum_{j=1}^{N} r_j \exp[-(t_aA(H_2O\%)^2/10^{j-1})\exp(-E/RT)] \qquad (9)$$

where $\underline{r}$ is the ratio $\underline{t}$ (at t_a)/t(at t_a = 0), $\underline{r_o}$ is the ratio MD_p^o/t(at t_a=0), and each $\underline{r_j}$ is the ratio MD_j^o/t(at t_a=0).

Discussion

Analysis of natural and accelerated aging data with equation (9) yields the following values for a "best fit":

$$N = 2 \quad r_o = 0.185 \quad r_1 = 0.300 \quad r_2 = 0.515$$
$$A = 2.9 \times 10^8 \text{Weeks}^{-1} \quad E = 16,160 \text{ cal mole}^{-1}\text{deg}^{-1}$$

It is remarkable that the pseudo-first order rate constants for both the fast and the slow processes have virtually identical second order dependencies on the water content and activation energies. Evidently an equilibrium is established between two moles of water and the chemi-sorptive sites prior to the deterioration of the sites. However, until the nature of the sites is well established, this remains speculation.

Use of equation (9) and the values above have provided[10] fairly good prediction of actual deterioration during prolonged storage under constant temperature conditions for experimental charcoals. For the more reasonable storage condition of a seasonably variable temperature the following must be considered. I assume a mechanism of the type

$$\text{Site} + 2H_2O \xrightarrow{k(t_a)} \text{Products}$$
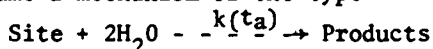
where $k(t_a)$ is a function of the aging time by virtue of $T=T(t_a)$. This mechanism gives for the ratio of sites remaining at time t_a to sites initially present the expression

$$\exp(-(H_2O\%)^2 \int_0^{t_a} k''(t)dt)$$

where $k''(t)$ is given by

$$k''(t) = A\exp(-E/RT''(t))$$

using these observations and an experimentally justifiable sinusoidal temperature-time relation, I have as an extension to equation (9) the relation

$$r = r_0 + r_1 \exp[-(H_2O\%)^2 A \int_0^{t_a} \exp[-E/R(T_m+T_c \sin(wt+\phi))]dt\}$$
$$+ r_2 \exp\{-(H_2O\%)^2 \frac{A}{10} \int_0^{t_a} \exp[-E/R(T_m+T_c \sin(wt+\phi))]dt\}. \quad (10)$$

Unfortunately the integrals can only be evaluated numerically, but this is no real obstacle with access to even a small desk-top programmable calculator. In equation (10) T_m is the median temperature of the cycle and T_c is the amplitude. The variables w and ϕ are the circular frequency and phase respectively. Further extensions to include smaller cycles on top of principal cycles (e.g. daily on top of yearly) seem unwarranted at least for my applications.

Appendix
    Equation (3) has the form

$$t = X\ell n(1+Y\exp(ZW)). \quad (A1)$$

For large $\underline{W}$ (large beds) $\underline{t}$ is found to be linear in $\underline{W}$. The slope of the life-weight curve $(\underline{t}$ vs $\underline{W})$ is given from (A1) as

$$\frac{dt}{dW} = \frac{XZY\exp(ZW)}{1+Y\exp(ZW)}. \quad (A2)$$

Empirically $Y\exp(ZW)$ is much larger than unity for large $\underline{W}$ so that equation (A2) becomes

$$\frac{dt}{dW} \cong XZ .$$

Therefore, from equations (A1) and (A3) and using $1+Y\exp(ZW)$ I have that

$$t \cong X\ell nY + ZW$$

which is a rearranged form of equation (4).

References
1. Summary Technical Report of Division 10, National Defense
    Research Committee, Vol 1, (1946) PB158505. Available from
    Clearing house for Federal Scientific and Technical Informa-
    tion, U.S. Department of Commerce, Springfield, VA 22151,
    Price: $31.00
2. Jonas, L. A. and Rehrmann, J., Carbon 10, 657 (1972).
3. Jonas, L. A. and Rehrmann, J., Carbon 12, 35 (1974).
4. Jonas, L. A., Boardway, J.C. and Meseke, E. L., J. Colloid
    & Interface Sci. 50, 538 (1975).
5. Wheeler, A. and Robell, A., J. Catal. 13, 299 (1969).
6. Dole, M. and Klotz, I., Ind. & Eng . Chem. 38, 1289 (1946).
7. Hutchins, R., Chem. Eng., p. 133, Aug 20, 1973.
8. Heister, N. K. and Vermaulen, T., Chem. Eng. Prog. 48, 506
    (1952).
9. Masamune, S. and Smith, J. M., A. I. Ch. E. J. 10, 246 (1964).
10. Magee, W. S., Baker, J. A., Poziomek, E. J., Boardway, J.C.
    and Ball, H., AROR 74-1, 419 (1974), Proceedings of the
    Nineteenth Conference on the Design of Experiments in Army
    Research, Development and Testing.

Carbon Materials in Large Volume Applications

ERLE I. SHOBERT, II

Stackpole Carbon Co., St. Marys, Pa. 15857

I. Introduction

A. **Economics**. The size and relative distribution of the business in the carbon field is shown in Table 1. These numbers include all but the carbon used in the manufacture of aluminum and magnesium in which Soderberg electrodes are used.

Carbon and Graphite Market
1974 - $400,000,000 Annually

Product	Percent
Brushes	14
Electrodes (Furnace)	45
Anodes (Chlorine)	5
Electrical Uses (Welding, Power Tubes, Illuminating)	8
Mechanical Uses (Seals, Discs, Vanes, Nozzles, etc.)	8
Nuclear (Piles and Moderators) and Aerospace	8
Chemical, Metallurgical Refractories, etc.	12

13,000 people; 2,000 technical

Table I

The percentages are based on industrial and government statistics. The number of people involved in the industry is an estimate as is the number of technical people which includes technical people in production and sales as well as those in research and engineering activities.

B. **Raw Materials**. Practically all of the raw materials used in the production of carbon and graphite are byproducts of

91

some other industry, Petroleum coke is the material left at the
end of the refining process of oil. Coal tar pitch comes from
the production of coke for the steel industry. The carbon black
and lampblack used in the carbon industry are but small percent-
ages of these materials which are produced primarily for the
rubber and printing industries. Natural graphite and various
resins and plastics are representative of the few materials used
by the carbon industry which are not just byproducts.
     This puts a definite constraint on the carbon industry in
that some changes which can take place in product quality are
not under the strict control of the people making carbon and
graphite. For example, the properties of hard pitch change with
the rate of production in the steel industry since this deter-
mines the manner in which the coke ovens are operated. The
quality of petroleum coke varies from oil field to oil field and
from refinery to refinery. It is also somewhat different de-
pending upon the mix of products from the refinery. A major part
of the art as well as the science of the carbon industry is in-
volved in producing uniform products from the variable raw ma-
terials which are available. These raw materials include:

Fillers	Binders
Petroleum Coke of Various Kinds	Hard Pitch
Carbon Black	Petroleum Pitch
Lampblack	Resins
Natural Graphite	Plastics
Artificial Graphite	
Charcoal	
Metallurgical Coke	

Impregnations	Other Additives
Metals: Cu, Ag, Sn, Babbit, Lead	Solid Lubricants: MoS_2, etc.
Lubricants	Abrasives
Resins and Plastics	Metal Powders for Sintered Ma-
Linseed Oil	terials: Cu, Ag

     C. Processes. The processes involved in the production of
tonnage amounts of carbon and graphite are those involved, in
general, in dealing with fillers and binders. The basic pro-
cesses are as follows:
     1. Raw Material Control and Test
     2. Raw Material Preparation: (a) Calcining; (b) Grinding
     3. Mixing: Hot and Cold
     4. Molding: Hot and Cold
     5. Extrusion
     6. Baking
     7. Graphitizing: Continuous and Batch
     8. Impregnating
     9. Finishing, Shapes and Hardware
Each of the variables must be under control to provide materials

which are uniform within themselves as well as from lot-to-lot
in a short time scale and from lot-to-lot over a long time scale.
The carbon industry must be able to produce carbon brush mater-
ials, for example, which are the same now as they were when they
were produced forty years ago since they must operate on the
same machines. Process flow charts for extruded and molded ma-
terials are shown in Figures 1 and 2.
     D. Operating Methods. The development and manufacture of
materials for commercial applications requires a great deal of
coordination within the various operating areas of the manufac-
turing organization. In general, these operating methods are as
follows:
     1. Determine requirements of the application;
     2. Choose the raw materials which best will provide these
         properties within cost limitations;
     3. Test full scale shapes and sizes;
     4. Change raw materials or modify processes to get the
         best results;
     5. Determine measurable properties of best material;
     6. Set up Q.C. to insure same raw materials, processing
         procedures, and final properties.
     Final properties alone will not determine in most applica-
tions whether a material is suitable. The same set of physical
properties--strength, hardness, density, porosity, conductivity,
etc.--can be achieved in many different ways, considering the
available materials and process variations, but the results on
a given application will not be the same; in fact, they could be
disastrous.
     The philosophy of carbon and graphite application takes into
account the fact that each of the various raw materials reacts
differently to the processes and each has its own characteristic
properties. This experience with all of these materials tells
the developer what to try first and then which direction to take
when improvement is required.
     These methods have resulted in low resistivity and high re-
sistivity; low thermal conductivity and high thermal conductivity;
low friction and high friction; high thermal shock resistance;
good resistance to oxidation; high contact voltage drop and low
contact voltage drop; and many more property ranges.
     In the short time available, we will touch on some of the
key technical aspects of each application, pointing out the
properties required as well as the problem involved.

II. Applications

     A. Electrodes. 1. Steel Arc Furnaces. The electric arc
steel furnace, Figure 3, is a dramatic use of graphite. Three
large electrodes enter the top of a pot and generate the three-
phase arc with the charge. The furnaces are charged hot or cold,
depending upon the application, and the cycle of operating
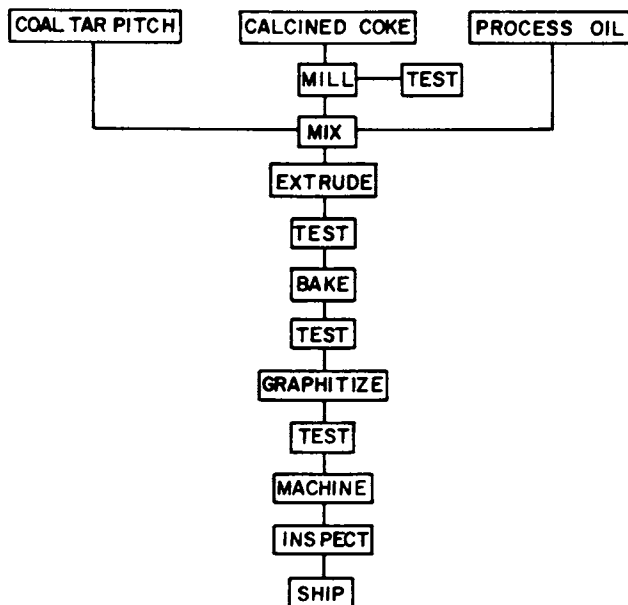
Figure 1. *Typical process for the manufacture of extruded graphite materials*
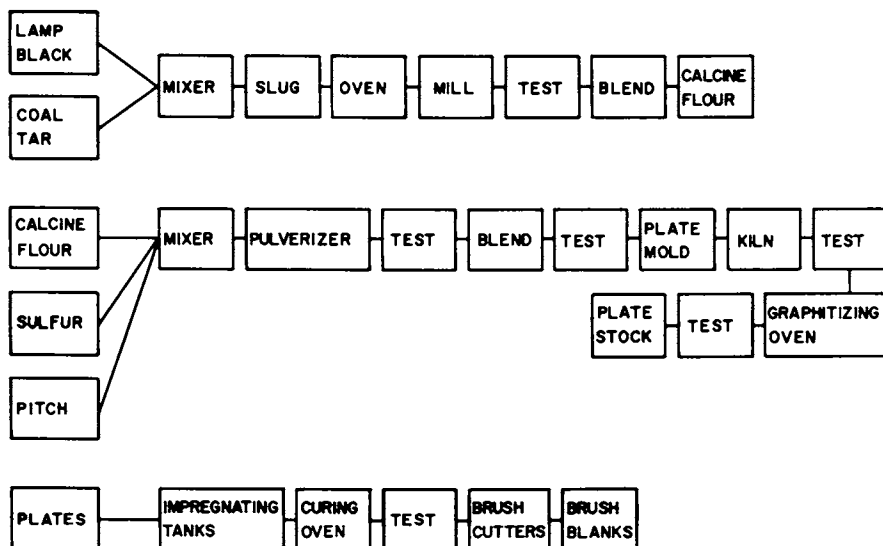
Figure 2. *Typical process for the manufacture of electrographitic brushes*

includes meltdown in which the arc is heating the metal to the
melting point. During this part of the cycle, it is possible
for large chunks of metal to fall onto the electrodes, causing
breakage.

When the charge is completely melted, there is a refining
period where the temperature is held and during which the metal
composition is adjusted. Adjustment to pouring temperature may
then be made, after which the electrodes are raised and the melt
is poured.

The diagram, Figure 4, shows the essential elements of the
electrode system with water cooled electrical connections to the
electrodes. The electrode sections are joined by means of graph-
ite nipples which must also be good thermal, electrical, and
mechanical connections. Because of the high currents, there are
thermal gradients, both radially and longitudinally in the elec-
trode which set up thermal stresses. Mechanical stress comes
from the charge.

The diagram shows the electrode tapered; this is because of
the oxidation on the sides of the electrode. The area at the
tip is of the order of one-half the area of the new electrode,
which means that about one-half of the material is lost by oxi-
dation from the sides. Arc spot temperatures of about 4000°C
cause erosion of the tip where the arc takes place. Current
densities in the arc cathode and anode spots are estimated be-
tween 10,000 and 50,000 apsi.

Suitable materials are those which have low electrical re-
sistance, high thermal shock resistance, and good oxidation re-
sistance. Thermal shock resistance includes the factors of
thermal conductivity and thermal expansion as well as heat capac-
ity.

These materials are produced by the extrusion of large
sections, baking, graphitizing, and subsequent machining.

2. Aluminum Refining. The diagram of an aluminum pot is
shown in Figure 5. In this case, the anode is the Soderberg
electrode. The steel case is made in sections and the carbon
mix is tamped in at the top. As the material wears away at the
face, steel and the anode material are dropped down and the dif-
ferent electrical connections are made.

The cathode is usually made from a petroleum coke pitch mix
which is tamped into the furnace shell against the insulation.
Steel rods are used for connections. In some cases, graphite
rods and plates are used to improve the conductivity of the cath-
ode.

As the anode material moves toward the hot part of the pot,
the pitch is carbonized, conductivity increases, and the carbon
material is available for conduction to the electrolyte. The
material in the cathode is cured in a similar manner by opera-
tion. The use of carbon and graphite in the aluminum industry is
important since it takes just somewhat less than one pound of
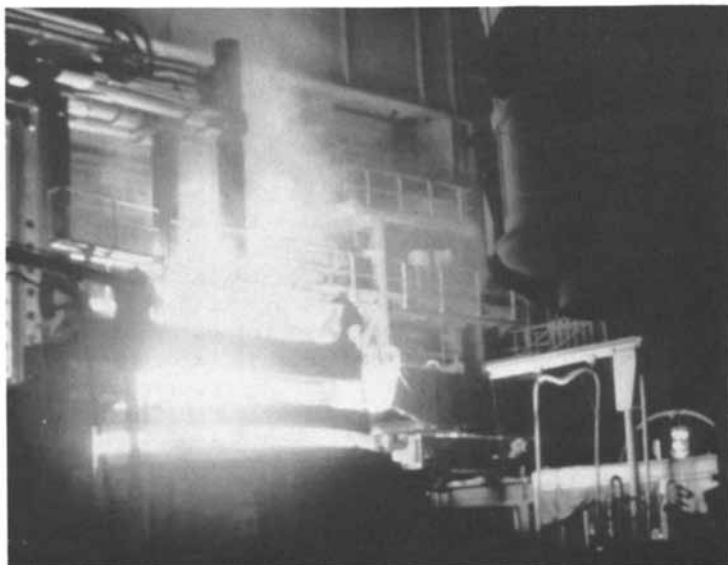
Figure 3.   Electric arc steel furnace in operation
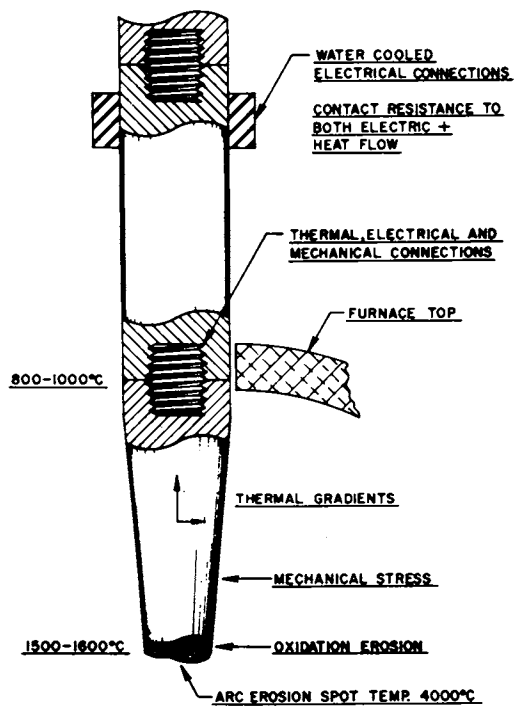
Figure 4.   Diagram of electric arc steel furnace electrodes

carbon to produce a pound of aluminum.

The production of the mix for the Soderberg cells involves control over the raw materials, mixing, and on the tamping operation into the steel shells.

B. Anodes. Until recently, the primary use of graphite in anodes was for the manufacture of chlorine. While there are still some cells in operation using graphite, there has been a major change in the case of mercury cells from the use of graphite to the use of a titanium metal screen holding precious metal oxides. While the initial cost of these so-called dimensionally stable anodes is high, depending upon the maintenance and power costs, there are installations where this is economical.

There are still some installations, however, where graphite is used in the conventional cells. In the mercury cell, chlorine is formed at the anode; and sodium, which dissolves in the mercury, is formed at the cathode. The mercury is circulated through a so-called denuder in which the sodium is reacted with water to form hydrogen and sodium hydroxide. The mercury is then returned to the cell.

In the mercury cell, Figure 6 , the anodes must be very low in vanadium content since this builds up in the system to the extent that the electrochemical relations at the cathode are changed and some hydrogen is formed which can react with the chlorine to cause an explosion. Graphite materials from these cells as well as for the diaphragm cells are produced by extrusion, baking, graphitizing, and machining.

A diaphragm cell is shown in Figure 7 in which the graphite anodes are cast in a lead base, standing vertically in the cell. The cathode is an iron screen covered with an asbestos diaphragm which separates the two halves of the cell. The chlorine is collected over the graphite and the hydrogen over the cathode.

C. Brushes. Brush materials are made by conventional carbon and graphite processes, using either extrusion or molding as the forming process. Metal graphite brushes are made by molding metal powders with graphite additions or by impregnating porous carbon and graphite materials with molten metal. A conventional process specification for brush materials is shown in Figure 2. There are several key points involved in the application of brushes which we may refer to the basic theory of contacts.

In the first place, a brush sliding on a metal surface produces a film which is partly oxide, partly graphite, partly lubricant (such as water), and which contains metallic conducting regions as shown in Figure 8. Current densities in the metallic conducting areas are of the order of 200,000 amp/cm^2. The resistance of these brushes, based on contact theory, depends upon the contact area as determined by the film, the specific resistance, and the effect of the hardness of the material as shown in Figure 9.
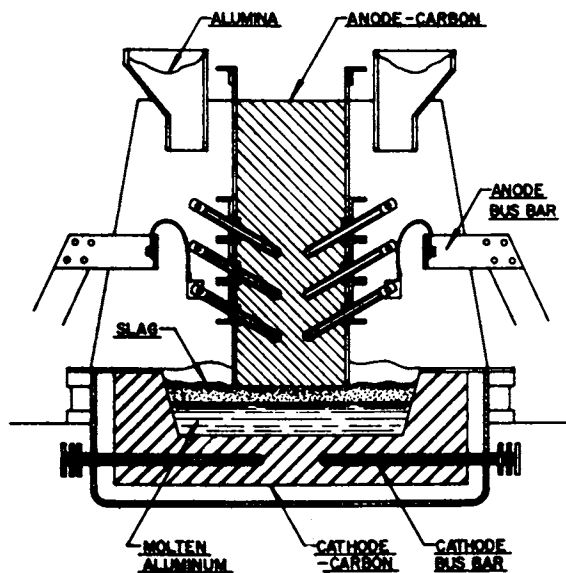
Figure 5.   Aluminum reduction pot
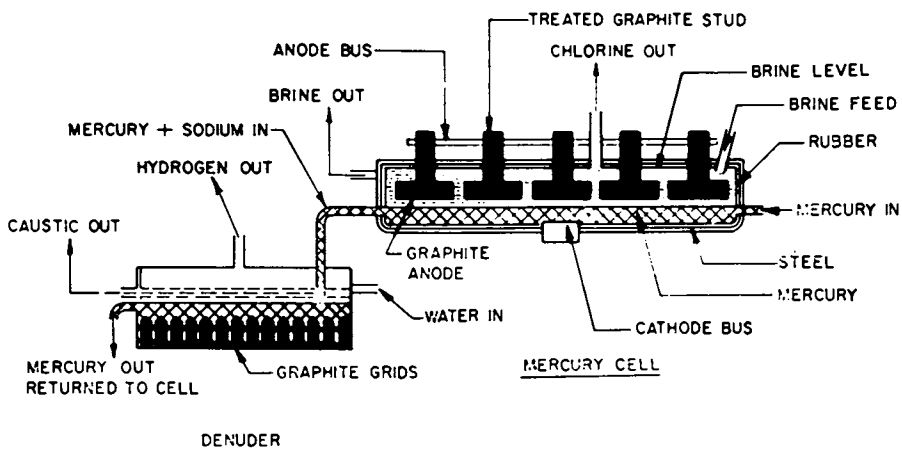
Figure 6.   Mercury cell for manufacture of chlorine from salt
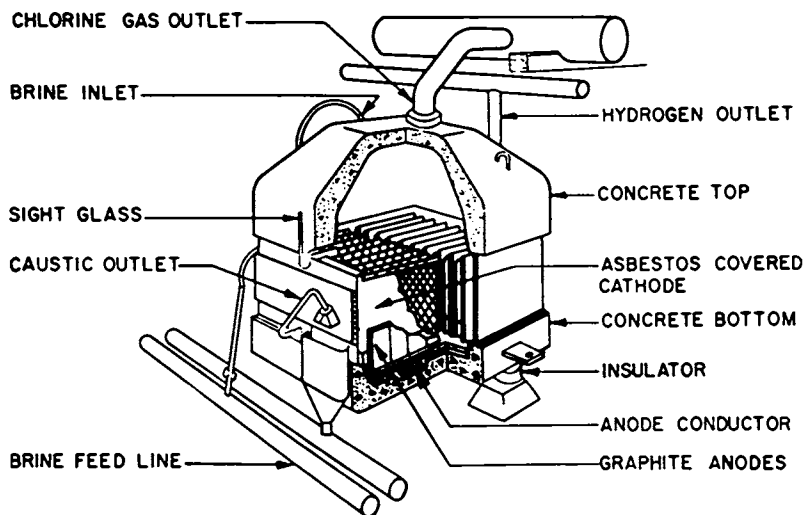
Figure 7.   *Diaphragm cell for the manufacture of chlorine from salt*
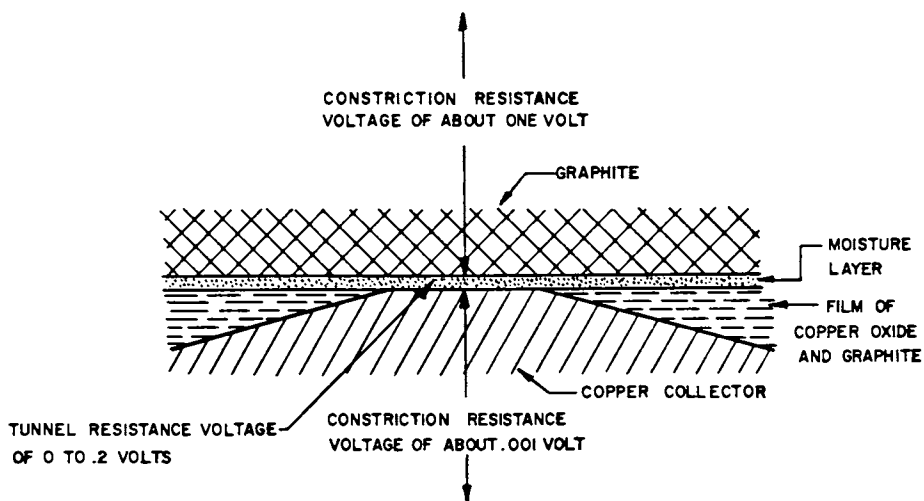
Figure 8.   *Schematic sliding contact surface*

The mechanical contact area under a brush is determined by the yield point and contact hardness. The electrical conducting regions are small parts of this mechanical surface. The final contact resistance is the result of an equilibrium between the tendency of the metal to oxidize and decrease these contact areas and the effect of the breakdown or fritting of the film which tends to increase these areas when the voltage at the immediate contacts reaches voltages of the order of .2 of a volt. The position of this equilibrium is further influenced by the abrasive nature of the brush and its materials which tend to increase the conducting areas and the presence of other lubricants which tend to decrease these areas. This equilibrium makes it appear that the brush might be acting as a semiconductor if tests are run for relatively long periods at each current. However, instantaneous changes in current indicate that the conduction is metallic as shown by the straight lines A and B in Figure 10, which are taken very quickly.

The necessity for lubrication is shown in Figure 11 in which brushes are run on a ring and the air is being dried. At a certain dryness, the wear increases drastically as the brushes essentially disappear in a cloud of dust, friction increases, and the contact resistance decreases. For high altitude and space applications, it is necessary to provide lubrication in another manner.

The conduction mechanism is purely metallic within the collector and the brush, that is, by means of the normal conduction electrons. The transfer takes place across the water or other lubricating film by means of the tunnel effect. The lubricating film separates the two material, carbon and metal, enough to prevent the mingling of their electron clouds which would result in welding or seizure, but it introduces a voltage drop only of the order of 0.1 volt from the electrical point of view.

Brush wear is shown in the general context of wear in Figure 12 which shows wear rates all the way from hydrodynamically lubricated bearings to chalk on the blackboard.

Commutation is an important aspect of brush operation, and the details of the electrical nature of commutation are shown in Figure 13.

One of the most important aspects of brushes has to do with mechanics. Various brush holder designs, shown in Figure 14, provide suitable means of holding brushes on the commutator, but the surface of the brush must adapt to the minute irregularities to provide this contact, as shown in Figure 15.

D. Seals, Bearings, and Brakes. Friction was not mentioned under brushes although this is an important part of successful brush operation. It is also important in seals and bearings that the friction be low, and that in the case of brakes, the friction be high. Figure 16 shows various seal

$$R = \frac{\rho}{2a} \qquad R = \frac{\rho}{2}\sqrt{\frac{\pi H}{P}}$$

$$\pi a^2 \cdot S = \frac{P}{H}$$

$$a = \sqrt{\frac{P}{\pi H}}$$

HARDNESS

COMPRESSIVE STRENGTH
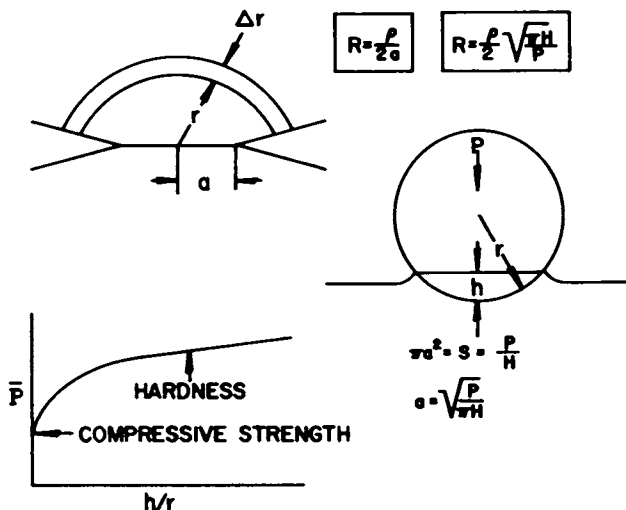
Figure 9. Contact resistance and hardness
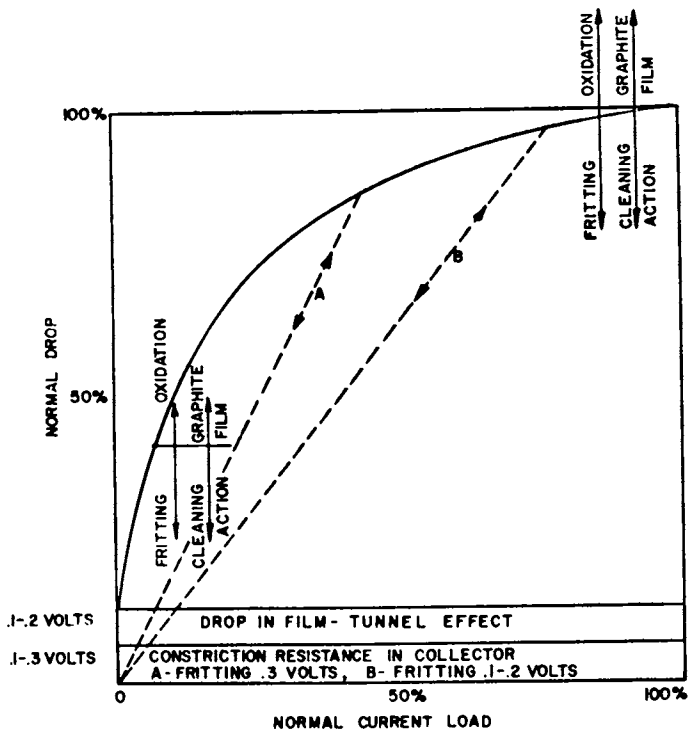
Figure 10. Schematic of contact resistance
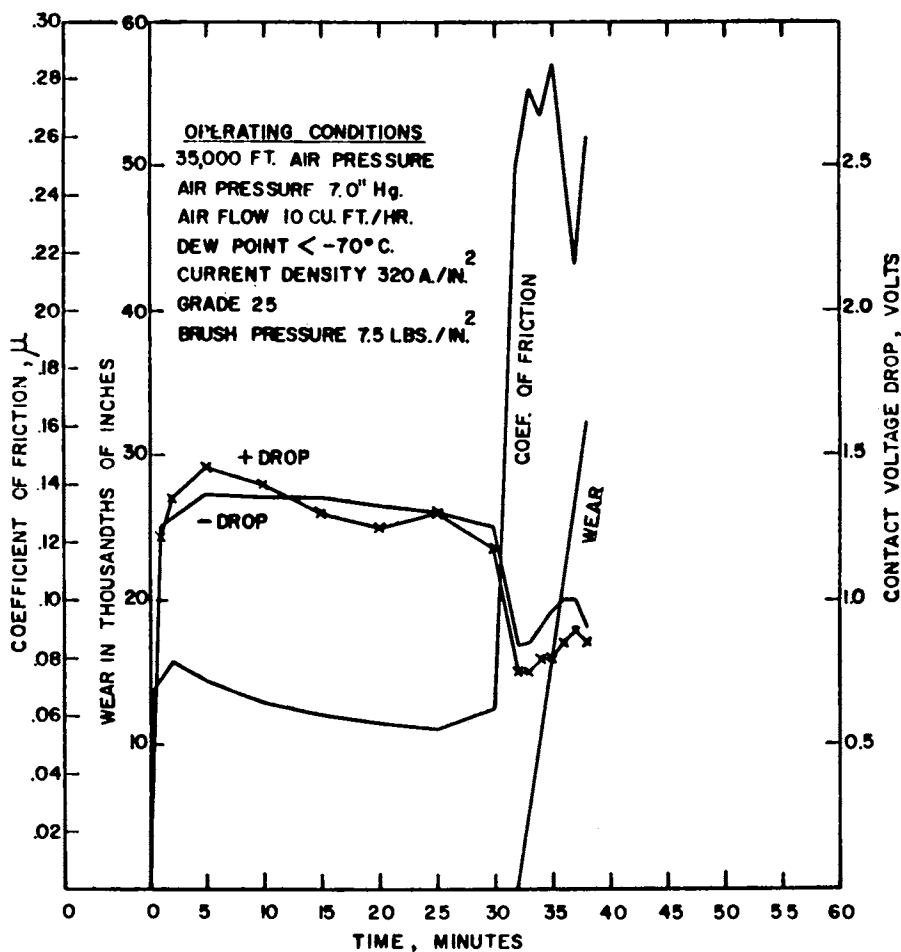
Figure 11.   *Effect of eliminating water vapor on sliding contacts*
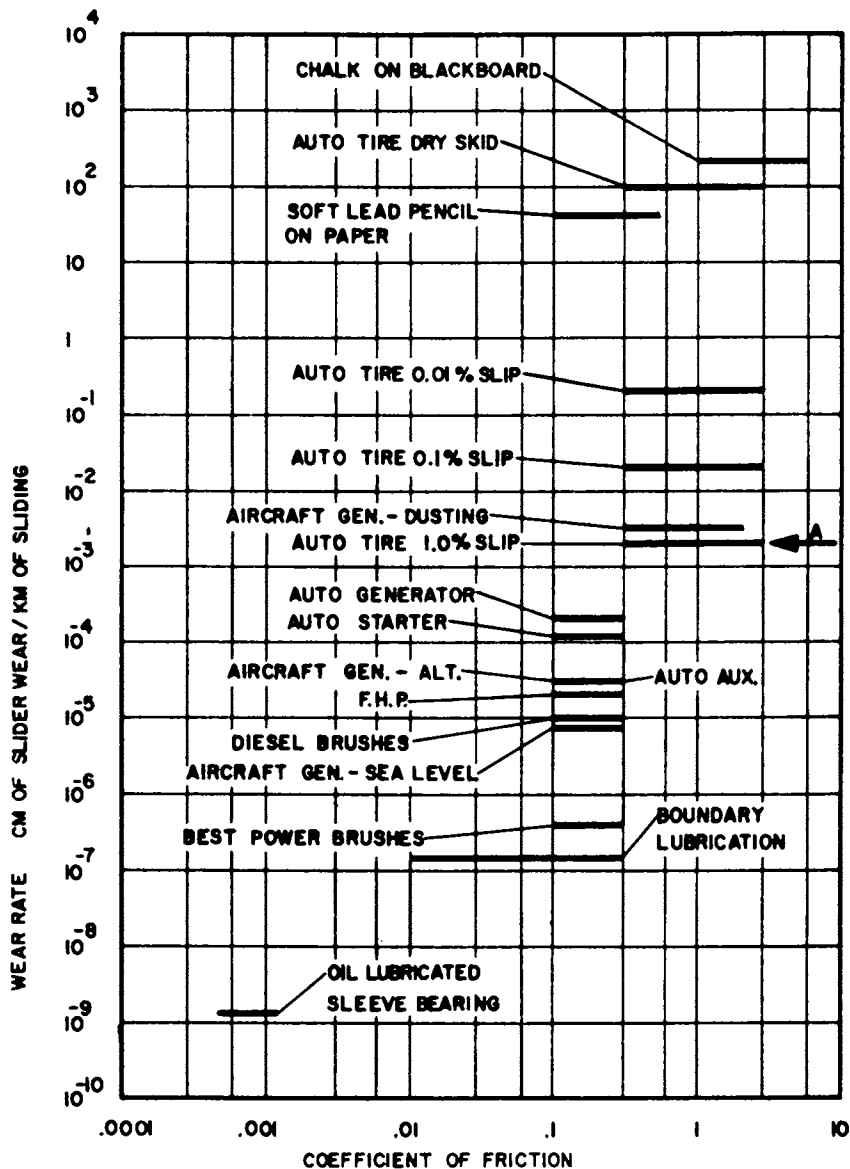
Figure 12.   Schematic of wear rates and coefficients of friction
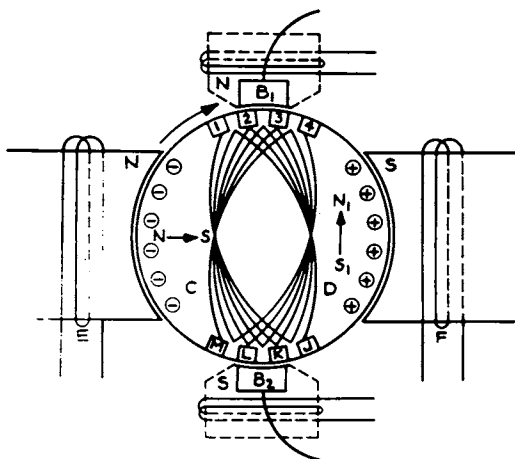
$$e = -nv\phi_r(t) + iR + L\frac{di}{dt} + \sum_q M_q \frac{di_q}{dt} \text{ volts}$$

Figure 13.   Circuits involved in commutation

REACTION HOLDER

RADIAL HOLDER

CARTRIDGE
HOLDER

TRAILING
HOLDER

CONSTANT PRESSURE
TRAILING HOLDER
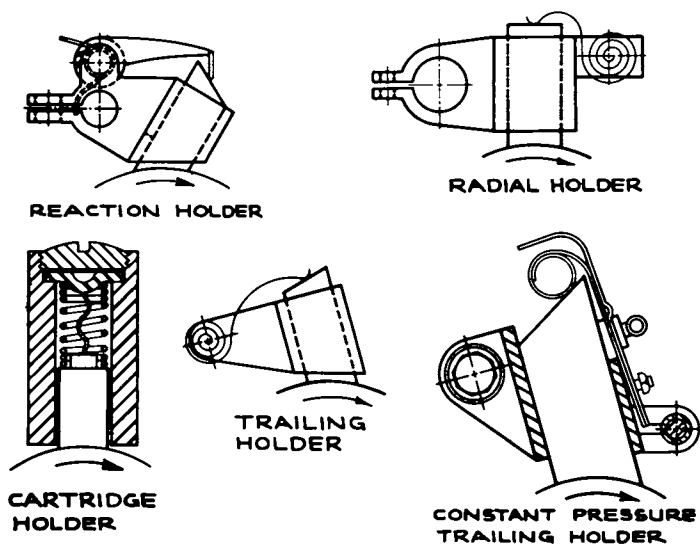
Figure 14.   Examples of brush holders

BRUSH FORCE = 4 LB.
BRUSH ELASTICITY = 100×10^6 g/cm^2

ELASTIC
PENETRATION

RADIUS OF
COLLECTOR= 4 IN.

RADIUS OF
BRUSH

RADIUS OF BRUSH	ELASTIC PENETRATION
4.04 IN.	0.000035 IN.
4.125 IN.	0.00006 IN.

RATE OF RECOVERY OF ELASTIC PENETRATION
ABOUT 1/10TH THE VELOCITY OF SOUND IN THE
BRUSH MATERIAL OR ABOUT 10^7 SEC. FOR 0.001 IN.
FASTEST COMMUTATOR BAR ABOUT 10^{-5} SEC.
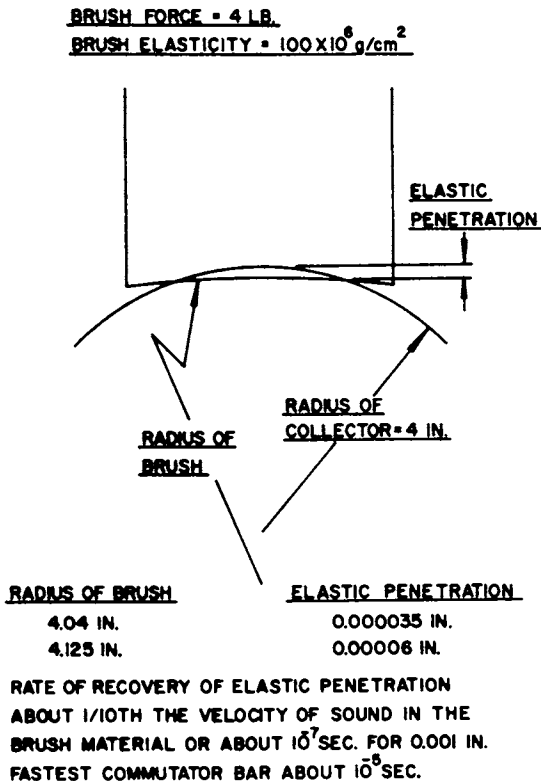
Figure 15.   Elasticity of the brush face
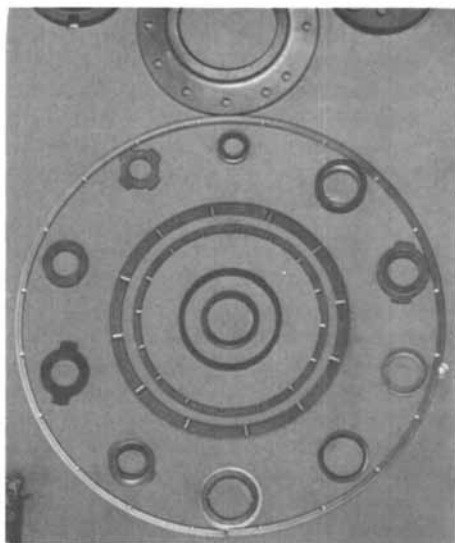
Figure 16.   Carbon seal rings for various purposes

materials that are used in a wide variety of applications. The largest seals are those used in jet aircraft engines between the various stages including those at the highest temperatures. The smaller seals are various types of face seals used for sealing liquids and gases.

Figure 17 shows three jet engine seals and the machining which must be provided on the surface to provide lubrication and the removal of wear particles. Figure 18 is a diagram of a carbon face seal which shows the elements used in a shaft seal. This type of seal is used for many different gases and liquids, and the materials of a seal and the face plate must be adjusted for these different materials. In the case of a face seal, friction and wear must be kept as low as possible to keep wear particles from interfering with the sealing action. The film which prevents the seizure of the carbon and metal face plate must be developed either from the liquid or material being sealed, or must be provided in the seal and face plate materials. For example, in sealing very dry gases, many of the same additives are used that are used in carbon brushes for high altitudes.

Carbon and graphite, while having low friction, under certain circumstances can also have high friction. This is developed in brake applications in which the constant friction, low wear, high thermal capacity, and high shock resistance of graphite materials are used for aircraft brakes. Materials for these applications have been developed in several different ways, some of which include graphite cloth and pyrolytic carbon and graphite materials.

E. Refractories. The refractory nature of carbon and graphite is used in many applications, particularly where oxidation is not present. Carbon brick is used for blast furnace liners. Glass mold faces are made with graphite; bearings that must run at high temperatures are made of graphite. Graphite is used for furnace boats and supports to a great extent in the semiconductor field and has the further advantage that it can be machined to very close tolerances for the support of these parts. Figure 19 shows some of the detail which can be achieved.

III. SUMMARY

In itself, the carbon industry is sizeable. Its materials are used in an essential way by many other industries with results that provide useful applications throughout our entire economy.

The technical nature of these applications is better understood, and the carbon industry can respond to application requirements more quickly and intelligently now than it could in the past. We have learned more about the nature of carbon and graphite, and we understand the requirements of the applications
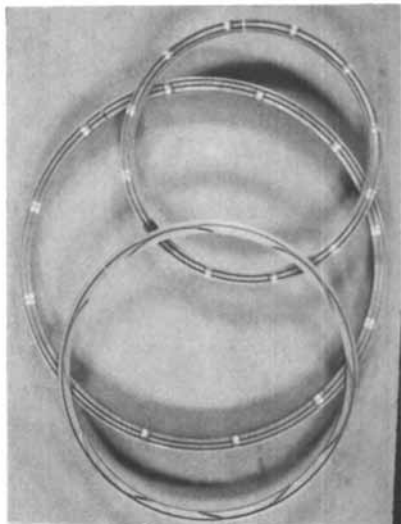
Figure 17.   Jet engine seals
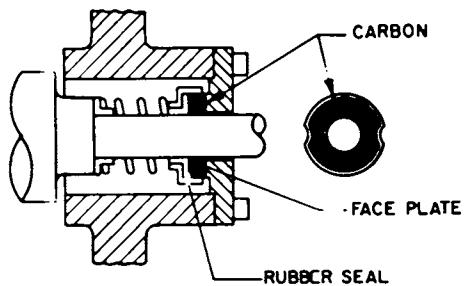
Figure 18.   Mechanical face seal
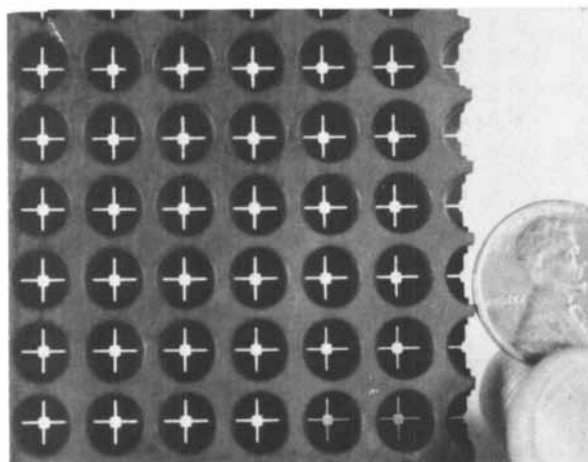
Figure 19.   Furnace brazing support

better.

With some few exceptions, most of the carbon used commer-
cially has come through the life cycle. Because of its high
binding energy, it tends to retain some of the structure of the
organic compound from which it was formed. This, together with
the processing possibilities, provides an infinite variety of
material properties. New technical opportunities are chal-
lenging the industry. It can and will respond constructively.

Literature Cited.

1. Shobert II, Erle I., "CARBON BRUSHES, The Physics
    and Chemistry of Sliding Contacts," Chemical Publish-
    ing Co., Inc., New York (1965).
2. Holm, Ragnar (in collaboration with Else Holm),
    "ELECTRIC CONTACTS, Theory and Application," 4th Ed.,
    Springer-Verlag New York, Inc., (1967).
3. Walker, Philip L., Ed. "CHEMISTRY AND PHYSICS OF
    CARBON," Marcel Dekker, Inc., New York (1965-73), 1-11.
4. "Proceedings of the Conferences on Carbon," University
    of Buffalo, Buffalo, No. 1-4. Waverly Press, Inc.,
    Baltimore, publishers of Conf. 1 and 2. Conference
    No. 5 Held at The Pennsylvania State University,
    University Park. Pergamon Press, New York, publishers
    of Conf. 3 to 5. (1953-1961).
5. Mrozowski, S., Ed., CARBON, Pergamon Press, New York,
    (1963 through present).
6. Houseman, D. H., "Some Factors Affecting Electrode
    Consumption in the Electric Arc Furnace," J. of the
    Iron and Steel Institute, (May, 1956), 183, 48-53.
7. Hearne, K. R., S. A. Nixon, and D. Whittaker, "Axial
    Temperature Distributions Along Thin Graphite Elec-
    trodes," J. Phys. D. Appl. Phys., (1972), 5, 710.
8. Bello, J. R., "Fundamentals of the Electric Arc Fur-
    nace," Paper No. EPC-12, The Metallurgical Society
    of AIME, New York.
9. Yavorsky, P. J. (American Smelting and Refining Co.,
    S. Plainfield, N.J.) and J. F. Elliott, (Professor,
    Dept. of Metallurgy and Materials Science, MIT,
    Cambridge,) "Observed and Predicted Temperatures in
    Large Arc Furnace Electrodes", from MIT Thesis, (1970)
10. Ciotti, J. A., "A New Era in Melting," J. of Metals,
    (April, 1971), 30-35.
11. Sundberg, "The Power Circuit of Arc Furnaces," Elektro-
    warme International (April, 1972) 30, B2, B93-B99.
12. Schwabe, W. E., "Measuring Problems and Techniques at
    A-C Furnace Arcs," National Carbon Research Laborator-
    ies, Cleveland (1954).

13. Holm, R., "Calculation of the Temperature Development in a Contact Heated in the Contact Surface, and Application to the Problem of the Temperature Rise in a Sliding Contact," J. App. Phys., (April, 1948), 19, 361-366.

14. Schwabe, W. E., "The Mechanics of Consumption of Graphite Electrodes in Electric Steel Furnaces," Presented at the 29th Electric Furnace Conference of the Metallurgical Society of AIME, Toronto, (December, 1971).

15. Rykalin, N. N., Nikolaev, A. V., and Goronkov, O.A., "Current Density at the Anodic Spot of an Arc," High Temperature (Sept. - Oct., 1971), 9, (5), 893-6.

16. "Some Factors Affecting the Wear of Graphite Electrodes in the Electric Arc Furnace," J. of the Iron and Steel Institute, (February, 1954), 176, 159-165.

17. Cosh, T. A., "Graphite Electrode Consumption in Electric Arc Furnaces," J. of the Iron and Steel Institute, (March, 1957), 185, 328-332.

18. Hering, C. "Laws of Electrode Losses in Electric Furnaces," Trans. Electrochemical Society, (1909), 16, 265-316.

19. Schwabe, W. E., "Experimental Results with Hollow Electrodes in Electric Steel Furnaces," Iron and Steel Engineer, (June, 1957), 34, (61), 84-91.

20. Schwabe, W. E., "Steelmaking in Ultra High Power Electric Arc Furnaces," Stahl u. Eisen, (August, 1969), 89, (17, 21), 927-937.

21. Ravenscroft, J., "Distribution of Electrode Consumption in an Electric Arc Furnace," Metallurgia V. (December, 1959), 60, 253-259.

22. Shobert II, Erle I., CARBON AND GRAPHITE, Chapter Printed in Modern Materials, Academic Press, New York, (1964), 4 , 1-99.

10

Laboratory and Plant Performance of Petroleum Pitch

J. W. PENDLEY and V. L. BULLOUGH

Reynolds Metals Co., Reduction Research Division, Sheffield, Ala. 35660

Approximately 0.5 pound of anode carbon is required for each pound of aluminum produced by the Hall-Heroult process. Since the metallic impurities in the carbon that are more noble than aluminum alloy with the product they should be kept at a minimum. Until the 1960's all anode carbon used to produce aluminum in this country contained coal tar pitch binder and petroleum coke aggregate.

Most of the petroleum coke used in the production of anodes is produced in delayed cokers. The quality of the coke varies with the combination of the properties of the coker feedstock. (1-3) The quality of the feedstock changes not only with geographic location of the crudes, and with operating parameters of the refinery, but also with the demand for the refiners product. (An example is the cyclic demand for asphalt in the summer and fuel oil in the winter.) As a general rule, refiners coke only refinery residuals that bring the least amount of profit and/or difficult to sell. These changes in the coker product plague the aluminum industry with a necessary raw material which has inconsistent properties. This past year has been no exception.

The green (uncalcined), coke is calcined in rotary kilns at 1200 - 1400°C to give a coke having a density of 2.03 to 2.08 g/cc. Calcined coke should have dimensional stability and good electrical conductivity to be suitable for electrodes.

For several years petroleum pitch has been evaluated in the laboratory at the bench scale (4,5) and in some plants on a small scale. (6) However, during the latter part of the 1960's the quality of the pitch and/or the economics of the production processes were developed to the extent that petroleum pitch entered the field as a substitute or as a replacement for coal tar pitch as an aggregate binder. (7,8) Petroleum pitch is produced by the thermal cracking of clarified slurry oil or other petroleum

residuals. (9)   Properties of petroleum pitch vary somewhat
with the geographic location of the crudes and with the manu-
facturing process.

Much effort has been exerted over the past two decades in a
search for analytical methods and techniques which will predict
the performance of the baked carbon by examining the pitch
binder.   Many of the investigators have attempted to relate
some physical property or properties to the physical properties
of the baked carbon. (10 - 13)   We have found, as well as others,
that the physical properties of the binder on which most specifi-
cations are written provide only a convenient means to deter-
mine changes in a pitch from a single source; and are not
meaningful for all pitches.

Laboratory Tests

For several years we have used an apparatus to assess the
quality of the binder by the performance of the carbon in the
electrolysis of molten salts. (14)   The assembly used in our
laboratory is illustrated in Figure 1.   The carbon specimen,
positioned between two pieces of boron nitride to confine elec-
trolysis to the vertical surface of the specimen, is suspended
beneath the surface of molten cryolite electrolyte.   A known
amount of current is passed through the system for a definite
period of time.   Carbon consumption is calculated from the
known current and the weight of carbon consumed during elec-
trolysis.

A number of petroleum pitches have been evaluated in our
laboratory in both prebake and Soderberg type carbon.   A
listing of all pitches evaluated would be time consuming and of
little interest to you, so we will confine our discussion to three
petroleum pitches produced by three different suppliers.   The
coal tar pitches used as controls were produced by a single
manufacturer which has supplied our company with pitch for
many years and the pitch is a plant proven binder.   Notice the
differences in the physical properties between the four pitches
presented in Table I.   These pitches were evaluated in our
laboratory at a pitch concentration of 25.5 w/o and an aggregate
distribution similar to that used in Soderberg type carbon.   The
samples were baked in a laboratory baking furnace. Performance
data and properties of the electrode samples are presented in
Table II.   The results reported are the average of duplicate
determinations.   It should be noted that although rather large
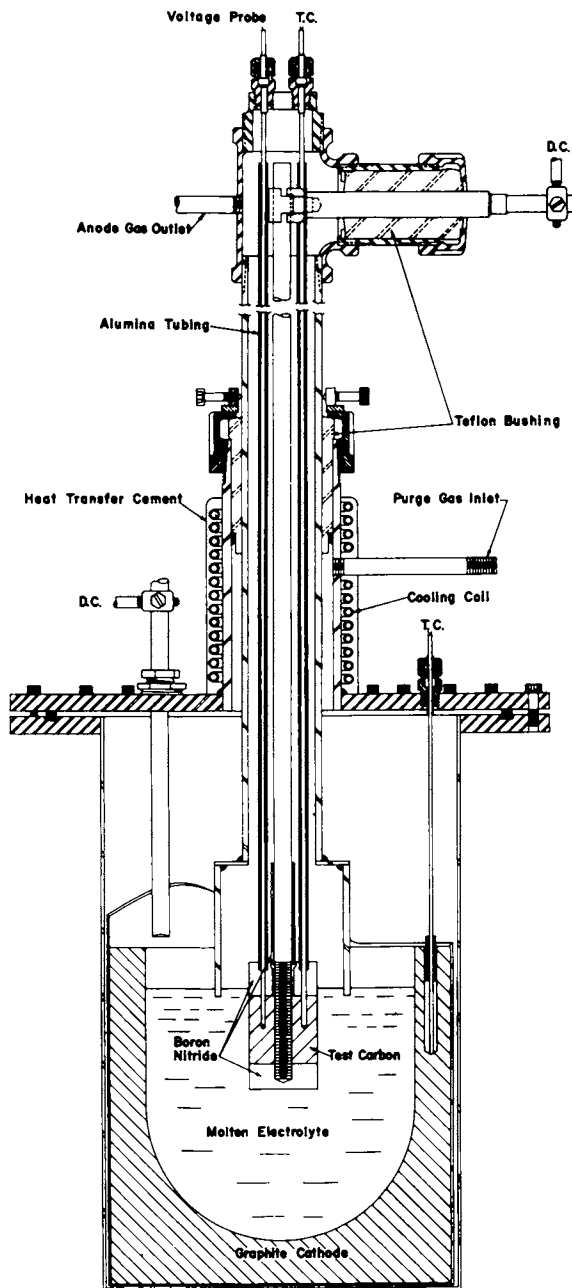
Figure 1.   Electrolytic consumption test cell

TABLE I.

PITCH ANALYSES

Pitch:	Petroleum		Coal Tar	
Pitch Supplier:	A	B	E	E_1
Softening Point, C/A, °C	121	119	120	106
Quinoline Insolubles, w/o	1.7	0.2	18.6	14.6
Benzene Insolubles, w/o	4.0	7.7	39.9	32.9
Ash, w/o	1.48	0.19	0.08	0.07
Coking Residue, Conradson, w/o	54	49	61	58
Sulfur, w/o	2.0	1.3	0.7	0.7
Specific Gravity, 25/25°C	1.15	1.24	1.34	1.34
Carbon Hydrogen Ratio, Atomic	1.33	1.44	1.79	1.86

differences existed in the properties of the pitches, and differ-
ence also existed in the physical properties of the carbon pro-
duced from the pitches, there is no difference between the
electrolytic reactivity of the carbons.

TABLE II.

LABORATORY PERFORMANCE OF BAKED
CARBON — SODERBERG TYPE

Pitch	Apparent Density, g/cc	Electrical Resistivity, Ohms/m/mm^2	Electrolytic Carbon Consumption, %
A	1.50	59	116
B	1.50	61	118
E	1.58	50	118
E$_1$	1.53	56	118

As mentioned earlier we have also evaluated petroleum
pitches in prebake type carbon in our laboratory.   The two
petroleum pitches listed in Table III are from different
suppliers.   Note the difference in the properties of these
pitches.   Carbons were prepared containing these petroleum
pitches at a concentration of 14.5 w/o and the controls at a
pitch concentration of 15.5 w/o.   The aggregate distribution
was similar to that used in prebake type carbon.   Performance
data and physical properties are presented in Table IV.
    In this evaluation, carbon containing pitch "B" was the
better performer.   You will again note that although pitch
properties were different, carbons containing three of the
pitches reacted the same in the electrolysis of molten salts.
    Electrolytic reactivity of laboratory prepared carbons also
agrees with the reactivity of plant prepared carbons.   Observe
the results presented in Table V.

TABLE III.

PITCH ANALYSES

Pitch:	Petroleum		Coal Tar	
Pitch Supplier:	B	F	E	E_1
Softening Point, C/A, °C	119	117	120	106
Quinoline Insolubles, w/o	0.2	9.3	18.6	14.6
Benzene Insolubles, w/o	7.7	29.3	39.9	32.9
Ash, w/o	0.19	0.07	0.08	0.07
Coking Residue, Conradson, w/o	49	58	61	58
Sulfur, w/o	1.3	1.0	0.7	0.7
Specific Gravity, 25/25°C	1.24	1.16	1.34	1.34
Carbon Hydrogen Ratio, Atomic	1.44	1.57	1.79	1.86

TABLE IV.

LABORATORY PERFORMANCE OF BAKED
CARBON — PREBAKE TYPE

Pitch	Apparent Density, g/cc	Electrical Resistivity, Ohms/m/mm^2	Electrolytic Carbon Consumption, %
B	1.52	61	109
F	1.54	63	112
E	1.54	55	112
E$_1$	1.57	62	113

TABLE V.

LABORATORY PERFORMANCE OF CORES FROM
PREBAKE ANODES CONTAINING
PETROLEUM PITCH

	Carbons Prepared In The Laboratory	Prebake Blocks Prepared in Plant
Apparent Density, g/cc	1.54	1.57
Electrical Resistivity, Ohms/m/mm^2	52	54
Electrolytic Reactivity, %	108	109

Plant Tests

During recent years five of the seven reduction plants operated by Reynolds Metals Company in the United States have tested petroleum pitch as an electrode binder. Some of these were 1 to 14 cell tests and one was an entire room, and then an entire line.

The use of petroleum pitch in the plant involved optimization of the binder to the particular aggregate being used and re-educating the carbon plant personnel from the old control of "operation by visual observation." Petroleum pitch has the characteristic of soaking into coke pores more than coal tar pitch during the mixing cycle giving a drier appearance. In prebake plants the excess pitch was driven from the aggregate during baking, and depending upon the excess used caused deformation of blocks and/or severe sticking of the packing material to the blocks.

The Soderberg plants testing petroleum pitch found the same deceptive appearance in their mixers as was seen in the prebake plants. However, here an excessive amount of pitch resulted in paste leaks and an added burden of pitch fumes on the fume recovery system. As a general rule operating personnel decreased the binder content by about 1.5 w/o when using petroleum pitch.

In addition to lower binder requirements one of the Soderberg plants found that they should decrease paste mixing temperature from 180°C to 160°C and decrease mixing time from 115 minutes to 45 minutes when using petroleum pitch. These findings agree with the work reported by Gyoerkoes. (6) These changes brought about an increase in the capacity of the carbon plant, and a savings in energy requirements, both mechanical and physical. This particular test included 14 cells and was conducted for about one year. Metal production figures showed that the cells containing petroleum pitch produced as much metal as the other cells in the room containing coal tar pitch.

Petroleum pitch tested in prebake type carbon was carried out at the room size and line size as reported by Alexander, et al. (8) Three different percentages of pitch, 14.5, 15.0 and 15.5 percent were tried in the initial evaluation. The number of blocks prepared and press data are presented in Table VI. Cull percentages are presented in Table VII. Adhesion of packing material was severe to blocks containing 15.0 and 15.5 percent pitch. This resulted in a burdensome cleaning problem.

TABLE VI.

PRESS   DATA

Percent Pitch	Average Mix Temp. (°C)	Average Press Temp. (°C)	Average Green Apparent Density	Average Bake Apparent Density	Approximate No. Pressed
		Petroleum Pitch Anodes			
14.5	162	130	1.63	1.62	8400
15.0	159	130	1.65	1.57	7900
15.5	163	130	1.69	- - -	4500
		Coal Tar Pitch Anodes			
16.0	160	133	1.68	1.64	- - - -

TABLE VII.

CULL PERCENTAGES AMONG PETROLEUM
PITCH ANODES

Percent Pitch	Cull Percentage*
14.5	4.86
15.0	7.14
15.5	10.14
Regular Blocks From Furnace	3.66

*The above percentages do not represent total culls by pitch percentage, but are the result of random samples taken over several days.

TABLE VIII.

CARBON CONSUMPTION

	Prior to Test (68 Days)		During Test (62 Days)	
	Room 8	Room 10	Room 8	Room 10
No. Set	13,865	14,265	12,702	12,674
Average Weight Per Block (Lbs.)	250.33	248.63	250.33	248.63
Carbon Consumption (Lbs. Carbon/ Lbs. Al.)	0.525	0.526	0.507	0.510
Overall Plant Consumption	0.514	0.514	0.511	0.511
Average Butt Weight (Lbs.)	74.64	75.40	78.67	79.12

The blocks containing petroleum pitch were set in Room 10 of the plant and the performance of these cells, over a period of 62 days, was compared with the performance of cells in Room 8 containing coal tar pitch, and also compared with the performance of cells in Room 10 prior to the test.   The results are presented in Table VIII.

Alexander concluded from this test "that petroleum pitch could be substituted satisfactorily for coal tar pitch."

As a note of interest this plant went to 100 percent petroleum pitch in 1971 and has operated with only small substitutions of coal tar pitch since that time.   The production record and carbon consumption of this plant is very good and they are completely satisfied with the performance of petroleum pitch.

ABSTRACT

Laboratory findings showed that carbon electrodes, both prebake and Soderberg type, containing petroleum pitch performed as well in the electrolysis of molten salts as carbon electrodes containing coal tar pitch.   Plant tests confirmed the laboratory findings that the consumption of carbon electrodes containing petroleum pitch was no different than the consumption of carbon electrodes containing coal tar pitch.

Electrolytic reactivity of cores obtained from carbon blocks manufactured in the plants agreed with the reactivity of laboratory prepared carbon.

The plants had a tendency to begin their tests with an excess of petroleum pitch which resulted in block deformation and/or severe sticking of packing material during the baking cycle; and resulted in paste leaks at the Soderberg cells.   As a general rule, when the petroleum pitch was optimized for a particular aggregate, the pitch requirement was decreased by 1 - 2 percent.

LITERATURE CITED

1. Scott, C. B., Chemistry and Industry, (1967), pp. 1124 - 1131.
2. Scott, C. B. and Folkins, H. O., "Effects of Major Processing Variables on Properties of Metallurgical Grade Petroleum Cokes," AIME paper presented at the Annual Meeting, San Francisco, Calif., February 20-24, (1972).

3. Pippin, B. H., "The Production of Petroleum Coke for Aluminum Cell Anodes," presented at the 100th Annual Meeting, American Institute of Mining, Metallurgical and Petroleum Engineers, Inc., New York, New York, March 1-4, (1971).

4. Reid, J. M. and Linden, H. R., "Production of High-Quality Electrode Binder Pitch by Cyclic Thermal Cracking of Heavy Petroleum Fractions," presented at the Meeting of the Division of Petroleum Chemistry, American Chemical Society, Pittsburgh, March (1966).

5. King, L. F. and Robertson, W. D., Fuel, 47, (1968), pp. 197-212.

6. Gyoerkoes, T., "Some Aspects of Petroleum Base Binders in Prebake Anode Fabrication," paper presented at the 98th Annual AIME Meeting, Washington, D. C., February (1969).

7. Ottewill, G. R., Metals Australia, October (1969), 325-27.

8. Alexander, C. D., Bullough, V. L., and Pendley, J. W., "Laboratory and Plant Performance of Petroleum Pitch," presented at the Annual AIME Meeting, New York, New York, March 1-4, (1971).

9. Ball, G. L., Gannon, C. R., and Newman, J. W., "Petroleum Pitch - A Major New Carbon Source," presented at the Annual AIME Meeting, San Francisco, California, February 20-24, (1972).

10. Chautte, L. P., and Beschofberger, G. P., Industr. Eng. Chem. 47, 1412, (1955).

11. Branscomb, J. A., Bullough, V. L., and Morrissey, H. A., "The Relationship of Pitch Properties to Anode Properties," paper presented at the Division of Gas and Fuel Chemistry, American Chemical Society, New York, New York, September (1960).

12. Dell, M. B., Fuel, 38, 183-87, (1959).

13. Bowitz, O., Eftestol, T., and Selvik, R. A., "New Methods for Testing Raw Materials for Anode Carbon Paste," Extractive Metallurgy of Aluminum, 2, 351-72, Interscience, (1963).

14. Bullough, V. L., Marshall, H. C., and Pendley, J. W., "Some Effects of Coke Calcination Temperature," paper presented at the Annual AIME Meeting, Dallas, Texas, (1974).

11

Machine-Fabricated Carbon and Graphite

DONALD E. CORAH and JOHN C. DAVIDSON

Technical Department, Airco Speer Carbon-Graphite, A Division of Airco, Inc.,
St. Marys, Pa. 15857

Information is presented on the fabrication of carbon and
graphite parts with specific properties for use in a variety of
mechanical, electrical, and chemical applications. Graphite is
manufactured with unique properties, which can be varied by the
method of manufacture and types of raw materials. Almost
every part is machined to some degree because of the high
percent of shrinkage, 3 to 10 percent, during the baking and
graphitizing operations. Different types of machining equipment
are used to obtain a desired shape and/or finish on graphite
parts.

Discussion

Manufacture and Properties. Figure 1 illustrates the
processing cycle for carbon and graphite, requiring up to nine
months to manufacture. Carbon is formed by either extruding
or molding primarily petroleum coke with a pitch binder and
thermally processing (baking and graphitizing) the formed
amorphous carbon to polycrystalline graphite. Lampblacks and
natural graphites are two alternate raw material fillers with
different electrical properties which are used primarily in
manufacturing brushes and electrical contacts. Pitch impreg-
nation is an optional step for densifying graphite.
Figure 2 shows a range of properties obtainable with
different graphites. Steel furnace electrodes are produced with
large carbon particles and a low CTE level for withstanding
thermal shock. Nuclear moderator blocks have a high density
for reflecting neutrons and are isotropic to increase irradiation
stability. Metal melting crucible graphite is fine grained to
resist metal penetration and oxidation. Molded high-density
graphite is used for rocket nozzles because of its flaw-free
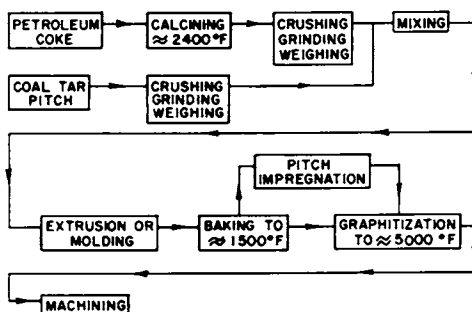
Figure 1.   Manufacture of graphite

Application	Electric steel furnace electrode	Nuclear moderator block	Metal melting crucible	Missile rocket nozzle	Electrical discharge machining electrodes
Forming Method	Extruded	Extruded	Extruded	Molded	Molded
Maximum Particle Size, in.	0.250	0.065	0.008	0.003	0.0008
Apparent Density, g/cc.	1.64	1.76	1.73	1.77	1.80
Specific Resistance, x 10^{-5} ohm. in.	35	36	40	48	42
Flexural Strength, psi With Grain	1100	2500	4300	3800	6800
Against Grain	900	2400	3700	3000	6600
CTE, x 10^{-6} C^{-1} With Grain	1.8	5.3	1.8	3.3	4.4
Against Grain	2.9	6.0	3.0	4.3	4.6
Scleroscope Hardness	30	45	50	45	65
Impurities, parts per million	6000	500	20	1000	1500

Figure 2.   Typical physical properties

structure and resistance to erosion. Ultrafine grain, high-
strength graphite is required for producing intricate detail in
electrical discharge machining electrodes.

Machining Graphite. Figure 3 shows typical tolerances
and finishes that are obtainable on graphite parts machined with
various types of equipment. The RMS surface finish is deter-
mined visually, as graphite's inherent porosity does not lend
itself to measuring the finish with a profilometer. The tool
types, feed rates, and machine speeds generally used in machin-
ing graphite on a production basis are shown. These operating
conditions are suitable for machining the majority of specialty
parts; and the machining methods depend on the configuration,
tolerances, and actual application. Graphites are readily
machinable with most cutting tools.

Fabricated Graphite With Specific Properties For
Numerous Applications. Figure 4 illustrates typical parts for
mechanical applications. Graphite is used as a nozzle in rocket
motors because of its ability to withstand temperatures above
5,000 F. The nozzle inside diameter is contoured on a lathe
using a tracer bar to accurately form the desired profile for
exiting hot gases during the firing of the rocket nozzle.
    The nonferrous metal continuous-casting die has a honed
inside diameter for producing a surface finish that increases
die life by reducing the coefficient of friction. The smooth
finish decreases the tendency of molten metal to adhere to the
graphite. Graphite's good lubricity enables metal bars to be
cast with smooth surfaces, free of tear marks.
    Graphite crucibles are excellent for melting, drawing,
and refining metals because of graphite's chemical inertness to
almost everything except very strong oxidizing agents. Some
crucibles are produced from high-purity graphite, containing
less than 20 parts per million total impurities, for processing
pure metals and isotopes. High-purity graphite is machined
without lubricants, handled with sanitary protective gloves, and
transferred in polyethylene bags to insure high purity.
    The semiconductor industry uses precision machined
fixtures having numerous holes requiring diameter and location
tolerances of plus or minus 0.001 inch or less. Graphite's
resistance to wetting by glass and its ease of machining to close
tolerances make it an excellent material for processing
hermetically sealed integrated circuits.
    Representative graphite parts for electrical applications

When you need a Workpiece with a RMS Finish of	With a range of Economical Tolerances	Use A	Tool Type	Under The Following Operating Conditions	
				Machine Settings	Machine Speed
350 to 600	0.0625 to 0.1875 in.	Bend saw	0.5 in. wide blade 4 teeth/in.	5000 FPM	Feed by hand
100 to 200	0.0312 to 0.0625 in.	Abrasive saw	0.06 in. thick by 10 in. diameter No. 36 grit silicon carbide wheel	1800 RPM	Feed by hand
200 to 300	0.008 to 0.0312 in.	Planer	36 in. long silicon carbide blades	2780 FPM	18 FPM
50 to 250	0.003 to 0.125 in.	Lathe	0.03 in. to 0.12 in. radius carbide tipped tools	500 RPM	0.008 in. to 0.018 in. per revolution
300 to 400	0.003 to 0.016 in.	Drill	High speed steel drills	500 RPM	Feed by hand
120 to 300	0.003 to 0.0625 in.	Mill	6 in. diameter fly cutter with 2 carbide bits	1880 FPM	0.75 FPM to 6 FPM
35 to 40	0.003 to 0.0625 in.	Wet centerless grinder	————	————	————
35 to 65	0.002 to 0.005 in.	High speed reamer	————	800 RPM	Feed by hand with 0.01 in. cut
15 to 30	0.001 to 0.003 in.	Lapping machine	No. 320 grit aluminum oxide wheels	40 psi pressure	Grind for one minute
20 to 32	0.001 to 0.003 in.	Hone	220-0 grit	1500 RPM with 18 psi pressure	Feed by hand

Figure 3.   Typical equipment and conditions for machining graphite

are shown in Figure 5. Graphite's low specific resistance and
strength that increases with temperature are desirable for
fabricating resistance furnace heaters. The heater shown
illustrates typical lathe and milling operations required in
machining graphite parts. Since the specific resistance of
graphite is not constant, as it is not a homogeneous material,
the heater diameter or the slot width has to be varied in machin-
ing to manufacture heaters to a desired total resistance.
Heaters are generally used in an inert atmosphere or vacuum
because graphite will oxidize at temperatures above 750 F.

     Carbons are used as sliding electrical contacts because
of their low wear rates. The pantograph shoe contact represents
a very hard carbon material not readily machinable. Diamond
tools are the practical way to machine carbon, generally gas-
baked materials, with a Scleroscope hardness over 70. Carbon
can be shaped to size in the green state, if liberal tolerances
are acceptable, before baking into a hard amorphous carbon.

     Graphite has electrical and mechanical properties ideal
for electrodes used in electrical discharge machining (EDM).
Graphite is machined into complex electrode designs, some
with cross sections as small as 0.005 inch. Graphite EDM
electrodes are used for machining complex mold and die cavities
at a very fast metal removal rate and low electrode wear com-
pared to metal electrodes.

     Graphite electrodes of much larger size and mass are
used for producing steel in electric arc furnaces. Graphite has
the ability to withstand thermal stresses over a 5,000 F. tem-
perature range. The electrode ends, along with a connecting
pin, are machined with precision threads for withstanding severe
mechanical stresses and for obtaining a low resistance joint.

     Figure 6 shows several graphite parts employed in the
chemical industry. Hexagonal shaped blocks with a grid of holes
are used as a core in nuclear reactors. Precision holes are
machined in the core by gun drills. Graphite is an excellent
nuclear core material because of its very low neutron capture
cross section.

     Graphite fluxing tubes are extruded to size on the outside
and inside diameters. The tube is suitable for use with a self-
tapping metal connector for attaching the gas line to the tube.
Graphite is inert to fluxing gases that are passed through molten
metal and will not contaminate the metal. Fluxing tubes are also
produced with a plugged end and radially drilled vent holes for
obtaining a better dispersion of fluxing gases.

     Anodes are used in the electrolytic process for chlorine

ROCKET NOZZLE

CASTING DIE

CRUCIBLE

FIXTURE
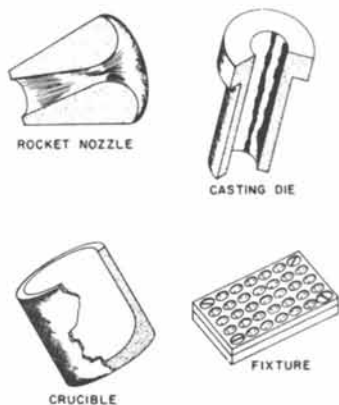
Figure 4.   Graphite for mechanical applications

HEATER

PANTOGRAPH CONTACT

E.D.M. ELECTRODE

STEEL FURNACE ELECTRODE
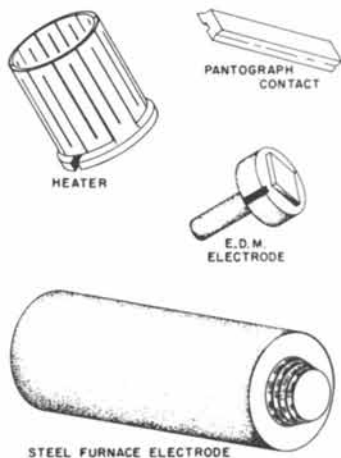
Figure 5.   Graphite for electrical applications

NUCLEAR REACTOR CORE

ELECTROLYTIC ANODE

HEAT EXCHANGER

FLUXING TUBE
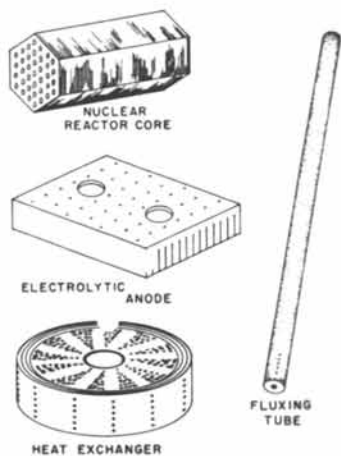
Figure 6.   Graphite for chemical applications

production.   Graphite is a preferred material because of its
electrical characteristics along with its good resistance to
chemical attack.   Various slot designs are machined into
graphite blocks for producing electrolytic cells.

Graphite, with its excellent resistance to corrosive fluids
and its high thermal conductivity of typically 100 BTU hr^{-1} ft^{-2}
F^{-1} ft, is used for heat exchangers.   Heat exchanger segments,
are precision machined and gang drilled so when stacked to-
gether they will produce a cylindrically shaped heat exchanger.
Two different fluids can be passed through radial and longitu-
dinal holes to effect heat transfer between the fluids without
cross contamination.

Conclusion

Graphite is manufactured with properties that make it a
versatile material for use in mechanical, electrical, and chem-
ical applications.   In general, all graphite parts require some
machining to obtain the multiplicity of diverse shapes, designs,
and tolerances required in industrial applications.   In contrast,
carbon has much more limited use and is generally made to
shape or shaped with diamond-tipped tools.

Graphites Fabricated from Green Petroleum Pitch Cokes

O. J. HORNE* and C. R. KENNEDY

Metals and Ceramics Division, Oak Ridge National Laboratory,** Oak Ridge, Tenn. 37830

Conventional graphite bodies are normally fabricated by com-
bining carbonized or graphitized filler materials with hydrocarbon
binders such as coal tar or petroleum pitches. During the sub-
sequent heat treatment to produce the final graphite body, the
filler undergoes little or no shrinkage, while pronounced shrink-
age of the binder material occurs, resulting in a final product
which contains a network of angular voids. This pore structure
weakens the overall structure and its ability to withstand
stressing.

The effect of pore morphology is particularly significant in
obtaining graphites with structures yielding high mechanical
integrity. These types of structure are very important when con-
sidering the resistance to differential crystallite growth during
nuclear irradiation and to resisting the high strains produced by
thermal stress or shock. Both types of problems can presumably
be solved by strengthening the interparticle boundaries and
reducing the role of pore structures to act as stress risers.
Thus, the desired structure is one having a monolithic character
with the pore texture smaller or less angular than the pores
inherently present in the coke structure.

One approach to obtain a monolithic-type structure with
smaller or less angular pores is to employ green coke as the
filler material. This approach offers at least two advantages.
First, the coke particle still retains some chemical reactivity
and will readily unite with the binder. Secondly, the volume
shrinkage of the green coke filler more nearly matches the binder
shrinkage during pyrolysis. Work reported by Kennedy and
Eatherly (1,2) has shown that graphite based on green cokes does
have the necessary monolithic structural characteristics and does
exhibit dramatic improvements in both irradiation and thermal
shock resistance.

Highly acicular green cokes have been employed in efforts to
obtain graphites with low thermal expansion and high thermal

*Present Address: Poco Graphite, Inc., P.O. Box 2121,
Decatur, TX 76234.

conductivity, which is essential for thermal shock resistance.
The search for highly acicular fillers led to the preparation of
green cokes from Ashland Oil Company's A-240 petroleum pitch.
Properties of graphites fabricated with the A-240-derived green
cokes were then compared with properties of graphites fabricated
using high quality acicular cokes graciously supplied by Union
Carbide Corporation, Carbon Products Division (UCC) and Great
Lakes Carbon Corporation (GLCC).

Experimental

A schematic view of the treatment and fabrication procedures
utilized in this study can be seen in Fig. 1. As indicated, both
the UCC and GLCC green cokes were fired for 1 hr at 500°C, pri-
marily to reduce moisture and/or volatile content to an acceptable
level for fabrication.

The A-240 cokes were prepared by firing approximately 1800 g
of A-240 pitch in carbon boats for 1 hr at 575, 600, 650, and
675°C under an inert atmosphere. A heating rate of approximately
5°C/min was used. Weight losses after firing the pitch to the
heat treatment temperature were 42.5, 43.9, 44.1, and 45.5%,
respectively.

An additional filler was prepared by heating A-240 pitch at
425°C for 24 hr with an initial room temperature argon pressure
of 2000 psi. The pressure-coked material was then fired at 500°C
for 5 hr.

After firing, the cokes were ground and appropriate quanti-
ties of the A-240 binder pitch were dry-mixed with the filler and
subsequently slurry blended using benzene until reasonably dry.
After grinding, the mix was warm-molded (approximately 95°C) at a
pressure of 2000 psi. The 1.6-in.-diam blocks were then placed
in a graphite sleeve and force-fitted into an Inconel outer
sleeve with graphite end plugs held tightly in place by a threaded
Inconel end cap. Before the end plugs were set in place, a mix-
ture of coarse-grain graphite filler and natural flake graphite
was placed between the end plug and the molded body. The end
plugs were then securely held in place with the threaded steel
end caps. An unassembled, along with a completed assembled,
restraining holder can be seen in Fig. 2.

The restrained blocks were then carbonized to 1000°C using a
controlled three-day cycle. After carbonization, the samples
were removed from the restraining holders and heated to 2800°C on
a one-day cycle. Specimens were then machined from the graph-
itized block for the various property measurements.

Results and Discussion

Typical microstructures for the graphites fabricated during
this study can be seen in Fig. 3. These graphites were typically
very uniform with a maximum particle size of approximately 120 μm.

GLCC, UCC
GREEN COKE

A-240 PITCH
COKED 1 HR
575, 600, 650
675°C

A-240 PITCH
COKED 24 HR
425°C, 2000 PSI

500°C, 1 HR

500°C, 5 HR

GROUND

10, 12, 14, 16 PPH
A-240 PITCH BINDER
2 PPH NITROBENZENE

SLURRY MIXED IN
HOBART MIXER USING
BENZENE

DRIED

GROUND

MOLDED, 95°C, 2000 PSI
AND HELD UNTIL COOLED
TO ROOM TEMPERATURE

PLACED IN RESTRAINTS

CARBONIZED

GRAPHITIZED
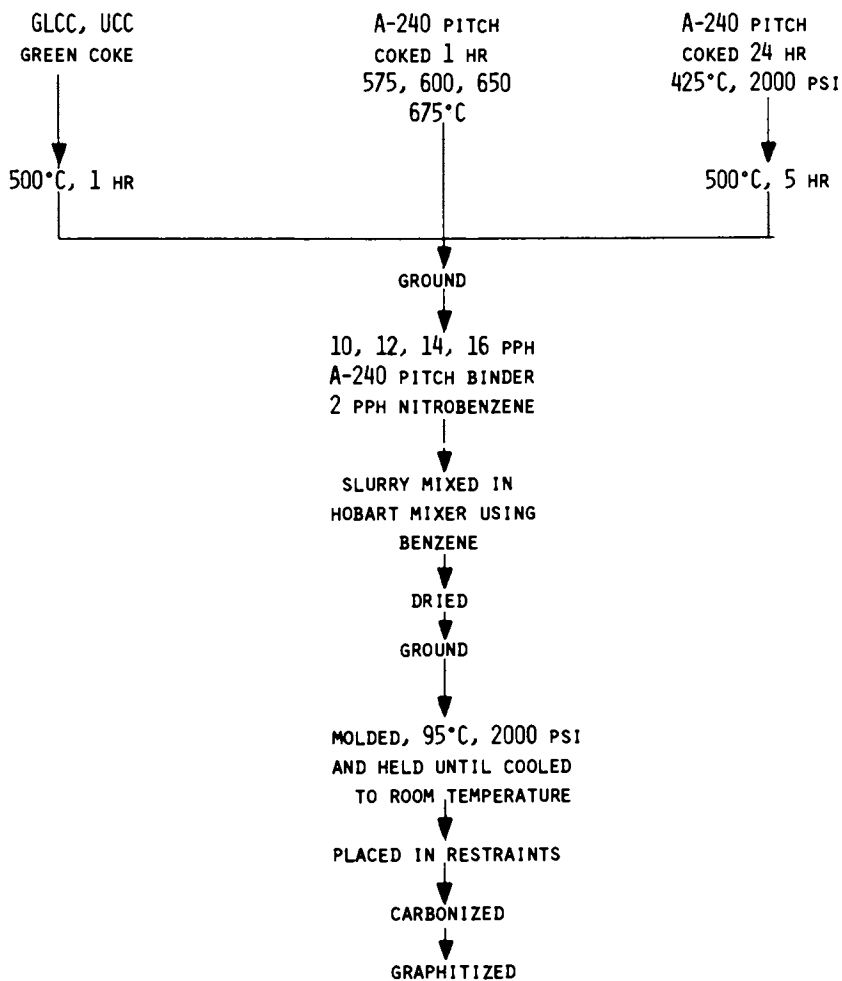
Figure 1.   Process description for the fabrication of the experimental graphites
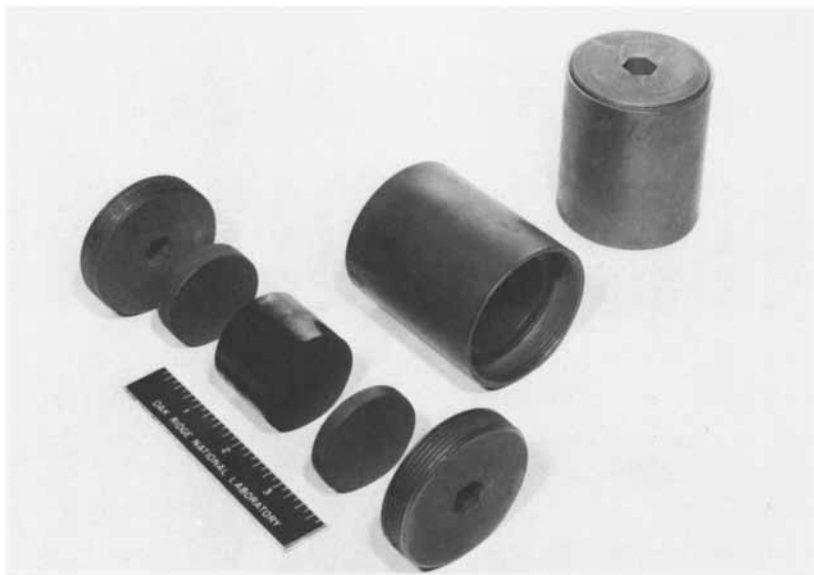
Figure 2.   Improved carbonizing block (1.6 in. dia. moldings)

Figure 3.   Typical microstructure of graphites fabricated using the experimental cokes

In general, properties of the graphites fabricated from the
UCC-, GLCC-, and A-240-derived cokes were quite similar and were
directly dependent upon the final graphitized density, which, in
turn, was dependent upon the initial green density. The greatest
difference between the A-240 cokes and the UCC and GLCC cokes was
the achievement of higher green densities of bodies fabricated
from the A-240 cokes prepared at the lower heat treatment
temperatures.

As indicated in Fig. 4, graphitized densities appeared to be
a linear function of green densities over the region studied. As
illustrated in this figure, as well as the rest of the figures,
the samples are identified according to filler. Thus, A-575
would denote the graphite fabricated from A-240 pitch heated at
575°C for 1 hr.

As shown in Fig. 5, graphitized densities for samples fabri-
cated from the A-240-derived fillers reached an apparent minimum
as the heat treatment temperature of the pitch approached the
650–675°C range. Though a dotted line is drawn below 600°C, data
seem to indicate that significant binder content effects are
present in samples fabricated from fillers prepared at tempera-
tures greater than 625°C. The graphitized densities and, thus,
the properties of the graphites can be improved by either single
or multiple impregnations.

As mentioned previously, the properties of the graphites were
directly dependent upon the final graphite density and the next
four figures emphasize this relationship.

Figure 6 shows that electrical resistivity values decrease
with increasing graphite density. The use of the term "normal"
refers to the with-grain direction. Though the relationships are
represented as linear functions, in actuality, an exponential
relationship exists. Highest resistivities resulted from A-650
and A-675 as expected from their low graphitized densities.
Resistivities of samples fabricated from the pressure-coked A-240
(I-A240) showed a similar type relationship, but yielded much
lower resistivities than were obtained for comparable graphite
density. For example, graphitized blocks fabricated from the
I-A240 with final densities of 1.63 and 1.67 g/cm^3 yielded with-/
across-grain resistivities of 810/1240 and 740/1090 µΩ-cm,
respectively.

As shown in Fig. 7, brittle ring strength increased linearly
over the region studied as the graphitized density increased.
Brittle ring strength is correlatable to 4-point beam loading and
tensile test values through a stress volume relationship. Because
of the lower stress volume, higher strengths are obtained from
brittle ring data than from either the 4-point loading or tensile
testing. Figure 8 shows a brittle ring specimen under compression.
Brittle ring data, modulli of elasticity, and fracture strains for
the I-A240 specimens show no significant deviation from the
density/property relationships exhibited by the other specimens.
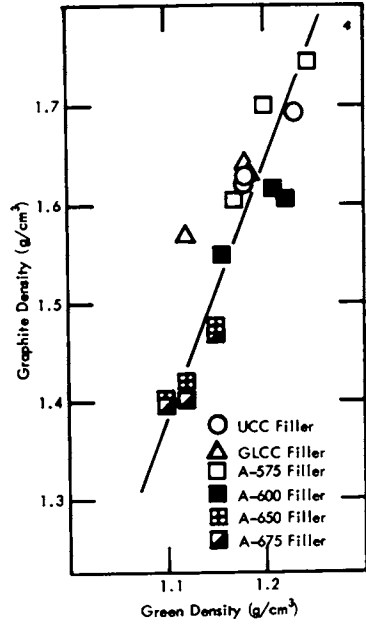
Figure 4.   The effect of green density on final density of graphites fabricated from green cokes
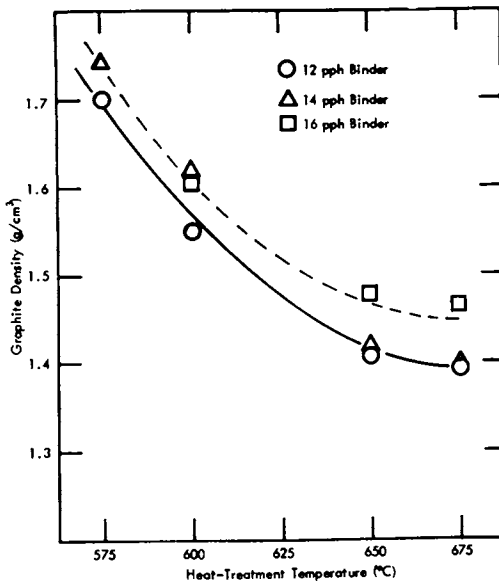
Figure 5.   The effect of the A-240 pitch heat-treatment temperature on the density of graphites fabricated from A-240-derived cokes
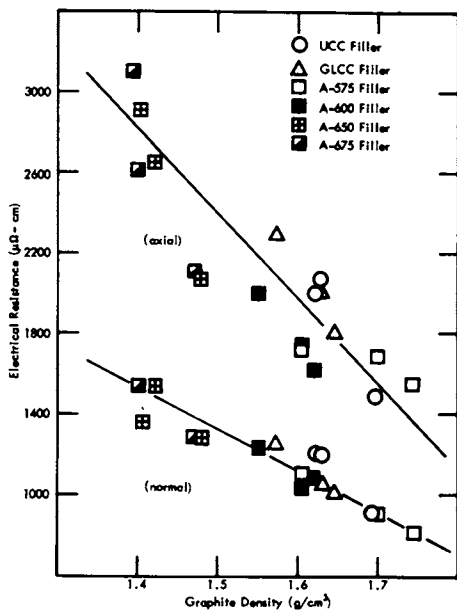
Figure 6. The effect of final graphite density on the electrical resistance of graphites fabricated from green cokes
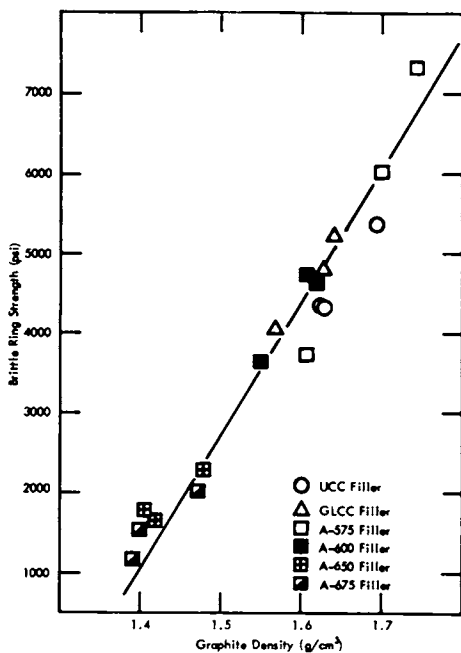
Figure 7. The effect of final graphite density on the strength of graphites fabricated from green cokes
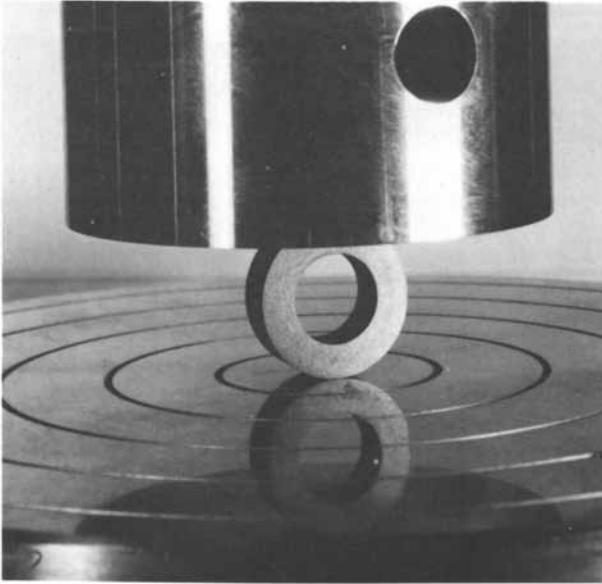
Figure 8.   Brittle ring sample under test
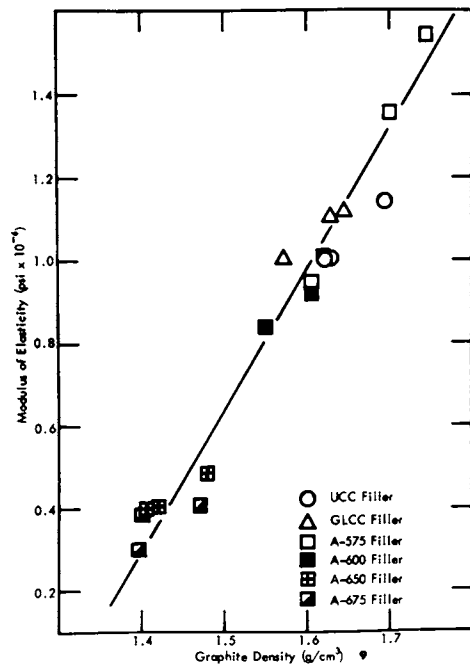
Figure 9.   The effect of final graphite density on the modulus of elasticity of graphites fabricated from green cokes
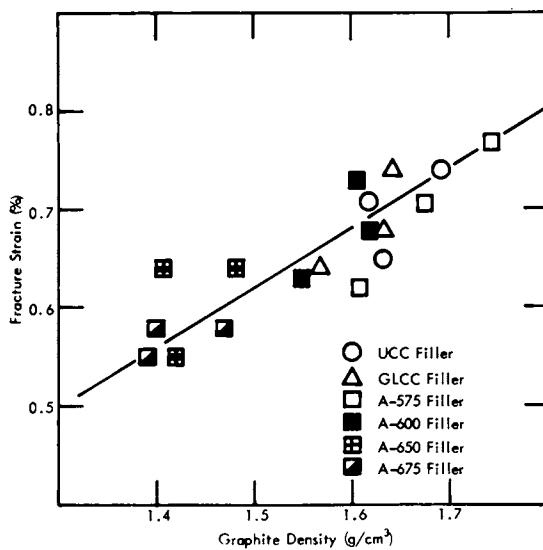
Figure 10. The effect of final graphite density on the fracture strain of graphites fabricated from green cokes

Figures 9 and 10 indicate that both the modulus of elasticity and fracture strain, respectively, increase as the graphite density increases.

Conclusions

In conclusion, graphites fabricated from A-240-derived green cokes show similar properties to graphites fabricated from high-quality acicular cokes. Graphite densities equal to or surpassing the densities of bodies fabricated using either the UCC or GLCC fillers were obtainable by the choice of the appropriate A-240 coke preparation temperature and the appropriate binder content. Properties of the graphites fabricated from the A-240-derived cokes were dependent upon achievement upon heat treatment temperature. Graphites fabricated from pressure-coked A-240 pitch yielded much lower electrical resistivities than expected from density/resistivity relationships. However, other properties were similar to those obtained from the UCC, GLCC, and other A-240-derived cokes. Thus, high-quality acicular cokes can be easily prepared from A-240 pitch and these cokes exhibit similar properties to other high-quality acicular cokes.

Literature Cited

1. Kennedy, C. R., and Eatherly, W. P., 11th Biennial Conference on Carbon, Gatlinburg, Tennessee, June 4, 1973, CONF-730601, p. 131.
2. Kennedy, C. R., and Eatherly, W. P., 11th Biennial Conference on Carbon, Gatlinburg, Tennessee, June 4, 1973, CONF-730601, p. 304.

Pressure Carbonization of Petroleum Pitches

R. L. BURNS and J. L. COOK

Fiber Materials, Inc., Biddeford, Maine 04005

Densification of graphite and woven fibrous composites is accomplished by the impregnation of the open porosity with a liquid carbon precursor and the conversion or carbonization in situ to a solid carbon and the transformation to graphite by heat treatment. Conventionally, the densification process is conducted at atmospheric pressure and must be repeated several times to reduce the porosity to an acceptable level. The multiplicity of cycles and the ensuing long process times are the result of the following characteristics: 1) low-carbon yield from the carbon-bearing liquid impregnant, 2) premature flow of the impregnant from the pores of an impregnated body during carbonization, 3) lack of sufficient impregnating pressure to thoroughly and uniformly impregnate a composite, 4) large volumetric shrinkage of the impregnant, 5) slow carbonization cycles required to obtain isothermal heating, and to minimize the effects of gas evolution from the carbonizing impregnant.

As the result of these limiting characteristics, a technique was developed by Cook and Lambdin(1) at the Oak Ridge Y-12 Plant, Oak Ridge, TN, which utilized an isostatic pressure to effectively impregnate carbon composites continuously during the melting and heating phase of the carbonization cycle. This work showed that carbon or graphite fibrous composites with a pitch binder could be successfully compacted and carbonized in a sealed can with 95% conversion of the carbon precursor binder to solid carbon. Further work both at Oak Ridge and Fiber Materials showed that the pressure carbonization technique with its characteristic high carbon yields was advantageous to the densification of woven carbon and graphite structures.

In related work, Price and Yates(2) baked graphite precursor composites to 800°C under pneumatic pressure at a temperature increase of 6°C per hour. This gave increased densities, reduced variability between samples, and permitted baking rates which, under normal conditions, would induce unacceptably high weight losses. Others(3) have used isostatic mechanical pressures up to 2200 psi by means of an impermeable, deformable sample container.

Equal gas pressure was maintained and controlled inside the
container by a separate connection until the desired process
temperature (590°C) was reached. The internal pressure was then
released which permitted compaction of the preformed specimen.
     Analagous processing(4) reveals the confining of a molded
composite of carbon in a substantially pressure-tight container
in which gaseous pressures above atmospheric can develop during
baking or by increasing the temperature.
     Recently, the studies of Dr. E. Fitzer and co-workers(5) in
Germany have confirmed the utility of the pressure-carbonization
technique. Also, they have shown that the extreme pressures
(15,000 psi) utilized in the early Oak Ridge studies were not
required to obtain the increased carbon yield.
     This paper discusses the effect of pressure, from 500 to
15,000 psi on densification rate, microstructure, and coking
yield for petroleum pitches. Microscopy is used to show the
development of a carbon from the liquid precursor.

Description of Pressure Carbonization

     Pressure-impregnation-carbonization (PIC) of pitch materials
as a technique for the densification of carbon/carbon composites
has received only a limited amount of attention. The PIC tech-
nique being employed by Fiber Materials is based on results of
previous works(1,5) and the confirming data presented in Table I.

Table I

Effects Of Pressure On The Densification Rate
For Pitch Impregnated C/C Composites

| Pressure (psi) | Coke Yield | Density (g/cc) | |
		Initial	Final
Atm.	51%	1.62	1.65
1,000	81%	1.51	1.58
7,500	88%	1.59	1.71
	89%	1.71	1.80
15,000	90%	1.66	1.78

     A schematic of the densification process is shown in Figure
1. A composite to be densified is initially vacuum-pressure im-
pregnated using conventional methods and carbonized while sub-
merged in the pitch impregnant. This initial cycle is not
performed under pressure to prevent damage or distortion to the
composite. When the part has completed this treatment, it has
the rigidity and strength to be processed through a PIC cycle.
The PIC cycle involves a stainless steel container holding the
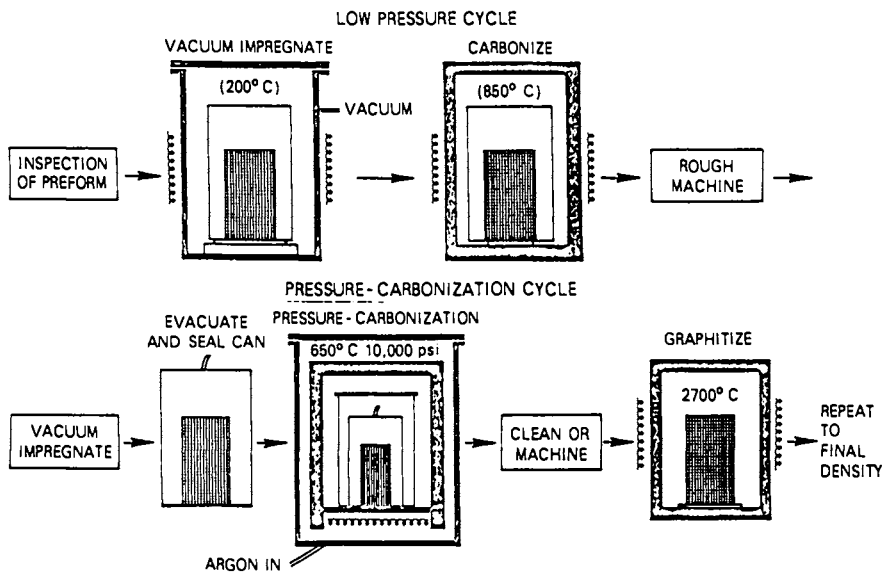
Figure 1. Densification of C/C material

composites which is then placed in a gas autoclave then heated
and pressurized at controlled rates. A typical PIC cycle requires
about 24 hours. The parts are removed from the inner container
and graphitized. The cycle is repeated until the final density is
obtained.

The rate of densification is dependent upon the type impreg-
nant, the coking yield of the impregnant, the volume of porosity
open to the impregnant, and the degrees of filling of this poro-
sity. For a typical petroleum pitch, the standard condition (1
atmosphere) coking yield is 45-55 weight percent. However, the
carbon content for such a pitch is usually greater than 90 percent.
Therefore, a significant amount of the available carbon is lost
during carbonization which results in a smaller density increase
for the composite. By the application of a gas overpressure, the
more volatile compounds forming within the heated pitch are pre-
vented from evaporating and likely form into higher molecular
weight polyaromatics.

Increased coking yield was initially considered the single
most important advantage of the PIC technique. However, as com-
posites were developed with smaller and more tortuous porosity,
the advantage of the isostatic pressure during the impregnation
phase of a PIC cycle was realized. As the petroleum pitch melts
and expands, the pressure on the container maintains a compressive
force on the pitch and thus, prevents runout from pores. In fact,
the pressure improves the uniformity of pore filling as the vis-
cosity of the petroleum pitch decreases with increasing tempera-
ture. This results in a more uniform composite microstructure as
the PIC cycles are repeated.

The final advantages of pressure carbonization will develop
as our understanding of the effects of pressure on carbon micro-
structure and composite performance evolves. For many years,
graphite fabricators have been able to tailor the microstructure
by altering the precursor material or using mechanical operations
such as grinding. The PIC technique may offer an additional con-
trol of the final product. This paper deals with a preliminary
examination of carbon precursors subjected to pressure carboniza-
tion.

Experimental

The objective of the experiments performed are to show (1)
microstructural changes during carbonization (2) effects of
pressure during carbonization on coking yield, microstructure,
density, and (3) comparison between petroleum pitch and other
precursor materials.

To compare the effects of pressure on physical properties,
pressure-carbonization of samples of Ashland Oil Company's Grade
240 petroleum pitch and Grade LS-24 were processed. A constant
pressure level was maintained on the samples as the temperature
was increased to 550 to 650°C. The coke formed from the two

materials was then evaluated. A comparison of physical proper-
ties for the unprocessed precursors is listed in Table II.

Table II

Comparision of Physical Properties of Ashland Oil Company's
Grade A-240 and LS-24 Petroleum Pitch

Property	A-240	LS-24
Benzene Insoluble (%)	4.8	4.2
Quinoline Insoluble (%)	Nil	Nil
Coking Value (%)	52.1	51.5
Ash (Wt. % Max.)	0.11	0.02
Sulfur (%)	1.6	0.05-0.1

After subjecting the samples to various pressures and
temperatures, the physical properties of the resulting coke and
graphite were compared. These properties included coke yield,
density and open porosity at each pressure of 500, 1000 and
10,000 psi.
     These same two materials were also examined for the develop-
ment of mesophase. In this experiment, equal weights of LS-24
and A-240 pitch were placed in stainless steel containers, each
having the same exposed surface area. A temperature of 350ºC
was arbitrarily chosen and the materials were baked until the
mosaic structure collapsed into a coke. Samples of the two
impregnants were removed at various intervals and examined for
the development of mesophase.
     Additional carbon precursors such as Allied Chemical
Company's Grade CP-277-15V coal tar pitch and Cinnamylideneindene
were processed at varying pressure levels and compared to the
baseline petroleum pitch materials.

Results

     In Tables III and IV are listed the density and porosity
measurements of A-240 and LS-24 processed at varying pressure
and temperature levels.

Table III

Comparison of Ashland Oil Company's Grade A-240 and LS-24
Carbonized at 550°C Under Noted Pressure Levels

Property	A-240			LS-24		
	500psi	1000psi	10,000psi	500psi	1000psi	10,000psi
Bulk Dens. (gm/cc)	0.85	0.75	1.04	0.79	0.72	0.87
Apparent Dens. (gm/cc)	1.37	1.33	1.31	1.37	1.34	1.36
Open Porosity (%)	37.9	43.6	20.4	42.5	46.0	35.8

Table IV

Comparison of Ashland Oil Company's Grade A-240 and LS-24
Carbonized at 550°C Under Noted Pressure Levels,
Subsequently Heat Treated to 2600°C

Property	A-240			LS-24		
	500psi	1000psi	10,000psi	500psi	1000psi	10,000psi
Bulk Dens. (gm/cc)	0.85	0.78	1.05	0.90	0.93	1.08
Apparent Dens. (gm/cc)	1.63	1.57	1.69	2.18	2.16	2.14
Open Porosity (%)	47.9	50.3	38.0	58.5	57.0	49.5

Table V lists the coke yield of A-240 and LS-24 at various pressures.

Table V

Pressure (psi)	Coke Yield (%)	
	A-240	LS-24
15	52.1	51.5
500	81.0	76.9
1000	81.3	79.8
10,000	--	80.5
15,000	86.2	--

It can be seen from the preceding tables that isostatic pressure during carbonization has a marked effect on the physical properties and char yields of carbon precursors. It also can be seen that minor variations in the pitch characteristics affect the physical properties of the processed coke.

To further explore pressure effects, the microstructures of the precursors were examined and also found to vary. Figures 2, 3, and 4 illustrate the microstructure of the cokes and graphites formed at various pressures.

Metallography showing the mesophase development for A-240 and LS-24 is compared in Figures 5, 6, 7 and 8. Figures 5 thru 7 compare the rate of growth and size of mesophase for A-240 and LS-24 pitch. As can be seen, mesophase formation from LS-24 shows a more rapid and uniform development than A-240 pitch.

Figure 8 shows the coalescence of mesophase droplets into larger structures. This SEM confirms the round shape of mesophase and the joining of smaller droplets into a larger mosaic structure.

Figure 9 compares three carbon precursors, petroleum pitch, coal tar pitch and a synthetic precursor. All were processed the same and all three cokes illustrated varying structures and grain sizes. Further work in this area must be performed to be able to correlate a resulting microstructure with the properties of the precursor.

Conclusion

The following conclusions can be made from the experiments conducted.

The microstructure of the coke has a definite relationship to the graphite formed. In the tests conducted, various structures of coke formed varying structures of graphite.

Increases in pressure of carbonization increase the coking yield. Lower pressures in the 500-1000psi region account for the most significant increases. Above 10,000psi, the increase in coking yield becomes negligible.

Increase in pressure of carbonization results in what appears to be a more graphitic structure. When the pressure of carbonization exceeds 2000psi, a more graphitic material was formed.

The grain size of the graphite was also related to pressure of carbonization. Higher pressures tend to form a finer grain material.

The experiments performed in this evaluation only provided qualitative inputs to the conclusions that were made. A detailed quantitive examination must be undertaken to define and correlate the effects of isostatic pressure on microstructure and composite performance. These tests and results were performed to provide guidelines for future development. As can be seen, mesophase from LS-24 shows more rapid and uniform development and growth than A-240.
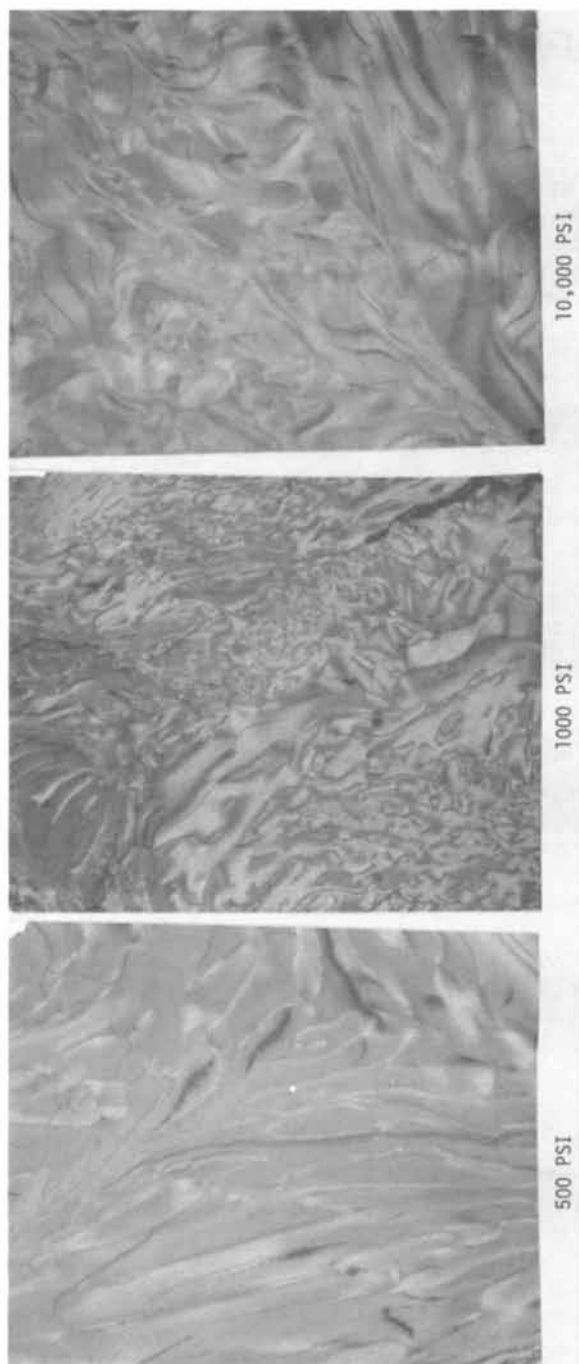
Figure 2. Microstructure of Ashland Oil Co.'s grade 240 petroleum pitch coked to 550°C under isostatic pressure of 500 psi, 1000 psi, and 10,000 psi (85×)
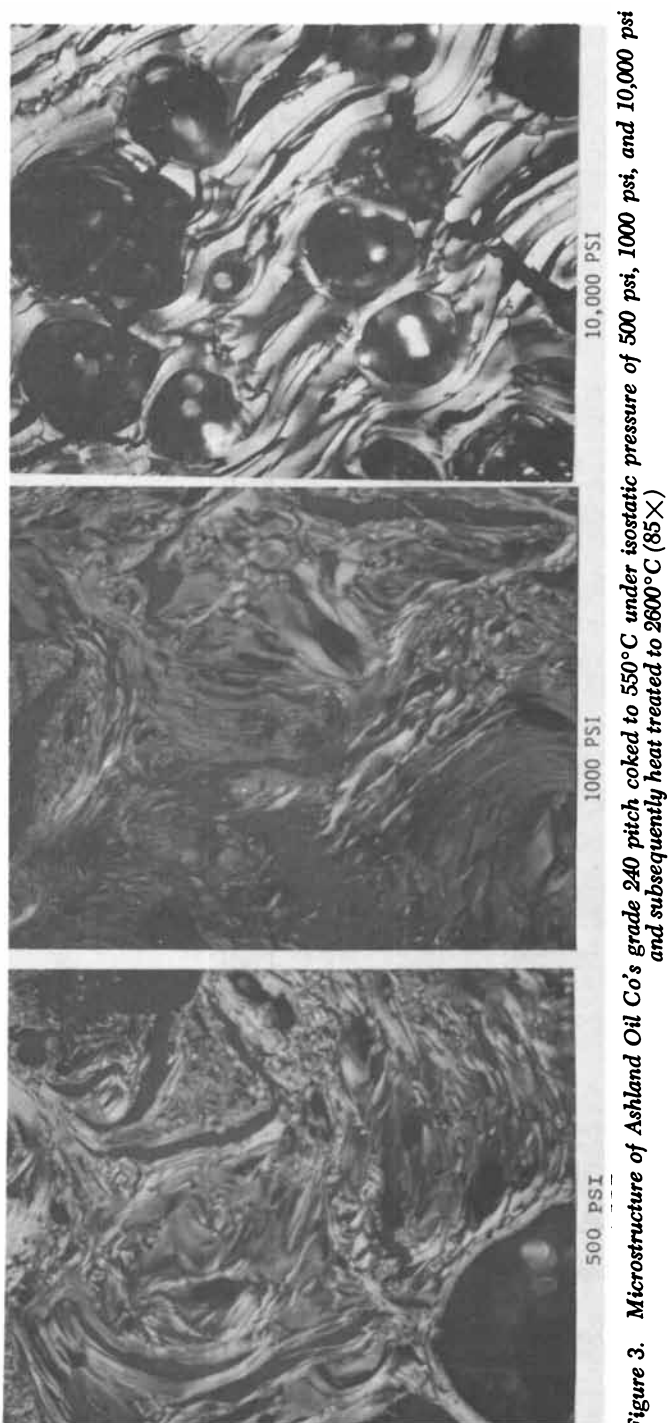
Figure 3. Microstructure of Ashland Oil Co's grade 240 pitch coked to 550°C under isostatic pressure of 500 psi, 1000 psi, and 10,000 psi and subsequently heat treated to 2600°C (85×)
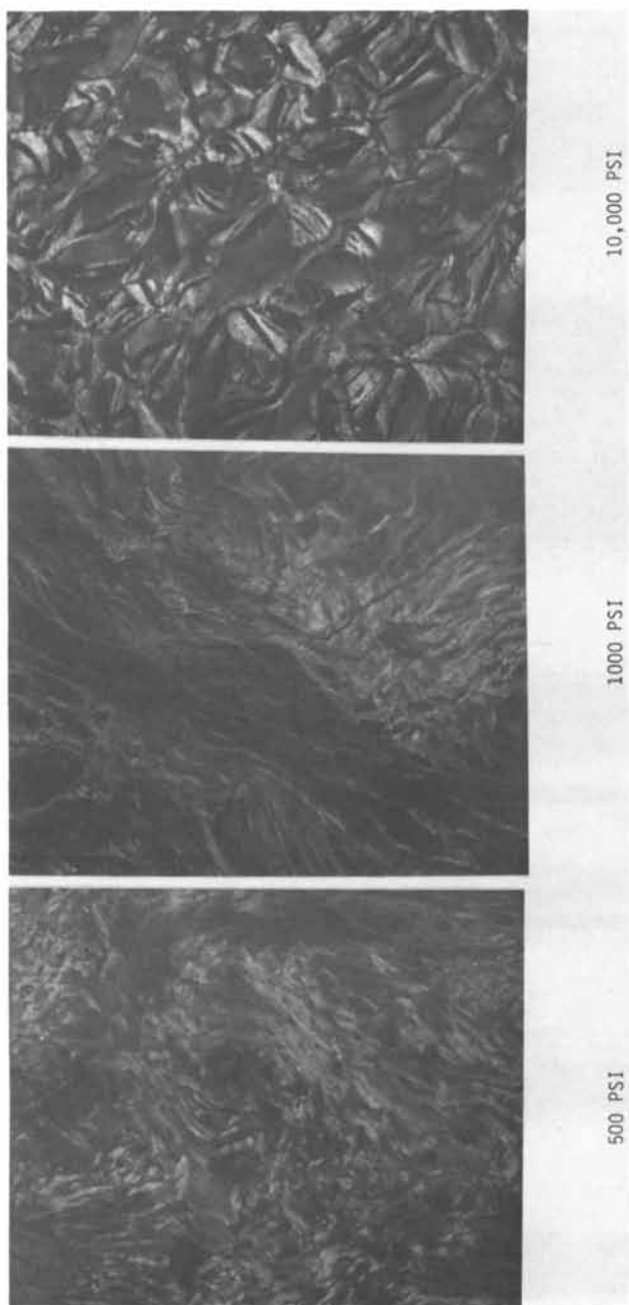
Figure 4. Ashland Oil Co.'s grade LS-24 coked to 550°C under isostatic pressure and subsequently graphitized to 2600°C (85X)
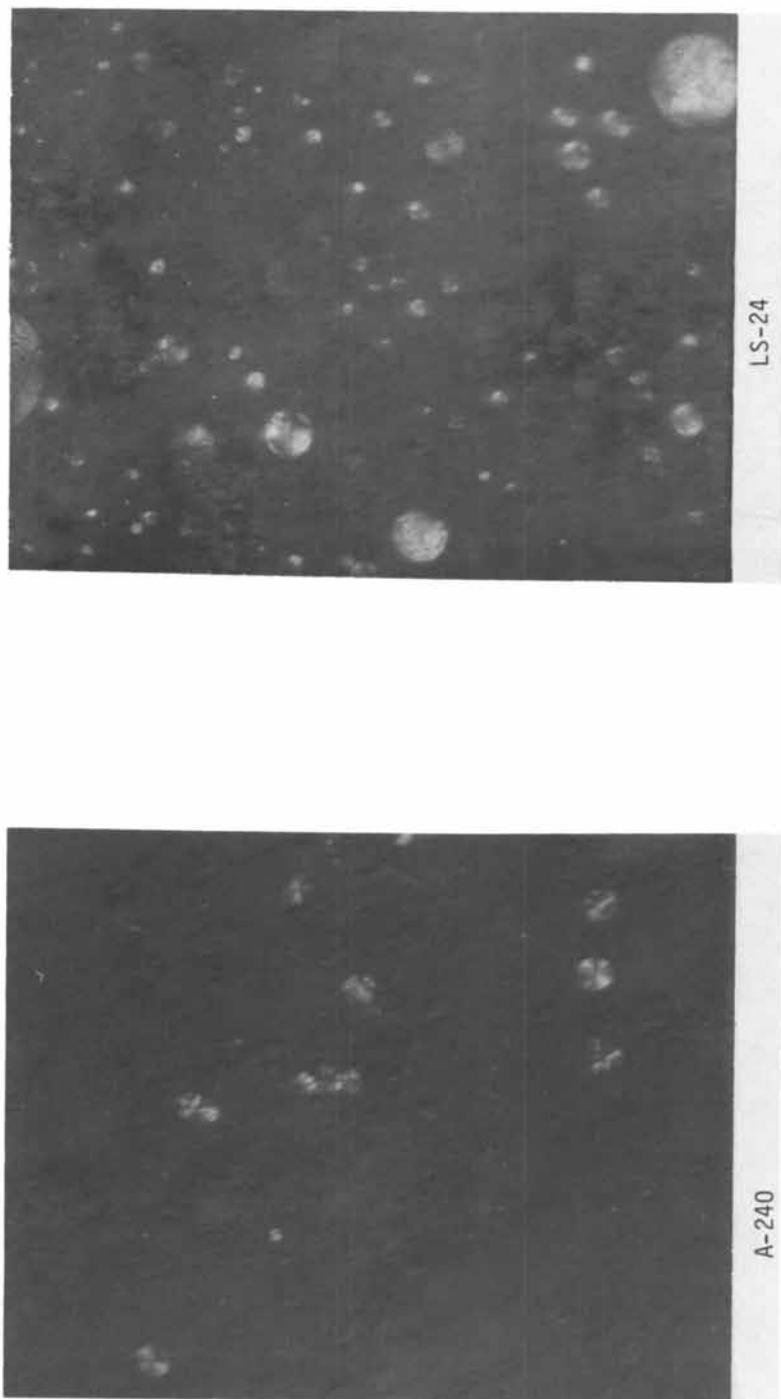
Figure 5.   Ashland Oil Co.'s grade A-240 and LS-24 heat treated at 350°C for 115 hr (340×).
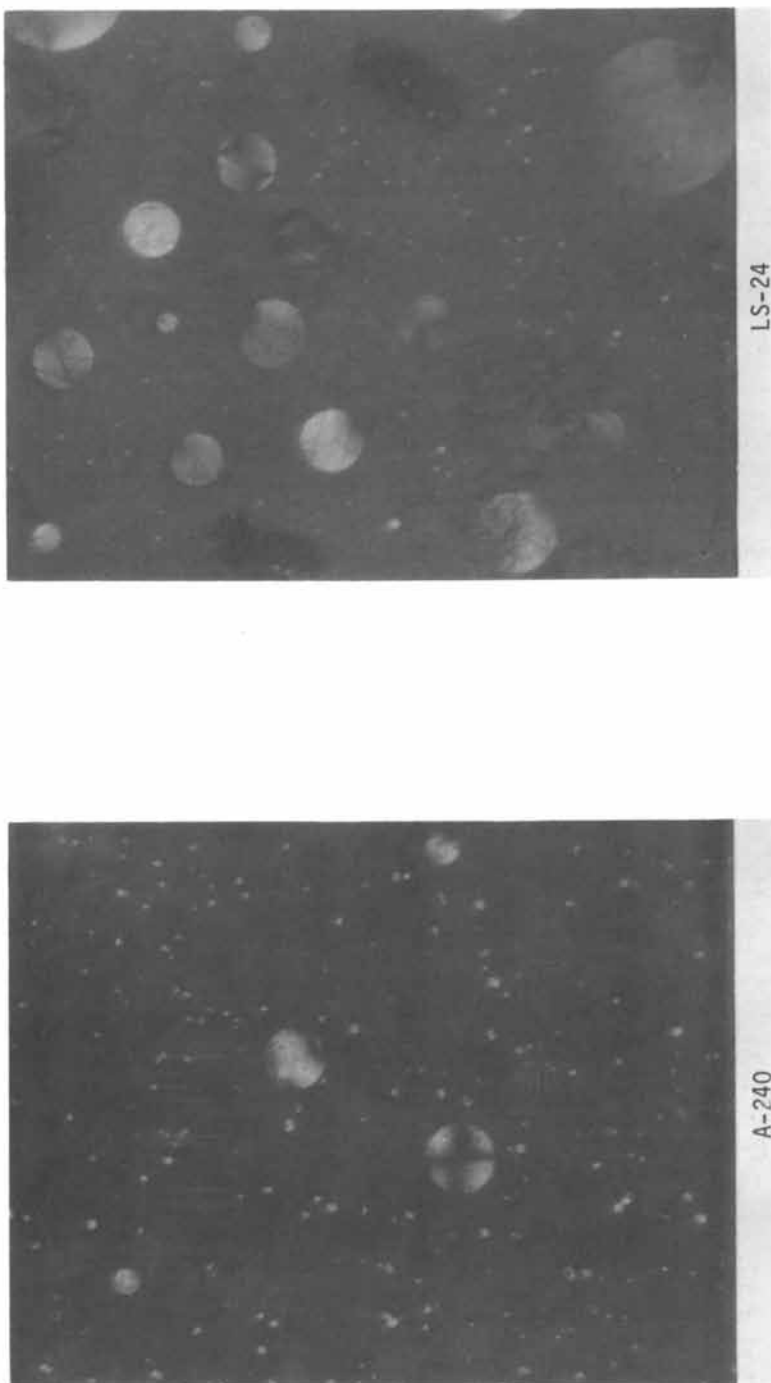
Figure 6. Ashland Oil Co.'s grade A-240 and LS-24 heat treated at 350°C for 161 hr (340×)
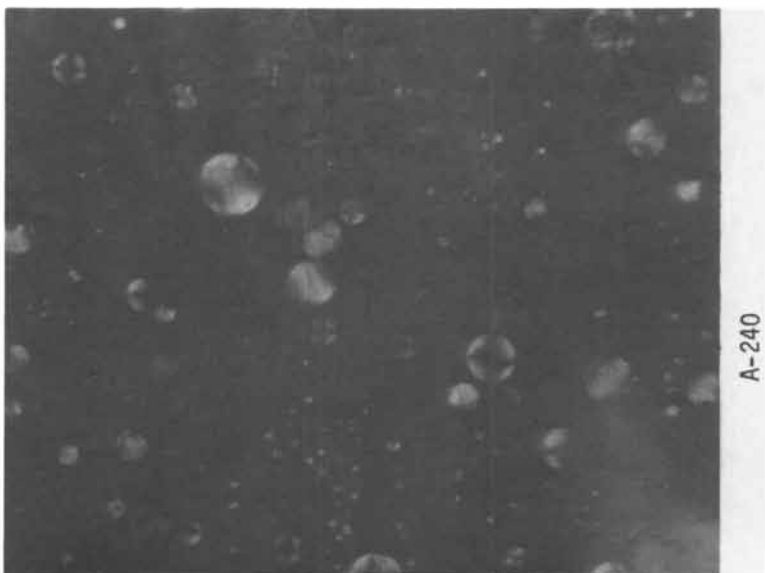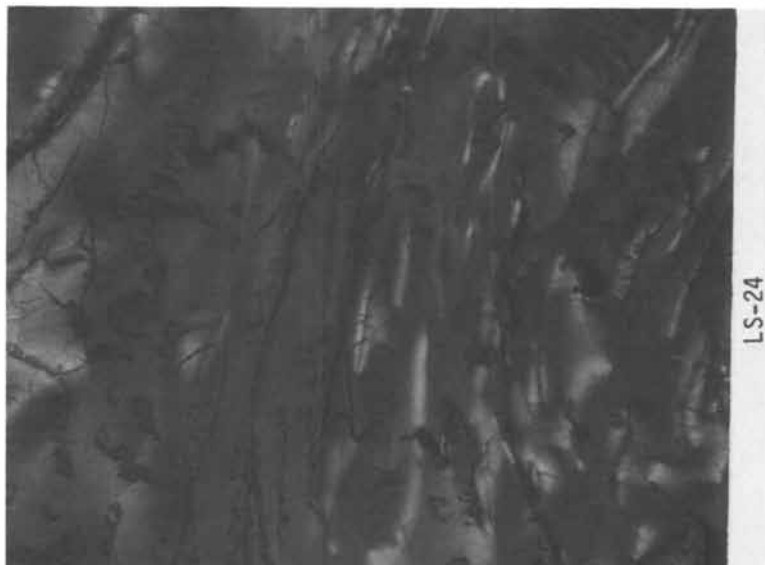
Figure 7. Ashland Oil Co.'s grade A-240 and LS-24 heat treated at 350°C for 204 hr (340×)
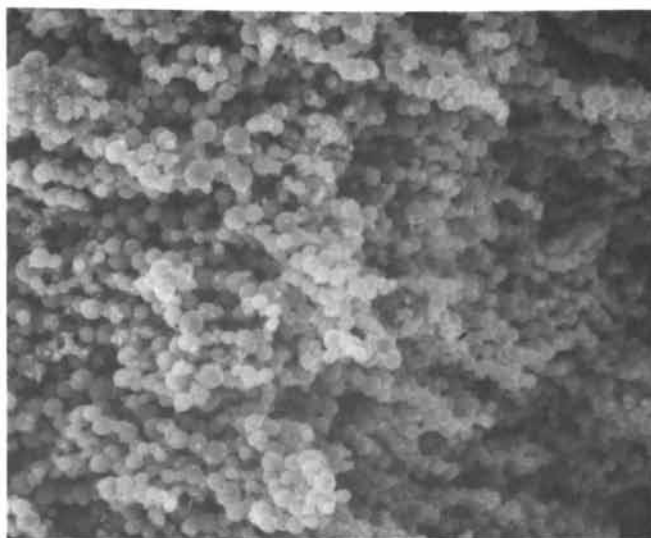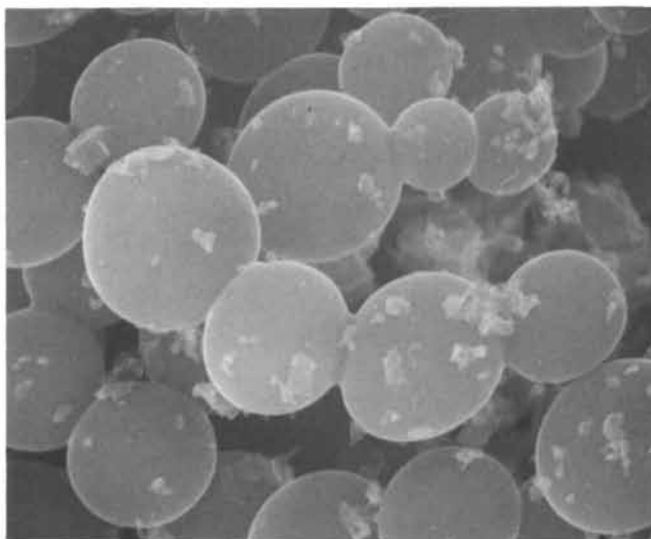
Figure 8. Ashland Oil Co.'s grade A-240 petroleum pitch—mesophase formation (left, 255×; right, 2550×)
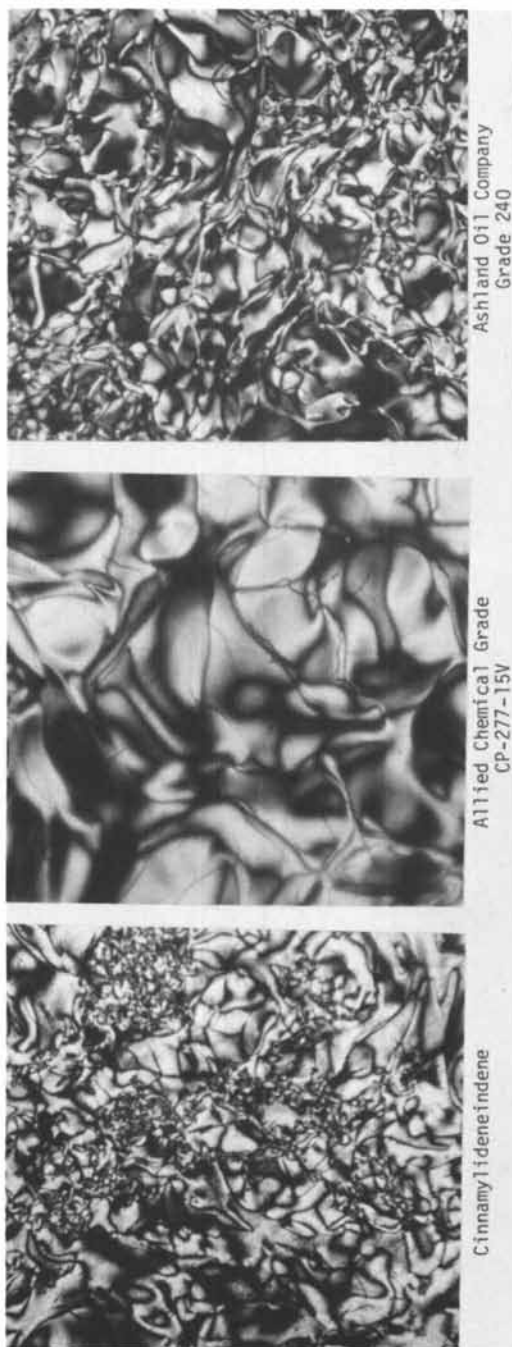
Figure 9. Comparison of microstructure for carbon precursors coked to 650°C under isostatic pressure of 750 psi (212×)

Literature Cited

(1) Cook, J.L. and Lambdin, F., "Fabrication of Discontinuous, High-Fiber Content, Isotropic Carbon/Carbon Composites", Report No. Y-1784, Oak Ridge Y-12 Plant, Oak Ridge, TN (1971).
(2) Price, M.S.T. and Yates, F.W.; Conference of Industrial Carbon and Graphite, pp 111-125; Society of Chemical Industry, London, England (1958)
(3) Pressure Baking, USAF Contract Number AF33 (657) 11738 with Great Lakes Research Corporation; Elizabethton, TN (1964)
(4) "Improvements in or Relating to Production of Carbon Masses", United Kingdom Patent 759, 160.
(5) Dr. E. Fitzer and B. Terwiesch, Carbon Vol. 11, pp 570-574 (1973).

14

Advanced High Pressure Graphite Processing Technology

WILLIAM CHARD, MICHAEL CONAWAY, and DALE NIESZ

Battelle, Columbus Laboratories, Columbus, Ohio 43201

Since the early 1800's when Sir Humphrey Davy utilized
carbonized-wood rods for generating an electric arc, the carbon
and graphite industry has grown steadily. Today the industry
supplies materials ranging from 55-in.-diameter graphite cylinders
for large metallurgical crucibles and arc-melting electrode
applications to 1/8-in.-diameter high-purity electrodes for arc
lights. In general, the materials supplied for these applications
are fabricated by conventional extrusion techniques. Special
molding and hot-working techniques have been developed for fabrica-
ting more homogeneous, refined graphite materials for certain
specialized applications such as ballistic-missile nose tips and
rocket nozzles. However, companies in the industry are slow to
accept new processing technology or to go outside of their own
organizations for advanced developments. The term "Black Art"
appropriately fits the industry, as considerable art and experience
are typically required to guide the manufacturing practices.
    This paper describes recently developed high-pressure
processing techniques utilizing hot-isostatic-pressing (HIP)
equipment and procedures for use in fabricating unique graphites
and carbon-carbon composites. This process is by no means a
laboratory curiosity. Several manufacturers are producing this
equipment and equipment systems commercially and autoclave or
pressure vessels with working areas as large as 4 ft in diameter
by 10 ft long are currently available at Battelle's Columbus
Laboratories for processing studies. This paper briefly reviews
the current graphite-processing technology, discusses the HIP
process, and summarizes some of the advantages of utilizing this
process to fabricate carbon and graphite structures.
    The graphite structures of most interest here are considered
to be specialty graphites. These are fine-grained, reasonably
isotropic, high-density, homogeneous, multigranular materials.
These materials are typically considered for use as aerospace and
reentry materials, bearing seals, special electrodes, nuclear

155

reactor components, semiconductor fixtures, and other applica-
tions where high-performance standards are required. Other
specialty carbon-base materials such as advanced carbon-carbon
reinforced structures, fiber-base graphites, and multiparticulate
composites are also included.

Conventional Graphite-Processing Techniques(1,2,3)

Certain inherent physical and chemical limitations have
been imposed on the organic presursors used to produce carbon
and graphite structures,which in turn impose restrictions on the
method of fabricating these material. The major areas of difficulty
are (1) the nature and amount of volatile outgassing constituents
evolved during the pyrolysis of organic precursors, (2) the
complex chemistry and wide variability of organic-base materials
used in processing carbon and graphite and their sensitivity to
pyrolysis environments, and (3) the limitation in equipment
available for processing these materials at temperatures up to
2800 C.

Bulk graphites are, in fact, composites of carbon particulates
bonded together by a second carbon-binder phase. Additional
carbon phases may be introduced by impregnation of an organic
material into the pore structure of a typically subdense multi-
granular bulk carbon or graphite. Fiber-base graphites are
composites that have a chopped fiber-filler substituted for a
particulate grain filler. Carbon-carbon composites are materials
that possess a continuous fiber structure which dominates or
defines the properties of the composites and the materials are
typically identified as "reinforced" structures because of the
carbon-fiber phase. A wide range of properties and character-
istics can be attained in carbon-base materials through the
selection of filler, binder, and impregnant precursor materials;
coking procedures; method of consolidating or forming (extrusion,
molding, hydropressing); processing-temperature sequences and
ultimate temperatures reached; manufactured-product size and shape
and other material and processing factors. These complex combina-
tions are not simple. Table 1 lists several typical commercial
carbon products with representative properties.

The conventional methods of processing commercial bulk
graphite are by an extrusion and molding technique with several
subsequent baking (pyrolysis) and impregnation steps, as
illustrated in Figure 1. Hydrostatic pressing and hot-working
methods have seen limited development within the last 20 years
and are applied basically to the manufacture of specialty,

---

(1)   Carbon and Graphite Handbook (1968), Interscience Publishers,
      Charles Mantell.
(2)   Carbon and Graphite (1965), Academic Press, E. I. Shobert.
(3)   The Industrial Graphite Engineering Handbook, Union
      Carbide.

TABLE 1. TYPICAL PROPERTIES OF SEVERAL COMMERCIAL CARBON-BASE MATERIALS

Designation	Forming Method	Grain Size, in.	Density, g/cc	Direction(a) of Property Measurement	Tensile Strength, psi	Flexure Strength, psi	Young's Modulus, 10^6 psi	Thermal Expansion at 0-212 F, 10^{-6}/in.
Pyrolytic	CVD[b]	—	2.25	W A	14,000 1,500	21,000 1,500	4.4 1.7	0.2 10.8
ATJ	Molded, impregnated	0.006	1.73	W A	4,200 3,000	4,100 3,600	1.4 1.1	1.2 1.9
ATJS	Molded, impregnated	0.006	1.85	W A	5,000 4,200	5,400 5,100	1.5 1.1	1.2 1.6
ZTA	Hot worked or recrystallized	0.006	1.95	W A	4,400 1,500	5,200 2,500	2.5 0.9	0.5 3.8
Graphitite G	Extruded, impregnated	0.03	1.89	W A	2,800 1,800	3,200 2,600	1.4 1.2	0.6 1.9
AXF-5Q	Hydrostatic pressed	0.001	1.85	W A	10,000 10,000	12,000 12,000	1.7 1.7	3.2 3.2
Glassy Carbon (GC-20)	Molded Resin	—	1.47	—	6,100	10,500	3.8	2.1
Carbitex 700	2DC/C cloth layup	—	1.42	W A	5,500 300	9,000 —	1.7 0.4	0.4 1.6
RPG	CVD C/C felt	—	1.8	W A	6,000 2,600	8,000 —	1.9 1.0	0.2 1.4
2.2.3	Woven 3DC/C, impregnated	—	1.85	x-y[c] z	18,000 35,000	— 27,000	8.0 15.0	-0.30 -0.20

(a) W - With the grain (a-b direction)
    A - Against the grain (c direction).

(b) Chemical vapor deposit.
(c) Fiber orientation, z indicates longitudinal.
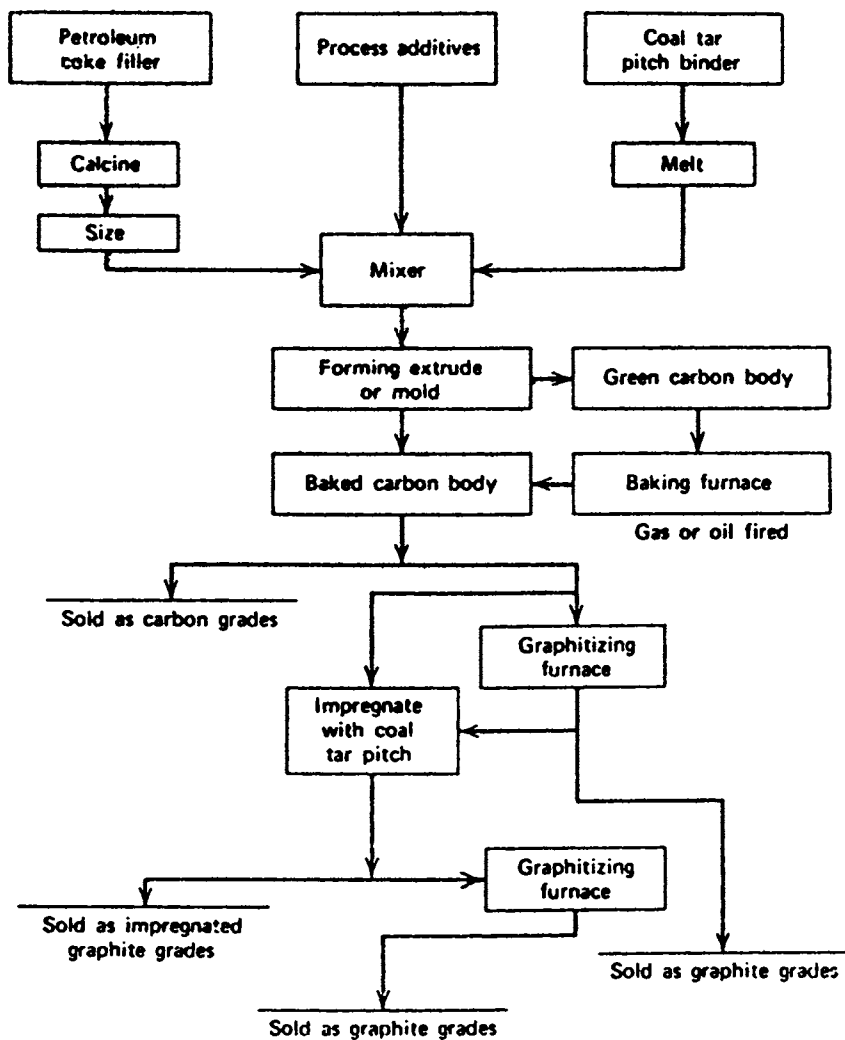
Figure 1.   Typical graphite manufacturing process

refined graphites. The fabrication process have several modifica-
tions which are employed to produce material of certain desirable
characteristics. All of these processes depend on consolidating
a thermoplastic carbon mass at either low temperatures, 150 to
250 C, or high temperatures, 1100 to 2600 C. These processes
typically require mixing of a coke or graphite flour with an
organic binder such as coal-tar pitch. Additives such as lamp or
carbon black are mixed in to obtain certain desirable properties.
The composition is mixed to blend the batch constituents before
heating to about 150 C, at which time the thermoplastic binder
allows the material to be consolidated by molding or extusion.
These green products are cooled and then baked or coked at about
950 C. This heat treatment allows the binder phase to lose its
volatile constituents and yields an extremely hard and porous,
solid, carbon mass. This operation may take an entire month to
complete. Multiple impregnation operations are commonly performed
with intermittent heat treatments to increase the density of the
material or decrease its permeability. The final thermal treat-
ment, graphitization, converts the hard noncrystalline carbon
article to softer crystalline graphite and is performed at around
2800 C. This conversion is very much dependent on the organic
precursor and the ultimate temperature attained. The cycle for
this operation may be 1 to 5 weeks.

   Hydrostatic-press-formed and hot-worked-recrystallized
graphites have been developed on a very limited basis to yield
certain specialized properties.(4) Hydrostatic-press-formed
graphites are reasonably isotropic, whereas moderately dense,
hot-worked-recrystallized graphites are anisotropic and of high
density. Typically, graphite materials receive several thermal
treatments and impregnations during their manufacture and total
processing times of up to 5 months may be experienced. The advent
of hot-isostatic-pressing (HIP) offers considerable potential for
fabricating a wide range of carbon-base materials with unique
refined and uniform microstructures in short processing times.

Advanced Processing Techniques

   Battelle's Columbus Laboratories initiated the development of
the hot-isostatic-pressing (HIP) process in the mid-1950's for
fabricating metal-clad nuclear-fuel elements.(5) Since that time,

---

(4)   "Research and Development on Advanced Graphite Materials,
      Volume VII-High Density Recrystallized Graphite by Hot-
      Forming", WADD-TR 61-72 (June, 1962).
(5)   Proceedings of the Second United Nations International
      Conference on the Peaceful Uses of Atomic Energy (September,
      1959), S. J. Paprocki, E. S. Hodge, and C. B. Boyer.

the process has developed into a commercially viable (6) technique
for fabricating specialty materials. The process is used
commercially to manufacture high-performance powder-metallurgy
materials with controlled homogeneous microstructures and out-
standing mechanical properties.
    The processing equipment consists of a large water-cooled
gas-pressure vessel with an internal furnace. A schematic of the
HIP processing system is shown in Figure 2, which typically
consists of a gas storage facility, high-pressure gas transfer
lines, a compressor, a high-pressure vessel or autoclave, and
an autocalve furnace. The material to be processed is typically
encapsulated in a hermatically sealed metal container and placed
in the autocalve for processing as shown schematically in
Figure 3. A schematic illustration of a high pressure autoclave
is shown in Figure 4. As the sample is heated, gas pressure is
applied to the sample container which consolidates or presses the
sample within. The gas is normally argon or helium, most of which
is reclaimed and reused (approximately 80 volume percent). At
elevated temperatures, the metal encapsulating container becomes
extremely plastic and acts like a "rubber bag", transmitting the
autoclave gas pressure to the sample and thus causing densifica-
tion. The diffusion rate of the autoclave gas through the
encapsulating metal container is normally very low and the hermatic
seal prevents gas from entering into the sample. The basic
advantages of the process are summarized as follows:
    (1) Effective consolidation utilizing high isostatic
        gas pressure for densification
    (2) The control of fabricated materials' microstructure
        with the use of high-isostatic-pressure consolida-
        tion and low sintering temperatures.
    (3) Precise control of process parameters
    (4) Versatility in the ability to process a wide
         range of materials at a wide range of processing
         parameters
    (5) The ability to process large and unusual geometric
         parts
    (6) The capability to process large parts with less
         concern for aspect ratios (length/diameter) or
         for size limitations found with unidirectional
         hot pressing
    (7) Production capability through large-volume
        capacities and short process turn-around times.

_____

(6)   "Solid-State Bonding and Consolidation of Powders Under
      Hot-Isostatic Pressure", C. Boyer, H. Hanes, K. Meiners,
      F. Orcutt, ASME Paper 71-WA Prod-20, July 15, 1971.
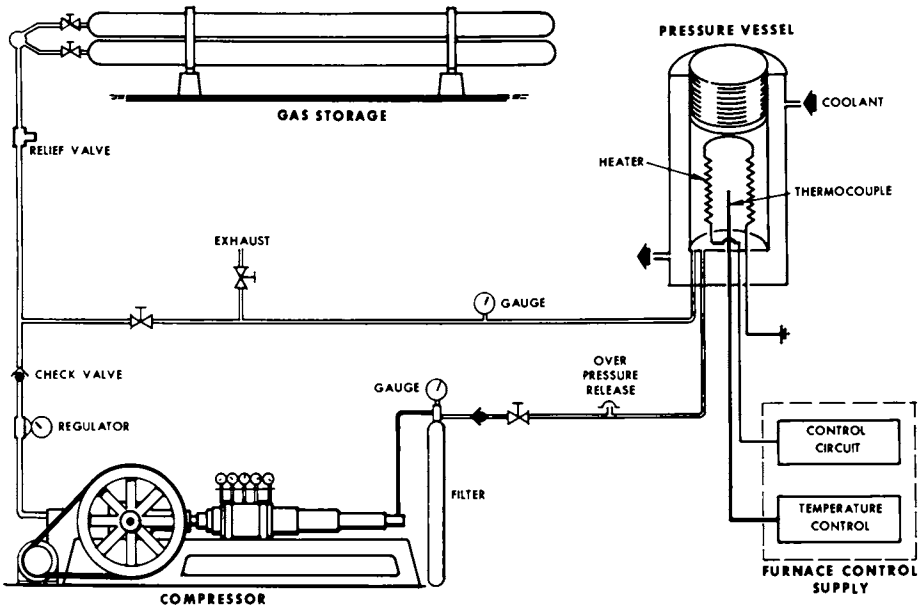
Figure 2. Simplified schematic of hot isostatic pressure system
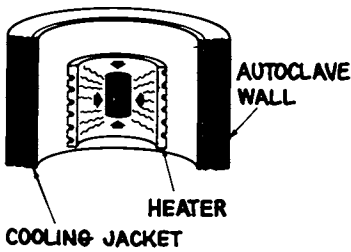
Figure 3. Schematic of high pressure process

INTERRUPTED THREAD CLOSURE

RUPTURE DISC ASS'Y.

COOLANT LINE

SPIRAL-GROOVED LINER

MICRO-QUARTZ

THERMOCOUPLES

ALUMINA

SPOOL HEATER

PLATE ELEMENT

PLUG-IN CONNECTOR PLATE

VACUUM LINE

ELECTRICAL LEADS FROM HEATER

MULTIPLE THERMOCOUPLE LEAD THROUGH
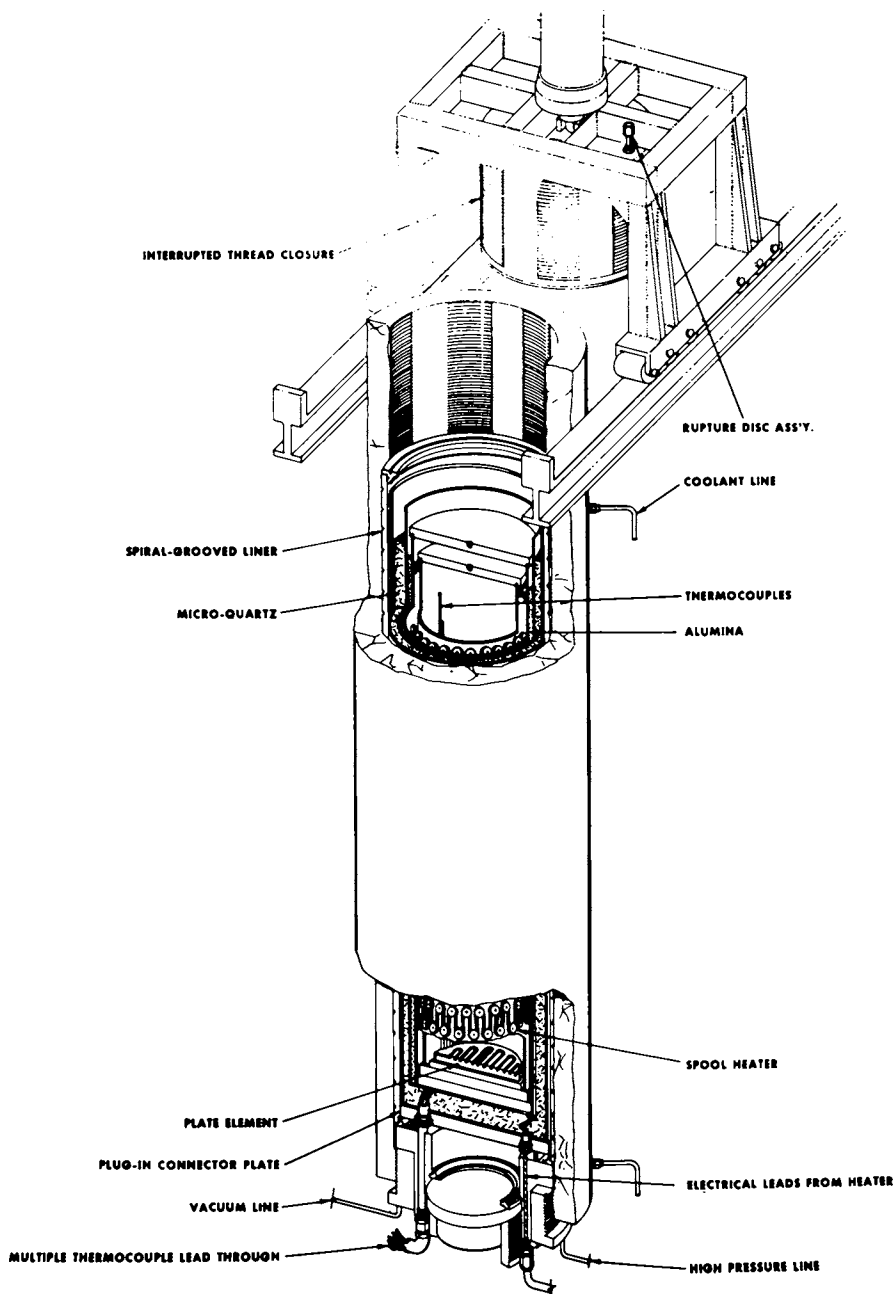
HIGH PRESSURE LINE

Figure 4.   Schematic of HIP processing equipment

A wide range of autoclave sizes are available, as indicated in Table 2, which briefly outlines the current capabilities of Battelle's Columbus Laboratories' high-pressure autoclave facility. The largest autoclave has a working area or processing zone 4-ft in diameter by 10 ft long with operational capabilities of 15,000 psi and temperatures up to 1260 C. The temperature uniformity within this working volume has been measured to be better than $\pm$ 10 C at 1260 C. The vessels at Battelle-Columbus are being modified to place the heater, pressure and instrumenta-tion feed throughs in the bottom of the autoclave in a simple automatic plug-in, plug-out arrangement as shown in Figure 3. This arrangement eliminates the necessity to manually connect and disconnect all feed throughs, with significant time savings in loading and unloading sequences. Encapsulated materials to be HIP consolidated are typically loaded into the autoclave within the heater assembly. The autoclave lid is merely screwed into place and the processing cycle is started. Although this process is a batch-type operation, techniques have been developed to make maximum effective use of the high-pressure autoclave working volume and in-use time. Automatic handling and operating equipment have also been developed to refine the process for production applications. Computer systems are now being used to control the pressure/temperature cycle sequence and for continual processing-data acquisition. Special procedures, such as dynamic outgassing or venting of encapsulating containers and high-pressure hydrostatic extrusion have been performed which further illustrate the versatility of the process.

Three basic approaches have been examined to date in developing HIP processing of graphite materials and two appear to offer considerable potential for fabricating improved homog-eneous carbon and graphite structures. The three basic approaches are:

(1) Consolidation of fibrous and particulate materials without any binder phase
(2) Densification of pregraphitized or carbonized solids
(3) High-pressure impregnation/carbonization.

Particulate Consolidation. Coke (graphite) powder or fibers are placed in selected metal processing containers and processed at temperatures up to 2650 C and 17,000 psi.(7,8) The particulate powders or fibers are typically pre-formed into a solid shape by

(7) "Hot Isostatic Compacting of Graphite", D. C. Carmichael, P. D. Ownby, E. S. Hodge, BMI-1746 (October, 1965).
(8) "Dense Isotropic Graphite Fabricated by Hot Isostatic Compaction", D. C. Carmichael, W. C. Chard, M. C. Brockway, BMI-1796 (March 31, 1967).

TABLE II

BATTELLE-COLUMBUS HIP PROCESSING CAPABILITY[a]

Processing Zone, in.		Pressure, psi	Temperature	
Diameter	Length		C	F
2.5	8	10,000	1650	3000
3.5	12	10,000	1260	2300
4	36	10,000	1260	2300
	15		1650	3000
5	30	15,000	1260	2300
	20		1650	3000
8	36	15,000	1260	2300
	15		1650	3000
18	72	15,000	1200	2200
3	16	50,000	1760	3200
3	3	20,000	2700	4900
13	50	30,000	1200	3000
48	120	15,000	1260	2300
1	3	150,000	1540	2800

(a) Specific capabilities are frequently extended and modified as required to meet research and development program needs.

hydrostatic pressing. To date, the materials have been processed without a binder phase, hence the term "binderless" graphites. The highest strength structures have been attained utilizing coke flour rather than a graphite flour as the powder precursor. The relative tensile strength of some of these materials is shown in Table 3. The coke flour is considered to be much more "active" than the graphite flour and is more easily "sinterable". Bonding between adjacent coke particles is thought to occur during HIP consolidation as a result of intensified interparticle pressure effects between the available carbon lattice bond sites in adjacent carbon particles. Graphite flours have been processed to higher densities owing to the softness and lubricity of the graphitized material, but lower strengths are attained due to the lack of available interparticle carbon bonding sites.

Binderless material has been processed at temperatures from 1800 to 2650 C and at pressures between 30,000 and 17,000 psi. The highest strength graphites have been obtained when processed at around 2600 C. Tantalum containers are used because of the high tantalum carbide-tantalum eutectic (2830 C). Reaction between sulfur in the carbon materials and the tantalum container at temperatures above 1500 C has caused premature failure of the tantalum cans. Such failure should be reduced by lowering the temperature of processing to 1000 to 1500 C and utilizing low-sulfur cokes. Less expensive encapsulating materials can be used at these lower temperatures and much larger processing capacities would be available. To date, the HIP process has been used most extensively for fabricating particulate graphite structures, but considerable potential exists for fabrication fiber-base structures.

The microstructures of several unique binderless graphite materials are shown in Figures 5, 6, and 7. Figure 7 illustrates a unidirectional graphite fiber structure with no binder phase. All of these materials are within 95 percent of theoretical density.

Two basic approaches are considered applicable for binder-less-type fabrication of carbon-base materials, high temperature and low temperature processing. The high-temperature process (1800-2600 C) is considered more for experimental studies and does not   considerable manufacturing potential. Both the temperature limitations (furnace design and size) and reaction problems are eminent. A low-sulfur (<0.5 wt %) graphitizable coke produced from a petroleum crude offers potential for reducing or eliminating the sulfur problem.

The most promising "binderless" approach is to use low temperatures when partially pyrolyzed (coked) organic precursors are used rather than totally coked flours. Partially coked materials offer considerable potential for reducing the processing temperature required to consolidate and bond the particulates together and, hence, decrease reaction problems and increase processing-size capabilities. Temperatures in the 800 to 1300 C range are

TABLE III

PROPERTIES OF SELECTED HOT-ISOSTATIC PRESSED AND COMMERCIAL AEROSPACE GRAPHITES

Material[a]	Density, g/cc (% of Theoretical)	Diametral Tensile Strength, psi
Densified Solids		
ATJS	1.68 (74)	1700
ATJS	1.82 (81)	3000
ATJS (HIP)	2.13 (94)	3400
AXF-5Q	1.83 (81)	3300
AXF-5Q (HIP)	2.13 (94)	5100
Compacted Powders		
Artificial Graphites (HIP)	2.20 (97)	500–1400
Petroleum Cokes (HIP)	2.13 (94)	1800–2500
Glassy Carbon (HIP)	1.74 (74)	2500
Diamond (HIP)	2.00 (89)	3300

(a) HIP indicates hot isostatically pressed. Commercial materials are unmarked.
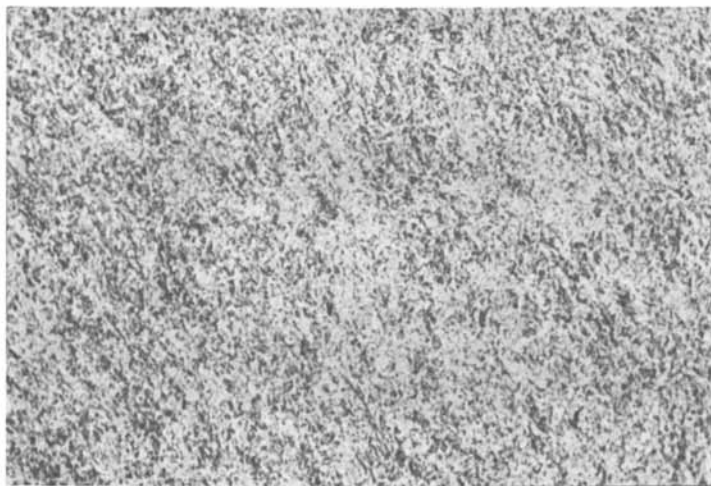
Figure 5.   Binder-free HIP graphite–coke precursor.   Density — 2.13 g/cm³.
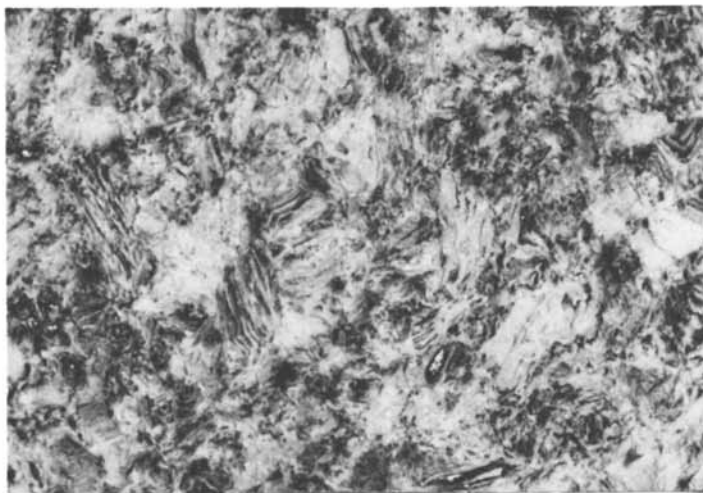
Figure 6. Binder-free HIP graphite–artificial graphite precursor. Density — 2.20 g/cm³.
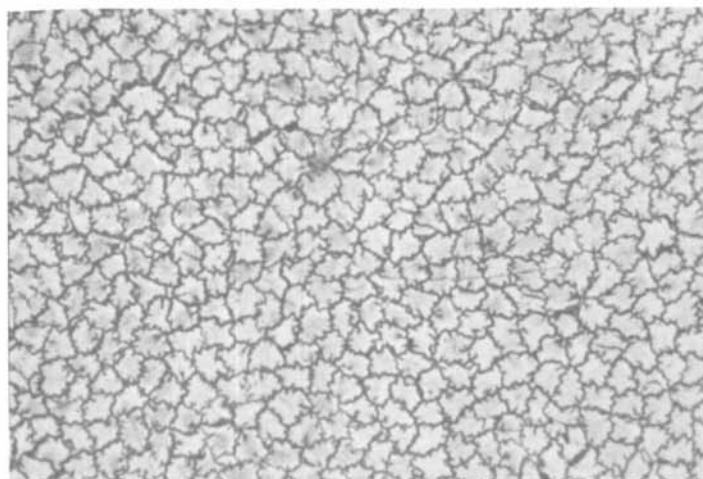
Figure 7. Unidirectional binder-free fiber graphite (T25). Density — 1.86 g/cm³.

considered appropriate. The pseudoplasticity of a partially
pyrolyzed flour under high pressure would allow for easier
densification and interparticle bonding. It is expected that a
one- or two-step process and a total processing time of 2 weeks
could be used to produce isotropic, homogeneous graphites of near
theoretical density. Another approach is to add only a small
amount of binder phase to a coke or graphite flour to assist in
promoting interparticle carbon bond formation and to generate
some lubricity in the consolidating compact. The selection of a
binder of the same composition as the coke precursor would be
extremely attractive. As discussed later, the volatile distilla-
tion products of decomposition during carbonization would be
diffused through the walls of the metal container, leaving behind
a high-density uniform-pore solid structure. A total HIP process-
ing time of two days could be utilized for these materials.

   Solid Densification. This operation is very similar to that
described previously except that a solid structure has been
attained prior to HIP densification. This solid may consist of
a graphitized solid, a carbonized solid, or a partially carbonized
solid. To date, only graphitized or carbonized solids have been
processed, and difficulties similar to those met in the particulate
approach have been experienced with these products--a reaction
problem with sulfur in the carbon-base precursors and the need
for high-temperature processing equipment. Solid carbon and
graphite structures have been densified to near theoretical
densities as shown in Table 3. Since significant plastic flow
in solid carbon occurs above 2200 C, elevated temperatures
appear to be required to significantly densify a reasonably solid
structure by a plastic-flow mechanism so as not to fracture
already attained interparticle carbon bonds. A partially
carbonized solid may offer potential as a precursor, however,
since pseudoplastic flow for densification may be initiated at
the interfaces of the particulate preform. This approach would,
therefore, be comparable to the high-temperature approach
described in the previous section.

   High-Pressure Impregnation/Carbonization. This process
incorporates impregnation and carbonization operations in the
same processing cycle. A porous preform, typically a woven
graphite-fiber carcass, is loaded into a steel processing
container and subjected to conventional atmospheric-pressure
impregnation of a liquid organic material (e.g., coal tar or
petroleum pitch). The pitch-impregnated structure is hermetically
sealed in the processing container and then hot-isostatically
pressed or carbonized at temperatures up to about 700 C and
pressures of about 15,000 psi. A schematic illustration of the
process is shown in Figure 8. The processing zone of Battelle's
current HIP carbonization unit is 16-in diameter by 55 in. long,
with a measured temperature variation of only $\pm$ 10 C at about

SAMPLE PREPARATION   CONVENTIONAL IMPREGNATION

EVACUATE AND
SEAL CAN

HIP CARBONIZATION

SAMPLE CLEAN-UP
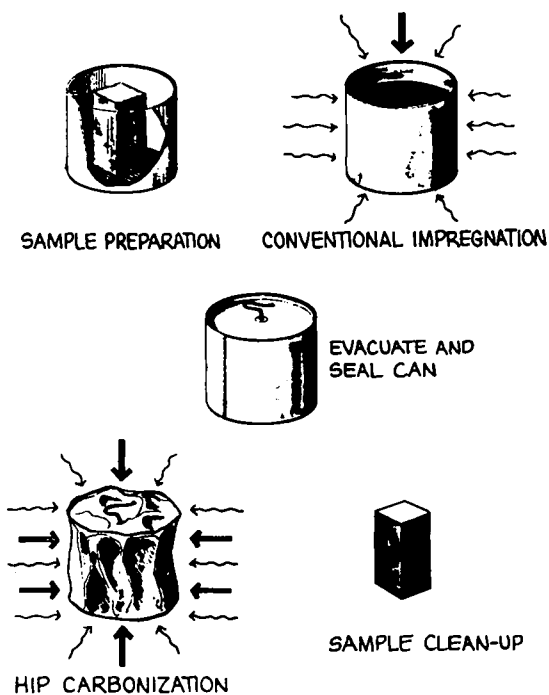
Figure 8. Schematic of high pressure impregnation/carbonization cycle

700 C. During heat-up, the impregnant becomes fluid and is forced
into small pores in the porous carcass not completely impregnated
by the atmospheric pressure technique. A pressure of 15,000 psi
is currently being used for this technique. Hence, more effective
and complete impregnation is accomplished than a conventional
2000- and 3000-psi manufacturing impregnation cycle. As the
impregnant is pyrolyzing at about 400 C, the volatile hydrogen
decomposition gas is diffused through the wall of the steel
container. A 91 weight percent coking yield is currently being
obtained by the process after heating under pressure to about
700 C. Thus, the process accomplishes an impregnation and a
carbonization step in the same cycle. After processing, the
metal can is removed by simple mechanical means and the excess
coke is chipped from the densified carcass.

     Multiple impregnation steps may be performed to densify
porous materials to almost any desired density level. With the
selection of high-carbon-yield precursors, it is envisioned that
a one- or two-step processing cycle could be performed to achieve
near theoretically dense solids. Total processing time is
estimated to be about 5 weeks with HIP cycles of about 30 to 60-
hr duration. This is the process currently used to densify high-
performance carbon-carbon composite materials for reentry applica-
tions. While it offers considerable potential for fabricating
both unique multigranular and carbon-carbon composites, only
limited development effort has been put forth to perfect or
optimize this technique.

     It should be pointed out that in all of the above discussions,
graphitization is performed at about 2700 C after selected
processing sequences.

     In conclusion, the hot-isostatic-pressing process appears
to offer considerable potential for fabricating unique graphite
materials and should be considered as a commercially viable
manufacturing process. Although in its infancy as a production
tool, the process is not just a laboratory curiosity. Develop-
ment efforts are required to establish and define the processing
procedures required for fabricating homogeneous reproducible
graphite materials. The HIP process offers the potential for
controlling processing parameters and, hence for achieving
material properties never before attained in the graphite industry.
It is not expected that this process will replace production
techniques for fabricating large 55-inch diameter coarse-grained
bulk graphite electrodes, but it is capable of producing smaller,
fine-grained, high-performance graphites and specialty carbon-
carbon composite materials. The capability of precision process
control, high isostatic forming pressure, versatility, extremely
high carbon yields, and short processing times make the HIP process
most attractive. As an extra bonus, the use of isostatic gas
pressure also allows shaped components to be directly fabricated
with little excess material to be removed by final machining.
These capabilities should allow for the fabrication of high-

performance carbon and graphite products with improved, homogeneous, and reproducible microstructural characteristics and physical properties. The process is considered most feasible for producing refined specialty bulk graphites for use as fixtures, boats, and susceptors in the semiconductor industry; for high-purity spectrographic electrodes; for high-strength seals and bearings; and for high-purity and high-performance nuclear and aerospace applications. Specialty carbon-carbon composite materials that could be processed would include materials for such applications as advanced high-speed aircraft disc brakes; thermal-stress-resistant nose tips, rocket nozzles, and heat shields for advanced missile systems; biocompatible prosthetics for bone and teeth implants; formed ablation-resistant high-temperature components for such applications as the space shuttle leading edge and others. It is expected that petroleum products will form an ever-increasing presursor(s) base for many specialty graphites. These petroleum products will include coke fillers as well as petroleum pitch binders and impregnants. Reproducibility and purity will be keys to the use of these materials as graphite and carbon-carbon composite constituents.

15

Structural Characterization of Graphitic Cokes and the Products Thereof

W. BRADSHAW and V. MAMONE

Lockheed Missiles & Space Co., Inc., Sunnyvale, Calif.

   In the utilization of graphites in an extreme environment where thermal shock may be severe, it is necessary to produce materials of high strain-to-failure and low thermal expansion coefficient with good thermal conductivity. The objective of this initial study was to characterize various bulk graphite precursor cokes and the effect of additions of several types of coke filler fines on the microstructural and mechanical properties of billets fabricated. The ultimate goal was to produce a material model for graphites with higher tensile strength and strain-to-failure, while maintaining a low thermal expansion coefficient and compatible thermal conductivity.

Approach

   Seven types of coke particles were subjected to extensive microstructural characterization with respect to density, morphology, crystalline characteristics, and porosity. From the seven filler precursors (See Table I), four were selected for further analysis in billet fabrication studies. Both isotropic and anisotropic filler precursors were used as particle additions (15%) in a conventional graphite process, i.e., molded and pressed into green graphite shapes, subjected to multiple bakes and reimpregnations and finally graphitized and reheat-treated. The material was tested for tensile strength and strain-to-failure during processing and after post-graphitization heat treatment.
   The microstructural characterization consisted of optical and scanning electron microscopy, density determinations by displacement in mercury and helium, evaluation of pore size and distribution by mercury porosimetry, and x-ray diffraction analysis.

172

Table I

MICROSTRUCTURE OF GRAPHITE PRECURSOR COKES

PRECURSOR	CRYSTAL HABIT	INTERLAYER SPACING, d (Å)	L_C (Å)	CRYSTALLITE DENSITY (gm/cc)	g FACTOR (AS REC'D)
CODE C	ACICULAR	3.49	44	2.18	-0.58
CODE D	ACICULAR	3.49	30	2.18	-0.58
FLUID COKE	SPHEROIDAL	3.49	27.5	2.18	-0.58
GILSO COKE	SPHEROIDAL	3.48	59	2.18	-0.46
INTERMEDIATE PETROLEUM COKE	SEMIACICULAR	3.44	42	2.21	0.0
GLASSY CARBON, 1400 GRADE	ANGULAR	3.66	16,13	2.07	-2.56
SANTA MARIA COKE, 1400 GRADE	SPHEROIDAL	3.44	33,59	2.10	0.0

Analysis during billet fabrication studies consisted of determination of density and tensile strength and strain-to-failure of in-process material after each fabrication step and after graphitization and final heat treatment.

Experimental Methods

Apparent crystallite size, L_C, and average crystallite diameter, L_A, were calculated from the x-ray line width $\beta_{1/2}$ of the 0002 and $11\bar{2}0$ x-ray reflections occuring at 26.6° and 77.8°, respectively, using the Sherrer formula (1, 2)

$$L = \frac{K\lambda}{\beta_{1/2} \cos \theta}$$

where K is a constant = 0.90 for L_C and 1.77 for L_A, λ is the wavelength of the analyzing radiation, $\beta_{1/2}$ is the peak half width corrected for instrumental broadening and 2θ is the respective diffraction angle for 0002 and $11\bar{2}0$ x-ray diffraction peaks. The data were uncorrected for strain broadening. Consequently, in the more disordered materials such as glassy carbon, the apparent crystallite size, L_C, is a measure of the degree of distortion in interlayer spacing, and the parameter, L_A, may be described as the average defect-free distance (3, 4).

The Maire-Méring g-factor, considered a measure of the degree of graphitization (4, 5, 6), was calculated from the following equation:

$$d_{0002} = 3.354\,g + 3.440\,(1-g)$$

where 3.354 and 3.440 are the interlayer spacings for graphite and turbostratic carbon, respectively, and d_{0002} is the interlayer spacing calculated from the observed diffractive peak, 2θ.

Apparent density, D_A, and real density, D_R, were calculated from mercury porosimetry where the apparent density is the weight in grams divided by the displacement volume in mercury at atmospheric pressure and real density, D_R, is the weight of the sample divided by the displacement volume in mercury at 5000 psi. Percent open porosity was calculated from the difference between the volume displacement in Hg at atmospheric pressure and the volume displacement after mercury intrusion at 5000 psi, i.e., the volume fraction pores with a diameter greater than 0.035 μm. He density is measured by volume displacement in helium gas and excludes open porosity greater than 2.5 A.

Tensile strength and strain-to-failure were measured at room temperature in the with-grain and across-grain directions using round tensile specimens with a gage length of 2.54 cm and a gage diameter of 0.475 cm. The specimens were generously radiused at the fillet areas to minimize stress concentration effects.

Experimental Results

■ Microstructure.* The microstructure of the various cokes is summarized in Table I. Code C and Code D cokes were acicular cokes which were anisotropic in nature as indicated by their optical activity in polarized light, Figures 1 and 2. Code C coke has a fine particle size and very fine granular structure within the particles. It was produced from intermediate petroleum coke, described below, by grinding after calcining. Code D coke has a very coarse granular structure (Figure 2) resembling coarse fibrous and nonfibrous mesophase cokes (7,8).

Both the fluid coke and Gilso coke are spheroidal, Figures 3 and 4. The fluid coke, which is formed in a fluidized bed (9), is in the shape of uncoalesced spheres, Figure 3. The Gilso coke appears to have been formed from coalesced mesophase spheres, Figure 4. The spheres themselves have a fine isotropic texture. They are joined by coarse isotropic mesophase with a slight tendency toward a fibrous texture at the surface of the spheres. The intermediate petroleum coke has both a needle-shaped texture and isotropic texture, Figure 5. This coke is the precursor of Code C coke which consist of fines sieved from ground intermediate petroleum coke.

Glassy carbon possesses no optical activity whatsoever and is completely isotropic (Figure 6). The particles shown here were produced by rapid curing and pyrolysis to promote cracking for easy attritioning into fines. Microporosity and internal flaws also developed. Glassy carbon produced in conventional long pyrolysis cycles does not have such flaws.

Santa Maria coke has a fine isotropic texture, strongly resembling mesophase graphite, in the as-received condition, Figure 7a. After calcining at 1400°C the isotropic grains are refined to smaller grain size and rosettes form in some areas, Figure 7b. The calcining also causes pores to form in association with the rosettes, Figure 7c.

With the exception of the intermediate petroleum coke and the Santa Maria coke, all the precursor materials were nongraphitic, i.e., had a d-spacing greater than 3.44 Å, Table I, Glassy carbon was the least graphitic with a d-spacing of 3.66 Å, an apparent crystallite size, L_C, of 16 Å and a g-factor of -2.56 after pyrolysis to 1000°C. The most graphitic materials with respect to g-factor were the Santa Maria coke and the intermediate petroleum coke. Gilso coke which had large mesophase spheres joined by coarse isotropic mesophase had the largest apparent crystallite size, L_C.

The texture of the cokes was evaluated by scanning electron microscopy. The Code C particles were extremely fine, Figure 8. The edges of the flakes had strong basal plane texture. The Code D particles are much larger and are obviously in an unground state, Figure 9.

───────────

*The authors wish to acknowledge the contributions of the Materials Science Analysis Laboratory, directed by W. C. Coons, who carried out the microscopy and the x-ray diffraction analysis.

Figure 1.   Microstructure of Code C coke

Figure 2. Microstructure of Code D coke

b. Bright Field

a. Polarized Light
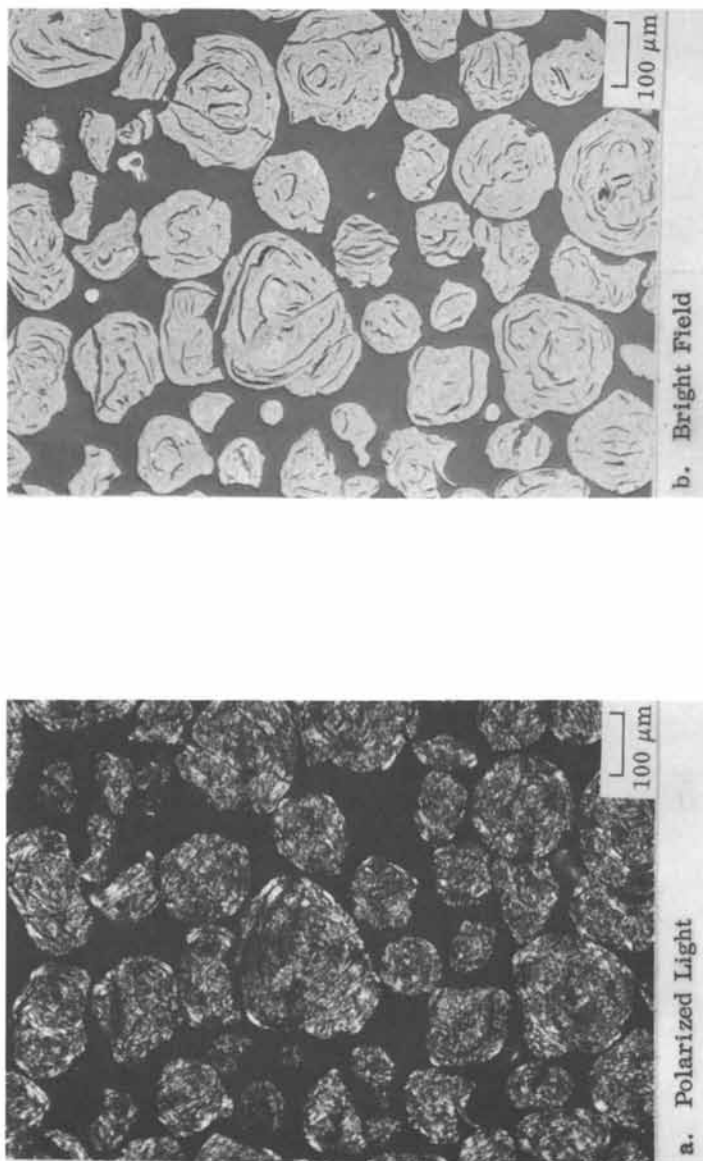
Figure 3. Microstructure of fluid coke
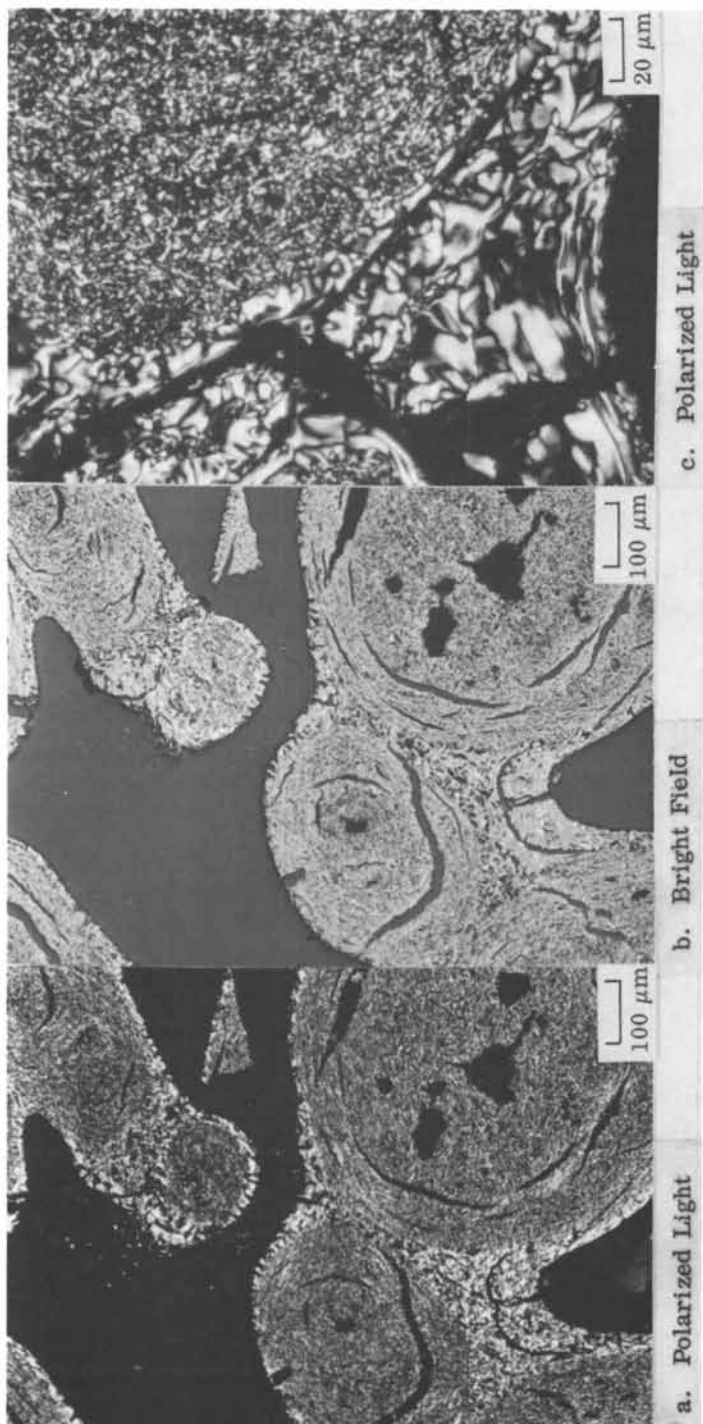
Figure 4. Microstructure of Gilso coke, as received

Figure 5. Microstructure of intermediate petroleum coke

a. Bright Field, showing sev-
eral particles with cracking
and microporosity developing
as a result of rapid pyrolysis,

b. Single particle of higher
magnification, Bright Field
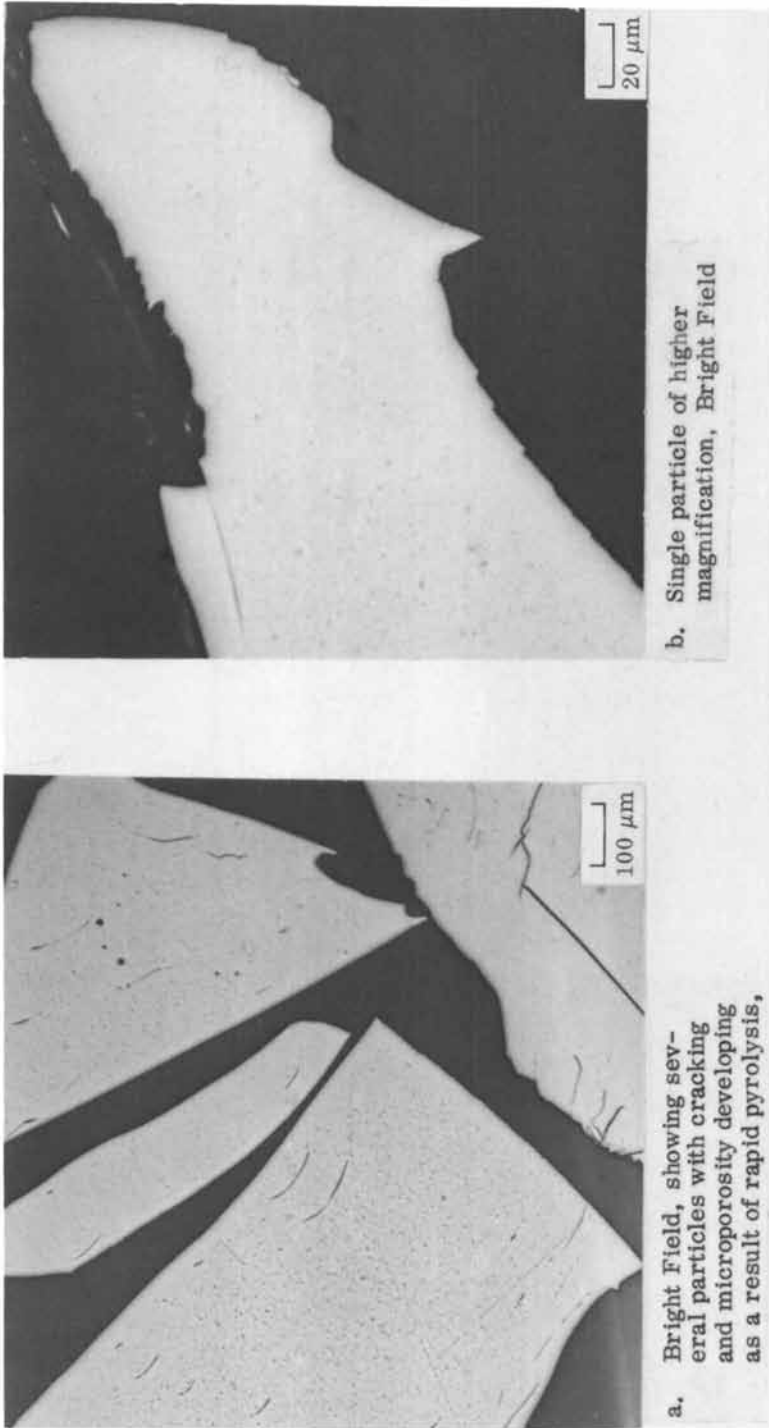
Figure 6.   Microstructure of particles of glassy carbon produced by rapid pyrolysis to 1000°C
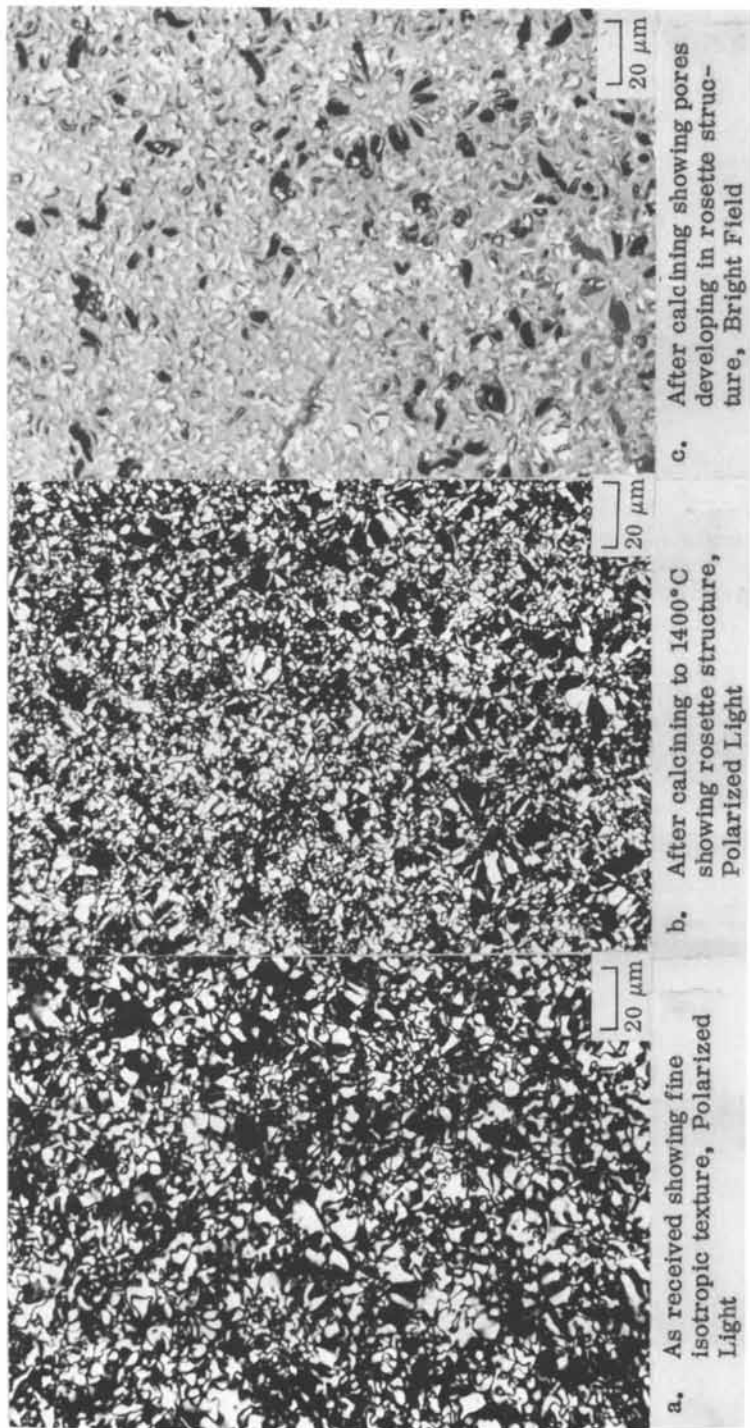
Figure 7. Microstructure of Santa Maria coke, as received and after calcining at 1400°C

a. As received showing fine isotropic texture, Polarized Light

b. After calcining to 1400°C showing rosette structure, Polarized Light

c. After calcining showing pores developing in rosette structure, Bright Field

a. Code C fines

b. Typical texture

c. Basal plane texture at edge of flake in central region of Figure b
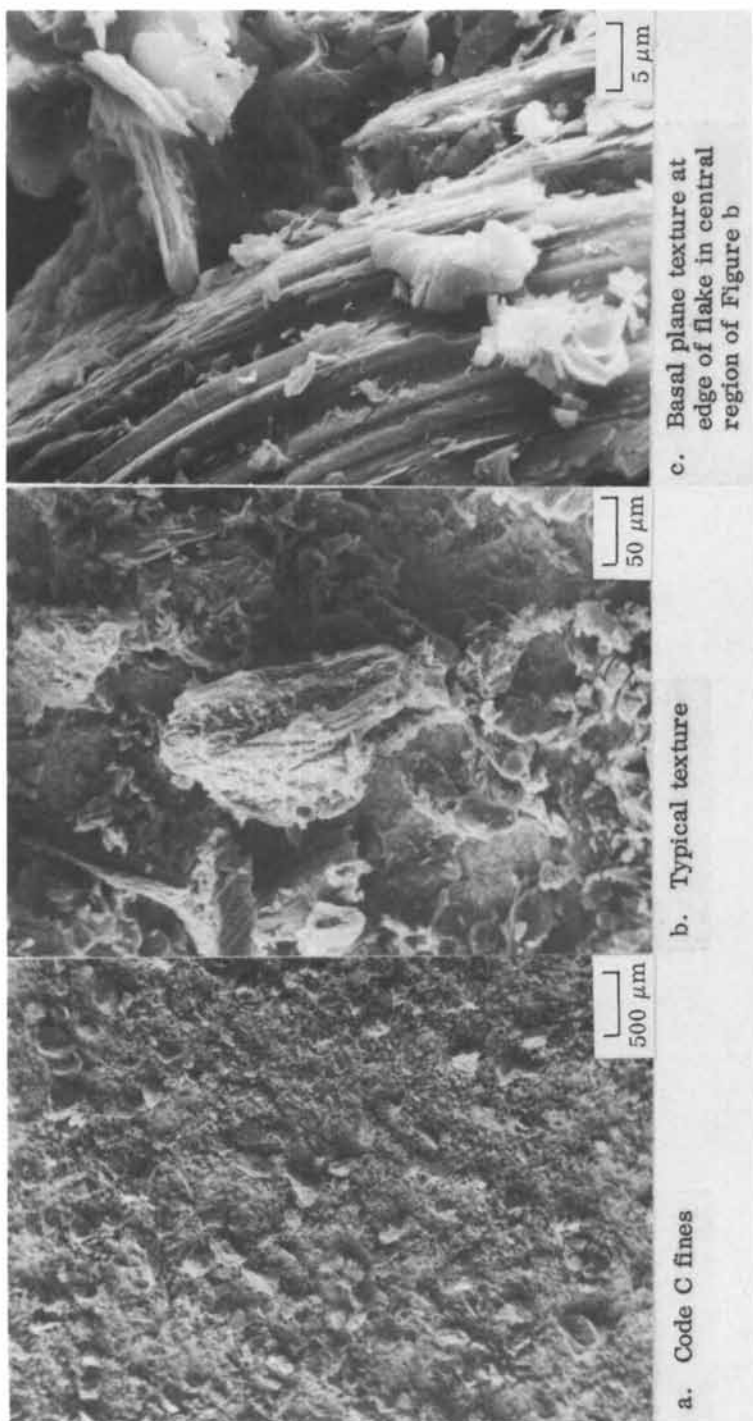
Figure 8. Surface texture of Code C coke particles showing strong basal plane texture

Figure 9. Surface texture of Code D coke showing microcracking parallel to basal planes

a. Code D coke b. Microcracking c. Fine microcracking

There is strong basal plane texture and considerable microcracking. The fluid coke consists of small spheres with an onionskin texture with the basal planes at the surface parallel to the surface of the spheres, Figure 10. A particle of Gilso coke is shown in Figure 11. It obviously is an aggregate of coalesced spheres. The microcracking indicates the spheres have a semi-onionskin texture. The cracking is random in the regions joining spheres. The intermediate petroleum coke has the most random texture, Figure 12. There are regions where the basal planes are parallel to particle surfaces, Figure 12b, and regions where the basal plane edges are exposed, Figure 12c. The glassy carbon particles produced by rapid pyrolysis to promote microcracking and ease of grinding exhibit typical brittle conchoidal fracture, Figure 13. The Santa Maria coke had a random particle distribution, Figure 14a, with isotropic particles clinging to the surface of the material, Figures 14b and 14c.

■ Effect of heat treatment* on weight loss, density, and porosity of coke precursors. The weight loss of various cokes when heat-treated independently is illustrated in Figure 15. Glassy carbon does not graphitize, except when in contact with graphite flake (10) or with metal carbide formers (11,12). Consequently, the particulate glassy carbon addition acted differently when processed in contact with graphite flake and pitch than it did when processed independently. The acicular large particle Code D coke lost only 4% weight after processing to 2750°C. Code C coke and intermediate petroleum coke behaved almost identically. The two spheroidal cokes, exhibited the most substantial weight loss with heat-treatment temperature.

Density data on the as-received cokes are reported in Table II. Code C coke, with an initial density of 1.47 gm/cc, had a large open porosity and exhibited considerable weight loss (8%) after heat treatment to 2750°C. There was a slight density decrease during heat treatment, Figure 16, and an increase in open porosity, Figure 17.

Code D coke which had a high starting density (1.91 gm/cc) and showed little weight loss during heat treatment (4%) also showed little change in density and open porosity, Figures 16 and 17. The fluid coke which consisted of small spheres with low porosity in the form of microcracks underwent substantial weight change, Figure 15, and decrease in density, Figure 16, with no substantial change in porosity, Figure 17. Both Code C coke and its precursor, intermediate petroleum coke, exhibited an intermediate weight loss, 8 to 9%, Figure 15. The density behavior of the two cokes, Code C and intermediate petroleum coke, was quite different, Figure 16. Code C coke had a low initial density of

---

*Heat-treatment experiments were carried out in a resistance furnace in an argon atmosphere. The 1000°C cycle was seven days to temperature and an 8-hr hold. The higher heat treatments were done with 6 hr to temperature and a 2-hr hold.
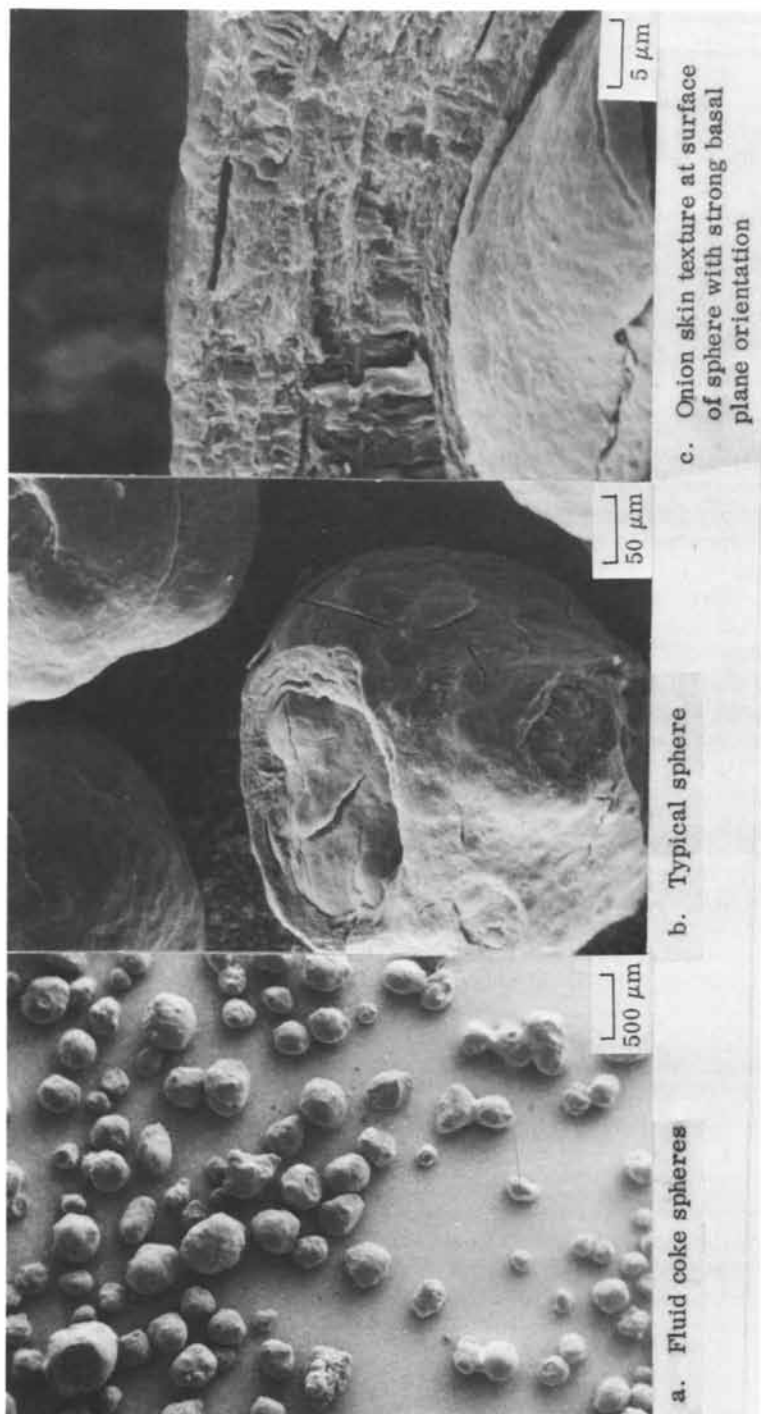
Figure 10.   Fluid coke texture showing minimal coalescence of spheres and onion skin texture at surface of sphere

a. Fluid coke spheres

b. Typical sphere

c. Onion skin texture at surface of sphere with strong basal plane orientation

a. Gilso coke particle   500 μm

b. Portion of sphere with semi-onion-skin texture   50 μm

c. Microcracking indicating poor basal plane texture   5 μm
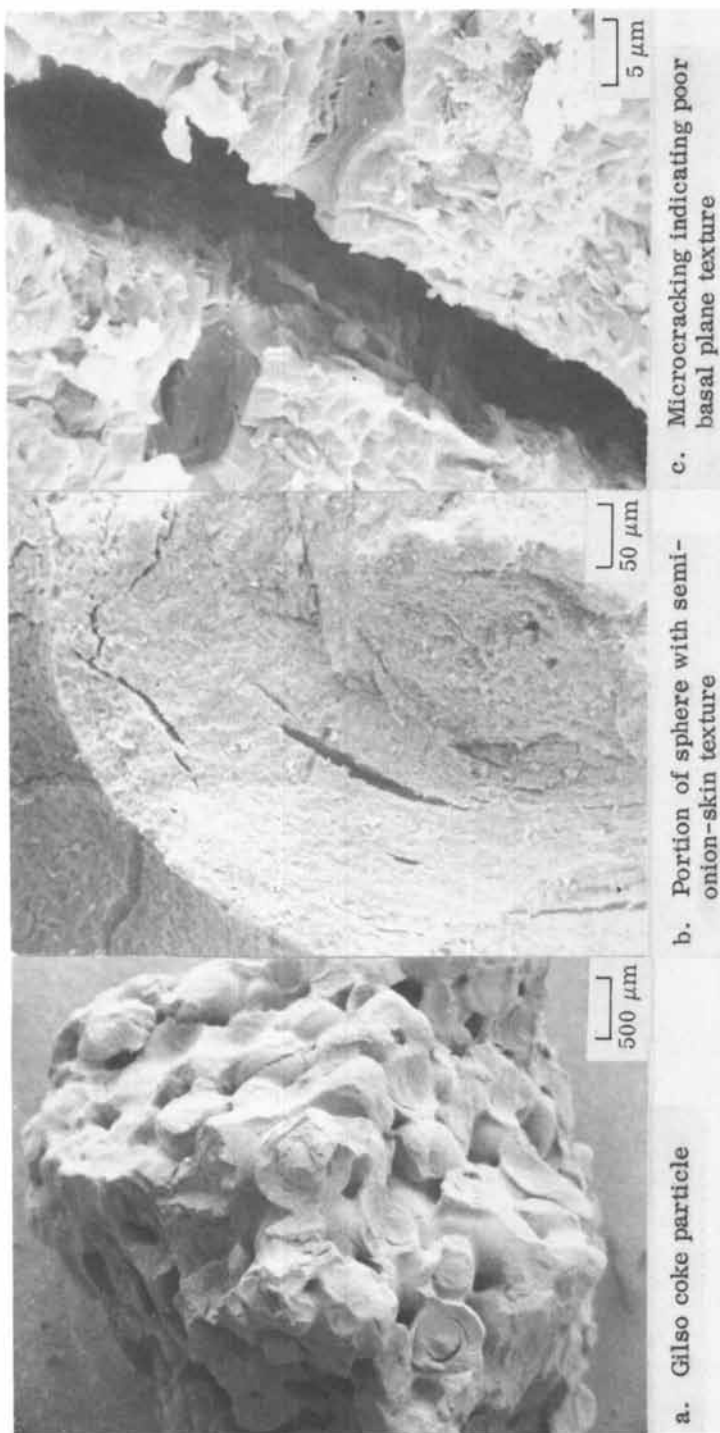
Figure 11. Gilso coke texture showing multicoalescence of spherical particles

a. Portion of coke particle

b. Region with basal plane parallel to particle surface

c. Region with basal planes perpendicular to particle surface

Figure 12. Intermediate petroleum coke with strong randomly oriented basal plane texture
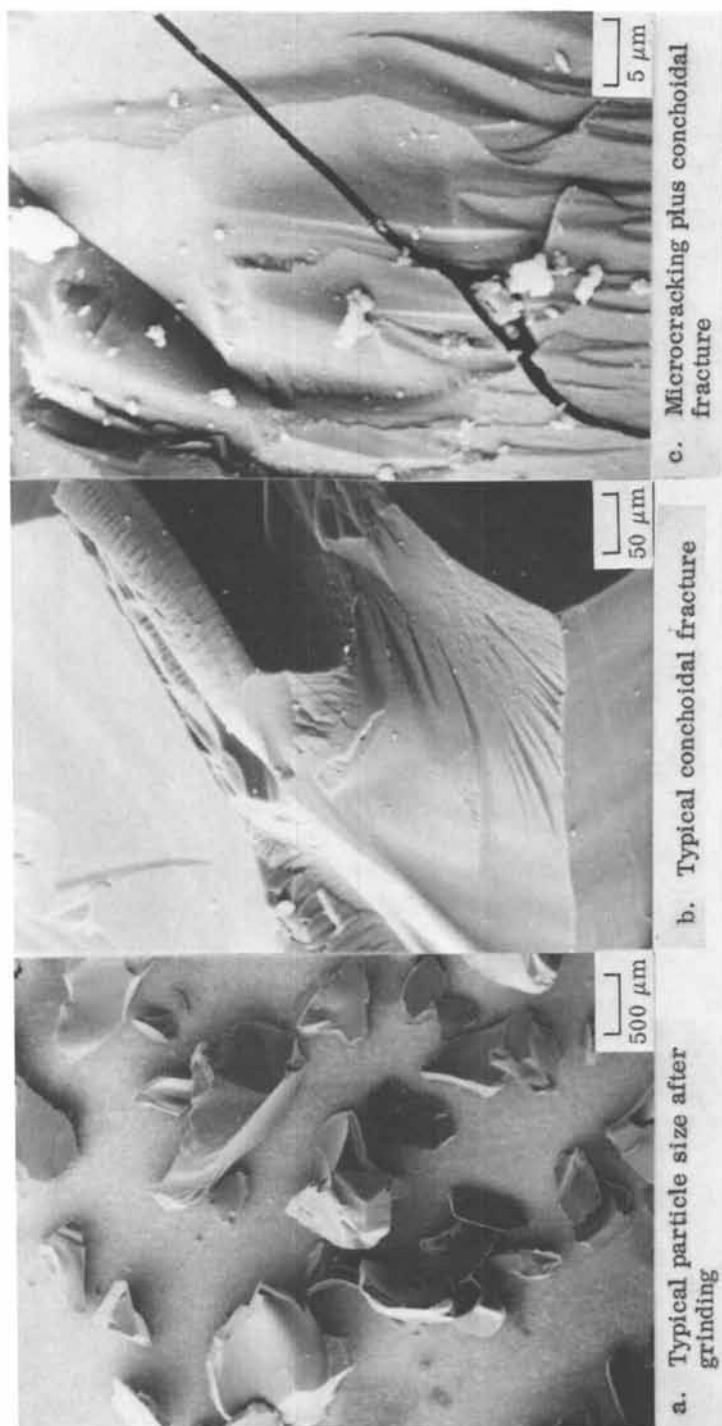
Figure 13. Glassy carbon powder rapidly pyrolyzed to 1000°C to promote microcracking for subsequent ease in communication, then calcined to 1400°C

c. Microcracking plus conchoidal fracture

b. Typical conchoidal fracture

a. Typical particle size after grinding

Figure 14. Santa Maria coke after calcining at 1400°C

a. Typical particle distribution b. Particle surface c. Isotropic nature of surface
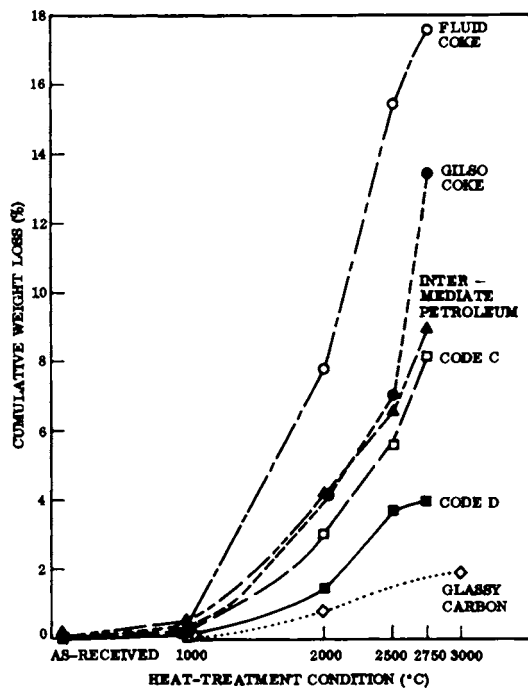
Figure 15. Effect of heat treatment on weight loss
of coke precursor
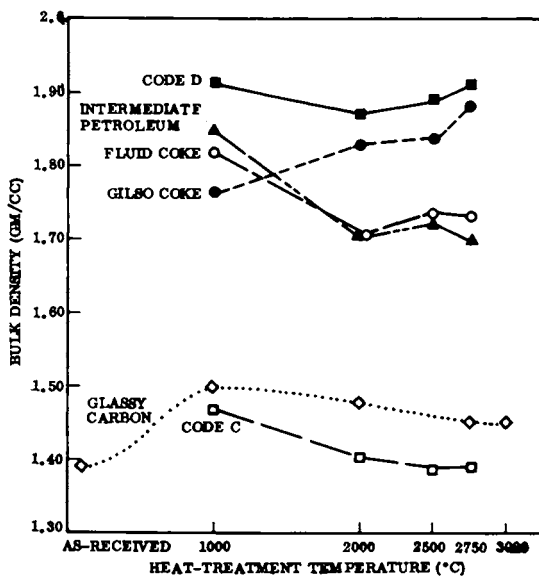
Figure 16. Effect of temperature on bulk density of
coke precursors

Table II

HELIUM DENSITY AND MERCURY POROSIMETRY OF COKES

Type	D_A* (g/cm^3)	D_R** (g/cm^3)	(%) Open Porosity	Pore Median Diameter (μm)	He Density (g/cm^3)
Code C	1.47	2.09	30	2.8	2.088
Code D	1.91	2.11	10	1.5	2.121
Intermediate Petroleum	1.85	2.06	10	1.7	2.060
Gilso	1.77	1.88	6	0.65	1.901
Fluid	1.82	1.96	7	0.86	1.928

*Apparent or bulk density.
**Real density, i.e., the density obtained after a Hg penetration at 5000 psi.

1.47 gm/cm^3 and this decreased with further heat treatment. The intermediate petroleum coke had a higher starting density, 1.85 gm/cm^3 which decreased to 1.70 gm/cm^3 after heat treatment to 2750°C. The open porosity of Code C coke was 30% in the as-received condition and it increased to about 39% after final heat treatment, Figure 17. The intermediate petroleum coke behaved like Code D coke with respect to porosity. These data indicate that the sieving and grinding operation cause a change in porosity and possibly some segregation of low-density particles. The real density D_R and the He density are the same for Code C, Code D, and intermediate petroleum coke indicating there is no fine porosity in the range between 350 and 2.5 Å.

The Gilso coke which consisted of large coalesced spheres, Figure 4, lost considerable weight during heat treatment, Figure 15, so that the density increased with heat treatment temperature, Figure 16, but the accessible porosity remained unchanged, Figure 17. Gilso coke had a substantial difference between real density and He density (Table II) indicating a fine porosity of 6.5%. Although not reported here, density fractionation studies showed that the Gilso coke consisted of particles with densities ranging from 1.5 to 2.0 gm/cc.

The data with respect to the effect of weight change, density, and porosity may be summarized as follows:

- The fine (Code C) and coarse (Code D) needle cokes exhibited substantially different behavior from each other.
  - Code C coke which has a very low apparent density does not undergo substantial weight or density changes when processed to 2750°C. There is an increase in open porosity associated with graphitization as discussed in the next section.
  - Code C coke has a high initial bulk density, undergoes little weight loss during heat treatment, and the density and open porosity remain substantially unchanged.

    — Intermediate petroleum coke, the coarse precursor for Code C coke exhibits similar weight loss with heat treatment, but different porosity and apparent density.
- The fine fluid coke and coarse Gilso coke were much more similar in their behavior during heat treatment.
  - Both underwent substantial weight decreases.
  - Both underwent little change in open porosity greater than 0.035 μm, i.e., that accessible to mercury at 5000 psi
  - The fine fluid coke underwent a decrease in density. As shown in the next section, it was the least graphitic of all five cokes examined in great detail
  - The coarse Gilso coke underwent an increase in density, which was associated with increasing graphitization
- Glassy carbon, an isotropic carbon generated from resin rather than pitch underwent the least weight change, density changes, and change in open porosity during heat treatment. It also is much less graphitizable, except when in the presence of graphite flake or metallic impurities.
- With the exception of glassy carbon, all the candidate precursor fillers had considerable accessible porosity.

■ Effect of heat-treatment temperature on the degree of graphitization. The effect of heat treatment on the degree of graphitization is illustrated in Figure 18. Code C coke is nongraphitic when heat-treated below 2000°C; but becomes slightly graphitic after heat treatment to 2500°C with little further change after heat treatment to 2750°C. becomes turbostratic after a 2000°C heat treatment and becomes more graphitic with each heat-treatment condition. The intermediate petroleum coke becomes graphitic after heat treatment to 2500°C, but the g-factor does not change with further heat treatment.

    The fluid coke is nongraphitic at lower heat-treatment temperatures, 1000° to 2000°C, and becomes turbostratic after heat treatment to 2750°C. Because the fluid coke particle is spherical with tightly packed lamallae to begin with, it cannot graphitize readily. The Gilso coke, which contains two types of mesophase, becomes graphitic after heat treatment to 2500°C and continues to become more graphitic with further heat treatment.

    Glassy carbon remains isotropic and nongraphitic when pyrolysed with contact with graphite. Santa Maria coke which is isotropic is nongraphitic in the as-received form but becomes graphitic after heat treatment to 1400°C.

    The effect of heat treatment on apparent crystallite thickness, L_C, i.e., decrease in stacking disorder, is shown in Figure 19. Code C coke reaches a crystallite thickness of 350 Å after heat treatment at 2500°C. Code D reaches a maximum crystallite thickness of 409 Å after heat treatment to 2750°C.

    Gilso coke, an agglomeration of spheres, reaches a maximum crystallite thickness of 280 Å after heat treatment to 2750°C. The fluid
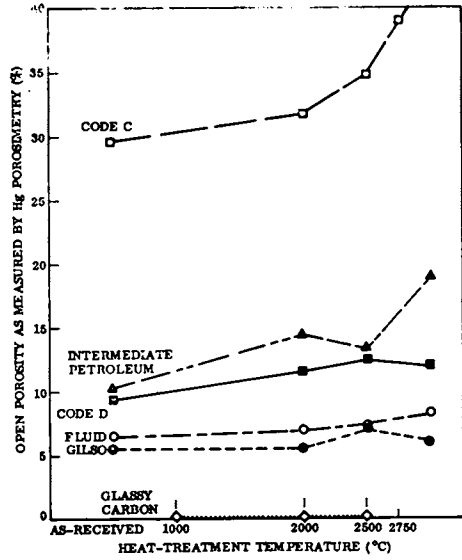
*Figure 17. Percent open porosity vs. heat
treatment temperature*
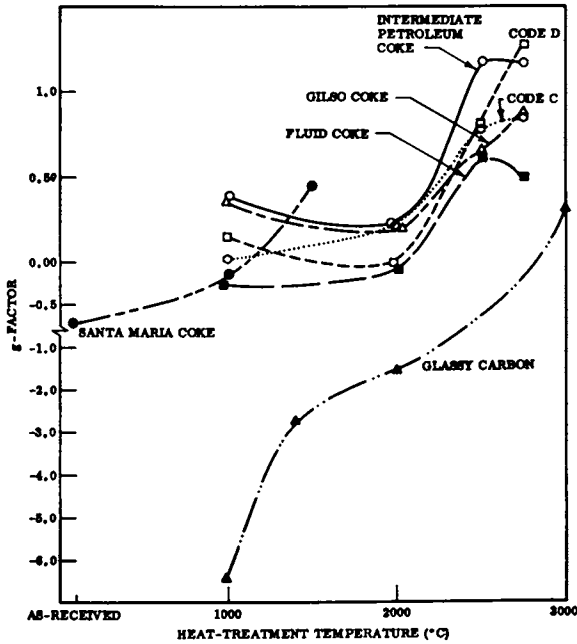
*Figure 18. Degree of graphitization as a function of heat
treatment temperature*

coke, consisting of very small spheres, had a maximum crystallite thickness of 215 A° reached after heat treatment to 2500 °C.

Santa Maria coke, an isotropic coke with a rosette structure, Figure 7, did not undergo any crystalline growth with heat treatment except the grain refinement observed during calcining; probably because intersecting randomly oriented crystallite boundaries inhibit such growth. Glassy carbon, a hard disordered carbon did not appear to undergo much growth in crystallite size. This material is a hard carbon with a high degree of disorder probably associated with strain broadening.* It underwent only slight increase in apparent crystallite size with increasing heat-treatment temperature.

The two needle cokes, the intermediate petroleum coke, and the two spheroidal cokes all underwent substantial increases in mean crystallite diameter, L_A, i.e., mean-defect distance, when heat-treated from 2500 °C to 2750 °C, Figure 20. The fluid coke, a small particle spheroidal coke, exhibited the least growth. Glassy carbon, which has a turbostratic structure (14), exhibits little two-dimensional order, hkl peaks are absent, and thus the L_A cannot be readily measured; i.e., the graphite layers are not in registration with each other (15) and consequently are not easily ordered unless stress is applied (11) or catalytic effects occur. Santa Maria coke also is turbostratic and has no significant hkl peak after calcining at 1400 °C. Its fine granular structure, visible optically, probably inhibits the development of large-diameter grains.

The degree of anisotropy developed as a result of crystalline growth is shown for five of the graphitizable cokes, Figure 21. The Code D coke was the most isotropic of the five evaluated. Code C coke, intermediate petroleum coke, fluid coke, and Gilso coke all underwent substantial increases in crystalline anisotropy when heat-treated above 2500 °C.

Our studies on the degree of graphitization may be summarized as follows:

- Maire-Méring Factor
  - Glassy carbon is nongraphitizing
  - Santa Maria coke starts out as nongraphitic but approaches d-spacing of 3.44 after calcining to 1400 °C
  - All other cokes appear to reach a maximum value at either 2500 ° or 2750 °C
- Apparent Crystallite Thickness, L_C (Å)
  - Glassy carbon exhibits very low crystallite size, probably due to strain broadening
  - The spheroidal cokes have intermediate L_C
  - The acicular cokes have the highest L_C and probably the least strain broadening

---

*We are currently studying the effects of this strain contribution using the method of Thrower and Nagle (13). Preliminary evidence indicates that the 004 and 006 peaks are so weak that the technique may not be applicable.
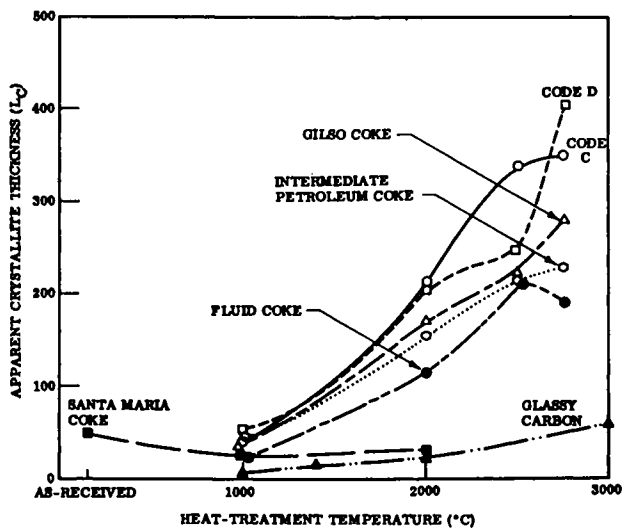
Figure 19. Apparent crystallite thickness vs. heat treatment temperature
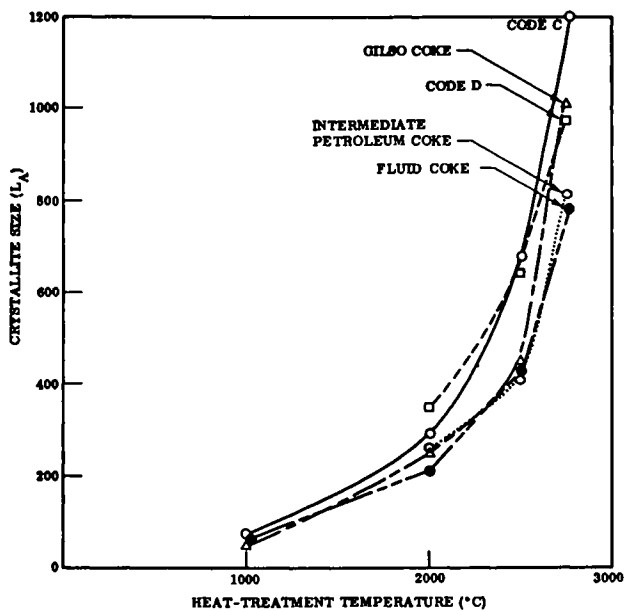
Figure 20. Apparent crystallite diameter as a function of heat treatment temperature

- Apparent Crystallite Width, L_A (Å)
  - Glassy carbon was not analyzed as the hkl reflection is non-detectable
  - In other cokes, L_A increases with heat-treatment temperature
- Anisotropy Ratio, L_A/L_C
  - Code D coke was the most isotropic of the five cokes evaluated
  - The anisotropy ratio of the other cokes increased greatly upon heat treatment to 2750°C
  - The spheroidal coke became the most anisotropic
  - The Code C coke was the least anisotropic of these four

■ Billet fabrication studies. This study was designed to determine the effect of various filler additions on the tensile strength and strain-to-failure of billets molded under similar conditions. The filler particles were added as 15% additions and in one case no fines were added. The base coke particles in all cases were Code C coke. The cokes selected for addition were the following:

- Code C coke, a graphitizable intermediate coke with some anisotropy, was added as 15% fines, ground to a 15-micron particle size
- Santa Maria coke, a graphitizable isotropic coke with a rosette structure, was added to determine the effect of additions of graphitizable isotropic fines
- Glassy carbon coke, a totally isotropic material, was added to determine the effect of nongraphitizable additions
- A control billet with no addition of fines was prepared in the same manner as the other experimental materials, and
- Another with 25% fines of the 15-micron Code C type coke was also prepared

Selected billets were subjected to a post-graphitization heat treatment of 2 hr at 3000°C with a 6-hr rise to heat-treatment temperature.

The analysis of the billets consisted of evaluation of density, tensile strength, and strain-to-failure after each processing step, graphitization, and post-graphitization heat treatment.

Density data are listed in Table III. All of the billets decreased in density between the 1st and 3rd bake. The fourth bake caused densification of billets with isotropic addition or no fines, no change with 15% fines, and a slight decrease with 25% fines. The graphitization caused the most significant densification. Post-graphitization heat treatment for 2 hr at 3000°C caused a slight decrease in density. The highest density after graphitization was obtained with 15% Code C fines

As seen in Figure 22, tensile strength increases with increasing densification. There seems to be little difference between the types of additives. Both with- and across-grain strength increase with each processing step. Strength increases as a function of graphitization and degree of densification. The increase in with-grain strength is higher than that of across-grain strength. Poorest results were obtained with
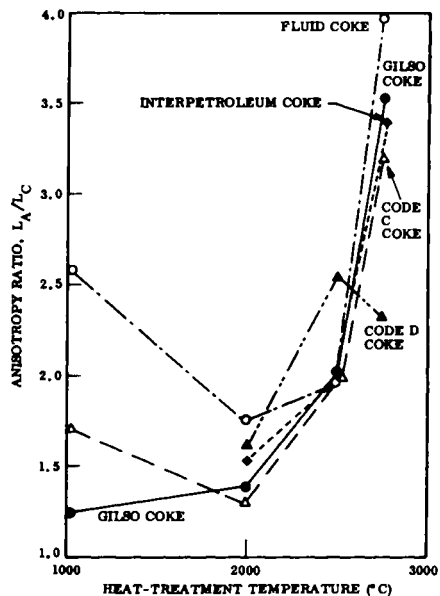
Figure 21. Crystalline anisotropy as a function of heat treatment temperature
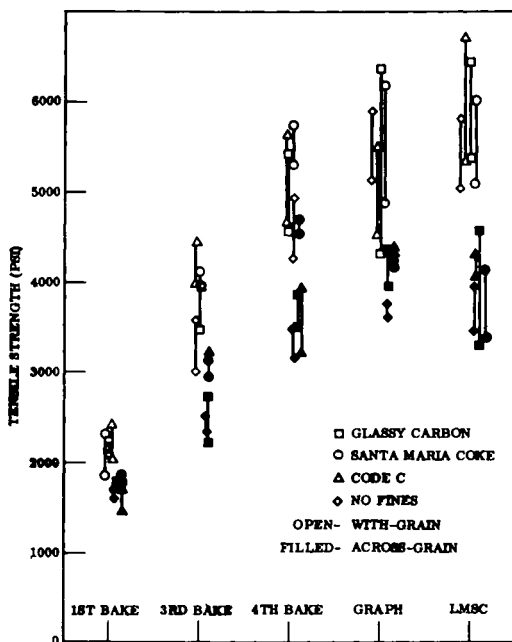
Figure 22. Tensile strength as a function of process cycle

Table III

DENSITY OF In PROCESS MATERIALS

Process Step

Type of Addition	1st Bake	3rd Bake	4th Bake	Graphitization	LMSC Heat Treatment (2 hr at 3000 °C)
Glassy Carbon	1.066	1.068	1.105	1.291	—
Santa Maria Coke	1.352	1.000	1.238	1.368	1.241
No Fines	1.000	1.000	1.110	1.385	1.372
15% Fines	1.375	1.200	1.200	1.568	1.438
25% Fines	1.235	1.200	0.958	1.425	1.200
Average Density	1.206	1.093	1.122	1.407	1.312

no fines, which also produced low density billets. Best results were ob-
tained with the addition of 15% Code C fines which had the highest billet
densities, Table III. Glassy carbon or Santa Maria coke additions pro-
duced properties which were intermediate between additions of aniso-
tropic fines and no fines. Glassy carbon which graphitized in the
presence of graphite flake resulted in a billet with somewhat lower den-
sity and greater data scatter in the across-grain direction. The addition
of Santa Maria coke caused uniformly lower results.

The effect of process cycle on strain-to-failure is shown in
Figure 23. It should be noted that the greatest increase in strain-to-
failure occurs in graphitization. Post-graphitization heat treatment
causes minor increases in the average with-grain strain-to-failure but
increases the standard deviation. Across-grain strains are higher than
with-grain strains. Across-grain strain generally increases faster
than with-grain strain. The increase in strain-to-failure observed dur-
ing graphitization was accompanied by a corresponding increase in
anisotropy, ϵ_a/ϵ_w, particularly with needle coke fines

Best results were obtained with Code C fines and no fines with re-
spect to uniformity of results and lowest minimum value.

Conclusions

The conclusions reached were as follows:

■ Effect of Particle Additions on Mechanical Properties.

● Neither the addition of 15% Santa Maria coke or 15% glassy carbon
had a significant effect
● Neither glassy carbon nor Santa Maria coke could be detected
optically in the graphitized billet; both had been graphitized by
graphite nucleation or stresses generated during the thermal
treatments and subsequent graphitization. This accounted for a
variable density increase which in turn, probably accounted for
greater scatter in the tensile data observed.
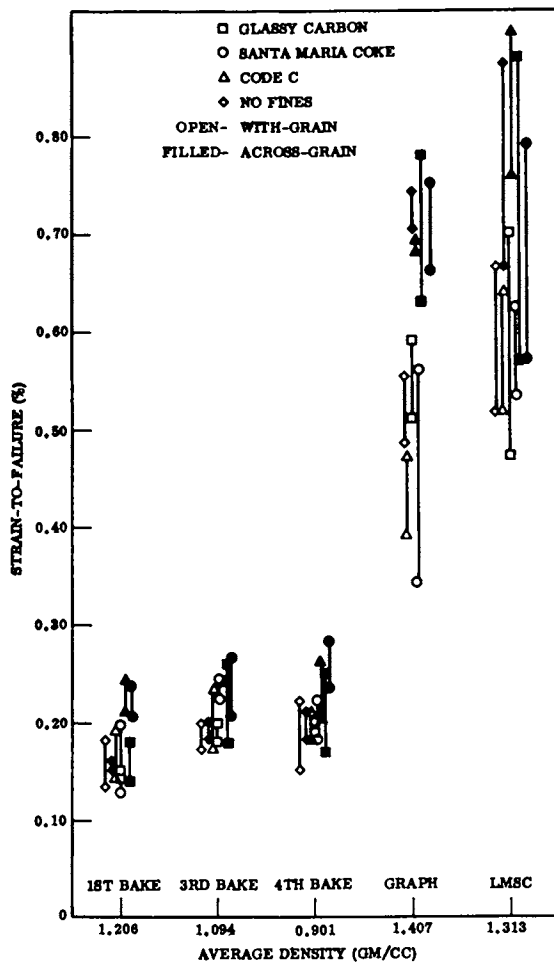
Figure 23.   Tensile strain-to-failure as a function of
process cycle

- Code C coke with and without fines appeared to have better properties with respect to average values and a minimum in data scatter

■ Tensile strain-to-failure.
  - The principal increase in strain-to-failure occurred during graphitization with only a slight additional increase with post-graphitization heat treatment, i.e., strain-to-failure increases with degree of graphitization
  - The increase in strain-to-failure was accompanied by an increase in anisotropy ϵ_a/ϵ_w
  - Across-grain strain increases more rapidly than with-grain strain
  - Post-graphitization heat treatment causes some small increases in strain-to-failure but with greater data scatter, possibly due to the enlargement of pore clusters which are critical flaws

■ Tensile strength.
  - Strength increases linearly with densification and graphitization. A post-graphitization heat treatment resulted in decreases in density with a decrease in data scatter but no substantial improvements in tensile strength
  - With-grain strength increases slightly faster than across-grain strength

■ Effect of particle morphology. The microstructure of additives of 15% or less has little significant effect on bulk properties, since these graphitize in the mix but not when processed separately. The effect of isotropic additions appears to be a decrease in density, accompanied by a greater scatter in tensile properties. The addition of 15% fines which were slightly anisotropic or no fines caused the greatest improvements in properties with respect to uniformity of data and highest minimum value in both the across-grain and with-grain direction.

Literature Cited

1. Klug, A. P., and Alexander, L. E., "X-Ray Diffraction Procedures," John Wiley, New York (1954), p. 512
2. Warren, B. E., Phys. Rev (1941), <u>59</u>, p. 693
3. Fischbach, D. B., in "Science and Technology of Carbon Materials, A Symposium at the University of California at San Francisco, Calif.," 14−16 Aug 1974 (1974), II-1 to II-21
4. Fitzer, E., Mueller, K., and Schaeffer, W., in "Chemistry and Physics of Carbon," Marcel Dekker, New York (1971), <u>7</u>, pp. 269−272
5. Blackman, L. C. F., "Modern Aspects of Graphite Technology," Academic, New York (1970), p. 9
6. Maire, J. and Méring, J., "Proc. Conf. Carbon 4th at Buffalo, New York," Pergamon Press, New York (1963), p. 345

7. White, J. L., "Preprint of ACS Symposium on Petroleum Derived Carbon, Phila, Pa." (1975), 19, pp. 440−443
8. White, J. L., Johnson, G., and Zimmer, E., "Extended Abstracts of 12th Biennial Conference on Carbon, Pittsburgh,Pa." (1975), American Carbon Society and University of Pittsburgh,REVMAT, Silver Springs, Md., pp. 221−222
9. Mantell, C. L., "Carbon and Graphite Handbook," Interscience Publishers, New York (1968), p. 152
10. Bradshaw, W. G. and Pinoli, P. C., "LMSC Glass-Like Carbon," Lockheed Palo Alto Research Laboratory, Palo Alto, Calif. (1969), pp. 11−12
11. Fischbach, D. B., in "Chemistry and Physics of Carbon," Marcel Dekker, New York (1971), 7, pp. 71−88
12. Fitzer, E. and Kegel, B., Carbon (1968), 6, p. 433
13. Thrower, P. A. and Nagle, D. C., Carbon (1973), 11, p. 663
14. Rothwell, W. S., J. App. Phys. (1958),39, pp. 1840−1845
15. Wignall, G. D. and Pings, C. J., Carbon (1974), pp. 51−55

Graphites for Thermostructural Application

C. A. PRATT, JR.

Air Force Materials Laboratory, Wright Patterson AFB, Ohio 45433

Materials for use as nosetips on ballistic re-
entry vehicles must be able to withstand the severe
conditions imposed by reentry. Two of the important
considerations are mass loss by ablation and resistance
to mechanical failure as a result of the steep tempera-
ture gradients generated within the material by reentry
heating. Of the materials which may be considered for
nosetip use (Figure 1), graphite has the best ablative
performance but is limited thermostructurally by its
allowable mechanical strain. The carbon-carbon mate-
rials which have good ablation and thermostructural
performance are somewhat handicapped by the complexi-
ties of fabrication which lead to costs approximately
thirty times that of graphite. In view of this situa-
tion it behooves the system designer to evaluate the
cost effectiveness of graphite for a particular system.
    Several changes in traditional design have been
made in an attempt to allow the use of graphite. One
of the most notable is the change from a shell type
tip to a plug (Figure 2). The primary difference is
the change from a principle maximum hoop strain to a
principle on axis strain with a resulting lower magni-
tude. Other changes such as comprehensive nondestruc-
tive inspection for materials truncation and methods
of establishing design allowables also have been uti-
lized. These, when incorporated with improved mate-
rials provide a substantial technology base for the
user.
    The approach taken to improve bulk graphite has
been an iterative event based on increasing the strain
allowable within a material while not allowing other
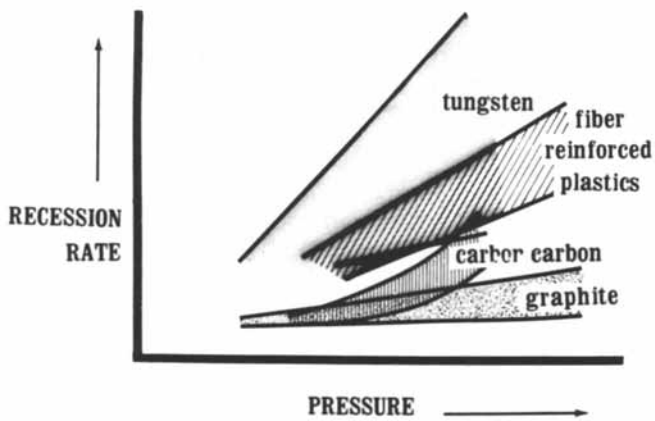
*Figure 1.   Compartive recession rates of high tem-
perature materials*
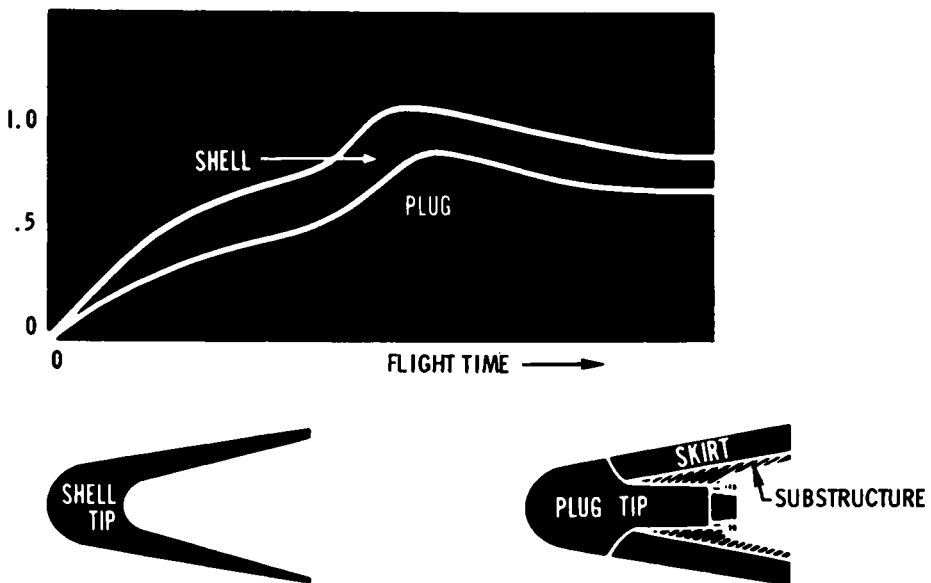
Figure 2.   Maximum strain/critical strain

properties to change in a deleterious manner. It has
also included a necessity to hold property variations
within a billet and from billet to billet to a minimum
and to work with fabrication processes that are well
established and understood. This has avoided to some
extent the possibility of having such things as for-
mulation changes masked by unknown processing events.
The original selection of baseline grades or materials
to optimize was made by examining microstructure,
crack propagation characteristics, and temperature
stress information (Figure 3). From these considera-
tions a decision was made to pursue optimization on
those materials having maximum particle sizes in the
60 to 100 micron range and microstructures that fit a
preconceived idea of the type required for load carry-
ing capability and relatively free of crack propaga-
tion sites. No attempt has been made to mathemati-
cally express these parameters in predictive or cor-
relative equations as has been done for other ceramics.
Figure 4 illustrates some of the pore distribution and
size problems that were of concern in the iteration
sequence. Figure 5 defines the load carrying capabi-
lity desired where curve B dramatizes the desirable.
Figure 6 illustrates the related process steps associ-
ated with determining various characteristics of the
graphite. It was through these steps that adjustments
such as volume per cent of fine particles in the mix
and amount of densification in each impregnation cycle
were examined.

Although higher graphitization temperature can be
used advantageously to increase strain it was never
seriously investigated to higher temperatures during
processing because of the difficulty in establishing
uniform, known temperatures (Figure 7) in available
equipment. The thought here was that higher tempera-
ture graphitizations would add more variability than
it would favorably increase strain. Figure 8 is the
flow diagram for the most recent iteration on the two
base grades designated as 994 and 1140. For 994 as
illustrated on the top line only a very minor adjust-
ment has been made to change the structure slightly.
Other graphites shown in the flow diagram have under-
gone more dramatic changes. Preliminary data for
these graphites are shown in Table I.
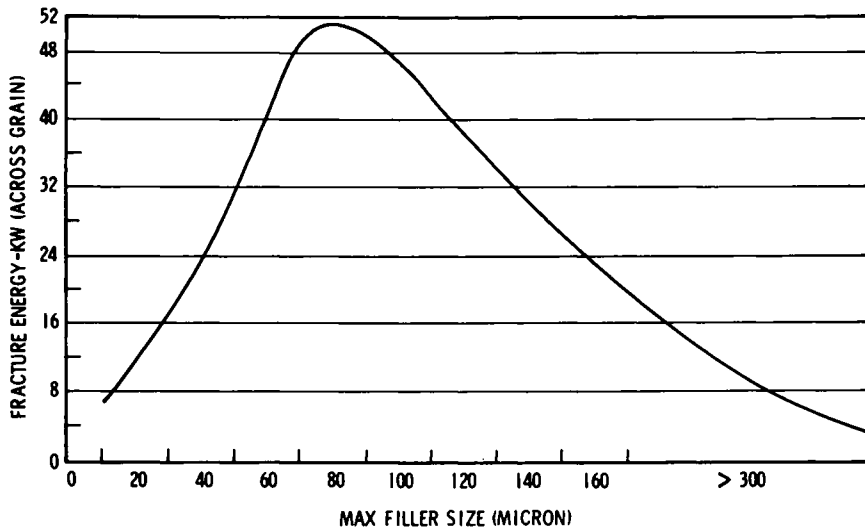
Figure 3.   Thermal stress resistance vs. maximum filler size and processing conditions
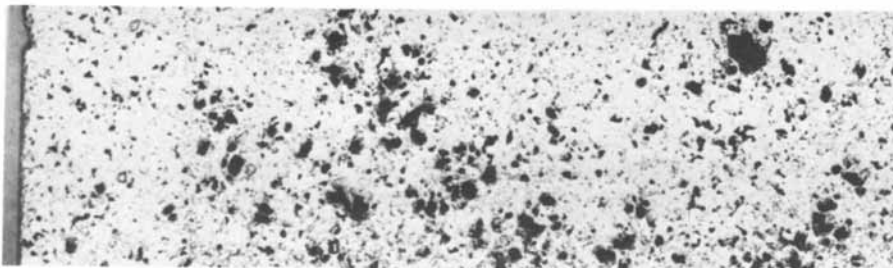
Figure 4.   85× photomicrograph of material 1140 (vacuum impregnated)
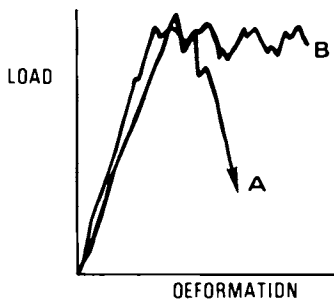
Figure 5. *Fracture toughness*

PARTICLES PREP	PRESS	HT	IMPREG CYCLES	GRAPHITIZATION
1. VOIDS 2. VOID CLUSTERS 3. INCLUSIONS 4. PORE SIZE 5. PORE SIZE DIST 6. PROFILES	1. INCLUSIONS 2. CRACKS 3. SOLID RESPONSE 4. STRIATIONS 5. PROFILE	1. CRACKS 2. SOLID RESPONSE	1. VOIDS 2. VOID CLUSTERS 3. CRACKS 4. SOLID RESPONSE 5. STRIATIONS 6. PORE SIZE 7. PORE SIZE DIST 8. PROFILES	1. CRACKS 2. SOLID RESPONSE
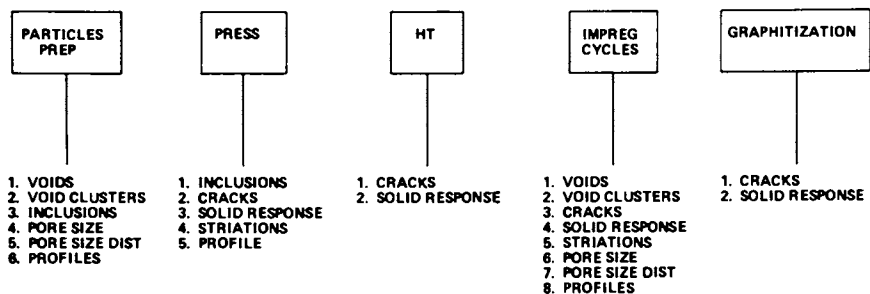
Figure 6. *Process anomalies*
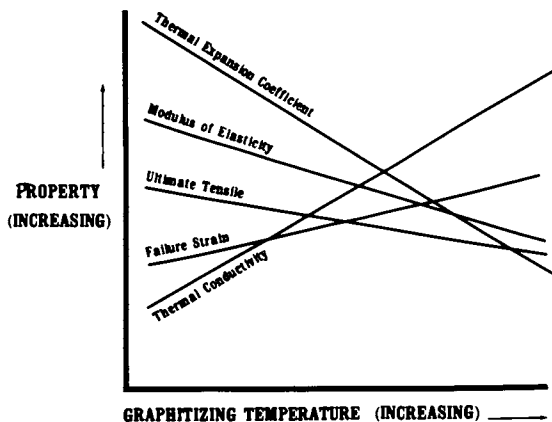
Figure 7.
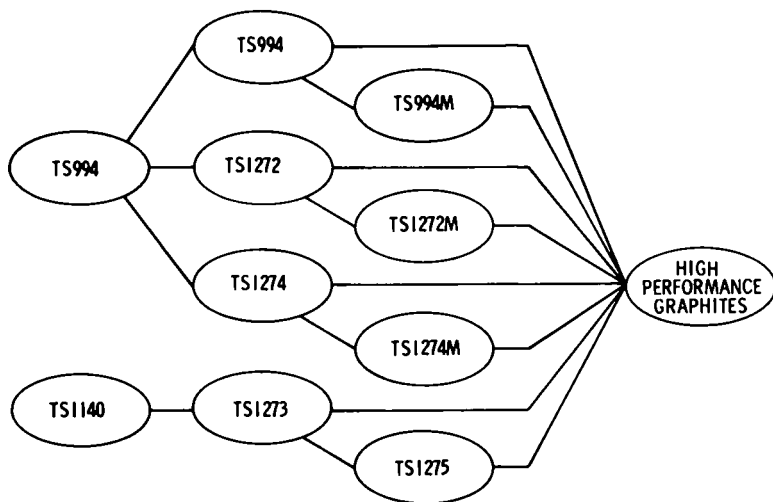
Figure 8.

TABLE 1

POLYCRYSTALLINE GRAPHITE

PROPERTY*	UNITS	PRODUCTION ATJS	TS1276	TS994	TS1272	TS1273	TS1274	TS1275
STRAIN TO FAILURE	MILS	5.1/4.2	5.9/4.6	7.3/5.4	8.59/5.81	7.37/4.62	8.06/5.75	7.45/5.15
TENSILE STRENGTH	PSI	4200/5200	4520/6080	4200/5700	4242/6070	3711/4815	3936/5689	2303/4769
EXPANSION (RT TO 5000°F)	MILS	16.6/13.1	16.6/13.0	16.0/11.7	18.0/11.8	17.9/12.3	17.7/11.4	18.1/12.1
DENSITY	g/cc	1.83	1.84	1.86	1.83	1.80	1.81	1.74
THERMAL STRESS	KW/IN²	6.3/9.5		10.4/18.3	11.3/19.5	13.1/18.5	13.1/20.0	10.8/17.6

* VALUES ARE ACROSS GRAIN/WITH GRAIN
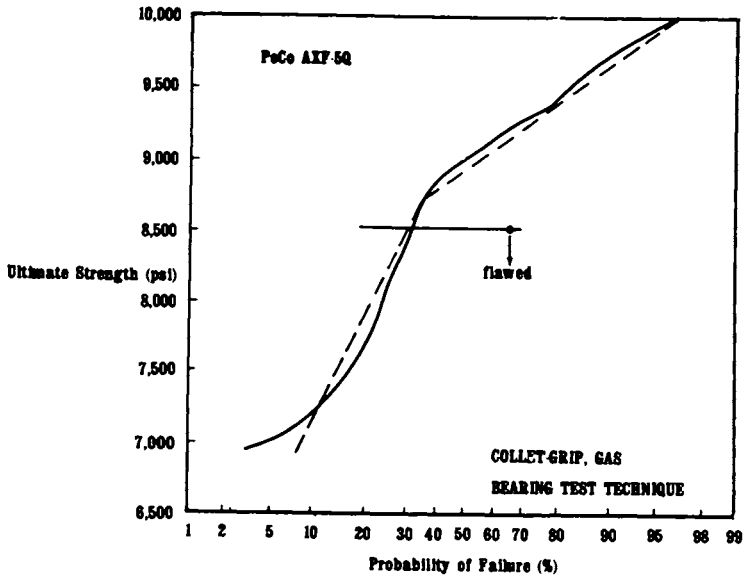
Figure 9. *Uniaxial ultimate strength vs. probability of failure*
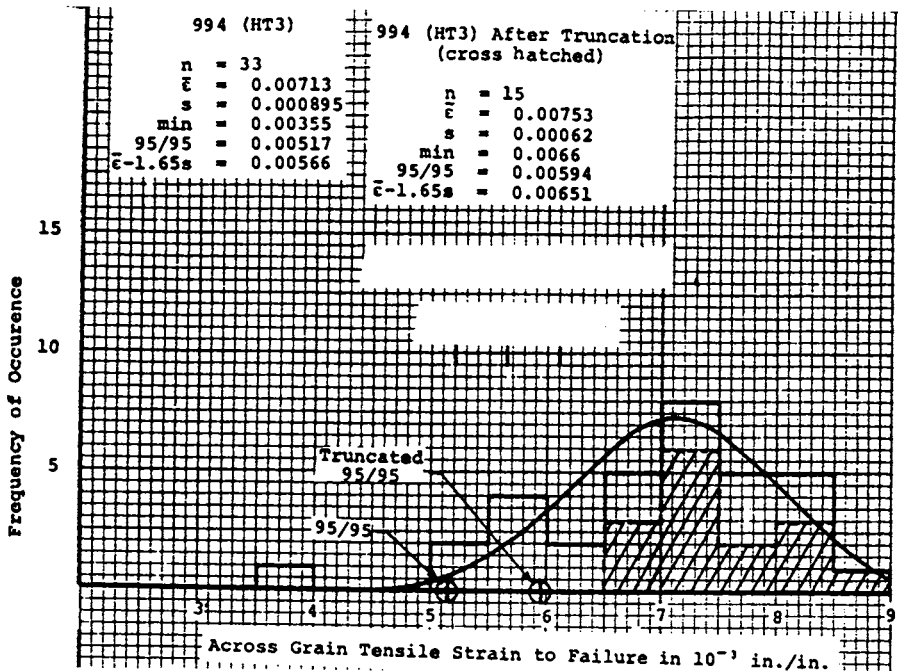
Figure 10.

TABLE 2

NDT DETECTION TECHNIQUES

FLAW TYPE   **NDT TECHNIQUE**

VOIDS ────────────────────────
X-RAY
PULSE-ECHO
ULTRASONIC ATTENUATION
SURFACE INSPECTIONS

VOID CLUSTERS ──────────────
X-RAY
PULSE-ECHO
ULTRASONIC ATTENUATION
SURFACE INSPECTIONS

INCLUSIONS ──────────────
(BONDED AND UNBONDED)
SELDOM X-RAY
SELDOM PULSE-ECHO
OCCASIONALLY ULTRASONIC ATTENUATION
SURFACE INSPECTIONS

CRACKS ───────────────────
SELDOM X-RAY
SELDOM PULSE-ECHO
ULTRASONIC ATTENUATION
SURFACE INSPECTIONS
PULSE-ECHO ───────── LOSS OF BE / SEE SAW

SOLID RESPONSE ────────────
OCCASIONALLY X-RAY
VELOCITY
ELECTRICAL RESISTIVITY
APPARENT DENSITY (POROSITY)

STRIATIONS ───────────────
OCCASIONALLY X-RAY
PULSE-ECHO – WEAK BE
ULTRASONIC ATTENUATION
SURFACE INSPECTIONS

PORE SIZE ─────────────────
SELDOM X-RAY
VELOCITY
ULTRASONIC ATTENUATION
OCCASIONALLY SURFACE INSPECTIONS
POROSITY/PERMEABILITY

PORE SIZE DISTRIBUTION ──────
OCCASIONALLY X-RAY
VELOCITY
ULTRASONIC ATTENUATION
OCCASIONALLY SURFACE INSPECTIONS
POROSITY/PERMEABILITY
DENSITY
PULSE-ECHO – WEAK BE

Concurrent with the initiation of the development of graphites with a higher strain capability, a comprehensive nondestructive testing program was started to find a way to reject flawed material from usage (Figure 9). Previous NDT programs had not provided success in this area because of attempted one-on-one correlations, i.e., one technique-one kind of flaw approach. The new approach included blind NDT where all standard techniques were utilized to examine many billets in several diameters. This information was then matched against destructive data both in singular fashion and in combinations to determine applicable techniques. The conclusion made from this investigation was that while some techniques appeared sensitive to the flaws listed in Figure 6, all techniques listed in Table II must be utilized for maximum impact on design allowables. The effect of being able to truncate materials by the use of NDT is illustrated in Figure 10 where the truncated population is compared with the total population. The strain minimum is moved from 3.5 mils to 6.6 mils and the design allowable 95/95 about 0.8 mil.

Another aspect which has been investigated because of necessity is the strain allowable at about 2000°F since this is the temperature at which critical strain occurs in many nosetips. With the graphites investigated, strain capability at this temperature was lower than room temperature which caused a design handicap. Heat treatments at well controlled temperature and time intervals were investigated and found to correct this problem. The HT3 on Figure 8 is a designation which reflects the heat treatment conditions.

Other aspects such as multiaxial response, volume effects, and improved predictive code capabilities have also added significantly to the capability of utilizing graphite for nosetips.

Acknowledgements

17

Formation of Carbon–Carbon Composite Materials by Pyrolytic Infiltration

J. J. GEBHARDT, E. R. STOVER, W. MUELLER, and J. YODSNUKIS

Advanced Materials Development Laboratory, General Electric Co.,
Re-Entry and Environmental Systems Division, Philadelphia, Penn. 19101

Carbon-carbon composites comprise a class of high tempera-
ture structurally efficient materials useful among other things,
for nose tips and thermal shields on high velocity re-entry
vehicles. They consist of polycrystalline graphite, the so-called
matrix phase, reinforced with a predetermined, prewoven three-
dimensional array of graphite or carbon fibers, having spacing,
packing, composition and geometry selected for optimum response
to certain anticipated thermomechanical service loads. Extensive
design and development work has led to two major approaches for
formation of the matrix phase, i.e., the graphite in the inter-
stices and within the fiber bundles, of prewoven fiber forms so
as to achieve maximum, uniform density throughout the structure
with minimum distortion of the geometry or damage to the fibers.
These are based respectively on multiple pitch impregnation/char/
graphitization cycles and on the pyrolytic decomposition of a
carbon precursor vapor at surfaces within the structure.

The two approaches can be combined for the purpose of
reducing the overall processing time for larger woven billets, by
first infiltrating and depositing from the vapor phase to a pre-
determined extent and then completing the densification by pitch
impregnation. The procedures used in a specific case are deter-
mined by the properties of the matrix achieved and whether or not
the combination of matrix, fiber and geometry can meet the per-
formance requirements of the mission for which the material is
intended.

Fiber Preforms

The graphite fiber preforms which constitute the reinforcing
component of carbon-carbon composites are prepared on the basis
of previously stipulated geometry, fiber packing ratios, spacings

212

and fiber selection. These are selected to provide optimum per-
formance under different service conditions in terms of strength,
thermal shock resistance, thermal conductivity, and ablation re-
sistance. Considerable prior development has been undertaken to
arrive at a number of weave geometries which have shown potential
for achieving composites in which the strength and modulus of the
fibers contribute to the properties of the composite. Several
of these geometric arrangements are shown schematically in
Figure 1.

The manner of weaving these configurations avoids sharp
bends and crimping of the fiber bundles; effectively the fiber
bundles are aligned along the principal axes of the selected con-
figuration and compressed to the desired spacing. The fiber
packing in any direction can be varied so that, for example, in
a three directional orthogonal array, the fiber bundles which lie
in the Z direction can contain several times the number of fila-
ments placed in the X or Y direction. Similarly, the fiber
bundles forming the orthogonals in the seven directional geometry
can be varied from those comprising the diagonal directions. By
such variations, the fiber volume in a so-called unit cell of the
repeating geometric pattern can be varied to provide a number of
different ratios of reinforcement between Z and X-Y directions
in the orthogonal case, or between orthogonals and diagonals in
the 7D case. The packing density, gross preform size and geometry
are important factors in the efficiency with which the geometric
interstices and fiber bundles can be filled with a matrix material,
graphitic in most instances of interest in aerospace uses, to
achieve a high density composite with the desired constellation
of properties.

The maximum strength of multidirectional reinforced carbon-
carbon composites lies in the direction of the reinforcing fiber
bundles. In a 3D orthogonal geometry, this is clearly in the
X, Y and X directions. The 7D structure is a combination of 3D
and 4D geometries, consisting of orthogonally arranged (X,Y,Z)
bundles with additional fiber bundles (T,U,V,W) running along all
four diagonals of the 3D unit cell cubes. This design provides
improved shear strength compared with the 3D material (1,2).

The cubic voids of the 3D structure share common corners,
while the voids of the 4D geometry share common sides, as is
shown in Figure 1. Hence the latter geometry is inherently more
permeable than the former. The 7D structure, a combination of
these geometries, would therefore be expected to be more permea-
ble than a purely 3D orthogonal. Because of the available
channels in the 7D structure, gas can continue to diffuse to
inner regions despite rapid deposition within the fiber bundles,
which quickly seals off the restricted access to corner-connected
cubic voids in 3D structures.

The remainder of this paper is concerned with densification
by pyrolytic carbon infiltration, of relatively large (4"x4"x8")
preforms containing graphite fiber bundles in a 7D geometry.*
Figures 2 and 3 show radiographic positive views of such a

3D ORTHOGONAL

UNIT CELL IN T DIRECTION

CONTACTS BETWEEN PRISMS

4D CUBIC

7D
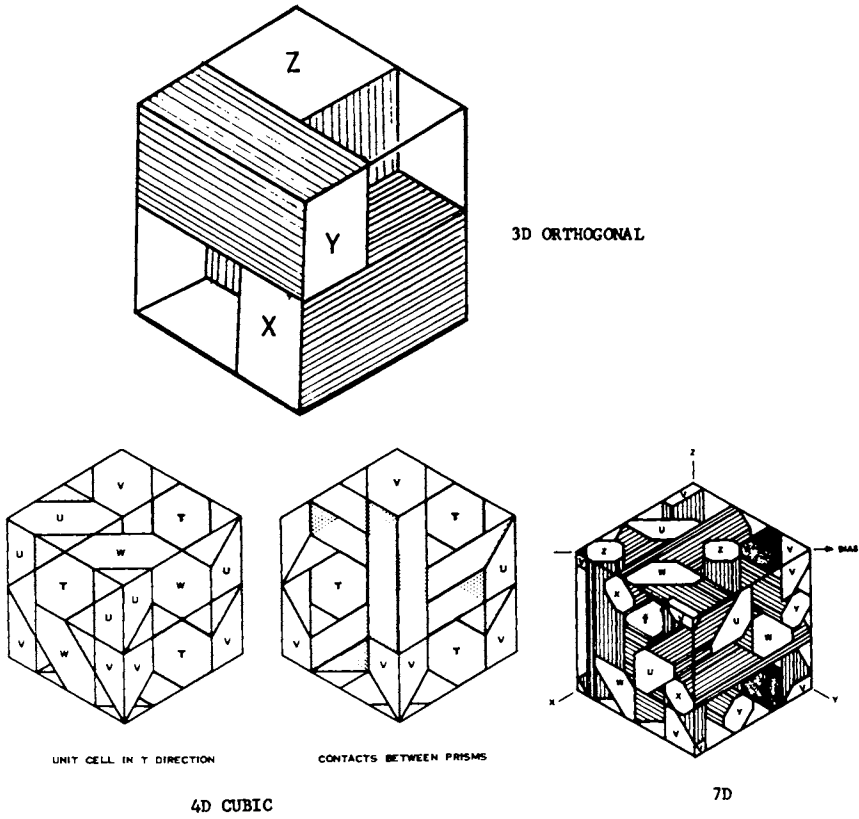
Figure 1. Fiber reinforcement geometries
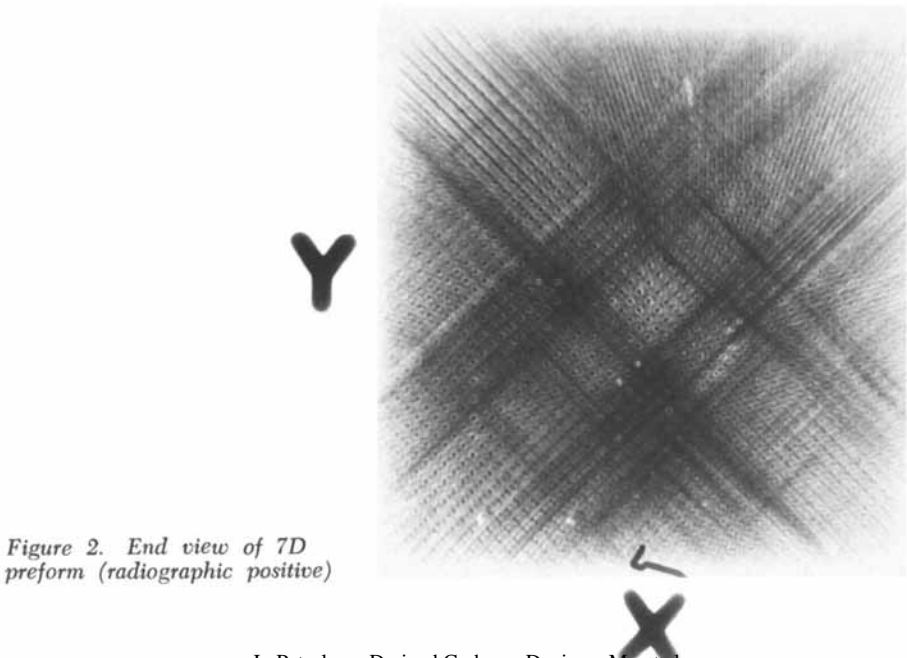
Figure 2. End view of 7D preform (radiographic positive)
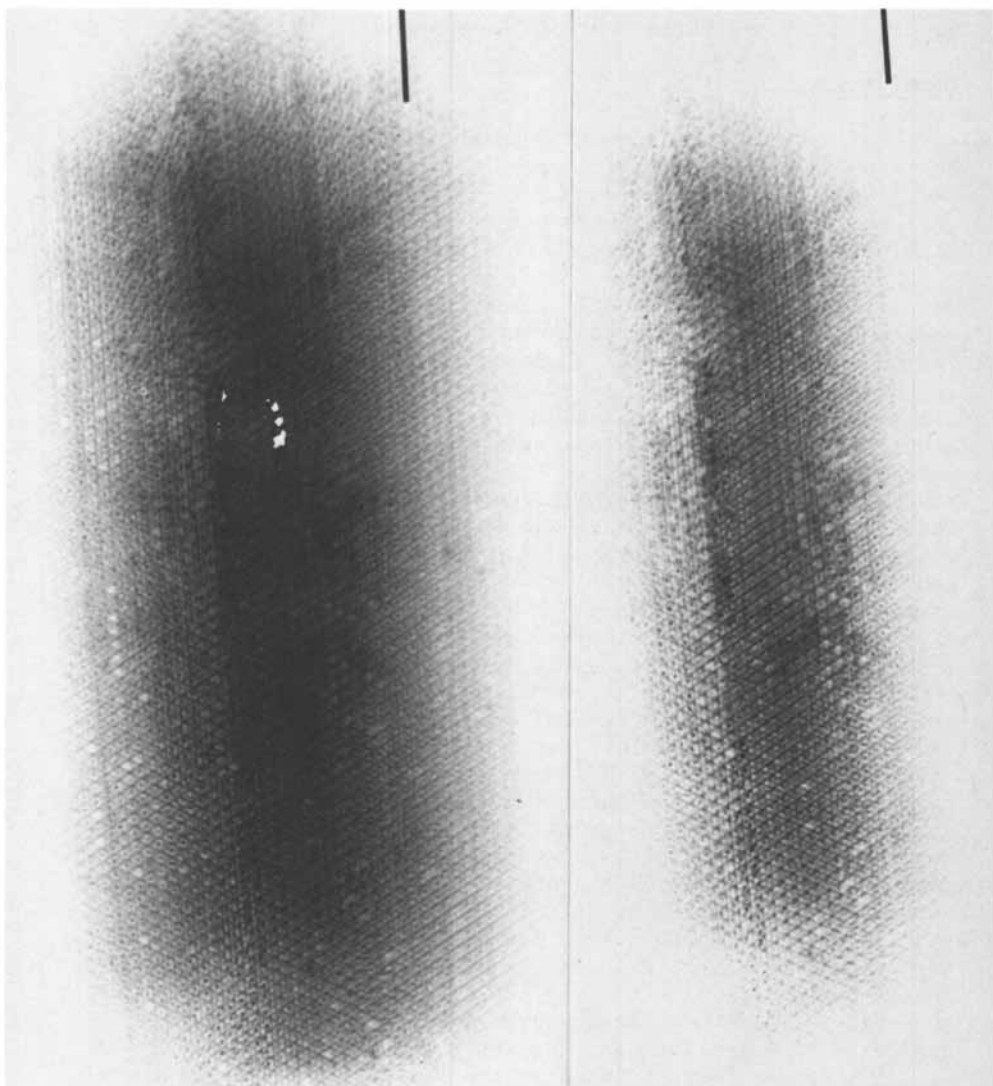
Figure 3. 7D graphite fiber preform viewed in one of the diagonal directions. Right view at lower intensity shows center region.

preform, taken from one end and from one of the diagonal positions
in which the dark spots are due to fiber bundles, viewed end-on,
while the dark lines represent fiber bundles viewed laterally.
The fibers were polyacrylonitrile (PAN) precursor material, two
thousand filaments per tow with four tows comprising the ortho-
gonal bundles and three tows in the diagonal direction (2).

Pyrolytic Infiltration

      The customary procedure by which both relatively porous and
quite dense bodies are infiltrated with carbon, using the thermal
decomposition of methane, consists of maintaining the entire body
at a uniform constant temperature, usually around 1050-1100°C, in
flowing methane at a pressure of 1 to 100 torr (3).
      In the process, the feed gas undergoes a series of vapor
phase interactions as it diffuses into the preform, forming inter-
mediate species which further react to deposit carbon on all
heated surfaces. The overall deposition rate is highly sensitive
to surface area, as well as concentration, so that clogging of
outer access paths is a problem when high infiltration densities
are called for. The driving force which causes the methane to
continue to enter the preform from the exterior gas phase is the
concentration gradient established between the outer surface and
locations within the preform where decomposition has depleted the
gas phase to varying extents. Simultaneously, hydrogen, which is
generated by the decomposition reactions, diffuses outward to the
exterior gas stream where the hydrogen content is close to zero,
if pure methane is used as the feed gas. Hydrogen also acts as
a deposition suppressant by its mass action effect on inter-
mediate reactions which generate it, and is sometimes added to
the feed mixture. As a result, a deposition gradient is estab-
lished within the preforms as a function of distance from the
outer surface. This is influenced by the geometry of the pre-
form as well as the concentration gradients so that deposition
gradients will vary with geometry under similar infiltration
conditions. As a result, in order to achieve high infiltration
densities, even with fiber preforms which have a well distributed
surface area, such as carbon felt, it is necessary to operate at
minimal deposition rates for long periods of time, with periodic
mechanical removal of the outer surface through which the gas no
longer has access. Because of the high cost of the preforms of
interest in this work, such a procedure is not suitable for
achieving high infiltration densities.
      A second procedure known as the 'thermal gradient approach'
(4) consists of maintaining the deposition region which is far-
thest away from the gas supply at the highest acceptable tempera-
ture, i.e., below that at which gas phase sooting occurs. This
is accomplished by placing the woven construction, which is to be
infiltrated, against a heated surface, thereby establishing a
temperature gradient within the structure. The gas flow is

relatively high and at approximately one atmosphere with some degree of dilution with either hydrogen or an inert gas. Deposition occurs on the back or hottest surface first and proceeds uniformly through the weave to the outer surface as the structure becomes denser and thermal conductivity improves. The method is most useful for relatively thin (e.g., up to 1 inch thick) structures. In the case of the larger three-dimensional structures such as the 7D billets of interest in the present work, the diffusion paths would be too long and deposition would occur principally in the outer regions, leaving a low density core. Furthermore, the larger cross-section of the specimen causes considerable gas turbulence and uncertain gas phase pyrolysis conditions.

A variation of the temperature gradient method was developed for the purpose of densifying woven structures of suitable size for fabrication of nose tips. This approach consists of coupling the fiber structure directly with the field produced within a r.f. coil. The densely packed graphite fibers conduct sufficiently well to heat the preform, in such a manner that the highest temperature produced is in the center of the preform. The temperature gradient between the hottest and the coolest surfaces of a fiber preform depends on the density of the preform, the fiber geometry and the thermal conductivity of the fibers themselves as well as the velocity with which gas is passed around the preform. In preforms comprised of randomly oriented short filaments, such as a carbon felt, the temperature gradient can be as high as several hundred degrees per inch, while in 3D orthogonal, tightly packed preforms, it can be as low as ten to twenty degrees per inch, from the center of the preform to the outer surface (5). By using a short coil, i.e., with only two or three turns, one end of the preform can be heated in this manner, and the billet can be drawn slowly through the coil so that eventually its entire length is heated in this manner. During this procedure, the process gas is passed around the preform at high velocity to provide high methane concentration at preform surface as well as maintain the steepest possible temperature gradient.

This method was explored in preliminary experiments using small (e.g., 0.5" square to 2" square) woven substrates of varying reinforcement geometry, mounted in a fixed position within the coil. The arrangement is shown schematically in Figure 4. The temperature of the hottest visible part of the billet within the coil was maintained at 1075–1100°C with an optical pyrometer and manual power supply control. The results of these experiments showed that at fixed temperature, gas flow and pressure, secondary effects such as geometry, packing density, and void size and shape govern the degree of densification achievable, as well as the uniformity of distribution of the pyrolytic carbon within the structure (5). Figure 5 relates some of these factors (unbroken lines) in terms of initial preform density and the

Specimen
Motion

To Vent

Woven Preform

R.F.Coil

Gas Container

Gas Inlet
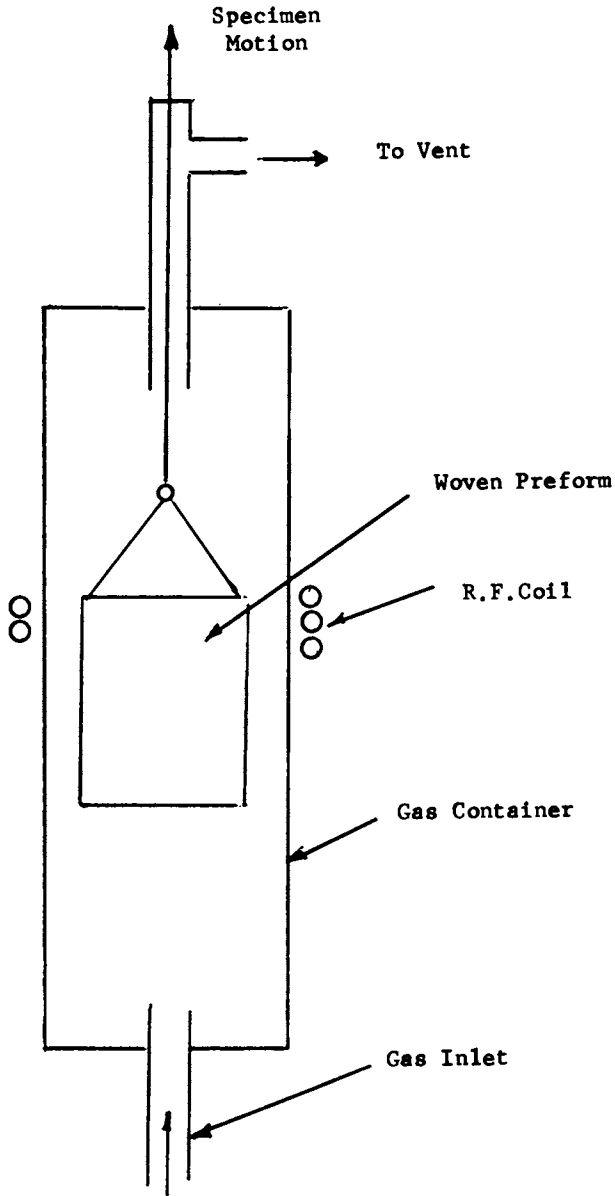
Figure 4.   Schematic of direct coupling infiltration
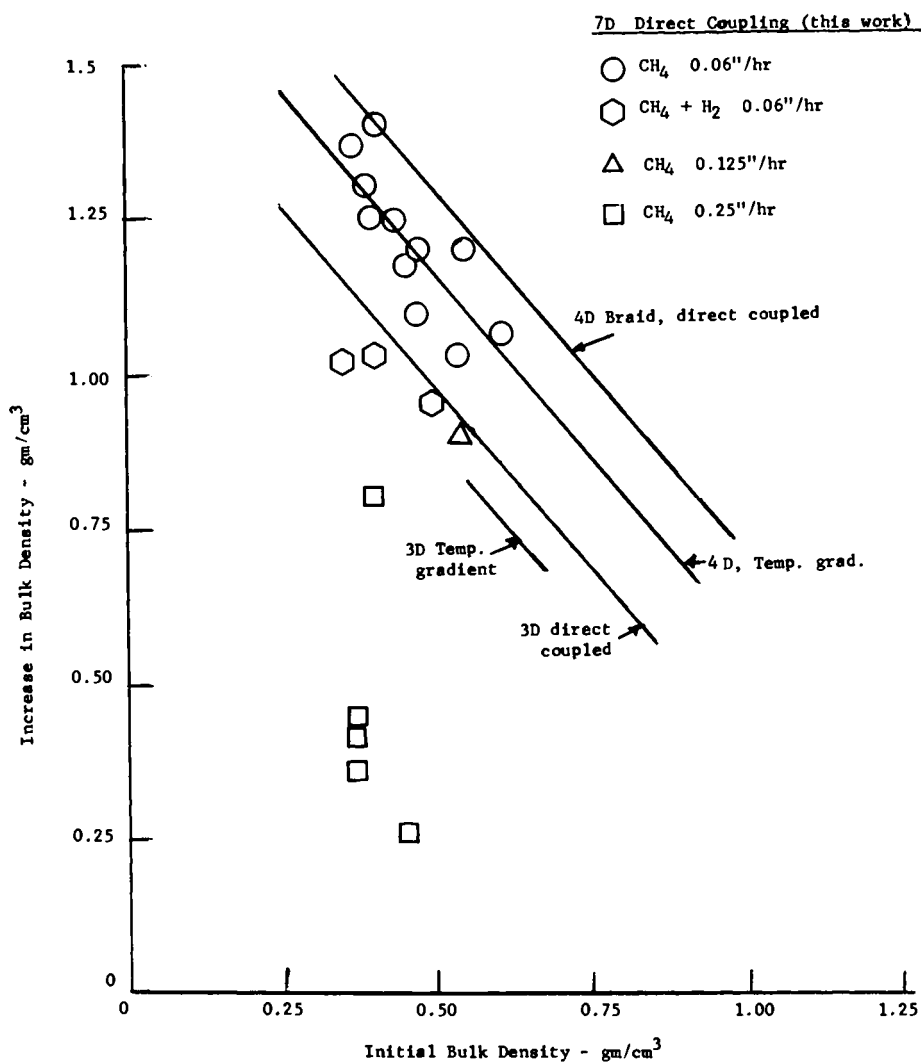
Figure 5. *Correlation between initial and final density for various weave geometries and infiltration methods*

increase in density achieved by the time deposition began to occur predominately on the outer surface. Several fiber geometries and methods were correlated in this manner, and in general indicated that higher infiltration densities could be achieved with relatively open accessible void structures, such as random fiber orientation (e.g., felt) or connected voids (e.g., non-cubic) when direct coupling was used (6). Infiltration of these geometries by the temperature gradient method yielded slightly lower density increases than did the direct coupling technique. The closed, cubic void structure of the 3D orthogonal structures was more difficult to densify by either method.

Preliminary experiments were conducted with materials which were about one square inch or slightly larger in cross-section, and which were drawn through the coil manually in batch fashion until the entire length of the specimen has been infiltrated. For the purpose of achieving uniformity from end to end with larger specimens, the 4" x4" x 6-8" billets processed in the scale-up work, were suspended from a motor driven lift and continuously raised through the coil during the entire infiltration. In several cases, the feed gas was diluted with hydrogen to repress premature deposition in the outer portions of the billets. The rate at which the billet was raised through the coil was also varied to provide specimens which would ultimately contain different ratios of pyrolytic to pitch-base graphite after impregnation and graphitization. Table 1 summarizes the process data and lists the results in terms of bulk density measured after removing the surface scale and lower density ends of the preforms. Referring to Figure 5, it is seen that the increases in average bulk density attained, represented by open symbols, agree fairly closely with the preliminary results, which are shown as solid lines. However, all of the finished materials contained density gradients from center to outside. Densities were estimated radiometrically to range from 1.2 to 1.4 gm/cm^3 at the center to 1.6 to 1.7 gm/cm^3 in the outer fiber region and at the corners in specimens drawn through the coil at .06 in./hour. Specimens infiltrated at higher draw speeds, e.g., 0.125 or 0.25 in/hour were less dense as is shown in Figure 6, but also had noticeable density gradients, ranging from about 0.85 to 1.20 gm/cm^3 through the thickness. This is illustrated in the radiograph shown in Figure 7. Hydrogen was added to the feed gas in an effort to repress premature deposition of carbon in the outer fiber region but this was not a wholly successful procedure, and radiographs of the infiltrated specimens showed significant density gradients existed. Figure 8 shows how the surface area sensitive nature of the pyrolytic infiltration process causes carbon to concentrate in the fiber bundles. Clogging of the access paths at intersections of the fiber bundles leaves the large interstitial voids incompletely filled. In Figure 9 at higher magnification, void regions can be seen among individual filaments within the fiber bundles.

TABLE I

PROCESS DATA FOR INFILTRATION OF 7D WOVEN CONSTRUCTIONS

Spec. No.	Cross Section (in.)	Draw Speed (in/hr)	Bulk Density (g/cm³)			After Pitch	Gas Comp. City plus	Density Gradient (g/cm³)
			Initial	Final	Incr.			
709A	1.52 x 1.41	.05	.39	1.86	1.12	----	----	
709B	1.25 x 1.25	.06	.43	1.69	1.26	----	----	
709E	1.30 x 1.30	.066	.38	1.63	1.25	----	----	
709G	1.90 x 1.90	.057	.41	1.67	1.27	----	----	
721	1.94 x 1.87	.06	.32	1.69	1.20	1.85	----	
731	1.20 x 1.19	.06	.54	1.74	1.37	1.85	----	
709F	1.33 x 1.33	.066	.40	1.46	1.06	----	----	
732T	1.0 x 1.0	.06	.47	1.76	1.29	1.86	20 % H$_2$	
732B	1.0 x 1.0	.125	.47	1.67	1.20	1.84	----	
733	1.0 x 1.0	.06	.35	1.70	1.35	1.84	----	
703	3.38 x 3.38	.05	.46	1.66	1.34	1.82	----	
705	3.33 x 3.33	.05	.44	1.54	1.10	1.82	20 % H$_2$	1.75 - 1.83
701	4.20 x 4.20	.06	.50	1.42	0.93	1.79	20 % H$_2$	1.2 - 1.7 (after CVD)
707	3.20 x 3.20	.057	.53	1.60	1.07	1.86	----	
710	3.40 x 3.40	.06	.48	1.57	1.09	1.82	----	
706	3.39 x 3.58	.125	.53	1.45	0.93	1.83	----	
720	3.33 x 3.40	.250	.38	1.16	0.78	----	----	
723A	3.40 x 3.38	.250	.37	.84	0.47	----	----	
723B	3.50 x 3.25	.250	.39	.78	0.39	----	----	
727	3.28 x 3.28	.250	.45	.73	0.28	----	----	
719	4.27 x 1.21	.250	.38	.79	0.41	----	----	

Conditions: Max. Temperature Approximately 1075-1100°C
Gas Velocity Approximately 165 cm/sec
Methane-City Gas, Phila. Gas Co., 1030 BTU/ft³, dried
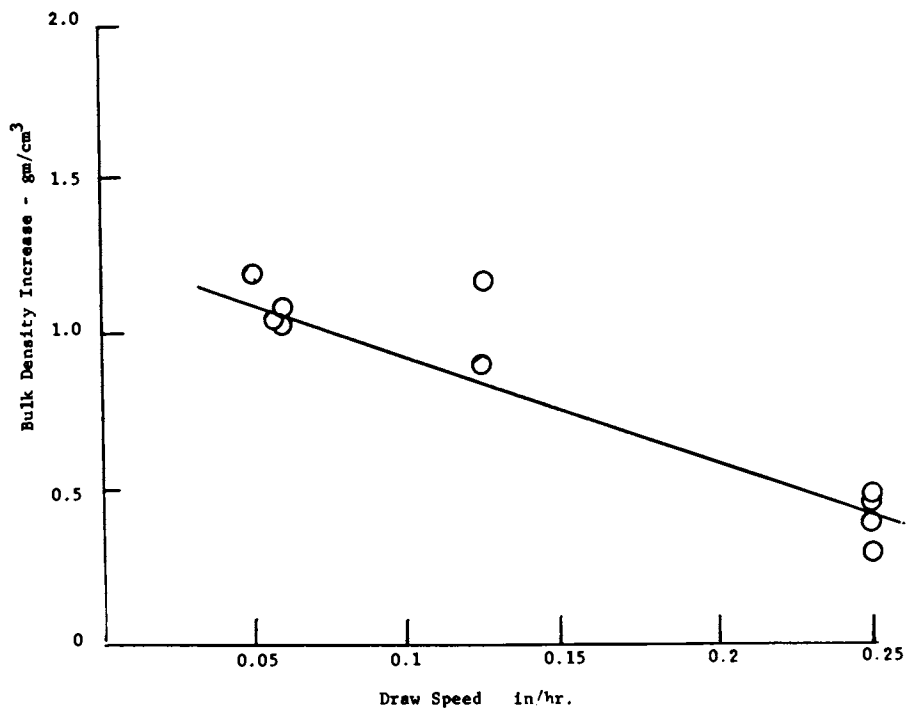
Figure 6.   *Correlation between specimen draw speed and density increase*
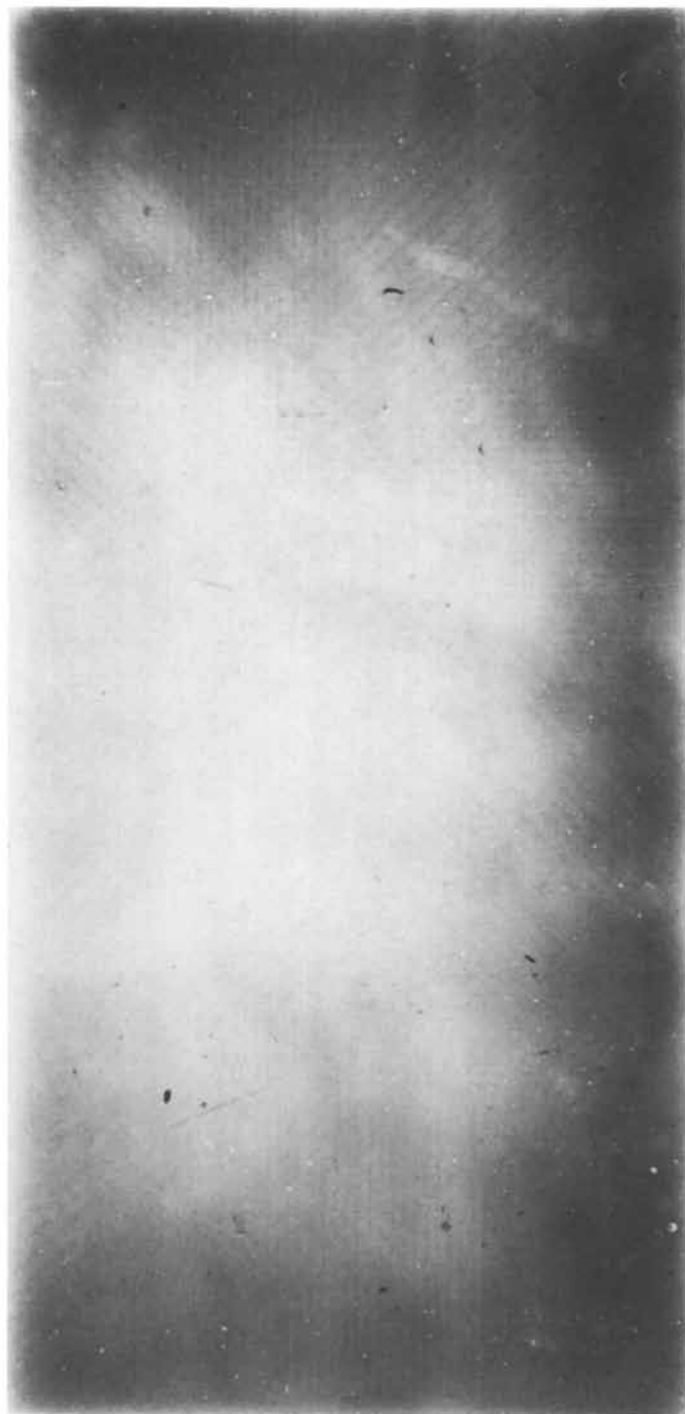
Figure 7. Radiographic positive of 7D graphite fiber preform after pyrolytic infiltration at 0.125 in./hr, showing density gradients
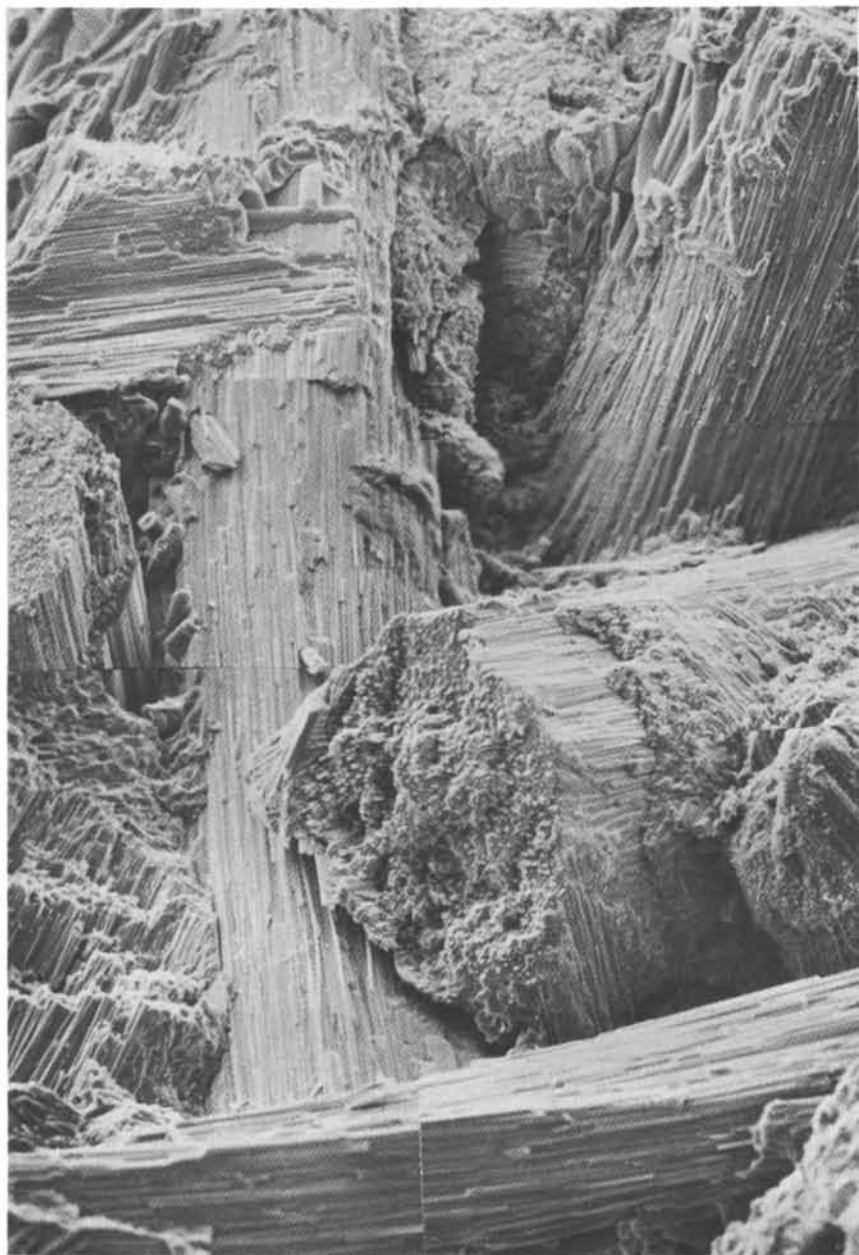
Figure 8. Scanning electron microscope montage of high density (1.73 gm/cm³) infiltrated 7D billet at fracture surface (76✕) showing concentration of infiltrated carbon within fiber bundles
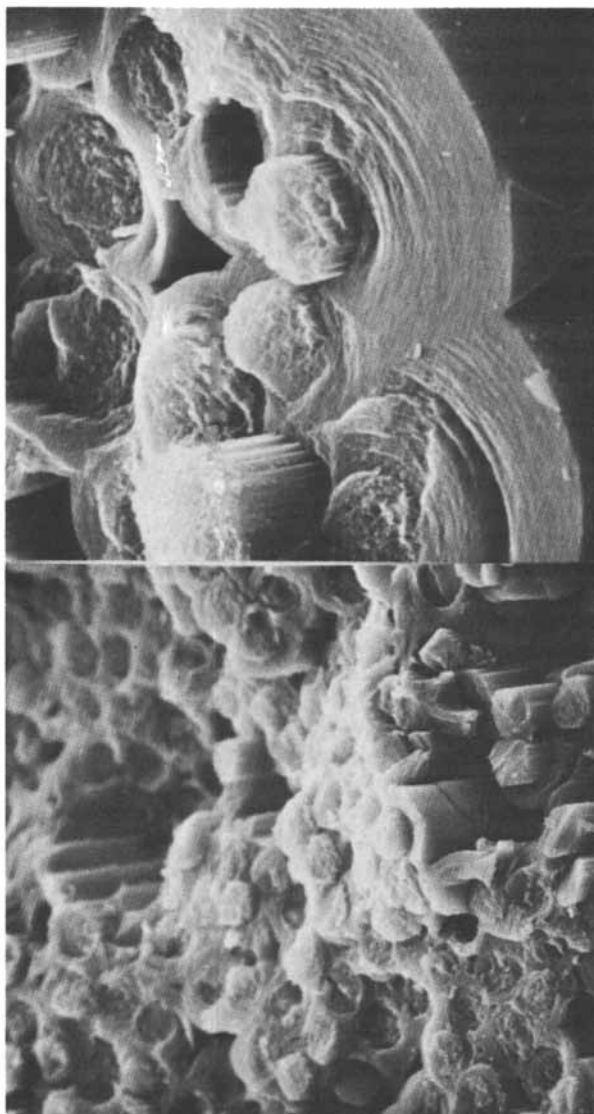
Figure 9. Scanning electron microscope views of pyrolytic carbon deposit within bundles in 7D billet (left, 850×; right, 2550×)

In subsequent processing, the infiltrated billets were impregnated with coal tar pitch at high pressure (1 Kbar), pyrolyzed at that pressure and then graphitized at 2800°C to convert the pyrolytic and pitch-base carbon to graphite.** Final densities were in the range of 1.75 to 1.83 gm/cm^3. Examination of the finished billets by x-radiography showed that density gradients remained even after impregnation, and that regions of the preforms which had been infiltrated the most now had the lower final densities. This is due to sealing of the void regions within fiber bundles by the pyrolytic coating, as is shown in Figure 9, preventing access of the pitch to these locations. Fiber bundles in the centers of the preforms, not being so heavily coated, permitted greater access of the pitch and thus higher final densities. Billets which were infiltrated at higher draw speeds, in which fiber bundles were not as heavily coated, were more uniform after impregnation.

Conclusions

Densification of carbon and graphite fiber three-dimensional preforms was carried out by pyrolysis of methane gas, with heating effected by direct interaction of the preforms with a r.f. field. The pyrolysis process was influenced primarily by concentration gradients within the preforms and by the greater available surface area within fiber bundles, as compared to interstitial void walls. Density gradients were substantially reduced by subsequent impregnation and pyrolysis of liquid coal tar pitch, although the initial gradient due to infiltration became reversed owing to decreased accessibility to pitch where fiber bundles were heavily coated. Selection of this approach to fabricating carbon-carbon composites would depend on the extent to which property variations within the finished material could be tolerated in the ultimate use of the composite.

Literature Cited

1. Stover, E.R. and Latva, J.D., Eleventh Biennial Conference on Carbon, Extended Abstracts, June 4-8, 1973, Paper No.FC-9, p. 277.
2. Stover, E.R., Roetling, J.A., Ruzauskas, E.J., Connell, W. and Hall, K.J., Ibid, Paper No. FC-22, pps. 335-6.
3. Kotlensky, W.V., "Deposition of Pyrolytic Carbon in Porous Solids", in "Chemistry and Physics of Carbon", Vol.9, ed. by P. L. Walker, Jr. and P. A. Thrower, pps. 191-198, Marcel Dekker, N.Y., 1973.
4. Ibid, pps. 198-202.
5. Gebhardt, J.J., Stover, E.R., and Yodsnukis, J.J., Proceedings of 4th National Technology Conf., Soc. Adv. Mat. Proc. Eng. (SAMPE), October 1972, Palo Alto, CA.

6. Gebhardt, J.J., Tenth Biennial Conference on Carbon, June
    1973, Lehigh University, Paper No. FC-33, Summary of Papers,
    Defense Ceramic Information Center.

---

*   Fiber Preforms were fabricated by Fiber Materials Inc.,
    Biddeford, ME, 04005
** Performed at the Y-12 Plant, Union Carbide Corporation,
    Nuclear Div., Oak Ridge, Tenn.

18

Factors Affecting the Structure and Properties of Pyrolytic Carbons

C. F. CULLIS

The City University, London, England

The structure and properties of pyrolytic carbons are considerably influenced by the conditions under which they are formed. In this respect, probably the most important single determining factor is the temperature of formation and here there is general agreement that both the size of the crystallites and their degree of preferred orientation increase with temperature, while the interlayer spacing decreases (1,2). Other factors which have received much less systematic attention include the presence of additives (3,4), the nature of the carrier gas (4,5) and the structure and chemical composition of the initial organic compound. As regards this last factor, the available evidence seems to show that, although the "charring" of solids and liquids yields carbons which bear some structural relationship to the source material (6,7), the pyrolysis of a wide variety of gaseous hydrocarbons at temperatures from 800 to 2000°C produces carbonaceous deposits which are generally very similar (7). However, although few relevant investigations have been made with compounds containing volatile heteroelements, there is evidence that these constituents can significantly influence the structure of the deposited carbon. Thus, for example, pyrolytic carbons obtained from pyridine and thiophene do not graphitise well (7), while the progressive replacement of hydrogen by chlorine in hydrocarbons leads to carbonaceous deposits in which both the size and the degree of preferred orientation of the crystallites are decreased (8).

In some recent work, carbons were formed by the pyrolysis at ca. 1000°C of a cyclic hydrocarbon, cyclopentadiene, and of ring compounds of formally similar structure, but containing different heteroelements, viz. furan, thiophene and pyrrole (9). Some typical values of the density, ρ, the crystallite diameter, L_a, and the crystallite height, L_c, are given in Table 1. These show that the carbons deposited from cyclopentadiene and furan are broadly similar; both materials graphitise readily on heat-treatment to 2700°C, the density approaching the value for ideal graphite (2.269 g cm^{-3}). In contrast, carbons from thiophene and

228

pyrrole differ not only from those derived from the other start-
ing compounds but also from one another. Thus these materials
do not graphitise at all on being heated to 2700°C. With thio-
phene carbons, there is a spectacular decrease in density; while
the carbons formed from pyrrole have an unusually high initial
density which remains almost unchanged on heat-treatment.

Table 1

Properties of pyrolytic carbons formed from different initial
organic compounds

Initial Compound	$\rho(g\ cm^{-3})$		$L_a(10^{-8}cm)$		$L_c(10^{-8}cm)$	
	I	II	I	II	I	II
Cyclopentadiene	1.926	2.261	39.0	>100	18.6	>200
Furan	1.944	2.268	40.1	>100	19.4	>200
Thiophene	1.951	<0.79	38.0	51	19.4	<200
Pyrrole	2.001	2.003	38.0	>100	21.0	>200

I. Carbons deposited at 930°C

II. I after being heated at 2700°C.

It seemed possible that the observed differences in carbon
properties might be related, in some measure, to the identity of
the carbon-hydrogen species formed during pyrolysis and subse-
quently involved in the carbon-forming process. Thus, in a
parallel study (10), analytical measurements were made of the
gaseous decomposition products formed under conditions similar to
those used for the production of the pyrolytic carbons. When a
heteroatom was present initially, this appeared in the gaseous
products almost entirely as water, hydrogen sulphide or hydrogen
cyanide and was nearly absent from the deposited carbon. In all
cases, however, the principal hydrocarbon products were methane,
acetylene, ethylene and benzene. The observed variation with
reaction time suggests, however, that methane is the principal
final product, benzene is a reasonably stable product and acety-
lene and ethylene are intermediates, as are ethane and various
C_3 and C_4 species formed in smaller amounts. Thermochemical
considerations make it likely that in all cases the ring opens by
fission of the C-X bond (where X = CH_2, NH, O or S). Following
isomerisation of the resulting biradical and fission of the
remaining C-X bond, a C_4 fragment is produced:
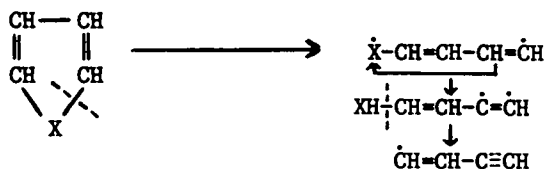
With each starting compound, this is probably $C_4H_3^{\cdot}$, which is believed to be of considerable mechanistic importance in carbon formation (11).

The observed variations in carbon properties may however be satisfactorily accounted for by the different extents to which dehydrogenation and hence crosslinking between the crystallites are produced by the scavenging effects of the different gaseous heteroatom-containing species formed. In general, density provides a measure of the closeness of packing of the carbon crystallites. At low deposition temperatures, close packing is prevented by the presence of hydrogen atoms and hydrocarbon fragments attached to the edges of the layer planes (12). As the temperature increases, dehydrogenation reactions reduce the number of peripheral species and crosslinking tends to occur between adjacent crystallites with a resulting increase in carbon density.

When cyclopentadiene is the starting compound, there is little interplanar or intercrystallite crosslinking in the initially deposited carbons since these materials graphitise readily on heat-treatment. The carbons derived from furan behave similarly, although the somewhat higher initial density suggests slightly more crosslinking as a result of the removal by oxygen-containing radicals of species attached to crystallite edges.

The presence of sulphur has a much more marked effect on carbon properties. Thus, on being heated to 2700°C, the carbons formed from thiophene "exfoliate" with a dramatic decrease in density. Here the HS· radical is probably, even at relatively low temperatures, an efficient scavenger of the blocking groups at crystallite edges and the forcible expulsion of these and other sulphur-containing species at higher temperatures causes complete disruption of the carbon structure.

Finally, nitrogen has perhaps the most pronounced effect on carbon properties. When pyrrole is the starting compound, the interplanar and intercrystallite links appear to be so extensive that the crystallites are locked into position as soon as they are deposited. Thus, heat treatment to 2700°C produces no appreciable increase in density and the carbons do not graphitise. The appearance of nitrogen in the products almost exclusively as hydrogen cyanide suggests that the scavenging in this case is brought about by the CN radical which, on thermochemical considerations, would be expected to be the most efficient of the species studied in removing peripheral fragments from crystallite edges.

The validity of a mechanism involving scavenging by heteroatom-containing radicals receives support from the observation (9) that carbons formed by pyrolysis of cyclopentadiene in the presence of added hydrogen sulphide (Table 2) are generally similar to those derived from thiophene (Table 1). In this connection, it is of interest to compare the influence of hydrogen

sulphide with that of another heteroatom-containing gas,
hydrogen chloride, which does not significantly affect the
properties of the resulting pyrolytic carbons (Table 2).   The
absence of any appreciable effect of the halogen compound
suggests that the chlorine atom is a relatively inefficient
scavenger of peripheral groups, although the presence of subs-
tantial amounts of chlorine in the initial organic compound
sometimes has a well-defined effect on the properties of the
resulting pyrolytic carbons (4,8).

<div align="center">Table 2</div>

Properties of pyrolytic carbons formed from cyclopentadiene in
the absence and presence of ca. 25 mol % of gaseous additives

Additive	$\rho(g\ cm^{-3})$		$L_a(10^{-8}cm)$		$L_c(10^{-8}cm)$	
	I	II	I	II	I	II
None	2.017	2.260	38.2	>100	23.5	>200
Hydrogen sulphide	2.088	<0.79	51.3	>100	24.5	<200
Hydrogen chloride	2.017	2.269	36.8	>100	22.3	>200

I.   Carbons deposited at 990°C

II.   I after being heated to 2700°C.

     In order to investigate further the apparently contrasting
effects of hydrogen sulphide and hydrogen chloride on carbon
formation and properties, studies were made of the surface top-
ography of pyrolytic carbons formed from cyclopentadiene both in
the absence and presence of these additives.   Thus samples of
thin-film carbon, formed by pyrolysis of the hydrocarbon at ca.
1000°C, were removed from the quartz plates which were used as
substrates for deposition and the surfaces which had been
exposed to the gas during pyrolysis were then shadowed with
silver and mounted in the vacuum chamber of a Stereoscan scanning
electron microscope.
     The surfaces of the carbons formed by the pyrolysis of
cyclopentadiene alone are comparatively smooth, although they
show a few protrusions and striations (Figure 1(a)).   Under
these conditions, gas-phase carbon is absent from the deposition
zone.   In contrast, the addition of hydrogen chloride causes
many such protrusions and the number of these depends on the
concentration of the additive (Figures 1(b)(c)).   As has already
been shown by other workers (4), the presence of the chlorine
compound causes considerable quantities of disordered gas-phase
carbon to be formed in the reaction zone (Figures 1(d)(e)).
The 'hillocks' observed most probably result from the growth of
surface carbon around soot particles which have been incorporated
in the deposited matrix.   As the pyrolysis continues, these soot
particles are covered by further surface carbon.
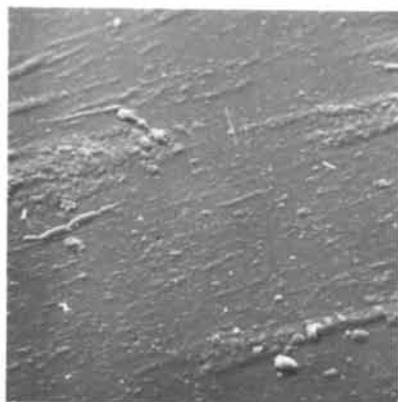
(a)
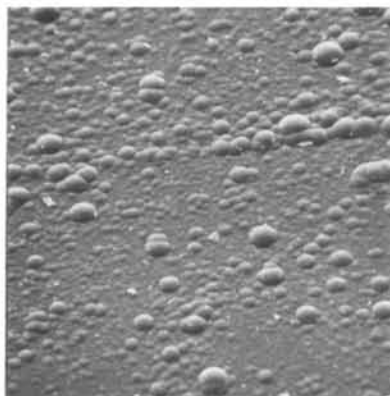
(b)
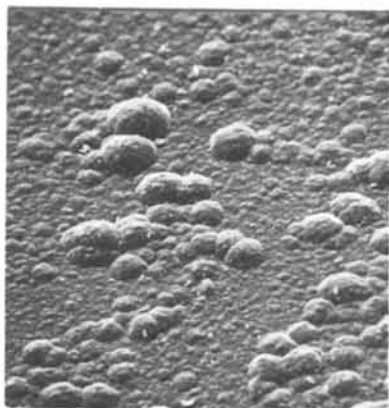
(c)
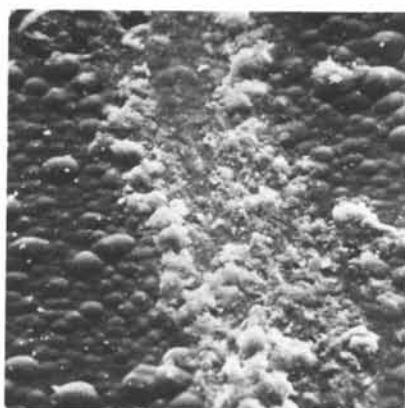
(d)
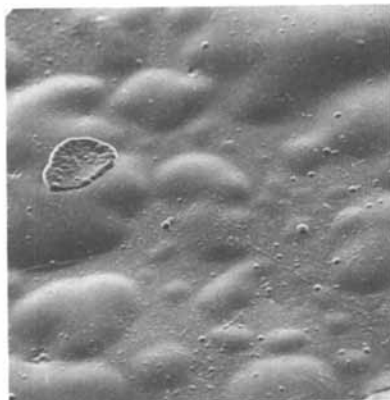
(e)   (f)

Figure 1. Electron micrographs of carbon formed by pyrolysis of cyclopentadiene at 990°C: (a) in absence of additives (mag. 244×); (b) in presence of 55.75 mol % hydrogen chloride (mag. 97×); (c) in presence of 24.66 mol % hydrogen chloride (mag. 104×); (d) in presence of 24.66 mol % hydrogen chloride (mag. 210×); (e) in presence of 24.66 mol % hydrogen chloride (mag. 840×); (f) in presence of 22.05 mol % hydrogen sulfide (mag. 47×)

For comparison, pyrolytic carbon was also produced from cyclopentadiene in the presence of hydrogen sulphide, an additive which inhibits the pyrolysis and reduces soot formation to a low level (9). In this case there are fewer protrusions than with cyclopentadiene alone but the surface of the carbon is covered by 'blisters' which almost certainly indicate an attempt to relieve strain within the structure during deposition (Figure 1(f)). This suggestion is supported by the 'exfoliation' or complete disruption of structure which occurs on heat-treatment of the samples to 2700°C (Table 2).

A possible explanation of the enhanced formation of gas-phase carbon in the presence of hydrogen chloride is that the latter compound is readily attacked by hydrocarbon radicals (13) to yield chlorine atoms:

$$R^{\cdot} \; + \; HCl \longrightarrow RH \; + \; Cl^{\cdot}$$

which then presumably react with acetylenic hydrocarbons (14,15) e.g.

$$Cl^{\cdot} \; + \; C_2H_2 \longrightarrow C_2H^{\cdot} \; + \; HCl$$
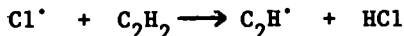
and thus promote formation of carbon via reactions of the ethynyl radical (16):

$$C_2H^{\cdot} \; + \; C_2H_2 \longrightarrow C_4H_2 \; + \; H^{\cdot}$$

$$C_2H^{\cdot} \; + \; C_4H_2 \longrightarrow C_6H_2 \; + \; H^{\cdot}$$
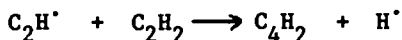
In contrast, hydrogen sulphide has a more complex effect on gas-phase pyrolysis reactions but it is known to be an efficient stabiliser of free radicals by hydrogen donation:

$$R^{\cdot} \; + \; H_2S \longrightarrow RH \; + \; HS^{\cdot}$$
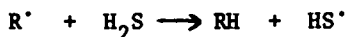
the above process requiring an activation energy of only 10-20 $kJ.mol^{-1}$ (17). The overall effect observed depends however on the subsequent reactions of the $HS^{\cdot}$ radical, which is clearly a much more effective scavenger of peripheral groups at crystallite edges than is the $Cl^{\cdot}$ atom (18). Thus the different influences produced by the two gaseous additives are probably attributable to the relative efficiencies with which free radicals derived from them either undergo deactivation by reacting with peripheral groups at crystallite edges or propagate chains leading to carbon formation in the gas phase. With hydrogen sulphide, removal of peripheral groups is preferred, but with hydrogen chloride gas-phase propagation reactions appear to be energetically favoured.

The presence of heteroelements either in the initial reactant or in the surrounding gaseous atmosphere may thus constitute an important factor in determining the structure and properties of pyrolytic carbons. It would now clearly be of considerable interest to discover also how the chemical reactivity of such carbons is affected by these same factors.

Abstract

   Studies have been made of the structure and physical
properties of pyrolytic carbons formed at ca. 1000°C both from
organic compounds containing volatile heteroatoms and from a
hydrocarbon in the presence of gaseous heteroelement-containing
additives.   Pyrolytic carbons formed from oxygen-containing
compounds are generally similar to those derived from hydro-
carbons but nitrogen and sulphur compounds yield carbons with
somewhat different properties and in particular much less ten-
dency to graphitise on heat-treatment.   The observed variation
in properties can be satisfactorily explained in terms of the
extents of dehydrogenation and hence crosslinking produced by
the different scavenging effects of heteroatom-containing free
radicals.   Sulphur- and nitrogen-containing radicals are
especially effective scavengers and their behaviour is compared
with that of other dehydrogenating species such as chlorine
atoms.

Literature Cited

(1)   Brown, A.R.G. and Watt, W., 1st. Ind. Carbon and Graphite
      Conf. p.86, Soc. Chem. Ind., (1958).
(2)   Blackman, L.C., Saunders, G. and Ubbelohde, A.R., Proc. Roy.
      Soc. (1961) A264, 19.
(3)   Frazee, J.D. and Anderson, R.C., 3rd. Biennial Carbon Conf.
      p.405, Pergamon Press (1959).
(4)   Higgs, P.H., Finicle, R.L., Bobka, R.J., Seldin, E.F. and
      Zeitsch, K.J., WADD Tech. Rept. (1964) 37, 61-72.
(5)   Tesner, P.A. and Rafalkes, I.S., Dokl. Akad. Nauk. SSSR,
      (1952) 87, 821.
(6)   Kinney, C.R., 1st. and 2nd. Biennial Carbon Conf. p.83,
      Pergamon Press (1956).
(7)   Conroy, J.S., Slysh, R.S., Murphy, B.D. and Kinney, C.R.,
      3rd. Biennial Carbon Conf. p.395.   Pergamon Press (1959).
(8)   Cullis, C.F., Manton, J.E., Thomas, G.B. and Wilman, H.,
      Acta Cryst. (1959) 12, 382.
(9)   Cullis, C.F. and Norris, A.C., 3rd. Ind. Carbon and Graphite
      Conf. p.235.   Soc. Chem. Ind. (1970).
(10) Cullis, C.F. and Norris, A.C., Carbon (1972) 10, 525.
(11) Gay, I.D., Kistiakowsky, G.B., Michael, J.V. and Niki, H.,
      J. Chem. Phys. (1965) 43, 1720.
(12) Grisdale, R.O., Pfister, A.C. and van Roosbroeck, W.,
      Bell System Tech. J. (1951) 30, 271.
(13) Anderson, K.H. and Benson, S.W., J. Chem. Phys. (1963) 39,
      1677.
(14) Cullis, C.F., Minkoff, G.J. and Nettleton M.A., Trans.
      Faraday Soc. (1962) 58, 117.
(15) Munson, M.S.B. and Anderson, R.C., J. Phys. Chem. (1963)
      67, 1582.

(16) Cullis, C.F., Hucknall, D.J. and Shepherd, J.V., Proc. Roy. Soc. (1973) A335, 525.

(17) Imai, N. and Toyama, O., Bull. Chem. Soc. Japan (1960) 33, 652.

(18) Cullis, C.F. and Norris, A.C., Carbon (1974) 12, 216.

Carbon In Prosthetic Devices

J. C. BOKROS, R. J. AKINS, H. S. SHIM, A. D. HAUBOLD, and
N. K. AGARWAL

General Atomic Co., San Diego, Calif. 92138

During the past decade, carbon has been evaluated and ac-
cepted as a material for use in the construction of implantable
prosthetic devices. The chain of events that led to this devel-
opment is intriguing because, as with many developments, the
pathway of progress contained curious combinations of coinci-
dences and misinterpretations.

In the early 1960s, Gott and his colleagues at the University
of Wisconsin set out to study the effect of electrical charges on
the blood-clotting properties of plastic materials (1). Recalling
Abramson's observations that the important components of blood are
negatively charged (2) and Sawyer's findings that the inside lin-
ing of blood vessels is negative relative to the outside (3-4),
Gott reasoned that the clotting of implanted foreign materials
should be influenced by their surface charge. He prepared con-
ductive test specimens by coating them with a graphite paint* and,
using a dry-cell battery, applied electrical charges to specimens
implanted in blood vessels. He found that when a positive charge
was applied to a specimen, it thrombosed, whereas when a negative
charge was imposed, the specimen remained clot-free. More impor-
tantly, however, was the chance finding that specimens with no
electrical connection did not clot (5). Apparently, the graphite
paint was antithrombogenic.

At about this same time, there was a parallel effort in the
nuclear field to develop radiation-stable, impermeable carbon
coatings for the nuclear fuel of high-temperature, gas-cooled,
atomic reactors (6). Soon after Gott's results were reported, a
mutual interest in carbon prompted, in 1965, a collaborative
effort between Gott's group at the University of Wisconsin and
the carbon group at General Atomic Company in San Diego to study
the compatibility of pyrolytic carbons and blood and to relate
the compatibility of carbon to its crystal structure and surface
properties.

---

*Dag 154 colloidal graphite paint manufactured by Acheson
Colloids Company, Port Huron, Michigan

Ironically, the inference by the early data that paint pigmented with colloidal graphite was antithrombogenic later proved to be false, and the antithrombogenic property of the graphite coatings was found to be due to a coincidental pretreatment procedure that was used before the specimens were implanted.

In the early tests, the coated specimens were sterilized by soaking in benzalkonium chloride and, just before implantation, were rinsed in a dilute solution of heparinized saline in order to minimize clotting during the placement (1). It was not until later that it was found that graphite paint alone or graphite paint treated with only a heparin rinse was thrombogenic and that only specimens that were coated with graphite paint, soaked in benzalkonium chloride, and then rinsed with heparin were antithrombogenic (7). The antithrombogenicity resulted from formation of a gelatinous complex of the benzalkonium ion with heparin that is not very soluable and was somehow bound to the graphite surface (8).

Initially, the bonding of heparin to graphite paint was thought to be due to a weak chemical linkage between the hydrophobic portion of the benzalkonium ion and the adsorptive, oleophilic graphite surface which, in turn, was linked to the highly negative heparin molecule via the cationic quaternary ammonium group. Actually, however, subsequent studies showed that the bonding between the gelatinous quaternary ammonium salt of heparin and the graphite paint was mechanical. The gelatinous benzalkonium-heparin salt was held in small surface pores in the graphite paint, and the amount of the complex that could be retained was directly dependent on the surface porosity (9-10). In fact, several porous substrates were found to be temporarily rendered antithrombogenic by successive pretreatments with benzalkonium chloride and heparin.

Only by chance was the conductive graphite paint selected for use in the early tests porous and rendered antithrombogenic by pretreatment with benzalkonium chloride and heparin; the high level of thromboresistance was not an inherent property of the graphite paint. In any event, Gott's early experiments (1) sparked interest in using a variety of carbons in prosthetics (9, 11).

The peculiar chain of events leading from the early studies of electrical effects using conductive graphite paint to the misleading result that suggested that graphite paint was inherently antithrombogenic provided the impetus to study the compatibility of the newly developed nuclear carbons. This, in turn, led to the surprising finding that clean, polished isotropic pyrolytic carbons deposited at relatively low temperature (LTI carbons)* in fluidized beds are inherently thromboresistant and that the

_____

*Available commercially under PYROLITE, registered trademark of General Atomic Company

thromboresistance is not enhanced by pretreatment with benzalkonium chloride or heparin (10).

Independently, in the autumn of 1967, Benson, while involved with the NASA Biomedical Applications Team, became interested in possible biomedical applications of carbons developed for the space program and began an extensive collaborative effort to evaluate the biocompatibility of vitreous and other carbons (12). This work was instrumental in advancing vitreous carbon as a material useful in a variety of transcutaneous applications including artificial tooth roots.

Although the usefulness of carbon as a biomaterial is a direct result of its biocompatibility, the breadth of its possible applications is a consequence of its other properties, which are tailorable and in combination make the material qualified for use in a variety of different applications.

For example, the benign properties of carbon have been demonstrated by early uses of lampblack as a pigment for tatoos (12). This ancient application not only demonstrates the biocompatibility of carbon but also provides evidence that carbon has the ability to resist the corrosive environment of the living body and not be biodegraded by it. Furthermore, the desirable engineering properties of carbon and its fabricability into a wide variety of useful shapes contribute to its versatility (13); e.g., carbon may be either porous or impermeable (14), and certain forms (the LTI carbons) have high strength (15-16) as well as wear and fatigue resistance (17-18). Benson's early survey (12) listed a wide variety of carbonaceous forms and projected many possible biomedical applications, some of which have been realized.

This paper is devoted primarily to the uses of pyrolytic carbons (the LTI carbons) since they have been clinically accepted and are used extensively in the construction of cardiovascular prosthetic devices. Applications of vitreous carbon as dental implants that are in a new-technique phase and some new forms of carbon that are under development are also discussed.

Properties

Biocompatibility. The biocompatibility of LTI carbons and its dependence on surface chemistry and surface topography have been studied extensively. Most of the early data was generated by NIH's Artificial Heart Program Contractors, the bulk of which has been published. The most important results have been summarized by Bruck and are listed in Table I (19-25).

The pure and silicon-alloyed varieties of LTI carbons exhibit a good to excellent degree of thromboresistance in both the vena cava test of Gott (20) and the renal embolus test of Kusserow (26). Although thromboresistance is of prime importance for biomaterials to be used in cardiovascular devices handling blood, other characteristics are also important. A material may be thromboresistant but still cause adverse reactions with cells or

TABLE I
BIOLOGICAL PROPERTIES OF LTI CARBONS (19)

Test	Result
In-Vivo (10, 20-21)	
Vena cava	
2 hr	Excellent
2 weeks	Excellent
Renal embolus	Very good
In-Vitro	
Effect on plasma proteins (22)	None
Effect on plasma enzymes (22)	None to slight
Calcium replacement clotting time (22)	Not prolonged
Adherence of:	
Erythrocytes (WB)	Light
Leukocytes (WB)	None
Platelets (PRP) (23)	Moderate
Platelet aggregation and activation (24)	Slight
Cell growth (amnion) (23)	Near 100%
Zeta potential (Krebs)	Negative
Critical surface tension (25)	50 dynes/cm

alter molecular elements of blood. Results of Hegyeli (23) and
Schoen (24) indicate that clean, polished LTI surfaces are not
only thromboresistant but also compatible with cellular elements
of blood. Halbert (22) and his coworkers showed further that LTI
carbon surfaces do not influence plasma proteins or alter the
activity of plasma enzymes.

There has been considerable speculation about the specific
combinations of surface properties that are responsible for the
compatibility of LTI carbons. The problem of interpretation is a
many-faceted and difficult one because blood compatibility infers
not only a compatibility with the various clotting factors but
also a broader compatibility with the formed cellular elements of
blood as well as a compatibility with the molecular species not
involved in clotting. It is thought that the compatibility of
carbon with blood may be due to an ability to maintain an inter-
mediate adsorbed layer of protein at the carbon-blood interface
without causing undesirable alterations which, for example, could
trigger the complex series of reactions that lead to thrombus
formation (25). Recent reports of the adsorptivity of albumin
on LTI carbons and the passification of the surface with regard to
platelet interactions are consistent with this general view (27-
29).

All of the results taken together suggest that the LTI carbons represent a significant advance in the search for blood-compatible materials. Because blood is probably the most finicky of the body's tissues, one may infer that the LTI carbons will also be inert in soft or hard tissue. This inference is being confirmed in applications described in later sections of this paper.

As alluded to above, biocompatibility and nonbiodegradability are not sufficient for materials that are to serve in devices that are subjected to mechanical abuse. In the following sections, the physical and mechanical properties that are relevant to usages in prosthetics are described.

Strength. The strength properties of carbon are structure-sensitive and vary with structure, e.g., density, degree of graphitization, preferred orientation, crystallite size, and microstructure (6). Of all of the bulk forms of carbons, including the pyrolytic graphites used in rocketry (30) and vitreous carbons (31), the pyrolytic carbons deposited in fluidized beds exhibit the highest strength and toughness.

Kaae has studied the mechanical properties of the LTI carbons and has related their strength to their density and crystallite size (15, 32). His data show that the fracture stress of the highest-density LTI carbons is above 70,000 psi, i.e., three or four times that of bone. The strength of the LTI carbons is enhanced by alloying with silicon (16), and, for concentrations less than about 20 wt % Si, the alloying addition does not detract from the biocompatibility (10).

It is worth comparing the strength of the LTI carbons with that of vitreous carbon since the latter has been used clinically in dental applications for several years (33) and is currently considered by the American Dental Association's Council on Dental Materials and Devices and Council on Dental Research to be in a new-technique phase. The strength properties of vitreous carbon and a high-density LTI carbon are listed in Table II. The combination of high strength and relatively low elastic modulus of the LTI carbon results in a high value of $\sigma^2/2E$, the strain energy to fracture, implying that it is tougher and less brittle than vitreous carbon.

The fact that the strength of LTI carbon is higher than that of vitreous carbon has been attributed to a basic difference in the microstructures that may be traced to differences in processing (34-35). Vitreous carbon is derived from a polymeric precursor by pyrolyzing at a slow rate, driving off volatile constituents, and leaving a glassy-appearing carbonaceous residue (31). These materials are typified by a low density near 1.5 g/cm^3. Their purity is variable, depending on the purity of the precursor polymer. A variety of defects identified in these materials have been attributed to residual impurities that are presumably present in the parent polymer (36). The presence of these defects may be

TABLE II
COMPARISON OF STRUCTURE AND PROPERTIES
OF VITREOUS (GLASSY) AND PYROLYTIC CARBONS

Property	Vitreous Carbon	Pyrolytic Carbon
Density, g/cm^3	1.5	1.0 to 2.2
Crystallite size (L_c), Å	10 to 30	20 to 200
Modulus of rupture, psi	20,000 to 30,000	50,000 to 100,000
Young's modulus, psi	3.5×10^6	2.0 to 5×10^6
Strain energy to fracture, $\sigma^2/2E \left(\times 10^2 \ \dfrac{in.-lb}{in.^3} \right)$	1	7

responsible for the highly variable, low strength of the vitreous
materials (37).

The LTI pyrolytic carbons are deposited at elevated tempera-
tures from a pure hydrocarbon gas onto a preformed refractory sub-
trate such as graphite. Under certain specific deposition con-
ditions, supersaturation occurs and gas-borne droplets are formed
(38). Deposition of LTI carbon onto the substrate is primarily
due to the deposition of droplets, the remnants of which have a
beneficial influence on the mechanical properties (15, 34). Be-
cause of the microstructural texture conferred by the droplets,
crack propagation in LTI carbon is difficult and torturous.

The fractographs in Figures 1a and 1b compare the smooth con-
coidal fracture surface of vitreous carbon with the rough fracture
surface of LTI carbon. The toughness and strength of the LTI car-
bon have been attributed to the large surface area and the asso-
ciated large amount of energy required to create the new surface
during fracture.

Fatigue and Wear. Although high fracture strengths and
toughness are important for materials called upon to sustain high
stresses in load-bearing devices, fatigue and wear are additional
considerations when materials are selected for use in devices sub-
jected to cyclic loading or abrasion, i.e., dental implants,
orthopedic devices, and artificial heart valves.

The fatigue properties of a variety of carbons with medical
applications have been studied as a function of their structure
(18, 39). Although the endurance limit varied over a wide range
from 25,000 psi for vitreous carbon to 80,000 psi for silicon-
alloyed LTI carbon, none of the materials exhibited a fatigue-type
failure. In every case, either the specimen fractured at its
normal single-cycle fracture stress or no failure occurred. The
data in Figure 2 for an LTI carbon with 8 wt % Si are typical.
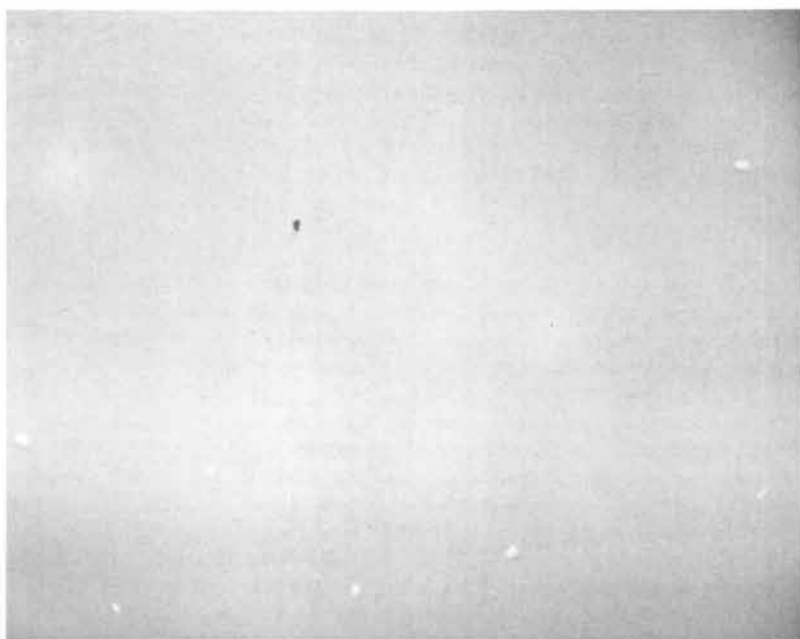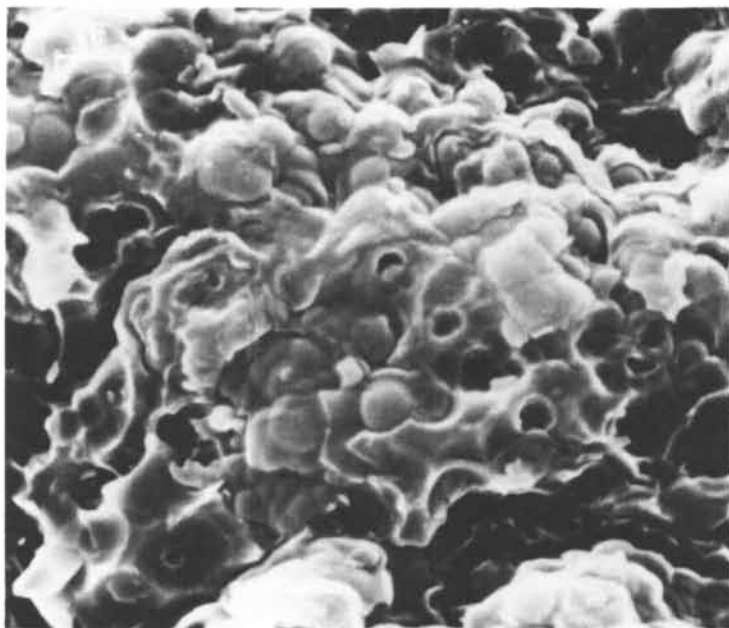
Figure 1. Comparison between the fracture surface of (a) (top) vitreous carbon and (b) (bottom) LTI carbon (both 920✕)

The lack of a dependence of the fracture stress on the number of stress excursions is, of course, an important advantage for the designer of prosthetic devices because large allowances for fatigue effects that are normally required for metals and polymers are not required in designs that use LTI carbons.

The dependence of the endurance limit on density and on silicon content in Figure 3 shows that, for a given low density, the endurance limit is increased by going from the glassy structure to structures containing droplet remnants and that there is a further increase with increasing density to about 50,000 psi. Codepositing silicon with carbon raises the endurance limit to 80,000 psi. Current specifications for the LTI carbons used in heart valve prostheses would include the two materials containing 8 and 15 wt % Si. All other deposits, excepting the deposit with 23 wt % Si, would be too soft and would wear at unacceptably high rates (discussed below). The material with 23 wt % Si, although its fracture strength is high, would lack toughness and would be too brittle for load-bearing applications.

The wear resistance of carbon is markedly dependent on its structures. The data in Figure 4 compare the wear rates caused by a high-density LTI carbon disk rubbing on various pure and silicon-alloyed LTI carbons and vitreous carbon (17). The initial drop in wear rate (open circles) with increasing hardness is due to an increase in the density of the LTI carbon. The low-density LTI carbon and the vitreous carbon both experienced high wear rates. A further but smaller decrease in wear rate is attainable by codepositing silicon with carbon; silicon also enhances strength (16-17). The specification for PYROLITE* carbons used clinically in heart valve applications requires that the hardness be between about 240 and 370 DPH (50-g loads).

A variety of other properties of pure and silicon-alloyed LTI carbons are listed in Table III.

Applications

Cardiovascular. The human heart consists of two pumping chambers, each of which is equipped with an inlet valve and an outlet valve. Disease can damage these valves, impairing their function, and can often require replacement with a prosthetic valve (see Figure 5).

The first implantation of an artificial valve was made in 1952 by Hufnagel in the descending aorta (40). The advent of open heart procedures made possible implantation in the normal position, and in 1960 Harken performed the first successful implantation of a caged-ball prosthesis in the aortic position (41). In the ensuing years, the clinical use of heart valve prostheses has proved the worth of these devices, salvaging otherwise hopeless patients. Experience has shown, however, that many problems remain, and the ideal prosthesis has yet to be proved.

*Registered trademark of General Atomic Company
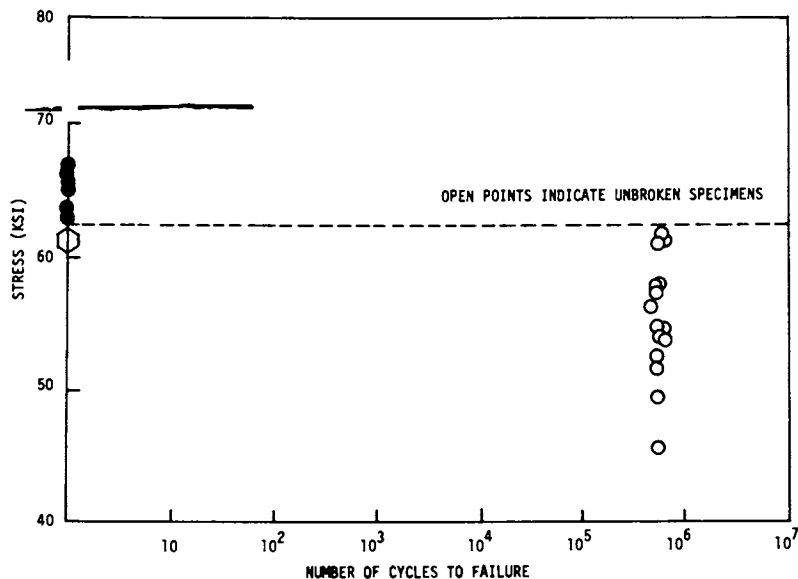
Figure 2. Cycles vs. stress for a silicon-alloyed pyrolytic carbon with 8 wt % silicon, a carbon matrix density of 1.97 g/cm³, and a DPH hardness number of 295; single-cycle fracture strength denoted by hexagon (18)
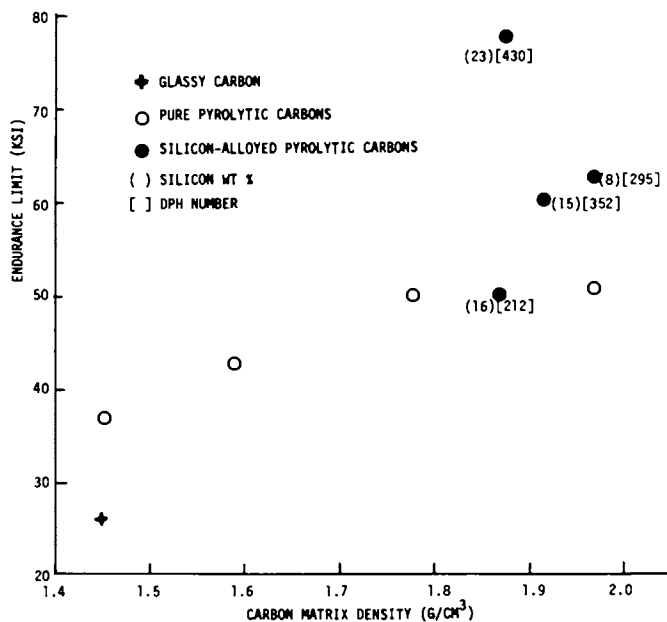
Figure 3. Endurance limit vs. carbon matrix density for pure and alloyed LTI carbon (18)
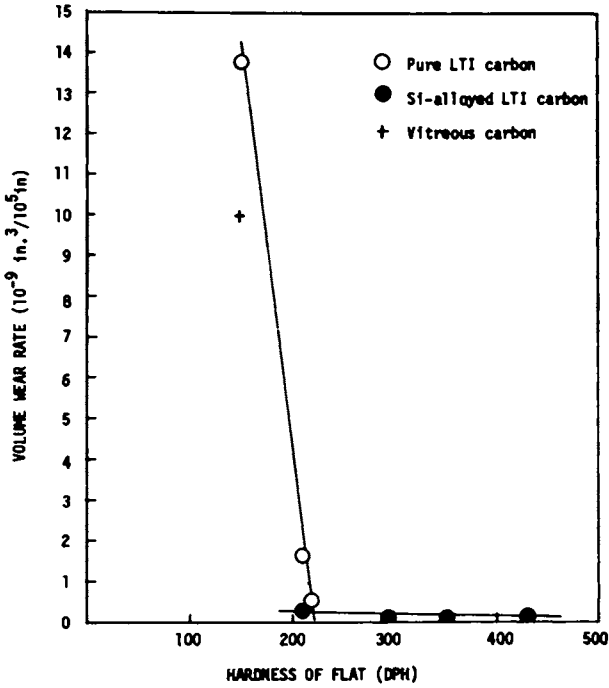
Figure 4. Wear rates caused by a high density LTI carbon disk rubbing on a variety of pure and alloyed carbon plates
(17)
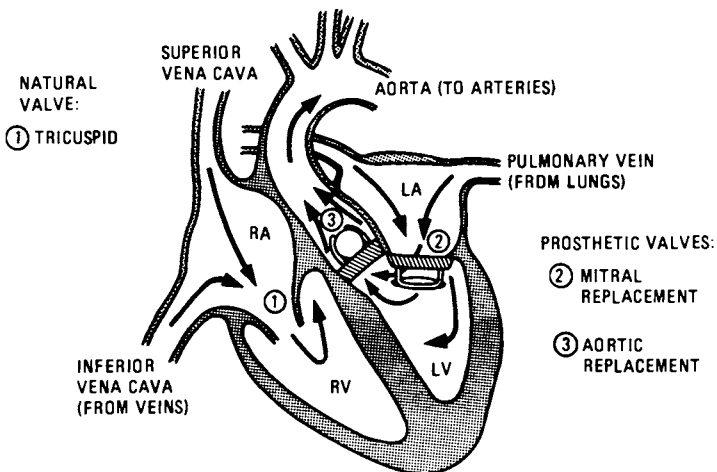
Figure 5. Schematic of heart illustrating function of prosthetic heart valves

TABLE III
PROPERTIES OF PURE AND SILICON-ALLOYED
LTI CARBONS

Property	Pure LTI Carbon	Silicon-Alloyed LTI Carbon
Density, g/cm^3	1.5 to 2.1	2.0 to 2.2
Crystallite size (L$_c$), $\overset{\circ}{A}$	30	30
Flexural strength, psi	40,000 to 70,000[a]	90,000
Young's modulus, psi	2.5 to 4 x 10^6[a]	5 x 10^6
Fatigue limit/flexural strength	1.0	1.0
Poisson's ratio	0.2	0.2
Hardness (DPH)	150 to 250[a]	350
Thermal expansion co-efficient (x 10^6 °C)	4 to 6[a]	5
Electrical resistivity at 20°C, ohm-cm	0.0005 to 0.002	0.0003 to 0.002
Thermal conductivity at 20°C, cal/cm-sec-°C	0.01	0.01
Silicon content, wt %	0.00	12
Impurity level, ppm	Less than 100	Less than 100

[a]The higher values are for carbons with the highest densities.

A review of the hemodynamic characteristic of prosthetic valves has recently been published (42) and may be consulted for functional characteristics of valves that were available in 1973.

Aside from the hemodynamic problems associated with the pumping of blood, there have been serious materials-related problems of biocompatibility and durability. Problems of thrombosis and mechanical failure, by wear or fatigue, of rubbing or flexing components of valves have been well-documented (43-62) and summarized (35).

The use of LTI carbon in the rigid components of prosthetic valves has virtually eliminated problems of wear, and results from in-vitro (35) and in-vivo animal tests suggest that significant wear will not occur even during the lifetime of a young patient (35, 63-69). Furthermore, the substitution of LTI carbon for polymeric occluders has eliminated problems of distortion and degradation that have been common with polymeric occluders (44-47, 57-58, 62, 70-75).

The wear resistance of LTI carbon, together with the fact that the material is not subject to fatigue or biodegradation, has made it the material of choice for long-term implantation in valves (63-69) or as the component of cardiac assist devices (76-77). At the time of our last reporting (35) (August 1971),

about 2000 components were delivered for clinical use in prosthet-
ic valves. Through June 1975, more than 110,000 components were
delivered. Very likely, 100,000 components have been implanted
since initial introduction, in 1969, of the hollow LTI carbon-
coated ball for the DeBakey-Surgitool aortic valve prosthesis.
About 40,000 components have been implanted for more than 2 yr.

Since 1969, there have been no failures of LTI carbon heart
valve components in normal function. The cause of four deaths due
to strut failure of the Model 105 Beall valve (78-80) was traced
to the application of excessive lateral forces onto the struts
during handling of the prosthesis before or at implantation, re-
sulting in cracks in the carbon coating with subsequent fatigue
failure of the underlying metal wire. As a result of this experi-
ence, a new package has been designed in which the valve can be
sterilized without being removed until time of implantation. In
addition, the diameter of the substrate wire that is carbon-coated
has been increased from 0.030 to 0.045 in., increasing the
strength of the struts in lateral bending by a factor of about 3.

During the past 2 yr, there have been several new innovations
in valves that utilize LTI carbon. Although the hollow balls for
the DeBakey aortic valve were rendered opaque by lining with tung-
sten screen (35), the occluders in all other clinical valves were
not readily visualizable with X rays. Recently, methods of fabri-
cating disc-type occluders containing opaque markers have been
developed, and marked discs are in test. The most promising
method utilizes a tantalum ribbon embedded in an annular groove in
the substrate graphite (see Figure 6a) which, in an X ray, is
visible as an opaque ring (see Figure 6b).

Recently, two new valves, the Cooley-Cutter aortic and mitral
valves, have been released for general clinical use (81). Both
valves use a hollow LTI carbon occluder lined with tungsten screen
to allow visualization of the occluder with X rays. The valves
have a double open-ended titanium cage with a full orifice (see
Figure 7). Other clinical valves that use LTI carbon components
are the Beall-Surgitool mitral valve (63), the Bjork-Shiley
mitral and aortic valves (35, 64-67), the Debakey-Surgitool aortic
valve (35), and the Lillehei-Kaster mitral and aortic valves (35,
68).

Transcutaneous Devices. Fifteen years ago, Murphy published
a section in Orthopaedic Appliance Atlas entitled "New Develop-
ments and Dreams" in which he predicted:

> In a less remote future, bioengineering research in bone
> plates and hip-replacement prostheses may well lead to
> ability to attach an inert material so securely and per-
> manently to bone that loads from a prosthesis could be
> transmitted directly to the skeleton. Research on eye
> implants, skeletal traction, and implant dentures might
> even give hope of infection-resistant passage of the
> prosthesis through the skin for a lifetime. After all,
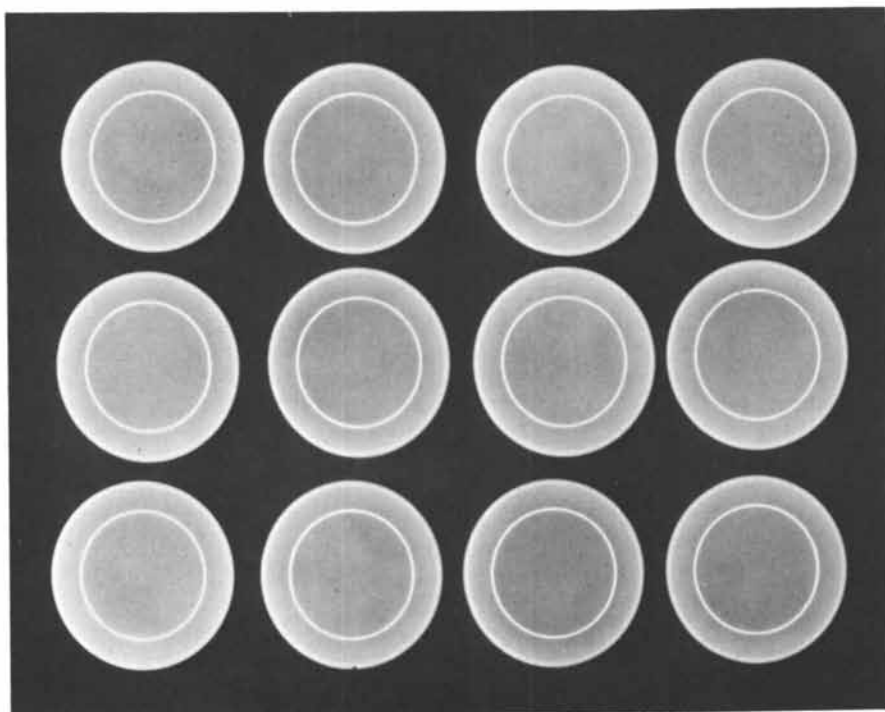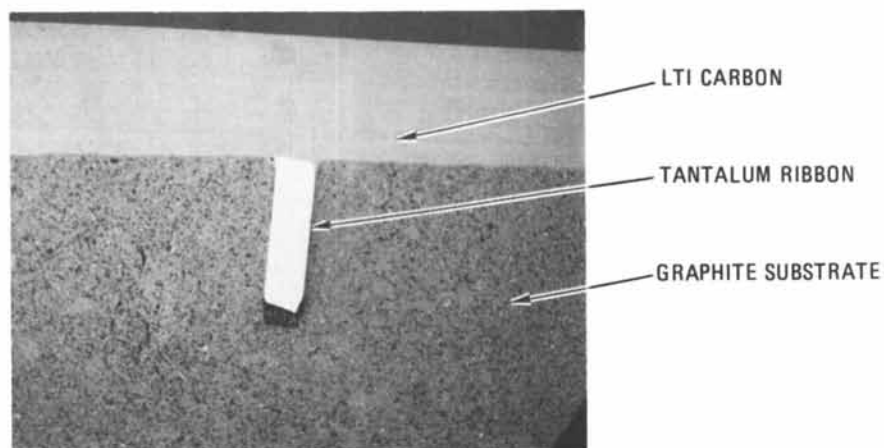
Figure 6. (a) (top) Photo micrograph of a section through the tantalum radio-opaque marker in a disc-type occluder (25✕); (b) (bottom) radiograph of discs marked with tantalum ribbons embedded in the graphite substrate

the present rate of resistance to infection successfully
combats vast numbers of bacteria during a few weeks of
skeletal traction or even a decade of use of implant
dentures with a very crude seal. More successful seal-
ing techniques, based on better engineering as well as
biological principles, might tip the scale enough to make
"limb fitting" of a skeletally attached device truly a
part of the surgeon's specialty. The prosthetist would
then be concerned with the alignment of the components to
be attached, by a bayonet lock, to the peg outside the
skin. Although small research efforts have been, and
again are being devoted to animal experiments on skeletal
attachment and related problems, and a few human experi-
ments are said to have been tried, this idea is still
considered highly experimental and is flatly condemned by
many surgeons.

The work initiated by Benson in 1967 showed that carbon might
provide the means for gaining permanent access through the skin
(12, 81), not only for direct attachment to the skeletal system
but also for providing a means of transmitting electrical leads
for powering implanted cardiac assist devices, neural stimulation,
and stimulation of bone growth, or for providing blood access for
renal dialysis. Although the optimum surface topography that is
required to form the best bacterial seal has not yet been identi-
fied (82), there is evidence that either vitreous carbon or LTI
carbon is sufficiently compatible with tissue to perform for long
periods in the transcutaneous situation (6, 12, 83-89). The
schematic in Figure 8 illustrates the use of a transcutaneous de-
vice to provide a lead-through for electrical leads.

Vitreous and LTI carbons have both been used in a variety of
transcutaneous devices. Vitreous carbon is somewhat limited when
load bearing is required because of its extreme brittleness (90).
In the following paragraphs, some of the newer transcutaneous de-
vices that use LTI carbon are described.

1. Skeletal Attachment: The Rehabilitation Engineering Cen-
ter at Rancho Los Amigos Hospital in Downey, California, has pio-
neered the search for a satisfactory method of attaching a pros-
thesis to the skeleton. In November 1974, the group inserted such
a device in the leg of an amputee. The prosthetic device (see
Figures 9 and 10) was designed in collaboration with the Kennedy
Space Center of NASA. The LTI carbon transcutaneous device is
cemented to a metallic latching device for attaching the below-
knee pylon prosthesis (see Figure 11). The skeletal prosthesis
attachment unit implanted in the leg of the amputee is depicted in
Figure 12 as it appeared immediately after surgery. The device is
performing satisfactorily at the time of this writing (9 months
after insertion) (91).

2. Dental Implants: Dental surgeons have sought for decades
for a material that could be fashioned into an artificial tooth
root, implanted through the gingiva into the jawbone, and provide
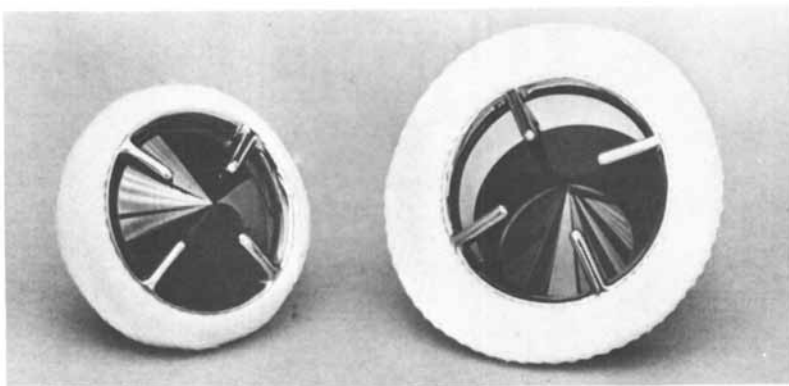
Figure 7. Cooley-Cutter aortic (right) and mitral (left) valve prostheses
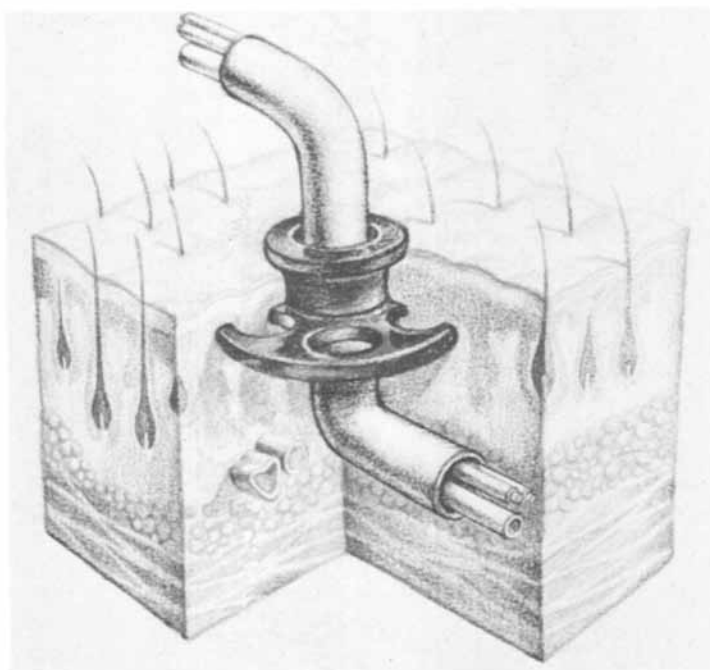
Figure 8. Carbon transcutaneous device
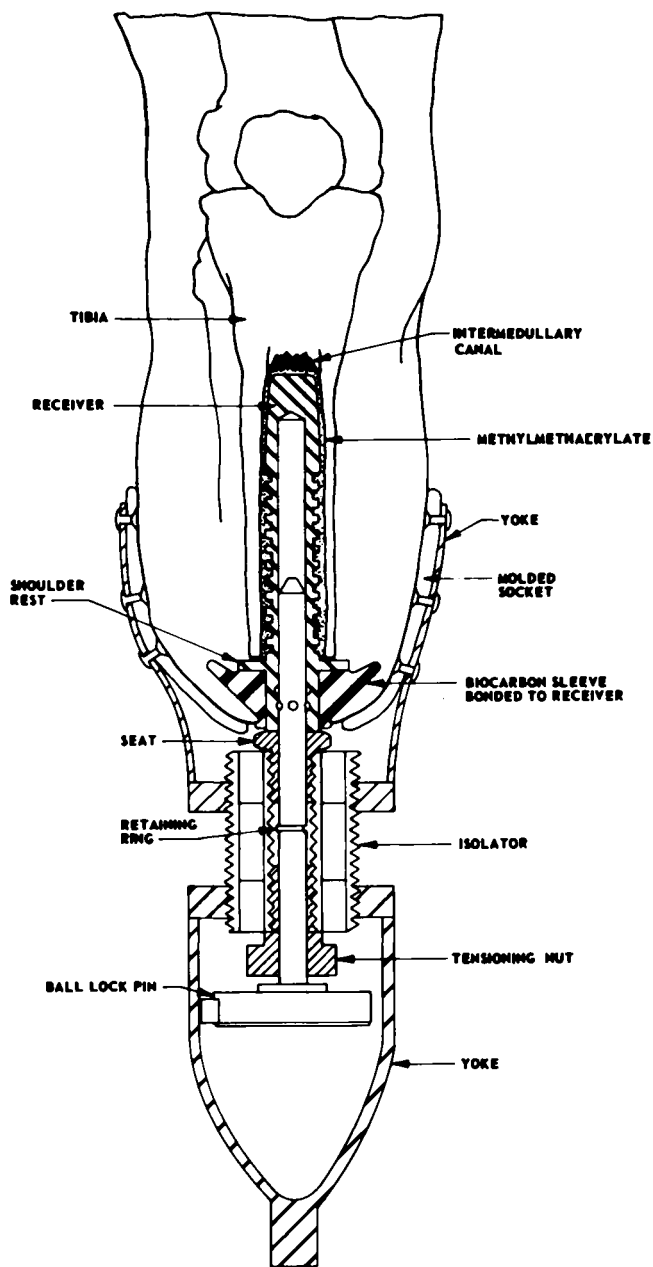
Figure 9.   Below-knee prosthetic attachment
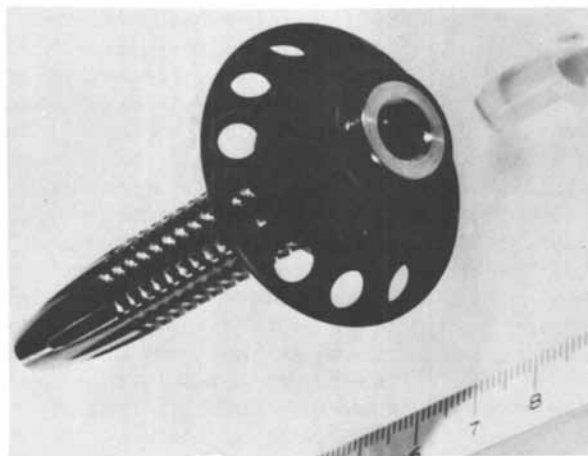
Figure 10. Skeletal prosthesis attachment; femoral implant fabricated by Kennedy Space Center, NASA; LTI flange carbon by General Atomic Co.

Figure 11. Below-knee pylon prosthesis with transparent socket, prepared for attachment

the support for a tooth, bridge, or complete denture. LTI carbon because of its strength, its ability to perform transcutaneously, and its elastic match with bone is especially suited for this application. Tests that were begun in 1971 in primates at the Southwest Foundation for Research and Education (87) explored a number of configurations and provided the basis for an expanded, intensive evaluation of blade-type endosseous implants at the Tulane University Delta Primate Center in Louisiana. Details of the design, mechanical properties, and animal results have been reported (92). The approach, illustrated by the schematic in Figure 13, uses an LTI carbon-coated graphite blade implanted in the mandible for the purpose of supporting a bridge. The blade is about 1.5 mm thick, and the base of the crown support at the plane of the gingiva is from 3.0 to 4.0 mm thick (see Figures 14a and 14b). The high strength of the LTI carbon allows much thinner sections than are possible with vitreous carbon, thus requiring that less bone be sacrificed when the device is implanted. Accordingly, implants can be made in alveolar ridges that have already undergone some degeneration. Even the thinnest blade designs can support four times the load in bending that would cause a Vitallium or titanium blade to bend over (92). Human trials have been initiated.

    3. _Artificial Hearing_: The University of Utah, in conjunction with the Otologic Medical Group in Los Angeles, has been exploring the feasibility of using the tonotopic spatial organization of the cochlea for artificial hearing (93). Subjects have been implanted with cochlear electrodes to define stimulation parameters and methods for pitch modulation necessary for designing permanent devices. LTI carbon transcutaneous buttons (see Figure 15) are currently being used to house the electrical connector. The LTI carbon button apparently forms a bacterial seal so that the connector is well-tolerated without infection. A connector implanted in a deaf volunteer is shown in Figure 16 as it appeared 10 days post-operative. The device is performing satisfactorily at the present time (4 months after insertion).

New Developments

    There are many cardiovascular, orthopedic, and dental devices that would be improved if carbon components could be used, but, because of shape, cost, and other factors, they cannot be made from LTI carbon, vitreous carbon, or other bulk forms of carbon. In order to meet these requirements, we are developing new processes that allow deposition of an adherent, thin, impermeable barrier layer of pure isotropic carbon on the surface of polymeric and intricate metallic substrates.

    For example, many intricate metallic heart valve housings have sections and shapes that make them unsuitable for coating with LTI carbon. The devices shown in Figures 17a, 17b, and 17c are experimental components for artificial valves and an emboli

Figure 12. Skeletal prosthesis attachment unit implanted in leg of amputee, immediately after operation
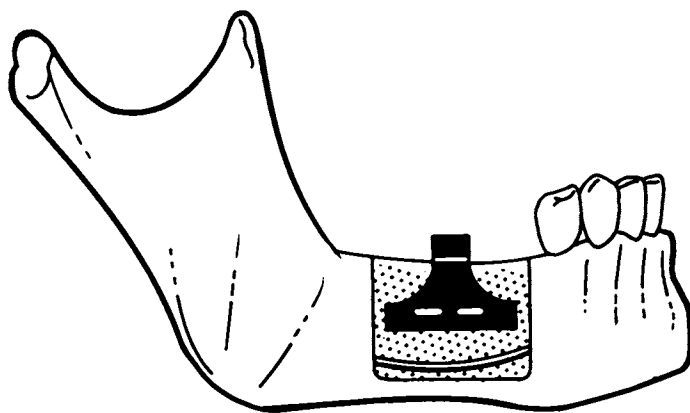
Figure 13. Schematic showing an LTI carbon blade-type implant in a mandible
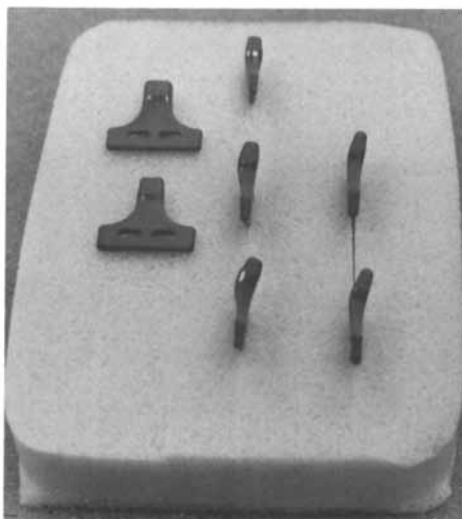
Figure 14 (a).   LTI carbon endosseous blade-
type dental implants
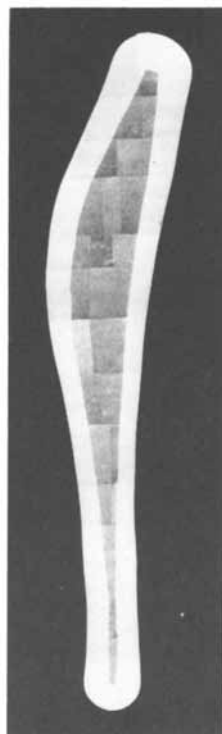
Figure 14 (b).   Cross section of dental implant showing in-
ternal graphite substrate and LTI carbon structural coating

Figure 15. LTI carbon transcutaneous buttons
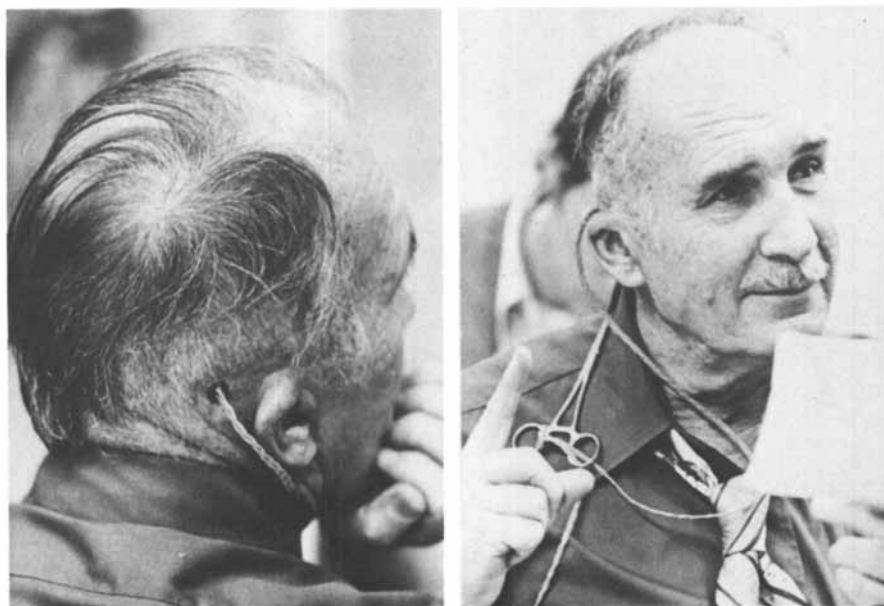
Figure 16. LTI carbon transcutaneous button installed in a cochlear stimulation experiment
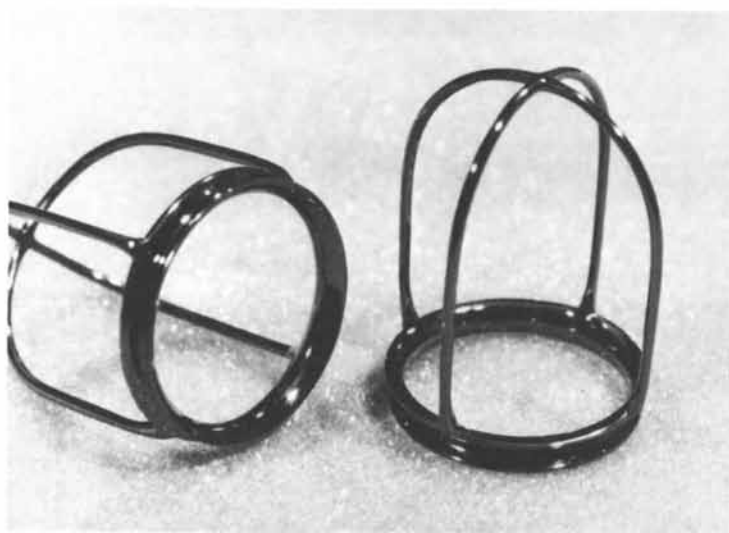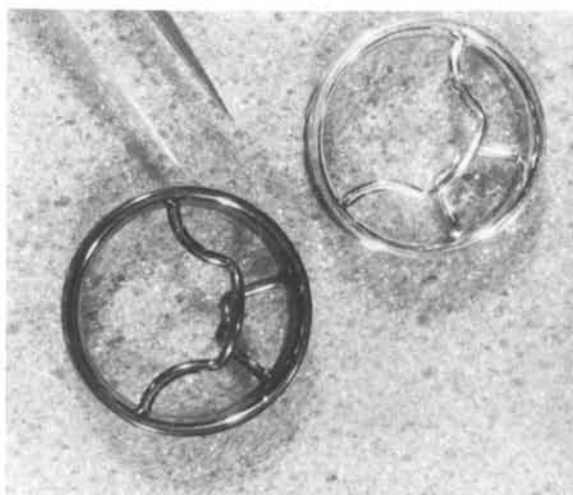
Figure 17 (a) and (b).   Experimental metallic prosthetic devices—heart valve housings coated with a thin, impermeable layer of isotropic carbon
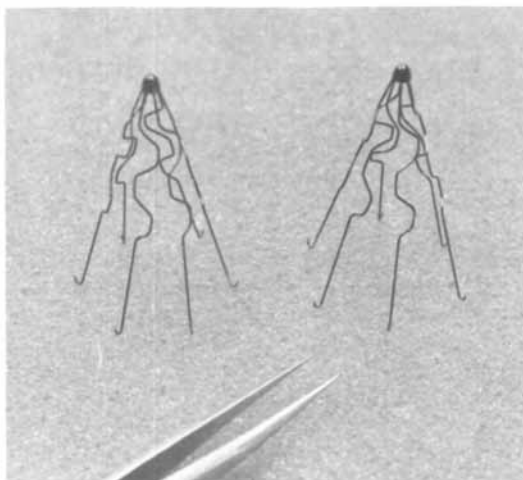
Figure 17 (c).   Experimental metallic prosthetic devices—coated stainless steel emboli filter

Figure 18.   A bone plate and screws coated with an adherent, thin layer of impermeable isotropic carbon

filter. The impermeable carbon coating is about 5000 Å thick and covers all exposed metallic substrates. Because the coating* is so thin, it will in time be worn off in localized areas that are continuously rubbed by the occluder. The major fraction of the coating, however, will remain. Since the coating is too thin to be structural, the mechanical properties of the coated device are the same as those of an uncoated device.

Another example is coating for orthopedic appliances (see Figure 18). The metallic parts retain all of the physical and strength properties of the uncoated metal, but, biochemically, the surrounding tissue is aware of only the inert carbon surface.

In this new process, the substrate material need not be subjected to high temperatures, so polymers may be coated. This means that low-cost molded articles can be coated, for example, for disposable blood-handling devices.

The present usage of carbon in medicine that was sparked by Gott's original experiments with graphite pigmented paint represents a significant advance in the search for materials to be used in fabricating spare parts and accessories for the body. The special compatibility of carbon, its nonbiodegradability, its mechanical likeness to bone, its good wear resistance, and its resistance to failure in fatigue taken together offer a unique combination of properties that makes carbon especially suited for use in prosthetic devices. The ability to provide a thin carbon "seal-coat" on polymer and intricate metal shapes should expand the usefulness of the material for even more applications.

Literature Cited

1. Gott, V. L., et al., "The Coating of Intravascular Plastic Prostheses with Colloidal Graphite," Surgery (1961), 50, 382.
2. Abramson, H. A., "The Influence of a Low Electromotive Force on the Electrophoresis of Lymphocytes of Different Ages," J. Exp. Med. (1925), 41, 445.
3. Sawyer, P. N., and J. W. Pate, "Bioelectric Phenomena as an Etilogic Factor in Intravascular Thrombosis," Am. J. Physiol. (1953), 175, 103.
4. Sawyer, P. N., J. W. Pate, and C. S. Weldon, "Relations of Abnormal and Injury Electric Potential Differences in Intravascular Thrombosis," Am. J. Physiol. (1953), 175, 108.
5. Gott, V. L., et al., "The Anticlot Properties of Graphite Coatings on Artificial Heart Valves," Carbon (1964), 1, 378.
6. Bokros, J. C., "The Preparation, Structure, and Properties of Pyrolytic Carbon," in Chemistry and Physics of Carbon, vol. 5 (P. L. Walker, Jr., ed.), chap. 1, Dekker, New York, 1969.
7. Whiffen, J. D., et al., "Heparin Application to Graphite-Coated Intravascular Prostheses," Surgery (1964), 56, 404.
8. Gott, V. L., et al., "Biophysical Studies on Various Graphite-Benzalkonium—Heparin Surfaces," in Biophysical Mechanisms in

*HEMOPLATE carbon: a trademark of General Atomic Company

Vascular Homostasis and Intravascular Thrombosis (P. N. Sawyer, ed.), pp. 297-305, Appleton-Century-Crofts, New York, 1970.

9. Bokros, J. C., et al., "Heparin Sorptivity and Blood Compatibility of Carbon Surfaces," J. Biomed. Mater. Res. (1970), 4, 145.

10. Bokros, J. C., L. D. LeGrange, and F. J. Schoen, "Control of Structure of Carbon for Use in Bioengineering," in Chemistry and Physics of Carbon, vol. 9 (P. L. Walker, Jr., and P. A. Thrower, eds.), pp. 103-171, Dekker, New York, 1972.

11. DeLaszlo, H. G., U. S. Patent 3,526,906, 1970 (filed October 10, 1966).

12. Benson, J., "Pre-Survey on Biomedical Applications of Carbon," North American Rockwell Corporation Report R-7855, 1969.

13. Bauer, D. W., and W. V. Kotlensky, "Relationship between Structure and Strength for CVD Carbon Infiltrated Substrates," presented at 23rd Pacific Coast Regional Meeting, American Ceramic Society, San Francisco, California, October 28-29, 1970.

14. Kotlensky, W. V., "Deposition of Pyrolytic Carbon in Porous Solids," in Chemistry and Physics of Carbon, vol. 9 (P. L. Walker, Jr., and P. A. Thrower, eds.), pp. 173-261, Dekker, New York, 1972.

15. Kaae, J. L., "The Mechanical Properties of Glassy and Isotropic Pyrolytic Carbons," J. Biomed. Mater. Res. (1972), 6, 279.

16. Kaae, J. L., and T. D. Gulden, "Structure and Mechanical Properties of Co-Deposited Pyrolytic C-SiC Alloys," J. Am. Ceram. Soc. (1971), 54, 606.

17. Shim, H. S., and F. J. Schoen, "The Wear Resistance of Pure and Silicon-Alloyed Isotropic Carbon," Biomater. Med. Devices Artificial Organs (1974), 2, 103.

18. Shim, H. S., "Behavior of Isotropic Pyrolytic Carbons under Cyclic Loading," Biomater. Med. Devices Artificial Organs (1974), 2, 55.

19. Bruck, S. D., S. Rabin, and R. J. Ferguson, "Evaluation of Biocompatible Materials," Biomater. Med. Devices Artificial Organs (1973), 1, 191.

20. Gott, V. L., and A. Furuse, "The Current Status of In-Vivo Screening of Synthetic Implant Materials for Blood Compatibility," Med. Instr. (1973), 7, 121.

21. Whalen, R. L., D. L. Jeffery, and J. C. Norman, "A New Method of In-Vivo Screening of Thromboresistant Biomaterials Utilizing Flow Measurement," Trans. Am. Soc. Artificial Internal Organs (1973), 19, 19.

22. Halbert, S. P., M. Anken, and A. E. Ushakoff, "Compatibility of Blood with Materials Useful in the Fabrication of Artificial Organs," Annual Report, Contract PH-43-66-980, National Heart and Lung Institute, National Institutes of Health, Bethesda, Maryland, 1969.

23. Hegyeli, R. J., R. Gallagher, and L. K. Peterson, "Further Studies of the Interaction of Blood and Tissue Cells with Artificial Heart Implant Candidate Materials In-Vitro," in Artificial Heart Program Conference, p. 203, National Institutes of Health, Bethesda, Maryland, 1969.

24. Schoen, F. J., "Surface Studies of Carbons for Prosthetic Applications," in Proceedings of 4th Annual Scanning Electron Microscope Symposium, part I, p. 385, IIT Research Institute, Chicago, 1971.

25. De Palma, V. A., et al., "Investigations of Three-Surface Properties of Several Metals and Their Relation to Blood Compatibility," J. Biomed. Mater. Res. Symp. (1972), 6, 37.

26. Kusserow, B. K., R. W. Larrow, and J. E. Nichols, "Analysis and Measurement of the Effects of Materials on Blood Leukocytes, Erythrocytes, and Platelets," Annual Report, Contract PH-43-68-1427, National Heart and Lung Institute, National Institutes of Health, Bethesda, Maryland, 1972.

27. Kim, S. W., University of Utah, private communication.

28. Smith, L. E., National Bureau of Standards, private communication.

29. Salzman, E. W., Beth Israel Hospital, private communication.

30. Gebhardt, J. J., and J. M. Berry, "The Mechanical Properties of Pyrolytic Graphite," AIAA J (1965), 3, 302.

31. Cowlard, F. C., "Materials Research Yields Versatile Carbonized Polymer," Design Eng. (March 1970), 49.

32. Kaae, J. L., "Relations between the Structure and Mechanical Properties of Fluidized-Bed Pyrolytic Carbons," Carbon (1971), 9, 291.

33. Dumos, M., and H. M. Myers, "The Vitreous Carbon Tooth Replacement System: A Surgical Discipline," Intern. J. Oral Surg. (1974), 3, 1.

34. Kaae, J. L., "Microstructure of Isotropic Pyrolytic Carbon," Carbon (1975), 13, 55.

35. Bokros, J. C., and R. J. Akins, "Applications of Pyrolytic Carbon in Artificial Heart Valves: A Status Report," in Proceedings of 4th Buhl Conference on Materials, p. 243, Carnegie Press, Pittsburgh, 1971.

36. Kaae, J. L., "Microstructural Observations on a Commercial Glassy Carbon," General Atomic Company Report GA-A13121, 1974 (to be published in Carbon).

37. Kenner, G. H., et al., "Biocompatibility and Static Fatigue Behavior of Glassy Carbon," J. Biomed. Mater. Res. (1975), 9, 111.

38. Bokros, J. C., "Variations in the Crystallinity of Pyrolytic Carbons Deposited in Fluidized Beds," Carbon (1965), 3, 201.

39. Schoen, F. J., "On the Fatigue Behavior of Pyrolytic Carbon," Carbon (1973), 11, 413.

40. Hufnagel, C. A., and W. P. Harvey, "Surgical Correction of Aortic Regurgitation," Bull. Georgetown Univ. Med. Center (1952), 4, 128.

41. Harken, D. E., *et al.*, "Partial and Complete Prosthesis in Aortic Insufficiency," J. Thoracic Cardiovascular Surg. (1960), 40, 744.
42. Roschke, E. J., "An Engineer's View of Prosthetic Heart Valves," Biomater. Med. Devices Artificial Organs (1973), 1, 249.
43. Brewer, L. A., Prosthetic Heart Valve, Charles C. Thomas, Springfield, Illinois, 1969.
44. Hylen, J. C., *et al.*, "Aortic Ball Valve Variance: Diagnosis and Treatment," Ann. Internal Med. (1970), 72, 1.
45. Roberts, W. C., and A. G. Morrow, "Fatal Degeneration of the Silicone Rubber Ball of the Starr-Edwards Prosthetic Aortic Valve," Am. J. Cardiol. (1968), 22, 614.
46. Mellenry, M. M., *et al.*, "Critical Obstruction of Prosthetic Heart Valves Due to Lipid Absorption by Silastic," J. Thoracic Cardiovascular Surg. (1970), 59, 113.
47. Hylen, J. C., "Durability of Prosthetic Heart Valves," Am. Heart J. (1971), 81, 299.
48. Cooley, D. A., *et al.*, "Aortic Valve Prosthesis Incorporating Lightweight Titanium Ball, Dacron Velour Covered Cage, and Seat," Trans. Am. Soc. Artificial Internal Organs (1967), 13, 93.
49. Starr, A., R. Herr, and J. H. Wood, "Accumulated Experience with the Starr-Edwards Prosthesis, 1960-1968" (cited in Reference 8, p. 468).
50. Detmer, D. E., and N. S. Braumwald, "The Metal Poppet and the Rigid Prosthetic Valve," J. Thoracic Cardiovascular Surg. (1971), 61, 175.
51. "Outlook for Prosthetic Heart Valves Patient Improves," J. Am. Med. Assoc. (1968), 205, 28.
52. Reis, R. L., *et al.*, "Clinical and Hemodynamic Assessments of Fabric-Covered Starr-Edwards Prosthetic Valves," J. Thoracic Cardiovascular Surg. (1970), 59, 84.
53. Schottenfeld, M., *et al.*, "Cloth Destruction and Haemolysis with Totally Cloth-Covered Starr-Edwards Prostheses," Thorax (1971), 26, 195.
54. Gunstensen, J., "Acute Dysfunction of the Starr-Edwards Mitral Prostheses," Thorax (1971), 26, 163.
55. Hughes, R. K., and J. S. Carey, "Experience with the Kay-Shiley Mitral Valve" (cited in Reference 8, p. 587).
56. Paton, B. C., *et al.*, "Follow-Up Results on the Kay-Shiley Valve" (cited in Reference 8, p. 598).
57. Hopeman, A. R., R. L. Treasure, and R. J. Hall, "Mechanical Dysfunction in Caged-Lens Prostheses," J. Thoracic Cardiovascular Surg. (1970), 60, 51.
58. Robinson, M. J., F. J. Hildner, and J. J. Greenberg, "Disc Variance of Beall Mitral Valve," Ann. Thoracic Surg. (1971), 11, 11.

59. Bjork, V. O., "Experience with the Wada-Cutter Valve Prosthe-
    sis in the Aortic Area," J. Thoracic Cardiovascular Surg.
    (1970), 60, 26.
60. Ress, J. R., et al., "Late Results of Valve Replacement,"
    Surgery (1970), 67, 141.
61. Aston, S. J., and D. G. Mulder, "Cardiac Valve Replacement:
    A Seven Year Follow-Up," J. Thoracic Cardiovascular Surg.
    (1971), 61, 547.
62. "Hazards of Heart Valve Replacement," Brit. Med. J. (June 20,
    1970), (5710), 677.
63. Beall, A. C., et al., "Clinical Experience with an Improved
    Mitral Valve Prosthesis," Ann. Thoracic Surg. (1973), 15,
    601.
64. Bjork, V. O., "The Pyrolytic Carbon Occluder for the Bjork-
    Shiley Tilting Disc Valve Prosthesis," Scand. J. Thoracic
    Cardiovascular Surg. (1972), 6, 109.
65. Lepley, D., Jr., et al., "Experience with the Bjork-Shiley
    Prosthetic Valve," Circulation (Supp. III) (July 1973), 48 and
    49, III-51.
66. Fernandez, J., et al., "The Bjork-Shiley Prosthesis," Ann.
    Thoracic Surg. (1972), 14, 527.
67. Pupello, D. F., et al., "Fifty-Two Consecutive Aortic Valve
    Replacements Employing Local Deep Hypothermia," Ann. Thoracic
    Surg. (1975), 19, 487.
68. Kaster, R. L., C. W. Lillehei, and P. J. K. Starek, "The
    Lillehei-Kaster Pivoting Disk Aortic Prosthesis and a Compara-
    tive Study of Its Pulsatile Flow Characteristics with Four
    Other Prostheses," Trans. Am. Soc. Artificial Internal Organs
    (1970), 16, 233.
69. Cooley, D. A., R. D. Leachman, and D. C. Wukasch, "Diffuse
    Muscular Subaortic Stenosis: Surgical Treatment," Am. J.
    Cardiol. (1973), 31, 1.
70. Messmer, B. J., M. Rothlin, and A. Senning, "Early Disc Dis-
    lodgement," J. Thoracic Cardiovascular Surg. (1973), 65, 386.
71. Larmi, T. K. I., and P. Karkola, "Shrinkage and Degradation of
    the Delrin Occluder in the Tilting-Disc Valve Prostheses,"
    J. Thoracic Cardiovascular Surg. (1974), 68, 66.
72. Hughes, D. A., et al., "Late Embolization of Prosthetic Mitral
    Valve Occluder with Survival Following Reoperation," Ann.
    Thoracic Surg. (1975), 19, 212.
73. Wukasch, D. C., et al., "Complications of Cloth-Covered Pros-
    thetic Valves: Results with a New Mitral Prosthesis," J.
    Thoracic Cardiovascular Surg. (1975), 69, 107.
74. duPriest, R. W., et al., "Sudden Death Due to Dislodgement of
    Disc Occluder of Wada-Cutter Prosthesis," J. Thoracic Cardio-
    vascular Surg. (1973), 66, 93.
75. Keen, G., "Late Death Due to Escape of Ball from Mitral Valve
    Prosthesis," J. Thoracic Cardiovascular Surg. (1974), 67, 202.

76. Rafferty, E. H., H. D. Kletschka, and D. A. Olsen, "Nonpulsa-
    tile Artificial Heart," J. Extra-Corp. Tech. (1973), 5 (2 and
    3).
77. Bernstein, E. F., et al., "A Compact, Low-Hemolysis, Non-
    Thrombogenic System for Non-Thoracotomy Prolonged Left Ven-
    tricular By-Pass," Trans. Am. Soc. Artificial Internal Organs
    (1974), 20, 643.
78. Nathan, M. J., "Strut Failure," Ann. Thoracic Surg. (1973),
    16, 610.
79. Gold, H., and L. Hertz, "Death Caused by Fracture of Beall
    Mitral Prosthesis," Am. J. Cardiol. (1974), 34, 371.
80. Brawley, R. K., J. S. Donahoo, and V. L. Gott, "Current Status
    of the Beall, Bjork-Shiley, Braunwald-Cutter, Lillehei-Kaster,
    and Smeloff-Cutter Cardiac Valve Prostheses," Am. J. Cardiol.
    (1975), 35, 855.
81. Benson, J., "Elemental Carbon as a Biomaterial," J. Biomed.
    Mater. Res. Symp. (1971), 5, 41.
82. Winter, G. D., "Transcutaneous Implants: Reactions of the
    Skin-Implant Interface," J. Biomed. Mater. Res. Symp. (1974),
    8, 99.
83. Grenoble, D. E., "Progress in the Evaluation of Vitreous Car-
    bon Endosteal Implant," Ariz. St. Dental J. (1973), 19, 12.
84. Mooney, V., and D. B. Hartman, "Clinical Experience in the Use
    of High Purity Carbon for Percutaneous Passage," Proc. 18th
    Nat. Soc. Aerospace Mater. Proc. Engs. Symp. (1973), 16, 268.
85. Grenoble, D. E., et al., "Development and Testing of Vitreous
    Carbon Dental Implant," Proc. 18th Nat. Soc. Aerospace Mater.
    Proc. Engs. Symp. (1973), 16, 276.
86. Benson, J., "Carbon Implant Research," Proc. 18th Nat. Soc.
    Aerospace Mater. Proc. Engs. Symp. (1973), 16, 244.
87. Hammer, J. E., and O. M. Reed, "Pyrolite Carbon Dental Im-
    plants in Baboons: A Preliminary Report," in Medical Prima-
    tology, part II, p. 177, S. Karger, Basel, Switzerland, 1973.
88. Huckee, E. E., R. A. Fuys, and R. G. Craig, "Glassy Carbon:
    A Potential Dental Implant Material," J. Biomed. Mater. Res.
    Symp. (1973), 7, 263.
89. Miller, J., Montreal General Hospital, private communication.
90. Stanitski, C. L., and V. Mooney, "Osseous Attachment to Vitre-
    ous Carbon," J. Biomed. Mater. Res. Symp. (1973), 7, 97.
91. Reswich, J. B., and V. Mooney, Amputee Clinics (1975), 7, 5.
92. Hulbert, S. F., et al., "Design and Evaluation of LTI-Si Car-
    bon Endosteal Implants: A Status Report," presented at 7th
    Annual International Biomaterials Symposium, Clemson Univer-
    sity, Clemson, South Carolina, April 28, 1975 (to be published
    in J. Biomed. Mater. Res.).
93. Mladejovsky, M. G., et al., "Artificial Hearing for the Deaf
    by Cochlear Stimulation: Pitch Modulation and Some Parametric
    Thresholds," presented at 21st Annual Meeting of ASAIO, Wash-
    ington, D. C., April 17-19, 1975 (to be published in the
    transactions).

20

Mesophase: The Precursor to Graphitizable Carbon

HARRY MARSH and CHRISTOPHER CORNFORD

Northern Coke Research Laboratories, School of Chemistry, University of
Newcastle upon Tyne, Newcastle upon Tyne, NE1 7RU, England

The great majority of organic materials carbonize, that is
they thermally decompose in an inert atmosphere, to provide
volatile compounds and black carbonaceous residues variously
called chars, charcoals, soots, carbons, semi-cokes or cokes.
Carbonization systems either pass through a fluid phase as with
petroleum and coal-tar pitch and some coals, or remain entirely
in the solid phase as with cellulose and coconut shell. Carbons
formed in the latter process are invariably non-graphitizing
because on heating to 3300 K they do not develop, to any signifi-
cant degree, an extensive, crystalline, three-dimensional,
graphite lattice. However, carbons formed in the former process,
with few exceptions such as from sugar, are graphitizing, because
on heating to 3300 K, they develop an extensive crystalline
structure and are essentially graphitic. The non-graphitizing
carbons are described as hard carbons, isotropic in bulk
properties and possess appreciable surface area and pore volume
within a microporous network. The graphitizing carbons are des-
cribed as soft carbons, anisotropic in properties and possess low
surface areas and little porosity. Clearly, there must exist
important differences between the structures of these two classes
of carbon which will explain these major differences in properties.
     All, soft, graphitizing carbons are not identical but exhibit
significant differences in the extent of development of their
graphitic properties, for example in the size and relative
orientations of the crystal(lite) components. These differences
are intimately associated with the chemical properties of the
parent material being carbonized, and are dependent on the con-
ditions of carbonization.
     This paper is concerned, in detail, with the mechanism of
formation of graphitizable, anisotropic carbons, and the factors
which influence the final, overall properties of these carbons.
In the studies of both classes of carbon, the optical microscope
has played a major role. Optical microscopy, using polarized
light and preferably a phase-sensitive plate, distinguishes these
two classes of carbon: the anisotropic structures rotate the

plane of the polarized light and exhibit extinction contours,
bands, nodes <u>etc</u>. With "tinted polarized light", obtained by
using a gypsum phase-sensitive plate, the anisotropic carbon
exhibits, from its polished surface, yellow, blue and red areas
which interchange colour on rotation of the specimen. Each colour
represents a section of a volume element of a given crystal
orientation. If the similarly orientated areas are of small
diameter ($<$ 5 μm) and appear with a sensitive-tint as a multi-
coloured mozaic, they are termed "mozaics": larger areas (5 to
100 μm) are termed "domains" and appear as large isochromatic
areas. The isotropic carbons exhibit a purple colour at all
orientations of the specimen. It is the shape, size and
structure of these anisotropic areas which essentially control the
properties of the heat-treated carbons. These shapes, sizes and
structures are themselves functions of the chemical and physical
properties of the carbonization system. It is the detailed
analysis of these functions which constitutes current research
themes and provide insight into a unique mechanism of formation of
anisotropic carbon via the nematic liquid crystal and mesophase,
as outlined below.

Liquid Crystals.

      The optical, anisotropic properties exhibited by carbons
which graphitize [1] imply that the lamellar structure of
graphite is already established in low temperature carbons (800 K),
albeit in a highly imperfect form. In order to understand how
such imperfect, lamellar structures form from an isotropic, fluid
phase of carbonization (pyrolysate), it is necessary, first of all,
to consider the properties of (nematic) liquid crystals. It was
Brooks and Taylor [2], of CSIRO, Australia who, by examining ani-
sotropic development of cokes in coal seams metamorphosed by
igneous intrusions, suggested an explanation of the growth of
anisotropy in terms of liquid crystals.
      Liquid crystal systems [3] have been recognized since 1888
[4]. The term was originally used to describe systems obtained
by melting such substances as cholesteryl benzoate which had
unusual fluid properties and which were anisotropic when viewed in
thin sections between the crossed-polarizers of an optical
microscope. Such systems possessed more structural order than
found in normal (isotropic) liquids, but were not genuinely
crystalline. In a debate on nomenclature, Friedel [5] suggested
that the term "mesophase" (intermediate state) would obviate the
apparent inconsistency of "a crystalline-liquid". But, mesophase
is rather too imprecise a term itself. However, its use as a
description of an intermediate phase in carbon formation is now
established and this current usage is discussed below.
      Of the several categories into which liquid crystals may be
placed, it is the nematic (thread-like) rather than the smectic
(soap-like) or cholesteric system which has relevance to

carbonization. The nematic liquid crystal may be distinguished
from others in the way it separates from the isotropic liquid as
spherical droplets which eventually coalesce to give a nematic
domain. These droplets are anisotropic. In the optical micro-
scope, such materials form domains of preferred orientation of
molecules, the domains being distinguished by boundaries which
appear as black lines (threads) in the field of view of the
microscope. The reticular net of extinction contours is the
manifestion of changes in the direction of molecule alignment and
such structural discontinuities, termed "disinclinations" [3] are
of considerable relevance to discussions of carbon formation.
     The arrangement of molecules, e.g. 6-methoxy-2-naphthoic
acid, in the nematic liquid crystal is usually envisaged as one in
which the molecules lie parallel to one another, but with no order
in the stacking sequence (Figure 1). Containing surfaces exert a
considerable influence, with constituent molecules near to the
surface/interface lying parallel to the surface (Figure 1).
Molecules which form nematic liquid crystals usually possess
features of common geometry. The molecules are usually
elongated or rectilinear. Flat segments such as benzene rings
enhance liquid crystallinity; the molecules are rigid along the
long axis and the existence of strong dipoles and easily
polarizable groups is important.

Mesophase.

     That nematic liquid crystals could be formed from the fluid
phase of certain carbonization systems was suggested by Brooks
and Taylor [2]. The immediate implication is that the stacking
sequence of molecules in such liquid crystals correspond to the
parallel imperfect stacking of molecules/lamellae in pregraphitic
carbons. Thus, the nematic liquid crystal formed during carbon-
ization processes came to be termed the mesophase (but see below).
It was Taylor [6] who made the relevant initial observations in
the Wongawilli coal seam of New South Wales. An igneous dyke, a
tongue of molten magma, had penetrated the coal seam and
established a positive thermal gradient through the coal seam to-
wards the dyke. The effect, over some hundreds of metres, was to
establish a very gradual thermal gradient reaching maximum
temperatures which passed through and exceeded the temperatures of
formation of anisotropic coke from coal. It was the slow rates of
heating and the identification of a very narrow temperature zone
of formation of anisotropic carbon which provided the first clues
of the dependence of anisotropic carbon formation upon a liquid-
crystal type precursor. Previous laboratory experiments had all
used too rapid a heating rate and the detail of formation of
anisotropic carbon was missed.
     Taylor [6] observed that, on approaching the dyke, small
spheres, initially micrometer size, were observed in the vitrinite.
Figure 2 shows similar spheres growing in laboratory carbonized

acenaphthylene. The spheres, in polished section, exhibited
rather unusual optical properties which were consistent with ani-
sotropic stacking of the constituent lamellae parallel to an
equatorial plane [6]. An alternative possibility of circum-
ferential stacking, as in an onion, was discounted. These
spheres, on further heating, grew at the expense of the vitrinite
and coalesced to form the mozaic structures. Taylor [6]
recognized that this anisotropic sphere was providing the clue to
the development of graphitizing carbons. The molecular arrange-
ments within the sphere, deduced from optical properties and
confirmed by electron diffraction, closely resembled that of the
nematic phase in substances which form liquid crystals. Hence,
the mechanism of formation of graphitizable carbons(via the
mesophase) came to be associated with properties of liquid
crystals.

Liquid Crystals and Mesophase.

The original suggestion by Brooks and Taylor [2] and taken up
by other workers [7-18] promoted considerations of the possibility
of close similarity in growth processes and properties between the
mesophase and nematic liquid crystals. It is now generally
accepted that the mesophase is a plastic, anisotropic phase which
grows from the fluid pyrolysate and solidifies to give the
anisotropic coke. The plastic properties of the mesophase [7],
its high degree of anisotropy [2], the effect of magnetic fields
which can align the constituent molecules of mesophase [19], the
orientation of molecules parallel to contained or confining
surfaces [13] and of eutectic effects [17] all fit in well with
the known properties of liquid crystals.
But, there exists other evidence which indicates that this
intermediate phase between the isotropic pyrolysate (e.g. plastic
coal or coal-tar pitch) and anisotropic coke is NOT a nematic
liquid crystal as such. For example, for almost all systems the
mesophase is formed irreversibly. It is relatively insoluble in
benzene and in pyridine [20]. Activation energies of formation of
140 to 180 kJ mol^{-1} correspond to chemical rather than to physical
processes [21]. Observed increases in molecular weight [2] and
C/H ratios [20] also indicate the chemical nature of the
processes leading to mesophase formation. The spacings between
constituent lamellae of the mesophase are known to decrease with
time at constant temperature [21], this also being indicative of
continuing chemical processes occurring within the mesophase after
its formation.
The above discussion suggests that the similarities with
nematic liquid crystals mainly concern the ordering or stacking
processes of mesophase growth, whilst the dissimilar properties
are indicative of chemical processes of mesophase formation and
change within the mesophase. It can be argued that, although
mesophase has structural similarities to nematic liquid crystals,

its formation and maturation is a chemical process. Hence, it is suggested as definitions of the two terms, that mesophase is a structural analogue and possibly a pseudomorph of an initial, transient, nematic liquid crystal phase in which only Van der Waals and dipole interactions orientate the molecules. Thus, a 'model process' for formation of nematic liquid crystals and then mesophase can be described as follows.

During the carbonization process of a parent substance, e.g. coal, coal-tar pitch, petroleum pitch etc., the various pyrolytic reactions of the carbonization result in an increase in the average molecular weight of the fluid, carbonization system. This is illustrated in the carbonization of anthracene in a closed system which leads to the formation of dianthryl and trianthryl [10] which further co-condense to produce large, planar molecules containing nine to about thirty hexagonal rings. With increasing carbonization temperature, increasing fluidity of the system increases the diffusivity of the constituent molecules leading to an enhanced probability of molecule-molecule inter-actions. That an anisotropic structure subsequently develops suggests that surface-to-surface interactions come first, with the edge-to-edge interactions coming later. This surface-to-surface interaction could resemble that of a physical adsorption process. Here, the larger is the adsorbed molecule, the higher is the molar enthalpy of adsorption. Associated with these higher enthalpies of adsorption are the longer residence times, or duration of stay, of the adsorbed molecule on the adsorbent sur-face [22]. In the carbonization systems, this physical inter-action results in the formation of the nematic liquid crystal from the planar (aromatic) molecules. If such attractive forces can withstand the disruptive forces of molecular collisions, then a relatively stable, stacked, molecular structure can exist within the pyrolysate. Additional molecules can be adsorbed, increasing the thickness and length of what is now an 'embryonic' nematic liquid crystal. At this stage, the liquid crystal may be reversibly dissociated [23]. But, if the duration of its existence is sufficiently long, perhaps milliseconds as distinct from nanoseconds (the duration of molecular collisions), then chemical bonding may occur between the constituent molecules of the 'embryonic' liquid crystal which now loses its ability to dissociate reversibly into its constituent molecules. The nematic liquid crystal then becomes a polymeric, anisotropic stable phase with a structure based upon that of the transitory liquid crystal. This polymeric phase is the mesophase, which with few exceptions [23] is detected and studied in the optical microscope.

Mesophase Growth and Coalescence.

The liquid crystal and mesophase thus originate by a process of homogeneous nucleation. Once formed, the mesophase spheres (shapes) continue to grow at the expense of the isotropic, fluid

phase of the carbonization system until they eventually touch each other. What happens at this stage is a function of the plasticity of the mesophase itself. Should it have retained sufficient plasticity during its growth period (and the carbonization conditions are not too turbulent) then the mesophase shape will have responded to the requirements of minimum surface energy and will have become spherical. When two spherical mesophase meet, then this facility to respond towards minimum surface energy again dictates that these two spheres adopt a single spherical shape, i.e. they coalesce. This coalescence probably occurs by a process similar to growth. The surface of a mesophase sphere is made of molecules with their planes at right angles to the sphere surface (Figure 3). During coalescence, the molecules initially overlap and adsorption/interaction is possible.

The degree of plasticity possessed by the mesophase at temperatures where coalescence occurs is a function of two properties of the mesophase. It is a function of the degree of polymerization or cross-linkage which exists within the mesophase. The higher the degree of polymerization, the lower is the plasticity of the mesophase. The degree of polymerization is dependent upon the chemical reactivity of the constituent molecules. If this reactivity is high, then at comparatively low temperatures the degree of polymerization is extensive and the mesophase has little plasticity. The degree of plasticity is, secondly, a function of the degree of non-planarity of constituent molecules. Such structures as "arm-chair" or "boat", while not preventing liquid crystal formation could inhibit the facility of relative movement (slip) within the mesophase, this movement being necessary to respond to the forces of coalescence. Whatever the relative importance of chemical or physical effects, mesophase of low plasticity will, consequently, grow with a non-spherical shape and when contact is made between mesophase shapes, then coalescence is severely restricted. As a result, only mozaics of fine-grained anisotropic material are formed, and NOT the large domains of anisotropic carbon.

Generally, the more aromatic is the parent substance, the greater is the plasticity of the resultant mesophase, and the greater is the temperature range over which the mesophase retains this plasticity. This is determined by the relatively low chemical reactivity of aromatic molecules and their greater planarity when compared with, e.g. the heterocyclic and substituted, unsaturated, non-planar molecules found in some petroleum derivatives and low-rank coals. Thus, in industrial situations, the coalesced mesophase generally retains sufficient plasticity to respond to the shear forces set up by thermal convection currents and volatile bubble movement through the systems and thus creates the flow-type anisotropy of coking coals or the needle-coke anisotropy of aromatic-rich petroleum sources. The needle-coke anisotropy from petroleum sources can be larger, by an order of
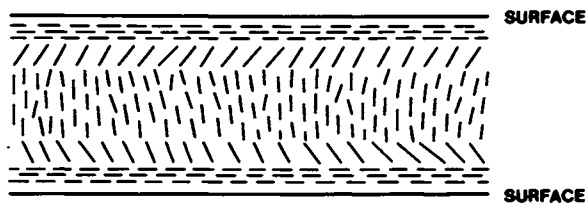
Figure 1. *Diagram of molecular arrangements within nematic liquid crystals*

25 μm
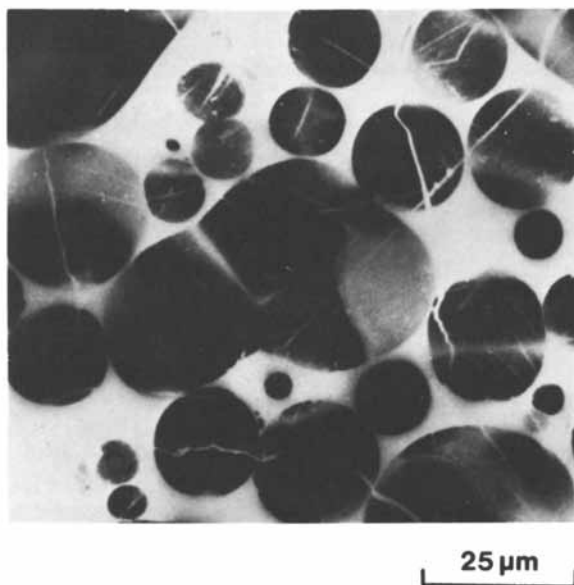
Figure 2. *Optical micrograph showing mesophase growth and coalescence from acenaphthylene*
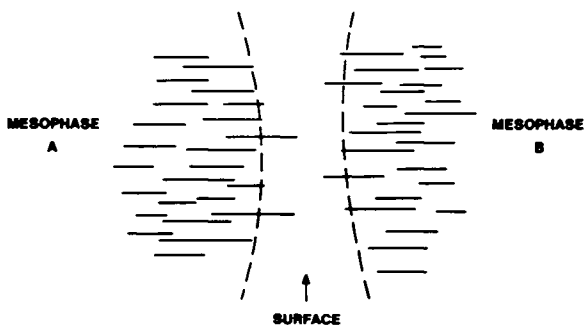
Figure 3. *Diagram of the initial stages of coalescence of mesophase spheres*

magnitude, than the flow-type anisotropy from coals.

For industrial situations, Patrick [24] has described meso-
phase growth during the carbonization of British coals and White
[7] has extensively examined mesophase from many petroleum
sources. Marsh and co-workers [8-17] carbonized model compounds
as well as coals and pitches in attempts to formulate the basic
principles which underlie mesophase growth characteristics in the
industrial situation. To study the growth processes usually re-
quires the preparation of polished samples for optical microscopy,
and this can be a tedious process. However, an observation by
Marsh, Walker et al. [16] that the mesophase coalescence can be
restricted by carbonization under pressures greater than about
70 MPa (10,000 p.s.i.) means that the shape and size of mesophase
can be monitored by the more convenient technique of scanning
electron microscopy (Figure 4). The detail of the many carbon-
izations, of single substances and mixtures of graphitizable and
non-graphitizable model compounds is published [8-16] from which
the following conclusions can be made explaining the wide
variation in size (0.3 to 100 μm) and shape (irregular, sphere,
needle-like) [13] of mesophase. These conclusions involve con-
siderations of carbonizing systems where processes other than
those discussed above may be operating, e.g. the presence of inert
solids and non-graphitizing compounds:

A. Flow-type or coalesced anisotropy results from:-

(i)   mobility of the developed mesophase anisotropic
structures over surfaces of solids (inerts) or at liquid/gas
interfaces, resulting in their coalescence and flow-type appear-
ance, often associated with convection currents within the plastic
phase.

(ii)   the growth, preferentially, of mesophase at surfaces,
rather than in the bulk of the isotropic liquid.

(iii) the enhanced plasticity of mesophase associated with
molecular aromaticity as in coal-tar pitch, or with the presence
of oxygen in heterocyclic, polycyclic systems which are known to
enhance the growth of mesophase [14,15]. A decrease in the com-
plexity of mixtures of molecular species associated with an
increase in the homogeneity of chemical reactivity also favours
coalesced anisotropy.

B. The non-coalescence of the mesophase structures can be
attributable to:-

(i)   colloidal solid impurities within the carbonizing
system being adsorbed on surfaces of mesophase.

(ii)   residual compounds, not forming liquid crystals, being
adsorbed on surfaces of growing liquid crystals.

(iii) physical separation by formation of isotropic carbon.

(iv)   low mobilities of molecules of high molecular weight

and low plasticity of mesophase restricting growth and coalescence
during the carbonization process.

C. The smaller sizes of anisotropic structures can be attribut-
able to:

     (i)   dilution of those compounds, which form liquid
crystals, in an isotropic liquid composed principally of com-
pounds capable of forming only isotropic carbon.
     (ii)   the existence of a range of temperature over which
constituent molecules of the carbonizing system separately form
liquid crystals. This can be associated with extensive re-
structuring of molecules in the carbonization process.
     (iii)   slow growth rates of liquid crystals resulting from
the high molecular weight of constituent molecules.
     Variations in carbonization characteristics between, e.g.
petroleum and coal-tar feedstocks can be attributed to
significant differences in chemical composition of these materials.
A more comprehensive understanding of these variations is
dependent upon an improved knowledge of the chemistry of these
materials. However, the complexity of petroleum feedstocks, in
particular, must not be underestimated.
     It has recently been observed by Isaacs [25] and Marsh et al.
[17] that mixtures of organic compounds, when co-carbonized, form
anisotropic carbon, despite the observation that when carbonized
singly, the organic compounds form only isotropic carbon, e.g.
co-carbonization of carbazole and pyromellitic dianhydride.
Perhaps intermolecular reactions between these two compounds pro-
duce a new series of molecules capable of forming liquid crystals
[25]. On the other hand, it may be that mixed nematic liquid
crystals form eutectics [17] stable at temperatures lower than the
temperatures of formation of liquid crystals from single compon-
ents. There is a relevance of these observations to carbonizations
of blends or mixes of fusible components.

Mesophase Structure and Graphitizability.

     In the above discussions, the argument is made that the
stacking sequences of constituent molecules in nematic liquid
crystals formed in the pyrolysate are maintained in the mesophase
and established in the anisotropic carbon. Thus, the anisotropic
carbons possess an imperfect, pregraphitic structure which is
progressively perfected, with increasing temperature, towards
graphite. Two factors significantly influence this graphiti-
zation process; first, the size of the anisotropy, (mozaic or
domain) is important since boundary conditions limit crystal
growth processes; second, the detail of the stacking sequences
influences graphitization which essentially is the removal of the
stacking defects in the original carbon. Stacking defects are
associated, not only with the relative positions of constituent

molecules, but also with the presence of heteroatoms, vacancies and lack of planarity in these large stacked molecules.

Consequently, the properties of a graphitized material must depend, closely, upon the structure of the mesophase (its extent of order and molecular perfection) this being dependent upon the chemical and structural properties of the constituent molecules of the pyrolysate and the carbonization conditions. To control the structure of the mesophase offers a method of controlling the properties of the graphitic material.

Marsh, Cornford and Crawford [26,27] use two techniques to analyze structure in mesophase and pregraphitic carbons. Optical microscopy, with quantitative reflectance measurements from polished surfaces, using polarized light provides information about the extent of conjugated bonding within constituent molecules of the pyrolysate/mesophase/carbon and about the stacking sequences of the molecules in establishing the anisotropic structure. High resolution, phase-contrast electron microscopy [28] of carbons can resolve the "lattice" of the stacked, constituent molecules as fringe images, so providing a direct visual description of structure within mesophase.

Marsh, Cornford and Crawford [29] using these two complementary techniques, examined structural changes occurring during the carbonization and graphitization of polyvinylchloride and a coal-tar pitch. Both techniques clearly support the model of mesophase growth and graphitization outlined above. The growth of conjugated molecules in the liquid pyrolysate is monitored, no marked conjugation is detected as mesophase is developed, but increased conjugation occurs as the plastic mesophase is converted to solid carbon. The electron microscope reveals the parallel stacking of molecules in mesophase from polyvinylchloride (Figure 5) so providing direct evidence of the structural orientation suggested by Brooks and Taylor [2] and others [7]. The perfection of stacking in the graphitized material (2673 K) is seen in Figure 6.

Structure within mesophase of different sizes has also been examined [26]. Mesophase mosaics, about 1 μm diameter, can be formed from the structurally complex compound 2-(o-hydroxyl-phenyl)-benzo-thiazole (I),(Figure 7) and mesophase, about 50 μm diameter can be formed from the planar molecules of acridine (II),(Figure 8). Preliminary results from a phase-contrast, electron microscope study of these two mesophase materials are as Figures 9 and 10, which also contain tracings from the fringe images. The stacking sequences and length of fringe in the mesophase prepared from (I) are less developed than in the mesophase prepared from acridine (II). This would suggest (albeit from an initial investigation) that differences in stacking development and molecular shape may be associated with mesophase of different sizes, and illustrates how correlations between mesophase characteristics (plasticity, coalescence and ordering) and graphitizability may be established.
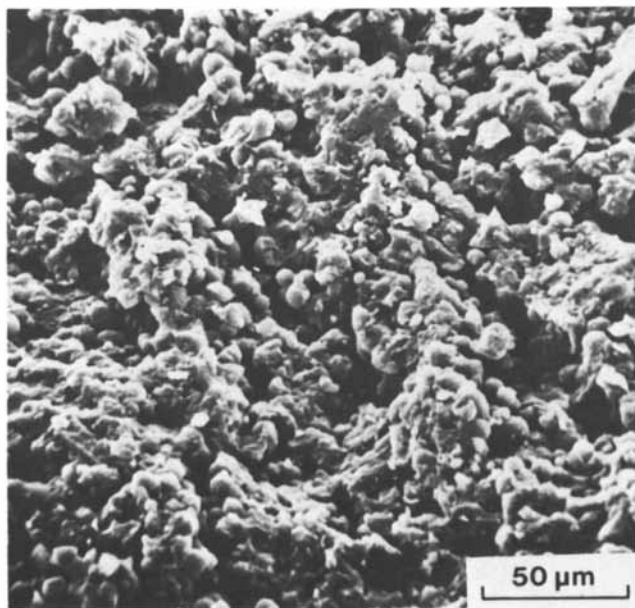
Figure 4. Stereoscan micrograph of botryoidal, non-coalesced mesophase produced by carbonizing a coal tar pitch under pressure
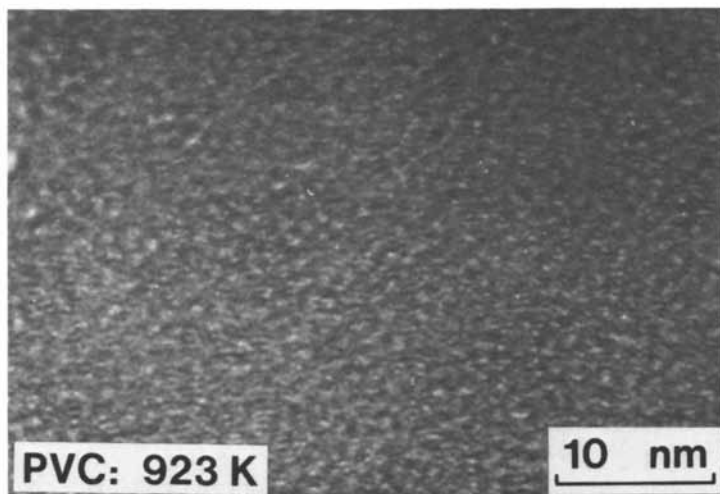
Figure 5. Phase-contrast electron micrograph showing lattice-fringes from carbon (poly-vinyl chloride, HTT 923 K)
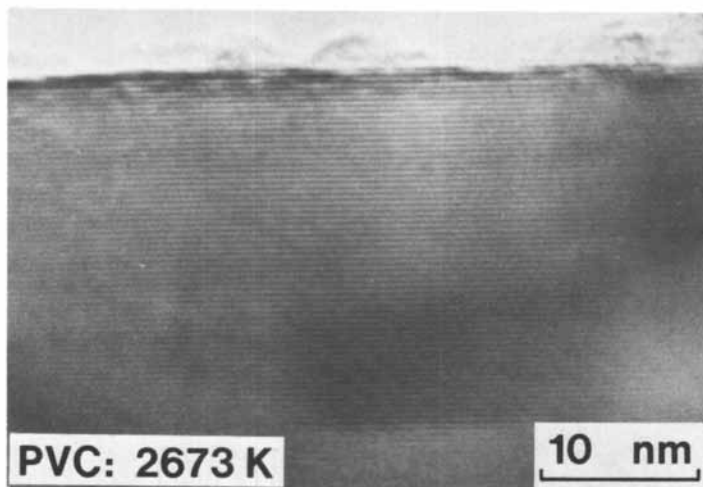
Figure 6.   Phase-contrast electron micrograph showing lattice-fringes from carbon (polyvinyl chloride, HTT 2673 K)
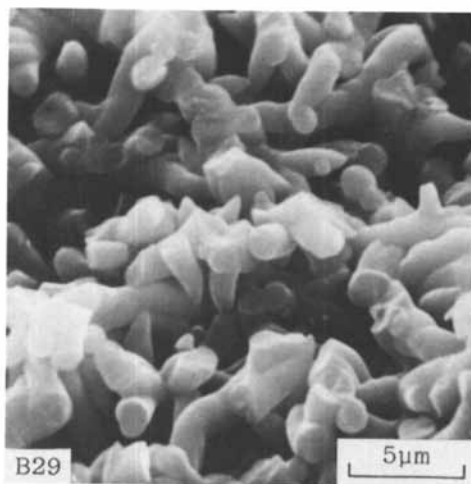
Figure 7.   Stereoscan micrograph of mesophase from   2-(o-hydroxylphenyl)benzothiazole,   HTT 850 K
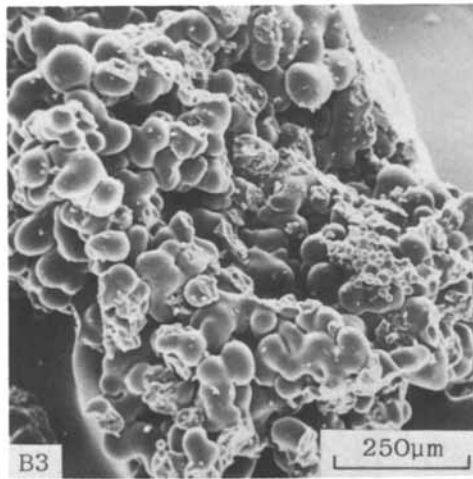
Figure 8. Stereoscan micrograph of mesophase from acridine, HTT 850 K
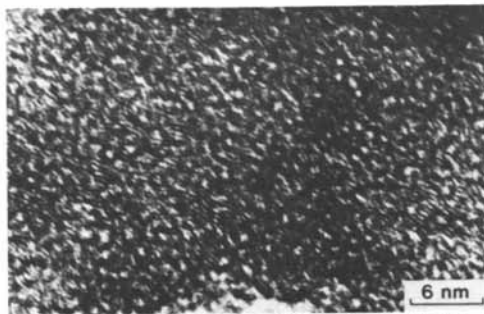
ELECTRON MICROGRAPH.   JEOL 100C.
– BENZO – THIAZOLE   850 K.
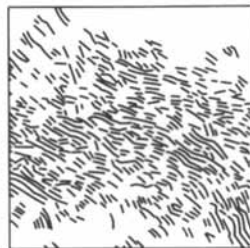
TRACED   FRINGE   PATTERNS.

Figure 9.   Phase-contrast electron micrograph showing lattice-fringes from carbon (2-(o-hydroxylphenyl)benzothiazole, HTT 850K)
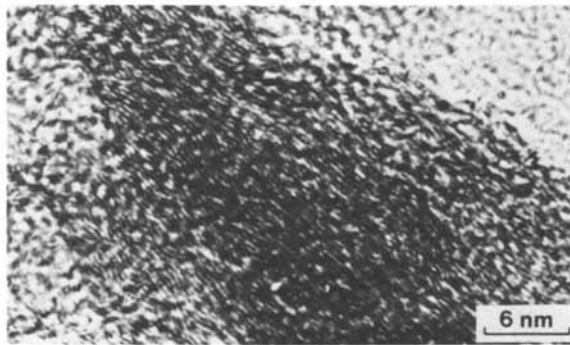
ELECTRON MICROGRAPH. JEOL 100C.

ACRIDINE 850 K.
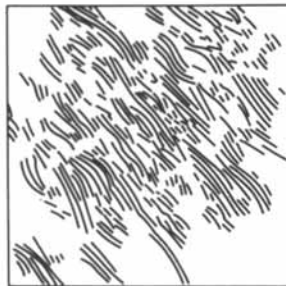
TRACED FRINGE PATTERNS.

Figure 10. Phase-contrast electron micrograph showing lattice-fringes from carbon (acridine, HTT 850 K)

Industrial Relevance.

    Studies of mesophase constitute a good example of "an
improvement in the quality of discussion of the process" leading,
it is hoped "to an improvement in the quality of the product of
the process". Examples where discussions of mesophase have
industrial relevance include:-
A. All aspects of production of commercial graphite; the
    processes within the delayed coker and other cokers used in
    production of petroleum coke; the production of specialized
    forms of coke; the carbonization of coal-tar pitch; the
    interaction of mesophase with the grist during the
    carbonization of blends; the properties of baked electrodes.
B. The isolation of mesophase, and its subsequent manipulation
    to produce graphitic material of controlled structure and
    properties e.g. industrial construction units.
C. The production of certain carbon blacks which possess
    considerable order of lamellar stacking parallel to
    surfaces [30,31].
D. Aspects of production of carbon fibres from petroleum and
    coal-tar pitch, and coal extracts.
E. Aspects of production of blast furnace coke from single
    coals and coal blends (important in countries with shortages
    of coking coals); coke strength could be related to growth
    and orientations of mesophase relative to surfaces of
    components of blends and vescicles [32].

Acknowledgements.

Summary: Mechanisms are discussed of the formation of graphiti-
zable anisotropic carbons from fluid pyrolysates in terms of
nematic liquid crystals and the mesophase. All graphitizable
carbons are not identical but exhibit significant differences in
the extent of development of graphitic properties; examples are
the size and relative orientation of the crystal components.
Explanations are advanced for the variations in size, shape,
coalescence and orientations of anisotropic mozaics and domains in
graphitizing carbons. The importance of the chemical composition
of parent substances in determining mesophase growth character-
istics is emphasized. The industrial relevance of mesophase in
carbon and graphite production is summarized.

Literature Cited.

1. Fischbach D.B., 'Chemistry and Physics of Carbon', Ed. P.L. Walker Jr., (1971) 7, 1, Edward Arnold, New York.
2. Brooks J.D. and Taylor G.H., 'Chemistry and Physics of Carbon', Ed. P.L. Walker Jr., (1968) 4. 243, Edward Arnold, New York.
3. Brown G.H., Doane J.W. and Neff V.D., 'Review of Structure and Properties of Liquid Crystals', Butterworths, 1971. De Gennes P.G., 'The Physics of Liquid Crystals', Clarendon, Oxford, 1974.
4. Reinitzer F., Monatsh, (1888) 9, 421.
5. Friedel G., An. Physique, (1922) 18, 273.
6. Taylor G.H., Fuel, London, (1961) 40, 465.
7. White, J.L., Progress in Solid State Chem., (1974) 9, 59.
8. Marsh H., Akitt J.W., Hurley J.M., Melvin J.M. and Warburton A.P., J. Applied Chemistry, (1971) 21, 251.
9. Marsh H., Dachille F., Melvin J.M. and Walker P.L., Carbon, (1971) 9, 159.
10. Evans S. and Marsh H., Carbon, (1971) 9, 733.
11. Evans S. and Marsh H., Carbon, (1971) 9, 747.
12. Marsh H., Foster J.M. and Hermon G., Carbon (1973) 11, 424.
13. Marsh H., Fuel, London, (1973) 52, 205.
14. Marsh H., Foster J.M., Hermon G. and Iley M., Fuel, London, (1973) 52, 234.
15. Marsh H. et al., Fuel, London, (1973) 52, 243.
16. Marsh H. et al., Fuel, London, (1973) 52, 253.
17. Marsh H., Cornford C. and Hermon G., Fuel, London, (1974) 53, 168.
18. Goodarzi F. et al., Fuel, London, (1975) 54, 105.
19. Sanada Y., Furuta T. and Kimura H., Carbon, (1972) 10, 644.
20. Huttinger K.J., Bitumen, Teere, Asphalte, (1973) 24, 255.
21. Honda H. et al., Carbon, (1970) 8, 181.
22. De Boer J.H., 'The Dynamical Character of Adsorption', Oxford University Press, London, 1968.
23. Lewis R.T., Abstracts of 12th Biennial Conf. on Carbon, Amer. Carbon Soc., Pittsburgh, 1975.
24. Patrick J.W. et al., Fuel, London, (1973) 52, 198.
25. Isaacs L.G., Carbon, (1968) 6, 765.
26. Marsh H., Augustyn D., Cornford C., Crawford D. and Hermon G., Abstracts of 12th Biennial Conf. on Carbon, Amer. Carbon Soc., Pittsburgh, 1975.
27. Marsh H. and Cornford C., Abstracts of 12th Biennial Conf. on Carbon, Amer. Carbon Soc., Pittsburgh, 1975.
28. Ban L.L., 'Surface and Defect Properties of Solids', (1972) 1, 54. The Chemical Society, London.
29. Marsh H., Cornford C. and Crawford D., Unpublished results.
30. Marsh H., Carbon, (1973) 11, 254.
31. Donnet J.B. et al., Carbon, (1974) 12, 212.
32. Cornford C. and Marsh H., Unpublished results.

21

Mesophase Mechanisms in the Formation of the Microstructure of Petroleum Coke

J. L. WHITE

The Aerospace Corp., P.O. Box 92957, Los Angeles, Calif. 90009

Carbon and graphite materials are required to withstand
increasingly severe conditions of thermal shock, stress, and re-
actor irradiation in the steelmaking, aluminum, aerospace, and
nuclear industries. The performance of these materials depends
to a large degree on the characteristics of the filler coke, which
is conventionally produced by the delayed coking of various heavy
refinery feedstocks. Thus more stringent demands are being
made on the quality of petroleum coke at the same time as the
supply patterns for the coking feedstocks are changing rapidly.
This situation has motivated the investigations summarized here,
which seek an understanding of how microstructures form in
order to assist in producing more homogeneous cokes of improved
quality.

Studies of the carbonization of coal and petroleum precur-
sors, as well as various model organic compounds, have con-
firmed and added much detail to the point first made by Brooks
and Taylor (1, 2), viz., that the principal features of graphitic
and pregraphitic microstructures are established in a relatively
narrow range of temperature near 450°C in which the pyrolyzing
mass exists as a viscous anisotropic liquid, i.e., as a "meso-
phase" in the terminology of liquid crystals. Petroleum-derived
starting materials yield a wide variety of mesophase morpholo-
gies, ranging from the fine isotropic microconstituents favored
in reactor graphites for their stability under neutron irradiation
to the acicular or needle-like microconstituents valued for the
thermal-shock resistance which they contribute to electrode or
aerospace graphites (3-6). These microconstituents are often
found in intimate and complex combination in petroleum coke,
thus reflecting the varied nature of the refinery streams fed to
the delayed coker.

This paper offers a review of work performed for the
EURATOM-Petten Research Centre (7, 8), the Gulf Oil Corpora-
tion (5, 9), and The Aerospace Corporation (6, 10, 11). The
results indicate that the formation of mesophase microstructures
in the coking of a wide range of feedstocks follows systematic

patterns which relate primarily to the plasticity of the mesophase
and the deformation experienced by the mesophase as it hardens
to a semi-coke within the coke drum.

Formation of Mesophase Structures

The formation of microstructure in graphitizable materials
has recently been reviewed (10). We summarize here some
points relevant to the carbonization of typical coker feedstocks.
Polarized-light micrography has proved valuable for car-
bonization studies because the optical anisotropy characteristic
of the graphite crystal begins with the parallel alignment of the
layer-like aromatic polymers to form the carbonaceous meso-
phase. In the early stages of the mesophase transformation, the
mesophase precipitates from the pyrolyzing matrix as small
spherules as illustrated by Figure 1. The polarized-light re-
sponse can be employed to map the orientations of the mesophase
layers relative to the plane of micrographic section (8). The
spherules display the characteristic Brooks-and-Taylor mor-
phology; within the central region the mesophase layers lie par-
allel to define the polar diameter but curve to meet the interface
with the pitch matrix at a high angle.
As pyrolysis proceeds the mesophase spherules grow and
sink through the pitch matrix. When spherules meet, coales-
cence often occurs to produce larger droplets of more complex
structure, as illustrated by Figure 2. Mapping of the extinction
contours reveals a lamelliform morphology with no trace of any
structure resembling a grain boundary at the coalescence junc-
ture. Thus the dominant structural feature of the carbonaceous
mesophase and its heat-treated fossils is the two-dimensional
mesophase layer rather than the three-dimensional crystal grain
of conventional polycrystalline materials.
As pyrolysis continues, the coalescence processes eventu-
ally produce bulk mesophase which often displays the complex
lamelliform morphology illustrated by Figure 3. Frank (12)
terms this morphology a Möbius body, and the manner in which
space is filled by the mesophase lamellae accounts for the arrays
of bends, folds, splays, and lamellar stacking defects (disclina-
tions) found in the various microconstituents of coke (10).
When the plane of polarization of the incident light is ro-
tated, the polarized-light extinction contours sweep across vari-
ous regions of the micrographic cross-section, but the nodes and
crosses remain fixed in position. Figure 4 shows how the
polarized-light response reflects the underlying lamelliform
structure (7). Thus detailed mapping procedures are not neces-
sary to characterize the microconstituents of coke; it is sufficient
for most purposes to define the structures in terms of the average
spacing and alignment of the extinction contours (5).
The nucleation, growth, and percolation of gas bubbles
within the mesophase can produce extensive plastic deformation,
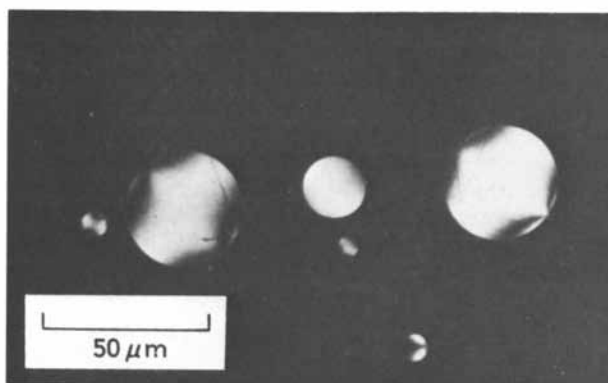
PHOTOMICROGRAPH OF
MESOPHASE SPHERULES

STRUCTURAL SKETCH OF
MESOPHASE SPHERULES

POLE
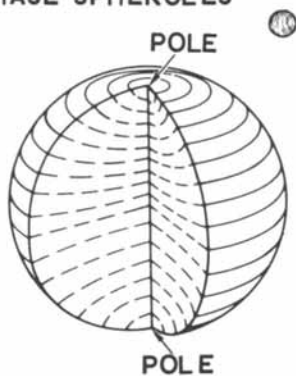
POLE
MESOPHASE SPHERE WITH
SECTION INCLUDING
POLAR DIAMETER

Metallography

*Figure 1.   The alignment of mesophase layers in spherules
precipitated by the pyrolysis of an extruded coal tar pitch (8).
Photomicrograph made with crossed polarizers.*
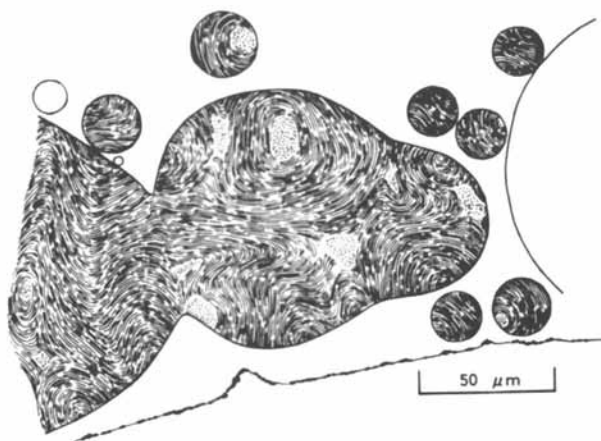
INDICATES REGION WHERE LAYERS LIE
PARALLEL TO PLANE OF SECTION
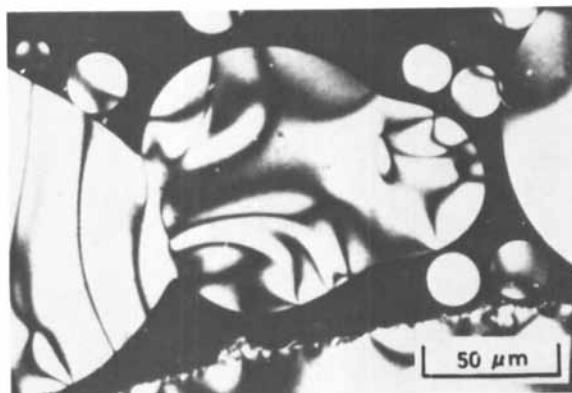
Metallography

*Figure 2.   Mesophase layer alignment in droplets at
two stages of coalescence (8). Photomicrograph made
with crossed polarizers.*

U   CO-ROTATING NODE
Y   COUNTER-ROTATING NODE
O   CO-ROTATING CROSS
X   COUNTER-ROTATING CROSS

100 μm
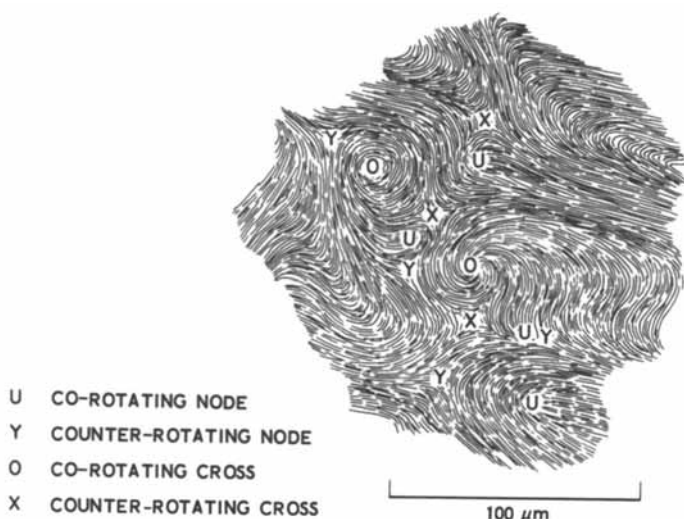
Journal de Chimie Physique

Figure 3. The Möbius morphology of bulk mesophase with a coarse structure (7). The structural sketch was mapped from a series of micrographs under conditions of crossed polarizers. The layer stacking defects (disclinations) are denoted in terms of their polarized light response (see Figure 4).

CO-ROTATING NODE

COUNTER-ROTATING
CROSS

COUNTER-ROTATING
NODE

SPACING OF EXTINCTION
CONTOURS

CO-ROTATING CROSS

TRANSITORY CROSS
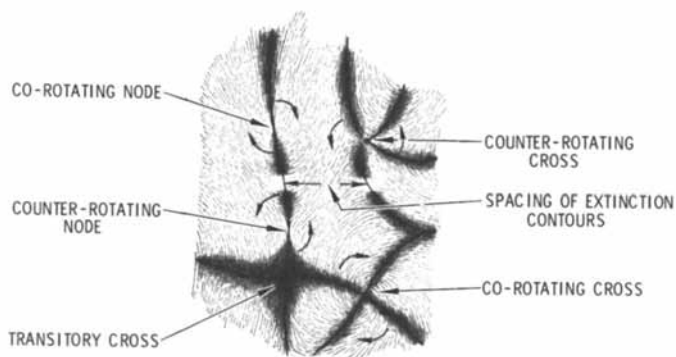
Journal de Chimie Physique

Figure 4. Polarized light response of a lamelliform structure with four common types of layer stacking defects (disclinations). The spacing of extinction contours offers a measure of the bend, twist, splay, and disclination density of a given microconstituent. The nature of each disclination may be determined from the rotation direction of the extinction contours when the plane of polarization of the incident light is rotated (7).

which constitutes a mechanism by which the microstructure is
both oriented and reduced to finer texture. Figure 5 illustrates
the fibrous appearance of the extinction contours at a relatively
modest extent of deformation. This array corresponds to the
oriented and folded layers of the structural sketch. Such micro-
constituents may be characterized by the average spacing of
extinction contours measured transverse to the preferred
orientation.

    The microstructural refinement can be intensified by pur-
posefully applying mechanical deformation to the mesophase
while it remains plastic (11). Figure 6 illustrates the fine tex-
ture of extinction contours on the transverse and longitudinal
cross-sections of a 3-mm rod drawn from a partially trans-
formed petroleum pitch (Ashland A-240) mesophase. The aver-
age spacing of extinction contours is about one micron. By
drawing to smaller diameters very fine fibrous textures similar
to those found in spun mesophase fibers (13, 14) can be produced.

Coke Microstructures

    In ordinary refinery practice, delayed coking is employed
to wring the last gas and liquid values from reduced petroleum
crudes. The product cokes usually display complex heteroge-
neous structures which are of little value for demanding applica-
tions; for example the microstructure of an ordinary low-sulfur
coke shown in Figure 7 contains coarse, fine isotropic, and some
deformed microconstituents. Most such cokes may be viewed as
lying between two extreme structural types: the fine isotropic
microstructure, which is typical of gilsonite coke but is also
found as a major microconstituent in most cokes produced from
reduced crudes (3, 5); and the acicular or fine fibrous micro-
structure found in the needle cokes produced from the more aro-
matic refinery streams from which the asphaltene components
have been removed by cracking and distillation (15). The most
common needle-coke precursors in current use are the decant
oils derived from fluidized catalytic cracking processes (16).

    The fine isotropic character of a "buckshot" coke is illus-
trated by Figure 8. The average spacing of extinction contours
in this unusually homogeneous microstructure is about 5 microns.
The buckshot cokes derive their name from the spherical aggre-
gates (diameters of the order of 5 mm) which usually character-
ize their macrostructures; they closely resemble gilsonite cokes
in particle shape and microstructure.

    Figures 9 and 10 illustrate the microstructure of a selected
needle-coke particle. Appreciable amounts of coarse mesophase
microconstituents are usually found in intimate association with
the needle-like regions (6). The needle appears fibrous in longi-
tudinal cross-section but fine isotropic in transverse cross-
section. The extinction contour spacing of about 2 microns is
typical of needle-like regions.
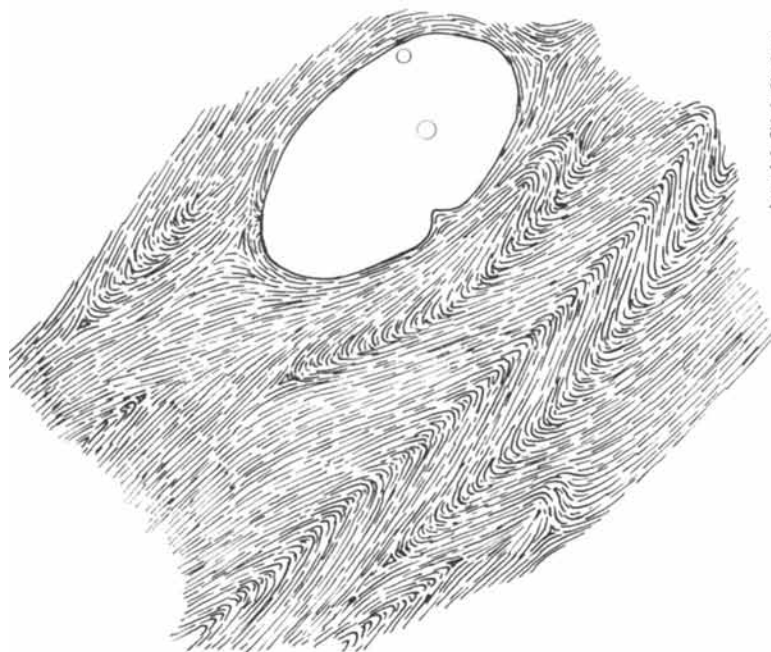
Journal de Chimie Physique

Figure 5. The development of deformed microconstituents in bulk mesophase by bubble percolation (7)
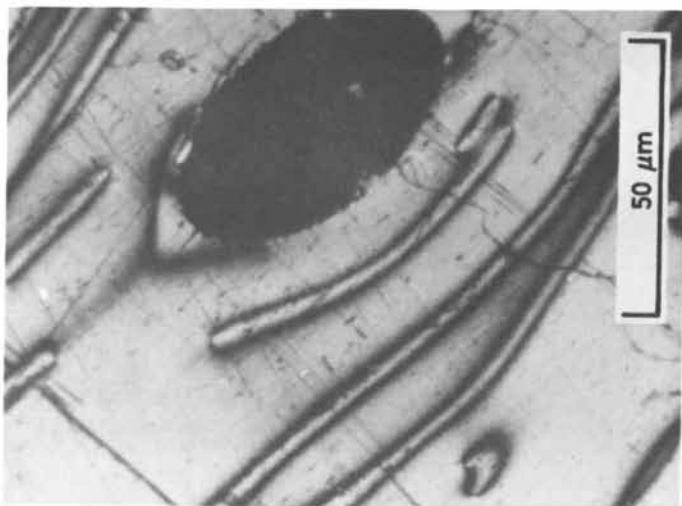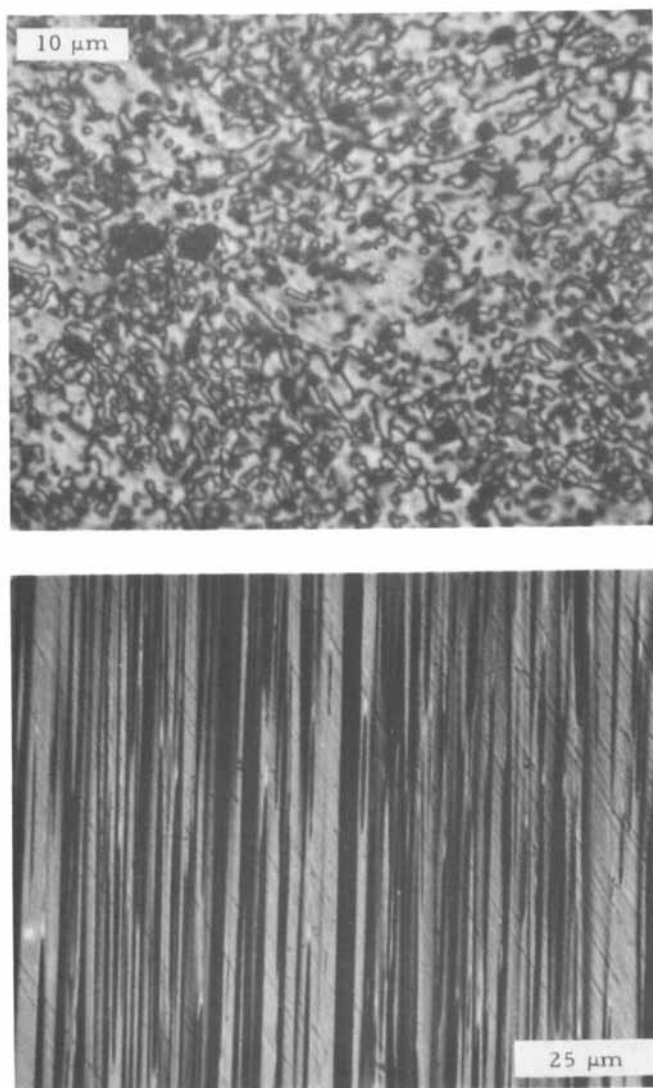
Figure 6. The fine deformed microstructure of a mesophase rod drawn from partially transformed Ashland A240 pitch. Crossed polarizers. Top, transverse to axis of rod; bottom, longitudinal section.
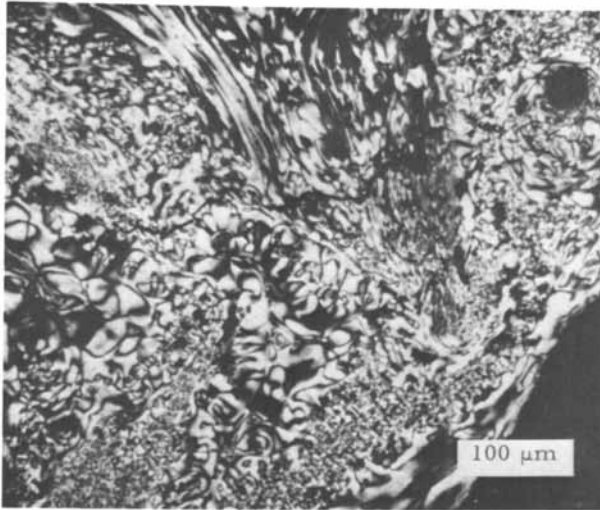
*Figure 7.   A typical microstructure of ordinary delayed coke.
Crossed polarizers.*
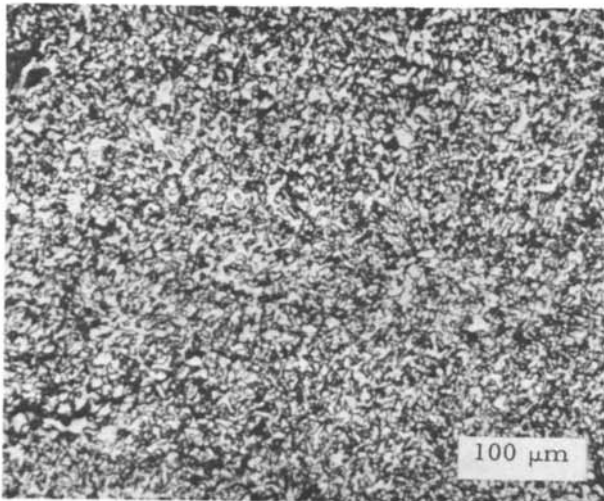
*Figure 8.   Fine isotropic microstructure of a "buckshot"-
type delayed coke. Crossed polarizers. Extinction contour
spacing — 5 μm.*

ORIENTATION OF
CROSSED
POLARIZERS

500 μm

SECTION PARALLEL
TO LENGTH OF
NEEDLE COKE
PARTICLE

EDGE

SECTION PERPENDICULAR
TO LENGTH OF NEEDLE
COKE PARTICLE

A
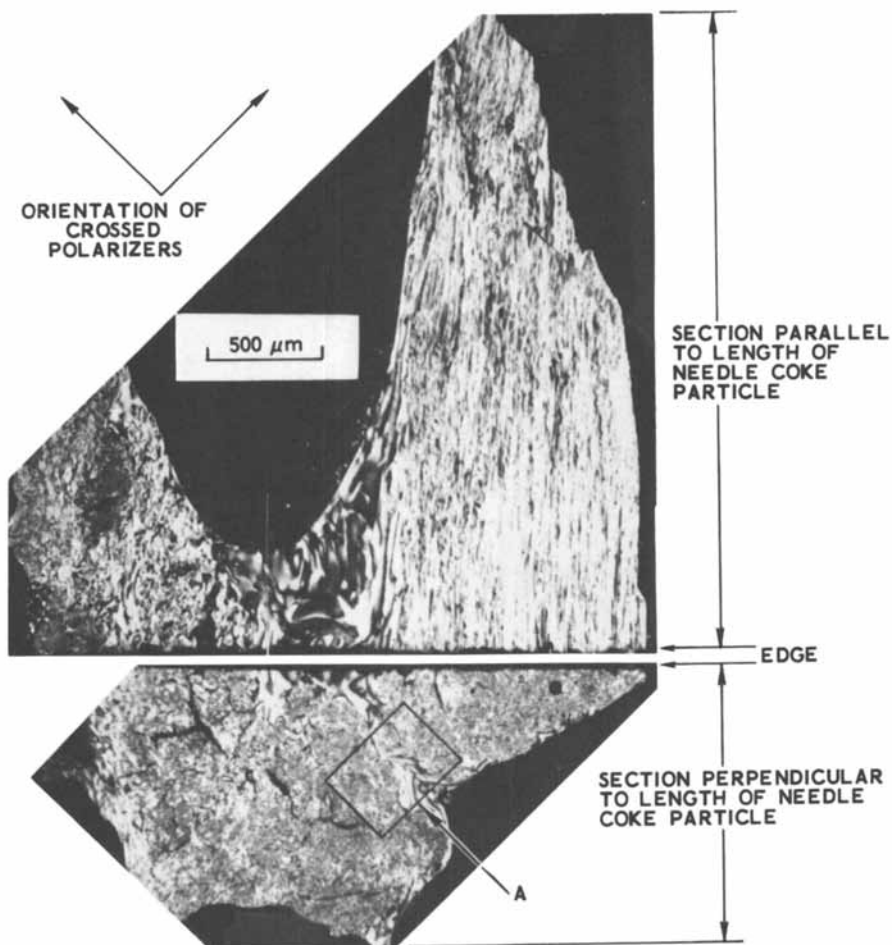
Figure 9.   The microstructure of a needle coke particle viewed parallel and perpendicular to the length of the particle. Crossed polarizers. The region indicated by A is shown at higher magnification in Figure 10.

Figure 10. The microstructure of a needle coke particle, viewed perpendicular to the length of the particle. Region A of Figure 9. Crossed polarizers.

Experimental Methods

A wide range of petroleum coker feedstocks as well as some coal-derived liquids have been surveyed for their characteristic mesophase microstructures. The materials listed in Table I were selected as representative of the range of coker feedstocks, and the formation of microstructure during the pyrolysis of these feedstocks has been studied in some detail.

Methods of incremental pyrolysis (5) are employed to obtain pyrolysis residues representative of all stages of interest. The pyrolysis furnace consists of a copper block with a number of penetrations for 25 mm diameter test tubes to permit the pyrolysis of a number of specimens under identical conditions. An inert atmosphere is used to prevent oxidation. The reflux condition can be varied by altering the flow rate of the inert gas and by use of an internal cell which prevents return of refluxed liquid to the pyrolysis cell. The temperature of the block is customarily programmed to rise at 20°C/hr to 360°C, and then at 5°C/hr to a maximum temperature of 600°C. Low heating rates are desirable to avoid excessive foaming in the later pyrolysis stages of some precursors.

Mesophase transformation curves are constructed from measurements of the residue yield and the quinoline insolubility by assuming that quinoline is a specific extractant for the untransformed pitch. The quinoline extraction is conducted at 75°C. The mesophase is recovered by centrifugation.

Micrographic preparations appropriate to the delicate nature of fresh mesophase (8) are applied to full vertical cross-sections to ensure evaluation of gravity segregation effects which are common in the pyrolysis of petroleum-based precursors (5). In partially transformed specimens, it is usually possible to identify the most recently transformed mesophase, i.e., the mesophase microconstituent formed just prior to removal of the specimen from the furnace, by its proximity to the mesophase-pitch interface. Mutually perpendicular cross-sections (e.g., see Figures 6, 9, and 19) have been found useful in understanding the morphology of deformed mesophase microstructures (6).

Results

Mesophase transformation curves for three typical coker feedstocks are given in Figure 11. The mesophase yield, assumed equal to the quinoline insolubles formed during pyrolysis, is computed from the product of the pyrolysis residue yield and the quinoline-insoluble content (corrected for the initial quinoline insolubles).

Mesophase transformation curves for two pitches commonly used in fabricating carbon and graphite artifacts are given in Figure 12. The coal-tar pitch contains appreciable insoluble particles which dominate the formation of microstructure

Table I. Precursors for Pyrolysis Studies

	Density (gm/cm3)	Sulfur Content (w/o)	Q. I.[d] (w/o)	Softening Point (°C)
Gilsonite American Gilsonite Co.	1.040	0.3[a]	0.3	149-154[a]
Air-Blown Asphalt Gulf Oil	1.019	4.4	0.2	85
Propane Asphalt Gulf Oil	1.026	1.1	0.1	65
Reduced Crude Gulf Oil	0.981	0.9	0.3	<20
Decant Oil Gulf Oil	1.068	2.3	<0.1	<20
Decant Oil Union Oil	1.070[a]	1.6[a]	b	4[c]
Petroleum Pitch (A240) Ashland Oil	1.220[a]	1.5[a]	Nil[a]	122[a]
Coal-Tar Pitch (30M) Allied Chemical	1.324[a]	b	12.5[a]	102[a]

Notes: a.   Typical values given by supplier
       b.   Not available
       c.   Pour point
       d.   Q. I. = Quinoline Insolubles
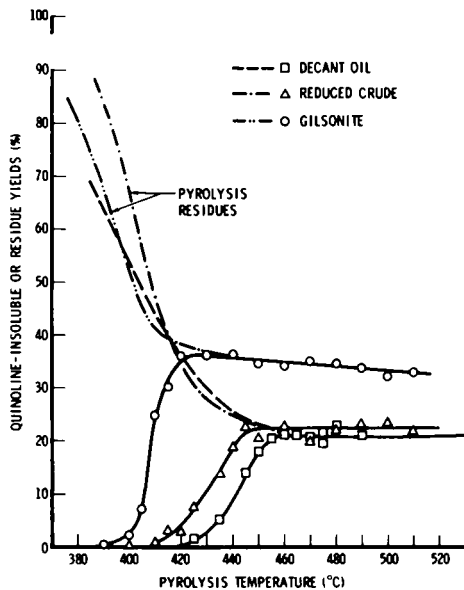
Figure 11. Yields of pyrolysis residue and mesophase for three petroleum based precursors—a decant oil (Union Oil), a reduced crude (Gulf Oil), and a Gilsonite (American Gilsonite Co.)
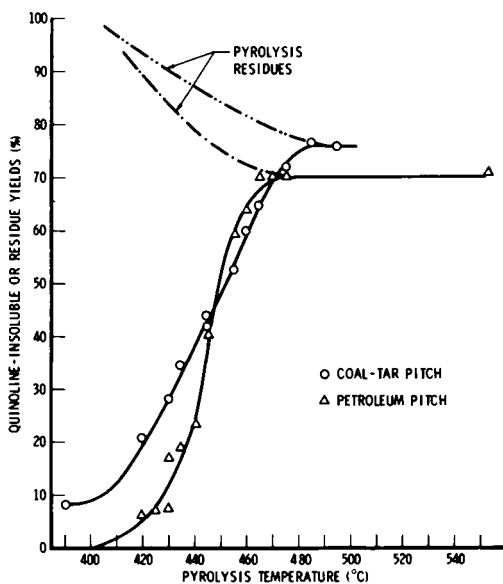
Figure 12. Yields of pyrolysis residue and mesophase for two fabrication pitches—a petroleum pitch (Ashland Oil A240) and a coal tar pitch (Allied Chemical 30M)

(<u>2</u>, <u>8</u>, <u>10</u>); the transformation takes place over a much wider range
of temperature than observed for the petroleum-based precursors.
In contrast, the petroleum pitch transforms over the same tem-
perature range, and forms the same series of microstructures,
as the petroleum-derived decant oils.

Each transformation curve may be characterized in terms
of the temperature at which 50 percent of the mesophase has
formed, T(50%), and the temperature range over which the
majority of the transformation takes place, i.e.,

$$\Delta T(80\%) = T(90\%) - T(10\%).$$

Data for T(50%) and ΔT(80%) are given in Table II.

Micrographic examination of the pyrolysis residues re-
vealed close similarities in the mesophase microconstituents
forming at equivalent temperatures. For the heating rate of
5°C/hr, 430°C appeared as a threshold temperature between the
formation of fine isotropic microconstituents and the formation
of coarser-textured mesophase which is deformable by the
stresses of bubble percolation.

The micrographs of Figure 13 offer examples of the simi-
lar fine-textured but heterogeneous microstructures which are
built up incrementally by the formation mechanisms operating
below 430°C. The initial transformation produces colonies or
clumps with polarized-light extinction contour spacings of about
1 micron. The mesophase precipitating at 410°C and coalescing
around the initial colonies displays contour spacings of the order
of 2.5 microns. Figure 14 illustrates a coarser but still ran-
domized microconstituent forming in a propane asphalt pyrolyzed
to 420°C; the average contour spacing is about 6 microns.

In general, the mesophase precipitated below 430°C forms
fine-textured isotropic microconstituents which vary in the spac-
ing of the polarized-light extinction contours from 0.8 micron
(i.e., near the limit of optical resolution) at 400°C to about 10
microns as the pyrolysis temperature increases to 430°C (<u>5</u>).
These spacings correlate approximately with the sizes of the
Brooks-and-Taylor spherules undergoing coalescence at each
temperature. The microconstituents appear to be built up by a
randomized coalescence process, and the mesophase is suffi-
ciently viscous to resist deformation by such forces as interfacial
tension or bubble percolation. To a first approximation, the
contour spacing for a given temperature of precipitation is inde-
pendent of the precursor, and the logarithm of the contour spac-
ing increases linearly with the precipitation temperature. The
fine isotropic microconstituents are thus randomized arrays
which are effectively isotropic on a scale of several times the
diameter of the coalescing spherules.

Isotropic microconstituents coarser than 10 microns in
contour spacing are usually present only to a minor degree be-
cause the coarse-textured mesophase is deformable by the

Table II. Mesophase Transformation Characteristics

| | Transformation | | Mesophase | |
	Temp. T(50%) (°C)	Range ΔT(80%) (°C)	Yield (max.) (w/o)	Ref.
Gilsonite American Gilsonite Co.	409	13	36.5[a]	5
Air-Blown Asphalt Gulf Oil	414	26	30.0[a]	5
Propane Asphalt Gulf Oil	427	26	32.4[a]	5
Reduced Crude Gulf Oil	431	26	22.6[a]	5
Decant Oil Gulf Oil	451	24	22.5[a]	5
Decant Oil Union Oil	441	25	21.0[b]	17
Petroleum Pitch (A240) Ashland Oil	444	34	70.0[b]	17
Coal-Tar Pitch (30M) Allied Chemical	444	56	68.0[b]	17

Notes: a. Pyrolyzed under conditions of high reflux
        b. Pyrolyzed under conditions of low reflux
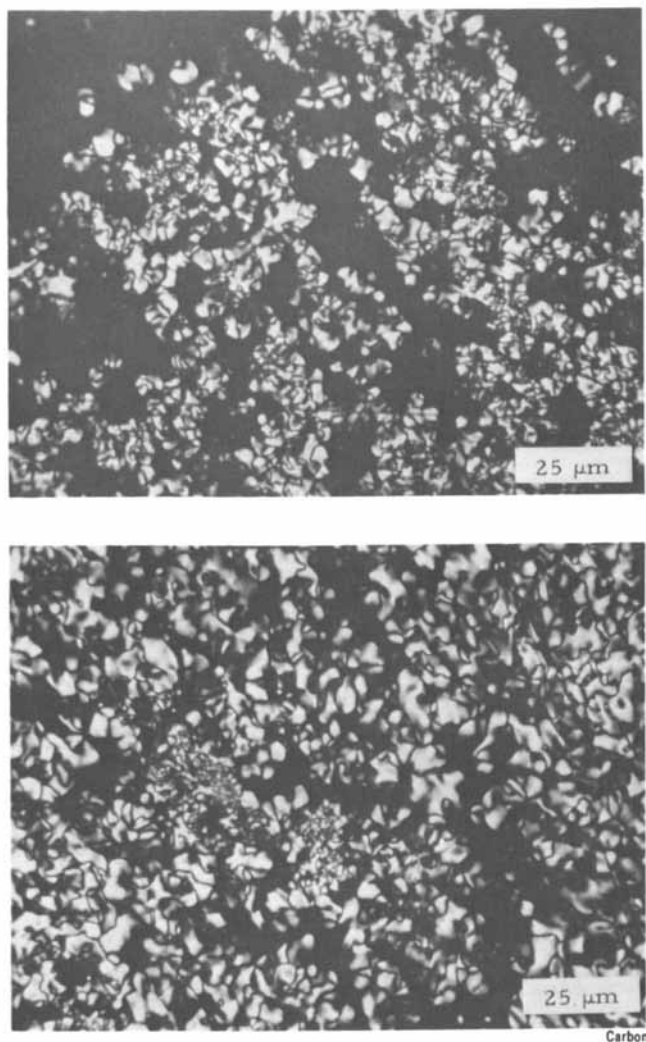
Figure 13. Two coker feedstocks pyrolyzed to 410°C (5). Crossed polarizers. Upper micrograph, air-blown asphalt, average contour spacing = 2μm; lower micrograph, Gilsonite, contour spacing of fresh mesophase = 3μm.

stresses of bubble percolation. This effect is illustrated by
Figure 15 for a reduced crude pyrolyzed above the 430°C thresh-
old temperature (5). A series of microconstituents are present,
ranging from fine isotropic to fine deformed and including some
undeformed coarse mesophase just coalesced from the pitch
matrix.

For feedstocks transforming above 430°C, the deformation
by bubble percolation can be extensive, producing eventually the
fine deformed textures of needle coke particles illustrated by
Figures 9 and 10. Owing to the premium value of needle cokes,
it is useful to distinguish between the coarse and fine deformed
microconstituents; a contour spacing of 10 microns has been
chosen as a convenient threshold value (5).

Although deformed structures appear in abundance above
430°C, the textures remain coarse until pyrolysis temperatures
of about 460°C are attained. This pattern of formation of the fine
deformed microstructures is illustrated by Figures 16 through 20
for a decant oil supplied by the Union Oil Co. Similar patterns
were observed for the Gulf decant oil (5) and the Ashland A240
petroleum pitch (17). Such precursors are sometimes described
as "clean" feedstocks (15); in terms of mesophase microconstit-
uents, this denotes that no fine isotropic mesophase is precipi-
tated in the early stages of coking.

Figure 16 (upper view) illustrates the coalescence to coarse
undeformed mesophase in the earliest stage of the transformation
in decant oil. Coarse deformed structures, of the type shown in
Figure 16 (lower view), appear as soon as the bulk mesophase
grows to sizes of the order of a millimeter.

Figure 17 demonstrates the strong refinement of the de-
formed microstructures which occurs between 455° and 465°C.
This refinement is coincident with the qualitative observation of
increasing mesophase viscosity as the bubbles percolate with
increasing difficulty through the pyrolyzing mass. The average
spacing of extinction contours drops rapidly below the 10-micron
threshold value as the pyrolysis temperature exceeds 460°C.
This structural refinement by bubble percolation may occur while
transformation is still incomplete. The mesophase transformed
above 460°C often appears in pores blown earlier in the fine de-
formed microconstituent; this mesophase thus forms under rela-
tively quiescent conditions and is readily distinguished by its
coarse structure (11) and alignment with the substrate coke (8).

Examination of the fine deformed microstructures (18) has
revealed a spectrum of fine deformed microconstituents ranging
from the fibrous structure of a coke needle to the lamellar struc-
ture of a bubble wall; compare Figures 9 and 18. The spacing of
extinction contours in a bubble wall appears to depend on the ex-
tent of deformation. The perpendicular cross-sections given in
Figure 19 demonstrate the significant difference between the fine
fibrous and the fine lamellar morphologies. The bubble wall dis-
plays similar lamellar microstructures on both cross-sections,
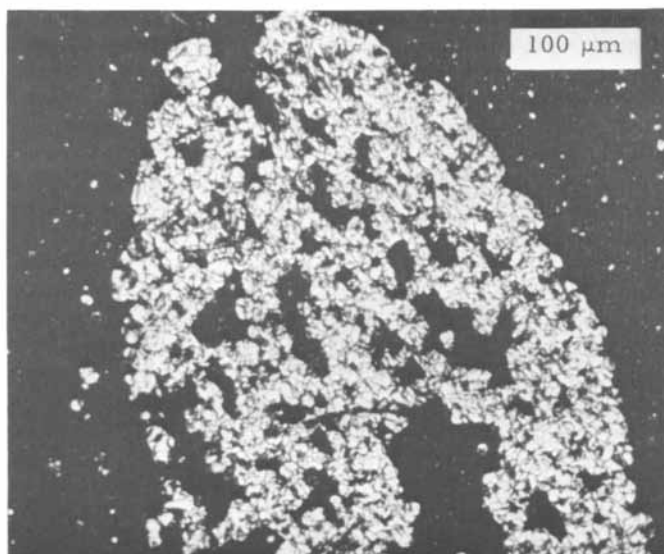
Figure 14. Propane asphalt pyrolyzed to 420°C. Crossed po-
larizers. Average spacing of extinction contours — 6 μm.
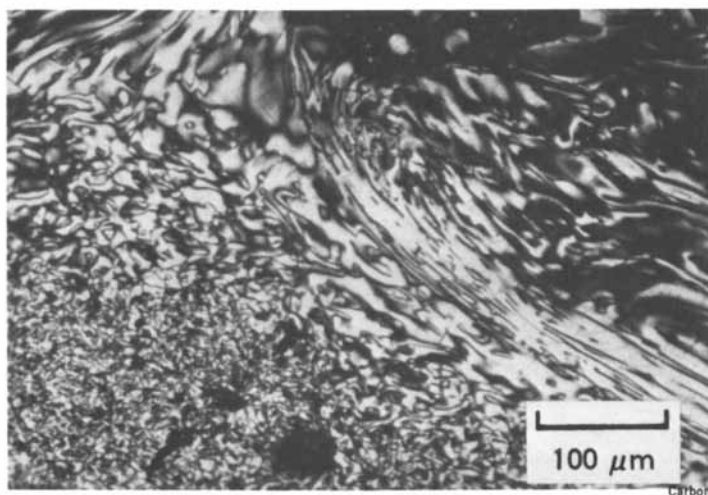
Figure 15. Reduced crude mix pyrolyzed above the threshold tem-
perature for formation of coarse and deformable mesophase (5).
Crossed polarizers.
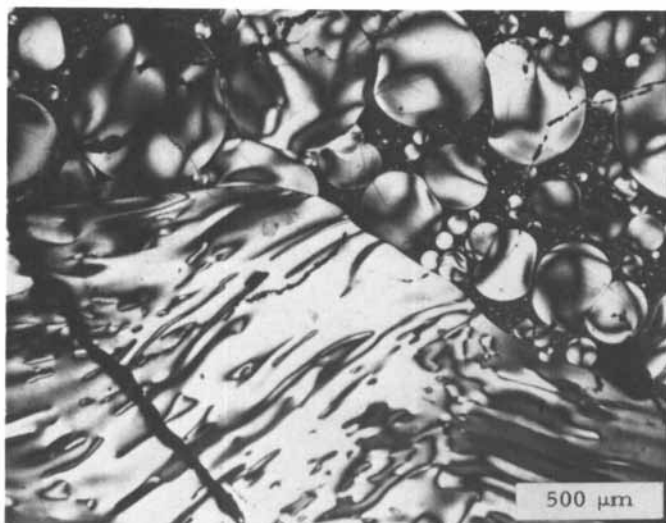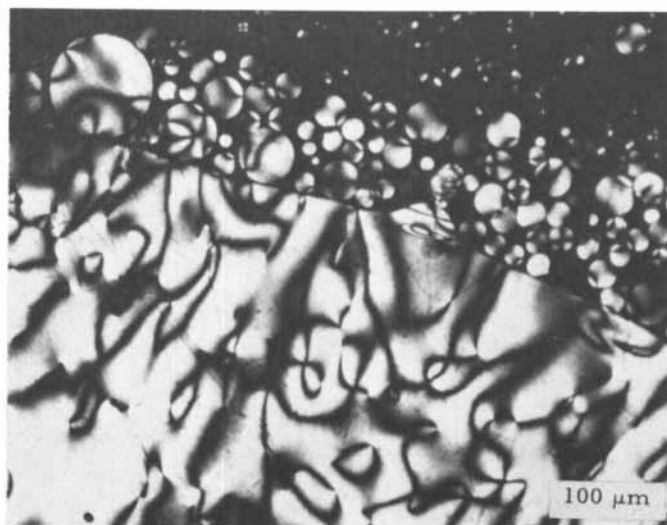
Figure 16. Coarse and coarse deformed microstructures formed in the pyrolysis of a decant oil. Crossed polarizers. Top: pyrolysis temperature = 430°C, extinction contour spacing = 50 μm. Bottom: pyrolysis temperature = 443°C.
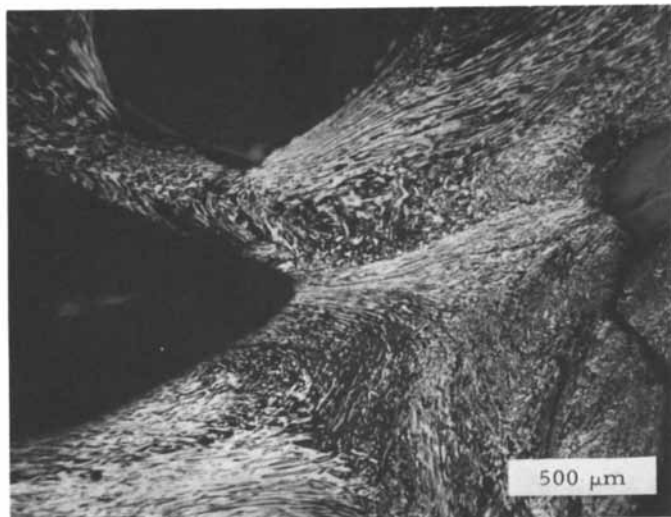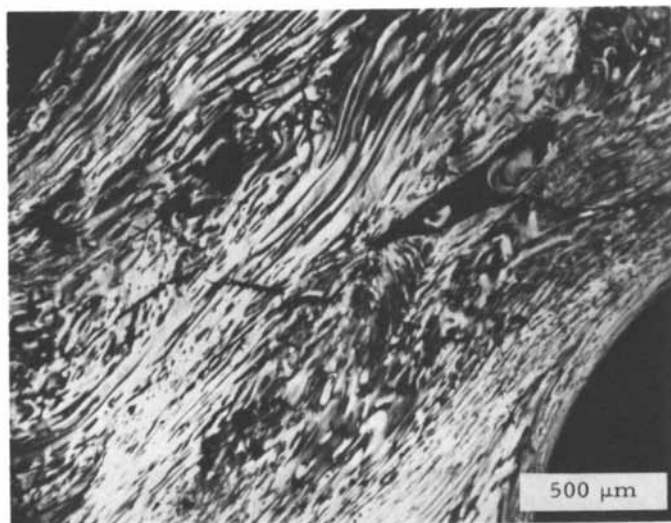
Figure 17. The refinement of microstructure by bubble percolation in a pyrolyzed decant oil. Crossed polarizers. Top, pyrolysis temperature ⎯ 455°C; bottom, pyrolysis temperature ⎯ 465°C.
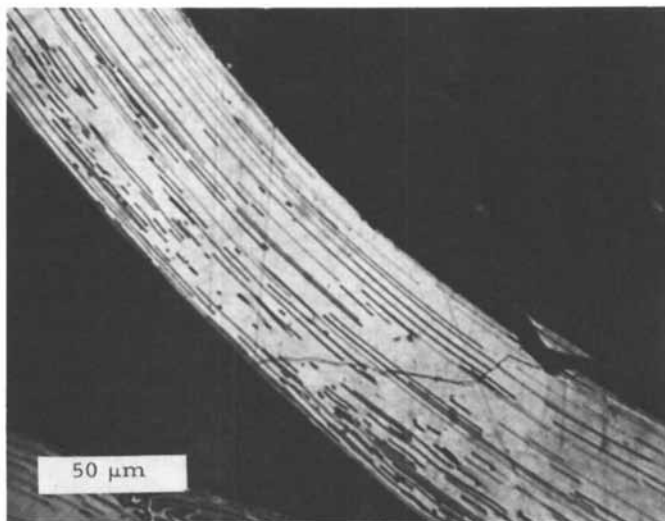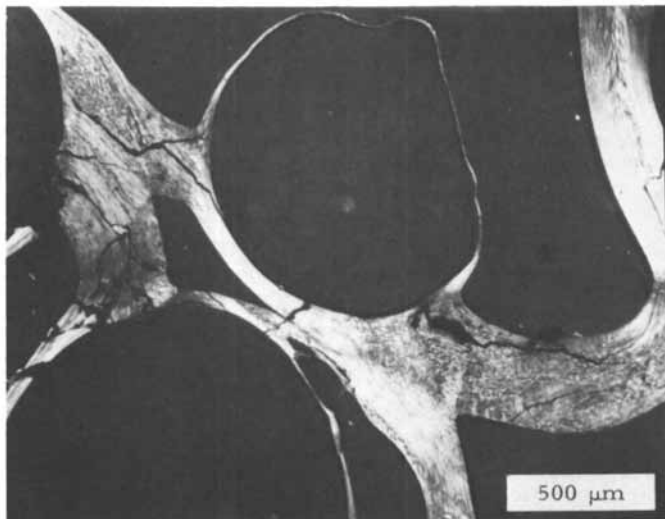
Figure 18. The fine lamellar microconstituents formed in the bubble walls of a decant oil pyrolyzed to 490°C. Crossed polarizers.

and the extinction contours can be traced over the edge at which
the perpendicular sections meet. Thus the fine lamellar micro-
constituent is symmetric around the normal to the bubble wall,
while the fine fibrous microconstituent displays a randomized
symmetry around the direction of the needle.

        Needle-forming precursors pyrolyzed above 460°C often
display fine buckled or corrugated structures of the type illus-
trated by Figure 20. In the case of bubble walls, the buckled
structures appear to result when the bubble breaks to release
the biaxial tensile stresses in the bubble wall. The mesophase
appears to be too viscous to rearrange its structure more than
indicated by the buckling or folding of the oriented layers. Thus,
for pyrolysis temperatures above 460°C, the mesophase has de-
veloped a memory, in effect, for the fibrous or lamellar micro-
structures induced by deformation processes.

        Figure 21 illustrates the coexistence of fine fibrous, fine
lamellar, and coarse microconstituents in a needle coke pre-
pared by the delayed coking of Ashland A240 petroleum pitch.
Note that the regions of apparent fine isotropic structure are
actually fine fibrous microconstituents sectioned transversely
to the fibrous direction since fine isotropic microconstituents
are not formed in the pyrolysis of A240 pitch. These micro-
graphs also illustrate some basic differences in the microscopic
appearance of fine fibrous and fine lamellar microconstituents
when observed with crossed polarizers. The extinction contours
of a fine fibrous region sectioned longitudinally (region F in Fig-
ure 21) are due to bands where the layers lie parallel to the plane
of section; accordingly the contours do not move as the plane of
polarization is rotated. On the other hand, the layers of the fine
lamellar microconstituent (region L) lie at approximately the
same high angle to the plane of section; the extinction contours
are more crisply defined and move when the plane of polarization
is rotated.

        This catalogue of mesophase microstructures recognized
in petroleum cokes is concluded by Figure 22, which illustrates
a globular array formed in an air-blown asphalt. The globular
microconstituent appears to result when the mesophase spherules
harden before coalescence can occur. Such structures are infre-
quent in cokes formed near atmospheric pressure but are a com-
mon product of high-pressure carbonization (19).

Discussion

        The foregoing results point to the existence of two system-
atic patterns for the formation of coke microstructures from the
conventional range of feedstocks fed to the delayed coker. For a
heating rate of 5°C/hr, the transition between patterns occurs at
a transformation temperature of 430°C, where the precipitating
mesophase is just sufficiently plastic to be deformable by the
stresses of ordinary bubble percolation. The schematic struc-
tural diagram of Figure 23 seeks to relate the structure of the
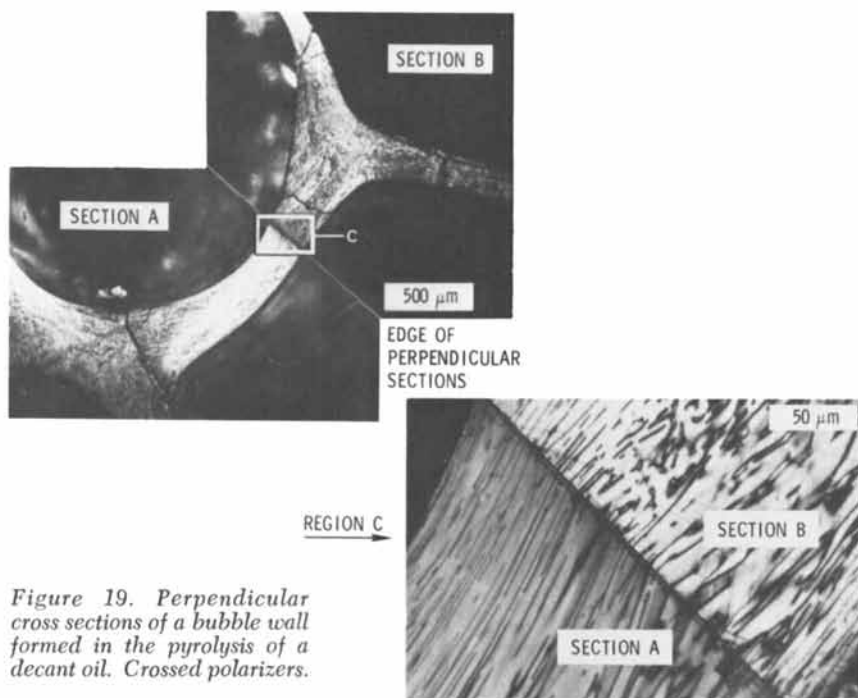
Figure 19. Perpendicular cross sections of a bubble wall formed in the pyrolysis of a decant oil. Crossed polarizers.
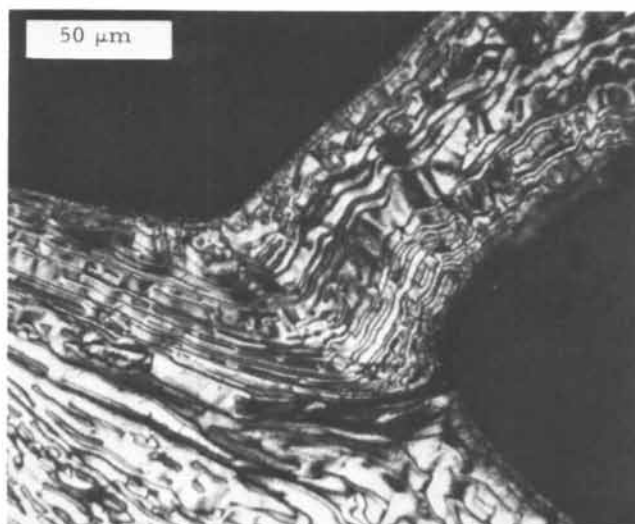
Figure 20. The buckled lamellar structure of a collapsed bubble wall. Decant oil pyrolyzed to 550°C. Crossed polarizers.
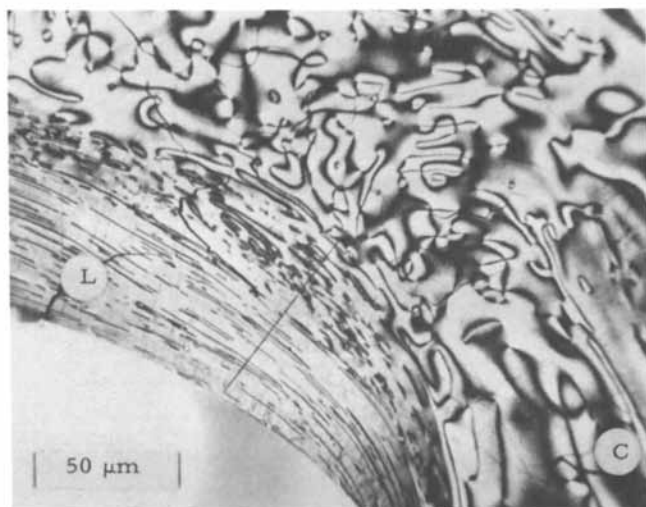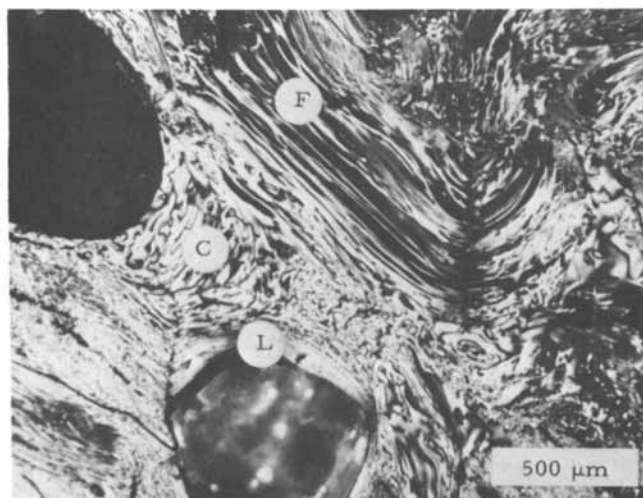
Figure 21. A needle coke produced by delayed coking of Ashland A240 petroleum pitch. Crossed polarizers. Some microconstituents are labeled—F, fibrous; L, fine lamellar; C, coarse.
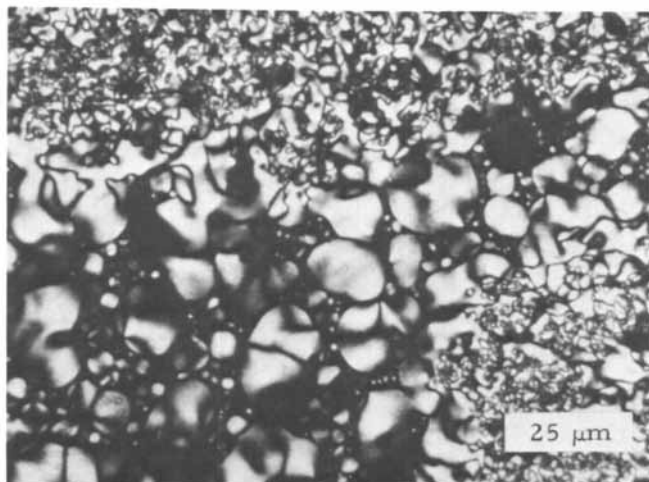
Carbon

Figure 22. The globular microconstituent formed in air-blown asphalt pyrolyzed to 430°C (5)
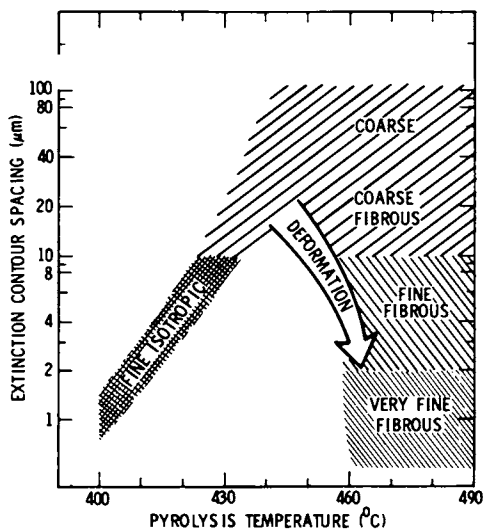
Figure 23. The relation of mesophase micro-constituents of coke to their temperatures of formation from precursors pyrolyzed at 5°C/hr

mesophase microconstituents, as indicated by the spacing and alignment of the polarized-light extinction contours, to the temperature of formation and the deformation experienced by the mesophase before hardening to semi-coke.

Although the chemical characteristics of the mesophase and its precursors appear to range over a continuous spectrum, it is convenient to follow Scott and Folkins (16) in distinguishing two general types of component molecules in the pyrolyzing precursors:

(1)   Rapid-reacting components that precipitate fine mesophase spherules under mild pyrolysis conditions. The spherules coalesce with little growth to produce randomized fine microconstituents that are not readily deformed. The fine-isotropic microstructure is established essentially by the coalescence process.

(2)   Slow-reacting components that precipitate mesophase spherules under more severe pyrolysis conditions. These spherules grow and coalesce to a coarse and more plastic bulk mesophase. In continued pyrolysis this mesophase can undergo extensive deformation by bubble percolation while the viscosity increases by aromatic polymerization within the mesophase.

During the coalescence stages, the only microscopic differences which have been distinguished between the mesophases formed by the two types of precursor components are in the scale of the coalescing spherules. A more significant difference appears to lie in the subsequent viscous behavior of the coalesced mesophases. The fine isotropic textures of the lower-temperature mesophases are frozen-in coincident with or soon after coalescence while the higher-temperature mesophases are more fluid and can rearrange or deform in response to the forces of interfacial tension or bubble percolation. In fact, for the decant oils and petroleum pitch studied here, deformation of coarse microconstituents begins almost as soon as spherule coalescence has produced a bulk mesophase. However, only the deformation experienced by this mesophase above 460°C is effective in producing the fine fibrous and lamellar microconstituents of needle coke. These fine structures are frozen into the final structure of the coke only when deformation is applied to the mesophase as it reaches a critical level of viscosity.

The experiments on the drawing of rods (11, 17) as well as the extensive work at the Union Carbide Corp. on the spinning of fibers (13, 14) from the mesophase, usually at a stage of partial transformation, confirm the role of mechanical deformation in producing the fine fibrous and lamellar microconstituents of needle coke. At least two modes of deformation in the process of delayed coking should be distinguished: uniaxial extension to produce fibrous or acicular structures symmetric about the fiber

axis, and biaxial extension to produce lamellar or plate-like structures. If bubble percolation is the dominant mechanism of deformation within the coke drum, the fibrous structures may be approximated from multiple sequential steps of biaxial deformation rather than by simple uniaxial extension.

Micrographic estimates have shown a useful degree of correlation between the microconstituents present in cokes produced from the same feedstock by laboratory pyrolysis, by pilot-scale coking, and by full-scale delayed coking ($\underline{5}$). On this basis, laboratory pyrolysis tests, including micrographic evaluation and construction of mesophase transformation curves, have been used to screen potential coker feedstocks. Table III lists the microconstituents which have been distinguished in applying quantitative micrography to rate the relative needle-like quality of cokes and pyrolysis residues ($\underline{5}$, $\underline{6}$, $\underline{17}$). This listing is not intended to imply the existence of distinct phases, but only to provide a descriptive classification of microconstituents which actually grade smoothly from one to another.

Some three-dimensional models of the morphologies bounding the spectrum of fine deformed microconstituents are sketched in Figures 24 and 25. The needle or acicular morphology suggests a complex array of folded curtains, the height of the curtains being much greater than the radii or spacings of the folds on the transverse section. The sketch will suggest how the intensity of folding is reflected by the spacing of polarized-light extinction contours on either transverse or longitudinal sections. Heat treatment of this structure beyond 600°C, and eventually to graphitization temperatures, introduces many interlamellar shrinkage cracks due to anisotropic shrinkage processes, but otherwise effects only minor displacements in the lamelliform geometry frozen into the mesophase as it congealed to a solid coke at temperatures just under 500°C ($\underline{6}$, $\underline{8}$, $\underline{18}$).

The lamellar morphology of a mesophase bubble wall is more ordered than a needle structure. Figure 25 emphasizes the characteristic feature of the lamellar morphology, viz., the sharp folds in each planar region bounded by a disclination loop ($\underline{17}$, $\underline{18}$). Thus most of the extinction contours in a bubble wall (see Figures 18 and 19) have a doublet structure (of the nature shown in Figure 5) that requires higher magnification for resolution.

Conclusions

The microstructures of most petroleum cokes produced by delayed coking are comprised of complex mixtures of microconstituents whose structures are established during the brief plastic lifetime of the carbonaceous mesophase. The experimental methods of incremental pyrolysis and polarized-light micrography have proved to be useful tools in understanding how the structures of each of these microconstituents are formed.

Table III. Mesophase Microconstituents in Petroleum Coke

Name	Preferred Orientation	Description	Examples[a]
Fine Isotropic	Randomized array	Polarized-light extinction contours spaced at < 10 microns	7, 8, 13, 14, 15, 22
Coarse	None to weak	Extinction contours spaced at > 10 microns	2, 3, 7, 9, 10, 15, 16a, 21
Coarse Deformed	Weak to moderate	Extinction contours, across fibrous bands, spaced at > 10 microns	7, 15, 16b, 17a
Fine Deformed: Fine Fibrous Fine Lamellar	Strong	Extinction contours spaced at > 10 microns Symmetric about fiber axis Symmetric about normal to lamellae	17b 6, 9, 10, 21, 24 5, 18, 19, 20, 21, 25
Globular	None	Spherules hardened before coalescence. Infrequent in delayed cokes.	22

Note: a. Figures in which the microconstituent is prominent

POLISHED
SECTION
VIEWED WITH
CROSSED POLARIZERS
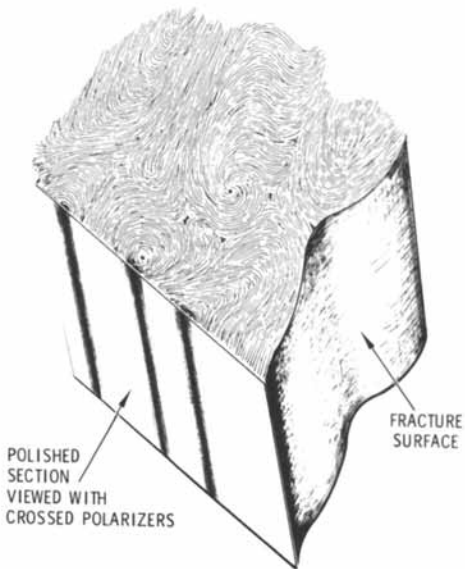
FRACTURE
SURFACE

Microstructure and Fracture
of Carbon Systems

Figure 24. The fine fibrous morphology of an acicular region of a needle coke particle (17)

PLANE OF FOLDING

DISCLINATION
LOOP

DISCLINATIONS
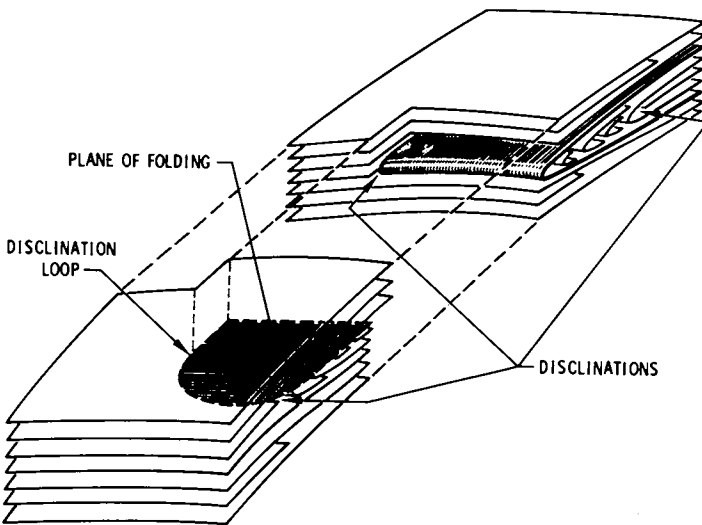
Microstructure and Fracture
of Carbon Systems

Figure 25. The fine lamellar morphology of a mesophase bubble wall (17)

The carbonaceous mesophase is a special class of liquid crystals which may be described as "lamellar nematic." Although detailed analyses of the bend, fold, splay, and disclination structures of the mesophase layers are no doubt far from complete, the relationships to the surface crystal structures important to biological processes (20, 21) suggest that attention should also be given to disclinations in the layers themselves. Phase-contrast electron microscopy (22, 23) offers a direct approach to understanding of the molecular arrays.

Two general types of mechanisms underlie the formation of structure in the various mesophase microconstituents. First must be listed the pyrolysis chemistry of the precursor molecules, which determines the pyrolysis conditions (e.g., the temperature at a given heating rate) for precipitation of the mesophase as well as the final structure of the fine isotropic microconstituents. The precursor chemistry also determines the viscosity of the coalesced mesophase and thus the susceptibility of its microstructure to modification by deformation. This deformation constitutes the second general structural mechanism. The experiments in drawing (11, 17) and the extensive work on spinning (13, 14) demonstrate that the mesophase, at proper levels of pyrolysis, can be subjected to high levels of extensive deformation to produce intense preferred orientations. These studies have also shown that deformation at a specific stage in coking is essential to the formation of needle coke and that the fine fibrous and fine lamellar microconstituents of needle coke can be produced, respectively, by uniaxial and biaxial extensive deformation.

Since the deformation experienced by the mesophase in delayed coking is only an incidental result of the flows of the incoming liquid and the evolved gas, this coking process does not appear well-suited to the preparation of improved needle cokes. The quality of the product is determined primarily by the feedstock selection, and the operator can have only limited further control by adjustment of pressure or recycle conditions (24). New coking methods designed to apply mechanical deformation at the appropriate stage in mesophase pyrolysis offer a more direct means for the further development of needle cokes. For this purpose, there is a present need for measurements of the relevant properties, e.g., the thermal expansion of the several microconstituents that can be produced by mechanical deformation.

Acknowledgements

Literature Cited

1. Brooks, J. D., and Taylor, G. H., Carbon (1965) 3, 1.
2. Brooks, J. D., and Taylor, G. H., Chem. and Phys. of Carbon (1968) 4, 243.
3. Whittaker, M. P., and Grindstaff, L. I., Carbon (1972) 10, 165.
4. Pietzka, G., Wilhelmi, G., and Pauls, H., Carbon '72 Preprints (1972), 397.
5. White, J. L., and Price, R. J., Carbon (1974) 12, 321.
6. Zimmer, J. E., and White, J. L., 12th Conf. on Carbon, Extended Abstracts (1975), 223.
7. White, J. L., Dubois, J., and Souillart, C., J. Chim. phys., special number (April, 1969), 33; available in English translation as EURATOM rept. 4094e (1969).
8. Dubois, J., Agace, C., and White, J. L., Metallography (1970) 3, 337.
9. White, J. L., Guthrie, G. L., and Gardner, J. O., Carbon (1967) 5, 517.
10. White, J. L., Prog. in Solid State Chem. (1974) 9, 59.
11. White, J. L., Johnson, G., and Zimmer, J. E., 12th Conf. on Carbon, Extended Abstracts (1975), 221.
12. Frank, F. C., Disc. Faraday Soc. (1958) 25, 19.
13. Didchenko, R., Barr, J. B., Chwastick, S., Lewis, I. C., Lewis, R. T., and Singer, L. S., 12th Conf. on Carbon, Extended Abstracts (1975), 331.
14. Union Carbide Corp., Netherlands Patent Appln. 73-04398, opened for inspection 2 October 1973.
15. Great Lakes Carbon Corp. vs. Continental Oil Co., et al., District Court, W. D. Louisiana, Lake Charles Div., 138 USPQ 613 (1963).
16. Scott, C. B., and Folkins, H. O., J. Metals (1972) 24 (5), 25.
17. Meyer, R. A., White, J. L., Zimmer, J. E., Evangelides, J. S., and Rubin, L., Microstructure and Fracture of Carbon Systems, Final Report, The Aerospace Corp. TOR-0076(6726-02)-2 (1975).
18. White, J. L., and Zimmer, J. E., to be published.

19.   Marsh, H., Dachille, F., Melvin, J., and Walker, P. L., Jr.,
        Carbon (1971) 9, 159.
20.   Harris, W. F., Surface and Defect Properties of Solids
        (1974) 3, 57.
21.   Harris, W. F., in "Fundamental Aspects of Dislocation
        Theory," edited by Simmons, J. A., et al., National
        Bureau of Standards Special Publication No. 317 (1970)
        1, 579.
22.   Marsh, H., Augustyn, D., Cornford, C., Crawford, D.,
        and Hermon, G., 12th Conf. on Carbon, Extended
        Abstracts (1975), 117.
23.   Marsh, H., proceedings of this conference.
24.   Stout, E. F., Janes, M., and Biehl, J. A., WADD Tech.
        Rept. 61-72, vol. 36 (1964).

High Modulus Carbon Fiber Processes

R. J. DIEFENDORF

Rensselaer Polytechnic Institute, Materials Engineering Department, Troy, N.Y. 12181

Although carbon fibers have been made inadvertent-
ly from natural fibers for thousands of years, it was
Edison (1) in 1878, who purposely took cotton fibers,
and later bamboo, to make carbon lamp filaments.
Interest in carbon fibers was renewed in the late
1950's, when synthetic cellulosics (rayons) in textile
forms were converted to carbon fibers. Although other
precursor fibers were studied, cellulosics remained the
main source for carbon fibers until the mid 1960's. All
these fibers had low stiffness, although some obscure
reports and related technology indicated that high
modulus carbon fibers could be made. In early 1964,
Bacon (2) made the first high modulus carbon fiber by
hot stretching rayon precursor carbon fibers. This was
followed by Watt (3), who made a high modulus carbon
fiber by retaining some of the original preferred
orientation of polyacrylonitrile in the carbon fiber.
Although other fiber types have been investigated for
precursors, the low cost of commercially available
fibers produced for textile uses has made rayon and
particularly polyacrylonitrile the main precursors for
carbon fiber production. More recently, in the late
1960's, the realization that truly widespread use of
carbon fibers for reinforcement would require lower
cost than that possible from the rayon or PAN processes
caused initiation of research on using petroleum pitches
to make carbon fibers. In addition to hot stretching,
two other processes (4,5) have been developed using
pitch precursors to make high modulus carbon fibers. In
the following sections, the rayon, PAN, and two pitch

processes for making carbon fiber will be described.

HIGH MODULUS CARBON FIBER PROCESSES

High modulus carbon fibers require that the stiff
layer planes of graphite be aligned parallel to the
fiber axis. Commercial processes develop this orien-
tation by plastic deformation. Since carbon fibers are
made from organic precursors, the preferred orientation
can be introduced in the precursor fibers and hopefully
preserved upon conversion to carbon. The preferred
orientation also may be introduced in the carbon fiber.
The precursor and carbon fibers are anisotropic on the
ultrascale, and the application of a tensile stress
will result in forces which will try to cause orien-
tation. In the case of a linear polymer, such as
polyacrylonitrile, a tensile load applied to the fiber
will attempt to align the zig-zag backbone of the
polymer parallel to the fiber axis. Similarly,graphite
basal planes or aromatic ring compounds will tend to
align parallel to the fiber axis, when plastically de-
formed under tension. The development of the high pre-
ferred orientation, which is required to make high
modulus carbon fibers, is accomplished by applying this
orienting stress, and then allowing substantial amounts
of plastic deformation. The deformation can occur in
the spinnerette and post-spinning stretch given the
precursor fiber, or during processing of carbon fiber,
or in the carbon fiber. This accounts for the differ-
ent high modulus carbon fiber processes.

A.   High Temperature Deformation of Carbon Fibers -
      Rayon Precursor Carbon Fibers

Graphite can only yield by basal plane slip at
room temperature. Hence, while a highly oriented
graphite like a single crystal can be bent at room
temperature, a carbon with random grain orientation, or
a structure that pins basal plane slip is brittle.
Deformation of these materials requires high tempera-
tures to either allow other slip systems to operate, or
diffusion to occur. Practically, for randomly oriented
structures, a temperature of 2800°C is required such
that the deformation can occur in short times (seconds)
when under high load. At lower temperatures, (2100 -

2400°C), the stress is limited by the strength of the filament in colder portions of the apparatus, and the diffusion activated creep is slow. At higher temperatures, the applied stress is limited by the strength (perhaps, stress rupture) of the fiber in the hot zone.

This process was developed to produce high modulus fibers from rayon precursor carbon fibers, but it is applicable to any carbon fiber provided it can withstand the required orienting stress (2,6). A schematic diagram for the rayon precursor process is shown in Fig. 1. Rayon is a thermoset, but charring agents and low temperature oxidation (stabilization) increase carbon yield upon pyrolysis (carbonization) to carbon fiber. Although the fiber is a shrunken idiomorph of the original highly crenulated rayon fiber, the pyrolysis chemistry is such that the original preferred orientation in the cellulosic structure cannot be transformed to an oriented graphite structure (3,4). Upon heat-treatment to 2800°C, ("graphitization"), the structure has been observed to consist of tangled ribbons of layer planes about 30Å wide and which resembles a bowl of spaghetti (9). When these fibers are strained at 2800°C, the tangled ribbons are observed to straighten. Almost perfect alignment of the basal planes parallel to the fiber axis is observed with strains of 180%. The process has been applied to unoriented pitch precursor carbon fibers (6) as well as rayon, and the process has produced the widest range of fiber moduli (6Msi to 120Msi). The application of stress during high temperature heat treatment of oriented carbon fibers also can result in significant improvements in moduli, and the strain and temperature requirements are lower. The main disadvantage of the process is the structural changes which occur upon heat treatment to 2800°C.

B.   Deformation of Aromatic Pitches - Pitch Precursor Fibers (3,10)

The introduction of preferred orientation in an aromatic pitch at low temperature, and the maintenance of at least part of this orientation during processing would seem to offer advantages over deformation at 2800°C. In addition, petroleum pitches are of interest because of low cost, high carbon yield, and, at least in the past, availability. In one process (4)(Fig.2),

FIBER ⟶ STABILIZE ⟶ CARBONIZE ⟶ GRAPHITIZE ↗

ORIENT
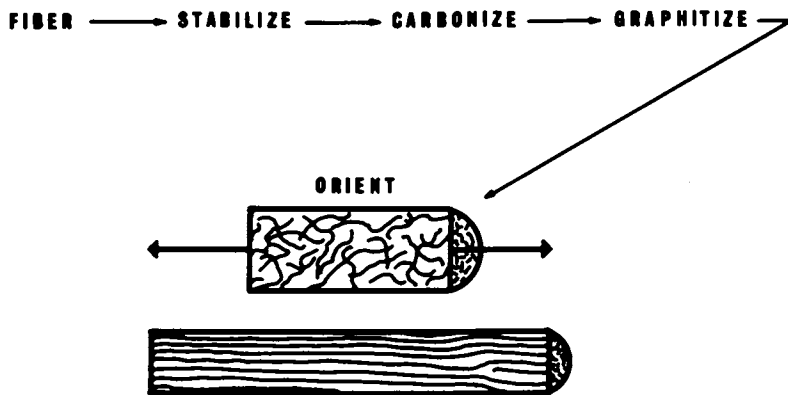
Figure 1. Rayon precursor process for carbon fibers. Rayon fibers are oxidized to increase carbon yield, slowly heated to 950°C to convert to carbon, and then strained at 2800°C to give a high modulus carbon fiber.

[ISOTROPIC LIQUID] High ė Spin ⟶ STABILIZE

CARBONIZE GRAPHITIZE Tension
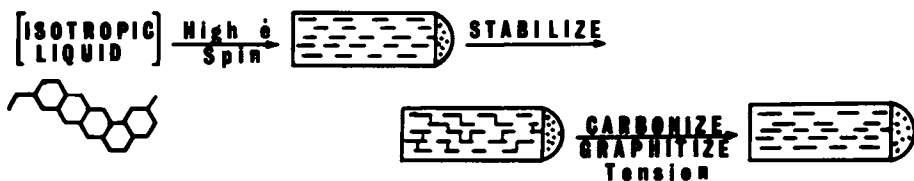
Figure 2. Isotropic pitch process for carbon fibers. An aromatic isotropic pitch is melt-spun at high strain rate to give an oriented fiber. The fiber is thermoset by oxidation and then heated under tension to maintain the preferred orientation.

an isotropic pitch is melt spun at very high strain
rates to align the aromatic molecules parallel to the
fiber axis and then the fiber is quench cooled to
retain the preferred orientation. This thermoplastic
fiber is carefully oxidized at low temperature to
crosslink the structure to an infusible fiber. The
oxidation is rather slow at low temperature but too
high a temperature causes the aromatic molecules to
relax to the isotropic state. Even with oxidative
stabilization, relaxation can occur when the oxidative
bonds are broken during carbonization. Hence, the pre-
ferred orientation is lost, unless an orienting stress
is applied during this critical period. Similarly, a
stress is found advantageous during the higher heat-
treatment temperatures (1700°C - 2200°C) to obtain com-
mercially practical moduli. This phenomena is the same
as described for aligned fibers in Section A. At
present, no fibers are commercially made by this pro-
cess, the major problem probably being the lengthy oxi-
dation step.

Higher molecular weight aromatic pitches often
form anisotropic liquids (mesophase, liquid crystals).
Mesophase is a thermodynamically stable structure, and
once formed will not relax to an isotropic liquid, un-
less heated above the mesophase-liquid transition tem-
perature. In general, this transition temperature is
above the decomposition temperature in petroleum
pitches, so that the high preferred orientation in the
mesophase is retained (partially) upon conversion to
carbon. In one commercial process (5) where the pitch
is partially mesophitic and partially isotropic, the
pitch is spun at sufficiently high temperature that
both the mesophase and isotropic pitches are deformed.
The pitch does not need to be spun at the high strain
rates and then quenched as in the prior example, since
the orientation in the mesophase is stable. The only
thing that is required is that the mesophase be
deformed sufficiently so that the aromatic molecules are
oriented parallel to the fiber axis. Since mesophase
is often spherical at lower volume fractions in pitches,
the deformation results in long cylinders of mesophase
in the more isotropic matrix of the fibers. At higher
volume fractions of mesophase, where it is a continuous
phase, or at higher strain rates, the fibers will
appear more homogeneous. Higher strain rates will
cause the isotropic component to orient, especially

because of the restraints of the neighboring mesophase,
so that it may not be distinguishable in the fiber. The
more isotropic matrix can be rapidly made infusible by
thermal oxidation at relatively high temperatures, be-
cause the orientation of the mesophase will not be lost
at oxidation temperatures. Although some orientation
is lost in the mesophase during carbonization, enough
remains, that further heat-treatment at higher tempera-
ture will redevelop a high preferred orientation. (Upon
heat-treatment, graphite will try to attain perfect
orientation (single crystal), provided enough orien-
tation is present to act as a director for further
growth.) The resulting fiber may resemble a mini-
composite with high-modulus fibrils (resulting from the
mesophase) embedded in a lower modulus matrix (which is
produced from the isotropic pitch), or it may be more
homogeneous in cross section with either basal planes
assuming an onion-skin or radial structure. A fiber
modulus range of 6 to 60 Msi has been produced.

C.   Deformation in Polymers - PAN Precursor Fibers

      Although linear organic molecules can be easily
oriented, this orientation would be lost on heating to
carbonization temperatures. Alternatively, a para-
ladder polymer, with a glass transition sufficiently
high to prevent loss in orientation, is considered un-
spinnable. Polyacrylonitrile offers an attractive
solution (Fig. 4). The initial stretching of the PAN
increases the axial alignment of the polymer molecules
backbone parallel to the fiber axis. Then the polymer
chains are cyclized by oxidation to form a ladder polymer.
During this oxidation, the fibers must be kept under
tension to maintain the alignment of the PAN, otherwise
relaxation occurs, and the resulting ladder polymer is
disoriented with respect to the fiber axis. After
stabilization, the fiber has an oriented ladder
structure with a sufficiently high glass transition
temperature, that it is not necessary to maintain
tension in the remaining processing (11). Considerable
nitrogen and hydrogen are still present in the naphthy-
ridene-type rings that form the basic units of the
polymer, and these elements are largely eliminated from
the structure during the carbonization stage (heating
to 1000°C)(12). The carbon atoms which remain are
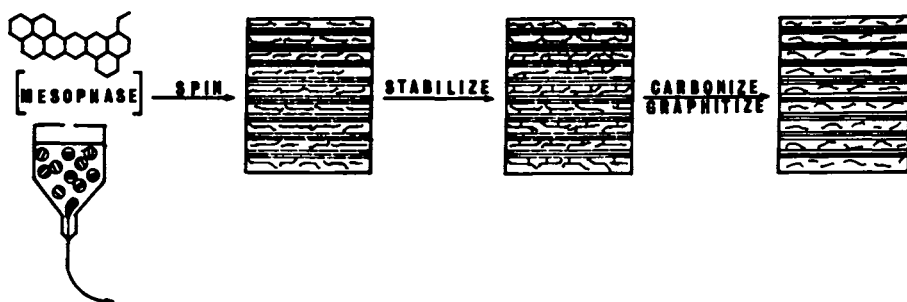
Figure 3. *Mesophase pitch process for carbon fibers. A pitch which is partially isotropic and partly liquid crystal is melt-spun to give a preferred orientation to the liquid crystal elongated domains. The fiber is oxidized to thermoset the isotropic pitch, and the fiber is heated to carbonize and develop the structure.*

POLYACRYLONITRILE   PROCESS
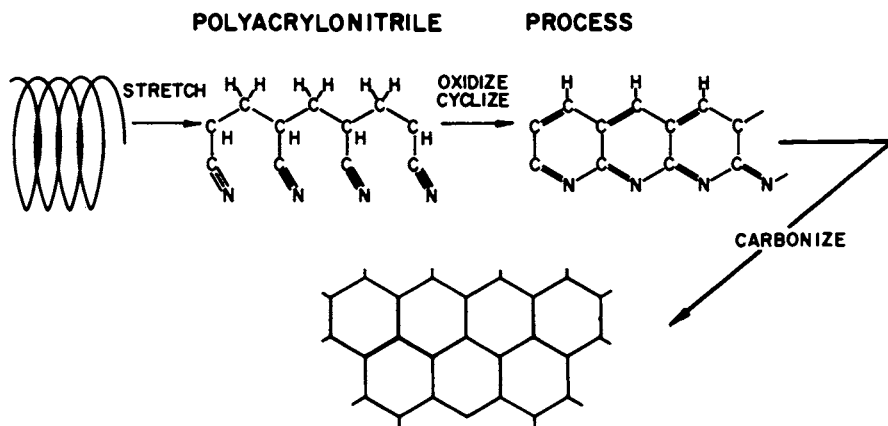
Figure 4. *Polyacrylonitrile precursor for carbon fibers. PAN fibers are stretched, converted to ladder polymer, and converted to carbon fiber. Remnants of the preferred orientation of the ladder polymer are retained in the carbon fiber.*

principally in the form of extended hexagonal ribbon
networks (13). Although these ribbons tend towards
alignment with the fiber axis, their degree of ordering
relative to each other and the fiber axis is relatively
low. However, the preferred orientation can be improved
by heat treatment to higher temperatures (14-16).
Moduli from approximately 6 to 75Msi can be obtained by
varying initial precursor orientation and heat-treat-
ment temperature.

SUMMARY

The processes that produce high modulus carbon
fibers all depend on plastic deformation to introduce
the required preferred orientation for high modulus. A
review of the processes shows that the preferred orien-
tation may be introduced into the precursor or the
carbon fiber itself. These processes produce fibers,
which have much improved structural efficiencies
compared to conventional materials. Processes, now in
development, promise substantially lower fiber costs.

LITERATURE CITED

1. Edison, T., "Electric Lamp", U.S. Patent 223,898,
    27 Jan. 1880.
2. Bacon, R., "Chemistry and Physics of Carbon", Vol.
    9, pp.1-102, Marcel Dekker, Inc.,N.Y. (1973).
3. Johnston, W., Phillips, L. and Watt, W., British
    Patent 1,110,791 (Appl.April 24 and Dec.29, 1964).
4. Kureha Kagaku Kagyo KK, Patent DT-2027384 (Dec.17,
    1970).
5. Singer, L., Netherlands Patent 239490(April 4,1972).
6. Hawthorne, H., Paper #13, Int.Conf.Carbon Fibres,
    Plastics Industry, London (1971).
7. Bacon, R., and Tang, M. M., Carbon, 2, 211 (1964).
8. Bacon, R., and Tang, M. M., Carbon, 2, 220 (1964).
9. Fourdeux, A., Perret, R., and Ruland, W., Paper #9
    Int. Conf. Carbon Fibres, Plastics Industry,
    London (1971).
10. Standege, A. E. and Prescott, R., British Appl.
    No. 49850/65 (Nov. 24, 1965).
11. LeMaistre, C. W., Ph.D. thesis, Rensselaer
    Polytechnic Institute (1971).
12. Watt, W., and Green, N., Paper #4, Int. Conf.
    Carbon Fibres, Plastics Industry, London (1971).

13. Johnson, D. J., Crawford, D., and Oates, C., "The Fine Structure of a Range of PAN-Based Carbon Fibers", Tenth Biennial Conf. on Carbon, Bethlehem, Pa. (June 1971).
14. Badami, D. V., Joiner, J. C., and Jones, G. A., Nature, 215, 386 (1967).
15. Ruland, W., "The Relationship Between Preferred Orientation and Young's Modulus of Carbon Fibers", presented at Am. Chem. Soc. Polym. Chem.Div. Conf., Atlantic City (Sept. 1968).
16. Brydges, W. T., Badami, D. V., Joiner, J. C. and Jones, G. A., Am. Chem. Soc., Polym. Chem. Div., Preprint 9, No. 2, 1310 (1968).

23

Recent Developments in Carbon Fiber Treatments

PIERRE EHRBURGER, JEAN-JACQUES HERQUE, and
JEAN-BAPTISTE DONNET

Centre de Recherches sur la Physico-Chimie des Surfaces Solides (CNRS),
24 Avenue du President Kennedy, 68200 Mulhouse, France

Carbon fibers have outstanding mechanical properties and, therefore, are of considerable interest in the field of composite materials. The performance of a fiber-resin composite depends not only on the tensile strength of the material, but to a large extent also on the coupling properties between the fiber and the matrix. In particular, the interactions occuring at the carbon-resin interface determine flexural strength, interlaminar shear strength and mode of failure of the composite.

Carbon fiber-epoxy resin composites have poor shear strength. This is generally attributed to a lack of cohesion between the reinforcing fiber and the organic matrix. As a result, considerable work has been done to change the surface properties of the fibers with a view to improve the interfacial bond. Oxidation treatments in gaseous (1) (2) and solution phases (3) (4) (5) as well as vapor phase deposition techniques (1) have been used with variable success. In the last few years, attention has been given to electrochemical etching which allows a continuous processing of the fibers (6) (7). In this study, the changes in surface properties of the filaments subjected to electrochemical etching will be examined. More specifically, the influence of the nature of the fiber as well as the influence of the electrolyte solution used for etching on the composite properties are investigated.

Anodic Etchings

Two types of carbon fibers made from an acrylic precursor have been studied. Their initial characteristics are listed in Table I.

The fiber denoted AG was heat treated at a temperature of 2000°C and is referred to as "graphitized fiber".

Anodic oxidation of the filaments was performed in dilute nitric acid (1% by weight) as well as in a normal sodium hydroxide solution. A graphite plate was used as cathode and the work

324

Table I - Characteristics of the Carbon Fibers

Fiber	HTT	Section	S_{BET}
AG	2500°C	95μm^2	0.4 m^2/g
AC	1100°C	120μm^2	0.3 m^2/g

potential was set at 2 volts and the current density close to 1 mA/cm^2.

AG Fibers. It has been shown previously in our laboratory (8) that graphitized carbon fibers form graphitic oxide when treated with appropriate oxidizing reagents. Therefore, AG fibers were submitted to an anodic etching in nitric acid in order to form a lamellar oxide layer on the surface of the fiber. In fact, X-ray patterns of oxidized samples exhibit the characteristic reflection of graphitic oxide after a few minutes of treatment.

With sodium hydroxide as electrolyte, AG fibers undergo a weight loss due mainly to carbon dioxide formation.

AC Fibers. The behavior of AC carbon fiber is quite different from that of the graphitized AG fiber. In fact, AC fiber possesses a less ordered crystalline microstructure and does not form lamellar oxide. As observed for other poorly crystalline carbons, such as carbon blacks, the main oxidation products are carbon dioxide and polycarboxylic acids which are called degradation products (9). These acids remain partially on the surface of the fibers especially during etching in acidic medium. The amount of polycarboxylic acids remained on the surface reaches 1% by weight after a treatment of 3 minutes (10). Repeated extractions of the fibers with hot alkaline solution ensure complete removal of these products from the fibers.

Properties of the Treated Fibers

The surface properties of the heated fibers were examined both chemically and physically.

The oxygen contents of the filaments were determined by elemental analysis and are given in Table II. The fibers are refered to the etching solution and the treatment time in minutes. It is seen that except for graphitized AG fibers etched in nitric acid, the oxygen content remains quite small and comparable to that of the non-heated fiber. In the particular case of the AG HNO3 fiber, it is known that the oxidation mechanism involves an intercalation process which fixes oxygen in the internal part of the fiber. In the AC HNO3 case, oxygen is only fixed on the surface and after removal of the degradation products, the oxygen content is less than 0.1%.

Table II - Oxygen Content of the Treated Fibers

Fibers	% Oxygen
AG non-treated	<0.1
AG HNO$_3$ 15 min	32.3
AG NaOH 10 min	<0.1
AC non-treated	<0.1
AC HNO$_3$ 10 min*	1.25
AC HNO$_3$ 10 min**	<0.1
AC NaOH 10 min**	<0.1

* before extraction
** after extraction

    It is well known that oxygen is partially present on the sur-
face in the form of acidic groups. According to Boehm (11), strong
acidic groups such as carboxylic acids or phenols are neutralized
by sodium hydroxide solution. The results of the titrations with
0.1 N NaOH are given in Table III.

Table III - Acidic Groups of the Treated Fibers

Fibers	Acidic Groups µeg/g
AG non-treated	3
AG NaOH 1 min	16
AG NaOH 10 min	16
AC non-treated	7
AC HNO$_3$ 1 min	14
AC HNO$_3$ 10 min	14
AC NaOH 2.5 min	16
AC NaOH 10 min	20

It appears that the increase in acidic group, occurs mainly in the
first few minutes of treatments and that the acidic groups content
is of the same order of magnitude in all the cases.
    The surface topography of the treated fibers was examined by
means of a scanning electron microscope (Figure 1 & 2). It is seen
that the untreated AC and AG fibers present longitudinal striations.
A smoothening of the surface is seen to occur upon etching and the

Non-treated AG fiber X5100

AG/NaOH 10 min. X5100
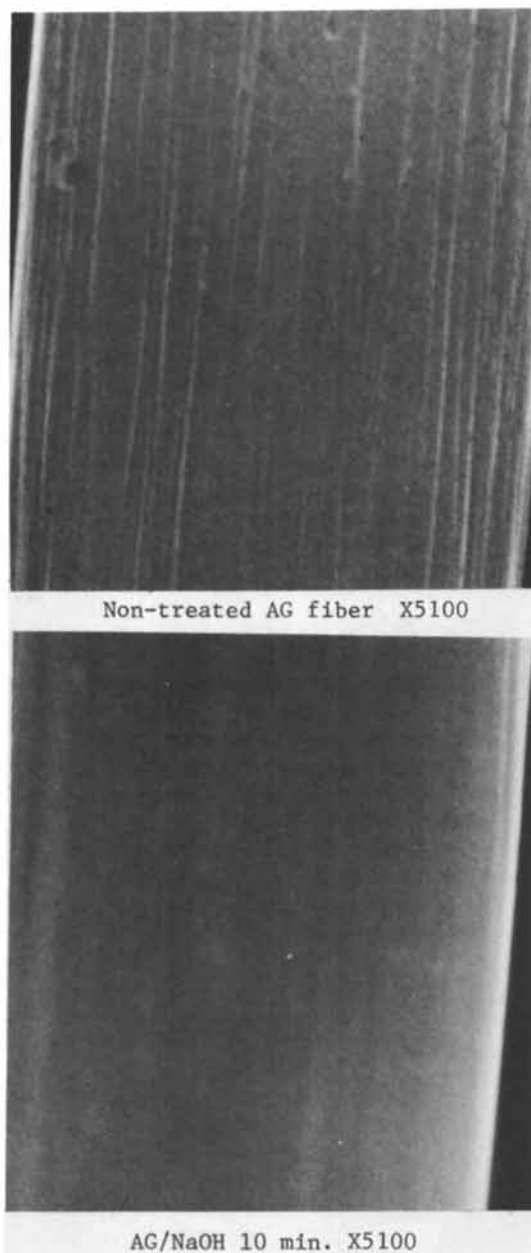
Figure 1. AG fiber
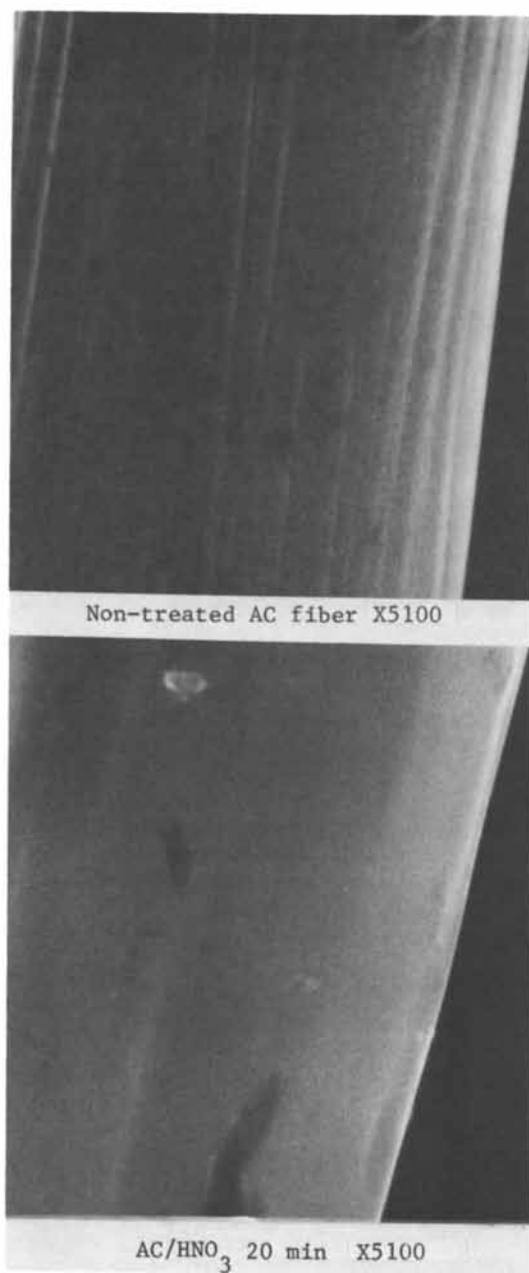
Figure 2.   AC fiber

surface becomes more uniform for both alkaline and acidic treatments.

Surface areas were measured by krypton adsorption at liquid nitrogen temperature. The results are shown in Table IV.

Table IV - Surface Areas of the Treated Fibers

Fibers	S_{BET} m^2/g
AG non-treated	0.43
AG NaOH 1 min	0.27
AG NaOH 10 min	0.22
AC non-treated	0.27
AC HNO$_3$ 1 min	0.35
AC HNO$_3$ 10 min	0.36
AC NaOH 2.5 min	0.32
AC NaOH 10 min	0.42

It is seen that there is no significant change in the specific surface. However, it is interesting to note that the specific area changes are quite different for the two fibers. The loss of surface area of the AG fibers may be explained by the removal of surface defects during the etching. In contrast, etching of AC fibers leads to an increase in microporosity as is usually observed with less organized carbons.

Modification of the surface properties may be accompanied by a marked decrease in tensile strength as a result of excessive degradation of the fiber. Therefore, tensile strength (σ_r) and Young's modulus (E) of the treated fibers were measured on monofilaments (Table V). It is noticed that even for short treatment times, AG fibers etched in nitric acid undergo a tremendous decrease in tensile strength. The reason for this behavior becomes evident when one realizes that the intercalation mechanism affects the internal parts of the fiber, thus resulting in a sharp decrease in the cohesion of the graphitic ribbons. In all other cases, treatments for short times i.e. 1 or 2 minutes do not significantly alter the mechanical properties of the fiber.

Properties of the Composites

Uniaxial fiber reinforced composites were made using treated fibers and an epoxy resin (Araldite LY556). Hot pressing was used for polymerization in the presence of a catalyst (Ciba HT 973). The fiber content in each composite was 75% by weight. Interlaminar shear strength (σ_c) of the composite was measured using a cant-

ilever test piece.

Table V - Mechanical Properties of the Treated Fibers

Fibers	σ_r psi	E psi
AG non-treated	$3.2\ 10^5$	$6.3\ 10^7$
AG HNO$_3$ 2 min	$1.4\ 10^5$	-
AG NaOH 1 min	$2.3\ 10^5$	$6.5\ 10^7$
AG NaOH 10 min	$2.4\ 10^5$	$6.4\ 10^7$
AC non-treated	$3.1\ 10^5$	$3.4\ 10^7$
AC HNO$_3$ 1 min	$3.0\ 10^5$	$3.4\ 10^7$
AC HNO$_3$ 10 min	$2.1\ 10^5$	$3.4\ 10^7$
AC NaOH 2.5 min	$2.8\ 10^5$	$2.8\ 10^7$
AC NaOH 10 min	$2.0\ 10^5$	$2.6\ 10^7$

Preliminary experiments were made to determine the influence of the degradation products present on the AC fibers on the bond strength of the composite. It appears that for non-purified fiber, which still contains degradation products, there is no improvement of the shear strength. In contrast, when extracted fibers are incorporated in the composite, there is a significant increase of σ_c, especially for short etching times.

Table VI - Influence of the Degradation Products on the Shear Strength of the Composites

Fibers	σ_c(psi) non-purified fiber	purified fiber
AC non-treated	7860	
AC HNO$_3$ 1 min	7550	12100
AC HNO$_3$ 5 min	7000	10020
AC HNO$_3$ 10 min	6850	9700

The maximum interlaminar shear strengths obtained in various treatment conditions are given in Table VII. It is seen that only a slight improvement in the shear strength of the composite containing nitric acid treated AG fibers is obtained. This is because the mechanical properties of these fibers have been considerably effected by the etching process. Furthermore, the increases in σ_c for the AC fibers are comparable for both acidic and alkaline treatments.

Table VII - Interlaminar Shear Strength of the Composites

Fibers	σ_c (psi)
AG non-treated	2000
AG HNO$_3$ 2 min	3860
AG NaOH 1 min	7860
AC non-treated	7860
AC HNO$_3$ 1 min[*]	12100
AC NaOH 2 min[*]	13100

[*] after extraction

The fractures of the composites after shear failure have been examined in a scanning electron microscope (figures 3, 4). It is seen that fiber pull-out before the failure still remains after acidic treatment. In contrast, after alkaline etching, the fracture surface becomes more smooth. Therefore it appears that for similar increase in shear strength, different failure modes of the composites may occur. Moreover, these results indicate that the surface properties of the fibers are differently modified by acidic and alkaline treatments.

The most important factors which been found to influence the fiberbond are chemical groups, specific area and rugosity. However, no correlation between these factors and the bond improvement has yet been found, especially for polyacrylonitrile based fiber. In order to investigate the role of the acidic groups, treated AC fibers were pyrolyzed at 1000°C in argon. This treatment is known to remove the strong acidic groups from the surface. After pyrolysis, the fibers were incorporated as previously in an epoxy matrix. As seen in Table VIII, pyrolysis of the etched fibers leads to a decrease in shear strength although the σ_c value is still greater than in the case of the untreated fibers.

Table VIII - Influence of the Acidic Groups of the
Shear Strength of the Composites

Fibers	Acidic groups µeg/g	σ_c psi
AC non-treated	7	7860
AC HNO$_3$ 1 min	14	12100
AC HNO$_3$ 1 min 1000°C	0	11000
AC NaOH 2.5 min	16	13100
AC NaOH 2.5 min 1000°C	0	11000

AG/HNO₃ X3400

AC/HNO₃ X2125

Figure 3.   Fracture of the composite after acidic etching of the fibers
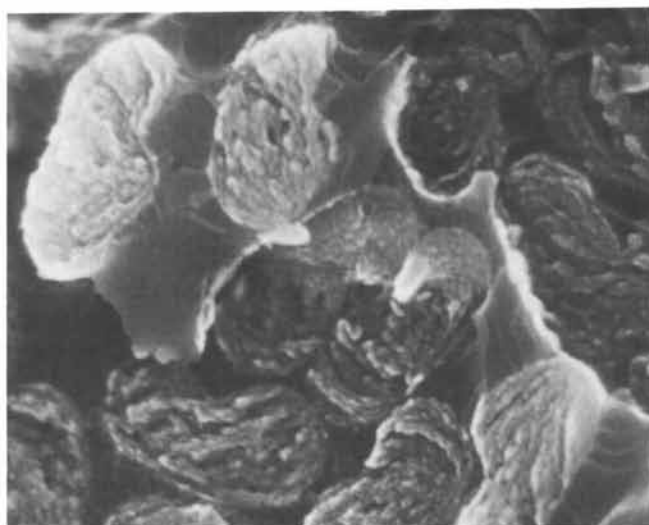
AG/NaOH X2125

AC/NaOH X3400

Figure 4. Fracture of the composite after alkaline etching of the fibers

The results of the present investigation show that acidic
groups strongly influence shear strength of the composites but
other factors such as the specific area affect the interfacial
bond strength. According to Mimeault (12), pyrolysis of carbon
fibers at 1000°C leads to an increase in specific area which in
our case may counterbalance partially the effect of the acidic
groups. However, the increase in specific area is mainly due to
an increase in microporosity and it is doubtfull that the resin
could penetrate in the micro pores. Therefore, we may attribute
the improvement of the interfacial bond strength partially to the
presence of acidic surface groups.

Conclusion

This study points out that electrochemical etching of graph-
ite and carbon fibers leads to significant improvement of the
interfacial bond strength between the fiber and the matrix. The
interactions of the fibers and the organic matrix are strongly
affected by the etching treatment. The influence of strong acidic
groups on the interlaminar shear strength has been established
in the case of carbon fibers.

Literature Cited

1. GOAN J. C., PROSEN S. P.: Interfaces in Composite ASTM Spe-
    cial Tech. Publ. 452, p. 3.
2. HERRICK, J. W., GRUBER P. E. Jr., MANSUR F. T.: Surface
    Treatment for Fibrous Carbon Reinforcements: (July 1966) AFML-
    TR-66-178 Part 1, Air Force Materials Laboratory.
3. HERRICK J. W.: 23rd Ann. Techn. Conf. SPI Reinforced Plastics/
    Composite Divisions, (February 1968) Section 1G-A.
4. AITKEN, I. D., RHODES G., SPENCER A. P.: 7th Int. Reinf. Plast.
    Conf. Brighton (Oct. 1970).
5. DAUKSCH M.: Thesis C.U.H.R. January 1973 Mulhouse (FRANCE).
6. COURTAULDS Ltd: U. K. Patent (1964) No. 14.4341.
7. RIEUX J. P., LEHUREAU J.: French Patent (1972) No. 72.14.950.
8. DONNET J. B., DAUKSCH H., PAPIRER E.: 11th Carbon Conference
    (1973) Gatlinburg (Ten), p. 172.
9. DONNET J. B., EHRBURGER P., ILVOAS A. M.: Bull Soc. Chim.
    France (1972), 6, 22.
10. EHRBURGER, P., HERQUE J. J., DONNET J. B.: Proceeding of the
    Fourth London Int. Carbon and Graphite Conf. (Sept. 1974) to
    be published.
11. BOEHM H. P., ECKEL M., SCHOLZ W.: Zeit fur Anorg. Chem.
    (1967), 353, 236.
12. MIMEAULT V. J., McKEE, D. W.: Nature (1969), 224, 793.

Mechanism of Nucleation and Growth of Carbon Black

J. LAHAYE and G. PRADO

Centre de Recherches sur la Physico-Chimie des Surfaces Solides,
24 Avenue du Président Kennedy, 68200 Mulhouse, France

Carbon blacks may be obtained from hydrocarbons either by pyrolysis or by partial combustion. The main question in the understanding of carbon black formation is to determine how hydrocarbon molecules which may be as simple as methane or benzene can, after vaporisation, lead in a few hundredths of a second to solid particles containing several tens of thousands of carbon atoms. Besides the chemical transformation of initial hydrocarbon, a phase change from gaseous to solid occurs, either directly or via a liquid phase. Various aspects of the subject have been reviewed during the last ten years (1-4). In a forthcoming comprehensive review (5), the nucleation and growth aspects of carbon formation are emphasized. The present paper will include the description of: the nature of the nuclei precursors; the kind of nuclei formed (liquid or solid) and the type of nucleation responsible for their formation; the growth of nuclei and their association during growth.

Nature of Nuclei Precursors

1. **Carbon Blacks Produced in Flames**. In the oxidation zone of a flame, concurrently with oxidation reactions and formation of ions, large hydrocarbon molecules are produced: polyacetylenes, polycyclic aromatics with or without side chains (6-9).

The work of Homann and Wagner (6-10) is particularly relevant to the role of these large hydrocarbon molecules in the formation of soot.

The authors studied a diffusion acetylene flame in which carbon black particles were formed. By direct probing in the flame and by extraction of the products adsorbed on soot, they could determine two types of aromatics:

a. Polycyclic aromatics without side chains such as: naphthalene (128 mass units), acenaphthylene (154), phenanthrene (178), pyrene (202) and coronene (300).

335

   b. Polycyclic aromatics with side chains. Their molecular
masses range from 150 up to 550.
   Contrary to the case of polyaromatics with side chains, it
appears that polyaromatics without side chains directly taken
from the flame are identical to those extracted from the soot
sampled at some distance from the oxidation zone. Their concen-
trations increase steadily following the oxidation zone without
going through any maximum. Therefore, the authors consider that
polyaromatic hydrocarbons with side chains are precursors of
carbon black particles while those without side chains are by-
products. These intermediate species may have two origins:
   a. The polymerization of acetylene or other unsaturated
compounds,
   b. The formation of benzyne type radicals.
Homann and Wagner consider that in the radical-rich oxidation
zone, polyacetylenes (Figure 1) are formed by reactions such as:

$$
{}^{\cdot}C_2H + C_2H_2 \longrightarrow \underset{\downarrow\ +H}{\overset{\overset{C_4H_2}{\uparrow}-H}{C_4\ H_3^{\cdot}}} \xrightarrow{\ +C_2H_2\ } \overset{\overset{C_6H_2}{\uparrow}-H}{C_6H_3(+H_2)} \xrightarrow{\ +C_2H_2\ } \quad \cdots
$$
$$
C_4H_4
$$
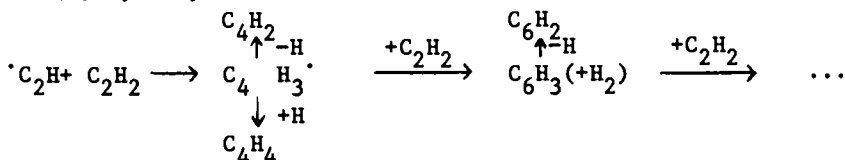
If a ${}^{\cdot}C_2H$ or any other radical attacks a polyacetylene molecule,
the probability that it will collide with one end decreases with
increasing chain length; thus, branched macroradicals are formed.
These radicals go on adding polyacetylenes and ring closures may
occur.
   Fields and Meyerson (11) investigated the pyrolysis of
aromatic compounds, unfortunately at a relatively low temperature
(700°C). They noticed that the formation of benzyne is almost as
universal as that of acetylene in the pyrolysis of aliphatic
compounds. It appears that only a fraction of aromatic nuclei
involves scission of C-C bonds.

INSERTION

C_6H_6 + BENZYNE

1-2 ADDITION

1-4 ADDITION

$\begin{array}{c}H\\|\\C\\|||\\C\\|\\H\end{array}$

(Fields and Meyerson)
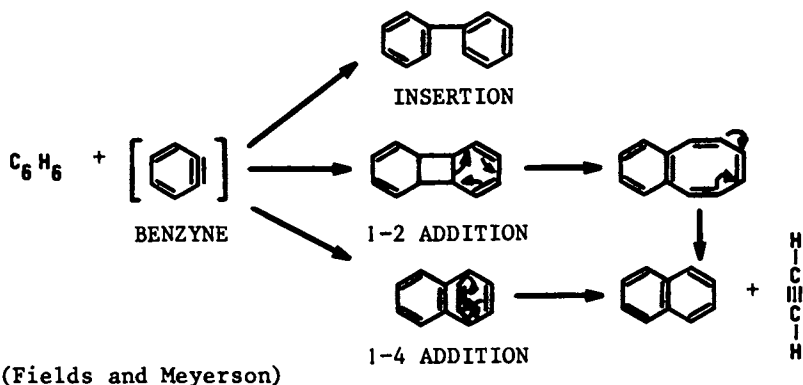
In the case of benzene flames, the formation of benzyne as intermediate might make it clear why the polycyclic aromatic hydrocarbons are formed in concentrations about 100 times larger than from aliphatic fuel for the same carbon to oxygen ratio in the unburnt gases.

Whatever the mechanism, polynuclear species, some with side chains, are formed in the oxidation zone of a flame. What about systems in which carbon blacks are formed under conditions of pure pyrolysis (thermal blacks) ?

2. <u>Carbon Blacks Produced by Pyrolysis of Hydrocarbons</u>.
The different intermediates proposed can be classified into two categories (<u>5</u>):
  a. unsaturated aliphatic or aromatic molecules.
  b. carbon vapor resulting from the dehydrogenation of initial hydrocarbons.
Palmer (<u>12</u>) estimates that polymerization reactions produce cyclic molecules, partly aromatic, as intermediates in carbon formation.

In studying the thermal decomposition of benzene, Prado (<u>13</u>) measured the yields of carbon and tar as a function of the reaction time (Figure 2). It appears that when the reaction time is increasing the tar yield reaches a maximum at the beginning of the carbon black formation, and rapidly decreases thereafter. There is no longer doubt that under usual pyrolysis conditions, the macromolecules formed in the gas phase are intermediates in carbon formation.

To our knowledge, there is no published work which demonstrates experimentally that carbon vapor is an intermediate in gas phase carbon formation, except the production of divided carbon by evaporation of graphite (<u>14</u>) and subsequent condensation, which does not concern carbon black production.

Nucleation and Growth Phenomena

At the end of the oxidation zone of a flame or in a thermal system at very small residence times, large polyaromatic molecules (to which we will refer as macromolecules) are present. They will form the primary nuclei. What type of nucleation is responsible for their formation? How are they going to grow?

1. <u>Carbon Blacks Produced in Thermal Systems</u>.
  a. <u>Theory involving solid nuclei</u>. In 1971, Samkhan et al. (<u>15</u>), referring to the work of Kargin et al. (<u>14</u>) gave a mathematical outline and equations for calculation of the rate of carbon black formation during the thermal decomposition of hydrocarbons. They identified the nuclei of the new phase as carbon black crystallites obtained by condensation of carbon vapor. Actually, we know that in the case of thermal blacks, they are not crystallites but large concentric layer planes (<u>16</u>, <u>17</u>). It is difficult to assume that carbon layers of the crystallites have enough mobility to be able to align in extended layers as large
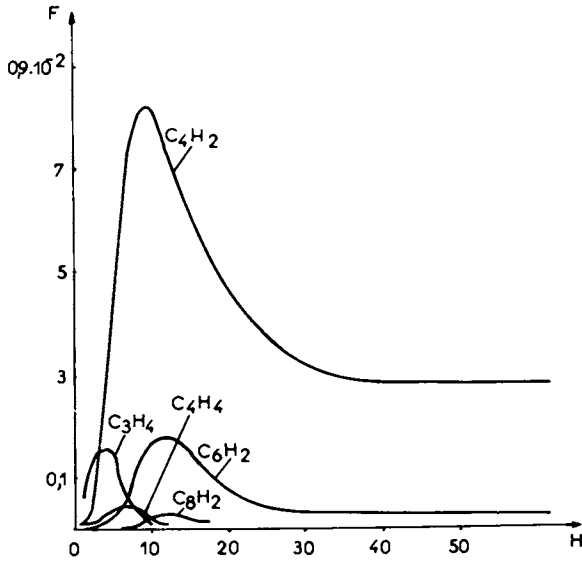
Figure 1.
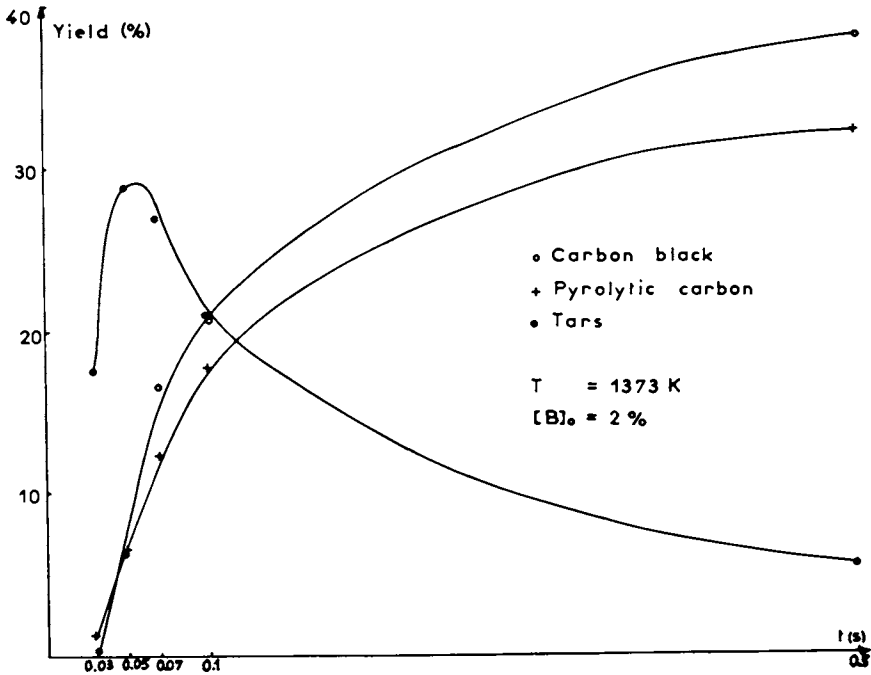
Figure 2.

and well organized as those encountered in thermal blacks.

    b. <u>Theory involving liquid nuclei</u>: Lahaye et al. (18, 19) studied the mechanism of carbon black formation by thermal decomposition in a flow system of benzene diluted in a stream of nitrogen. The carbon black particles were collected at the end of the heated tube. The number and the size of the particles have been determined for different molal fractions of hydrocarbon, residence times and temperatures. The number of particles gives information on the nucleation step and the size essentially on the growth step.

    One important result of this study is the observation of the constancy of the number of nuclei when the molal fraction (Table I) and the residence time (Table II) vary, for a given temperature (as a first approximation each nucleus is assumed to lead to one carbon black particle). Without going into details of the explanation of these results (5,13,19) worked out with the help of the classical theory of nucleation (20-22), they can be explained as follows:

    The initial hydrocarbon is transformed by gas phase reactions into macromolecules as already mentioned. The partial pressure of macromolecules increases with reaction time until supersaturation is high enough to induce the condensation of macromolecules into liquid microdroplets (critical nuclei). Since no additional nuclei are formed, we may conclude that supersaturation is not high enough any more to induce the formation of new nuclei. This means that the rate of formation of macromolecules is smaller than the rate of growth of the nuclei present.

    If the critical nuclei were microcrystallites in the first st-age of growth, they would yield crystallites which could develop in two different ways : a) growth and formation of an anisotropic macroscopic crystalline structure, which has never been observed in such a systems; and b) collision and agglomeration thus forming a particle. As previously pointed out, it is difficult to imagine the reorganization of individual crystallites into large con-centric carbon layers.

<div align="center">

Table I

Number of nuclei N formed per cc of gas TPN as a function
of the initial molal fraction of benzene $[B]_0$.

t = 0.5 s   T = 1100°C

</div>

$[B]_0$ (%)	1	2	4	6	8	10
$N \times 10^{-10}$	0.78	0.79	0.83	0.87	0.72	0.72

<div align="center">

Table II

Number of nuclei N formed per cc of gas (TPN)
for different reaction time t

$[B]_0 = 6\%$ T = 1100°C

</div>

t (s)	0.1	0.3	0.5	1.0
$N \times 10^{-10}$	0.87	0.91	0.87	0.75

Electron microscopy of samples collected at very low residence time, while not being a direct proof of the existence of liquid intermediates, is a good illustration of the liquid state of the nuclei. The liquid nuclei grow by adding macromolecules which continue to be produced. The kinetics of nuclear growth is in agreement with this description of the phenomena. The liquid nuclei are pyrolyzed into solid particles (dehydrogenation).

A statistical study of the diameter distribution curves of carbon black samples gives additional information on nucleation and growth of the particles formed in the experiments carried out by Prado (13). Generally, dispersed systems follow a statistical size distribution law which is either normal(Gaussian) or lognormal (23). The distribution law can be characterized by the parameters D_A, D_g, σA, and σg which are the arithmetic and geometric average diameters, the arithmetic and geometric standard deviations, respectively. For each distribution curve, a χ^2 test was carried out by assuming the distribution to be either normal (χ_N^2) or lognormal (χ^2 L.N.). Experimentally, the following has been shown:

a. The size distributions are neither perfectly normal nor perfectly lognormal.

b. The nearer the sample approaches the condition at the moment of nucleation, the closer the curve resembles a normal distribution; conversely, the more significant the particle growth, the closer the curve resembles a lognormal distribution.

c. For samples obtained under different conditions of molal fractions and temperature $\frac{DA}{\sigma A}$ and Log σg remain constant, within experimental error (Table III). Wersborg, Howard and Williams (24) found an identical result for carbon black samples formed in a flat acetylene-oxygen flame. What is the meaning of the constancy of $\frac{DA}{\sigma A}$ and in σg ? A sufficient prerequisite for these two relations to be constant is that, on a statistical point of view, each particle grows proportionately to its diameter ($D (t_1) = k D (t_2)$). It has been shown (19) that it will be the case if in each elemental volume ("slice" of the gas stream) where N_i nuclei appear, all of the particles have the same diameter after growth. Nucleation being a random phenomenon, N_i is randomly distributed. It means that the distribution of particle diameters of a given sample is not the result of a random distribution of the size of the particles in an element volume but of the random distribution of their numbers in the different elemental volumes. An evident consequence of this theory is that, in each volume of the gas stream, particles have all the same size and, therefore, by collision they form aggregates containing particles with the same size, even if the entire sample is very polydispersed. This consequence is in good agreement with observation carried out with industrial carbon blacks as well as with carbon blacks prepared on a laboratory scale.

Another consequence seems to be in contradiction with some of the results obtained. Indeed, it may be derived that the growth of

the particles proportional to their diameters maintains the normality of the size distribution (19). The distortion of the distribution curves appears as a secondary phenomenon which will be shown to be a partial coalescence or association between microdroplets or growing solid particles (25).

In carbon-black-producing system the mean free path of nuclei is several orders of magnitude large than the nuclei diameter; therefore, the interactions between nuclei are negligible and the nuclei population can be considered as a Maxwell gas (25, 26). The number of particles N of the system as a function of the duration of aggregation t can be computed using the kinetic theory of gases. The following expression has been established:

$$N = No \ (1 + 8 \times 10^{-12} No^{5/6} T^{1/2} Co^{1/6} ct)^{-6/5}$$

where No = number of particles per cc before aggregation
   T = Temperature in °K
   c = sticking coefficient
   Co= number of benzene molecules giving carbon black

(per cc). The exact value of the sticking coefficient is not known, and ct has been used as a variable of the expression of N.

Each distribution curve being characterized by a x^2 test, the smaller the ratio $\frac{x^2 LN}{x^2 N}$ the closer the curve resembles a lognormal distribution.

The value of N has been computed from a purely normal initial population. The ratio $x^2 LN/x^2 N$ and the variation of N have been computed when ct varies from 10^{-2} to 10^{-3}á, before and after growth (Table IV). In both cases, for values of ct below $10^{-2}s$, the diameter distribution tends towards a lognormal distribution, though the percentage of association is less or equal to 20% (20% is the experimental uncertainty in the determination of the number of particles formed, in Lahaye and Prado's work).

Table III
Statistical particle parameters calculated from experimental
data (19)

(B)₀ (%)	0.5	1	2	4	6
t (s)	0.5	0.5	0.5	0.5	0.5
T (°C)	1100	1100	1100	1100	1100
D_A (Å)	377.4	524.1	717.0	913.2	972.5
σ_A (Å)	69.1	90.2	115.5	168.5	171.6
D_A/σ_A	5.46	5.81	6.21	5.42	5.67
ln σ_g	0.188	0.176	0.167	0.182	0.171
$\frac{x^2 L.N.}{x^2 N}$	2.68	1.48	1.50	1.26	0.37

$$\frac{DA}{\sigma_A} = \frac{\sum ni \ d_i}{\sqrt{\sum (n_i (d_i - D_A)^2) \times \sum n_i}} \ ; \ \ln \sigma_g = \frac{\sqrt{\sum ni (\text{Log } d_i - \text{Log } Dg)^2}}{\sum n_i}$$

n_i = number of particles in an interval centered on d_i.

Therefore, association of particles explains why a normal population becomes, after growth, a lognormal one. This study demonstrates another important point. For a reaction time of a few milliseconds, the nuclei are still liquid and it can be assumed that the sticking coefficient is close to 1 and ct corresponds to the reaction time. It means that the association phenomena occur very quickly after the nucleation of microdroplets. However, immediately after association, as diameters of the associated particles can be individually measured, the population remains normal; after growth the associated particles lose their individuality and each primary cluster becomes a single particle more or less spherical (the primary clusters containing a few nuclei must not be confused with the particle aggregates constituting the final population). Growth acts as a "developer" of association which occurred much earlier in the process of nuclear formation.

Phase contrast electron microscopy brings some proofs of association phenomena.

Table IV
Theoretical computation of association of particles

	Before growth			
ct (s)	10^{-3}	5×10^{-3}	8×10^{-3}	10^{-2}
% association	2.6	11.4	16.9	20.1
D_A (A°)	151.4	156.4	159.9	162.2
ΔD_M (A°)	0.0	0.0	0.0	0.0
ΔD_A (A°)	30.0	30.3	30.4	30.5
D_A/σ_A	5.0	5.16	5.25	5.32
ln σg	0.208	0.199	0.193	0.189
χ^2 LN/χ^2N	104.5	1.5	0.60	0.47
	After growth			
ct (s)	10^{-3}	5×10^{-3}	8×10^{-3}	10^{-2}
% association	2.6	11.4	16.9	20.1
D_A (A°)	1517	1575	1614	1639
ΔD_M (A°)	1350	1350	1350	1350
ΔD_A (A°)	294.5	277.2	267.3	261.5
D_A/σ_A	5.15	5.68	6.04	6.27
ln σg	0.204	0.181	0.169	0.162
χ^2 LN/χ^2N	16.7	1.82	1.28	1.12

2. Carbon blacks produced in flames
    a. Nucleation step : Three separate theories have been developed to explain carbon nuclei formation in the pyrolysis zone (yellow colored) of a flame namely -"chemical nucleation"-, physical nucleation on ions and homogeneous physical nucleation.
    b. Chemical nucleation : "Chemical nucleation" refers to the progressive transformation by chemical reaction of the polynuclear molecules into more and more condensed ones, reaching

the carbon nucleus in the final steps. This mechanism, advanced
by Homann and Wagner (6), does not explain the discontinuous
character of carbon formation. These authors themselves observed
that after the appearance of carbon "no new nuclei were formed,
although relatively large quantities of polyacetylenes were still
present". Furthermore, there is a large gap between the larger
molecules identified (with a mass of about 600) and the smaller
carbon particles with masses of about 40,000 for particles of
about 40 Å diameter. A sequence of radical chemical reactions can
hardly explain this discontinuity. Thus, it appears that chemical
nucleation cannot be responsible for the phenomena observed.

　　c. Physical nucleation on ions : It has been shown that ions
are formed in the oxidation zone. Many authors indicate that some
particles are electrically charged. In particular, Weinberg et al.
(27) studied the influence of electrical fields on the formation
of carbon in flames.

　　The authors pointed out that in changing the direction of the
electrical field, the direction of migration of the particles also
changed. They concluded that the positive ions present in the
flame probably act as nuclei for carbon formation.

　　An electrical field, however, very quickly carries the ions
out of the oxidation zone, preventing their eventual neutralisa-
tion. Under these conditions, the ion concentration in the
pyrolysis zone becomes much higher, strongly changing the
conditions of nucleation. Moreover, the carbon particles form
aggregates requiring only one of its particles to be charged to
migrate in the gaseous flux. Therefore, it is not evident that all
particles nucleate on ions. More recently, Howard et al. (24)
measured the fraction of particles charged in a premixed flame of
acetylene. Their average number fraction is 30%.

　　If ionic nucleation is the predominant nucleation mechanism,
the measured 70% average fraction of neutral particles requires
that the charges be rapidly neutralised under the investigated
flame condition.

　　In the case of flames, ionic nucleation may be important,
but a firm conclusion is however, not yet possible.

　　d. Homogeneous nucleation : Homann and Wagner (6) noticed an
increase of the polyaromatic molecules concentration at the
beginning of the zone of soot formation. The supersaturation of
these species increases and when it is high enough, condensation
may occur according to homogeneous physical process. This theory
developed for the case of thermal systems (19) allows the
explanation of the formation of soot particles in flames through
the intermediate form of droplets which, after growth and chemical
transformation, give solid carbon particles. Ulrich (28) considers
that this mechanism of appearance of solids in flames is general
(silica, carbon black, etc.). It is noteworthy that this theory,
recently proven for the case of thermal systems, had been assumed
a long time ago : it is the well-known "oil droplet theory"
(29,30).

e. Growth step : It has been known for many years (31) that
an individual carbon black particle usually has several "centers".
Investigations by phase contrast electron microscopy (17) sustain
this observation. It is actually impossible to exclude the
possibility for the "centers" to be graphitization centers formed
during the transformation of a single liquid droplet into a solid
particle. It appears more likely that they are growth centers
corresponding to primary particles which subsequently associated.
The presence of partially coalesced particles observed in thermal
black samples (13,25) agrees with this hypothesis. Moreover,
particle aggregation is much more important for carbon blacks
formed in flames than for thermal blacks. Any theoretical calcula-
tion of particle growth must take into account the phenomena of
deposit on the particle surface and of association. In that
respect, Wersborg's model is interesting (24). It includes
nucleation, coagulation (association) and surface growth. For
practical purposes the rate of nucleation is defined as the rate
of appearance of the smallest observable particles (15Å).
Experimentally coagulation rate constants were obtained by
assuming a monodisperse system and expressing the coagulation rate
according to the oversimplified Smoluchoski's (32) theory.

A fairly good agreement with the equations was observed. It
appears that the main interest of this study is the possibility
of differentiating the nucleation zone from the growth zone. It
shows also clearly both ways of growth of a particle in flames.
In other investigations, systems were studied in which one type
of growth is predominant, hiding the influence of the other. In
this way, Ulrich (28), referring to the calculation of Brock and
Hidy (33-36) established the equations describing association
process for silica formation in flames. For carbon blacks, the
problem becomes somewhat more complicated since there is more than
one reaction and macromolecules continue being produced after
nucleation. This leads, as already pointed out, to surface
deposits. For thermal blacks (13,18,19) surface growth predomi-
nates and for carbons formed in flames association phenomena
predominates.

Gilyzaetdinov (37) also considered the kinetics of formation,
growth and coagulation of growing carbon black particles by means
of the active collision theory. He concluded that coagulation of
growing particles of carbon black aerosols has a significant role.

The influence of electrical forces on particle growth (24,
38) will not be discussed in the present review. As noticed by
Ulrich (39), the evidence used to support ionic effects in carbon
black formation can be applied with equal weight to support a
theory of growth through random collisions. Thus for example,
extensive work by Vold (40), Medalia (41), Sutherland (42) and
Ravey (43) using computer simulation has shown that aggregates
synthesized through random sticking collision resemble the chain-
like carbon black aggregates observed by electron microscopy.
Therefore, ionization may not play a key role in carbon black

growth, but it may inhibit growth and agglomeration somewhat when the ion particle number becomes large.

CONCLUSIONS

Carbon blacks may be produced by thermal treatment of hydrocarbons in the absence of oxygen as well as by their partial combustion.

In the case of thermal systems, it appears to be well established at present that the initial hydrocarbon is being transformed by complex reactions into large polyaromatic molecules which condense into liquid microdroplets, precursors of the ultimate carbon black particles. The growth consists of simultaneous associations of small nuclei and deposit of large polyaromatic molecules at their surface. For thermal blacks the deposit is the main growth step. Some associations which occur have the effect of transformation of the particle size distribution from normal (Gaussian), found immediately after nucleation, to a lognormal distribution.

In the case of carbon blacks produced in flames, the general mechanism of carbon black formation as indicated for thermal systems appear to be valid. The intermediate species between the initial hydrocarbon and the large aromatic molecules are polyacetylenes. For benzene and aromatic hydrocarbons in general, the benzyne radical might be an important intermediate.

Association of particles appears much more important in flames than in thermal systems.

According to some investigators, the ions present in flames play an important role in the nucleation of liquid microdroplets and in growth and formation of aggregates. Additional work is required to establish the significance of nucleation on ions.

Literature Cited

(1) Palmer, H.B., and Cullis, C.F., Chemistry and Physics of Carbon, Vol. 1 (P.L. Walker, Jr., Ed.) Dekker, New York, (1965), p. 265.
(2) Donnet, J.B., "Les Carbones", Masson Ed. Paris, Tome II, (1965), 712.
(3) Feugier, A., Rev. Inst. Fr. Petr., (1969), XXIV, 11, 1374.
(4) Gaydon, A.G., and Wolfhard, H.G., "Flames" 3rd edition, Chapman and Hall, Ed., London, (1970).
(5) Lahaye, J., and Prado, G., Chemistry and Physics of Carbon, Vol. 13 (P.L. Walker, Jr., Ed.) Dekker, New York (to be published).
(6) Homann, K.H., and Wagner, H.G., 11th Symp. (Intern.) on Combustion. The Combustion Institute, Pittsburgh, Pa., (1967), p. 371.
(7) Palmer, H.B., Voet, A., and Lahaye, J., Carbon (1968), 6, 65.
(8) Ray, S.K., and Long, R., Combust. Flame, (1964), 8, 139; ibid., (1968), 12(3), 226.

(9) Crittenden, B.D., and Long, R., ibid., (1973), 20, 359.

(10) Homann, K.H., ibid., (1967), 11, 265.

(11) Fields, E.K., and Meyerson, S., Accounts of Chemical Research, (1969), Vol. 2, 9, 273.

(12) Palmer, H.B., J. Chim. Phys., April (Special Issue), (1969), p. 87.

(13) Prado, G., Ph. D. Dissertation Thesis, C.U.H.R. and U.L.P. of Strasbourg (1972).

(14) Kargin, V.A., Berestneva, Z. Ya., Safronov, N.Ya., and Zhilkina, V.I., Kolloid. Zh., (1967), 29(3), 342.

(15) Samkhan, I.I., Tsvetkov, Yu.V., Petrunichev, V.A., and Glushko, I.K., ibid., (1971), 33(6), 885.

(16) Ban, L.L., "Surface and Defect Properties of Solids", Roberts, M.W., and Thomas, J.M., ed., (1972), Vol. 1, p. 54, Chem.Soc.

(17) Marsh, P.A., Voet, A., Mullens, T.J., and Price, L.D., Carbon, (1971), 9, 797.

(18) Prado, G., and Lahaye, J., C.R. Acad. Sci. Paris (1972), 274, 569; ibid., (1972), 274, 1880.

(19) Lahaye, J., Prado, G., and Donnet, J.B., Carbon, (1974), 12, 27-35.

(20) Volmer, M., and Weber, A., Z. Physik. Chem. Leipzig, (1926), 119, 277.

(21) Becker, R., and Doering, W., Ann. Phys., (1935), 24, 719.

(22) Zel'dovitch, J.B., J. Exp. Theoret. Phys., (1942), 12, 525 ; Act. Phys. Chem. SSSR, (1943), 18, 1.

(23) Smith, J.E., and Jordan, M.L., J. Coll. Sci., (1964), 19(6), 540.

(24) Wersborg, B.L., Howard, J.B., and Williams, G.C., 14th Symp. (Intern.) on Combustion. The Combustion Institute, (1973) p. 929.

(25) Prado, G., and Lahaye, J., J. Chim. Phys. (1975), 4, 483.

(26) Benson, S.W., "The Foundations of Chemical Kinetics", Graw-Hill Book Company, Inc., (1960), p. 135.

(27) Place, E.R., and Weinberg, F.J., 11th Symp. (Intern) on Combustion. The Combustion Institute, (1967), p. 245.

(28) Ulrich, G.D., Comb. Sci. Techn. (1971), 4, 47.

(29) Parker, W.G., and Wolfhard, H.G., J. Chem. Soc., (1950), 2038.

(30) Sweitzer, C.W., and Heller, G.L., Rubber World, (1956), 134, 855.

(31) Donnet, J.B., Bouland, J.C., and Jaeger, J., C.R. Acad. Sci. Paris, (1963), 256, 5340.

(32) Smoluchowski, M., Z. Phys. Chem., (1917), 92, 129.

(33) Brock, J.R., and Hidy, G.M., J. Appl. Phys., (1965), 36, 1957.

(34) Hidy, G.M., J. Colloid Sci., (1965), 20, 123.

(35) Hidy, G.M., and Brock, J.R., ibid., (1965), 20, 447.

(36) Hidy, G.M., and Lilly, D.K., ibid., (1965), 20, 867.

(37) Gilyazetdinov, L., Zh. Fiz. Khim., (1970), 44(7), 1828.

(38) Wersborg, B.L., Howard, J.B., and Williams, G.C., Technical Report, Dept. of Chem. Eng. Massachusetts Inst. of Techn., Cambridge, December (1972).

(39) Ulrich, G.D., 12th Symp. (Intern.) on Combustion. The Combustion Institute, Pittsburgh, (1969), p. 884.

(40) Vold, M.J., J. Colloid Sci., (1963), 18, 684.

(41) Medalia, A.I., ibid., (1967), 24, 393; Carbon, (1969), 7, 567.

(42) Sutherland, D.N., J. Colloid Interf. Sci., (1967), 25, 373.

(43) Ravey, J.C., Ph. D. Dissertation Thesis Nancy (France)(1973).

25

Role of Acetylenic Species in Carbon Formation

C. F. CULLIS

The City University, London, England

    A fundamental problem in the formation of carbon from gases
is the elucidation of the mechanism whereby reactant molecules
containing only a few carbon atoms and a considerable proportion
of other elements are converted into particles of carbon or carbon
-rich solids, which contain tens or hundreds of thousands of
carbon atoms and relatively little else.
    The overall process of carbon formation which can be
represented diagrammatically as shown below:
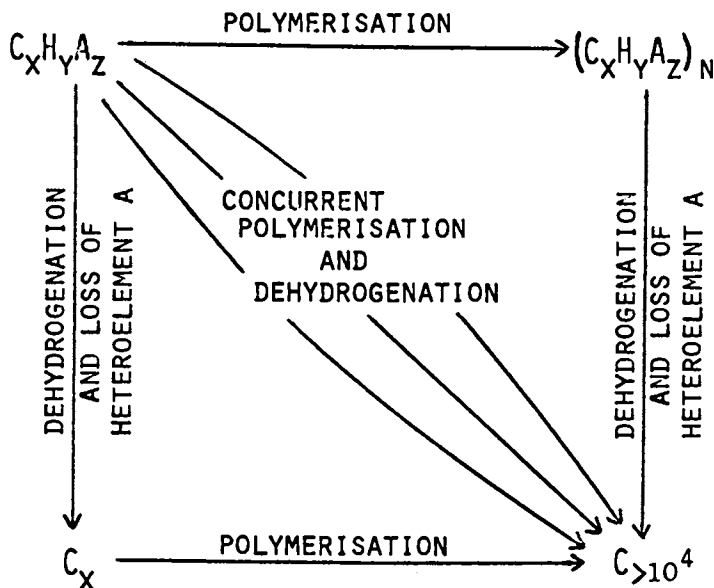
must of course involve both <u>dehydrogenation</u> (including the removal
of other volatile heteroelements) and <u>polymerisation</u>. Some of
the early 'theories' of carbon formation postulated that these two

processes took place consecutively, there being some disagreement
as to whether dehydrogenation or polymerisation occurred first.
Later it was proposed that the two processes are in fact simultan-
eous, and Porter - principally on the basis of some studies of the
flash photolysis of ketene (1) - revived an idea which had its
origins in the last century, namely that hydrocarbon-based fuels
are initially degraded to acetylene and that carbon is formed from
this compound by a series of rapid reactions involving concurrent
dehydrogenation and polymerisation.

Acetylene is certainly a common product of the decomposition
of hydrocarbons under carbon-forming conditions at elevated
temperatures (2-5) and studies of low-pressure hydrocarbon flames
have also shown that this compound is present among the reaction
products (6,7). However, what is perhaps now rather more firmly
established experimentally is the importance of polyacetylenes in
carbon formation. Bonne, Homann and Wagner (8), using mass-
spectrometry, were able to identify and follow the concentrations
of the species C_2H_2, C_4H_2, C_6H_2 and $C_{10}H_2$ throughout the reaction
zone of a flat premixed low-pressure acetylene flame under sooting
conditions. At the same time, it was possible to measure by
electron microscopy the total concentration, density and particle
size of the carbon formed. It was shown that equilibrium
relationships exist among the various acetylenic species and that,
when carbon starts to be formed, the concentrations of all such
species decrease, levelling off when carbon formation has
virtually ceased. These relationships are quantitative in the
sense that no other hydrocarbons are present in the carbon-growth
region in concentrations sufficient to account for the growth.
Nor is there any significant relationship between the carbon
monoxide concentration and the extent of carbon formation.

The view which has emerged from these observations is that,
despite the possible importance of acetylene as an intermediate
in many carbon-forming systems, this compound is required only to
form polyacetylenic species and, if these can be produced by other
easier routes, then the presence of acetylene itself is not
essential. Thus, for example, the powerful sooting tendency of
benzene has been ascribed (9) to the ease with which ring-opening
and fragmentation produce $C_2H\cdot$ and $C_4H_3\cdot$ radicals and it is
believed that acetylene itself is not necessarily involved in the
reaction. Certainly radicals such as $C_2H\cdot$, $C_2H_3\cdot$ and $C_4H_3\cdot$ have
been detected in the reaction zones of certain hydrocarbon flames
under sooting conditions (10,11) but, although Homann and Wagner
(12,13) have discussed at some length the further reactions which
such radicals may undergo, there is little quantitative kinetic
information about such reactions or the extent to which they may
be involved in carbon formation.

Results

Some recent studies of the reactions of the ethynyl radical,
$C_2H\cdot$, with acetylenic hydrocarbons (14,15) are of some relevance

to mechanisms of carbon formation in gases. Ethynyl radicals
were generated by the photolysis at 253.7 nm of monobromoacetylene
in the presence of nitric oxide, to 'mop up' bromine atoms, and a
large excess of an inert gas (nitrogen), to remove excess trans-
lational energy from the newly produced free radicals (16). A
relatively simple mechanism:

$$C_2HBr + h\nu \longrightarrow C_2H^{\cdot} + Br^{\cdot} \qquad 1)$$

$$C_2H^{\cdot} + C_2HBr \longrightarrow C_4H_2 + Br^{\cdot} \qquad 2)$$

$$C_2H^{\cdot} + C_2HBr \longrightarrow C_2H_2 + C_2Br^{\cdot} \qquad 3)$$

$$Br^{\cdot} + NO + C_2HBr \longrightarrow BrCN + CO + HBr \qquad 4)$$
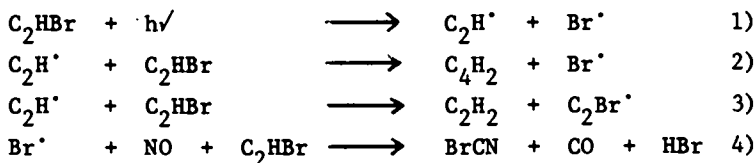
was found to account for the primary products formed. Since a
linear relationship existed between the rate of formation of
diacetylene and that of acetylene at various initial concentra-
tions of monobromoacetylene (Figure 1), it was clear that the
recombination of ethynyl radicals did not occur to any appreci-
able extent.

When ethynyl radicals react with acetylene, they can
presumably either abstract or displace hydrogen atoms:

$$C_2H^{\cdot} + C_2H_2 \longrightarrow C_2H_2 + C_2H^{\cdot}$$

$$C_2H^{\cdot} + C_2H_2 \longrightarrow C_4H_2 + H^{\cdot}$$
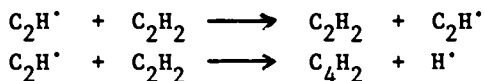
It is clearly not possible to follow the course of the first
reaction, as the reactants and products are identical; experiments
with monobromoacetylene-nitric oxide mixtures containing acetylene
alone thus provide no useful information. If, on the other hand,
acetylene-d_2 is added, the relative rates of hydrogen transfer and
hydrogen displacement:

$$C_2H^{\cdot} + C_2D_2 \longrightarrow C_2HD + C_2D^{\cdot} \qquad 5)$$

$$C_2H^{\cdot} + C_2D_2 \longrightarrow C_4HD + D^{\cdot} \qquad 6)$$
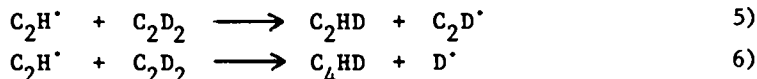
can be obtained from the amounts of acetylene-d_1 and diacetylene-
d_1 formed. Experiment shows that k_5/k_6 is ca. 0.4 at $25^{\circ}C$.

In the presence of added methylacetylene, ethynyl radicals
react to form acetylene, diacetylene and penta-1,3-diyne, which
presumably result from reactions involving hydrogen transfer,
methyl displacement and hydrogen displacement respectively:

$$C_2H^{\cdot} + C_3H_4 \longrightarrow C_2H_2 + C_3H_3^{\cdot} \qquad 7)$$

$$C_2H^{\cdot} + C_3H_4 \longrightarrow C_4H_2 + CH_3^{\cdot} \qquad 8)$$
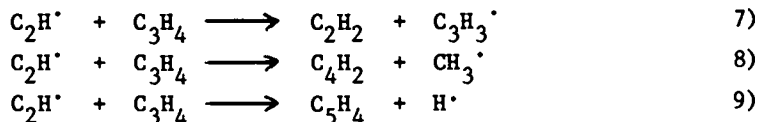
$$C_2H^{\cdot} + C_3H_4 \longrightarrow C_5H_4 + H^{\cdot} \qquad 9)$$

If reaction 9) is the sole source of penta-1,3 diyne and reactions
3) and 7) are the only sources of acetylene, it follows that:

$$\frac{[C_5H_4]}{[C_2H_2]} = \frac{k_9[C_2H^\cdot][C_3H_4]}{k_3[C_2H^\cdot][C_2HBr] + k_7[C_2H^\cdot][C_3H_4]}$$

$$= \frac{k_9[C_3H_4]/[C_2HBr]}{k_3 + k_7[C_3H_4]/[C_2HBr]}$$

If $[C_5H_4]/[C_2H_2]$ = a and $[C_3H_4]/[C_2HBr]$ = b,

then: $\quad \dfrac{b}{a} = \dfrac{k_7}{k_9} b + \dfrac{k_3}{k_9}$

A linear relationship is indeed found between b/a and b (Figure 2) from which it can be shown that k_7/k_9 at 25°C is ca. 25. However measurements at temperatures up to ca. 250°C show that this ratio gradually decreases with increasing temperature (Figure 3), indicating that hydrogen displacement (which involves lengthening of the carbon chain) becomes increasingly important as more realistic carbon-forming temperatures are attained. Both these competing reactions have appreciable activation energies, that for reaction (9) being ca. 4 kJ.mol^{-1} greater than that for reaction (7). An exactly analogous treatment shows that k_8/k_9 is ca.10 at 25°C, but again this ratio slowly decreases, and hence diacetylene formation increases, as the temperature is raised.

The ethynyl radical may, of course, also add across the triple bond in methylacetylene:

$$C_2H^\cdot + CH_3C{\equiv}CH \longrightarrow CH_3\overset{\cdot}{C}{=}CH{-}C{\equiv}CH$$

$$\text{or} \quad CH_3C{=}\overset{\cdot}{C}H$$
$$\underset{C{\equiv}CH}{|} \qquad\qquad 10)$$
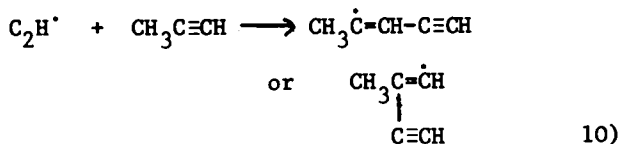
Now, if enough methylacetylene is present, then effectively all the $C_2H^\cdot$ radicals will react with it according to reactions 7) - 9) as well as by reaction 10). The sum of the partial pressures of acetylene, diacetylene and penta-1,3-diyne, when plotted against the pressure of added methylacetylene (Figure 4), falls eventually to a value of 1 x 10^{-2} mm Hg, which presumably represents the limiting contribution of reactions 7), 8) and 9). When no methylacetylene is present, the sum of the partial pressures of acetylene and dicetylene formed under the same experimental conditions (by reactions 2) and 3)) is ca. 4 x 10^{-2} mm Hg. The difference between these two quantities, viz. 3 x 10^{-2} mm Hg, should provide a measure of the extent of occurrence of reaction 10).
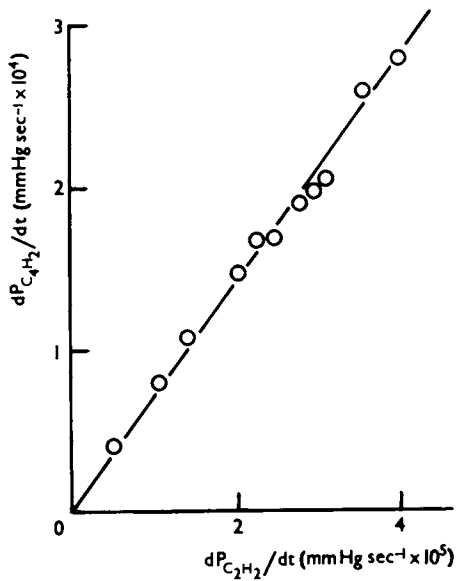
Figure 1. Formation of acetylene and diacetylene at different initial pressures of monobromoacetylene. Temperature, 25°C.
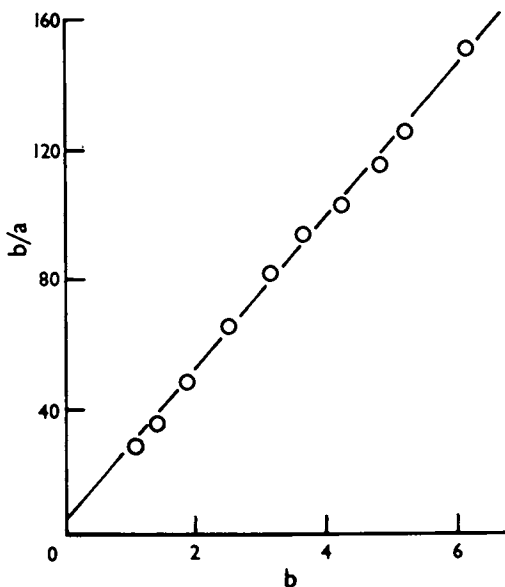
Figure 2. Variation of b/a with b where b — $[C_4H_4]/[C_2HBr]$ and a — $[C_6H_4]/[C_2H_2]$. Temperature, 25°C.
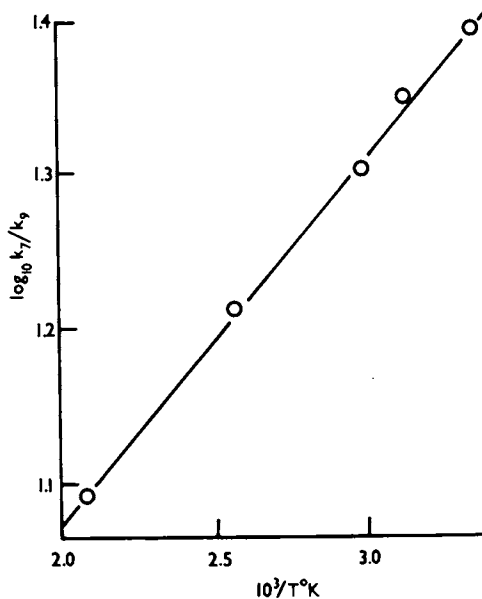
Figure 3.   Variation of k_7/k_9 with temperature
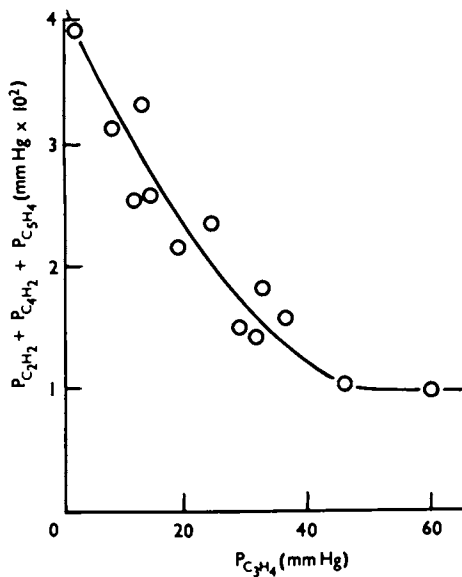
Figure 4.   Variation of sum of partial pressures of acetylene, diacetylene, and penta-1,3-diyne with initial pressure of methylacetylene

Thus: $\dfrac{k_{10}}{k_7 + k_8 + k_9} = 3$

and, since $k_8/k_7 \simeq 0.1$ and $k_9/k_7 \simeq 0.04$, it follows that

$$\frac{k_{10}}{k_7} \simeq 3.4$$

At room temperature, therefore, addition reactions of ethynyl radicals appear to occur somewhat more rapidly than hydrogen-transfer and hydrogen-displacement reactions. In general however addition reactions would be expected to decrease in importance as the temperature increases (17) and transfer and displacement reactions thus probably constitute the principal fate of ethynyl radicals under carbon-forming conditions.

When ethynyl radicals react with diacetylene, measurements of the relative rates of formation of acetylene and hexatriyne

$$C_2H^{\cdot} + C_4H_2 \longrightarrow C_2H_2 + C_4H^{\cdot} \qquad \text{11)}$$

$$C_2H^{\cdot} + C_4H_2 \longrightarrow C_6H_2 + H^{\cdot} \qquad \text{12)}$$
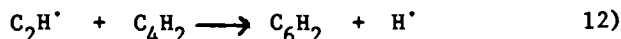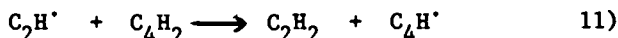
show, in much the same way as for the methylacetylene system, that k_{12}/k_{11} is ca. 1 at 25°C

Discussion

The result of this work which probably has most direct relevance to the early stages of carbon formation is that ethynyl radicals evidently do react with low molecular weight acetylenic hydrocarbons to form polyacetylenic species. However, hydrogen displacement reactions, which lead to a lengthening of the carbon chain:

$$C_2H^{\cdot} + C_2H_2 \longrightarrow C_4H_2 + H^{\cdot}$$

$$C_2H^{\cdot} + C_4H_2 \longrightarrow C_6H_2 + H^{\cdot}$$

$$C_2H^{\cdot} + C_6H_2 \longrightarrow C_8H_2 + H^{\cdot}$$

take place, even at the temperatures likely to be encountered under carbon-forming conditions, to an extent only comparable with that of hydrogen transfer reactions, e.g.

$$C_2H^{\cdot} + C_4H_2 \longrightarrow C_2H_2 + C_4H^{\cdot}$$

The simultaneous occurrence of reactions of the latter type does not, however, prevent the formation of higher polyacetylenic species, since free radicals will be formed which will undergo, to some extent, further hydrogen displacement reactions, e.g.

$$C_4H^\cdot + C_4H_2 \longrightarrow C_8H_2 + H^\cdot$$

Furthermore, simple acetylenic radicals such as $C_2H^\cdot$ and $C_4H^\cdot$ presumably also add on to polyacetylenes already present in the system. Thus, in one way or another, there is a tendency for polyacetylenic species to grow steadily larger.

However, due to the rigidity of the polyacetylenes and the fact that free radical addition reactions inevitably lead to a reduction in the degree of conjugation in an unsaturated molecule, the resulting higher molecular weight species are not likely to undergo ring closure to form aromatic structures. Thus, for example, ethynyl radicals may add to diacetylene:

$$HC\equiv C-C\equiv CH + C_2H^\cdot$$

$$HC\equiv C-\overset{\cdot}{C}\bullet CH-C\equiv CH \qquad\qquad HC\equiv C-C-C\equiv CH$$

$$+C_2H^\cdot \downarrow \qquad\qquad\qquad +C_2H^\cdot \downarrow$$

$$HC\equiv C-\overset{\cdot}{C}\bullet CH-\overset{\cdot}{C}\bullet CH-C\equiv CH \qquad HC\equiv C-C-C=\overset{\cdot}{C}H$$

Further growth then occurs mainly by addition, displacement and recombination reactions, and intermediates may perhaps eventually be formed which correspond to the 'carbon precursors' of molecular weight from 250–500 found in acetylene flames by Homann and Wagner (18). These are not aromatic compounds and their concentration runs parallel with that of 'young' carbon particles. Polycyclic aromatic hydrocarbons are, however, formed at the same time, but are not subsequently consumed in the carbon-forming region of the flame (18), suggesting that they grow by separate non-radical processes, possibly involving Diels-Alder condensation.

Nevertheless, the present kinetic results and especially the evidence of constant competition between hydrogen transfer and hydrogen displacement reactions strongly suggest that the growth of polyacetylenic species does not occur sufficiently rapidly to account, for example, for the almost instantaneous formation of carbon in a sooting flame. Thus there seems little doubt that, although reactions of simple acetylenic radicals with simple acetylenic molecules do lead to the production of higher poly-acetylenic species, other processes, including perhaps ion-

molecule reactions, must be largely responsible for the extremely
rapid formation of carbon observed under certain experimental
conditions.

Clearly, it is now desirable to obtain kinetic information
about the reactions of the higher homologues of ethynyl radicals.
As a prerequisite to this, however, it will be necessary to
devise satisfactory methods for the artificial generation of such
radicals in a reasonably high state of purity.

Abstract

Although acetylene itself is not necessarily involved in
carbon formation, the polyacetylenic species generally present
under carbon-forming conditions might be expected to be produced
by further reactions of small acetylenic free radicals.   Kinetic
studies of the reactions of ethynyl radicals ($C_2H^{\cdot}$) with low
molecular weight acetylenic molecules show that hydrogen displace
—ment reactions, which result in a lengthening of the carbon
chain, generally occur to an extent roughly comparable with that
of hydrogen transfer reactions, which do not lead to chain growth.
Thus, the general conclusion is that, although polyacetylenes can
be formed by the interaction of small acetylenic radicals with
acetylenic molecules, other considerably more facile reactions
must be responsible for the very rapid formation of carbon which
occurs, for example, in sooting flames.

Literature Cited

(1)   Knox, K., Norrish, R.G.W. and Porter, G., J. Chem. Soc.(1952)
      1477.
(2)   Greene, E.F., Taylor, R.L. and Patterson, W.L., J. Phys.Chem.
      (1958) 62, 238.
(3)   Glick, H.S.   Seventh International Symposium on Combustion,
      p.98, Butterworths, 1959.
(4)   Skinner, G.B. and Sokoloski, E.M., J. Phys. Chem. (1960) 64,
      1028, 1952.
(5)   Kozlov, G.I. and Knorre, V.G., Combustion and Flame, (1962)
      6, 253.
(6)   Foner, S.N. and Hudson, R.L., J. Chem. Phys. (1953) 21, 1374.
(7)   Prescott, R., Hudson, R.L., Foner, S.N. and Avery, W.H.,
      J. Chem. Phys. (1954) 22, 145.
(8)   Bonne, U., Homann, K.H. and Wagner, H.Gg., Tenth Inter-
      national Symposium on Combustion, p.503. The Combustion
      Institute, 1965.
(9)   Hou, K.C.and Palmer, H.B., J. Phys. Chem. (1965) 69, 863.
(10) Homann, K.H., Mochizuki, M. and Wagner, H.Gg., Z. Phys.
      Chem. (1963) 37, 299.
(11) Homann, K.H. and Wagner, H.Gg., Ber. Bunsengesellschaft,
      (1965) 69, 20.
(12) Homann, K.H., Combustion and Flame, (1967) 11, 265.

(13) Homann, K.H. and Wagner, H.Gg., Eleventh International Symposium on Combustion, p.371. The Combustion Institute, 1967.

(14) Cullis, C.F., Hucknall, D.J. and Shepherd, J.V., Combustion Institute European Symposium (Sheffield 1973), p.111. Academic Press 1973.

(15) Cullis, C.F., Hucknall, D.J. and Shepherd, J.V., Proc. Roy. Soc. (1973) A335, 525 (1973).

(16) Tarr, A.M., Strausz, O.P. and Gunning, H.E., Trans. Faraday Soc. (1965) 61, 1946.

(17) Trotman-Dickenson, A.F. and Milne, G.S., "Tables of Bi-molecular Gas Reactions", NSRDS - NBS 9, 1967; Kerr, J.A. and Parsonage, M.J., "Evaluated Kinetics Data on Gas-phase Addition Reactions", Butterworths, London 1972.

(18) Homann, K.H., and Wagner, H.Gg., Proc. Roy. Soc. (1968) A307, 141.

26

Microstructure and Morphology of Carbon Blacks

L. L. BAN and W. M. HESS

Cities Service Co., Petrochemicals Research, Drawer #4, Cranbury, N.J. 08512

Carbon blacks exist in many diverse morphological
forms which make them ideal objects for electron micro-
scope study. Because of the advent of high resolution
electron microscopy, the microstructure of these
carbons can also be viewed in a completely new light.

X-Ray Diffraction Studies. Warren, from his
atomic radial distribution studies, indicated that
carbon blacks are not composed of three-dimensional
graphite crystals ($\underline{1}$). Instead, he proposed that they
are composed of small graphite-like layers with the
same atomic positions within the layers as in graphite.
He further inferred that the layers are parallel but
rotated around the C-axis. The theory of the diffrac-
tion of X-rays by random layer lattices developed by
Warren ($\underline{2}$), and applied by Biscoe and Warren to the
study of carbon blacks ($\underline{3}$) showed that these carbons
produced (00.ℓ) three-dimensional and (hk) two-
dimensional reflections. The position of the (00.ℓ)
reflections indicated that the layers were further
apart than in graphite (e.g., 3.35Å vs. 3.6Å). Crystal
size along the C-axis, L_c, was determined from the
(00.ℓ) reflections, notably from the (00.2) and (00.4),
using the Scherrer equation. Crystal size in the
plane of the layers, L_a, was derived from the (hk) (10)
or ($\underline{11}$) reflections. Major refinements now exist in
analyzing the diffraction patterns of carbons and a
large literature of the published findings exist ($\underline{4,5}$).
The recent developments in analyzing the atomic radial
distribution of carbons indicate that the layers are
much larger than one would obtain from the two-dimen-
sional (hk) reflections ($\underline{4}$).

358

Electron Microscope Studies.   Electron microscopy
of carbons proceeded with the assumption that the find-
ings of the X-ray L$_a$ and L$_c$ measurements were correct.
The electron microscope was used to locate these
crystallites.   One of the first to attempt to resolve
and locate crystallites in carbon black was Hall ([6]),
who formed dark field images with the (00.2) reflec-
tions.   He reported that the images of very large
thermal black particles showed a concentric orienta-
tion of crystallites, with the graphitic layers
parallel to the surface.   At the time Hall was not
able to determine whether a similar orientation
existed for small particle size carbon blacks.   Later
electron microscope studies on treated thermal carbon
blacks (e.g. oxidation and high temperature graphiti-
zation) supported the findings of Hall ([7]).   It was
not until the application of high resolution dark field
microscopy, however, that Hall's hypothesis was shown
to be valid for all types of carbon black in their
initial untreated state ([8], [9]).

High Resolution Electron Microscopy

Using high-resolution (lattice image) phase con-
trast microscopy, the graphitic layer lattice was
resolved in a heat treated carbon black (2600°C) by
the interference of the (00.2) diffracted beam with
the (000) beam (Figure 1) ([10]).   These images showed
the extensive bending and continuity of the layer
planes.   The imaging of layer planes in every type of
carbon black followed this initial study ([11], [12], [13]).
In Figures 2 and 3, the orientation of the graphitic
layers is apparent.   The layer planes appear to orient
around growth centers.   The earlier dark field images
of these carbon blacks only showed small segments of
the continuous layer structure (See Figures 4, 5).
The size of the layers varies, but does extend up to
several hundred Angstroms.   Also, many of the layers
continue from one growth center to the other.   The
shape of the layers appears to be either ribbon or
disc, which are distorted and warped.   The size of the
layers perpendicular to and at different angles of the
projected images can be as large as the projected
lengths shown.   Also, the size of the layers seems to
be independent of the radius of the growth centers.
The absence of layer detail close to and in the center
of the growth centers indicates that they are either
hollow or composed of disorganized carbon (possibly
mixed with some inorganic impurities).   From these
studies, we conclude that the primary microstructural
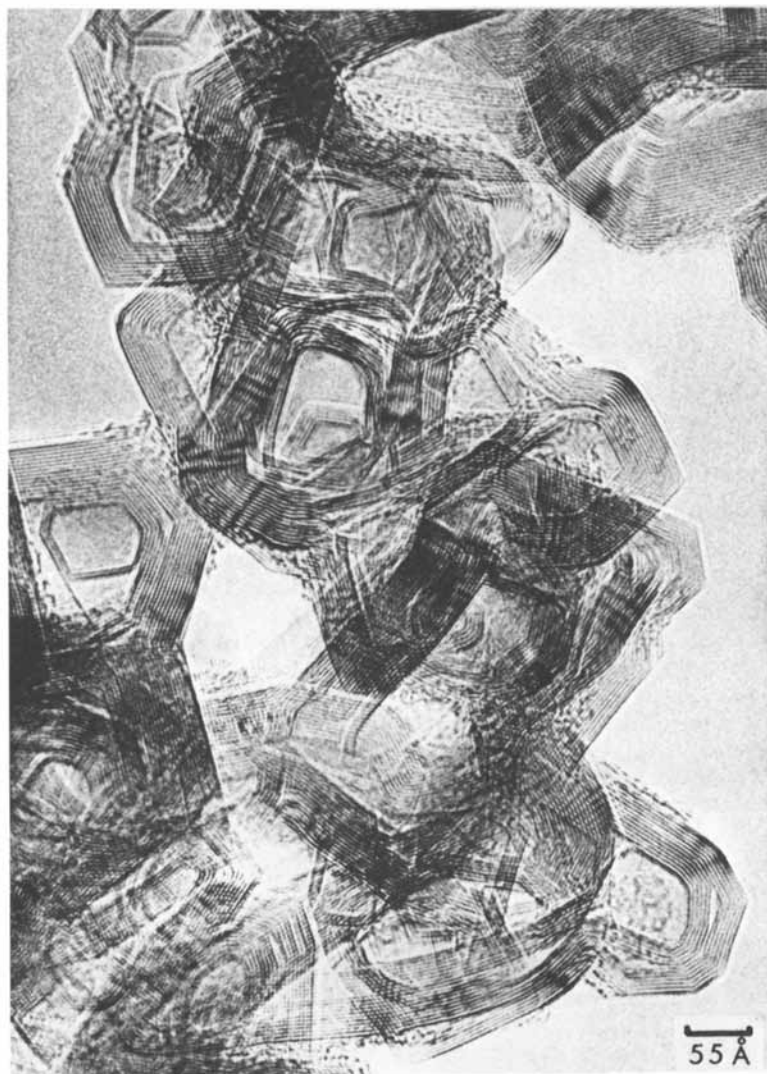
Figure 1. High resolution lattice image of a graphitized (3000°C) ISAF
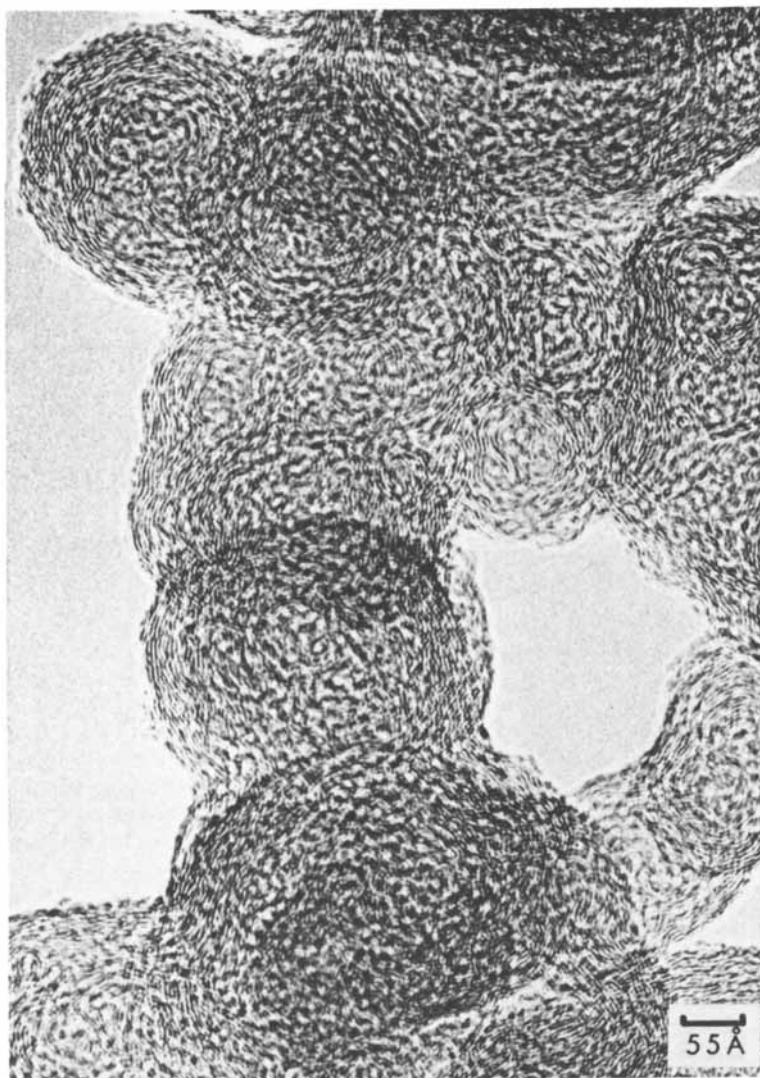
Figure 2. High resolution lattice image of an HAF
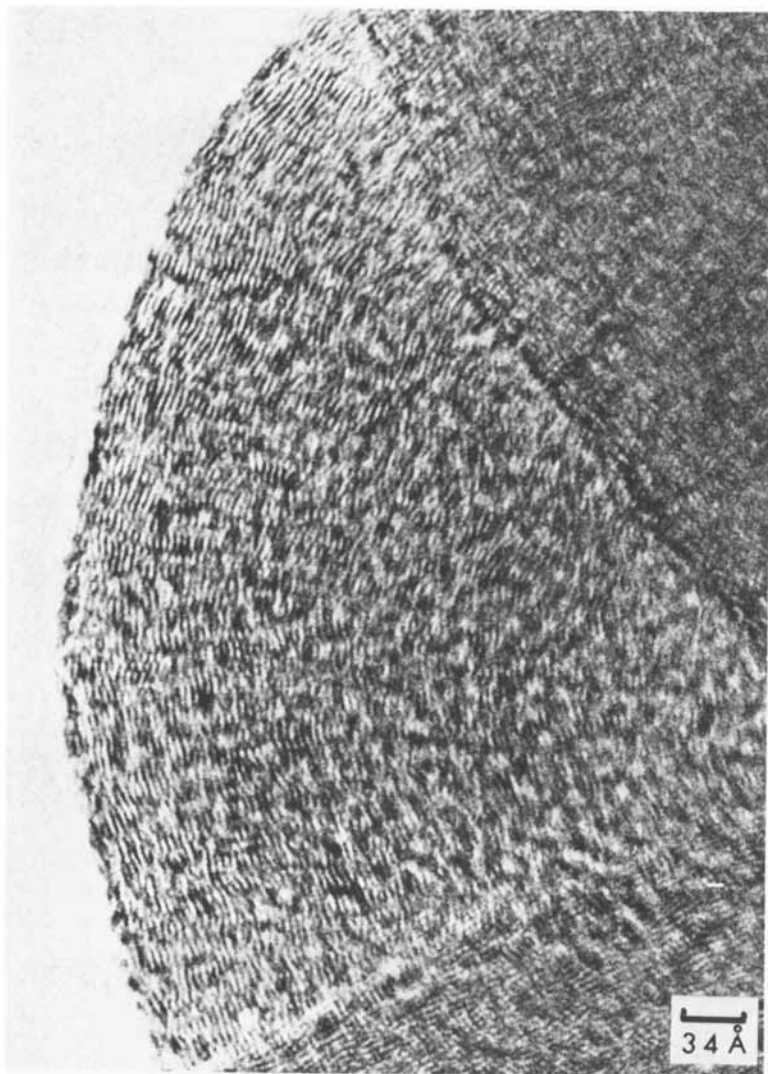
Figure 3. High resolution lattice image of MT
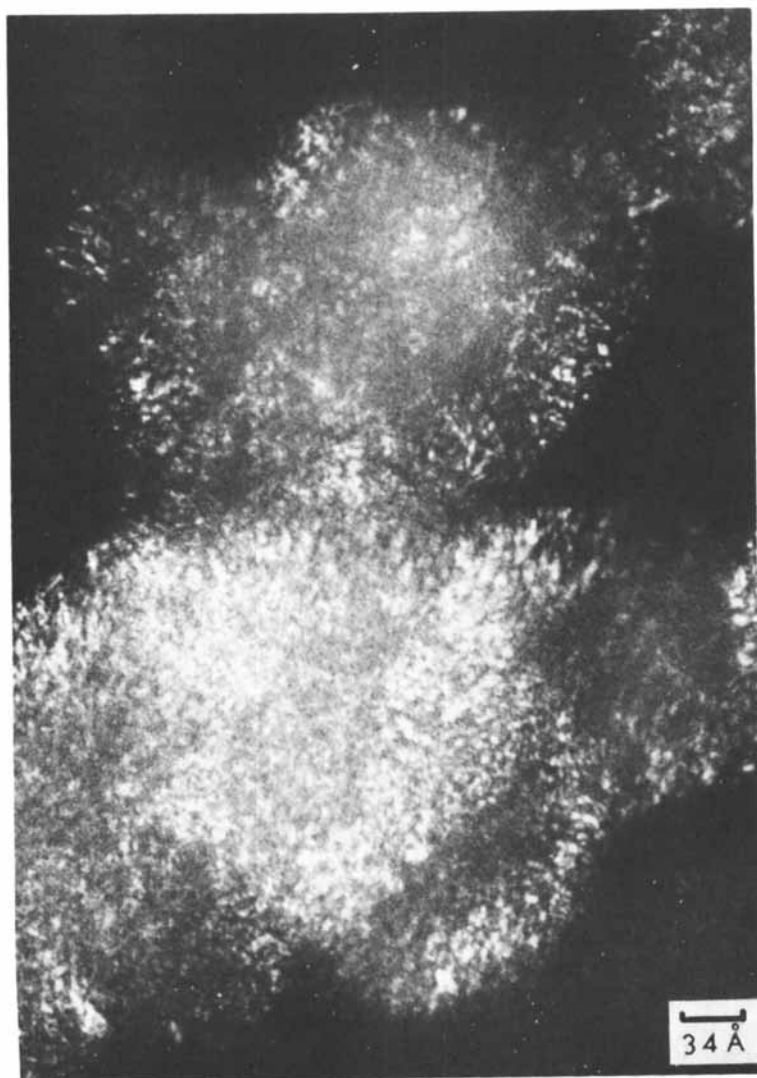
Figure 4. High resolution dark field (00.2) image of an HAF
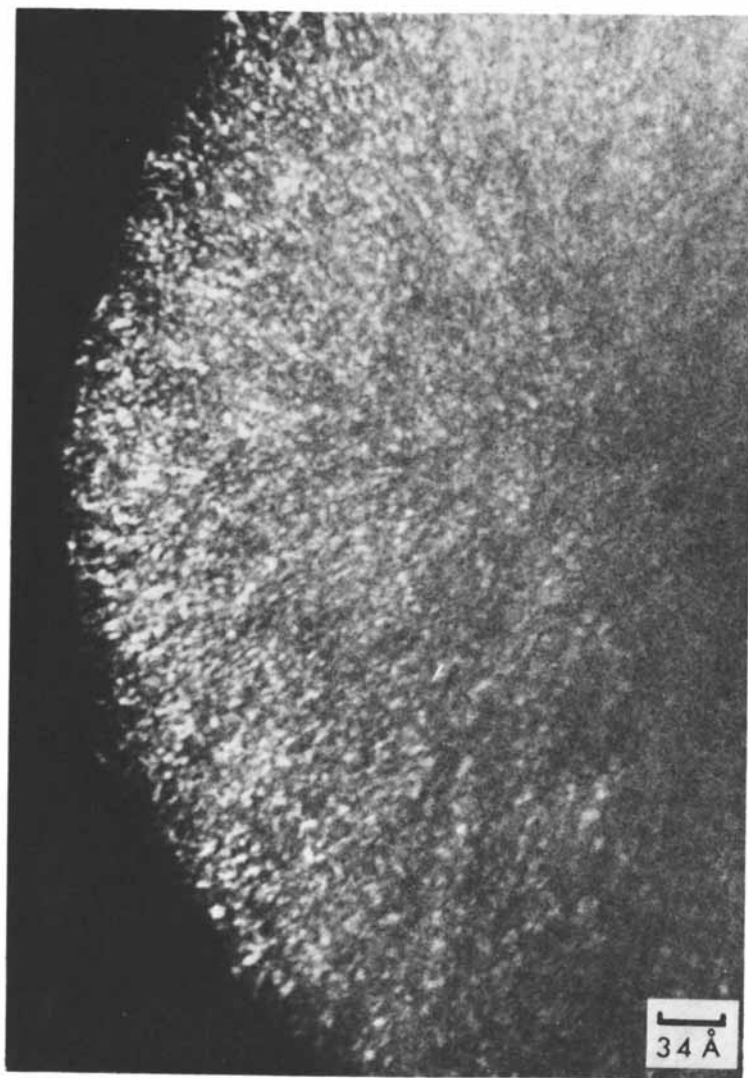
Figure 5. High resolution dark field (00.2) image of MT

units are the large distorted graphitic layers and not
the small 3-dimensional "crystallites" as had been
proposed by the X-ray diffraction studies. The thermal
black process tends to form single particles, with one
growth center. The furnace and channel black processes
predominately form irregular primary units with multi-
ple growth centers. These exist in a variety of shapes
which can be broadly grouped on the basis of spherical,
clustered or fibrous habits. These primary units can
now be considered as single graphitic paracrystals
which are composed of large distorted graphitic
layers (11, 14).
     The differences in microstructure, e.g. inter-
layer spacings and size of layers, do not seem to be
significant among different types of furnace blacks
(13). However, there appears to be a narrower dis-
tribution of interlayer spacings for the channel and
thermal blacks than for furnace blacks (12, 15).
During the incipient stages of graphitization (900-
1400°C) the layer planes in carbon blacks maintain
their orientation around the original growth centers.
The size of the layers does not appear to change, but
new types of distortions between layers and layer
groups are introduced (12, 15). Along with introduc-
tion of these new distortions, the bulk of the layers
tend to form straighter segments in comparison to the
untreated samples. The straightening of the graphitic
layers indicates that atomic rearrangement is taking
place within them. The large extent of the layers
seems to rule out growth by joining to neighboring
stacked layers. If layer growth does take place, it
most likely occurs between layers that are positioned
edge on, i.e., close to being in the same plane.

The Formation Of Carbon Blacks

     From their microstructure and general morphology,
carbon blacks appear to form from hydrocarbon droplets
(16, 17) which are most likely composed of small aro-
matic layers and possibly in a liquid crystalline
phase. The formation of the primary droplets appears
to be a homogeneous process (e.g. see the presence of
growth centers in Figures 2 and 3), while the encapsu-
lation of droplets by the addition of more aromatic
layers after collision has taken place is a heteroge-
neous process (18). It is unlikely that the growth
centers in furnace blacks exist in other than a liquid
state before "structure" formation, as indicated by
some workers (13, 19). The high resolution images in-
dicate that material flow has taken place between growth

centers before the completion of carbonization. Marsh
suggested recently that the liquid droplets are iso-
tropic and only in the process of further pyrolysis
do they form liquid crystals (20). However, Sweitzer
and Heller, in their experiments with the furnace
process, showed that the oily matter collected before
carbonization contained mostly large aromatic molecules
(17). This fact indicates to us that in the liquid
droplets these aromatic molecules align parallel to
each other in order to form the lowest free energy
state. They must also orient tangentially to the sur-
face, since carbonization is very rapid after the
collision of the liquid droplets. During carboniza-
tion, the polycyclic aromatic molecules can grow edge-
wise within the parallel layers by losing their edge
volatile components (e.g. hydrogen). The extent to
which the molecules can combine is probably governed
by their shape and the speed of carbonization. After
carbonization, it is also likely that the graphitic
structure contains many intralayer vacancies. Un-
fortunately, because of the absence of three-dimen-
sional ordering of the layers (turbostratic rotation),
these vacancies cannot be detected with high resolution
lattice imaging.

     It was indicated earlier that the formation of
liquid droplets appears to be homogeneous condensation
(18). However, one can also assume that there are
hydrocarbon ions present in the furnace flame which
can act as nucleating centers. In this case, conden-
sation is heterogeneous (21), which greatly complicates
the explanation of the formation of the liquid droplets
in hydrocarbon flames.

Size And Shape Of Primary Paracrystals

     The size and shape of the primary graphitic para-
crystals (units) of a carbon black are governed by the
reactor conditions under which it is made. Smaller
primary units (high surface area) are formed under
higher temperature conditions with diminishing contact
time. Irregular shape (e.g. high structure) is favored
by high concentrations of feedstock to increase the
tendency for collision and fusion of the hydrocarbon
droplets prior to carbonization.

     The characterization of carbon black unit size and
shape can now be accomplished very efficiently by
direct, automated electron microscope image analysis
(22, 23). The primary units may be rapidly classified
in terms of a number of geometric properties such as:
1. volume (V), 2. longest dimension (L), 3. average

width (W), 4. projected 2-dimensional area (A) and
5. perimeter (P). By combining some of these measure-
ments, shape information can be obtained. Linear
anisometry or form factor (F) is derived from L/W,
while 3-dimensional irregularity (relative to a sphere)
is obtained from $P^3/V \div 6\pi^2$. The latter has shown a
good correlation with the absorptive capacity (e.g.
DBP) of different carbon blacks (24).

Field specific image analysis provides only
average values for the above dimensional properties,
while feature specific analysis enables comparison of
different measurements on individual black units.
Feature specific analyses enable classification into
different shape categories (e.g. spherical, ellipsoi-
dal, fibrous) by means of pattern recognition tech-
niques (22).

Dry Black Measurements. Dry black samples (as
manufactured) may be prepared for image analysis by
ultrasonic dispersion in chloroform, followed by depo-
sition onto specimen grids coated with thin carbon sub-
strates (Figure 6). Typical measurements on a variety
of rubber grade carbon blacks are listed in Table I.
Unit size (volume) shows a particularly wide range
from below $2 \times 10^5 nm^3$ for the finest black (N-110) to
above $100 \times 10^5 nm^3$ for some of the coarser grades
(e.g. N-990). Linear anisometry varies from below 2.0
to above 4.0. Surface area (EMSA) is derived from
unit perimeter as related to volume and specific
gravity (25). This type of surface area determination
is particularly useful in that it can be employed to
measure the black surface area as it exists in a
rubber compound. Other types of surface area measure-
ments (e.g. nitrogen adsorption or the early EM
particle size model) are not capable of doing this.
Unit surface area distributional information also can
be obtained.

Morphological Breakdown. Whether or not carbon
black primary units actually fracture and reduce
their size during mixing into different systems such
as elastomers has been a subject of some controversy.
Gessler's studies, based on blacks extracted from
rubber compounds, indicated significantly lower oil
adsorption in comparison to the dry state (26).
Breakdown was greater for high structure blacks, and
also increased in the direction of higher black load-
ings. Gessler also hypothesized that active sites
were formed on the black surface as a result of
fracture of primary structure.
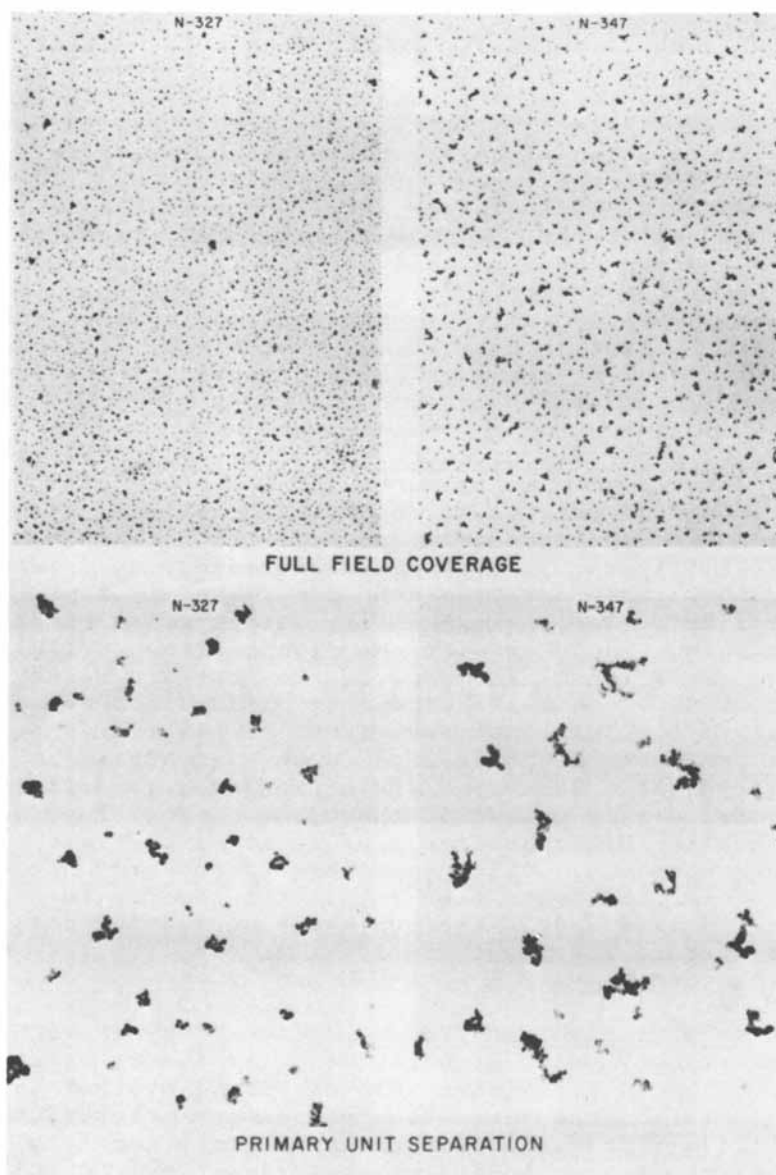
Figure 6.   Ultrasonic dispersions of HAF carbon blacks

Extensive morphological breakdown was also
reported by Medalia and Heckman based on electron
microscopy of black-elastomer mixtures (27). Their
work indicated higher breakdown for finer tread blacks
(ISAF) in comparison to coarser grades (HAF), inde-
pendent of DBP level.

Hess and coworkers demonstrated significant
morphological breakdown for a variety of carbon blacks
employing EM image analysis of microtomed vulcanizate
sections (28). All but very low DBP blacks (e.g.
N-327, N-770) showed a loss in unit length ranging
from about 30-40%. Studies on four polymer systems
(NR, SBR, BR and SBR/BR) were inconclusive in resolv-
ing breakdown differences related to polymer type.
Voet, Aboytes and Marsh (30) reported similar reduc-
tions in unit length in their EM studies on high
structure blacks in SBR (39). However, their inter-
pretation of the results differed quite markedly.
They attributed the change to a reduction of the so-
called secondary carbon black structure caused by
physically bonded black units, rather than actual
fracture of the primary units. We disagree with this
conclusion because of the magnitude of the changes
that have been recorded. Ban, et al. have also
resolved actual primary unit fracture in rubber by
means of high resolution electron microscopy (30).
It is difficult, however, to accurately measure the
total extent of fracture because one can never fully
eliminate microagglomeration of carbon black in the
dry state. Therefore, rather than argue the semantics
of what constitutes the true primary state of a carbon
black, it appears more reasonable to specify the con-
ditions under which the sample was prepared and
measured, i.e., ultrasonic dispersion of dry black,
microtomed section of a particular vehicle, etc.

Improved Methods For Analyzing Blacks In Rubber.
About 90% or more of the world's total carbon black
production (now in the range of 7 billion pounds) is
utilized in rubber applications, much of this being
automotive. It is not surprising then, that the
majority of the studies on blacks in end use applica-
tions apply to rubber.

Two new methods for the analysis of blacks in
elastomer compounds were introduced during 1973 and
1974. These are the thin layer pyrolysis and dis-
persed carbon gel techniques for separating the black
from the polymer (31, 30). The thin layer pyrolysis
technique can be applied to either vulcanizates or
raw stocks and is a modified version of the standard

ASTM pyrolysis procedure for rubber (32). Pyrolysis
is carried out slowly on microtomed sections (10-15μ
thick) of the compound to minimize sintering due to
carbonization. However, the latter cannot be
eliminated completely and weight average dimensional
properties were found to be the most suitable for
characterizing different blacks in comparison to the
dry state (31). The method appears to be the best
developed to date for identifying unknown carbon
blacks in vulcanizates and is also useful for compar-
ing the microagglomeration and network forming
characteristics of different blacks (25). The dis-
persed gel procedure is based on ultrasonic separation
of the carbon black primary units from the final raw
stock in a good solvent. This is generally accom-
plished using samples prepared by the procedure for
measuring bound rubber (e.g., overnight benzene
swelling of small bits of the compound in wire
baskets). The gel is readily broken down ultrasonical-
ly and separated into the primary black units that
exist in the mixed compound. A typical gel dispersion
for a high structure HAF carbon black, in comparison
to the dry state, is illustrated in Figure 7. The gel
specimen was pyrolyzed to remove any residual polymer.
A significant reduction in the unit size of the black
is apparent.

     The dispersed gel procedure thus far appears to
be the most accurate for obtaining black morphological
information in rubber. It is less influenced by micro-
dispersion effects in comparison to thin layer pyroly-
sis and is not subject to the contrast and orientation
problems associated with the direct microtome section-
ing approach (28).

     The relative breakdown characteristics (% retained
average unit volume in comparison to the dry state) of
a series of HAF blacks of varied DBP absorption, are
illustrated in Figure 8. The blacks are compared at a
70 phr loading in SBR-1712 and a 70/30 blend of SBR-
1712 and BR (both systems containing 37.5 phr of oil).
Breakdown increased in the direction of higher DBP
absorption and, for all but N-326, was higher in BR/OEP.
The polymer effect on breakdown appears to be attribut-
able to a higher black-polymer interaction with BR,
i.e., strong bonding to the polymer favors breakage
of the black units and less tendency toward micro-
agglomeration (30). However, no conclusive relation-
ship between black breakdown and interaction was
established when a variety of conventional and improved
tread blacks were compared in this BR/OEP formation (25).
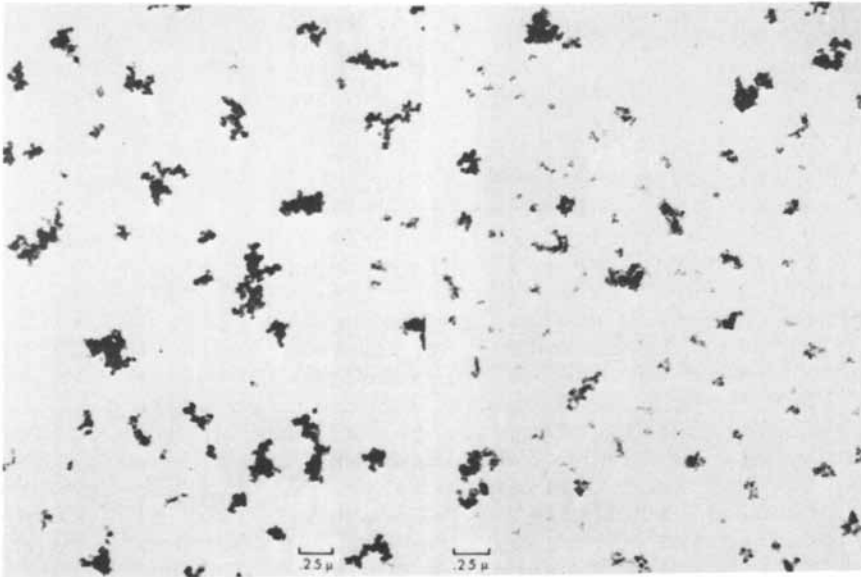
Figure 7. Morphological breakdown of EX-1 (155 DBP) in SBR-1500
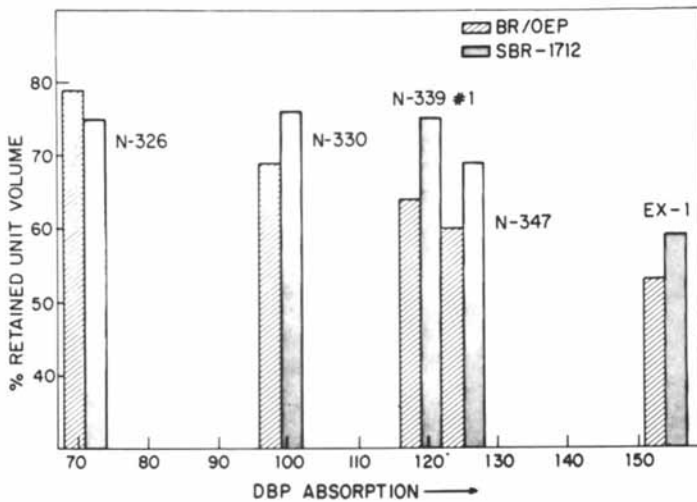
Figure 8. Relative breakdown of HAF carbon blacks as a function of DBP absorption

The dimensional characteristics for some of these blacks are listed in Table II, which can be compared to Table I (dry blacks) for the magnitude of the change.

Carbon Black Surface Activity

Following its morphological properties, the surface activity of a carbon black is its next most important characteristic, but remains somewhat vague in definition. Many different types of oxygen functional groups have been identified on the black surface. However, their significance has been questionable, with the exception of black usage in certain polar paint and ink vehicles and in low unsaturation rubbers in the presence of a chemical promotor (33, 34). The heterogeneity of the surface graphitic layer structure is known to be important in the bonding of carbon blacks to different polymers, at least from a physical standpoint (35). However, direct high resolution electron microscopy has not yet provided a suitable quantitative technique for measuring surface activity differences among most commercial blacks. On the other hand, high temperature heat treatment (partial graphitization) of any carbon black is known to drastically lower its surface activity. Any changes in black end use performance as a result of heat treatment, were associated with concomitant changes in the graphitic layer structure which could be resolved by high resolution electron microscopy (9).

To date, the most successful methods of assessing carbon black surface activity or interaction are those relating to specific systems in which the black has been mixed. Again, most of the efforts have been directed at elastomer systems. The bound rubber test measures that portion of the polymer that has been insolubilized during mixing (36, 37). Vulcanizate modulus changes as a function of the partial graphitization of a black have also been used to define its "activity index" (9, 38). Direct studies on black-polymer adhesion have been carried out by means of EM analysis of extraction replicas of vulcanizate specimens under strain (39).

All of the above procedures are either limited in their sensitivity or are also influenced by other factors that are not related to carbon black surface activity. A more direct measure of black interaction in elastomer systems can now be obtained by measuring the amount of polymer remaining on the black surface in the dispersed carbon gel (30). The change in the

HIGH RESOLUTION ELECTRON MICROGRAPHS
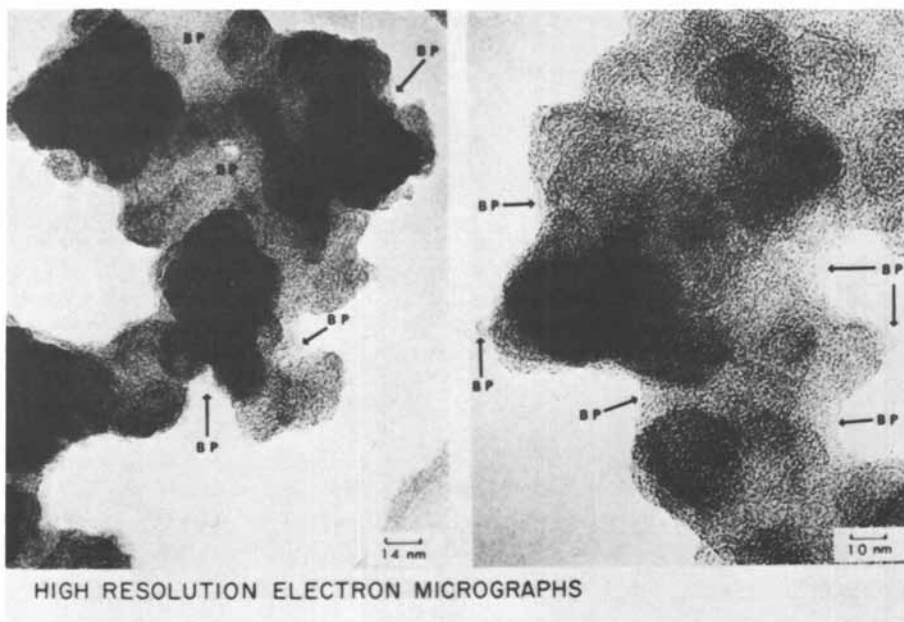
Figure 9.   Dispersed carbon gel showing residual adsorbed polymer.   High resolution electron micrographs.

TABLE I
MORPHOLOGICAL PROPERTIES OF RUBBER GRADE CARBON BLACKS
IN DRY STATE

ASTM NO.	$V \times 10^{-3} (nm^3)$	L(nm)	W(nm)	F	P^3/V	EMSA($M^2/g.$)
N-121	284	157	40.2	3.91	8.41	134
N-110	235	139	39.5	3.51	6.71	144
ISAF Imp.	310	152	41.7	3.65	6.55	119
N-220	288	145	40.9	3.55	6.25	119
N-339	423	180	43.1	3.99	8.61	105
N-347	611	203	49.2	4.13	9.30	94
N-330	570	187	51.2	3.65	6.40	85
N-326	336	145	47.9	3.02	4.45	89
N-550	6888	431	108.4	3.98	7.52	41
N-601	4292	314	106.2	2.96	3.65	37
N-660	9142	453	125.8	3.60	6.15	32
N-765	11382	502	132.6	3.79	6.21	32
N-770	6327	348	120.4	2.89	3.41	29
N-761	8017	363	135.1	2.69	2.82	24
N-990	11847	320	174.6	1.83	1.10	11

(NUMBER AVERAGE VALUES FOR DIMENSIONAL MEASUREMENTS)

TABLE II

MORPHOLOGICAL PROPERTIES OF IMPROVED AND CONVENTIONAL TREAD BLACKS
IN A 70/30 SBR-1712/BR COMPOUND

ASTM. NO.	$V \times 10^{-3} (nm^3)$	L(nm)	W(nm)	F	EMSA($M^2/g.$)	T(nm)
N-121	267	144	37.4	3.86	141	3.8
N-110	188	123	36.7	3.35	137	2.5
ISAF Imp.	252	134	39.3	3.36	128	3.4
N-220	221	129	38.0	3.38	125	2.7
N-339	351	161	44.0	3.66	111	2.7
N-347	460	180	47.3	3.81	98	1.9
N-330	420	159	47.8	3.33	89	1.4
N-326	246	129	45.2	2.86	86	0.6

(NUMBER AVERAGE VALUES FOR DIMENSIONAL MEASUREMENTS)

chord length distribution from image analyses is used to obtain the average polymer layer thickness, T. The value of T is calculated as half the difference in the mean chord (average width) of the black units before and after pyrolysis. The distribution of T is non-uniform as illustrated by high resolution electron micrographs in Figure 9 and also from measured changes in the specific shape of the black units following pyrolysis (25, 22). The frequency % increase from shape category 2 (ellipsoidal) to types 6, 7 and 8 (fibrous), following pyrolysis, is indicative of significant polymer removal from concave regions on the unit surfaces. A uniformly distributed surface polymer layer would not cause any shape category changes.

The average values of T in SBR and SBR/BR blends range from about 0.5 nm for inactive graphitized blacks (and very low DBP types) to above 3.0 nm for many of the improved tread grades (Table II). T increases (to a limiting value) as a function of increasing black loading and mixing time and decreasing extender oil content. Measurably higher values were obtained in a 70/30 SBR-1712/BR blend in comparison to SBR-1712 alone, both systems containing the same black and oil content.

Problems That Remain

A detailed knowledge of carbon black surface interaction is still lacking. A complete understanding of surface microstructure is necessary for a better understanding of interaction phenomena. At the present time, high resolution electron microscopy is limited to projections of the microstructure and surface detail cannot yet be resolved in these images. The formation mechanism of carbon blacks in high temperatures furnaces is still a challenging problem. We feel that a complete understanding of how carbon blacks form would be a great asset to the industry both scientifically and economically.

LITERATURE CITED

1. Warren, B.E., J. Chem. Phys.,(1934), 2, 551.
2. Warren, B.E., Phys. Rev.,(1941), 59, 693.
3. Biscoe, F. and Warren, B.E., J. Appl. Phys. (1942) 13, 364.
4. Ergun, S., in Walker, P.L. ed., "Chemistry and Physics of Carbon", Vol. 3, p.211-288, Marcel Dekker, New York, 1968.

5. Rouland, W., in Walker , P.L. ed., "Chemistry and
    Physics of Carbon", Vol. 4, p. 1-84, Marcel
    Dekker, New York, 1968.
6. Hall, C.E., J. Appl. Phys., (1948), 19, 271.
7. Heckman , F.A., Rubber Chem. Technol., (1964),
    37, 245.
8. Hess, W.M. and Ban, L.L. in R. Uyeda ed.,
    "Electron Microscopy", Vol. 1, p. 569, Maruzen,
    Tokyo, 1966.
9. Hess, W.M., Ban, L.L., Eckert, F.J., and
    Chirico, V.E., Rubber Chem. Technol., (1968),
    41, 356.
10. Heindenreich, R.D., Hess, W.M. and Ban, L.L., J.
    Appl. Crystl., (1968), 1, 1.
11. Ban, L.L. and Hess, W.M., 9th Biennial Conf. of
    Carbon, Columbus, Ohio, Battelle's Laboratories:
    Defense Ceramic Inf. Center, p. 162-163, 1969.
12. Ban, L.L., in M.W. Roberts and Thomas, J.M. ed.,
    "Surface and Defect Properties of Solids",
    Vol. 1, p. 54-91, The Chemical Society (London),
    1972.
13. Marsh, P.A., Voet, A., Mullen, T.J., and Price,
    L.D., Carbon, (1971), 9, 797.
14. Burgess, K.A., Scott, C.E. and Hess, W.M., Rubber
    Chem. Technol., (1971), 44, 230.
15. Ban, L.L. and Hess, W.M., 10th Biennial Conf. of
    Carbon, Columbus, Ohio, Battelle's Laboratories:
    Defense Ceramic Inf. Center, p. 159-160, 1971.
16. Grisdale, R.O., J. Appl. Physics,(1953), 24, 1082.
17. Sweitzer, C.W. and Heller, G.L., Rubber World,
    (1956), 134, 855.
18. Lahaye, J., Prado, G., and Donnet, J.B., Carbon,
    (1974), 12, 27.
19. Donnet, J.B., Lahaye, J., Voet A., and Prado,
    G., Carbon, (1974), 12, 212.
20. Marsh, H., Carbon, (1973), 11, 254.
21. Pound, G.M., J. Phys. Chem. Ref. Data, (1972),
    1, 119.
22. Hess, W.M., McDonald, G.C. and Urban, E., Rubber
    Chem. and Technol., Vol. 1 (1973), 46, 204.
23. Hess, W.M. and McDonald, G.C., ASTM, STP-553,
    1974.
24. Ulmer, J.D., Hess, W.M. and Chirico, V.E., Rubber
    Chem. and Technol., No. 3 (1974), 47, 629.
25. Hess, W.M., Chirico, V.E., Ban, L.L. and Ulmer,
    J.D., "The Influence of Black Morphology and
    Elastomer Interaction on Reinforcement Proper-
    ties", Intl. Rubber Conf., Munich, Germany,
    Sept. 1974.

26. Gessler, A.M., Rubber Chem. and Technol.,(1970), 43, No. 5, 943.
27. Heckman, F.A., and Medalia, A.I., J. of the IRI, (1969), 3, No. 2, 66.
28. Hess, W.M., Chirico, V.E., and Burgess, K.A., Kautschuk u. Gummi Kunststoffe,(1973), 26, 344.
29. Voet, A, Aboytes, P. and Marsh, P.A., Rubber Age (1969), 101, 78.
30. Ban, L.L., Hess, W.M., and Papazian, L.L., Rubber Chem. and Technol., No. 3 (1974), 47, 858.
31. Hess, W.M., Chirico, V.E., and Burgess, K.A., "Morphological Characterization of Carbon Black in Elastomer Vulcanizates", Intl. Rubber Conf., Prague, Czechoslovakia, Sept., 1973.
32. Banminger, B.B. and Pon Hon, F.C.J., Supplement to Back of ASTM Standards, Part 9, 1960.
33. Gessler, A.M., Rubber Age (1960), 87, 64.
34. Ford, W.E., Callan, J.E. and Hess, W.M., ibid., 92, (1963), No. 5, 738.
35. Sweitzer, C.W., Burgess, K.A. and Lyon, F., Rubber World (1961), 143, No. 5, 73.
36. Dannenberg, E.M., Rubber Age (1966), 98, No. 9, 82; No. 10, 81.
37. Gessler, A.M., ibid.,(1969), 101, No. 12, 54.
38. Hess, W.M., Burgess, K.A., Lyon, F., and Chirico, V.E., Kautschuk u. Gummi Kunststoffe (1968), 21, 689.
39. Hess, W.M., Lyon F. and Burgess, K.A., ibid., (1967), 20, No. 3, 135.

27

Review of Electrical and Thermal Properties of Carbon and Graphite

JOHN A. WOOLLAM

NASA Lewis Research Center, Cleveland, Ohio 44135

This paper reviews some of the electrical and
thermal properties of ordered, and partially ordered
carbons. Included are the following areas: 1) Conduc-
tion in crystalline graphite, and highly oriented pyro-
lytic graphite; 2) Conduction in pregraphitic carbons,
including negative magnetoresistance effects; 3) Thermal
and other electronic properties of pregraphitic carbons,
especially the work of Mrozowski and collaborators;
4) Josephson Junction-like behavior, as well as elec-
tronic switching, in carbon films; and 5) Compound
conductors formed from carbon, which have useful and/or
scientifically interesting properties, such as compound
superconductors, and high conductivity intercalated
fibers. The purpose of this paper is to put together
information and references on research not previously
reviewed, and to include topics which may not be famil-
iar to persons active in other aspects of carbon
research.

The processes for formation of various carbons
from solid or liquid hydrocarbons have been studied for
many years (1). Generally, carbons are either graphi-
tizable (sometimes called soft carbons), or non-graphi-
tizable (called hard carbons, glassy carbons, or
vitreous carbons). By graphitization is meant the
formation of the layered hexagonal crystal structure of
graphite (figure 1) and the alignment of regions having
this structure. This alignment is usually brought
about by applying heat and/or pressure. A non-graphi-
tizing carbon does not achieve overall alignment by
heating. Using electron microscopy, Marsh and colla-
borators have bound the structure of a non-graphitizing
carbon to be interlinking planes of aggregates in a
very tangled geometry, as shown in figure 2 (2). It
has been found that almost all graphitizing carbons go

378
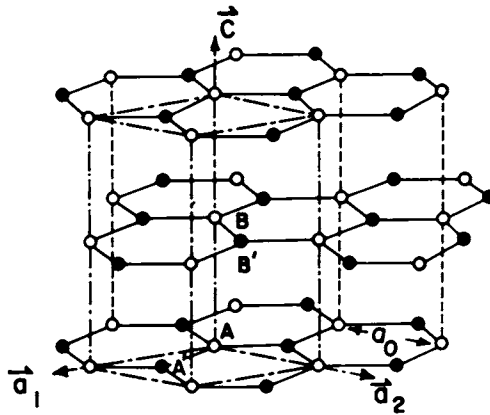
Chemistry and Physics of Carbon

Figure 1. Hexagonal structure of crystalline graphite showing ABABA layering, $\bar{c}$ and $\bar{a}$ axes (5)
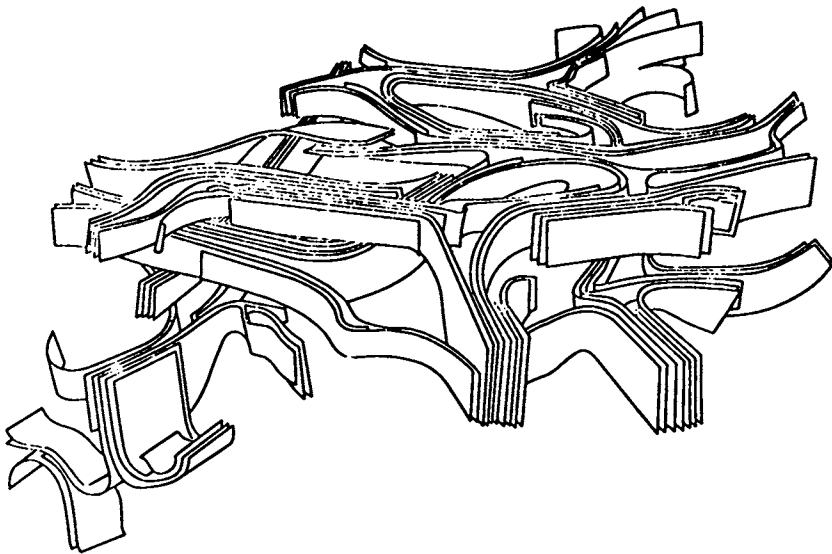
12th Biennial Conference on Carbon

Figure 2. Schematic from electron microscope observations of PVDC (glassy) carbons, HTT 2973°K (2700°C) (2)

through a "mesophase," or liquid crystal phase upon heating of liquid hydrocarbons (called "pitch") to 673 to 773 K (400 to 500 C)(3).

The maximum temperature to which carbon is heated is called the heat treatment temperature (HTT). In graphitizable carbons there is a change towards the more ordered graphite structure as HTT is increased, or as the time at any one HTT increases. After a long enough time (usually several hours) at one temperature, the structural changes are very much slower than at first. For this reason, as long as several hours are taken for heat treatment, the structure and properties are determined mainly by the HTT. Heat treatment is usually done at atmospheric pressure and can be made up to about 3773 K (3500 C) before substantial carbon sublimation takes place. Properties, such as the X-ray line structure, or electronic properties like the Hall effect, can be reproducibly related to the HTT.

In most carbon, hydrogen, oxygen, and nitrogen are removed from the starting hydrocarbon (pitch) after heat treatment to about 1473 K (1200 C). By 2273 K (2000 C) the material is quite pure, but further purification can be accomplished by chemical treatment.

In addition to the method of heat treating pitch, well graphitized carbons can be formed by pyrolysis (usually of methane) onto substrates above 2273 K (2000 C), followed sometimes by annealling under pressure. This procedure leads to a highly oriented graphite called pyrolytic graphite (PG). Some of the most highly perfected PG is called HOPG by its developer A. Moore (4).

The ability to uniformly and irreversibly change the degree of structural order as a function of HTT over a range of 2000 degrees K is peculiar to carbon, and makes carbon an opportune system for the study of the physics and chemistry of disordered solids.

Three basic types of carbon: 1) graphitizable, 2) non-graphitizable (glassy), and 3) pyrolytic (especially HOPG), will appear in the five topic areas listed at the beginning of this introduction. These five areas will now be discussed.

Conduction in Highly Oriented Graphite

Highly oriented graphite can be single crystalline (found in nature only), as well as polycrystalline. Because periodicity of the lattice greatly simplifies the theory of electronic properties, single crystal graphite behavior is relatively well understood.

Several good reviews of single crystal theory are
available (5,6), so single crystal theory will be
discussed mainly in its relation to HOPG graphite
(highly oriented pyrolytic graphite).

The atomic structure of single crystal graphite is
shown in figure 1. The $\bar{a}_1$ and $\bar{a}_2$ axes are in the basal
plane, and the $\bar{c}$ axis is perpendicular to the planes.
HOPG graphite is well characterized by specifying the
grain size in the basal plane, and the half angle of
the distribution of crystallite $\bar{c}$ axis directions. The
half angle is defined as the angular width at half
maximum intensity of the (002) diffracted X-ray line
after uniform rotation of the X-ray beam direction (4).
Typical HOPG specimens have grains up to 100μm across
(as measured by electron microscopy). The $\bar{c}$ axis dis-
tribution half angles of the best samples have half
angles as low as 0.2 degrees. Larger grains can be
obtained if larger angular distributions can be
tolerated (4).

The high degree of anisotropy in the structure of
single crystal graphite is reflected in the anisotropy
of its electrical and thermal properties. For example,
the ratio of electrical conductivity parallel to the
layers to that perpendicular is highest at low tempera-
ture and can be as high as 10^5 at cryogenic tempera-
tures (5). The corresponding ratio in the thermal
conductivity is as high as 300 but is higher at room
temperature than at cryogenic temperatures (7), and
generally has a maximum near 100 K.

HOPG and natural single crystal (NSC) graphite
are semimetals with less than 0.04 electron volt over-
lap of valence and conduction bands. From quantum
oscillatory galvano- and thermomagnetic (8,9), and
diamagnetic effects (10), and from recent magneto-
reflection studies (11), it is known that the elec-
tronic energy band structures of HOPG and NSC graphite
are nearly identical. Particularly sensitive evidence
for this comes from studies of minority carriers by
quantum oscillatory effects (12). An example of
minority carrier oscillatory effects is shown in
figure 3 where the thermoelectric power is plotted as
as function of field applied parallel to the $\bar{c}$ axis.
The thermoelectric quantum effects have the same
origins as the Shubnikov-de Haas effects (13), but are
more pronounced than Shubnikov-de Haas effects in
graphite. The higher frequency oscillations in figure
3 are from the majority carriers, the lower frequency
ones from minority carriers (marked by arrows) and are
superimposed. For small angles between the field and

the average HOPG layer plane direction, the majority
oscillation amplitudes are smaller than the minority
oscillations, making the study of minority effects
accurate and convenient. The data in figure 3 are on
a HOPG sample, and when these and other data are com-
pared to results on a NSC, it is concluded that the
energy band structure of HOPG and NSC are the same.

The energy band structure was calculated by
Slonczewski and Weiss (14), and parameterized by
McClure (15), (and is thus called the SWM band model).
The calculated bands near the vertical edge of the
Brillouin zone, as well as the Brillouin zone, are
shown in figure 4a and b (6), where energy is plotted
against momentum vector along k_z (parallel to $\overline{c}$) and
along k_x near the Brillouin zone edge (in the basal
plane). The valence and conduction bands are degene-
rate along E_3 at $k_x=k_y=0$ where k_x and k_y are measured
from the zone edge. Thus graphite would be a zero
band gap semiconductor with touching valence and con-
duction bands for all k_z values, if it weren't for the
small band overlap, given by $|2\gamma_2|$. This small over-
lap gives pure graphite metallic-like behavior, where
there are nearly equal electron and hole carrier
densities of about 10^{24} per cubic meter.

The overlap of the E_2 band with the E_3 bands is
small, and this gives rise to minority carriers near
the H points of the Brillouin zone.

The seven parameters of the SWM model have been
determined quite accurately by experiment (16), with
most of the last major discrepancies being explained
by including "trigonal warping" of the bands (17, 18,
19). The best values for these parameters, and their
physical interpretation are presented in Table I (16).

Electrical conductivity, σ, is determined by
two factors: carrier concentration n_e, n_h; and
mobility μ_e, μ_h; as expressed by (20):

$$\sigma = n_e e \mu_e + n_h e \mu_h \tag{1}$$

where the e subscript stands for electron and h for
hole in a two band system. The values of the quantities
in equation (1) depend on direction of current flow
relative to the crystal axes, but current will be
assumed to be in the basal plane for this discussion.
Carrier concentration is determined by band structure
for pure material, as well as by impurity doping for
non-pure material (21). To first order, the main
effect of impurities is to change the Fermi level
relative to the E_3 bands, and the relative number of

THERMOELECTRIC
POWER,
(ARBITRARY
SCALE)

MINORITY CARRIER
OSCILLATION MINIMA

0   .4   .8   .12   .16   .20   .24
MAGNETIC FIELD, TESLA
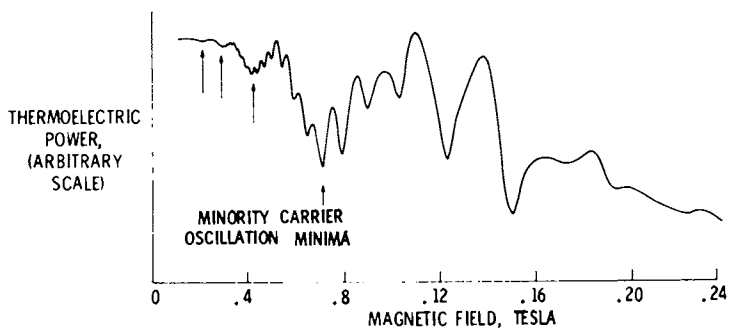
Physical Review

Figure 3.   *Thermoelectric power vs. magnetic field at 1.2 K in compressively annealed HOPG showing majority and minority carrier quantum oscillations superimposed* (12)
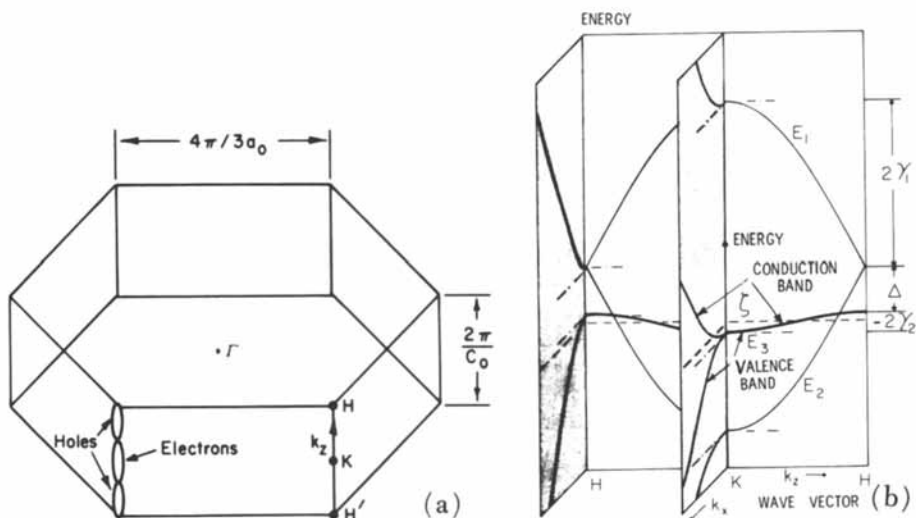
Figure 4.   *Brillouin zone of graphite (a) and energy bands of graphite (b) along edge of Brillouin zone. k_z is perpendicular to layers, k_x is in layer plane. Greek constants are given in Table I* (5,6).

TABLE I (From Reference 16)

Band Parameters--Their Order of Magnitudes
and Physical Origin

Band Parameter	Range of Magnitudes (electron volts)	Physical Origin
γ_0	$3.05 \rightarrow 3.20$	Overlap of neighboring atoms in a single layer plane
γ_1	$0.37 \rightarrow 0.41$	Overlap of orbitals associated with A and A' atoms located one above the other on adjacent layer planes
γ_2	$-0.018 \rightarrow -0.021$	Interactions between atoms in next nearest layers and from coupling between π and σ bands
γ_3	$.20 \rightarrow .34$	Coupling between the two E_3 bands by a momentum matrix element
γ_4	$.16 \rightarrow .25$	Coupling of E_3 bands to E_1 and E_2 bands by a momentum matrix element
γ_5	$\sim \gamma_2$	Interactions between second nearest layer planes. Introduction in E_1 and E_2 in second order of Fourier expansion to be consistent with E_3
Δ	$-0.02 \rightarrow 0.02$	Difference in crystalline fields experienced by A and B atoms

electrons and holes. For the remainder of this section
it is assumed that $n_e = n_h$ and the material is pure.
The second factor for determining σ is the mobility,
where

$$\mu_e = e\tau_e/m_e \qquad (2)$$

and where τ_e is the average time between collisions
and m_e^* is the "band" effective mass. At low tempera-
ture, τ_e is determined by defects and impurities and
is nearly temperature independent. At higher tempera-
ture τ_e is predominantly determined by phonon scatter-
ing. The effective mass is determined by the band
structure. In a magnetic field the conductivity is
tensorial even for a fixed direction of current flow,
and depends on magnetic field direction and magnitude,
as well as on n and μ .
       The average mobility, $\bar{\mu}$, is defined from

$$\bar{\mu} = \frac{1}{H}\left(\frac{\rho(H) - \rho(0)}{\rho(0)}\right)^{\frac{1}{2}} \qquad (3)$$

where $\rho(H)$ is the resistivity in a field H, for current
in the layer planes. Plots of $\bar{\mu}$ are shown in figure
5 as a function of temperature for a NSC, as well as
for HOPG graphite (5). The power law temperature
dependence results from in-plane and out-of-plane
acoustic phonon scattering. The low temperature (near
constant) dependence results from crystallite boundary
scattering and dislocation scattering, as discussed by
Sugihara and Sato (22) and by Spain (5). The smaller
the grain, or greater the number of defects of any
kind, the higher is the temperature below which mobili-
ty becomes constant.
       Looking then at the basal plane resistivity of
HOPG normalized to room temperature, $\rho \simeq 1/\sigma$ in zero
magnetic field, as shown in figure 6 (23), the tempera-
ture dependence is metallic-like for large grain size
HOPG and NSC (samples 4 through 14), and the resistivi-
ty drops by as much as a factor of 40 from 300 K to
4.2 K in some NSC samples (5). In figure 6 the
greatest resistivity drops are for the samples with
the lowest defect concentrations, and these result
from an increase of $\bar{\mu}$ which changes more rapidly
than the decrease in n as the temperature drops (5)
(see Equation 1). The sample with apparently the
least perfection (X-ray data is not available) is
labeled #1 and was prepared by methane pyrolysis and
pressure anneal to 3073 K (2800 C)(4). The best
pyrolytic sample (labeled #12 in figure 6) was
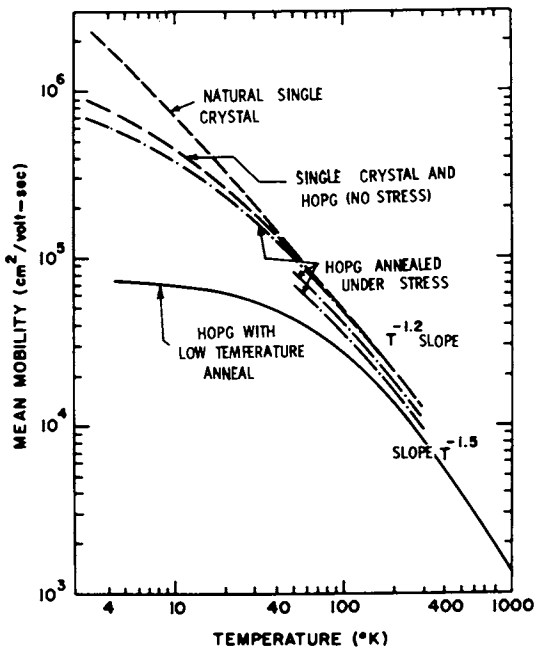
Chemistry and Physics of Carbon

Figure 5. Smoothed lines through experimental data of the log mobility $\bar{\mu}$ vs. log temperature for NSC (Soule) and several HOPG samples (5)
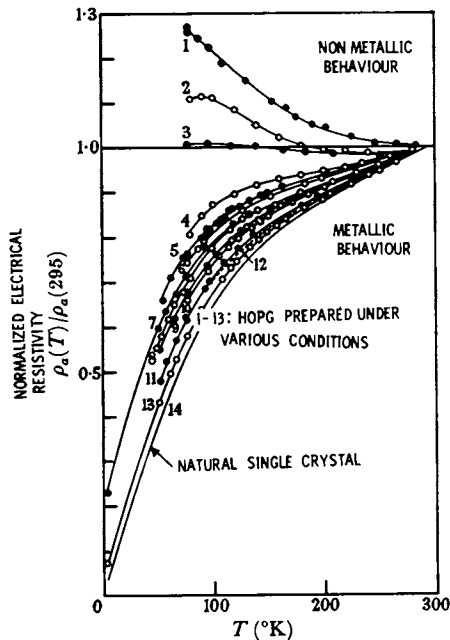
Proceedings of the Royal Society

Figure 6. Normalized resistance vs. temperature for various HOPG and NSC samples (23)

prepared from a stress recrystallization process called
ILPG by Moore (4). The highest perfection HOPG sample
yet found (21) has a 300 K to 4.2 K resistivity ratio
of 18, a factor of 2 less than that for the best NSC,
but a factor of 2 to 4 greater than commonly found (9).

In an intrinsic semiconductor, carriers must be
thermally excited (in absence of radiation) across an
energy gap to be effective in carrying current. This
results in a resistivity which increases as temperature
is reduced. The behavior in samples 1, 2, and 3 in
figure 6 is reminiscent of this type temperature depen-
dence, and these samples all had relatively low values
of temperature during preparations. That is, only HOPG
with high anneal temperature (above about 3073 K (2800
C)) have semimetallic conductivity. The possible exis-
tence of an energy gap for low anneal temperature pyro-
lytic graphite (PG) has been discussed (24) and is
debated (25). Klein (26) analyzed his resistivity data
on HOPG assuming the rise in ρ as T decreased was due
to the drop in n, rather than to the increase in μ.
There was difficulty with a fit of the data at low
temperature, however.

Conduction in Pregraphitic Carbons. Negative Magneto-resistance

In this section, I will discuss conduction in
graphitizable carbons produced by heating of petroleum
or coal tar pitch. Electron microscopy shows a gradual
increase in alignment of $\vec{c}$ axes and an increase in area
of the basal planes as a function of HTT (27, 28). The
key to understanding electronic behavior is probably
contained in the unusual structure of these incompletely
graphitized carbons.

A model for electronic energy band width as a func-
tion of HTT [for HTT between 373 K and 3473 K (100 C
and 3200 C)] in graphitizable carbons has been proposed
by Mrozowski, and this model shows band overlap for
HTT down to about 2473 K (2200 C), as seen in figure 7
(29). The increase of resistivity with decreasing
temperature, as observed for HTT below about 3073 K
(2800 C) is due to a temperature dependent scattering,
rather than to an energy gap phenomenon in this model.
Many experimental data have been compared with this
model. Mention should also be made of the ideas presen-
ted by Delhaes (46), which cover the region of the
question mark in figure 7.

A further complication occurs, as seen in figure 8
(30), which shows the onset of negative transverse
magnetoresistance for HTT less than about 2673 K
(2400 C). There is probably a negative component for
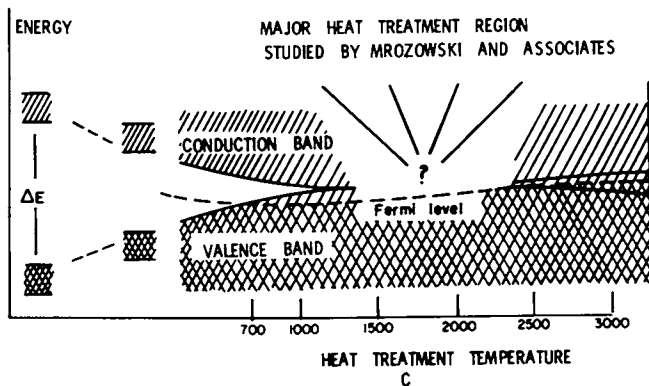
Carbon

Figure 7. Mrozowski band width model for graphitizable carbon with various HTT's (29)
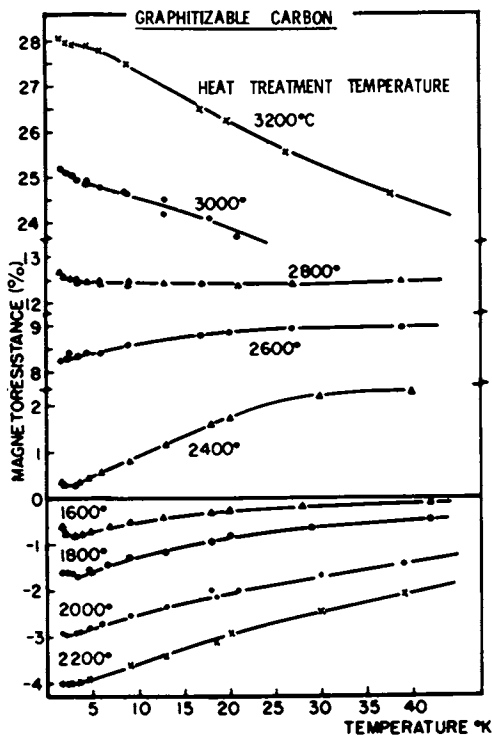
Carbon

Figure 8. Magnetoresistance of graphitizable carbon with various HTT's vs. temperature (20, 30)

the higher HTT's in figure 8. Other workers have found
negative magnetoresistance components (at low tempera-
tures and fields) in samples with HTT up to 3200 C.
(See also references 31 and 32.)

Negative magnetoresistance (MR) has been reviewed
by Delhaes (20) and will be only briefly summarized
here. The origins can be from several possible sources.
For specimens homogeneous on the scale of sample dimen-
sions, the origins of negative magnetoresistance (MR)
are in the change of n or μ with field. An appealing
mechanism is the presence of localized magnetic moments
in a narrow band, which affect scattering via exchange
coupling with itinerate conduction electron spins. The
application of a magnetic field reduces the conduction
electron scattering from magnetic spins because of
saturation of the localized moments by the field. As
covered in the next section, ESR has shown an increasing
number of localized spins in carbon with decreasing HTT
(33). Hishiyama, et al. (32) find evidence against this
interpretation: In neutron irradiated polycrystalline
graphite they find that negative magnetoresistance (and
the number of localized spins) increases with irradia-
tion dose, but does not go completely away upon anneal-
ling, even though the number of localized spins becomes
undetectable. In dilute alloys of transition metals in
noble metals an extremely small concentration of local-
ized spins causes negative MR (34). Negative MR is also
found in PG (24), and reference (24) discusses further
some of the possible origins.

Most industrially important carbons have HTT well
below 3073 K (2800 C), and among the more important pro-
perties are electrical and thermal conductivities.
Crystalline graphite conduction is relatively well
understood. The electronic properties of industrial,
or lower HTT carbon, is not nearly as well understood.
Some of the thermal and magnetic anomalies of low HTT
carbon will be discussed next.

Thermal and Other Properties of Pregraphitic and of Glassy Carbons

This section will discuss the work on thermal and
magnetic properties of carbons with heat treatment
temperatures (HTT) between 873 and 2273 K (600 and
2000 C). This includes especially the heat capacity,
ESR, and susceptibility studies. Two groups have been
very active in this area: Mrozowski, and Delhaes (29,33
35, 36, 37, 38, 39, 40). Numerous papers have
appeared, but the phenomena found have not been too

well understood, and no complete reviews have been made.

   A. <u>Experimental Results</u>. The theoretical, low
temperature specific heat of a nonmagnetic material
with free carriers has a temperature dependence given
by

$$C = \gamma T + \alpha T^3 \tag{4}$$

for $T \ll \Theta_D$ where T is temperature and Θ_D is the
characteristic Debye temperature and γ and α are
constants. The linear term is due to free carriers
and is linear by the following physical argument.
Because of the exclusion principle, the only electrons
which can gain energy are those within kT of the
Fermi energy, E_F. The number of these is the product
 $D(E_F)kT$, where $D(E_F)$ is the number of states per
unit energy at the Fermi energy. The thermally
excited carriers each have an energy increase of about
 kT. Thus the energy gain of the system is

$$U \simeq D(E_F)k^2T^2 \tag{5}$$

The heat capacity is thus

$$C = \partial U / \partial T \simeq 2D(E_F)k^2T \tag{6}$$

which is linear in T.
   The cubic term is the contribution from lattice
vibrations and is cubic because of the three dimension-
ality of the lattice.
   To determine γ and α , data are taken at cryo-
genic temperatures and plotted as C/T vs. T^2 which
should be a straight line with slope α and intercept
 γ . Plots of this type are shown in figure 9 for
graphitizable carbons for various heat treatment tem-
peratures between 873 and 3373 K (600 and 3100 C)(33).
Three major observations: 1) The coefficient α
decreases with increasing HTT. 2) Not so obvious in
figure 9 is that γ at first is about constant (HTT
600 to 800 C) and then decreases with increasing HTT.
Plots of γ vs. HTT are shown in figure 10 (33, 38).
If one studies electron spin resonance (ESR) the number
of magnetic spins contributing to the resonance can be
determined from the strength of the signal. Mrozowski,
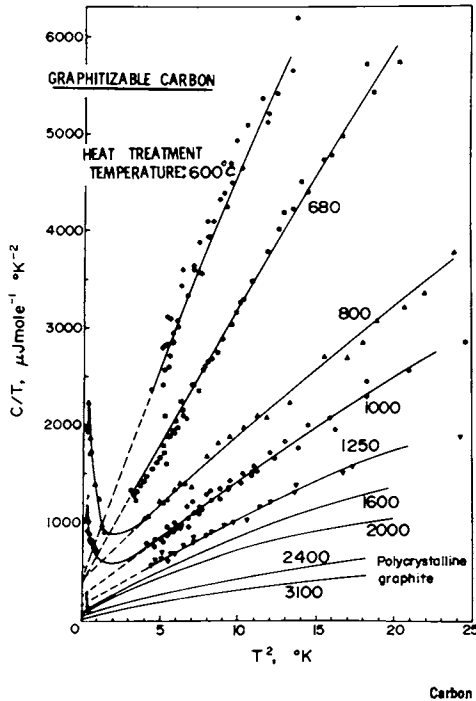
Carbon

*Figure 9. Heat capacity divided by tempera-
ture vs. T^2 for various HTT carbons. Data
points have been removed from best fits for
HTT 1600°–3100°C (33)*

Carbon
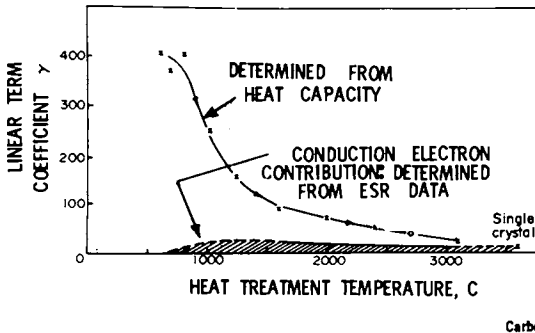
*Figure 10. Linear term coefficient γ in the heat
capacity and separation into free carrier and nonfree
carrier parts using temperature dependent ESR (33)*

et al. obtained an estimate of the γ term by studying
the temperature dependence of the ESR signal strength.
If they assume the localized magnetic spin centers obey
a Curie T^{-1} law, and the free carrier magnetic moments
are temperature independent, then the γ coefficient in
the specific heat can be obtained from the temperature
independent part of the ESR signal. (There can be
temperature independent contributions from local mag-
netic moments, and temperature dependent contributions
from free carriers (42), so this separation is an
approximation.) The ESR results are also shown in the
shaded area in figure 10. Thus, much of the linear
term is not due to free carriers, and the differences
are greater with lower HTT carbons. In a natural
single crystal, the ESR and heat capacity derived
γ 's agree with each other and with energy band
structure calculations; thus, the anomalies are not
intrinsic to crystalline graphite, but a result of the
structure of low HTT carbons.

The third major observation from figure 9 is the
rapid rise in C/T vs. T^2 at the lower temperatures.
The data actually go through a maximum below 1 Kelvin.
A plot of recent data on an expanded scale (figure 11)
shows the details of C/T peaks, where much of the heat
capacity anomaly is seen (44).

Results on glassy carbon are shown in figures 12
and 13 (37). Figure 12, like figure 9 (for graphitiz-
able carbon),shows a heat capacity anomaly at low
temperatures. The peak in GC is at lower temperatures
than for graphitizable carbon. Figure 13, like figure
10 (for graphitizable carbon), shows a maximum in γ
vs. HTT. However, the maxima are at very different
HTT. In soft carbon it occurs at about 873 K (600 C)
HTT and in GC one appears near 1973 K (1700 C) HTT.

To help reveal the origin of these peaks,
Mrozowski et al. neutron irradiated both soft and GC
carbon with various doses. Figure 14 shows results
for polycrystalline (high HTT) carbon. It was found the
γ term increased smoothly with irradiation. The
low temperature peak was larger for greater doses, and
the peak was not present in similar, but unirradiated
carbon. This showed that the peak was due to disorder
and not to impurities. The temperature locations of
the peak and qualitative features were essentially the
same for irradiated carbons as for carbons with various
HTT's, so peaks in both types of materials were attri-
buted to disorder and not to impurities; i.e.,
Mrozowski feels that both heat capacity peaks have the
same origin (25).
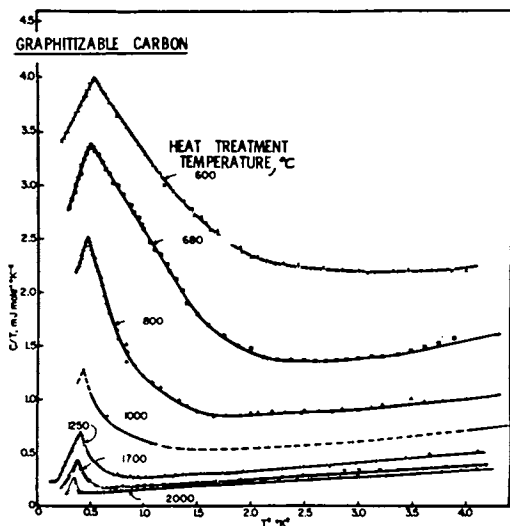
12th Biennial Conference on Carbon

Figure 11. Heat capacity divided by temperature vs. T^2 for graphitizable carbons heat treated from $873°K (600°C)$ to $2273°K (2000°C)$ (44)
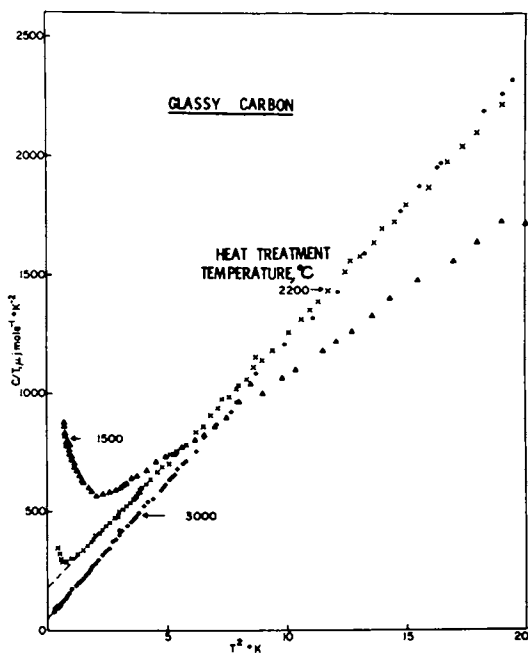
Carbon

Figure 12. Heat capacity divided by temperature vs. T^2 for several glassy carbons heat treated to temperatures indicated (37)
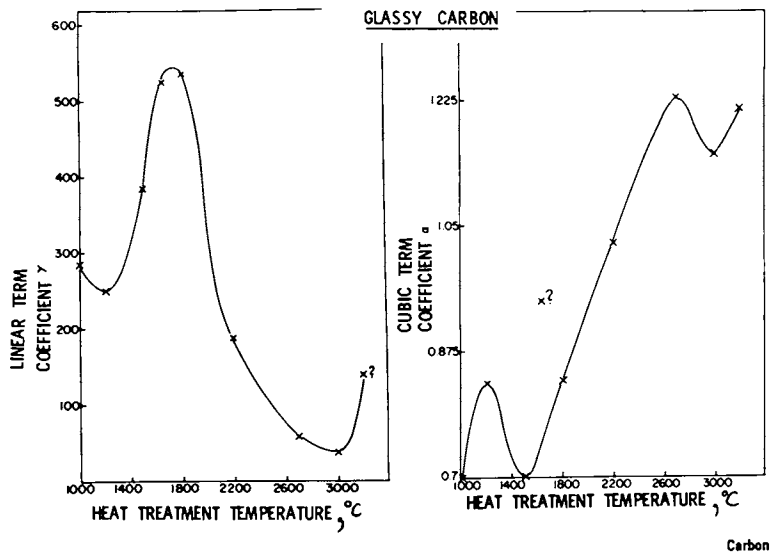
Figure 13. Linear term coefficients, γ, and cubic term coefficient, α, in
heat capacity vs. heat treatment temperature, HTT, for glassy carbon (37)
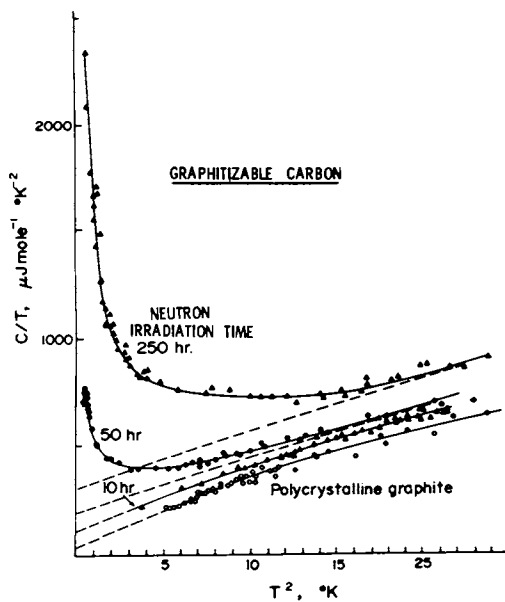
Figure 14. Heat capacity divided by temperature
vs. T² for several neutron irradiation times for
graphitizable carbon (33)
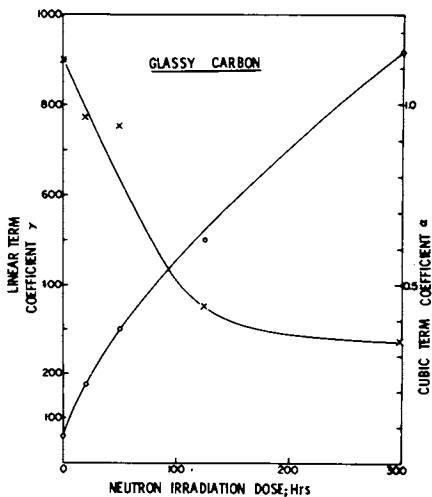
Carbon

Figure 15.   The coefficients of the linear and cubic terms in heat capacity vs. irradiation time in glassy carbon. ($\gamma(0)$ and α (x)) (36)
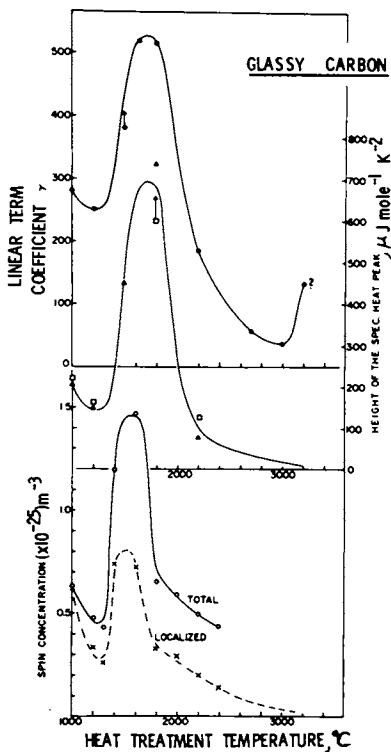
Carbon

Figure 16.   Linear term coefficient, γ, in heat capacity, height of specific heat anomaly, and spin concentration vs. HTT for glassy carbon (36)

A further study of heat capacity was made on glassy carbon with various HTT's and irradiations, and correlations made. The dependence of γ and α on irradiation in glassy carbon are shown in figure 15 (33). Notice that when δ goes up α goes down. Similar behavior is found for irradiated polycrystalline graphite. Further correlations are shown in figure 16, where the γ term, the height of the heat capacity peak, and the spin concentration are plotted against HTT of glassy carbon, showing the <u>strong correlations among these terms</u>. Another way of seeing correlations is shown in figure 17, for soft carbon (36), where the δ terms are monatonically increasing with heat capacity peak height.

The next obvious measurements to make are to: a) go to lower temperatures in order to completely fit the heat capacity peaks to models; b) study the effect of magnetic field on heat capacity; and c) measure the magnetic moment as a function of temperature. The a) measurements are now being made at the NASA Lewis Research Center using a large volume dilution refrigerator capable of reaching 0.02 K. An initial discovery by L. Kreps et al. is a new and large heat capacity maximum in glassy carbon below 0.1 K (43). Measurements of the magnetic moment at temperatures below 1 Kelvin have not been done but they would be quite revealing. The susceptibility has been measured above 1 K by the Delhaes group and the <u>Curie constant in the paramagnetic susceptibility is found to scale linearly with δ</u> (40).

Initial experiments on the field dependence of the heat capacity anomaly occurring near 0.7 K have been completed for graphitizable carbon heat treated to 1523 K (1250 C)(44). The peak rises with field, and the peak position moves up in temperature with increasing field. Mrozowski and Vagh have also investigated (in a magnetic field) an irradiated graphite and compared their data with data taken by the Delhaes group at higher temperature (39). The Delhaes data show that rapid rises in heat capacity with field are taking place. This heat capacity rise was attributed by Delhaes to a magnetic field induced Schottky anomaly.

B. <u>Interpretations of Data on Pregraphitic and Glassy Carbons</u>. The degree of graphitization, and the degree of disorder, depends on HTT. Disorder is also introduced by neutron irradiation. The structure of GC is very different from graphitizable carbon, and the similarity of many of the above results for graphitizable carbon and GC are surprising. The carbons studied by Mrozowski and by Delhaes are "pure" carbon systems, and because the position of the heat capacity

peak is weakly independent of HTT, and because neutron
irradiation introduces a very similar peak, Mrozowski
believes that these peaks are not due to impurities,
but to the presence of localized spins (25).

One can speculate on the origin of localized spins.
They may possibly be due to unpaired electron spins
trapped in sites of high stress in the disordered
lattice, or due to vacancies, or due to positively
charged interstitial carbon ions. In ordered carbon
there are no localized spins and the diamagnetism domi-
nates. Thus the number of trapped, unpaired electrons
should depend on the degree of disorder, but possibly
not in a smooth way. Thus in figure 10 the number of
localized spins has a maximum near 873 K (600 C) HTT,
and decreases with increasing HTT. The drop in local-
ized spins with increasing HTT is reasonable in view
of the decreasing volume of disordered structure avail-
able for forming localized spin sites. The situation
in GC is probably more complicated, because the struc-
ture changes less rapidly (but it does change)(27) with
HTT, yet the number of localized spins varies rapidly.

In short, the number of localized spin sites
depends in some (possibly complicated) way on defect
structure. These sites give rise to local magnetic
moments which produce a linear term (greater than that
expected for free carriers) in the heat capacity.
These moments have a Curie law dependence (susceptibil-
ity proportional to inverse temperature) above 1K and
give rise to two heat capacity anomalies below 1K.

Delhaes et al. have interpreted the results
summarized in the last paragraph based on a paper by
Kaplan, Mahanti and Hartman (45) which treats a system
of localized electrons in a narrow energy band using
the Hubbard Hamiltonian. An important feature of the
Kaplan, et al. model is the inclusion of strong
electron-electron correlations. The model predicts a
Curie law susceptibility (observed in carbon by
Delhaes et al. (40)), and a specific heat which is
linear in temperature and not due solely to free
carriers. (This was observed in carbon by Mrozowski
et al. (figure 10).) In the Kaplan et al. model, the
Curie law results from a lower probability of finding
two electrons in a localized state than of finding one,
due to the repulsive coulomb force between electrons
built into the Hubbard Hamiltonian. Other theories
have predicted linear temperature behavior for specific
heats, including theories for disordered systems. The
Kaplan et al. model is appealing because it predicts
both a Curie law susceptibility and a linear in T
dependence of the heat capacity. It also predicts a

Schottky heat capacity anomaly in a magnetic field (45),
but none in zero field. Blondet-Gonte, Delhaes and
Daurel experimentally find a heat capacity peak which
is present only in an applied field, and appears
between 2 and 4 Kelvin. This peak increases and shifts
with increasing field, which they attribute to a
Schottky anomaly such as predicted by the Kaplan et al.
theory (46). One cannot attribute the C_p peak near
0.7 K in disordered graphitizable carbon to the Kaplan
et al. term, because a peak in zero field is not
predicted by the theory. Further difficulty with
explaining the 0.7 K anomaly on the basis of electronic
band effects arises because of the complete absence of
any anomalies in electrical resistance vs. temperature
data in the region near 0.7 K (47).

Other interpretations of results in disordered
carbons which could be considered include the possi-
bility of: a spin glass system, superparamagnetism,
or a Kondo system. There are no resistivity anomalies
as a function of temperature (47), so this is not a
likely Kondo system. In the first two types of inter-
acting spin systems, the heat capacity anomaly falls
off as T^{-2} on the high temperature side of a peak.
This is not found for the carbon anomalies, especially
for graphitizable carbons.

Numerous other experiments have been performed on
partially disordered carbons. These include the Hall
effect and magnetoresistance, in pure and doped
materials, and some of these were reviewed by Mrozowski
in 1969 (29). An energy band model for HTT between
1273 and 2473 K (1000 and 2200 C) is still not com-
pletely formulated, but the model of Kaplan, Mahanti
and Hartman in predicting the observed Curie law sus-
ceptibility, an added linear term in the heat capacity,
and a field induced Schottky heat capacity anomaly, is
presently the most inclusive theory of possible appli-
cability. Unknown is the origin of the two very low
temperature heat capacity anomalies. Double heat
capacity maxima have been seen in antiferromagnetic
salts where one dimensional magnetic chains order at
temperatures above the three dimensional ordering tran-
sition (49). Graphite, being layered, may possibly
order magnetically in two dimensions at temperatures
above a three dimensional ordering temperature. The
magnitude of an antiferromagnetic heat capacity anomaly
at a three dimensional ordering transition in a typical
salt is usually weakly dependent on field (50) whereas
the transition seen by Mrozowski and Vagh (44) is
fairly strongly field dependent. Mrozowski (25)
believes the transition at 0.7 K is antiferromagnetic,

based on a cubic temperature dependence of the heat
capacity on the low temperature side of the anomaly.
A cubic temperature dependence is predicted from spin
wave theory, but should only be valid at very low
temperatures compared with the anomaly temperature.
The experimental data cover only the temperature region
with 20 percent of the peak, so I feel that conven-
tional antiferromagnetism may not be the complete
explanation. Further, the system considered is dis-
ordered, and the theory is for an ordered system.
Magnetic susceptibility and/or magnetic moment measure-
ments would aid greatly in determining the origin of
the heat capacity peaks.

Josephson Junction-Like Phenomena and Electronic Switching

Antonowicz has observed phenomena in carbon which
resemble Josephson Junction (J) effects (51, 52). In
the J effect (53) superconducting pairs of electrons
tunnel through a very thin insulating barrier ($\sim 10^{-9}$
m thick) between two superconductors. Current will
flow with no applied voltage until a maximum current
I_J is reached at which the material becomes ohmic.
This is the dc J effect. The dependence of I_J at field
is quite unusual: I_J goes periodically to zero as a
function of field.
In the ac J effect a dc voltage across a junction
causes radiation at the frequency

$$\omega \quad = \quad (q/\hbar) \, V_0 \qquad\qquad (7)$$

where V_0 is the voltage and q is twice the electron
charge. This is really an expression of conservation
of energy: $E = \hbar\omega = qV_0$. As a result of the ac J
effect, if radiation of frequency $n\omega$, where n is
an integer, is applied to the junction there will be
steps (whose form is dependent on the type of circuit
used) in the I V characteristics, and this process is
called "locking." The incident radiation modulates the
supercurrent resulting in a frequency modulation which
causes the steps. This effect is very useful in high
frequency electronics. The junction becomes a voltage
tunable oscillator and mixer.
Josephson junctions have many applications (volt-
meters, mixers, detectors, radiation sources, computer
elements, etc.). However, their biggest limiting fac-
tor is the need to operate below 20 K. This is the
significance of the Antonowicz discovery of J-like
effects in disordered carbon at room temperature.

Antonowicz's material is certainly not a room tempera-
ture superconductor (at least not a kind as we now know
them) and the effects observed are not likely due to
the J effect, but for applications, only the results
are important. One important present limitation for
possible use of the carbon junction is the long time
response ($\sim$ minutes).

The Antonowicz junctions are Al-C-Al prepared in
the following manner. Al is evaporated onto a porcelain
substrate, then covered with polyfurfuryl alcohol and
heated to 893 K (620 C) to form a carbon layer (there
likely is some organic material remaining). Then a
final aluminum evaporation is made. I V curves were
taken with 3 minute waits between voltage steps
($R \simeq 10^8$ ohms) to achieve equilibrium. At high enough
voltages a maximum current was reached. Repeating the
process in various fields gave an interference pattern
periodic in field, similar to the J effect. The period-
icity is $\sim$ 0.42 gauss for the example shown in figure
18 (51).

Next, Antonowicz irradiated the Al-C-Al junction
with 10 GHz microwaves, and I V curves were taken with
3 minute waits at each point. Weak steps or kinks at
2e ΔV = $\Delta n \hbar \omega$ were seen, and this behavior is much
like that of a J junction. However, these steps are
about 10^3 too large to be from a superconducting J
effect. This topic has been covered because it is an
interesting and possibly useful application of carbon.
Repeats of the experiments under various carbon prepar-
ation and experimental conditions are needed. For
example, microwave radiation with various frequencies
and intensities should be tried.

Closely related to the J-like behavior, and
actually discovered first in similar type sandwiches,
is electronic switching (54, 55). Switching was first
made famous by the discovery of very fast and large
changes in resistance of certain ternary and quaternary
chalcogenide glasses, upon application of a voltage
(56). These glasses could be made to switch from
insulating to conducting states and back again, by the
application of voltage pulses. Certain types would
remain in one state after the voltage was returned to
zero (memory type), others would switch back (threshold
type). The usefulness of these effects for computer
memory are obvious. They were amorphous so performance
was not changed by irradiation as is desirable for
certain applications.

Antonowicz et al. reported similar behavior in
Al-C-Al sandwiches prepared by deposition of evaporated
carbon in an argon atmosphere where changes of resis-
tance were as high as factors of 1000 (54, 55). Both
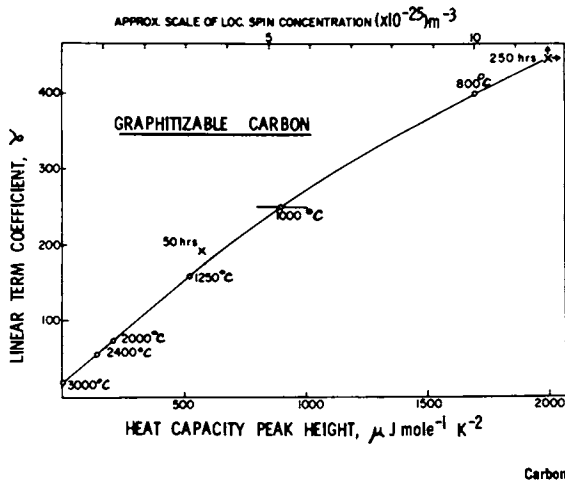
Figure 17. *Linear term coefficient, γ, in heat capacity vs. height of specific heat anomaly and localized spin concentration for graphitizable carbons with indicated HTT's and neutron irradiation times* (36)
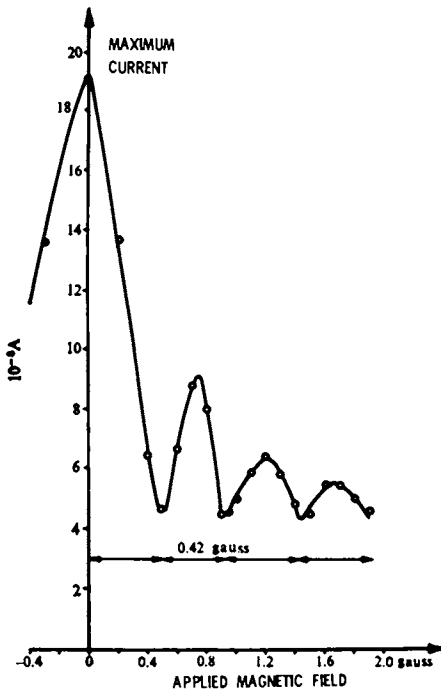
Figure 18. *Maximum current vs. applied field in Antonowicz Al-C-Al sandwich* (51)

"threshold" and "memory" types were found, and memories
as long as a few days were obtained. As many as
100,000 switchings on a device could be obtained.
Switching, again, is a potentially useful application
of disordered carbon. Both the J-like and switching
experiments should be repeated very carefully to
further document experimental conditions.

Compound Conductors Formed from Carbon

    A. Niobium Carbonitride Superconducting Fibers.
The applications of superconductivity became signifi-
cant in the early 1960's with the discovery that
Nb_3Sn superconducted below 18 K, and would stay
superconducting in very high magnetic fields, even
when carrying large currents (57). Magnets were con-
structed which could reach 14 tesla (140,000 gauss)
but which took tens of hours to charge (58). The
problem involved the motion of magnetic flux which
penetrates type II superconductors.
    In the past few years, it has been realized that
the problems of flux motion could be minimized by
carrying the superconducting current in small diameter
filaments (multifilamentary superconductors)(59). Due
to the brittleness of Nb_3Sn, the construction of multi-
filamentary superconductors is a difficulty metallurgi-
cal problem.
    A very novel approach to the problem of making
multifilamentary superconductors was carried out by
Lin et al. during 1973-1974 (60). They reacted niobium
pentachloride with carbon fiber precursor in the
presence of hydrogen and nitrogen at about 1873 K
(1600 C). The result was a film of niobium carboni-
tride about 1 micrometer thick formed on the surface
of the roughly 7 micrometer diameter carbon filaments.
The fibers came in yarn containing 720 filaments, and
the result was a multifilamentary superconductor with
superconducting transition temperatures in zero field
of about 16 Kelvin, critical fields at 4.2 Kelvin of
11.0 tesla (110,000 gauss) and critical current densi-
ties over 10^6 amp/cm^2. One unique aspect is that the
very high tensile strength of the fibers is decreased
by less than 30 percent. A similar fiber structure has
recently been formed using chemical vapor deposition
to form niobium carbon nitride on the surface of carbon
fibers by gas phase reaction, rather than by reaction
with the carbon in the fiber (61). The critical
temperature is less than 12 K, but slightly greater
critical fields and critical currents are found.
    The resultant material has not yet been wound

into a magnet, but the very small filament diameter
improves the chances for high field stability. The
critical field and temperature are not as high as Nb_3Sn,
but the stability and the high tensile strength may
make this superconductor useful in special applications.
An important point is that with some imagination, many
new and potentially useful applications for carbon can
be found. It appears from this, and other examples,
that these new productive areas may come from a
combining of research experiences.

   B. Intercalation Compounds from Carbon Fibers.
Intercalation compounds of carbon have been around for
a long time. Some of these are reviewed in Ubbelohde
and Lewis' book, Graphite and Its Crystal Compounds
(62). More recently, Hooley has written a review in
The Chemistry and Physics of Carbon on intercalation
isotherms in graphite (63), and in the same series are
articles by Marchand (64), and by Robert et al. (65)
dealing with changes in the electronic properties by
doping. As shown in figure 19, quite large drops in
resistivities, and high resultant conductivities can
be obtained in intercalation compounds.
   What is new in this area is that conductivities
at room temperature as high as that of copper at room
temperature have been found. Fibers can be made into
long lengths, are flexible, lightweight, and relatively
inexpensive. The possibility exists then of forming
useful cable to replace copper wire in such applications
as space and aircraft. In both these applications
weight is important, and carbon is light relative to
copper. In aircraft, very long lengths of wire are
used so both the cost and the weight of wire is signi-
ficant. This work is currently being pursued at the
University of Pennsylvania, and parts of the work were
discussed by Drs. Vogel (66) and Fisher (67) in this
"Petroleum Derived Carbons" symposium.

   C. Superconducting Intercalation Compounds. In
the mid-1960's it was discovered that alkali metal
intercalation compounds of pyrolytic graphite were
superconducting below 1 K (68, 69). The structure of
one such intercalation compound, C_8K, is shown in
figure 20 (62). Since then, a large number of super-
conducting intercalation compounds have been formed
from other layer structure host materials. Super-
conducting intercalation compounds are of interest
because of the high anisotropy and possible two dimen-
sionality. For practical applications they are of
interest because of the very high critical magnetic
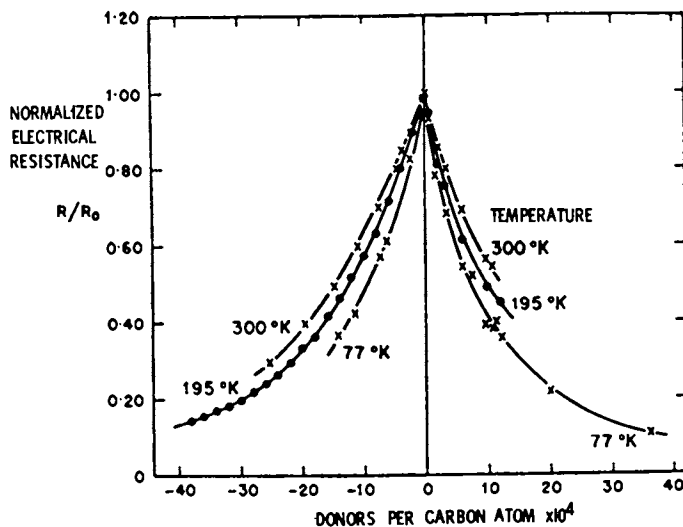
Graphite and Its Crystal Compounds

Figure 19. Change in resistance normalized to the undoped value of graphite with donor or acceptor doping (62)
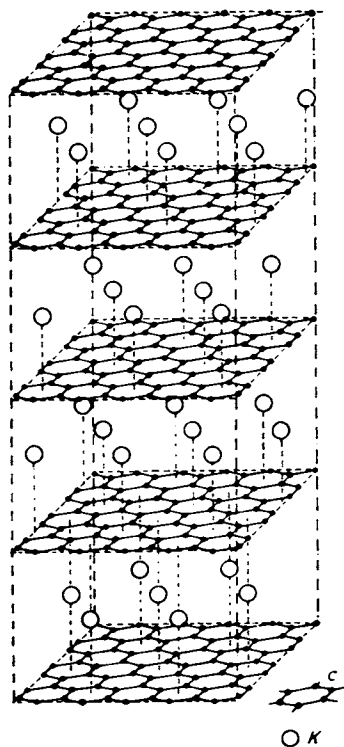
Graphite and Its Crystal Compounds

Figure 20. Structure of potassium intercalated graphite C_8K (62)

fields possible and potential use in Josephson Junction
devices. No study of critical fields in alkali com-
pounds of graphite has been made, however. The unique
situation for graphite superconducting compounds is
that they can be formed in fibers. As potentially
useful superconductors this is a good area for research.
Superconducting intercalation compounds remain an
active area of basic research, and the compounds of
graphite have not yet been well explored for their
superconductivity.

Final Statements and Suggestions for Further Research

        This paper has attempted to review some early
work, but with special emphasis on some areas of current
research. Due to the newness and complexity of many
of these areas, the results are not always completely
understood, nor have these areas been completely
explored experimentally.
        Of the areas needing further research, the third
topic area covered (thermal and other electronic
properties of pregraphitic carbons) is the least
understood. Especially, the origin of the two heat
capacity anomalies below 1 K is not known. Anomalies
have been observed only in the heat capacity, and no
unusual effects were found in the electrical conduc-
tivity (47), or thermal conductivity (25). If the
origin of the anomalies is possibly magnetic, then
obviously, data on the magnetization and/or magnetic
susceptibility vs. temperature and magnetic field
would help reveal this origin. Theoretically, various
mechanisms should be considered which could give rise
to the diversity of unusual effects seen in low HTT
carbons. Structural studies, such as those begun by
Marsh and collaborators (27) would help the theorest.
For example, it should be established whether there
are conducting regions separated by poorly conducting
regions in low HTT carbons (an "inhomogeneous model"
(70)), or whether low HTT carbon is homogeneously
amorphous.
        The fourth topic area of this paper concerned
Josephson Junction-like behavior, as well as electronic
switching. Since both Josephson-like phenomena and
electronic switching in carbon could be technologically
useful, it is important that these experiments be
repeated under a variety of experimental conditions,
and for various purities and thicknesses of carbon
films. If Josephson-like phenomena really exist in
carbon then there is a need for a theoretical explana-
tion.

Carbon is an ideal material for the study of superconducting intercalates because all other layer structure materials which will intercalate are compounds (71). Superconductivity in the intercalated compounds can never be two-dimensional because of the structural width of the layers. Layers of graphite, however, can be a single atom thick and the concept of a two-dimensional superconductor could be tested. So far, only the alkali metal intercalates have been studied and this was in pyrolytic graphite inferior to today's best HOPG. Superconducting graphite intercalates could have both technological and basic scientific importance.

Further studies of the electrical and thermal properties of carbon and graphite should lead to new and interesting physical phenomena, as well as new applications for carbon.

Acknowledgements

Abstract

Several current, as well as earlier, research areas are reviewed: electrical properties of pyrolytic and polycrystalline graphite; thermal, electrical and magnetic properties of graphitizable and glassy carbon with heat treatment temperatures between 873 K (600 C) and 2773 K (2500 C); Josephson Junction-like and switching behavior in carbon films; and some high conductivity, as well as superconducting, compounds formed from carbon. Suggestions for needed research are made.

Literature Cited

1.   Blackman, L. C. F., ed., "Modern Aspects of Graphite Technology," Academic Press, New York, 1970, 37.
2.   Ban, L. L.; Crawford, D.; and Marsh, H.: Extended Abstracts and Program of 12th Biennial Conference on Carbon, Pittsburgh (1975), p. 119, unpublished.
3.   Brooks, J. D.; and Taylor, G. H.: "The Formation of Some Graphitizing Carbons" in "Chemistry and Physics of Carbon," Vol. 4, pp. 243-286, Marcel Dekker, Inc., New York, 1968. Walker, P.L., ed.
4.   Moore, A. W.: "Highly Oriented Pyrolytic Graphite" in "Chemistry and Physics of Carbon," Vol.11,pp. 69-187, Marcel Dekker, Inc., New York, 1973.
5.   Spain, I. L.: "The Electronic Properties of Graphite" in "Chemistry and Physics of Carbon," Vol.12, pp. 1-147, Marcel Dekker, Inc., New York, 1973.
6.   McClure, J. W.: "Energy Band Structure of Graphite" in "The Physics of Semimetals and Narrow-Gap Semiconductors," p. 127, Pergammon Press, New York, 1971.
7.   Kelly, B. T.: "The Thermal Conductivity of Graphite" in "Chemistry and Physics of Carbon," Vol. 5, pp. 119-216, Marcel Dekker, Inc., New York, 1969. Walker, P. L., Jr., ed.
8.   Woollam, J. A.: Phys. Rev. Letters (1970), 25, 810.
9.   Woollam, J. A.: Phys. Rev.   (1971), B3, 1148.
10.   Williamson, S. J.; Foner, S.; and Dresselhaus, M. S.: Phys. Rev. (1965), 140A, 1429.
11.   Toy, W. W.; Hewes, C. R.; and Dresselhaus, M. S.: Carbon (1973), 11, 575.

12. Woollam, J. A.: Phys. Rev. (1971) B4, 3393.
13. Roth, L. M.; and Argyres, P. N.: "Semiconductors and Semimetals," (Willardson, R.K. and Beer, A. C., eds.), Vol. 1, p. 159, Academic Press, New York, 1966.
14. Slonczewski, J. C.; and Weiss, P. R.: Phys. Rev. (1958), 109, 272.
15. McClure, J. W.: Phys. Rev. (1957), 108, 612.
16. Dresselhaus, M. S.: "Status Report on Electronic Properties of Graphite," Proceedings of the Conference on the Physics of Semimetals and Narrow Gap Semiconductors, 1974, to be published.
17. Dillon, R.: Ph.D. Thesis, U. of Md., 1974.
18. McClure, J. W.: Phys. Rev. (1974), 9, 2467.
19. Dresselhaus, G.: To be published in Phys. Rev.
20. Delhaes, P.: "Positive and Negative Magneto-resistances in Carbons" in "Chemistry and Physics of Carbon," Vol. 7, pp. 193-235, Marcel Dekker, Inc., New York, 1971. Walker, P.L., Jr., ed.
21. Dillon, R. O.; Spain, I. L.; and Woollam, J. A.: To be published.
22. Sugihara, Ko; and Sato, Hisanao: J. of Phys. Soc. of Japan (1963), 18, 332.
23. Spain, I. L.; Ubbelhode, A. R.; and Young, D. A.: Proc. Roy. Soc. (1967), 262, 345.
24. Delhaes, P.; deKepper, P.; and Uhlrich, M.: Phil. Mag. (1974), 29, 1301.
25. Mrozowski, S.: Private communication.
26. Klein, C. A.: Rev. Mod. Physics (1962), 34, 56.
27. Marsh, H.: Lectures at the 12th Biennial Carbon Conference, Pittsburgh, 1975 (unpublished) and at NASA Lewis Research Center, 1975.
28. Marsh, H.: "Graphitizability and Liquid Crystal Development: Factors Influencing Growth and Structural Characteristics," Symposium on Petroleum Derived Carbon, April 1975.
29. Mrozowski, S.: Carbon (1971), 9, 97-109.
30. Inagaki, M.; Komatsu, Yi; and Zanchetta, J. V.: Carbon (1969), 7, 163.
31. Mrozowski, S.; and Chaberski, A.: Phys. Rev. (1956), 104, 74.
32. Hishiyama, Y.; Mrozowski, S.; and Vagh, A.S.: Carbon (1971), 9, 367.
33. Kamiya, K.; Mrozowski, S.; and Vagh, A. S.: Carbon (1972), 10, 267-275.
34. Van Den Berg, G. J.: "Anomalies in Dilute Metallic Solutions of Transition Elements" in "Progress in Low Temperature Physics," C. J. Gorter, ed., North-Holland Publishing Co., Amsterdam, 1964, Vol. 4.

35. Delhaes, P.; and Hishiyama, Y.: Carbon (1970), 8, 31-38.
36. Mrozowski, S.; Orzeszko, S.; and Vagh, A. S.: Carbon (1974), 12, 651-656.
37. Vagh, A. S.; Carton, B.; and Mrozowski, S.: Carbon (1974) 12, 645-650.
38. Delhaes, P.; Lemerle, Michel-Yves; and Blondet-Gonte, G.: C. R. Acad. Sc., Paris, Series B, (1971), 272, 1285-1288.
39. Blondet-Gonte, G.; Delhaes, P.; and Daurel, M.: Solid State Comm. (1972), 10, 819-822.
40. Delhaes, P.; and Blondet-Gonte, G.: Phys. Letters (1972), 40A, 242-244.
41. Kittel, C.: "Introduction to Solid State Physics," 4th Edition, Chapters 6 and 7, John Wiley and Sons, Inc., New York, 1971.
42. Morrish, A. H.: "The Physical Principles of Magnetism," Chapter 5, John Wiley and Sons, Inc., New York, 1965.
43. Kreps, L.; Vagh, A. S.; and Mrozowski, S.: Unpublished results.
44. Vagh, A.; and Mrozowski, S.: Extended Abstracts and Program of 12th Biennial Conference on Carbon, Pittsburgh, 1975, p. 55 (unpublished).
45. Kaplan, T. A.; Mahanti, S. D.; and Hartmann, W. M.: Phys. Rev. Letters (1971), 27, 1796.
46. Delhaes, P.: "On Electronic Band Model in Carbons" in "Summary of Papers, 11th Biennial Conference on Carbon," Gatlinburg, Tenn., 1973 (unpublished). Paper EP-4.
47. Dillon, R. O.; and Woollam, J. A.: unpublished results.
48. Toyozawa, Y.: J. Phys. Soc. Japan (1962), 17, 579.
49. Smith, T.; and Friedberg, S. A.: Phys. Rev. (1968), 176, 660. Unpublished data on the same material show a heat capacity maxima as well as the susceptibility maximum. (H. Forstat, private communication.
50. Schelleng, J. H.; and Friedberg, S. A.: Phys. Rev. (1969), 185, 728.
51. Antonowicz, K.: Nature (1974), 247, 358.
52. Antonowicz, K.: Physia Status Solidi (1975), A28, 497.
53. Solymar, Laszlo: "Superconductive Tunneling and Applications," Wiley Interscience, New York, 1972.
54. Antonowicz, K.; Jesmanowicz, A.; and Wieczorek, J.: Carbon (1972), 10, 81-86.
55. Antonowicz, K.; Cacha, L.; and Turlo, J.: Carbon (1973), 11, 1.

56. A short review and references can be found in:
    Adler, David: Electronics (1970), 43, 61.
57. Kunzler, J. E.; Buehler, E., Hsu, F. S. L.; and
    Wernick, J. H.: Phys. Rev. Letters (1961), 6,
    89.
58. Coles, W. D.; Schrader, E. R.; Thompson, P. A.:
    NASA TM X-52330 (1967).
59. "Applied Superconductivity Conference 1974,"
    IEEE Trans. on Magnetics (1975), 11.
60. Lin, R. Y.; Smith, W. D.; Coppola, J.; Economy,J.:
    AFML-TR-74-113 (1974)
61. Pike, G. E.; Mullendore, A. W.; Schirber, J. E.;
    Napier, J.: "Applied Superconductivity Conf.
    1974," IEEE Trans. on Magnetics (1975), 11, 187.
62. Ubbelode, A. R.; and Lewis, F. A.: "Graphite and
    Its Crystal Compounds," Oxford University Press,
    Oxford, 1960.
63. Hooley, J. G.: "Intercalation Isotherms on
    Natural and Pyrolytic Graphite" in "Chemistry and
    Physics of Carbon," Vol. 5, pp. 321-370, Marcel
    Dekker, Inc., New York, 1969.
64. Marchand, A.: "Electronic Properties of Doped
    Carbons" in "Chemistry and Physics of Carbon,"
    Vol. 7, p. 155, Marcel Dekker, Inc., New York,
    1971. Walker, P. L., Jr., ed.
65. Robert, M. C.; Oberlin, M.; and Mering, J.:
    "Lamellar Reactions in Graphitizable Carbons" in
    "Chemistry and Physics of Carbon," Vol. 10, p.141,
    Marcel Dekker, Inc., New York. Walker, P.L., ed.
66. Vogel, F. L., Jr.; and Popowich, R'Sue: "Changes
    in the Electrical Resistivity and Structure of
    Graphite with Intercalation by Nitric Acid,"
    Symposium on Petroleum Derived Carbon, April
    1975.
67. Fisher, J. E.; and Thompson, T. E.: "Free
    Carrier Plasma in Graphite Nitrate" in Symposium
    on Petroleum Derived Carbon, April 1975.
68. Hannay, N. B.; Geballe, T. H., Matthias, B. T.;
    Andres, K.; and MacNair, D.: Phys. Rev. Letters
    (1965), 14, 225.
69. Salzano, F. J.; and Strongin, M.: Phys. Rev.
    (1967), 153, 533.
70. Carmona, F.; and Delhaes, P.: Extended Abstracts
    and Program of 12th Biennial Conference on Carbon,
    Pittsburgh, 1975, p. 233, (unpublished).
71. Wilson, J. A.; and Yoffe, A. D.: Adv. Physics
    (1969), 18, 193.

Changes of Electrical Resistivity of Graphite Fibers with Nitration

F. LINCOLN VOGEL and R'SUE POPOWICH

Moore School of Electrical Engineering and Laboratory for Research on the Structure of Matter, University of Pennsylvania, Philadelphia, Penn. 19174

Pure single crystal graphite is a moderately good conductor of electricity having a resistivity of 4×10^{-5} Ω cm in the cystallographic "a" direction (1). That is approximately twenty times the resistivity of pure copper which is 1.67×10^{-6} Ω cm at room temperature (2). The electrical carrier concentration in graphite, composed of equal numbers of holes and electrons, is $3 \times 10^{19}/cm^3$ and the carrier mobility, high compared to any metal, is in excess of 10,000 cm^2/volt sec at room temperature (3). This high value is interpreted as due to the low scattering offered by the orderly resonant bond structure of the hexagonal graphite rings. By comparison, the free electron concentration of copper is approximately $10^{23}/cm^3$ with a mobility of 35 cm^2/volt-sec.

The formation of a graphite intercalation compound leads to a decrease in the electrical resistivity as has been shown by many workers in this field. Ubbelohde, for instance, has demonstrated this with a variety of intercalants such as bromine (4), bisulfate (5), nitric acid and a number of others (6), (7). Group I elements from the Periodic Table (see for example, Herold (8)) have been examined as intercalants in graphite and found to produce donor behaviour whereas the aforementioned acid intercalants, sulfuric and nitric, act as acceptors.

The largest change of resistivity in the conversion to an intercalation compound reported in the literature is for a Stage II compound of N_2O_5–H_2O (9) where the resistivity at $0^{\circ}C$ is approximately two micro ohm cm. The generally accepted mechanism for increase of conductivity in graphite intercalation compounds is the transfer of charge from the nitrate to the graphite transforming the latter into a giant cation. In these terms then, the stronger the acid–greater the ionization and the higher the conductivity. This paper describes some work in the initial phase of a program to determine the highest conductivity that can be achieved by using very strong acids as intercalants in graphite. "Graphite" fibers, particularly the high modulus type used to reinforce polymers and metals represent a convenient form

in which to conduct electrical resistivity experiments. The geo-
metric form of filaments allows for easy calculation of resis-
tivity values. Further, the high modulus fibers are fairly well
structured graphites having the normals to the crystallographic
"C" axis lying parallel to the fiber axis. (10) Since the
direction of highest conductivity is normal to the "C" axis
this orientation configuration is fortunate for maximizing con-
ductivity in the fiber. Probably the most important advantage
of the filaments is the ability to make satisfactory contacts
in a way that does not call the effects of high anisotrophy into
question. The work reported here will concentrate on commerially
obtained Thornel 75 fibers since they were found to be well struc-
tured and typical of high grade fibers.

The experiments described herein were done in the initial
part of our program to determine the intercalation character-
istics of "graphite" fibers with red fuming nitric acid.

Experimental Work

Working with individual graphite fibers having diameters
somewhat less than 10 μ diam presents the investigator with a
number of difficulties, especially considering the necessity for
maintaining multiple electrical contacts after treatment with
very strong acids. The method devised consisted of mounting
and soldering an inch long fiber of known cross sectional area
to a substrate and measuring the resistivity. After acid treat-
ment the resistivity of the same fiber sample was determined again
thus placing reliance on the resistivity change rather than the
magnitude of the absolute values.

Resistivity Measurements: Figure 1 illustrates the four-
point mounting of graphite fibers on the holder plate. The
plate itself is alundum with platinum connecting strips silk
screened on and then baked. The fiber is laid across the plati-
num strips, a dab of 80 Au-20Sn solder paste put at each con-
tact point and a short length of Pt wire is put over the fiber
and solder paste. When the solder is melted, a secure joint is
made holding the fiber between the platinum strip and platinum
wire. The choice of materials was governed mainly by the nec-
essity for maintaining electrical contact after repeated ex-
posures to highly reactive environments.

With a fiber so mounted, it is possible to make a four
point resistivity measurement conveniently. The outside con-
tacts are connected to the current source through a Keithley
Electrometer to measure the current. The voltage drop is measured
between the two inside contacts with a null voltmeter. For con-
venience in calculating resistivities the distance between the
voltage drop contacts is one centimeter.

The resistivity, defined as the resistance of a volume of
material having a cross section 1 cm x 1 cm and 1 cm in length,
is calculated from:

$$\rho = \frac{R \cdot A}{1}$$

where: R = resistance in ohms
        ρ = resistivity in ohm cm
        A = cross section in cm^2
        1 = length in cm

Since the main interest in this study was in determining the resistivity change that could be produced by treating fibers, it was essential to know the resistance before and after treatment, but the geometric quantities of length and area have to be known exactly only for calculation of absolute values of resistivity. Because the cross sections of the fibers are very often irregular their areas are most accurately determined by examination at high magnification in a scanning electron microscope. Because of the inconvenience and expense of this electron microscope measurement, it could not be used routinely on every sample measured. Rather, the cross section shape was determined for each fiber type and a correction factor applied to the circular area derived from the diameter measured by viewing from the side in a conventional light microscope.

Chemical Treatment: Intercalations of the fibers for both the resistivity experiments and the weight change experiments were done by immersion. The immersions were accomplished simply by submerging the mounted fibers in about 20 cc of the acid solution--red fuming nitric acid with a specific gravity of about 1.60--under controlled temperature conditions. This was followed by washing in water and acetone before measurement. In general, nitration by this method produced visible results in a matter of a few minutes.

Procedures: For the resistivity measurements a single graphite fiber selected for study was mounted on a contact substrate and soldered in position. Two small lengths--about 3mm long were broken off either end and retained for diameter and cross section measurement. The resistance of the centimeter long center section of the test piece was determined by passing a current in the 10^{-5} ampere range producing a voltage drop in the millivolt range. Smaller voltage drops were avoided to prevent interference from thermal and electrochemical EMF's. The sample is then treated with the acid for a specified length of time, cleaned and remeasured. The anticipated problem of large dimension changes or disintegration with intercalation was not encountered under the conditions employed in all of these experiments.

For the weight change experiments a bundle of fibers about an inch long weighing about 0.1 gram was loaded into a noble metal boat that had been baked to constant weight. The boats were provided with numerous holes which allowed them to fill and drain rapidly when placed in liquid for either nitration treat-

ment or rinsing in water and acetone. The procedure then was
to load a boat, weigh to the nearest tenth of a milligram, immerse
in acid, rinse, dry and weigh again. For other than room temper-
ature determinations the acid container was immersed in a larger
bath maintained at the appropriate temperature.

Experimental Results:

The changes in resistivity that were observed after treat-
ment of the Thornel 75 fibers with red fuming nitric acid are
shown in Table I.

TABLE I

RESISTIVITIES OF THORNEL 75 FIBERS
INTERCALATED BY IMMERSION IN HNO_3

TEMPERATURE °C	RESISTIVITY Ωcm		RESISTIVITY RATIO
	INITIAL	FINAL	
80	8.5×10^{-4}	1.2×10^{-4}	7
57	8.0×10^{-4}	6.0×10^{-5}	12
27	6.1×10^{-4}	8.1×10^{-5}	8

After intercalation these fiber resistivities are changed by
about an order of magnitude and there appears to be a pronounced
effect of temperature of treatment on the change in resistivity.
The weight change experiments shed further light on the
what is occurring during intercalation with red fuming nitric
acid. Figure 2 is a plot of the uptake of weight during this
acid treatment. The kinetics are characterized by an initial
increase which is sensitive to temperature followed by leveling
off which is roughly the same for the three temperatures, 2°,
22° and 57°C. These initial rates of weight increase are shown in
Table II and plotted against the reciprocal of the absolute
temperature of the reaction in Figure 3. The calculated activ-
ation energy of 20,000 cal/°C mol is indicative of the rate
limiting step of the formation reaction - possibly the step
involving indiffusion of the acid molecules.

TABLE II

RESISTIVITIES OF THORNEL 75 FIBERS
INTERCALATED BY IMMERSION IN HNO_3

TEMPERATURE °C	RATE % PER MINUTE
57	88
42	50
22	1.8
2	0.3
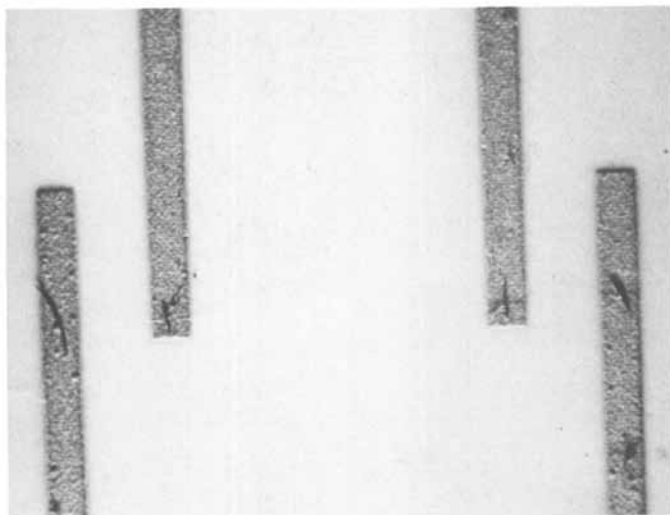
Figure 1. Four contact mounting substrate with graphite fiber soldered in place (3.8×)
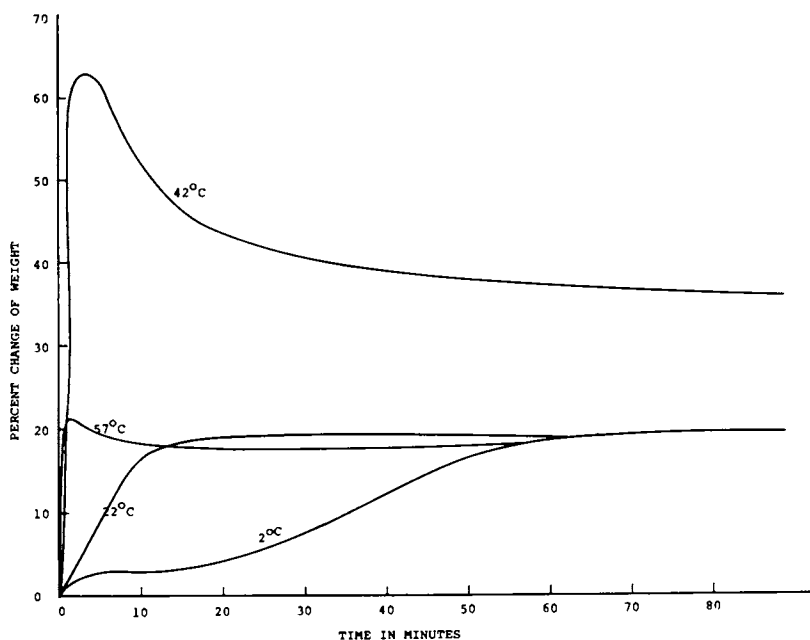
Figure 2. Intercalation of graphite fibers with red fuming nitric acid
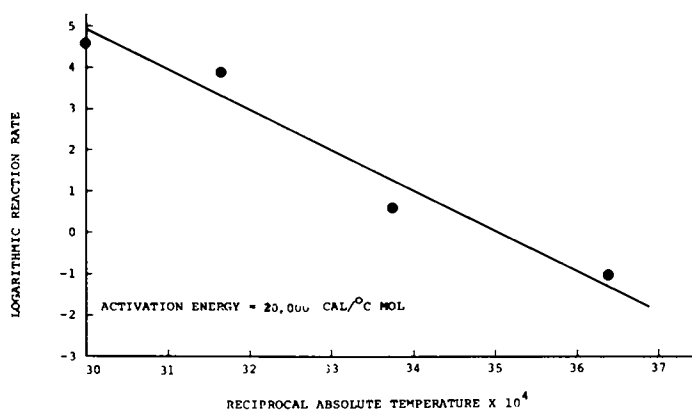
Figure 3. Intercalation of graphite fibers with red fuming nitric acid

Discussion and Conclusions

It seems clear from the data presented here that "graphite" fibers can be readily intercalated with red fuming nitric acid and that the resistivity changes that take place are comparable with those experienced in more perfect graphitic materials such as the stress annealed pyrolytic graphite crystals. The variations of conductivity that occur with variation of treatment temperature can be ascribed to concentration of intercalant changes. The weight change experiments agree with the resistivity experiments in a qualitative sense but the temperatures of maximization are not in agreement. Lacking in our understanding here is a knowledge of the exact species that resides in the lattice interstitially after intercalation is complete. The possibilities are numerous including all of the oxides of nitrogen, nitric acid, water or any combination of these. Careful and exact determination of these species must be done before an adquate structure of graphite nitrate can be deduced.

Literature Cited

(1). I.L. Spain, A.R. Ubbelohde and D. A. Young in Proc. 2nd Int. Carbon and Graphite, (1967).
(2). Metals Handbook, 8th Edition, Volume 1, Properties and Selection of Metals, Taylor Lyman Ed.
(3). I.L. Spain, Chemistry and Physics of Carbon, ed. by P.L. Walker and P.A. Thrower (Marcel Dekker, Inc. New York 1973) Vol. 8, p. 1
(4). L.C.F. Blackman, J.F. Mathews and A. R. Ubbelohde, Proc. Roy Soc A258, (1960)
(5). A. R. Ubbelohde, Proc. Roy Soc. A321,445 (1971)
(6). A. R. Ubbelohde, Proc. Roy Soc. A304, 25 (1968)
(7). B. Bach and A. R. Ubbelohde, Proc. Roy Soc. A325, 437 (1971)
(8). Herold, A. Bull, Soc. Chem., France p. 999 (1955).
(9). Fuzellier, H. Doctoral Thesis Presented to University of Nancy, France (1974).
(10).Fourdeaux A, Perret,R and Ruland, W. Conf. on Carbon Fibers Plastics Institute, London (1971)
(11). G. M. Jenkins, K. Kawamura and L.L. Baw, Proc. Roy Soc. A327, 501 (1972).

29

Free Carrier Plasma in Graphite Compounds

JOHN E. FISCHER, THOMAS E. THOMPSON, and F. LINCOLN VOGEL

Moore School of Electrical Engineering and Laboratory for Research on the
Structure of Matter, University of Pennsylvania, Philadelphia, Penn. 19174

The intercalation compounds of graphite are materials in
which layers of atoms or molecules lie between aromatic layers
of carbon atoms.(1)(2) Systematic x-ray studies (2)(3) have
shown that each layer of carbon atoms retains the original hexa-
gonal lattice of graphite with little or no change in the carbon -
carbon bond distance but the distance between the carbon layers,
i.e. the separation distance along the c-axis, is altered to
allow for the insertion of the intercalate. Such compounds can
exist in different stages of intercalation: stage one where the
intercalated specie lies between every other layer of carbon
atoms, stage two where there are two layers of carbon atoms be-
tween the intercalate layers, stage N where there are N carbon
layers between the intercalate layers, etc. As an example we
show the structure of the first stage compound C8K in Figure 1.
    A number of graphite intercalation compounds are metallic
in nature (5)(6) as indicated by their paramagnetism and electri-
cal conductivities (pristine graphite is a diamagnetic semimetal.)
Whereas the room-temperature electrical conductivity of stress-
annealed pyrolytic graphite parallel to the basal planes (per-
pendicular to the c-axis) can be 1/25 of the electrical conduc-
tivity of OFHC copper (or better), the conductivities of some
graphite intercalation compounds are an order of magnitude higher,
approaching half that of Cu. This is the case, for instance, for
the intercalates of sulfuric and nitric acid. The increase in
basal plane conductivity can be explained in terms of increased
carrier concentration in the graphite layers due to charge trans-
fer between the intercalate and the host lattice. At room temper-
ature crystalline graphite has a carrier concentration (N = P,
since its a semimetal) of approximately 10^{19} cm^{-3} (compared to
10^{23} cm^{-3} for Cu) and an average basal plane mobility of 10^4 cm^2/
Vs (compared to 35 cm^2/Vs for Cu). Hall effect measurements in-
dicate that a fractional charge transfer occurs when sulfuric or
nitric acid is intercalated into graphite leaving the graphite
layers with additional holes and, therefore, an increased con-
ductivity. This fact raises the obvious question: Can one find

an intercalate which will give enough of a carrier increase to
make the conductivity even better than that of Cu? Since a
charge transfer mechanism is involved, perhaps a stronger acid,
one with more ionizing ability, would be most effective. The
work of Vogel (7) has given some indication that this is indeed
the case.

Despite a large amount of effort on the synthesis and physi-
cal measurements of graphite intercalation compounds, the detailed
influence of the intercalate on the electronic properties of the
resulting compound remains largely unexplained. One would hope
to be able to understand the electrical conduction in terms of
such familiar concepts as carrier density, mobility and energy
band structure. Measurements of conductivity, Hall effect and
magnetoresistance have not provided a general model or set of
models to describe the interplay between charge transfer and
changes in mobility. To our knowledge, the Shubnikov-deHaas
experiment of Bender and Young (8) on dilute bromine-graphite is
the only case where a detailed correlation can be made between
intercalation and the electronic structure.

The research reported here are some initial results of a
program of experiments designed to probe the electronic struc-
ture and conduction processes of these synthetic metals. One
component of this program is optical and modulation spectroscopy,
the goals of which are to observe plasma oscillations associated
with conduction electrons and/or holes, and to follow key inter-
band transitions versus intercalation in order to deduce Fermi
level shifts, changes in bandwidths, and contributions of new
bands derived from the intercalating specie. We have begun this
work with a study of the optical reflectivity and thermoreflec-
tance of graphite intercalated with HNO_3 and SbF_5.

In the following section we present some ideas on the effect
of intercalation on the conduction processes in graphite com-
pounds. This is followed by a description of the relationship
between optical reflectivity and electronic conduction. Follow-
ing this is a description of our experiments with a summary and
conclusions.

Conductivity - A Simple Model

One of the most striking features of intercalation compounds
is the large increase in a-axis (basal plane) conductivity rela-
tive to that of pure graphite. (5)(6) It is of fundamental im-
portance to understand the dependence of conductivity on inter-
calating specie and concentration. In this section we present
a simple model for the concentration dependence which, despite
its limitations, brings out two important features: the inter-
play between increases in free carrier density and electron-
phonon scattering rate, and the influence of dimensionality.

The dc conductivity of a simple free-electron metal is

given by

$$\sigma = Ne\mu = Ne^2\tau/m^* \tag{1}$$

where N is the carrier density, μ is the mobility, τ is the mean
time between collisions and m^* the effective mass. At room tem-
perature the conductivity of most metals is limited by collisions
with thermal vibrations of the lattice atoms (phonons), so the
scattering rate $1/\tau$ is governed by the net interaction between all
the electrons and phonons in the system. The effective mass
accounts approximately for the influence of the periodic crystal
potential on electron motion. In free space $m^* = m_e$, the true
electron mass, whereas electrons in solids can have m^* greater or
less than m_e. Since m^* depends on crystal potential it can be
anisotropic and lead to anisotropy in σ through Eq. (1).
    The energy band structure determines the parameters N, τ and
m^* so once we assume a model for the effect of intercalation on
band structure, we can use it to estimate the change in conduc-
tivity. The electron density N is proportional to the k-space
volume enclosed by the Fermi surface; if N increases (e.g. upon
intercalation), this volume, hence the Fermi energy E_f, increases.
The electron-phonon scattering rate $1/\tau$ is determined by the num-
bers of electrons and phonons that are able to interact while
simultaneously conserving energy and momentum. Since phonon
energies are small compared to the Fermi energy, and since the
Fermi-Dirac distribution function governs electron occupancy, only
electrons within a few kT of E_f participate in collisions with
phonons. Thus $1/\tau$ is roughly proportional to the area of the
Fermi surface. The effective mass m^* is inversely proportional to
the curvature of the energy bands, which in turn is determined
by the crystal potential. In graphite, the strong sp^2 bonds with-
in the sheets give a large energy bandwidth, which leads to a
small m^* and therefore a large σ, for electron motion parallel
to the sheets. The much weaker p_z overlap between sheets gives a
bigger mass, hence lower σ for motion along the c-axis (additional
anisotropy in the scattering rate further enhances the anisotropy
in σ).
    Consider first a crystal with simple isotropic energy bands
such that $E(\bar{k}) = \hbar^2\bar{k}^2/2m^*$. The Fermi surface for this case is
spherical, with a radius given by $k_f = (2m^* E_f/\hbar^2)^{\frac{1}{2}}$. The electron
density is proportional to the volume:

$$N \propto k_f^{\ 3}, \tag{2}$$

while the scattering rate goes as the area:

$$1/\tau \propto k_f^{\ 2}. \tag{3}$$

Suppose we "intercalate" with donors, obtaining one additional
electron for each intercalated ion dependent of concentration X.

The Fermi surface will grow to accomodate the added electrons. If $N = N_0 + X$, the Fermi radius increases $k_f \propto (N_0 + X)^{1/3}$, according to ($\underline{2}$). At the same time, the scattering rate will increase due to the larger number of electrons with energies kT about E_f. Neglecting changes in the phonon density of states we have from ($\underline{3}$) that $1/\tau \propto (N_0 + X)^{2/3}$. Assuming m* is unchanged, the net dependence on concentration is

$$\sigma_{3D}(X) \propto (N_0 + X)^{1/3}. \tag{4}$$

We now consider the effects of anisotropy. The Fermi surface for a two-dimensional or layer structure crystal can be approximated by a cylinder, the component of the m* tensor perpendicular to the layers being very large. If the material remains two-dimensional after intercalation, we have $N = N_0 + X \propto 4\pi k_f^2 H$, where $4\pi k_f^2$ is the cross-sectional area and H the height of the Fermi cylinder ($H \gg k_f$). Now the scattering rate goes as $1/\tau \propto 2\pi k_f H \propto (N_0 + X)^{1/2}$, and the net dependence becomes

$$\sigma_{2D}(X) \propto (N_0 + X)^{\frac{1}{2}}, \tag{5}$$

a more rapid increase with X than the isotropic case, Eq. (4). Similarly, one-dimensional solids (such as the charge transfer salt TTF: TCNQ or the linear chain polymer $(SN)_x$) might be expected to behave as:

$$\sigma_{1D}(X) \propto (N_0 + X), \tag{6}$$

the strongest dependence of all. The implication is quite straightforward: In order to maximize conductivity by accepting the smallest degradation in τ for a given increase in N, the lowest dimensionality should give the best result.

The above model is based on many assumptions, not all of which are justified in the specific case of graphite. Eq. (1) assumes that only one type of carrier is important. This is certainly not true for pure graphite, in which the conductivity is the sum of roughly equal contributions from electrons and holes, however in low stage compounds where the conductivity has increased by an order of magnitude the carrier density must be more than ten times the initial value since τ is certainly lower (as will be shown later). Thus we can assume that one type of carrier will dominate σ in the compounds. The assumption that the fractional charge transfer per ion (or degree of ionization) is independent of concentration is probably the least justified. This assumption places two unrealistic constraints on the band structure of the compound: the energy levels introduced by the intercalant must be far in energy from E_f so they do not hybridize with the carbon bands near E_f, and the carbon band structure must itself be unchanged by intercalation. The latter is particularly weak, since the interplanar separation changes by more than a

factor of two in some cases, which will have a profound influence
on the bandwidths along the c-axis. The change in bandwidth will
also change m*, contrary to another of our assumptions. Changes
in phonon density of states are probably negligible to first
order, since even in stage 1 compounds 75% or more of the bonds
are essentially unaffected (the basal plane lattice parameter
changes by only a few percent).

The final arbiter of our simple picture is of course compari-
sion with experiment. Ubbelohde and co-workers have published
$\sigma(x)$ data for many intercalating species in graphite, most of
which show rapid increases in σ up to stage 4 or 5, followed by
saturation or even decreases upon further intercalation. A
most curious result is that $IC\ell$ intercalation approximately
follows our free-electron, $\sigma \sim X^{\frac{1}{2}}$ prediction while the chemically
similar Br_2 system reaches its maximum conductivity at about
stage 5 and then saturates. It's clear that many subtle effects
play a role, and therefore a more penetrating theoretical effort
is required.

Conduction Processes from Optical Reflectivity

Reflection of light from a non-magnetic conducting surface
is a classical electromagnetic field problem. The reflectivity
(fraction of energy reflected from the surface) can be written
in terms of a complex dielectric function and/or a complex
refraction index. The complex dielectric response function $\tilde{\varepsilon}(\omega)$
is defined by one of Maxwell's equations:

$$c \nabla \times H = 4\pi J + {}^{\partial D}/\partial\tau = \tilde{\varepsilon}(\omega)^{\partial E}/\partial\tau \ . \tag{7}$$

Assuming a sinusoidal time dependence $e^{-i\omega t}$, a free carrier
current linearly dependent on the electric field $J = \sigma E$, and that
the polarization of the lattice can be described by a lattice
dielectric constant $D = \varepsilon_0 E$, the dielectric function takes the
form

$$\tilde{\varepsilon}(\omega) = \varepsilon_0 + i4\pi\sigma/\omega. \tag{8}$$

The complex dielectric function is simply related to the complex
index of refraction $\tilde{\varepsilon} = (\eta + ik)^2$, and the normal incidence re-
flection is given by Fresnel's equation:

$$R = \frac{(\eta - \eta')^2 + (k - k')^2}{(\eta \quad \eta \ )^2 + (k - k')^2} \ , \tag{9}$$

where the primed indices refer to the medium outside the conductor.
For reflection from a sample in vacuum $\eta' = 1$ and $k' = 0$.

Within the relaxation time approximation the single carrier
ac conductivity is given:

$$\sigma = \frac{Ne^2\tau/m^*}{(1 + i\omega\tau)} \qquad (10)$$

Substitution of (8) and (10) into Fresnel's equation results in a distinctive shape for reflectivity versus photon energy: R $\sim$ 100% at low energy, then drops abruptly to a small value, the drop occuring over an energy range governed by ε_o and $\hbar/\tau$, and located in the vicinity of the "plasma frequency" given by

$$\omega_p = (4\pi Ne^2/m^*)^{\frac{1}{2}}, \qquad (11)$$

if ε_o is not much greater than unity. By fitting the Fresnel's equation to experimental reflectivity data, values for ε_o, τ and ω_p can be obtained. From these parameters the conductivity can be found: $\sigma = \omega_p^2 \tau/4\pi$. If the effective mass is known, these parameters can be further related to the carrier concentration and mobility: $N = \omega_p^2 m^* (4\pi e^2)^{-1}$, $\mu = e \tau/m^*$.

In this paper we analyze the optical reflectivity data of several graphite intercalation compounds in the vicinity of the plasma edge in order to determine the effect of intercalation on the conduction processes. Even though we are not certain as to the exact value of m*, we can identify trends in σ among various compounds from optical measurements alone, a great help given the difficulty of accurate and reliable σ measurements on these highly anisotropic crystals.

One complication in our analysis arises from the fact that ε_o is frequency dependent due to resonances or interband transitions associated with the electrons on the ion core. Such effects, however, don't mask the basic "edge" in reflectivity at the plasma frequency.

Experimental Methods and Results

In this section we present results of optical reflectance and thermoreflectance experiments on several acid intercalation compounds. These provide information on conductivity changes via Eq. 11 and also give clues concerning band structure and Fermi level position in the compounds.

Sample Preparation.

Intercalation compounds were made from stress-annealed pyrolytic graphite (9), which consists of 1-10 micron crystallites with their c-axes aligned to within a fraction of a degree, although the a-axes of the individual crystallites are randomly oriented in the basal plane. Rectangular bars were cut from larger plates using a diamond wire saw. Intercalation was performed by immersing the bars in red fuming nitric acid at room temperature for several hours. Expansion along the c-axis was dramatic and readily observable. While in the acid, the bars

separated into 50-100μm thick sheets; the c-faces thus exposed
were blotted dry and used directly for optical measurements.
X-ray diffractometer data indicated a well-defined single phase
stage 4 compound (c-axis repeat distance 17.8Å). The intercala-
tion specie has previoulsy been proposed (10) as NO_3^-.$3HNO_3$.
Intercalation with SbF_5 was carried out (11) in sealed copper
tubes containing graphite bars and a preweighed amount of liquid
SbF_5. The tubes were heated to 500K for several hours. The
superacid $HSbF_6$ was made by condensing HF gas into a Kel-F tube,
then adding an equal mole fraction of liquid SbF_5. Graphite
bars were immersed directly in this mixture for several hours at
300K. X-ray analysis indicated stage 1 with c-axis repeat dis-
tance 8.38 Å, very close to the 8.41Å value reported by Mélin and
Herold (12) for SbF_5 intercalation without HF. This is larger
than the 7.75A value for stage 1 nitrate and is consistent with
SbF_6^- as the intercalated specie, since NO_3^- is planar whereas
SbF_6^- is octahedral (13). To the best of our knowledge, this is
the first example of graphite intercalated with a mixture of a
Lewis acid and a Bronsted acid (13)

Optical Reflectance Spectra.

Reflectance spectra were measured using a prism monochromator
interfaced to a programmable calculator. For reflectance spectra,
the reflected intensity was measured at up to 500 energy values,
first from the sample, then from an aluminum mirror. The ratio
was then calculated and plotted automatically. Once the data
was obtained, further processing such as smoothing, differentia-
tion, multiple plots etc. could be performed.

Experiments were mostly limited to room temperature since our
cooling system requires that the sample be in a vacuum environment.
This was found to lead to rapid degradation of the acid intercala-
tion compounds. The sample space was thus filled with dry N_2 gas.
Unpolarized light at near-normal incidence on to basal planes
correspond to the electric field being perpendicular to the c-axis
for all data reported here.

Figure 2 shows the 300K reflectance of stage 4 graphite ni-
trate. The reflectance of pure graphite is roughly constant at
40% in this region. We associate the minimum near 1.1eV with
a plasma oscillation of free holes. The origin of the minimum
at 0.5eV isn't clear; its position and strength vary from sample
to sample. Included in Figure 2 is a theoretical curve based on
Eqs. (8), (9) and (10), with the parameters $\hbar\omega_p$ = 3.2 eV, $\omega_p\tau$ = 25
and ε_0 = 10. Comparisons with theory are only useful for illustra-
ting trends and should not be regarded as curve fits in the usual
sense. The comparison is quite good at low energy and in the
edge region. Near 0.5eV, the comparison suggests a second ab-
sorption process which produces a negative peak in the metallic
reflectance. The increase in R above the plasma minimum can be
explained by the onset of interband transitions, which lead to a
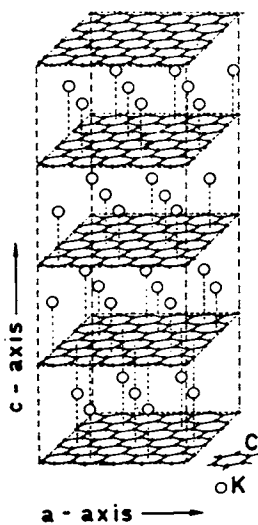
Figure 1. The first stage compound C_8K (after Ref. 4)
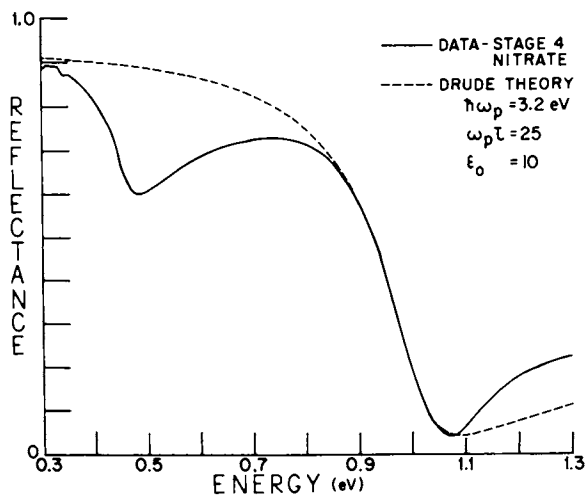
Figure 2. Reflectance of stage 4 graphite nitrate

frequency dependent ε_0.

Figure 3 compares spectra from several SbF_5 compounds, with and without HF. Variations in absolute reflectance are probably due to variations in flatness and surface quality. The reflectance minimum shifts systematically to higher energy with increasing acid strength. We also studied the sensitivity of the $SbF_5 + HF$ compound to ambient air; a further increase in the energy of the reflectance minimum was noticed when the sample was transferred into the spectrometer under N_2 gas. The low energy structure is seen to be quite variable in amplitude and energy, being almost absent in the unexposed superacid sample.

Table I summarizes the parameters obtained from preliminary analysis of reflectance spectra. Comparative values $\hbar\omega_p$ and τ in Table I were obtained for the various compounds keeping $\varepsilon_0 = 10$. Trends among the compounds are more significant than absolute values. The last three entries were obtained from the same intercalated sample; the reflectance of the free surface in contact with the acid was very low, but the reflectance minimum occurred at 2 eV. The variation in ω_p among the last three samples is most likely due to nonuniform intercalant concentration arising from an incomplete chemical reaction. (12)

One would like first of all to compare values in Table I with the corresponding values for pure graphite. This isn't strictly possible because the expected plasma edge associated with the $10^{19} cm^{-3}$ free electrons and holes is obscured in reflectivity by strong interband transitions. (This point is discussed more fully in the next section.) We can, however, estimate ω_p and $\omega_p\tau$ from measured values of N, P, m* and τ. Such an estimate shows that ω_p increases and τ decreases with intercalation, as expected from our earlier analysis. Detailed comparisons are unwise due to the fact that σ becomes complex and strongly frequency-dependent for frequencies near and above ω_p.

Thermoreflectance Spectra.

Thermoreflectance, the derivative of the reflectivity with respect to temperature, was measured by the direct heating method whereby a square wave current waveform was passed through the sample, producing peak Joule heating of approximately 0.2 W which gives an alternating ΔT of the order of 1K and an average temperature increase of 5K. The modulating frequency was 13 Hz. Optical and electronic details are given elsewhere (14). These experiments were also carried out at room temperature with near-normal-incidence unpolarized light.

Thermoreflectance experiments were undertaken in order to study variations in π bandwidth due to intercalation. In pure graphite the electronic band structure near the Fermi energy, E_f, consists of three overlapping bands which have their origin in the $2p^2$ atomic wave functions of the carbon atoms, the π electrons. The interaction between carbon layers splits the degeneracy of

these bands, giving the energy vs crystal momentum curves shown in
Figure 4. The π bandwidth is thus a measure of the innerplanar
interaction of the carbon layers. The energies E_1 and E_2 shown
on Figure 4 represent transitions from the bottom of the π_2 band
to E_f and from E_f to the top of the π_1 band, respectively. Thus
$E_1 + E_2 = 4\gamma$ gives a direct measure of the π bandwidth.

Figure 5a is a thermoreflectance spectrum of one of our pure
graphite samples. This data agrees with the results of Guizzetti
et al. (15), giving a value $\gamma_1 = 0.4eV$. Figure 5b shows a thermo-
reflectance spectrum for a stage 4 nitrate compound. The spectrum
is dominated by the thermal derivative of the plasma edge at 1.1eV
(see Figure 2) with weaker structure below (0.6 and 0.7 eV) and
above (1.7 and 2.1 eV). The two lower peaks might be interpreted
as analogs of E_1 and E_2, giving $\gamma_1 = 0.32eV$ for stage 4 nitrate.
This suggestion must remain tentative, pending a systematic study
of a range of compounds of varying stage and d spacing.

The shape of the down-up structure at 1.1eV in Fig. 5b agrees
well with that predicted from the temperature derivative of the
reflectance equation, supporting the identification of this
structure (and the associated minimum in reflectance) as a plasma
edge.

Figure 6 shows the logarithmic derivative with respect to
energy, $d(\ln R)/dE$, obtained by the calculator from the data of
Figure 2 (stage 4 nitrate). Comparing the plasma response near
1.1eV with the corresponding thermoreflectance spectrum in Fig.
5b, we notice that the positive peak is larger relative to the
negative peak in $d(\ln R)/dE$ than in $\Delta R/R$ (thermo.). This is be-
cause the former includes the effect of interband transitions
associated with the increase in R above 1.1eV whereas these tran-
sitions do not contribute strongly to thermoreflectance since they
are not associated with high-symmetry points in the zone. The
value of such data is twofold. First, the amplitude of the nega-
tive peak gives an accurate direct measure of τ if $\omega_p\tau > 5$, with-
out recourse to detailed curve fitting. Second, detailed study of
secondary structure (i.e. 0.45 eV in Figure 6) is greatly aided
by derivative techniques since it is now well-separated from the
main response. It is somewhat disturbing that the other peaks in
Figure 5b don't show up in $d(\ln R)/dE$, which makes their inter-
pretation even more tentative.

Discussion and Conclusions

The principal result of this paper is the observation of
metallic edges in reflectance spectra of intercalation compounds.
These are related to the "transmission windows" reported by
Hennig (16). The plasma edge interpretation is based upon the
following arguments: 1) general agreement with the shape predicted
by the Drude equation; 2) a temperature coefficient $d\omega_p/dT$ of
-3×10^{-4} eV/K, consistent with the influence of lattice dilation on
carrier density in simple metals; 3) thermoreflectance lineshapes
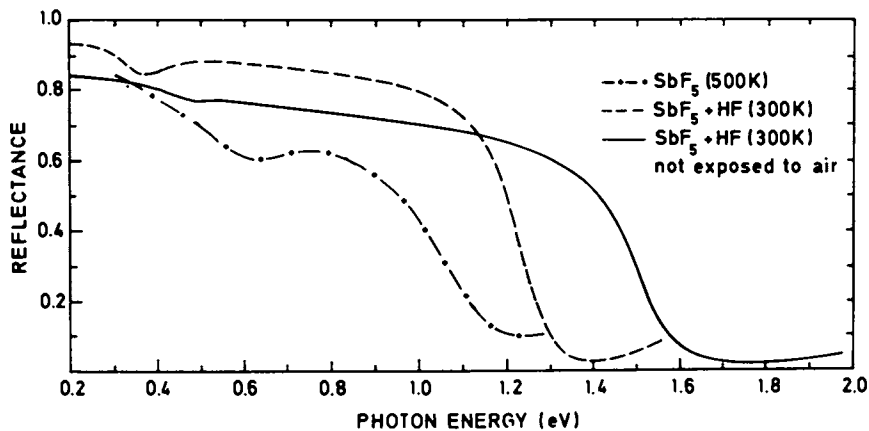
Figure 3.   Reflectance of several SbF₅ graphite compounds
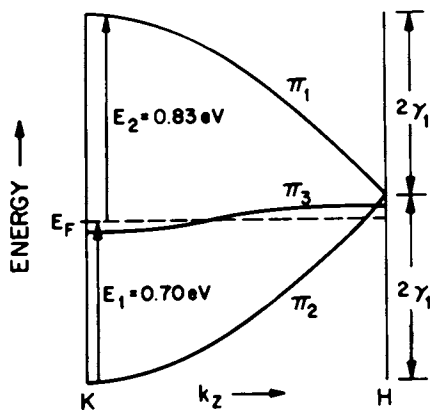
Figure 4.   Energy band structure near Eₗ
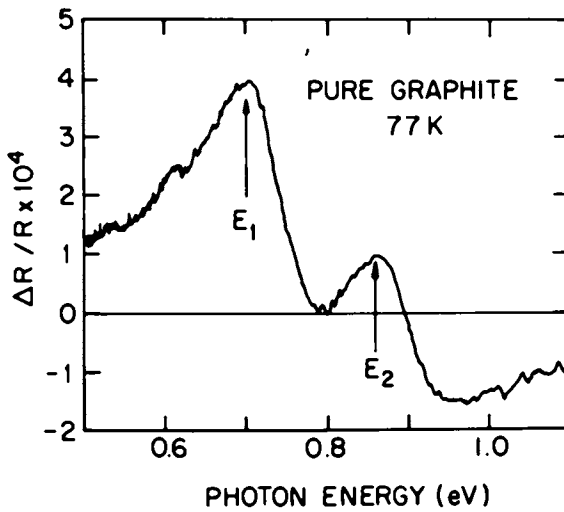
Figure 5a. *Thermoreflectance of pure graphite*
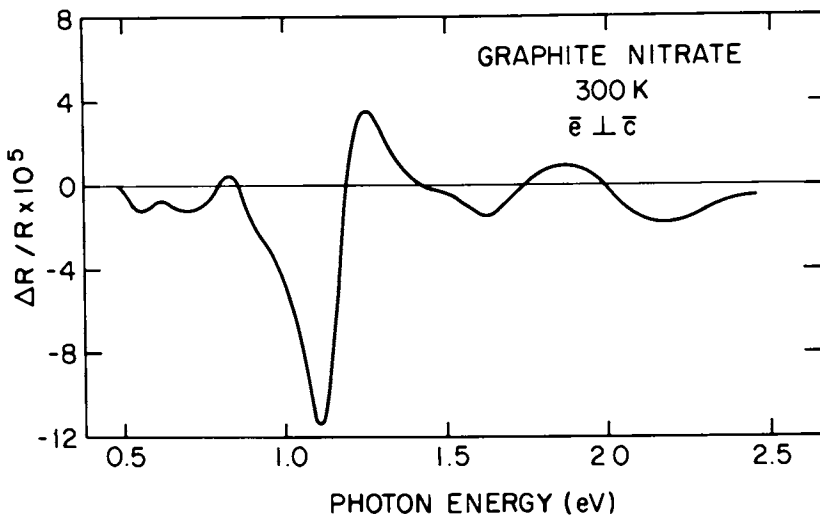
Figure 5b. *Thermoreflectance of graphite nitrate*
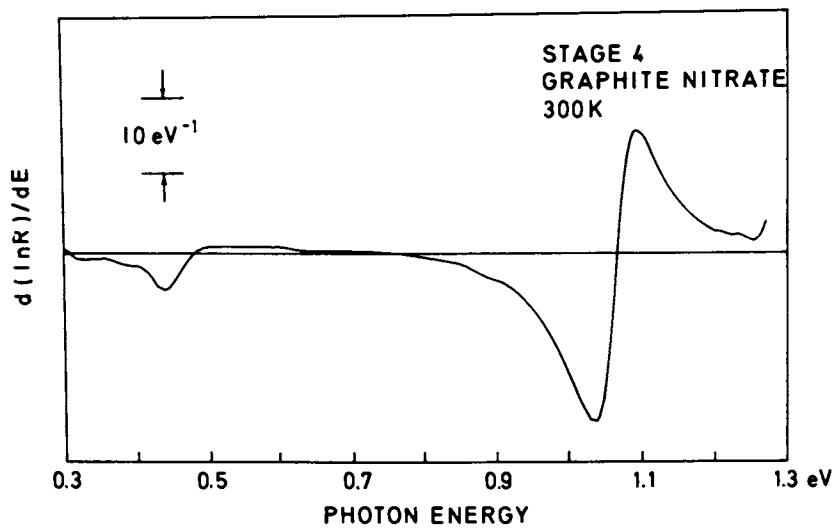
Figure 6. *Computer derivative of Figure 2*

in agreement with the temperature derivative of the Drude equation, 4) a higher plasma frequency in the SbF_5 compound compared to nitrate, consistent with preliminary measurements (7) which indicate that the former has higher conductivity.

An interesting result is obtained by comparing SbF_5+HF with HNO_3 compounds via Table I and Eqs. (1) and (11):

$$\frac{\sigma(SbF_5+HF)}{\sigma(HNO_3)} = \frac{\omega_p^2 \tau \ (SbF_5+HF)}{\omega_p^2 \tau \ (HNO_3)} \tag{12}$$

$$= (\frac{6}{3.2})^2 = 3.5.$$

According to Ubbelohde (6), $\sigma(HNO_3)/\sigma(graphite) = 12$, thus the implied conductivity increase for stage 1 SbF_5+HF is 3.5 x 12 = 42 times. Since $\sigma(copper)/\sigma(graphite) = 30$, this in turn implies that $\sigma(SbF_5+HF)$ is 40% higher than that of copper, larger than any value reported for graphite intercalation compounds, or indeed for any synthetic metal. This result is independent of the details of the reflectivity fits as long as ε_0 is approximately the same for the two compounds, because the reflectance minimum ω_0 is given by $\omega_p^2 = \omega_0^2 \ \varepsilon_0$. This prediction is of course amenable to test by direct conductivity measurements. The optical experiment has the advantages that contacts are not required and the results are not affected by anisotropy.

It would be premature at this point to attempt to partition the ω_p increase between N and m^*. We certainly expect N to increase upon intercalation, but the behavior of m^* is less predictable. For example, the above comparison between SbF_5+HF (stage 1) and HNO_3 (stage 4) could naively be interpreted as an increase in N of a factor 3.5, close to the value 4 which would be obtained if the degree of ionization and the density of ions within a plane are both independent of concentration. (Neither of these suppositions are justified.) Furthermore, Ubbelohde has shown that $\sigma(HNO_3)$ decreases slightly for concentrations beyond stage 4.

A clue can be obtained as follows. In pure graphite, the free carrier plasma is obscured by interband transitions, but the π valence (bound) electrons exhibit a resonance at 7eV. If we suppose that the 6eV plasma frequency for the stage 1 SbF_5+HF compound represents 1 free hole per 8 carbon atoms, then we can estimate (accounting for the decreased density of carbon atoms) that the average m^* for this compound is roughly 0.1 m_e. If the charge transfer is less than 1 per intercalant molecule, m^* becomes even smaller. It appears, therefore, that m^* in the compounds remains substantially smaller than the free-electron value, contrary to a suggestion by Hennig (16).

The ultimate usefulness of free-carrier plasma analysis will come from a combination of experiments which give an overdetermi-

TABLE I

Material	Comments		C-I-C Distance (Å)	$\hbar\omega_p$ (eV)	τ(sec.)
HNO$_3$ Stage 4	air-exposed		7.75	3.2	3 x 10^{-15}
SbF$_5$	air-exposed		8.41	3.5	3 x 10^{-15}
SbF$_5$ + HF	air-exposed		8.38	4.0	6 x 10^{-15}
Stage 1	N$_2$ gas ambient	center of bar		4.7	3 x 10^{-15}
		just below surface		4.9	3 x 10^{-15}
		original surface		6	-

Table II

Material		σ/σ(cu) a-axis 300K
graphite		1/30
C$_8$K	- stage 1	1/6
HNO$_3$	- stage 4	1/3
BF$_3$	- ?	5/6
SbF$_5$ + HF	- stage 1	(1.4)*

* predicted from ω_p

ned set of one-electron parameters. This procedure will be necessary to provide justification for the use of single-particle theory in the first place. (It may turn out that the d.č. conductivity is enhanced by collective phenomena.)

We have noted previously that the free carrier plasma in pure graphite does not produce the expected Drude edge in reflectance. Physically, this arises from the fact that the threshold for interband transitions in ǒnly 0.02eV so the interband strength is very large by the time ω reaches 0.4eV, the location of the expected minimum. Analytically the effect of a complex ε_0 is identical to a very small τ in Eq. (10), such that the resonance is broadened out. The observation of plasma edges in reflectance spectra of intercalation compounds thus implies that the interband strength is quite small for ω below 1.2eV. The reduction in bandwidth mentioned earlier would oppose this effect; the net result must be due to the shift in E_f.

The present work, coupled with earlier studies by Vogel on BF_3 compounds, clearly demonstrates that strong acids lead to larger conductivity increases than reported heretofore. It would be extremely interesting to learn to what extent this is due to larger fractional charge transfer and/or to large d-spacing hence a large density of states at the Fermi level. It will also be important to find out if there are any real differences between SbF_5 alone and with HF. The d-spacings are quite similar, and the differences in plasma energies shown in Figure 3 could in principle be due to contamination effects. The bandwidth hypothesis could be tested on stage 1 $SbCl_5$ for which d=9.36Å (although this compound may be difficult to synthesize).

Table II summarizes the 300K conductivities of several compounds. Values are given relative to copper to emphasize the practical possibilities. At this point we cannot estimate the maximum conductivity achievable via intercalated graphite, because we have yet to identify the limiting factors and appropriate models.

Literature Cited

(1). Hennig, G.R., *Progress in Inorganic Chemistry*, edited by F. A. Cotton (Interscience, New York, 1959), Vol. I, p. 125.
(2). Rüdorff, W., *Advances in Inorganic Chemistry and Radiochemistry*, edited by H. J. Emeleus and A. G. Sharpe (Academic Press, New York, 1959), Vol. 1, p. 223.
(3). Nixon, D. E. and Parry, G. S., J. Phys. C **2**, 1732 (1969).
(4). Rüdorff, W. and Schulze, E., Z. Anorg. Allgem. Chem. **277**, 156 (1954).
(5). Ubbelohde, A. R., Proc. Roy. Soc. (London) A **309**, 297 (1969).
(6). Ubbelohde, A. R., Proc. Roy Soc. (London) A **327**, 289 (1972).

(7). Vogel, F. L., (Unpublished).

(8). Bender, A. S. and Young, D. A., J. Phys. C 5, 2163 (1972).

(9). Moore, A. W., Chemistry and Physics of Carbon, edited by
P. L. Walker and P. A. Thrower (Marcel Dekker Inc., New York,
1973), Vol. 11, p. 69. We are grateful to Dr. Moore of Union
Carbide for providing us with aligned graphite specimens.

(10). Ubbelohde, A. R., Proc. Roy. Soc., A 304, 25, (1968).

(11). La Lancette, J. M. and La Fontaine, J., Chem. Commun. 815,
(1973).

(12). Mélin, J. and Herold, A., C. R. Acad. Sc. Paris 280, 641
(1975).

(13). Gillespie, R. J. and Peel, T. E., Advances in Physical and
Organic Chemistry (Academic Press, New York, 1971), Vol. 9, p. 1.

(14). Loughin, S., Yang, C. Y. and Fischer, J. E., Appl. Opt. 14,
1373 (1975).

(15). Guizzetti, G. Nosenzo, L., Reguzzoni, E. and Samoggia, G.,
Phys. Rev. Letters 31, 154 (1973).

(16). Hennig, G. R., J. Chem. Phys. 43, 1201 (1965).

Effect of Carbon Reactivity on the Operation of Carbon Reductants in the Iron Blast Furnace—A Comparative Study by Reflectance Microscopy

ROBERT T. JOSEPH
FMC Corp., Princeton, N.J. 08540

WILLIAM F. BERRY
W. F. Berry Associates, Murrysville, Penn. 15668

The use of carbon to smelt iron from its oxide ores is pre-historic in nature and probably began with the observation that the residue from a fire on certain soils contained a hard, non-breakable substance that could be fashioned into a weapon or tool. The carbon source was, most likely, charcoal, and because the initial process discovery remained traditional, charcoal remained the reductant used in the iron ore reaction system which can be described in its most simplistic form for hematitic iron as:

$$2Fe_2O_3 + 3C \rightarrow 2Fe + 3CO_2$$
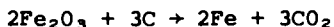
While this reaction might have been sufficient to describe what occurred in the production of iron up to the introduction of the blast furnace, the only common characteristic with present-day iron making is the use of carbon as a reductant. Even the nature of the carbon used across the centuries varied with the availability of the source and supply at any given point in time or geography.

This change in the types of carbon used is a progression from wood charcoal, to reasonably hard coals, to coke produced by thermal decomposition of soft coals, to the production of a new type of reductant by synthetic agglomeration of carbon containing materials that cannot be agglomerated by thermal decomposition alone.

The change in the physical and chemical characteristics of carbon with this progression resulted from the raw materials used and processing conditions required to make a blast furnace reductant out of that raw material. While the physical strength, shape and size are of prominent importance in specifying reductant quality for present-day coal cokes, the control by chemical characteristic has been largely implied as being the "reactivity" of the contained carbon. (1)

Reactivity of carbon is defined, for the purposes of this paper, as the comparative rate at which solid-state carbon reacts chemically with any other atom under any given arbitrary set of

environmental conditions. Since conditions are arbitrary, all
measurements of carbon reactivity are relative and bear meaning
only to results obtained through that prescribed system for
measuring reactivity.

Reactivity of carbons has been measured in the laboratory and
in actual operating commercial equipment. The work described
herein presents information from both sources.

Generally speaking, in making laboratory reactivity measure-
ments, the environment of the reaction may be varied in tempera-
ture and the substance used to react with the carbon. The nature
of this substance and the conditions imposed on the test are
usually selected to match the actual operation practiced as
closely as possible. Temperatures may be varied from 1000 to
3000°F. The reactants are usually the oxide of any atom that is
involved in the actual operation, i.e. oxides of hydrogen, carbon,
iron, etc. The systems used usually measure the amount of gas
evolved or the weight of carbon lost and, from such information, one can
calculate a reaction rate on some relative basis. That is, one
carbon is compared to another or to some arbitrarily selected
standard carbon.

The information collected may be used in formal kinetic
studies, but from the standpoint of practical application, the
data on reactivity reported here are not readily suitable for such
an analysis.

In production, the measurement of the reactivity of carbon is
carried out during production in production or semi-production
equipment. Individual carbon behavior is observed in cupolas or
blast furnaces, and the effect of reactivity is measured by com-
parison against a baseline period in terms of changes in yield,
mass balance, ease of operation and rate of production.

Some reactivities for the carbons used in the work described
herein have been determined in the laboratory by a specific stand-
ardized, but unpublished, in-house method at given temperatures,
and results are listed in Table I.

TABLE I

COMPARATIVE REACTIVITIES

Carbon Source	Intended Use	Reactivity in 10% Carbon Dioxide 1650°F 2400°F (Wt. % Loss Per Hour Reaction Time)	
		1650°F	2400°F
Formcoke (Briquetted Carbon Reductant)	Iron Blast Furnace	22	619
By-Product Oven Coke	Iron Blast Furnace	0.6	79
Beehive Oven Coke	Foundry Cupola	0.1	45

This information leaves no doubt that the formcoke, a briquetted coal-carbon reductant, is much more reactive than comparable cokes from thermal decomposition in by-product or beehive ovens.

Since the results from production practice were obtained by using by-product oven coke and formcoke of the same size in the same production equipment, the comparison of these operational results is valid regardless of the source of coal or process variation in the methods of production. What is being compared is the effect of reactivity values and not the cause of those values.

However, because the formcoke's high relative rate of carbon consumption at low reaction temperature, 1650°F, in carbon dioxide and because the 10 percent concentration is a reasonably good simulation of gas composition from the top to the bottom of the blast furnace atmosphere, extrapolation of this formcoke characteristic to expected blast furnace operation resulted in the following assumptions of probable behavior in the blast furnace: (2) (3)

1. The required formcoke per ton of hot metal produced would go up because of excess carbon gasification in the top regions of the furnace before temperatures occur where iron ore reduction could begin.

2. The pellet (briquet) strength would be eroded because of the intrapellet reaction with carbon dioxide and water vapor which would destroy the bonds that formed the pellet and produce particulate matter that is carried out with the gas stream; this assumes binder coke to be more reactive than coal cokes.

3. The pellet would absorb iron and slag at a much greater rate, because of this attack on its particulate micropore structure, than would oven coke - which is derived from a coalesced molten coal and has little or no micropore volume - and would allow considerable penetration by the molten iron and slag.

In the case of studies to determine the effect of solid carbon reactivity on cupola operation, in the middle and late 60's, considerable commercial scale experiments were carried out and reported in the literature of various meetings in Great Britain and on the Continent. These efforts indicated that reactive coke, did not perform as well as did the baseline coke. Off-gas analyses showed an increase in CO/CO_2 ratio indicating less heat released in the cupola which resulted in lower yields of molten metal for foundry casting. With respect to the chemistry of subsequent iron, there appeared to be insufficient carbon pickup to produce gray iron which was attributed to the lower hot metal temperature as a result of the carbon gasification due to higher reactivity.

While there was no comparison to formcokes or to highly reactive formcokes, the conclusion based on the oven coke work was applied to formcokes and extrapolated from cupola to blast furnace.

These conclusions, based on variation in reactivity of oven cokes, necessitated proof that the highly reactive formcoke would not cause an adverse effect on blast furnace operation. With this factor in mind and the drive to use low-rank coals that could not be part of any oven charge, the British Steel Corporation embarked on a blast furnace test program to determine whether or not formcokes made from these low-rank coals could be used as the carbon source for reducing iron.

Three thousand tons of briquets, which were produced in Southwest Wyoming from a coal that does not melt and coalesce, were tested in a week-long campaign in a blast furnace in Cardiff, South Wales. (4)

The results from this test show that these predicted descriptions of the behavior of the reactive formcoke briquets in the blast furnace did not occur.

In fact, the information collected indicates these briquets to have performed to the contrary. The behavior of the briquets was compared to the behavior of a high-grade furnace coke made from a coal that melted and coalesced in a by-product oven under closely controlled furnace conditions. Some results from this test, pertinent to the topic of this paper, are listed.

TABLE II

ABBREVIATED RESULTS,
COMPARATIVE OPERATION OF
BRITISH STEEL CORPORATION NO. 3 BLAST FURNACE
AT CARDIFF, WALES

Type of Coke	Furnace Coke	Formcoke
Reactivity of Coke at 1650°F in 10% CO_2 (Wt. % loss per hour reaction time)	0.6	22
Size of Coke (Nominal mm)	44	38 x 38 x 25
Carbon Rate (Kg of carbon/metric ton of iron)	479	471
Production Rate (Metric tons of iron per day)	805	873

As can be seen, despite this great difference in reactivity of the coke carbon at 1650°F, the formcoke required per ton of hot metal was a bit less. However, the yield of iron was greater in the period when formcoke briquets were the reductant.

It may be argued with some validity that the reactivities of coal carbons tends to merge as the reaction temperature in an oxidizing atmosphere increases. An attempt to demonstrate this by an in-house experiment in a 10 percent CO_2/90 percent nitrogen atmosphere was made. Results are shown as a complete curve of weight loss rate versus reaction temperature, on an equal exposed surface basis. Figure 1 presents these results.
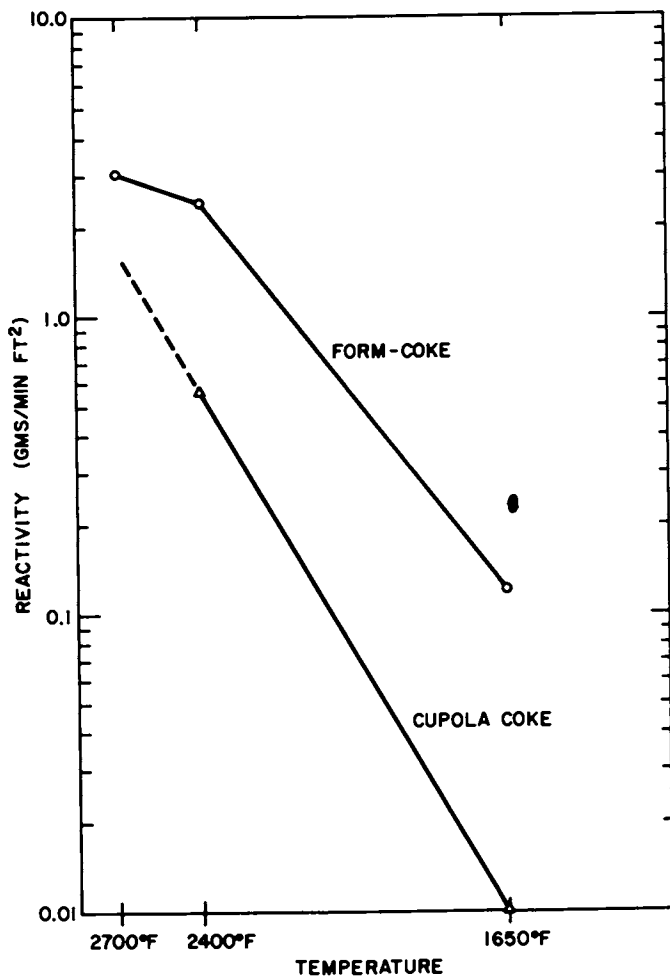
Figure 1. *Form-coke vs. oven-coke. Effect of temperature on re-activity in 10% CO₂.*

Notice how the rate loss curves tend to merge as the temperature approaches 2700°F which is about 300°F above the molten temperature of reduced iron. In the region of 2400°F, consumption of solid carbon in formcoke falls off by a factor of about two. This is attributed to a change in reaction mechanism from rate to diffusion·control. The practical importance of this is that under furnace conditions at these elevated temperatures, the oxidizing gases – carbon dioxide and water vapor – do not penetrate the formcoke structure and react internally. Therefore, it can be expected that the briquet will hold its shape and strength throughout its history in the furnace. While work in Japan (2) has indicated – with oven cokes – higher reactivity results in lower strength at high temperatures under furnace conditions (micro-strength), the data contained herein predict otherwise. When coupled with the slightly lower amount of formcoke necessary per ton of hot metal, it would appear that the formcoke iron ore chemistry must be different from oven coke iron ore chemistry; that high rate reduction of iron ore by the formcoke used takes place at a much lower temperature than when using oven cokes. Table III compares the rate of reducing iron ores by this type of formcoke – made from a broad rank selection of coals – with "high-grade" oven coke.

TABLE III

COMPARATIVE IRON ORE REDUCTION
FORMCOKE VS. OVEN COKE

Coal From Which Reductant Was Produced	Rank of Coal (ASTM)	10% CO_2 Reactivity %/Hr @ 1800°F	% Reduction 60 Minutes @ 1800°F
Appalachain Coking Coal Blend	(Produced in By-Product Oven)	2.7	39.4
South Africa	MVB	10.0	90.0
Kentucky	HVAB	24.6	90.8
Illinois No. 6	HVAB	22.3	93.8
Utah	Sub-bituminous A	24.3	89.0
Wyoming	Sub-bituminous B	23.5	91.6
Texas	Lignite	57.2	94.2

In the American counterpart to this British effort, (5) 20,000 tons of formcoke briquets were charged, and the test was considered successful. The test was run for one month on Inland Steel's No. 5 furnace at better than 100,000 ACFM blast rate.

During each of these tests, samples of the carbon reductants that were charged, were taken; samples of each reductant were recovered from the coke that had been through the entire furnace and escaped out the tap hole with the molten metal with each cast to remove hot iron from the furnace. These samples were examined by reflectance microscopy using a method described in the literature (6) after which were developed the ASTM Standards D-2796, D-2797, D-2798 and D-2799-72.

Essentially, the method consists of embedding a sample of the coke in some suitable plastic, polishing and embedded sample to an optical flat, observing the sample, which is illuminated by a light source of 548 nanometers wave length and recording the mean maximum reflectance, γ_o, at different stage angles. During this analytical procedure some 1,000 photomicrographs, at different magnifications were taken and analyzed. Of all the photomicrographs studied, Plates I through XVII were selected as best illustrating the general conclusions drawn from this work and presented here:

I. Formcoke Briquets Charged to the Furnace.

1. These formcoke briquets, in all cases, appear individually as a uniform structure throughout. The carbon from the binder source amounts to about 5 percent of the carbon content of the briquet and is equivalent to approximately 15 percent binder in the original undevolatilized specimen.

2. The formcoke briquets, in all cases, are strong with a total internal porosity of approximately 40 to 45 percent. The briquets are relatively dense in appearance and result from an apparently well-mixed, well-bonded uniform mass. The pore volume is in a micropore structure and not the result of large, interconnected holes. This is the basis for the briquet strength which translates to an ability to support 4,000 pounds per square inch at furnace operating temperature.

3. As a result of this uniformity, the reactivity of the entire briquet is equal as the briquet enters the furnace, and any changes in reactivity as the briquet passes through the furnace can be expected to be uniform.

4. The internal structure appears free from cracks and flaws.

II. Partially Consumed Formcoke Briquets Recovered From the Top of the Molten Iron Cast.

1. The recovered formcoke briquets retain uniformity, strength, and have increased in microporosity by only 4 percent.

2. The oxidation of the briquet carbon is strictly topo-chemical with penetration not exceeding 1 mm uniformly, even with specimens that have been 90 percent consumed. The topochemical reaction process applies to all reactions including the alkali attack on anisotropic carbon to form alkali-carbides. The unreacted portion of the briquet appears about the same in structure as the briquets before charging to the furnace.

III. By-product Oven Furnace Coke Charged to the Furnace.

1. The oven coke charged appears strong and uniform with a porosity of about 30 percent. This porosity is developed in the macropore structure and results in the very small surface area measured in most oven cokes, about 2 to 3 sq. meters per gram.

2. There appears to be a reasonably small amount of aniso-tropic carbon, but what amount is present appears to be non-uniformly distributed.

3. There is a basic crack system that appears through the coke which does not appear to effect the cold strength of the coke.

IV. Partially Consumed By-product Oven Coke Recovered From the Top of the Molten Iron Cast.

1. The structure and porosity of the oven coke allowed a complete internal reaction with all internal surface areas of the coke. This should be compared to the strictly topochemical reactions displayed by the formcoke samples exposed to the same process.

2. This extensive internal reaction has weakened the remaining coke structure to the point where the burden support necessary in the blast furnace is impared.

3. There is deep and extensive penetration of the oven coke by iron, slag, and alkali-carbides into the internal coke structure.

4. Alkali-carbide deposition is apparent throughout the entire structure of the oven coke, and the deposition of the alkalies appears to have a strong affinity to the anisotropic carbon forms of the coke.

5. Penetration of vapor or liquid phase iron, appears to cause a strong carbon reaction around the area of penetration leading to graphite formation.

6. Penetration of slag into the coke's structure seems to be unrelated to any carbon reaction within the coke. The slag appears to seal off the coke porosity.

As best as can be determined by the analyses of the photo-micrographs, with formcoke briquets the chemistry within the blast furnace is strictly surface - - - topochemical - - - wherein the original formcoke strength properties are retained over the whole reaction period. The comparable furnace chemistry for by-product oven coke indicates nonuniform but deep penetration into the center of the coke piece that tends to destroy the original coke structure, reduce the strength, and permit almost saturation of coke by slag and iron which seal off pores and slow down or stop the reaction.

LITERATURE CITED

1. Thompson, R. R., Mantione, A. F., Aikman, R. P., Blast Furnace Steel Plant, "Improvement of Coke Uniformity Through Measurement of Coke Reactivity", (March, 1971).

2. Nippon Steel Corporation/FMC Corporation, Private Communication, "NSC's View as to the Correlation Between the Coke Strength and Reactivity", (May, 1971).

3. Price, J. D., Proceedings of American Institute of Mechanical Engineers, "Coke Combustibility: A Neglected Characteristic", (February, 1959).

4. Holgate, J. K., Pinchbeck, P. H., Journal of the Iron and Steel Institute, "Use of Formed Coke: BSC Experience 1971/1972", (August, 1973), pp 547-566.

5. Laursen, F. W., Engineering and Mining Journal, "News Release", (February, 1975), 176, (2).

6. Gray, R. J., Schapiro, N., Blast Furnace and Steel Plant, "Relation of Coke Structure to Reactivity", (April, 1963) pp 273-280.

31

Comparision of Evolution of Heteroatoms from Coal and Petroleum Based Electrode Cokes

GEOFFREY M. KIMBER and M. DAVID GRAY

National Coal Board, Research Establishment, Cheltenham, England

The National Coal Board, England, are presently developing a process for the production of electrode coke from coal utilising solvent extraction under non-hydrogenating conditions.

Potential markets include both the graphite and carbon electrode industries which supply arc steel and aluminium smelters and use, at present, varying grades of petroleum coke.

In order to assess the quality of the electrode coke from coal, it was necessary for the National Coal Board to build up background knowledge not only by using the empirical tests developed for petroleum coke, which may not necessarily be relevant, but also by investigating more fundamental aspects.

This paper reports results of investigations into reactions which occur when calcined electrode cokes, both coal extract and petroleum based, are heated to graphitising temperatures. It shows that although there are differences between the types of coke, there are potential advantages in using a coal-based coke.

Experimental

The coal extract was made from a bituminous British coal by solvent extraction by anthracene oil at around 400°C for about 1 hour. The resulting coal digest was filtered and solvent recovered from the filtrate; coking at about 500°C under atmospheric pressure followed the solvent recovery. Much research on these stages has been done at the Coal Research Establishment, some of which has been described by Gray and Owen (1). A petroleum thermal tar (a feedstock for premium electrode coke manufacture) was subjected to a similar coking treatment (giving a 34% green coke yield). The resultant green cokes were calcined at 1300°C prior to kinetic studies at temperatures up to 3000°C.

In this study the necessary heating and cooling rates were achieved by using the apparatus shown in Figure 1. This consists of a graphite susceptor, weighing when loaded less than 100g, insulated with carbon black and inductively heated using a
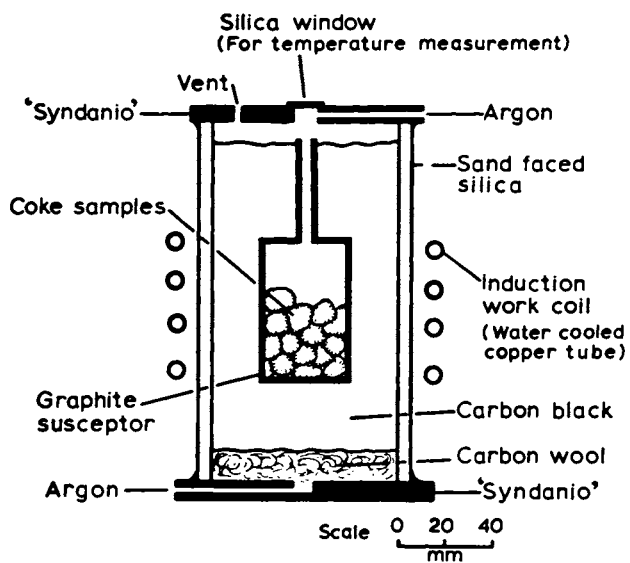
Figure 1.   Heat treatment furnace

450 MHZ 'Radyne' generator. The input power to the susceptor
was varied manually, up to a maximum of 8 kW, to give rates of
heating of 100°C min⁻¹ up to 1200°C and 50°C min⁻¹ thereafter;
the residence time at the heat treatment temperature (HTT) was
normally 10 min. The cooling rate was about 100°C min⁻¹ from
2500°C reducing to 50°C min⁻¹ at 1500°C. For each test the
susceptor was loaded with about ten individually identified and
weighed pieces of coke, including one piece of the 'control'
petroleum coke so as to avoid the inherent difficulties in
reproducing heat treatments at elevated temperatures.

        After heat treatment the coke pieces were reweighed and
prepared for elemental analyses and in the case of extract cokes,
where sample size permitted, for determination of density by
immersion in water. All samples were subjected to X-ray
diffraction tests using a Guinier de Wolff quadruple focussing
camera with highly crystalline quartz as a standard. Mean
crystallite heights and diameters (L_c and L_a respectively) were
calculated from the measured half peak widths.

Results and Discussion

        The results of these tests are shown in Table I and
Figures 2 and 3.

        Sulphur. Although the sulphur contents of the two types of
calcined coke are the same, coal extract cokes evolve their
sulphur at a lower temperature, losing over 90% after 10 min.
at 2500°C; in contrast, after 10 min. at 3000°C, 25% of a
petroleum coke's sulphur still remains. This indicates that the
sulphur is relatively less strongly bound in the coal extract
coke structure and thus, when being evolved, is likely to cause
less disruption to the structure. It is perhaps not surprising
therefore that it is possible to graphitise a carbon artefact
made from coal extract coke without needing any additive to
prevent puffing which normally occurs when petroleum cokes are
used.

        Nitrogen. The nitrogen content of the coal extract coke is
the higher, but most of it is evolved before 2000°C is reached
when the level is the same as for petroleum coke.

        Weight Loss. It will be seen from Table I that during heat
treatment coal extract cokes lose more mass than petroleum coke.
If these results are viewed in conjunction with the heteroatom
evolution it will be seen from Figure 2 that whereas petroleum
coke loses only its heteroatoms ($\triangle N + \triangle S = \triangle W$) the coal extract
coke evolves on average about 1½ atoms of carbon with every
heteroatom ($\triangle N + \triangle S \simeq \triangle W/2$) regardless of whether nitrogen,
at 1300-1750°C, or sulphur, at 2000-2500°C, is the major hetero-
atom being driven off. Whether this is because, in the release

Table I

Heat Treatment		Weight Loss above 1300°C		Density	Analyses of Heat-treated Cokes on dry ash free basis				
Temperature	Time	Average	Mean Deviation		C	H	N	S	O
°C	min.	%	%	mg mm^{-3}	%	%	%	%	%
Coal Extract Coke									
1300	10	0.621	0.098	2.084	98.6	0.1	0.65	0.60	0.2
1590	10	1.286	0.047	2.126	98.6	<0.1	0.40	0.70	0.2
1750	100	1.776	0.134	2.148	98.9	0.1	0.12	0.60	0.1
1740	10	1.900	0.121	2.145	99.1	0.1	0.04	0.60	0.2
1950	10	2.308	0.206	2.163	99.3	<0.1	0.02	0.40	<0.1
2210	10	2.495	0.136	2.172	99.6	<0.1	0.03	0.30	<0.1
2480	10	2.5	0.3	2.196	99.9	<0.1	0.04	0.05	
3000									
Petroleum Coke									
1300	10	0.141			99.1	<0.1	0.20	0.70	0.1
1590	10	0.152					0.09	0.70	
1750	10	0.181					0.05	0.70	
1740	100	0.50					0.02	0.60	
2210	10	0.43					0.04	0.45	
2480	10	0.70					0.04	0.40	
3000	10							0.20	

Figure 2. *Weight loss from calcined cokes*
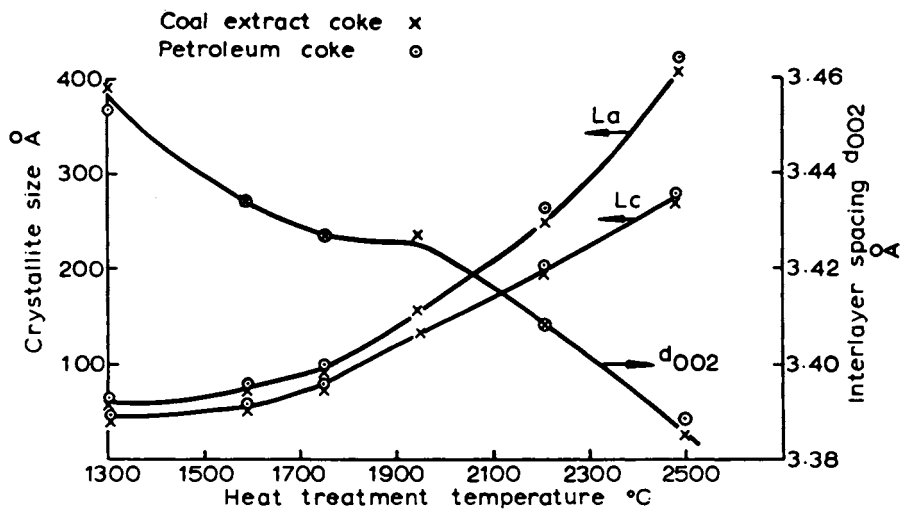
Figure 3. *Effect of heat treatment on crystallite dimensions*

of nitrogen or sulphur, carbon to carbon bonds are being broken rather than carbon to heteroatom ones, has not been positively identified but there is no doubt that the coal extract hetero-atoms are bound differently in the coke structure to those of petroleum coke.

It is of interest to note that 100 min. at 1740°C are equivalent to 10 min. at about 1880°C in respect of weight loss. Although this is the early stages of graphitisation, it is equivalent to an activation energy of 140 kcals mole^{-1}, a value not in conflict with values given by Hutcheon (2).

Density. Water displacement density (Table I) of coal extract cokes increases progressively from 2.084 mg.mm^{-3} after heating to 1300°C (within the normal specification for a premium grade electrode coke) to almost 2.20 mg.mm^{-3} after heat treatment at 2480°C. The bulk density of the coal extract cokes was similar to that of the petroleum coke used as standard. The dimensional stability on heating to 2500°C was good, i.e. a volume change of less than ½%.

Crystallite dimensions. Although it has recently been reported by several investigators, including Evans et al (3), working on coal extract coke heat treated to 2400°C, that high resolution electron microscopy shows the existence of graphitic crystallites an order of magnitude larger than the average calculated from x-ray diffractograms, this does not discount the use of the much simpler x-ray technique for comparative studies such as reported here.

It will be seen from Figure 3 that although petroleum coke always exhibits a larger crystallite size, the differences are hardly significant, reducing from 10% at 1300°C to a mere 3% at 2500°C. Thus, no alteration in current graphitising procedure would appear to be necessary if a change were made to coal extract coke based artificial graphites.

Of the original calcined cokes, the coal extract based material had the larger interlayer spacing (see Figure 3), indicating a wider divergence from true graphitic spacing probably due to its higher heteroatom content. However, it will be noted that by 2500°C the positions are reversed with the petroleum based material exhibiting both the larger interlayer spacing and heteroatom content.

Conclusions

Sulphur evolution from coal extract cokes takes place with less disruption to the carbon structure than in petroleum cokes; puffing inhibitors are unlikely to be needed in artificial graphite production using coal extract cokes. In addition to identifying this processing advantage the study has shown that coal extract coke has the potential necessary to make a good

electrode in that it graphitises as well as petroleum coke.

Acknowledgments

Abstract

A route for making, from coal, a high-purity coke suitable for the manufacture of both graphite and carbon electrodes has been developed. This process for electrode coke involves the solvent extraction of coal and is part of a wider National Coal Board programme into the beneficiation of coal which includes, besides electrode coke, hydrocarbon products, chemicals and carbon fibres. This paper describes the heat treatment of cokes in the range 1300-3000°C and shows that the heteroatoms in coal-based extract cokes are bound to the carbon structure in a different manner to those in petroleum coke. By measuring the growth of graphitic crystallites by X-ray diffraction, it is also shown that the rates of graphitisation are similar for both types of coke.

Literature cited

1.   Gray, M.D. and Owen, J. "Liquid Solvent Extraction of Coal - Influence of Process Conditions on Extract Properties", presented at Round Table Discussion "Chemical and Physical Valorisation of Coal", Rome, September, (1973).
2.   Hutcheon, J.M. "Modern Aspects of Graphite Technology", 18 Academic press London,(1970).
3.   Evans, E.L., Jenkins, J.L. and Thomas, J.M., Carbon (1972), 10, 637-42.

Plate I.   British steel test—Cardiff, Wales (July 1972).   Formcoke reductant before charge to furnace.

Location of photomicrograph—edge to 1 mm deep. Magnification—414×. The plastic embedding material (P) can be seen as a background of dark red. The dust suppressant (E) is almost the same shade of red as the plastic but appears as a very thin edge layer that penetrates to the 1 mm depth boundary. Char (C), the de-volatilized coal particle, is light red. The char particles, which were originally 2000–20 μ, appear to be a continuous phase interrupted only by occasional voids which appear as dark, almost black, areas throughout the plate. Voids are pointed out instead of pores, because the pore structure in this material is below 10 μ in average diameter and is not delineated by the method used to produce the plate. The yellow spot at 11 o'clock is the residue from original coal mineral matter. The relative homogeneity of this part of the specimen is consistent throughout the entire sample and from sample to sample.
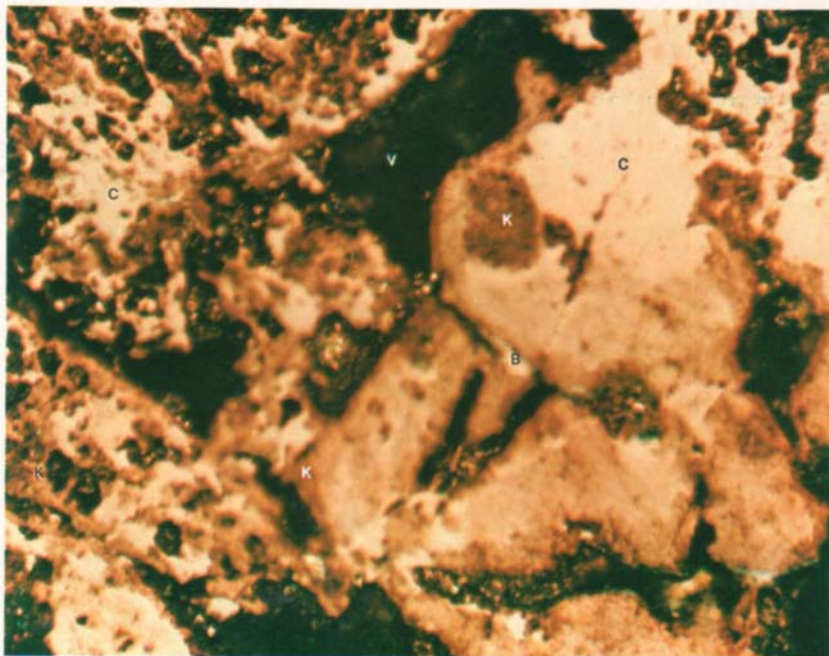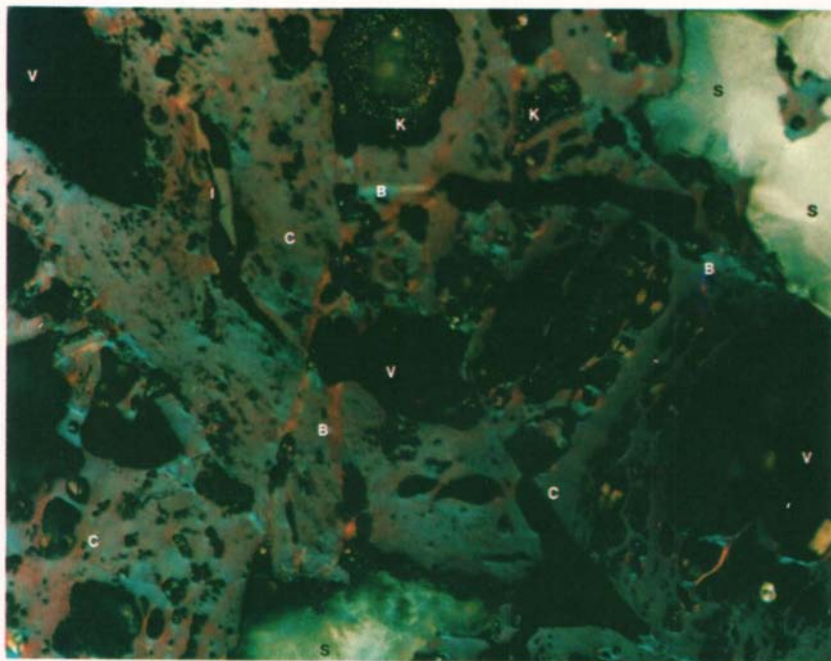
Plate II. *British steel test—Cardiff, Wales (July 1972). Formcoke reductant recovered from the ladle.*

Location of photomicrograph—edge to 1 mm deep. Magnification—180×. This plate shows the reaction area and the unattacked interior of the recovered specimen. In the upper left corner (C) is a char particle at the sample edge that has seen reaction to the furnace environment. It was penetrated almost completely causing pockets of alkali (K) to form. This char particle was 0.5 mm before attack. Just in from this reaction area is the unattacked char mass (C). Reaction has begun at the particle edges, but the binder bridges (B) appear as solid areas of pale yellow. Because of the sample orientation, alkali (K) from reaction occurring perpendicular to the plate plane is noted at any area bordering the voids (V). The mechanics by which reaction occurs is easily concluded to be the layer reaction (topochemical).

Plate III. British steel test—Cardiff, Wales (July 1972). Formcoke reductant recovered from the ladle.

Location of photomicrograph—edge to 1 mm deep. Magnification—310×. The persistence of binder–char bridges even after the intense reaction and violent environment of passage through the blast furnace is demonstrated. Binder residue coke (B) is apparent as both light-blue and pink areas that bond together char particles (C) throughout the plate. Again, the area viewed is at the 1-mm deep limit from the bottom at the right side of the plate. A very small area of iron (I), appears at 11 o'clock and is presumed to have been an occlusion in the original formcoke. The large ring of alkali at 12 o'clock is a mixed carbide and appears to be at the reaction limit of penetration. The light white–blue material at the upper right-hand corner and bottom center is slag (S) penetration following the reacting away of that char layer by the furnace atmosphere and charge. Even in this reacted area, char particles (C) appear undisturbed and strongly bound to other char particles. Note that this reaction is 1 mm deep at most.
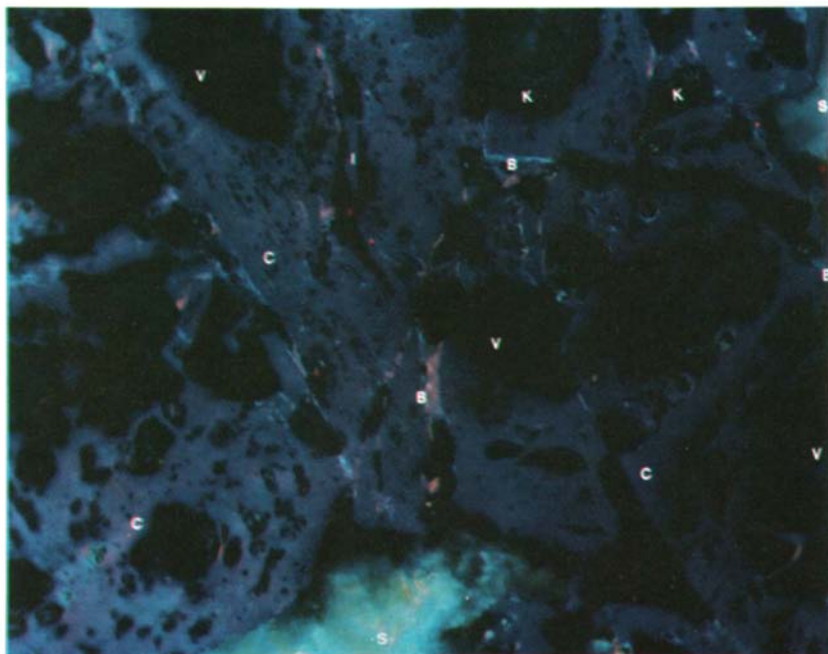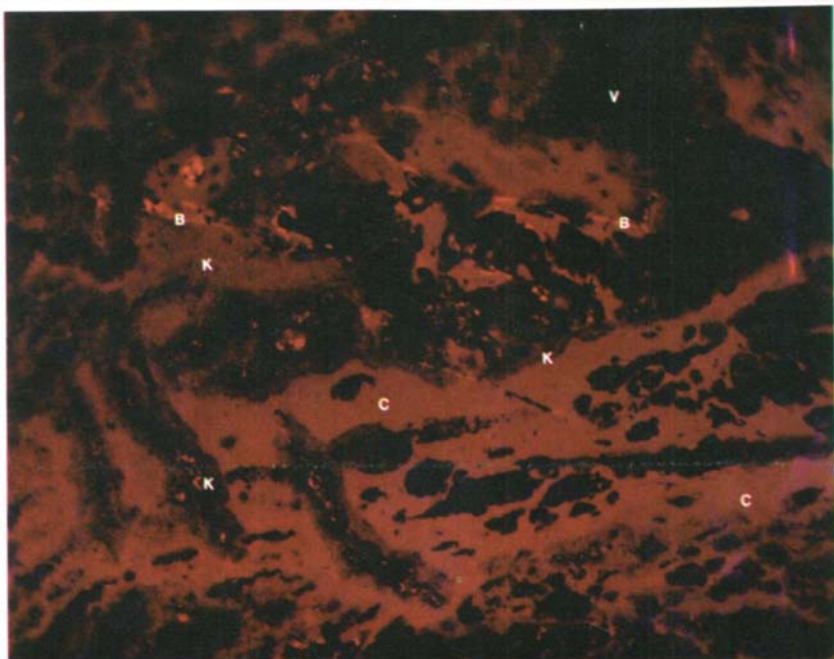
Plate IV. British steel test—Cardiff, Wales (July 1972). Formcoke reductant recovered from the ladle.

Location of photomicrograph—about at sample center. Magnification—414×. This plate carries the area viewed further in toward the specimen center and presents more and stronger evidence of the relatively homogeneous structure of the formcoke not more than 1 mm from the violent oxidation occurring at the specimen surface. Filters were changed to highlight binder coke (B) pink and blue bridges between char pieces, very firmly joining char particles (C) throughout the slide. The voids (V) occur regularly throughout the plate, and the char and binder coke are equally firm and unattacked. Again, this area is not more than 1 mm from the edge. Slag, alkali, and iron inclusions are muted by the filter.

Plate V. *British steel test—Cardiff, Wales (July 1972). Formcoke reductant recovered from the ladle.*

Location of photomicrograph—about at sample center. Magnification—414×. This plate displays the center of a formcoke briquet after the specimen had passed through the entire furnace and was about 80% consumed. The binder coke bridges (B) to char particles (C) are still as sound as in the original formcoke. The fact that this specimen was through the furnaces and had seen a temperature history of 3000–4000°F in an oxidizing atmosphere with respect to carbon is attested to by the formation of alkali carbides (K) in the area of the specimen center as a result of original coal mineral matter residue reacting with char (C). The absence of iron or slag penetration is again evidence that the reaction mechanics, with respect to blast furnace environment, is strictly topochemical.
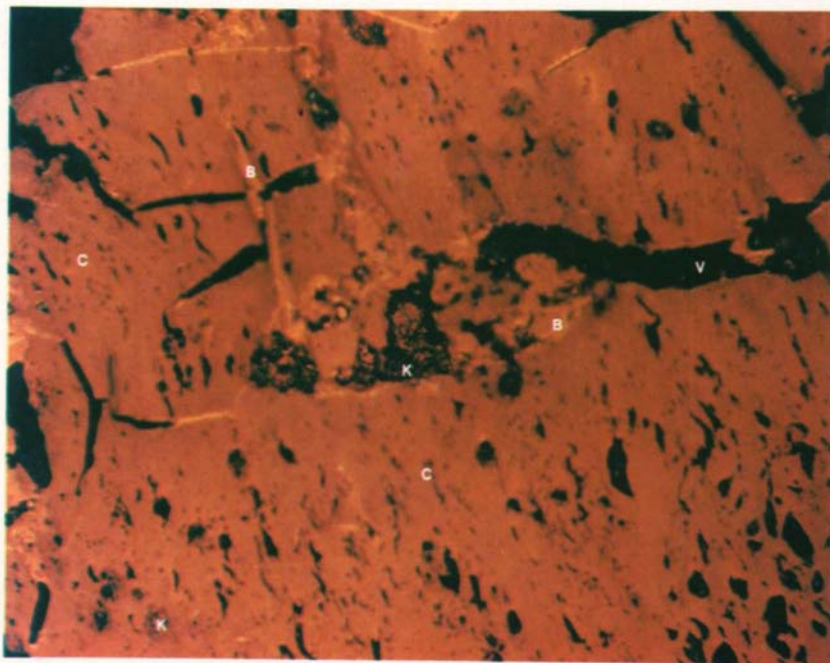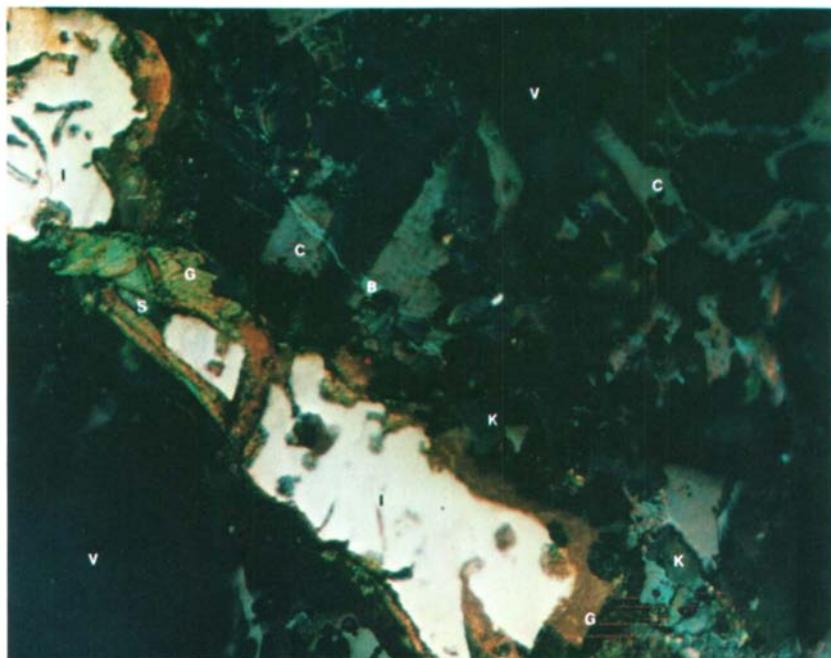
Plate VI. British steel test—Cardiff, Wales (July 1972). Formcoke reductant recovered from the ladle.

Location of photomicrograph—about at sample center. Magnification—414×. This plate, like Plate V, is at the center of a recovered specimen. The filters were changed to enhance the appearance of the alkali carbides (K) and to show that these occlusions were just that. No apparent connection with the reaction occurring at the surface could be found. Again, the binder coke–char bond is still intact and appears the same as similar bonds observed in the unreacted sample charged to the furnace.

Plate VII. *British steel test—Cardiff, Wales (July 1972). Formcoke reductant recovered from Tuyeres.*

Location of photomicrograph—edge to 1 mm deep. Magnification—414×. During the test some samples were obtained from the Tuyeres where specimens appear to have not lost any shape even though being reduced in size by reaction. This plate views an area to 1 mm in from the edge which lay at the lower right-hand corner and shows an iron–slag–graphite–alkali structure formed as a result of intense reaction at the surface. Graphite (G) occurs as a bridge between two segments of iron (I). Since alkali (K) is always associated with the graphite formation in all the photomicrographs studied, the alkali carbides may be either catalysts or forerunners to synthetic graphite development; that the reaction is limited to the depth of about 1 mm can be seen from the solid bond of char particle to char particle by binder coke (B), a pinkish-blue bridge between them.
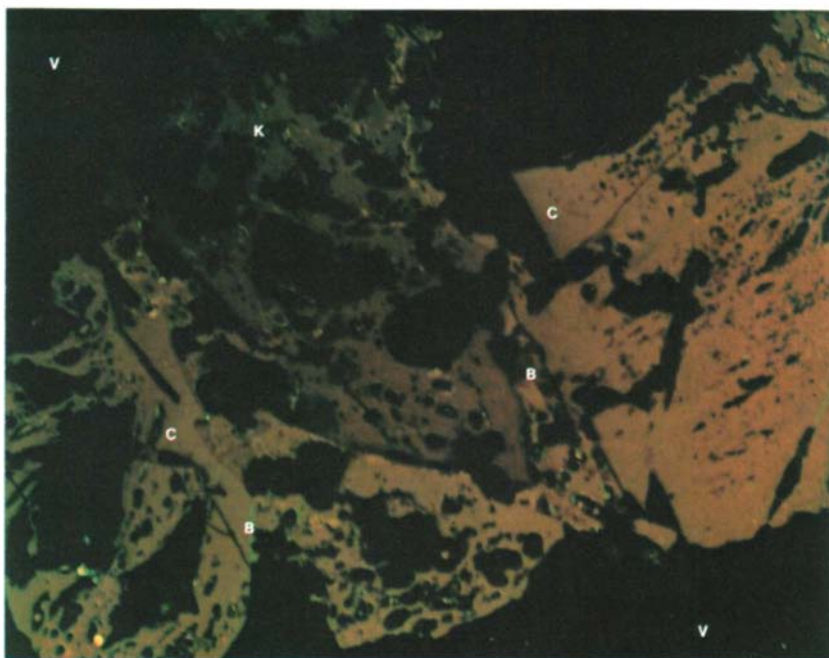
Plate VIII. *British steel test—Cardiff, Wales (July 1972). Formcoke reductant recovered from Tuyeres.*

Location of photomicrograph—edge to 1 mm deep. Magnification—414×. This plate emphasizes the fact that reaction occurs only on the surface of this highly reactive reductant. The surface is at the upper left-hand corner of the plate. The most obvious structures are the partially reacted particles (C) to the left of the plate and the unreacted particle to the right. The areas marked V are voids. Binder coke bridges (B) bond particles even in the reacted areas as long as there is unreacted material present. In short, even within the small particle, the carbon structure is such that only the surface reacts. An explanation for this may be postulated from Figure 1. In this type of formcoke, there is an extensive micropore system. This system is not a connected structure, but each pore or group of pores is isolated one from the other. Above 2400°F, Figure 1 shows that a diffusion controlled reaction appears to be limiting wherein gaseous products are prevented from penetrating beyond the surface.
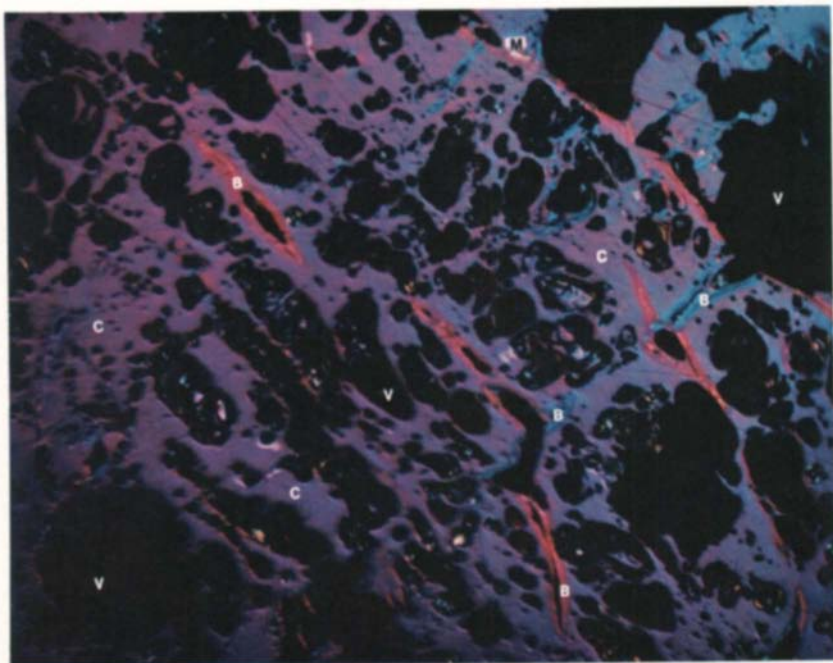
Plate IX. British steel test—Cardiff, Wales (July 1972). Formcoke reductant recovered from Tuyeres.

Location of photomicrograph—edge to 1 mm deep. Magnification—202×. By proper selection of color filters, binder–coke bridges (B) can be seen throughout the plate. The edge of the specimen is at the upper right-hand corner, and a partially reacted area is seen as an isthmus connecting two large voids (V). Each of the char particles (C) of original size or crushed by the processing, can be seen bound, at its limits, to another char particle by binder coke. Again, this specimen has passed through the furnace and only reacted at the edge. The interior seems to have been unaffected by the occurrences at the surface. This plate emphasizes the reason for continued specimen strength even though about 50% of this sample had been reacted.
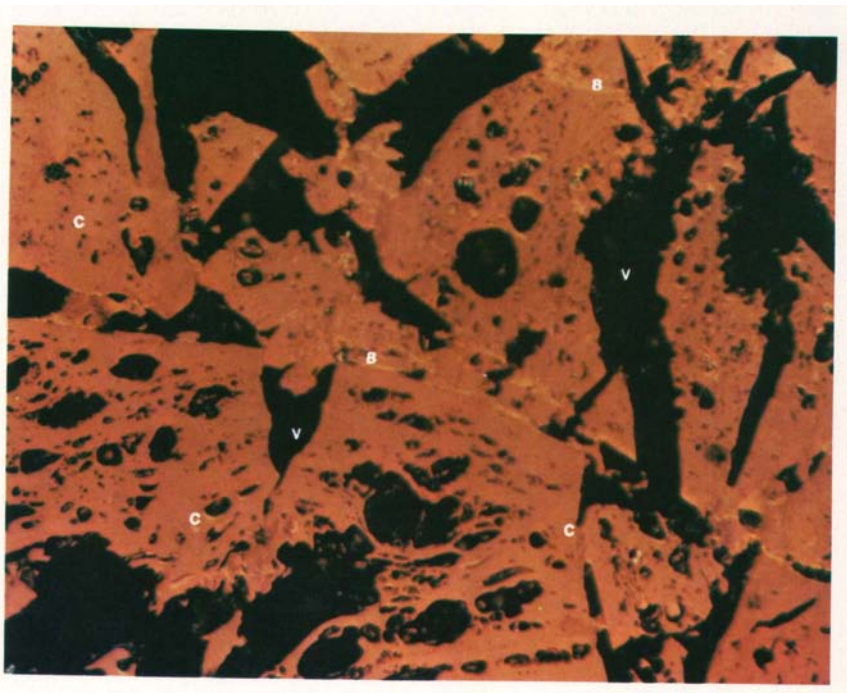
Plate X.   British steel test—Cardiff, Wales (July 1972). Formcoke reductant recovered from Tuyeres.

Location of photomicrograph—about at sample center. Magnification—414×. The center of this sample was about 25% consumed. The presence of unreacted char particles (C) and binder–coke bridges (B) serves to confirm again the surface nature of the furnace environment reaction to this formcoke.
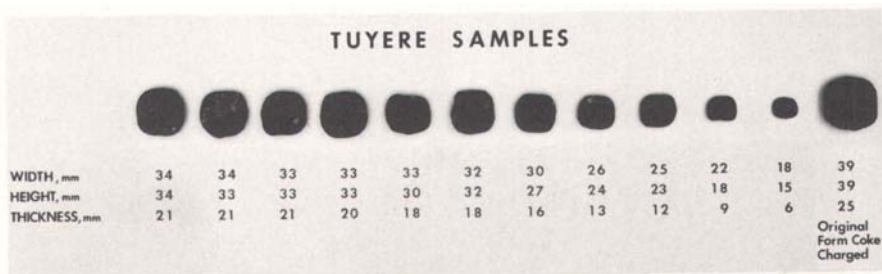
TUYERE SAMPLES

WIDTH, mm	34	34	33	33	33	32	30	26	25	22	18	39
HEIGHT, mm	34	33	33	33	30	32	27	24	23	18	15	39
THICKNESS, mm	21	21	21	20	18	18	16	13	12	9	6	25

Original Form Coke Charged

Plate XI. British steel test (July 1972). Formcoke reductant recovered from the Tuyeres.

The specimens show that, despite predictions that high reactivity would permit corrosion of the binding bonds and reduce the specimen to rust, the formcoke was consumed equally from all directions and maintained shape and internal structure. Microporosity increased by only about 3%. The density remains about the same on the average from the sample recovered: 0.9–1.0 g/ml.
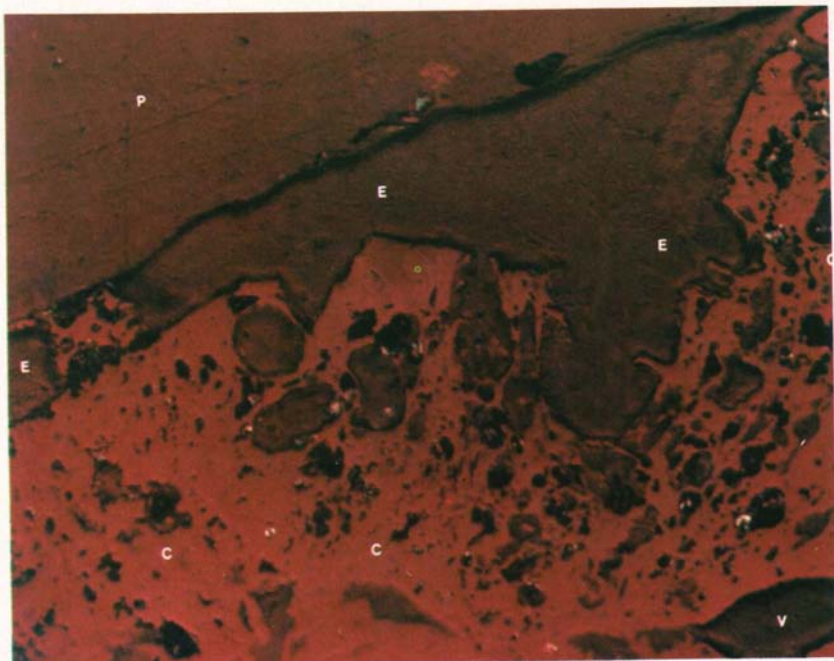

Plate XII. Inland steel test—S. Chicago, Ind. Formcoke reductant before charge to blast furnace.

Location of photomicrograph—edge to 1 mm deep. Magnification—414×. The dust suppressant coating is shown as a layer (E) at the outer edge, next to the embedding plastic (P). The char particles appear as a continuous phase (C). Voids (V) are large and unconnected. The spots of yellow are the mineral matter residue, ash, from the parent coal.
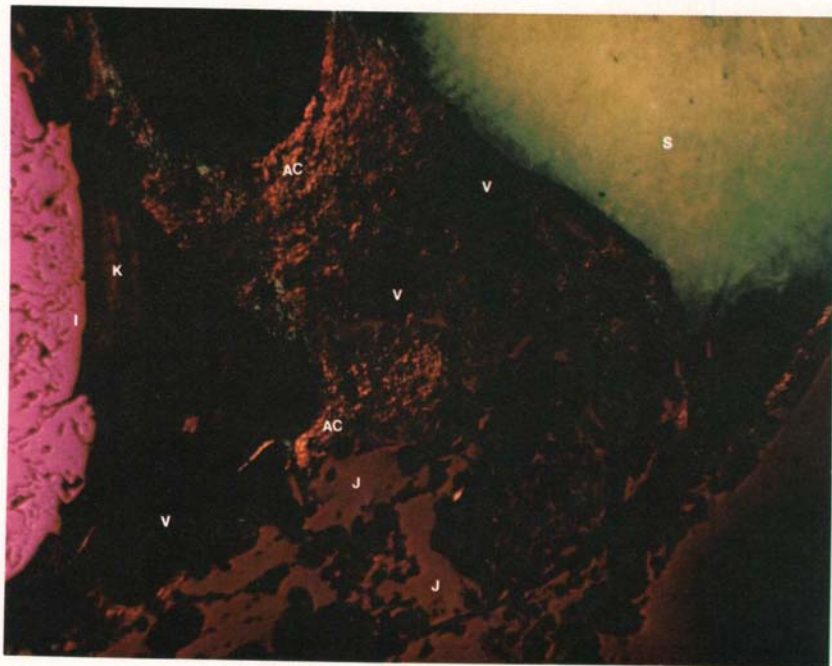
Plate XIII. *Inland steel test—S. Chicago, Ind. Formcoke reductant recovered from the ladle.*

Location of photomicrograph—edge to 1 mm deep. Magnification—414×. The specimen edge on this plate is at the upper right-hand corner, and the plate itself covers an area whose boundary from the edge is 1 mm. The reaction has caused an incursion of slag (S) at the right upper corner. The area AC is a char particle partially reacted and the beginning formation of graphite as anisotropic carbon. Unreacted char appears as a bright-pink arc at the plate left with a small amount of alkali (K) visible at its right edge and in the associated void (V). Isotropic carbon appears at the bottom of the plate and across the center contiguous with the anisotropic area to the top and slag to the right. Since this area is about 1 mm deep, the changes result from the surface reaction taking place.

Plate XIV. *Inland steel test—S. Chicago, Ind. Formcoke reductant recovered from the ladle.*

Location of photomicrograph—edge to 1 mm deep. Magnification—414×. This specimen was about 50% consumed, and the plate is oriented so that the specimen edge is at the upper left-hand corner. Again, the area covered extends inward about 1 mm to the partially reacted char particle (C) that appears at the bottom right as a mottled pink. The diagonal streak of bright white through the plate center consists of graphite (G) formed adjacent and bound to alkali (K) on its top and bottom sides and to the iron incursions on the diagonal. Slag (S) has penetrated about 1 mm to the edge of the partly reacted char particle (in the lower left). Beyond this boundary, the specimen was unreacted.
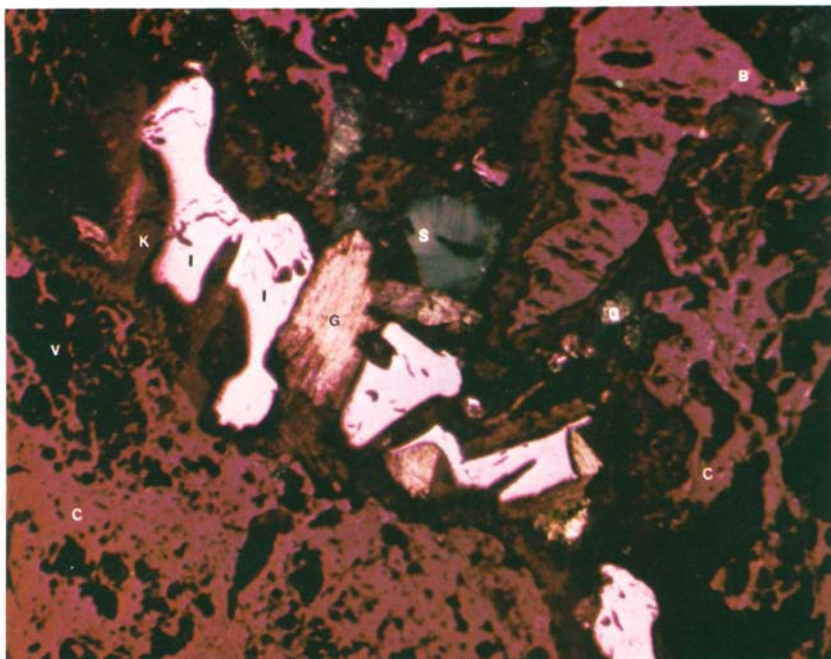
Plate XV. Inland steel test—S. Chicago, Ind. Oven coke reductant recovered from the ladle.

Location of photomicrograph—about at sample center. Magnification—414×. This plate is a section of a recovered oven coke specimen which was about 35 × 35 × 35 mm. Since oven coke is produced from a coal charge that melts, coalesces, and devolatilizes, that constituent of the coal that melts has a reflectance that reads out as binder (B) shown at the plate's upper right. Reacted carbon (C) from that constituent of the coal that does not melt looks almost like the binder constituent but does have a different reflectance. The predominant feature of the slide is the iron (I)–graphite (G)–alkali (K) complex that runs diagonally. This sequence always occurs, regardless of the carbon source. Alkali, probably washed from the furnace walls, has penetrated to the center of the specimen as slag and iron. The specimen was honeycombed with this type of structure. The void areas (V) were almost equal to the solid area and were connected, one to the other, out to the specimen edge about 15–20 mm away.
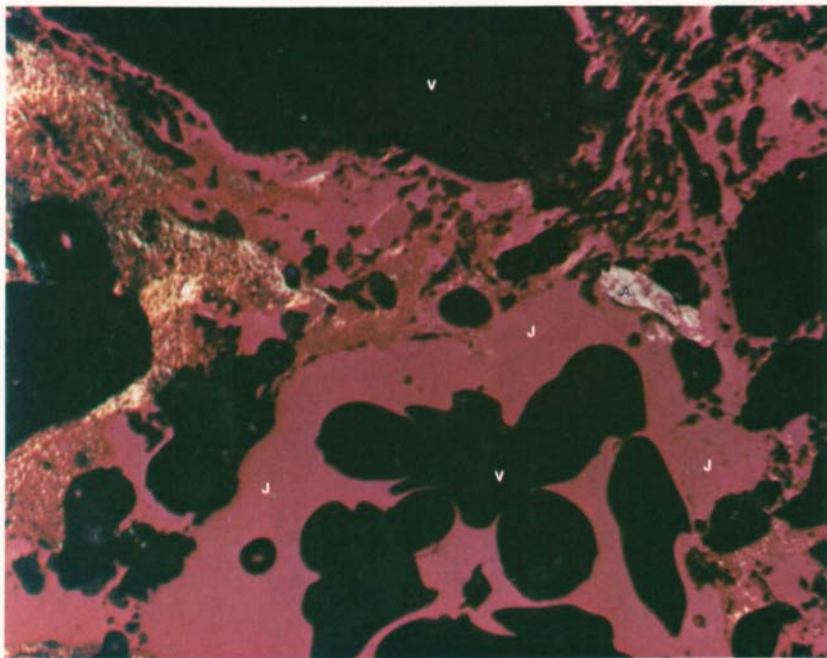
Plate XVI. Inland steel test—S. Chicago, Ind. Oven coke reductant recovered from the ladle.

Location of photomicrograph—about at sample center. Magnification—414×. Predominant on this plate are the voids (V) that have been generated at the center of the sample which was about 50% consumed—from approximately a 60 mm cube to about a 40 mm cube on the outside. There is anisotropic carbon (A) either formed or present as a residue in the original unreactive oven coke. However, the large masses of isotropic carbon (J) at the specimen center is honey-combed with voids and has been drastically reduced in strength; all the voids are connected to the surface. This reacted piece of oven coke, which was originally very strong, has lost at least 50% of its carbon density and even more of its strength.
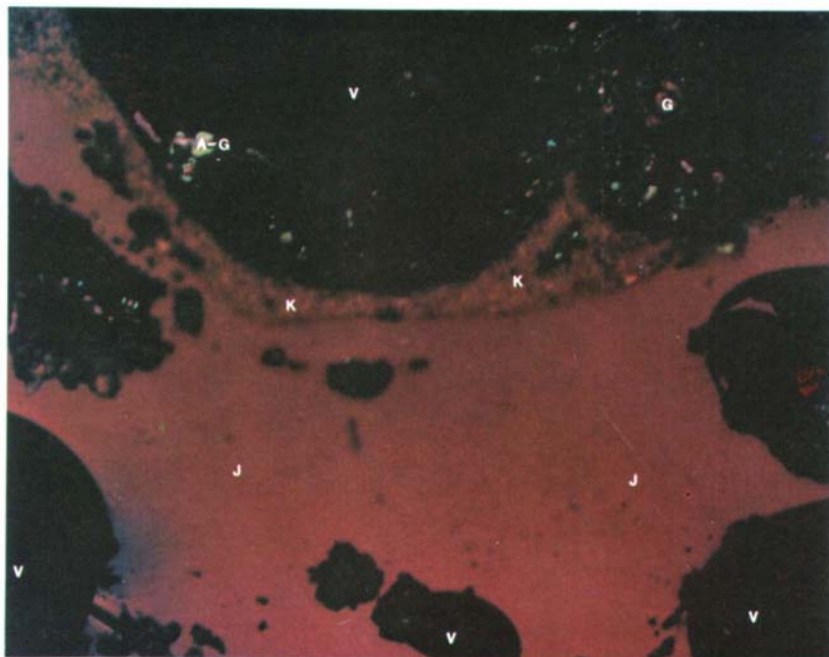
Plate XVII. *Inland steel test—S. Chicago, Ind. Oven coke reductant recovered from the ladle.*

Location of photomicrograph—edge to 1 mm deep. Magnification—414×. This photomicrograph seems to be a more dramatic display of the violent reaction that takes place in the center of each lump of oven coke as it passes through the blast furnace. Reactivity in oven coke, unlike reactivity in formcoke, is a function of internal surface area. Since the oven coke used in this test was of low reactivity, the effect of the furnace environment on coke structure is relatively less than on a similar piece of oven coke of twice this specimen's reactivity. Obviously, an oven coke with twice this specimen's reactivity would be almost completely reduced to fines and be plugged by iron and slag penetration. The area labeled J is isotropic carbon in transition; K is the alkali formation that is always present during the iron reduction reaction. Voids (V) cover about 40% of the plate area. This piece of oven coke is about to disintegrate to fines.